

Lecture Notes in Civil Engineering

Arvind Kumar Agnihotri
Krishna R. Reddy
H. S. Chore *Editors*

Proceedings of Indian
Geotechnical and
Geoenvironmental
Engineering
Conference
(IGGEC) 2021, Vol. 1

 Springer

Lecture Notes in Civil Engineering

Volume 280

Series Editors

Marco di Prisco, Politecnico di Milano, Milano, Italy

Sheng-Hong Chen, School of Water Resources and Hydropower Engineering,
Wuhan University, Wuhan, China

Ioannis Vayas, Institute of Steel Structures, National Technical University of
Athens, Athens, Greece

Sanjay Kumar Shukla, School of Engineering, Edith Cowan University, Joondalup,
WA, Australia

Anuj Sharma, Iowa State University, Ames, IA, USA

Nagesh Kumar, Department of Civil Engineering, Indian Institute of Science
Bangalore, Bengaluru, Karnataka, India

Chien Ming Wang, School of Civil Engineering, The University of Queensland,
Brisbane, QLD, Australia

Lecture Notes in Civil Engineering (LNCE) publishes the latest developments in Civil Engineering—quickly, informally and in top quality. Though original research reported in proceedings and post-proceedings represents the core of LNCE, edited volumes of exceptionally high quality and interest may also be considered for publication. Volumes published in LNCE embrace all aspects and subfields of, as well as new challenges in, Civil Engineering. Topics in the series include:

- Construction and Structural Mechanics
- Building Materials
- Concrete, Steel and Timber Structures
- Geotechnical Engineering
- Earthquake Engineering
- Coastal Engineering
- Ocean and Offshore Engineering; Ships and Floating Structures
- Hydraulics, Hydrology and Water Resources Engineering
- Environmental Engineering and Sustainability
- Structural Health and Monitoring
- Surveying and Geographical Information Systems
- Indoor Environments
- Transportation and Traffic
- Risk Analysis
- Safety and Security

To submit a proposal or request further information, please contact the appropriate Springer Editor:

- Pierpaolo Riva at pierpaolo.riva@springer.com (Europe and Americas);
- Swati Meherishi at swati.meherishi@springer.com (Asia—except China, Australia, and New Zealand);
- Wayne Hu at wayne.hu@springer.com (China).

All books in the series now indexed by Scopus and EI Compendex database!

Arvind Kumar Agnihotri · Krishna R. Reddy ·
H. S. Chore
Editors

Proceedings of Indian
Geotechnical
and Geoenvironmental
Engineering Conference
(IGGEC) 2021, Vol. 1

 Springer

Editors

Arvind Kumar Agnihotri
Department of Civil Engineering
Dr. B. R. Ambedkar National Institute
of Technology
Jalandhar, Punjab, India

Krishna R. Reddy
Department of Civil, Materials
and Environmental Engineering
University of Illinois at Chicago
Chicago, IL, USA

H. S. Chore
Department of Civil Engineering
Dr. B. R. Ambedkar National Institute
of Technology
Jalandhar, Punjab, India

ISSN 2366-2557

ISSN 2366-2565 (electronic)

Lecture Notes in Civil Engineering

ISBN 978-981-19-4738-4

ISBN 978-981-19-4739-1 (eBook)

<https://doi.org/10.1007/978-981-19-4739-1>

© The Editor(s) (if applicable) and The Author(s), under exclusive license to Springer Nature Singapore Pte Ltd. 2023

This work is subject to copyright. All rights are solely and exclusively licensed by the Publisher, whether the whole or part of the material is concerned, specifically the rights of translation, reprinting, reuse of illustrations, recitation, broadcasting, reproduction on microfilms or in any other physical way, and transmission or information storage and retrieval, electronic adaptation, computer software, or by similar or dissimilar methodology now known or hereafter developed.

The use of general descriptive names, registered names, trademarks, service marks, etc. in this publication does not imply, even in the absence of a specific statement, that such names are exempt from the relevant protective laws and regulations and therefore free for general use.

The publisher, the authors, and the editors are safe to assume that the advice and information in this book are believed to be true and accurate at the date of publication. Neither the publisher nor the authors or the editors give a warranty, expressed or implied, with respect to the material contained herein or for any errors or omissions that may have been made. The publisher remains neutral with regard to jurisdictional claims in published maps and institutional affiliations.

This Springer imprint is published by the registered company Springer Nature Singapore Pte Ltd.

The registered company address is: 152 Beach Road, #21-01/04 Gateway East, Singapore 189721, Singapore

Committees

Organizing Committee

Patron

Prof. R. K. Garg (Director)

Chairman

Prof. Arvind Kumar Agnihotri

Co-chairman and Principal Organizing Secretary

Dr. H. S. Chore

Convener

Dr. Davinder Singh

Organizing Secretary

Dr. Mrs. Rupali S.

Joint Organizing Secretaries

Dr. K. Senthil

Dr. Kanish Kapoor

Advisory Committee

Prof. N. K. Samadhiya (President, IGS), IIT Roorkee

Prof. G. L. Sivakumar Babu (Immediate Past President, IGS), IISc, Bangalore

Prof. J. T. Shahu (Honorary Secretary, IGS), IIT Delhi

Prof. Krishna R. Reddy, University of Illinois, Chicago (USA)

Prof. D. M. Dewaikar (Retd. Emeritus Fellow), IIT Bombay

Prof. J. N. Mandal (Retd. Emeritus Fellow), IIT Bombay

Prof. A. P. Singh, NIT Jalandhar

Prof. S. P. Singh, NIT Jalandhar

Prof. Raman Parti, NIT, Hamirpur
 Prof. S. K. Tiwari, MNIT Jaipur
 Prof. B. V. S. Visvanadham, IIT Bombay
 Prof. R. K. Ingle, VNIT, Nagpur
 Prof. G .R. Dodagoudar, IIT Madras
 Prof. G. Madhavi Latha, IISc, Bangalore
 Dr. Sanjay Kumar Shukla, Edith Cowan University, Perth, Australia
 Dr. Prabir K. Kolay, Southern Illinois University Carbondale (USA)
 Prof .Deepankar Choudhary, IIT Bombay
 Prof. K. G. Guptha, GCE, Farmagudi, Goa
 Prof. Vasant Matsagar, IIT Delhi
 Dr. Sanjay Nimbalkar, University of Technology Sydney, Australia
 Dr. S. K. Mukherjee, Retd., Secretary, PWD, Maharashtra
 Dr. I. K. Pateriya, NRRDA, New Delhi
 Dr. S. K. Ukarande, KJSIEIT, Mumbai (University of Mumbai)
 Dr. Sunil Basarkar, AFCONS, Mumbai
 Dr. C. R. Parthasarthy, Sarathy Geotech, Bangalore
 Dr. V. B. Ashtankar, MCGM Mumbai

Technical Committee

Prof. R. K. Sharma, NIT, Hamirpur
 Prof. Vishwas A. Sawant, IIT Roorkee
 Prof. C. H. Solanki, SVNIT Surat
 Prof. P. T. Ravichandran, SRMIST, Kattankulathur
 Dr. Kousik Deb, IIT Kharagpur
 Dr. Mrs. Sunita Kumari, NIT Patna
 Dr. Nilima Satyam, IIT Indore
 Dr. M. D. Goel, VNIT, Nagpur
 Dr. Sreevalsa Kolathayar, NITK Surathkal
 Dr. G. Kalyan Kumar, NIT, Warangal
 Dr. Sharbony Adhikary, VNIT, Nagpur
 Dr. Purnachandra Savoikar, GCE, Farmagudi, Goa
 Dr. V. B. Deshmukh, VJTI, Mumbai
 Dr. Mrs. Smita Patil, DMCE New Mumbai (University of Mumbai)
 Dr. R. B. Magar, AIKTC Panvel (University of Mumbai)
 Dr. Rajiv Chauhan, IKGPTU, Kapurthala
 Prof. Amit Srivastava, LPU, Phagwara
 Dr. Sanjeev Naval, DAVIET, Jalandhar
 Dr. Sudhir Arora, DAV University, Jalandhar
 Dr. Rajiv Bhatiya, MCP, Jalandhar
 Mr. K. K. Kanji, K. K. Spun Pvt. Ltd., Delhi
 Mr. S. K. Gupta, Mega Metro Pvt. Ltd., Delhi

Mrs. Minimol Korulla, MACCAFERRI Environmental Solutions Pvt. Ltd.,
Gurugram

Dr. Dulal Chandra Saha, Infrastructure Design Consultants Pvt. Ltd., Mumbai

Mr. Hemant Gor, Petrofac International Ltd., Sharjah (UAE)

Preface

Indian Geotechnical Society's, Jalandhar Chapter, was established in February 2020. After inception, the chapter conducted few workshops, seminars and expert lectures. As a major initiative in furthering the activities of the chapter, it in association with the Department of Civil Engineering of Dr. B. R. Ambedkar National Institute of Technology Jalandhar recently organized "First Indian Geotechnical and Geoenvironmental Engineering Conference-2021 (IGGEC-21021)". The conference was organized on 19–20 November 2021.

The conference aimed at bringing together leading academicians, scientists, researchers and field professionals including research scholars to exchange and share their ideas, experiences and research inputs pertaining to all aspects of geotechnical and geoenvironmental engineering, waste management and sustainable engineering. It also aimed at providing the premier interdisciplinary forum for researchers, practitioners and educators to present and discuss the most recent innovations, trends and concerns, practical challenges encountered and the solutions adopted in this field.

The papers received for the conference and selected after thorough review are grouped together under the following six themes.

The papers on following themes have been called and received

- Theme 1: Behaviour of Geomaterials and Geotechnical Investigation
- Theme 2: Soil-Structure Interaction, Earthquake Engineering and Computational Geo-mechanics
- Theme 3: Ground Improvement and Transportation Geotechnics
- Theme 4: Environmental Geotechnology
- Theme 5: Recycled Waste Materials
- Theme 6: Sustainable Infrastructure Engineering and Others.

Apart from the key note lecture, totally 96 papers covering the wide spectrum of the geotechnical engineering and the allied fields contributed by the authors are included in the proceedings.

Jalandhar, India
Chicago, USA
Jalandhar, India

Arvind Kumar Agnihotri
Krishna R. Reddy
H. S. Chore

About IGS, Jalandhar Chapter

The Indian Geotechnical Society (IGS) was established in the year 1948 with the purpose of advancement and dissemination of knowledge in different fields of geotechnical engineering. IGS, Jalandhar was established recently, i.e. in February 2020 under the flagship of IGS, New Delhi. The chapter was inaugurated by Prof. G. L. S. SivaKumar Babu, the erstwhile president of Indian Geotechnical Society, and Prof. N. K. Samadhiya (the current president of Indian Geotechnical Society). Prof. Arvind Kumar Agnihotri, the founder chairman, and Dr. H. S. Chore, the founder secretary along with their executive committee members, are putting in their best efforts to establish the chapter as the medium for disseminating knowledge in the field of geotechnical engineering and allied fields through workshops, seminars and short-term courses by inviting the eminent personalities in the field from country as well as from abroad. The group of the academicians led by Prof. Arvind Kumar Agnihotri in association with Prof. Krishna R. Reddy of University of Illinois, Chicago (USA), was instrumental in initiating the Environmental Geotechnology Recycled Waste Materials and Sustainable Engineering (EGRWSE).

Contents

Behaviour of Geomaterials and Geotechnical Investigation	
Sustainability Assessment of Controlled Low Strength Materials Utilizing Various Industrial Waste Materials	3
Sasha Simon, Luke Zaroni, Alex Young, Patrick Hulsebosch, Jyoti K. Chetri, and Krishna R. Reddy	
Effect of Fiber Reinforcement on the Direct Tensile Strength of Fiber-Reinforced Black Cotton Soil	17
Uma Chaduvula, B. V. S. Viswanadham, and Jayantha Kodikara	
Studies on Sugar Cane Bagasse Ash and Blast Furnace Slag-Based Geomaterial	25
H. R. Nikhade and B. Ram Rathan Lal	
Swelling Behaviour of Expansive Soil Reinforced with Geocell and Jute Fibres	33
Sanjeev Kumar, Sanjeev Naval, and Anil Kumar Sahu	
Stabilization of Black Cotton Soil by Using RBI Grade-81: A Review ...	53
Dharmendra Singh and Vijay Kumar	
Geotechnical Investigation of Soil for Construction of a Court Building	61
Nadeem Akhtar, Md. Intekhab Sami, Vaqar Sultan, and Zoha Khairoowala	
Application of Electrical Resistivity in Site Investigation at Ground Profile	73
Swati Ganesh Sonawane, A. B. Saner, Harshal Sarjerao Desale, and S. R. Joshi	
A Review on Various Geotechnical and Geophysical Investigations for a Dam Rehabilitation Project	83
Harshit Srivastava, R. P. Tiwari, Vijay Kumar, and Dharmendra Singh	

Investigation of Geotechnical Factors Affecting Electrical Resistivity of Soil	95
Suraj Sukhadev Vankamble and Rupa S. Dalvi	
Predicting Compaction Parameters of Silty Soil by Nonlinear Multivariable Approach	103
Shivani S. Gour, Vijay V. Muthekar, and A. B. Saner	
Study of Arch Formation in Basalt Rock—A Case Study	115
Tejal K. Khule and Rupa S. Dalvi	
Consolidation of Layered Soils with Variable Compressibility	127
Deepak Kumar Singh, Chitranshu Kumawat, and Siddharth Mehndiratta	
1D Consolidation of Silty Clay Subject to Different Ramp Loadings	141
Sumanta Roy and Sibapriya Mukherjee	
Assessment of Effective Shear Strength Parameters in Triaxial CU Shear Test	151
Suresh Maurya	
Geotechnical Properties of Copper Slag, Rice Husk Ash Blended with Lime, Cement and Geopolymer—A Comparative Study	163
Kuldeep Sharma and Arvind Kumar	
Effect of Addition of Slag on Engineering Properties of Clayey Soil	175
Aditya D. Ahirwar and H. S. Chore	
Analysis of Bearing Capacity and Settlement from Cone Penetration Test Results at an Irrigation Project	181
J. Sumalatha and J. Suresh Babu	
Soil-Structure Interaction, Earthquake Engineering and Computational Geo-mechanics	
Influence of Burial Depth of Soil on Reinforced Concrete Tunnel Against the Impact and Blast Loading	193
K. Senthil, Keshav Saini, and Manish Kumar	
Plate Load Tests on the Ring and Circular Footings	209
Vaibhav Sharma and Arvind Kumar	
Analytical Study on Soil-Structure Interaction of Framed Structure with Isolated Footing Resting on Silty Sand	219
R. Chaitra, R. Sridhar, and B. M. Ramesh	
Simulation of Load Bearing Capacity of a Single Pile in a Multi-layered Soil	229
Pratyusha Bandaru and Hemaraju Pollayi	

Studies on Evaluation of Effect of Sloping Ground on Lateral Pile Response: A Brief Review 235
 Nitesh Thakur and Hemant Chore

Numerical Modelling of Coal Mine Overburden Dump Slopes: Developments and Current State-of-the-Art 241
 Madhumita Mohanty, Rajib Sarkar, Sarat Kumar Das, and Krishna R. Reddy

Slope Stability Analysis of Highway Embankment by Using GEO5 Software 249
 Dharmendra Singh and Vijay Kumar

Prediction of Unconfined Compressive Strength of Clayey Soil Stabilized with Steel Slag and Cement 259
 Aditya D. Ahirwar and H. S. Chore

Experimental and Analytic Study of the Uplift Capacity of a Horizontal Plate Anchor Embedded in Geo-Reinforced Sand 267
 K. B. Akbar Husain and Samirsinh P. Parmar

Finite Element Analysis (FEA) of Geocell Reinforced Pavement in Hilly Terrain 291
 Aman Kashyap, Vijayasri Thanikella, G. Bharat, and Kranthi Kumar Kuna

Plaxis 2D Numerical Analysis of Encased Stone Column in Soft Clay ... 303
 Sanket S. Mudekar, Vidya N. Patil, Hemant S. Chore, and Vishwas A. Sawant

Multiple Linear Regression Analysis for Predicting Unconfined Compressive Strength of Fiber Reinforced Fly Ash Stabilized Lateritic Soil 315
 Hemant S. Chore, Swati Yede, Bhupati Kannur, and Rakesh Kumar

Prediction of Unconfined Compressive Strength of Fly Ash–Soil–Lime–Fiber System Using Multiple Regression Analysis 323
 Hemant S. Chore, Swati Yede, Bhupati Kannur, and Rakesh Kumar

ANN Model for Prediction of Compressive and Tensile Strength of Bacterial Concrete 333
 S. Varadharajan, S. V. Kirthanashri, Mohammad Shahban, Bishnu Kant Shukla, and Gaurav Bharti

Ring Foundation—A Review 341
 Prince Karandeep Singh and Arvind Kumar

Seismic Site Response and Liquefaction Potential for Proposed Underground Parking Site in Saharanpur (U.P.) 361
 Manish Bhutani and Sanjeev Naval

ANN Model for Evaluation of Seismic Behavior of Irregular Steel Building Frames 373
S. Varadharajan, S. V. Kirthanashri, Mrityunjai Govind Rao, Animesh Jaiswal, and Bishnu Kant Shukla

Deterministic Seismic Hazard Analysis for Amritsar, Punjab, India 381
Nikhil Bhatti, Sanjeev Naval, and Gagan Deep

Ground Improvement and Transportation Geotechnics

Effect of Sand Blanket Reinforced with Geogrid Over the Stone Column in Compressible Clay Soils: 3D Numerical Study 397
Sudheer Kumar Jala, Sudhanshu Sharma, and Aijaz H. Bhat

Use of Chitosan Biopolymer and Fly Ash to Enhance Mechanical Properties of Soil 407
Rohan M. Shinde, Shweta G. Jambhulkar, and Rupa S. Dalvi

Analyze of Subgrade Soil Behavior Blended with Phosphogypsum and Fly Ash as Additive 421
Priyanka Saha and Vidya Sagar Khanduri

Evaluation of Deviator Stress of Lime-Alcofine-Stabilized Fly Ash from Ultrasonic Pulse Wave Velocity 427
Rakesh Kumar Dutta and Jitendra Singh Yadav

Strength Behaviour of Dredged Soil Stabilized with Cement and Fly Ash 435
Razia Sultan and M. Y. Shah

An Experimental Study on the Effect of RBI Grade 81 Additive on the Engineering Properties of Clayey Soils 447
Manisha Gunturi and P. T. Ravichandran

A Study on the Effectiveness on the Polyethylene Strips in Cement-Treated Soil 457
Manisha Gunturi and Goutham Sarang

Shear Strength Characteristics of Marble Dust-Lime Stabilized Marine Clay 467
B. Manjula Devi and H. S. Chore

Evaluation of Bagasse Ash in Stabilization of Pavement Sub-Grade 477
Ridhi H. Jethwa, Sharmeen S. Momin, B. Manjula Devi, and H. S. Chore

An Experimental Study on the Strength Behaviour of Black Cotton Soil Stabilized with Industrial Waste Material (Zinc Slag) for Pavement Construction 483
 Mohini Patel, P. S. Prasad, Pranav R. T. Peddinti, and Vijai Kumar Kanaujia

Effect of Resilient Modulus on Inverted Base Pavements—A Theoretical Study 493
 Swagata Mishra, Pratik Jaiswal, and D. Sitarami Reddy

Identification and Analysis of Factors of Delay in Road Construction Projects 505
 Bishnu Kant Shukla, Vaishnavi Bansal, S. Varadharajan, Gaurav Bharti, Aparupa Shenoy, Udit Kumar Singh, and S. V. Kirthanashri

Effect of Curing on Strength of Clayey Soil Stabilized with Marble Dust 513
 Aditya D. Ahirwar and H. S. Chore

Analysis of Bagasse Ash with GBFS as a Cement-Treated Sub-Base 519
 B. Manjuladevi and H. S. Chore

Strength Characteristics of Copper Slag and Lime Stabilized Clayey Soil 531
 Aditya D. Ahirwar and H. S. Chore

Influence of Fines Content on the Strength and Compaction of the Poorly Graded Soil 539
 Vaibhav Sharma, Arvind Kumar, Pritesh Patel, and Dheeraj Kumar

Modification of Engineering Properties of Soil Using Waste Materials: A Review 549
 Alka Shah and Tejas Thaker

Suction Analysis at Soil-Geocell Interface for a Clayey Soil 561
 Bhavita S. Dave, Chandresh H. Solanki, and Atul K. Desai

Potential of Coconut Shell Powder on Geotechnical Characteristics of Stabilized Soil 569
 Pratik Ranjan Yadav and Mahesh Patel

Unconfined Compressive Strength of Fly Ash-Soil-lime-Fiber System 581
 Bhupati Kannur, Hemant S. Chore, and Swati Yede

Bearing Capacity of Geocell Reinforced Model Fly Ash Slope 591
 Vidya N. Patil, Hemant S. Chore, and Vishwas A. Sawant

**Unconfined Compressive Strength of Clayey Soil Stabilized
with Marble Dust 601**
H. S. Chore, Anurag M. Khadse, and Aditya D. Ahirwar

About the Editors

Prof. Arvind Kumar Agnihotri is Professor of Civil Engineering at NIT Jalandhar. He completed his Ph.D. from University of Roorkee (1998), M.Tech. from NIT Kurukshetra (1989) and B.E. from Panjab University Chandigarh (1987). He possesses a work experience of around 32 years in research, teaching and academic administration, with several years spent holding key leadership positions. His areas of interest are Geotechnical and Geo-Environmental Engineering, Reinforced Earth (Geo-Synthetics and Geofibers), Ground Improvement and Soil-Structure-interaction. He has supervised 12 Ph.D. Thesis and 4 more are in progress. He has guided 52 M.Tech. dissertations. He has published more than 135 papers out of which about 85 in referred international and National journals and 50 in conferences and 5 edited books/conference proceedings. He served as Head of Civil Engineering, Dean Academic, Dean (Planning and Development) at prestigious Dr. B. R. Ambedkar National Institute of Technology, Jalandhar. He is fellow/member of many professional organizations like ASCE, IGS, ISTE, Institution of Engineers, International Society of Soil Mechanics and Geotechnical Engineering and Indian Roads Congress. He is reviewer of many international journals of repute.

Dr. Krishna R. Reddy is a Professor of Civil, materials and Environmental Engineering, the Director of Sustainable Engineering Research Laboratory and also the Director of the Geotechnical and Geo-Environmental Engineering Laboratory in the Department of Civil, materials and Environmental Engineering at the University of Illinois at Chicago. Dr. Reddy received Ph.D. in Civil Engineering from the Illinois Institute of Technology, Chicago, USA. He received gold medals for being first in his class of B.S. (Civil Engineering) at Osmania University, India, and M.S. (Civil Engineering) at the Indian Institute of Technology, Roorkee.

Dr. Reddy is the author of four major books: (1) Geoenvironmental Engineering: Site Remediation, Waste Containment, and Emerging Waste Management Technologies, (2) Sustainable Engineering: Drivers, Metrics, Tools, and Applications, (3) Sustainable Remediation of Contaminated Sites, and (4) Electrochemical Remediation Technologies for Polluted Soils, Sediments and Groundwater. He is also author of 262 journal papers, 27 edited books/conference proceedings, 2 book chapters,

and 226 full conference papers (with h-index of 65 with over 14,000 citations). Dr. Reddy has given 231 invited presentations in the USA and 21 other countries (Argentina, Brazil, Canada, China, Colombia, France, Germany, Greece, Hong Kong, India, Italy, Japan, Kuwait, Macedonia, Mexico, Spain, Sri Lanka, South Korea, Turkey, Thailand, and UK). Dr. Reddy has served or currently serves as an Associate Editor or Editorial Board Member of over 10 different journals, including *ASCE Journal of Geotechnical and Geoenvironmental Engineering*, *ASTM Geotechnical Testing Journal*, *ASCE Journal of Hazardous, Toxic and Radioactive Waste*, *Journal of Hazardous Materials*, among others. He has also served on various professional committees, including the Geoenvironmental Engineering Committee and Technical Coordinating Council of Geo-Institute (GI) of the American Society of Civil Engineers (ASCE) and the Environmental Geotechnics Committee of International Society of Soil Mechanics and Geotechnical Engineering (ISSMGE). Dr. Reddy has received several awards for excellence in research and teaching, including ASCE Wesley W. Horner Award, ASTM Hogentogler Award, UIC Distinguished Researcher Award, University of Illinois Scholar Award, and University of Illinois Award for Excellence in Teaching. He is a Fellow of the American Society of Civil Engineers (FASCE), a Diplomate of Geotechnical Engineering (DGE), and a Board Certified Environmental Engineer (BCEE). He is also a registered Professional Civil Engineer (PE) and an Envision™ Sustainability Professional (ENV SP).

Dr. H. S. Chore Associate Professor and Head of Civil Engineering Department at NIT Jalandhar, received his B.E. from Nagpur University, Completed Masters from IIT Bombay and Doctoral Studies from VNIT Nagpur. His total teaching experience spans over 26 years. He has 244 publications to his credit with 58 research papers in the reputed refereed Journals; 91 papers in International Conference and 95, in National Conferences. He has guided 06 Ph.D. students and 06 more are in progress. He has guided 44 M.Tech. dissertations. He is member of many professional organizations like ACI, IGS, ISTE, Institution of Engineers, and Indian Roads Congress. He is reviewer of many international journals of repute.

Behaviour of Geomaterials and Geotechnical Investigation

Sustainability Assessment of Controlled Low Strength Materials Utilizing Various Industrial Waste Materials



Sasha Simon, Luke Zanoni, Alex Young, Patrick Hulsebosch, Jyoti K. Chetri, and Krishna R. Reddy

Abstract Controlled low strength material (CLSM) can be used as backfill material for utility trench construction. Many researchers proposed CLSM using industrial waste materials as part of the designs of these cementitious mixes. In this study, a comparative sustainability assessment of different CLSM designs that incorporate industrial byproducts is performed and compared to a conventional aggregate backfill design. This study also assessed the comparative sustainability of CLSM and conventional aggregate as trench backfill for a utility pipe installation on a roadway/drainage improvement project. The project includes 1.5 miles of utility trenching of a proposed frontage road and drainage improvement in the Chicago metropolitan area. The sustainability assessments include evaluating the environmental, economic, and social (triple bottom line) impacts of the alternate CLSM and conventional trench backfill options. A single sustainability index for each backfill design is computed using a multi-criteria decision analysis methodology and compared to identify the most sustainable CLSM design option.

Keywords Backfill · Industrial waste · LCA · Sustainability · Utility trenches

1 Introduction

The construction sector is responsible for a major portion of the global output of green-house gas (GHG) emissions. As environmental concerns continue to grow, it is important that the most sustainable methods prevail. Sustainability should be sought in even the most minute details. Backfilling methods, often times overlooked in the grand scheme of construction operations, can even be utilized to incorporate sustainability into a project plan. An alternative backfilling method that has arisen in recent years has been controlled low strength material (CLSM), which offers a possible sustainable solution where previously not thought possible. CLSM, also

S. Simon · L. Zanoni · A. Young · P. Hulsebosch · J. K. Chetri · K. R. Reddy (✉)
Department of Civil, Materials, and Environmental Engineering, University of Illinois, 842 West Taylor Street, Chicago, IL 60607, USA
e-mail: kreddy@uic.edu

© The Author(s), under exclusive license to Springer Nature Singapore Pte Ltd. 2023
A. K. Agnihotri et al. (eds.), *Proceedings of Indian Geotechnical and Geoenvironmental Engineering Conference (IGGEC) 2021, Vol. 1*, Lecture Notes in Civil Engineering 280, https://doi.org/10.1007/978-981-19-4739-1_1

known as flowable fill, is a permitted alternative to the conventional aggregate backfilling method used to fill utility trenches and other excavations at construction sites. A CLSM is a highly flowable and self-leveling material, usually composed of water, cement, and a fine aggregate material such as fly ash or other byproduct materials. The American Concrete Institute (ACI) defines a CLSM as a self-compacting, flowable, durable, and strong cementitious material with the compressive strength of the material being 8.3 MPa or lower. Compared with a conventional backfill, the advantages of a CLSM are no vibration compaction, less manpower, a narrower trench, easy distribution in complex sites (as it is flowable), no settlement due to low compressive strengths, durability, flexibility, and the ability to be combined with otherwise useless waste byproducts which would otherwise go to landfills. The disadvantages of CLSM involve possible increases in emissions and energy usage depending on the amount of cement in the mix design as well as the amount, and mode of transportation involved for the raw materials that compose the mix. The overall goal of this life cycle sustainability assessment is to determine the sustainability of CLSMs compared to conventional backfilling methods and to determine which CLSM mix design, if any, best reflects the three pillars of sustainability (environmental, economic, and social).

In this project, the life cycle sustainability assessment is performed in two parts. The first part considered was an isolated analysis of seven mix designs as well as the conventional backfilling method. The transportation costs for raw materials in the different mix designs were not considered. Without transportation costs, a clearer picture is painted of the individual effects different mix designs might have. The second part of analysis pertained to a specific application. For the specific application, seven CLSM mix designs were considered along with the conventional backfill as well. The transportation logistics in this part were considered, as well as the distinguishing or unique equipment required as part of the individual backfill options. This study contemplates comparing the use of different trench backfill methods on a roadway/drainage improvement located in Maywood, Illinois, USA. The study includes 1.5 miles of utility trenching in the right-of-way of Bataan Drive that acts as a frontage and eventual access route to I-290 (Eisenhower Expressway). The trench will encompass a 24" Reinforced Concrete Pipe that is being added for drainage issue mitigation in the surrounding community [5].

2 Project Background

Underground utilities (combined sewer, sanitary sewer, storm sewer, water main, individual utility services, gas, electric, telecommunications, etc.) crisscross our communities and often require protection using a select backfill material. The conventional method of backfilling a utility trench is to bed and trench the utility in granular coarse aggregate in 8"–12" lifts, with each lift requiring compaction to the applicable government agency standard. Typically, a greater area of land than required to solely lay the utility must be disturbed in order to allow for compaction equipment to fit and operate within the trench. Further, the time spent compacting can become

lengthy as the trench increases in depth, causing a significant increase in the duration of the project. The conventional method has a lower direct cost and thus is the most commonly applied technique; however, alternative methods (such as CLSMs that integrate waste products instead of virgin aggregate) may be a better alternative when evaluating the sustainability through the framework of the triple bottom line.

The purpose of this project is to evaluate alternative utility trench backfilling methods for their sustainability. However, the scope of this project does not include the actual design and testing of the mixes themselves. Instead, various mix designs from a literature review are selected and compared with each other. To increase the sustainability of the CLSM alternative designs, this study evaluated designs that integrate waste byproducts from industrial activities. This not only has the benefits associated with the reduction of production of new materials, but it can also result in a decrease in waste management-related issues associated with waste products. Essentially, by using waste products in a CLSM design, it is possible to find a use for material that would otherwise go directly to landfills.

3 Technical Alternatives and Design

An isolated analysis that contemplates the optimal mixes selected from the literature review in “isolation” (no transportation considerations) was first completed for the purposes of understanding how the environmental impacts and costs of the 7 CLSM mixes compared to the conventional method of backfilling. This approach provided results that show how sustainable the mixes could be. Obviously, emissions can be a large contributing factor to both economic and environmental sustainability, so in reality, the haul distances must be considered. However, the isolated approach was essential for providing information regarding how sustainable the admixture could be if sourced locally. The technical design for the isolated analysis of the utility trench for a 24 in. reinforced concrete pipe of length 1000 ft included a 5.5 ft wide trench, 15.26 ft³/ft of fill, or 15258 ft³ of total fill volume in conventional design. Similarly, for the same utility trench, the CLSM design resulted in a trench of 4.67 ft width, 12.20 ft³/ft, or 12202 ft³ of fill volume.

It should be noted that the only significant difference between the two designs is the width of the trench. Due to the self-leveling and self-compacting nature of the CLSMs, it is not necessary to over excavate the utility trench to allow for maneuverability of compaction equipment [6]. For isolated analysis, the materials of each mix design for a 1000-foot long trench are considered, whereas the specific project analysis took into consideration the full 1.5-mile length and transportation inputs. The materials quantities for each mix design were multiplied by a factor to convert to the specific analysis. These conversion factors were 27 for the conventional backfill and 28.1 for CLSM designs.

The seven CLSM mixes were selected specifically because they were the most sustainable with the lowest cement content, based on the published research studies. It should be noted, however, that the research studies dealing with CLSMs was not

necessarily to create a mix design with low emissions (e.g., one study tried to provide a very strong CLSM, which required high amount of cement), so the study was not able to compare like for like the material properties of the CLSM finished product. There is still the possibility that the same materials used in the mix designs could be used to create a very sustainable design if that was the design approach. Table 1 shows the mix designs selected for use in the sustainability analysis, along with their research source which can be referred to for additional information regarding the particular CLSM design.

The density and the material proportions allowed for the mixes to be batched or scaled for the analysis in this study. For each CLSM mix design, it was assumed that placement and mixing energy would be relatively similar; they would not change the relative sustainability between each mix design. The major component, other than material inputs that would vary, is the transportation quantities of the source materials. Table 2 shows the transportation quantities used for this project.

The specific project analysis takes transportation distances into account (for CLSM, from waste material source to the mix plant location) as well as from mix plant to project site. Additionally, total materials required for each alternative for the 1.5-mile length of trench are calculated.

Table 1 Summary of CLSM mixes selected based on published research studies

CLSM	Source	Selection	Properties		
			Strength (28 days)	Density (28 days)	Fresh density
			kPa	Kg/m ³	Kg/m ³
Bottom ash (mix 1)	Naganathan et al. [7]	5A	240	1508	1629
Fly ash + Sludge (mix 2)	Gabr and Bowders [4]	Conclusion recommended	550	2345	2142
Mine tailings (mix 3)	Bouzalakos et al. [2]	Optimized mix 2	1380	2600	2890
Recycled fine aggregates (mix 4)	Etxeberria et al. [3]	30% recycled aggregate	720	1700	1549
Stainless steel reducing slag (mix 5)	Sheen et al. [10]	M34/30	595		2056
Bottom ash and sediment (mix 6)	Naganathan et al. [7]	5D	670	1948	1797
Paper mill products (mix 7)	Wu et al. [11]	Optimal (g12)	640		2297

Table 2 Summary of transportation quantities for specific project analysis

Item	Entity	Location	Distance to site (miles)	Method
Project site	I-290/Bataan Rd	Maywood, IL		
Mix plant	Ozinga Plant	McCook, IL	6.3 miles	Truck
Aggregate	Vulcan Materials	McCook, IL	0.0	Truck
Quarry dust	Vulcan Materials	McCook, IL	0.0	Truck
Cement	Illinois Cement Co	LaSalle, IL	84	Barge
Fly ash	Will County Generating Station	Romeoville, IL	21.2	Barge
Slag	Beemsterboer Slag Corp	East Chicago, IN	39.9	Truck
Bottom ash	Will County Generating Station	Romeoville, IL	21	Barge
Paper sludge	Alsip MiniMill, LLC	Alsip, IL	15.5	Truck
AMD sludge	Alsip MiniMill, LLC	Alsip, IL	15.5	Truck
Mine tailing	Super Fund Site	Galena, IL	70	Truck

4 Sustainability Assessment Methodology

4.1 Environmental Sustainability

The environmental sustainability assessment was completed for the isolated analysis and specific project application by life cycle assessment (LCA) using SimaPro software. For this project, the emissions of waste materials were not considered, and emissions associated with the materials specifically produced for the backfill alternative are considered. For the specific project application, SimaPro software is also used to determine the environmental impacts of each of the 7 CLSM alternatives and conventional backfill. Material quantities and transportation distances are used as inputs. TRACI analysis method was utilized for all analyses in this study.

4.2 Economic Sustainability

This sustainability assessment featured an isolated analysis, excluding transportation costs, and a specific analysis tied to an actual ongoing project in Maywood, IL, USA. For direct costs, material and labor costs were the same for both economic assessments only differing in their quantities. The quantity of materials for each analysis was determined by the amount of material needed for the size of the trench, the different densities of each material, and then the individual breakdowns of each mix design. Material costs were determined using industry standards and prices with the majority of the prices obtained directly from local building material companies to ensure accuracy for the specific analysis. The cost of water was

ascertained via the Illinois Department of Natural Resources. The mining byproducts, acid mine drainage, AMD, sludge, and mine tailings, were estimated based on the published sources which were as follows: AMD sludge \$22.5/CY, bottom ash \$8/ton, cement \$126.5/ton, fly ash \$90/ton, mine tailings \$10.91/ton, natural aggregate \$12/ton, quarry dust \$3.25/CY, recycled aggregate \$15/ton, SSRS \$3.75/ton, and water \$14.53/1000 gallon.

Conventional backfill is not self-leveling like CLSM so it requires a lot of manpower to compact it in layers. These layers are usually every 6–12". In addition, more equipment is needed for conventional backfill to help place it and compact it. Equipment includes backhoes, vibrating compactors, and hand compactors. Fuel costs for the different equipment were determined by the fuel economy of the specific equipment and how long it was in operation for. In order to operate this equipment, skilled laborers were needed further adding to the labor costs. For the 1000-foot-long trench in the isolated analysis, a total of 90 man hours was determined, whereas 713 man hours were needed for the 1.5-mile-long trench in the specific analysis. The transportation costs for the specific project analysis were taken directly from statistics provided by the U.S. Department of Transportation which were \$0.03/ton-mile for rail, \$0.1/ton-mile for barge, and \$0.37/ton-mile for truck. The preferred modes of transportation of material were barge and rail as they are the much cheaper alternative as well as the more environmentally friendly alternatives with higher carrying capacity and less emissions. The second portion calculations were the distances materials had to travel to reach the concrete mixing plant and their mode of transportation. The majority of the materials were within reasonable distances except the mining byproducts which had to be transported by truck from a mine in Galena, IL which is 170 miles away. The recycled aggregate had minimal transportation costs, only concrete was considered, as both types of aggregate were on site. The quantity of materials, in tons, and the miles were then multiplied together with the product again being multiplied by the intermodal costs to obtain the final transportation costs in dollar amounts.

For indirect costs, SimaPro's stepwise method was used to estimate monetized environmental costs based on cumulative impacts of the assemblies and processes within our specific project analysis. This takes into account the transportation emissions, material emissions, as well as equipment emissions among other processes. These contributions from impact categories and impact pathways are summed and represented in various equivalent units. Monetary values are assigned using the "Single Score" function and output monetary values as USD 2002 were converted to 2020 values, via an inflation value of 43%. For comparison, other cost estimates included the U.S. EPA's cost of carbon as well as the State of Illinois' cost of carbon which were \$42/kg-CO₂ and \$16.5/kg-CO₂, respectively. The stepwise numbers were higher than both of these but still followed the same trends. In an effort of being conservative with cost estimates, the study chose to use the stepwise numbers in the final results.

4.3 Social Sustainability

Social sustainability can be difficult to quantitate due to social factors being qualitative in nature. For converting the qualitative factors to quantitative data, the social sustainability evaluation matrix (SSEM) was used [9]. The SSEM method breaks social sustainability into four different dimensions: social-individual, socio-institutional, socio-economic, and socio-environmental. Each of the dimensions consist of several key themes also known as social indicators. Social indicators are measures that are used to assist in quantifying the wellbeing of individuals and the community surrounding a project [9]. The social indicator categories selected for this study included social, socio-institutional, socio-environmental and socio-economic. Some of the indicators under each category were effect of proposed backfill technique on quality-of-life issues during construction, incorporation of green and sustainable infrastructure, degree of protection afforded to utility trench backfill workers by proposed activity and third-party business generation related to trench backfill, respectively. Each category had 5–6 such indicators.

Using the indicators as a template, a survey was created and sent out to 18 technical personnel experts with the scoring system ranging from -2 to 2 . For this project, the ratings of 1 and 2 have a positive social impact. A positive social impact shows that the project has a social benefit. While a negative social impact, -1 and -2 score, creates a negative social impact for the project [9].

The responses were sorted into spreadsheets depending on which dimension the question was in. Each dimension took the average score and standard deviation for each of the mix designs. The average score was added up for each of the mix designs, and this score was used for the final analysis. Standard deviation was used to see how spread the answers were. If the standard deviation was equal or less than 1 , the dimension had valid questions.

4.4 Integrated Sustainability Assessment

In order to develop a single sustainability index score for each mix design, a quantitative assessment method called QUALICS was used [8]. Equal weightages were assigned to each indicator. The methodology includes: (a) defining the tendency of the value function, (b) identifying the limits of maximum satisfaction and minimum satisfaction, (c) defining the shape of the value function, and (d) defining the mathematical expression of the value function. The mathematical function chosen for this project was a function proposed by which is dependent upon shape factors based on the chosen tendency and shape of the function. For environmental, economic and social impacts, a decreasing trend and concave shape were chosen in calculating value function [1].

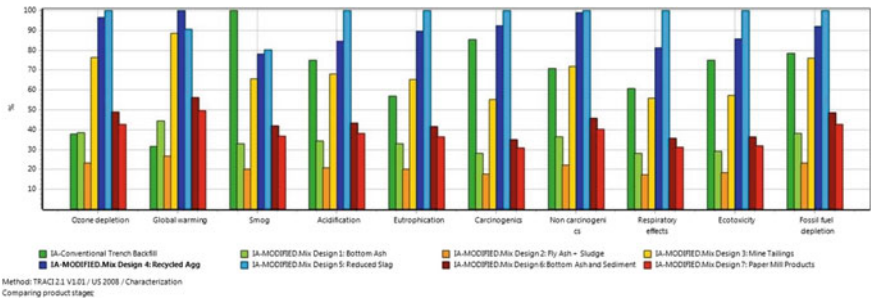


Fig. 1 Isolated analysis environmental results based on SimaPro

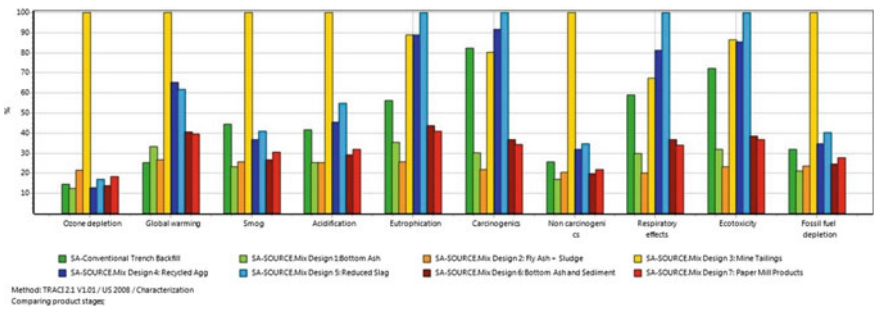


Fig. 2 Specific project analysis environmental results based on SimaPro

5 Results and Discussion

5.1 Environmental Sustainability

The results in Fig. 1 outline the isolated analysis which only evaluates the emissions of the virgin materials used in the alternatives. The results of the specific project application are summarized in Fig. 2. It is important to note that the specific project application considers material sourcing. The distances some of the materials were hauled created an incredibly large impact on the environment, rendering various mixes more sustainable than others just due to the fact of material sourcing.

5.2 Economic Sustainability

The isolated analysis was used to determine how sustainable the admixture could be if sourced locally with no transportation costs considered. The conventional backfill (\$14,814) fared well against the CLSM mix designs (ranged from \$12,344 to \$47,331) with the second cheapest method. The most expensive CLSM mix design

was the mix design 2 which featured fly ash and acid mine drainage sludge (\$47,331). This mix design tested well for environmental sustainability due to its high concentration of fly ash, an otherwise useless waste byproduct, but this came at a high cost due to the growing market value of fly ash. The three best CLSM mix designs were the recycled aggregate (12,344), bottom ash (\$24,164) and sediment (15,399), and paper mill products (\$16,980). These three featured similar strength profiles at a fraction of the cost to the other CLSM mix designs due to their cheaper materials.

Figure 3 the total costs associated with each method from the specific analysis. Similar to the isolated analysis, the material costs followed the same trends with the fly ash mix design surpassing all other backfill methods by a wide margin topping one million dollars. However, unlike the isolated analysis, the indirect and transportation costs were also considered which had significant effects. For example, the mode of transport and distance played a considerable role in the indirect costs. As Fig. 4 shows, the third CLSM mix design, featuring mine tailings as the primary component, incurred the highest indirect costs which was mainly due to transportation. Transportation by truck meant more trucks were needed to handle the amount of mine tailings which ultimately translated to higher costs and emissions. The mine tailings, traveling 170 miles via truck, were too far away to be considered economically sustainable. The second mix design of fly ash and AMD sludge did have the lowest indirect costs due to its environmentally friendly materials of waste byproducts and equally environmentally friendly modes of transportation. However, the lower indirect costs were still not enough to offset some of the material costs incurred from the expensive fly ash, and it still ended up as one of the most expensive backfill methods second only to the third mix design of mine tailings.

Similar to the isolated analysis, the three best CLSM mix designs were the recycled aggregate, bottom ash and sediment, and paper mill products. All three featured mostly sustainable forms of transportation modes, rail and barge, saving money on

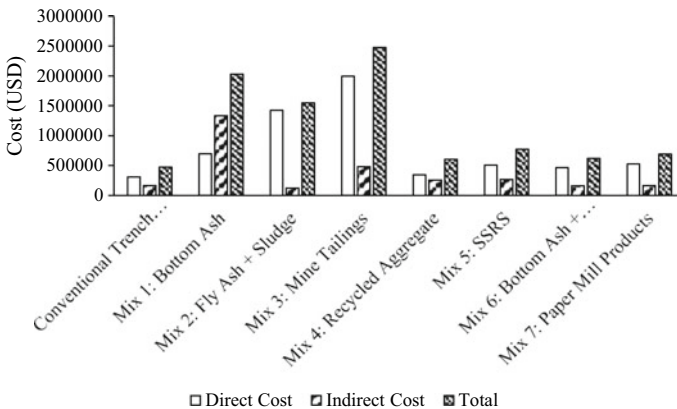


Fig. 3 Total costs summary for specific analysis

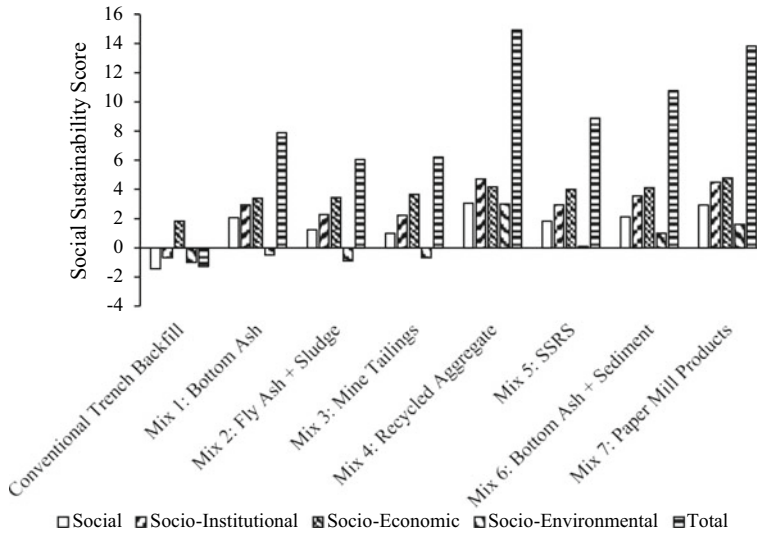


Fig. 4 Social sustainability scores

transportation costs as well as avoiding higher indirect costs associated with emissions. Lastly, the conventional backfill method turned out to be the cheapest as labor costs tended to even out as the project scope increased. With minimal transportation distances, conventional backfill had low indirect cost trailing only the first and second CLSM mix designs. As technology advances, CLSM mix designs may close the gap become more economically viable than conventional backfill. A healthy first step would include more environmentally sustainable methods of concrete production, possibly concentrated solar power technology which has had recent breakthroughs reaching high enough temperatures to produce concrete, which would save on material costs as well as indirect costs incurred from emissions. A second step might include electrical vehicles expanding to the truck industry, with advancing battery technologies, which could save on transportation costs as well as indirect costs incurred from emissions.

5.3 Social Sustainability

Figure 4 shows the average dimension scores for each mix design. Each of the dimension averages were averaged for the final overall score of each of the mix designs. Using the same method as the SSEM scoring with positive scores have a beneficial social impact, and negative scores cause a social deficit.

The mix design with the largest social benefit is the design using the recycled aggregate. With the mix design using paper mill products was the next highest. All of the CLSM mix designs had a positive overall score, while the conventional trench

backfill method was the only mix design to have an overall negative score. All but one of the standard deviations were within the range of less than or equal to one. The only standard deviation out of the range was socio-environmental with a standard deviation of 1.045.

5.4 Integrated Sustainability Assessment

The result of the integrated sustainability assessment using the QUALICS methodology is shown in Fig. 5. Scenario (a) portrays the results of the analysis for equal weighting across triple bottom line. Scenarios (b), (c), and (d) portray the results of the analysis for greater weighting on environmental, economic, and social factors, respectively. In all scenarios, Mix 3 is the least sustainable. For the equal weighting scenario, Mix 7 is the most sustainable with Mixes 1 and 6 also scoring as high sustainability. For the scenario that emphasizes environmental scores, Mix 7 is the most sustainable with Mixes 1 and 6 also scoring as high sustainability. For the scenario that emphasizes economic scores, Mix 1 and 6 are the most sustainable with Mix 7 also scoring as high sustainability. For the scenario that emphasizes social scores, Mix 7 is the most sustainable with Mixes 6 and 4 as also scoring as highly sustainable. Thus, the most sustainable trench backfill option can depend on the particular triple bottom line emphasis of the stakeholders, owners, or project managers.

6 Conclusion

The following conclusions can be drawn from the different approaches and assessments completed on the seven CLSM mixes and conventional aggregate trench backfill alternatives:

- The best design from an environmental assessment was Mix 1—bottom ash + fly ash.
- The best design from an economic point of view was conventional aggregate trench backfill.
- The best design from a social point of view was Mix—4 recycled aggregate.
- The best design using the MIVES methodology and weighing social, environmental, and economic impacts equally was Mix 7—paper sludge.
- The best design across each of the three different scenarios shown for the MIVES methodology was Mix 7—paper sludge.

Ultimately, the results yielded that not one single trench backfill alternative can be called the most sustainable in all aspects or all scenarios, and it is essential to consider the triple bottom line for each unique scenario. Furthermore, various methods that are sustainable in isolation can be the least sustainable option in other cases. However,

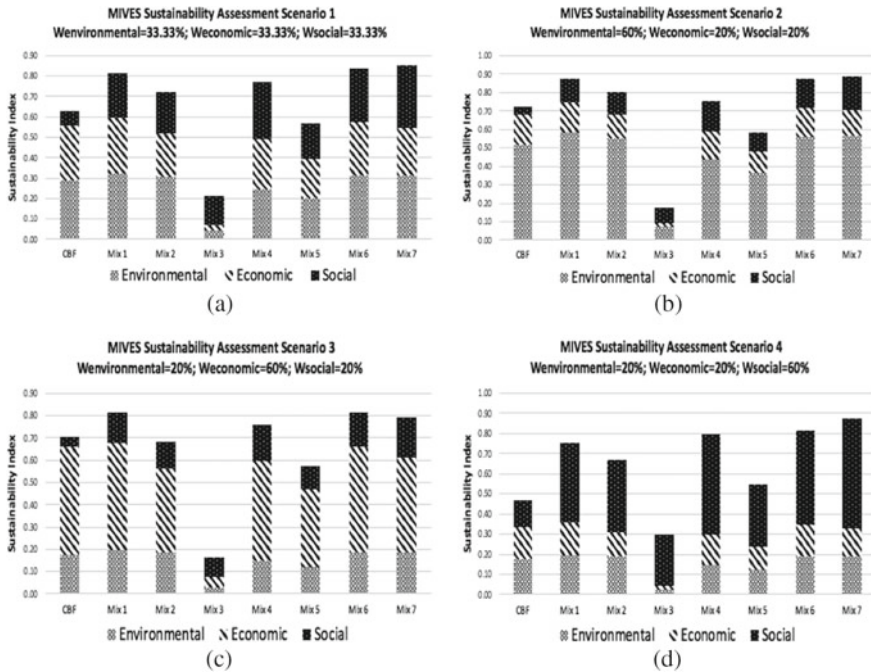


Fig. 5 Integrated sustainability assessment results for different weighting cases

by considering an integrated approach to sustainability, it is possible to design more reliable, sustainable, and better infrastructure systems that will help move toward a more sustainable future.

References

1. Alarcon B, Manga R, Josa A, Aguado A (2010) A value function for assessing sustainability: application to industrial buildings. *Sustainability* 3(1):35–50
2. Bouzalakos S, Dudeney AWL, Chan BKC (2013) Formulating and optimising the compressive strength of controlled low-strength materials containing mine tailings by mixture design and response surface methods. *Miner Eng* 53:48–56
3. Etxeberria M, Ainchil J, Pérez M, González A (2013) Use of recycled fine aggregates for control low strength materials (CLSMs) production. *Constr Build Mater* 44:142–148
4. Gabr MA, Bowders JJ (2000) Controlled low-strength material using fly ash and AMD sludge. *J Hazard Mater* 76(2):251–263
5. Illinois Department of Transportation (2016a) I-290 Eisenhower expressway: environmental resources, impacts, and mitigation
6. Illinois Department of Transportation (2016b) Standard specifications for road and bridge construction
7. Naganathan S, Razak HA, Hamid SNA (2012) Properties of controlled low-strength material made using industrial waste incineration bottom ash and quarry dust. *Mater Des* 33:56–63

8. Reddy KR, Cameselle C, Adams JA (2019) Sustainable engineering: drivers, metrics, tools, engineering practices, and applications. John Wiley & Sons, Incorporated, Newark
9. Reddy et al. (2014) Social sustainability evaluation matrix (SSEM) to quantify social aspects of sustainable remediation. In: ICSI 2014: creating infrastructure for a sustainable world, ASCE, pp 831–841
10. Sheen Y, Huang L, Wang H, Le D (2014) Experimental study and strength formulation of soil-based controlled low-strength material containing stainless steel reducing slag. *Constr Build Mater* 54:1–9
11. Wu H, Huang B, Shu X, Yin J (2016) Utilization of solid wastes/byproducts from paper mills in controlled low strength material (CLSM). *Constr Build Mater* 118:155–163

Effect of Fiber Reinforcement on the Direct Tensile Strength of Fiber-Reinforced Black Cotton Soil



Uma Chaduvula , B. V. S. Viswanadham , and Jayantha Kodikara 

Abstract The performance of geotechnical structures is a function of the tensile strength of the soil. Soils compacted at their desired density values in various geotechnical structures face the problem of cracking due to cracking failure. Lately, the technique of fiber reinforcement in mitigation of desiccation cracking is adopted by researchers. In this study, the influence of percentage dosage of the fiber on the direct tensile strength value of black cotton soil has been investigated. Polypropylene fibers of special trilobal cross section were used. The percentage fiber content was varied as 0, 0.25, 0.5, and 0.75% by the dry weight of the soil. The tensile strength was measured in a modified direct tensile strength test apparatus. The results indicate a rise in tensile strength and change in the failure pattern due to fiber inclusion. However, an optimum fiber content of 0.5% is observed, after which the tensile strength decreases. Due to fiber inclusion, the tensile strength increases by 67%.

Keywords Black cotton soil · Tensile-strength · Fiber reinforcement

1 Introduction

The performance of geotechnical structures essentially hinges on the shear strength parameters like shear strength, cohesion, and tensile and compressive strength. The tensile strength of the soil is a decisive factor in the overall stability of the structures

U. Chaduvula (✉)
Pandit Deendayal Energy University, Gandhinagar, Gujarat 382007, India
e-mail: uma.chaduvula@tot.pdpu.ac.in

B. V. S. Viswanadham
Indian Institute of Technology Bombay, Mumbai 400076, India

J. Kodikara
Monash University, Victoria 3800, Australia

like dams, levees, bridges, landfill liners, and containment ponds. Due to differential stresses, the soil undergoes tensile cracking. The cracks severely affect the strength, permeability, consolidation, and compression characteristics of the soil. Tensile strength tests have been done in both engineering and practice in brittle materials like concrete and rock. However, due to lack of uniformity and lower tensile strength values, the tests are difficult to be performed.

Various test methods are available to evaluate the tensile strength of the soil, viz. Brazilian split tensile strength test, double punch test, hollow cylinder test, and flexural beam test). Direct methods provide true uniaxial tension without any bending or torsional stresses. Recently, the tensile strength improvement of the soil with the use of fiber reinforcement method has been studied by the researchers [5, 8–10, 12–14]. The discrete and randomly distributed fibers in the soil matrix increase the overall strength of the soil by bridging action. This method is preferred over conventional planar geosynthetics, as there is no single potential failure plane.

The addition of fibers increases the tensile strength, reduces swelling potential, increases compressive strength, and improves consolidation characteristics [1–4, 6, 7, 11, 15]. In the current paper, the influence of fiber reinforcement on the direct tensile strength improvement of a locally available black cotton (BC) soil is studied. The influence of increase in fiber content is studied in the fiber-reinforced (FR) specimens and compared with the unreinforced (UR) specimens.

2 Materials

Black cotton soil

In the present study, the BC soil procured from a construction site in Pune, Maharashtra, India, was used. The X-ray diffraction (XRD) spectra revealed that the clay is composed of 49.31% montmorillonite, which is responsible for its expansive nature. Based on the physical properties and the Fress Swell Index of 125%, the soil was identified as CH. The clay was found to be slightly alkaline ($\text{pH} = 8$) in nature.

Fibers

Polypropylene (PP) fibers were used in this study. As the specific gravity, G_s , of PP fibers is low ($G_s = 0.91$), larger volume of fiber is present in a given mass of fibers as compared to polyester fibers ($G_s = 1.25$), and hence, the number of fibers is more for the same fiber content, $f\%$. The PP fibers have a special geometry consisting of tri-angle with rounded edges, called trilobal cross section. The effective diameter of the fiber is $\sim 40 \mu\text{m}$. The unique geometry offers better interlocking between the soil particles and fiber. The properties of the polypropylene fibers as provided by the manufacturer are shown in Table 1.

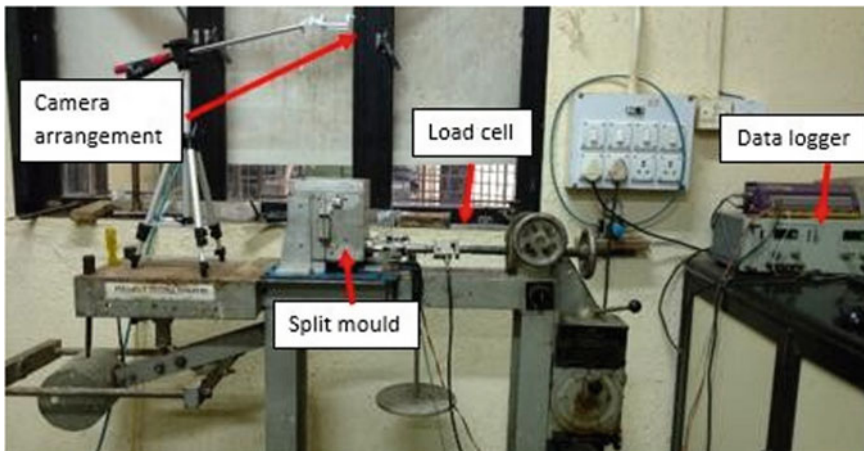
Table 1 Properties of the PP fibers (M/s. Recron 3s, Reliance Industries, Mumbai, India)

Properties	Unit	Value
Specific gravity	–	0.90–0.91
Linear density	Tex	0.4
Melting point	°C	160–165
Tenacity	gm per denier	4–6
Elongation	%	60–90
Alkaline stability	–	Very good

3 Methodology

The tensile strength improvement of fiber-reinforced BC clay was investigated with the help of planned experimental series of tests. The influence of fibers can be quantified by comparing the direct tensile strength of UR and FR specimens. The BC soil was reinforced with polypropylene fibers of cut lengths of 12, 30, and 50 mm at the fiber contents of 0, 0.25, 0.5, and 0.75% by weight of dry soil. A direct shear test apparatus was modified for testing the tensile strength. The test setup is shown in Fig. 1. The test setup consists of a split mold of dimensions $152 \times 152 \times 152$ mm consisting of a movable and open top section on a bottom section with a horizontal plate [5]. The bottom half is fixed on the horizontal plate which is attached to the base. The top half section is freely movable in the longitudinal direction along the guiderails on the horizontal platform.

The water content was considered as OMC-5% i.e., at 30% to understand the tensile behavior of FR soil mix. The wet mixes were wrapped in polybags and left to hydrate uniformly for 24 hours before compaction. A strain rate of 1.25 mm/min

**Fig. 1** Test setup for tensile-strength test

was adopted, and the test was continued till the soil entirely separated from the splitting side. The thickness of the specimen was maintained 100 mm for the tensile tests conducted. The specimen was compacted with the help of special X-shaped compacter for uniformity.

Mixing method

The black cotton soil was oven dried and sieved for preparing the specimens. The UR clay specimens were prepared by add water to the clay to reach close to its optimum moisture content. And, for preparing fiber-reinforced soil specimens, required amount of fibers were mixed with clay, and slowly water was added to the mix ensuring uniform mixing and distribution (Fig. 2). Fibers, being almost weight-less, do not significantly alter the density parameters of the soil. Therefore, maximum dry density (MDD), the specific gravity, and optimum moisture content (OMC) of the clay remain unaltered on addition of fibers.

The load taken by the soil specimen measured through the S-shaped load cell is divided by the area of cross A_c . The area of cross section is a product of the width of the soil specimen in a direction perpendicular to the movement of specimen and the height of the specimen. The tensile stress generated in the plane perpendicular to the direction of applied load is logged continuously (Fig. 1).

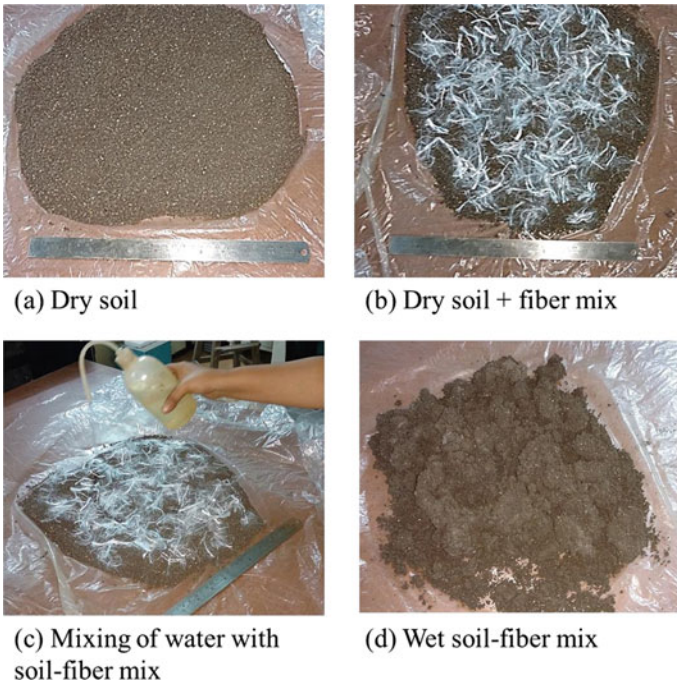


Fig. 2 Procedure of specimen preparation

4 Results and Discussions

Figure 3 shows the tensile stress versus displacement curves for the fiber length $l = 30$ mm and $w = 30\%$ for varying fiber-content of $f = 0.25, 0.5,$ and 0.75% . The value of direct tensile stress for the UR and FR specimens increases with an increase in the displacement value. At the peak stress, the stresses in the soil specimen overpass the tensile strength of the clay. The increase in the tensile stress causes formation of tensile cracks, which occurs abruptly in case of UR specimens. This behavior is found to be delayed in case of FR specimens indicating ductile failure, unlike brittle type of failure in UR specimens. The widened plateau and delay in stress–strain curve is due to the addition of tensile strength of the clay matrix due to the random distribution of fibers, which are acting as tensile elements. The delayed failure can be of utmost importance in problems where the soil is undergoing large strains, viz. differential settlement, slope failures, and tensile cracking in retaining structures, etc.

The tension cracks formed on the failed specimens reveal that the UR soil specimen and FR soil specimen with $f = 0.5\%$ and $l = 12$ mm undergo brittle failure. The FR soil specimens with $f = 0.5\%, l = 30$ mm and $f = 0.5\%, l = 50$ mm undergo a late and ductile failure, as the fibers hold the soil undergoing tension crack.

Figure 4 displays the deviation of peak tensile strength with varying fiber lengths for different fiber contents. As observed visually and through the values of tensile strength values, the longer fiber lengths are observed to perform better against large

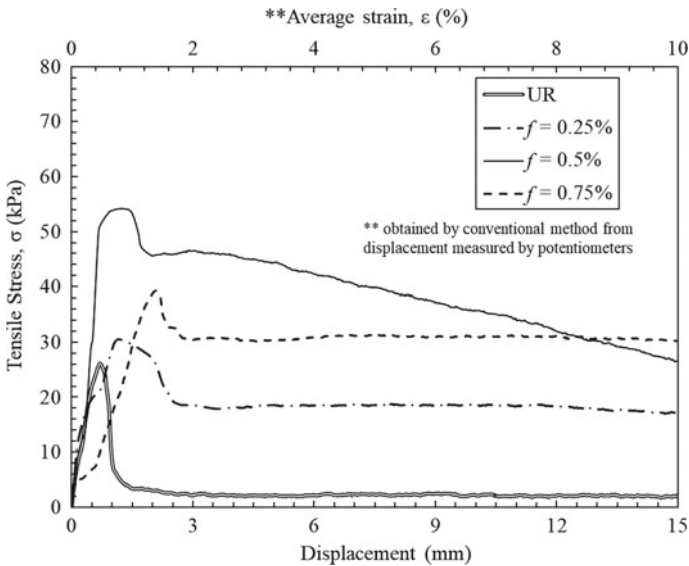


Fig. 3 Tensile stress versus displacement curve for fiber length, $l = 30$ mm and $w = 30\%$ for varying fiber content

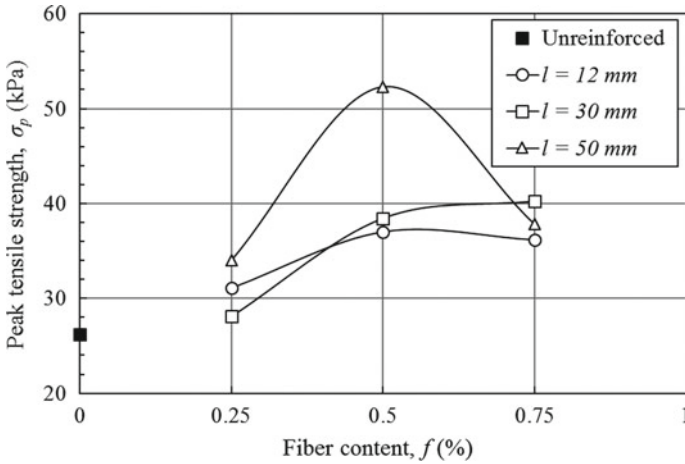


Fig. 4 Variation of peak tensile strength for specimens with varying fiber content for different fiber lengths

deformations like in the case of direct tensile strength tests. The bond length offered by the reinforcing fibers plays a critical role in the ductile behavior of FR clay.

The fiber at the crack takes the entire tensile load during cracking, and the fiber gets extended. If the length of the fiber in the stationary portion of the soil specimen is enough to offer the required bond strength, the fiber successfully mitigates the crack formation. If the fiber is not sufficiently long, the fiber gets pulled out at the crack. The fibers get pulled out when the tensile strength of the fibers is great that the bond strength. Shorter fibers (fiber length, $l = 12$ mm) get pulled out at the crack, as their pull-out strength is lesser than their tensile strength, as shown in Figure 5.

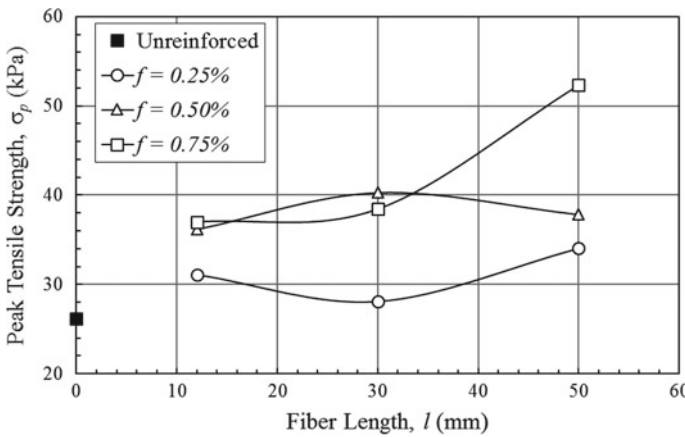


Fig. 5 Variation of peak tensile strength with varying fiber lengths for different fiber contents

5 Conclusion

The series of tensile strength tests indicate tensile strength improvement due to addition of tensile fibers. The specimens undergo an increase of tensile stress till a peak level is reached, and tensile cracks are formed. The brittle failure in UR specimens does allow any further extension of the specimens under deformation. The fiber-reinforced specimens reach to a higher peak stress value and exhibits a plastic deformation and gradual loss in the strength, while the fibers are get pulled out. The improved ductile behavior of the soil can be utilized in geotechnical structures subjected to large tensile stresses.

References

1. Chaduvula U, Viswanadham BVS, Kodikara J (2016a) A study on desiccation cracking behavior of polyester fiber-reinforced expansive clay. *Appl Clay Sci* 142(1):1–10. <https://doi.org/10.1016/j.clay.2017.02.008>
2. Chaduvula U, Viswanadham BVS, Kodikara J (2016b) Desiccation cracking behaviour of geofiber-reinforced expansive clay. In: *Geo-Chicago 2016. Geotechnical Special Publication*, vol 271, pp 368–377
3. Chaduvula U (2019) Experimental studies on the cracking behaviour of geofiber reinforced expansive soils. IITB Monash Research Academy
4. Consoli NC, de Moraes RR, Festugato L (2011) Split tensile strength of monofilament polypropylene fiber-reinforced cemented sandy soils. *Geosynth Int* 18(2):57–62
5. Divya PV, Viswanadham BVS, Gourc JP (2014) Evaluation of tensile strength-strain characteristics of fiber-reinforced soil through laboratory tests. *J Mater Civ Eng ASCE* 26(1):14–23. [https://doi.org/10.1061/\(ASCE\)MT.1943-5533.0000772](https://doi.org/10.1061/(ASCE)MT.1943-5533.0000772)
6. Divya PV, Viswanadham BVS, Gourc JP (2018) Hydraulic conductivity behaviour of soil blended with geofiber inclusions. *Geotextiles Geomembr* 46(2):121–130. <https://doi.org/10.1016/j.geotexmem.2017.10.008>
7. El Hajjar A, Ouahbi T, Taibi S, Eid J, Hattab M, Fleureau JM (2021) Assessing crack initiation and propagation in flax fiber reinforced clay subjected to desiccation. *Constr Build Mater* 278(April):122392. <https://doi.org/10.1016/j.conbuildmat.2021.122392>
8. Li J, Tang C, Wang D, Pei X, Shi B (2014) Effect of discrete fibre reinforcement on soil tensile strength. *J Rock Mech Geotech Eng* 6(2):133–137. <https://doi.org/10.1016/j.jrmge.2014.01.003>
9. Nahlawi H, Kodikara JK (2006) Laboratory experiments on desiccation cracking of thin soil layers. *Geotech Geol Eng* 24(6):1641–1664. <https://doi.org/10.1007/s10706-005-4894-4>
10. Nahlawi H, Chakrabarti S, Kodikara J (2004) A direct tensile strength testing method for unsaturated geomaterials. *Geotech Testing J*, ASTM 27(4):1–6
11. Phanikumar BR (2006) Prediction of swelling characteristics with free swell index. <http://www.crcnetbase.com.ezproxy.lib.rmit.edu.au/>. <https://doi.org/10.1201/9780203968079.ch13>
12. Rifai SM, Miller CJ (2009) Theoretical assessment of increased tensile strength, no. December, pp 1857–1862
13. Shannon B, Kodikara J, Rajeev P (2015) The use of restrained ring test method for soil desiccation studies. *Geotech Test J* 38(1):20130131. <https://doi.org/10.1520/GTJ20130131>
14. Stirling RA, Hughes P, Davie CT, Glendinning S (2015) Tensile behaviour of unsaturated compacted clay soils—a direct assessment method. *Appl Clay Sci* 112–113(1):123–133. <https://doi.org/10.1016/j.clay.2015.04.011>

15. Viswanadham BVSVS, Phanikumar BRR, Mukherjee RV (2009) Swelling behaviour of a geofiber-reinforced expansive soil. *Geotextiles and Geomembr* 27(1):73–76. <https://doi.org/10.1016/j.geotexmem.2008.06.002>

Studies on Sugar Cane Bagasse Ash and Blast Furnace Slag-Based Geomaterial



H. R. Nikhade  and B. Ram Rathan Lal

Abstract The proposed materials were prepared by the addition of sugar cane bagasse ash (SCBA), glass fibre, blast furnace slag and ordinary Portland cement. The glass fibre-to-sugar cane bagasse ash as mix ratio (GF/SCBA) was 0.2, 0.4, 0.6, 0.8 and 1.0%. The mix proportion blast furnace-to-sugar cane bagasse ash was 10% for present study. The cement-to-sugar cane bagasse ash ($C/SCBA$) ratio is taken 10, 15 and 20%. The compressive strength of prepared materials was examined after 7, 14 and 28 days, respectively. The effect of add-on of mix ratio on compressive strength, density and stress–strain behaviour was studied. The experimental results indicate that the density of prepared materials was decreased with the addition of glass fibre. The compressive strength of prepared material at mix ratio, 0.6% with 20% cement shows maximum value. The stress–strain behaviour for all mix ratio was observed to nonlinear.

Keywords Sugar cane bagasse ash · Compressive strength · Density · Glass fibre

1 Introduction

Use of conventional materials like sand, murum and aggregate is to increase day by day in the civil engineering works; due to rapid infrastructural growth, there has been shortage of this conventional material, and this leads to increase in the cost of conventional fill materials, which ultimately increase the cost of construction. After few years, there will be depletion of these conventional fill materials. Every year

H. R. Nikhade (✉)

Kavikulguru Institute of Technology and Science, Parsoda, Maharashtra, India
e-mail: harshal.nikhade@rediffmail.com

Department of Civil Engineering, Yeshwantrao Chavan College of Engineering, RTMNU, Nagpur, India

B. R. R. Lal

Department of Civil Engineering, Kavikulguru Institute of Technology and Science, RTMNU, Ramtek, India

large quantity of agricultural waste all over the world produce enormous quantity of ash and facing serious problems of handling and disposal. The large quantity of availability waste material like agricultural waste or industrial waste is another big environmental issue faced today. These wastes are normally burnt or dumped in low-laying areas or in open field. Some of these waste materials are disposed into rivers and canal which causes the outbreak of diseases. The sugar cane is most important crop produced in the world. Its production is 30.0 crore tonnes per year and 1.0 crore tonnes as sugar cane bagasse ash as waste [1, 2]. After extraction of sugar from sugarcane, fibrous and tough waste is formed. The fibrous residue is used for heat generation in the boilers. Ash is an extra earned from the burning of fibrous residue in boilers. Ash is deposited in low lying areas causing heaps in that area. The efficient use of this waste only solves its removal problem but also gives a cheap construction material. This paper objective principally focussed on the behaviour of development of new material using waste as SCBA, BF slag and glass fibre and binder as OPC.

BF slag is the excess material, containing primarily of CaO , SiO_2 , Al_2O_3 and MgO , generated from the iron-making blast furnaces. It is in the beginning liquid form but is lastly disposed as a solid subsequently cooling (IS 10447:1983). According to American Concrete Institute (ACI) committee, it mainly consists of silica and calcium developed in molten state (ACI 233 [3]). As per cooling method, three forms of slag created: air-cooled slag, granulated slag and expanded slag. Blast furnace slag is a consistent waste produced in enormous quantities by the iron and steel production industries in India. The use of waste not only helps in reducing greenhouse gases but also prevents in making it as biologically friendly construction materials. The BF slag is used as replacement of fine aggregate in concrete which contributes the compressive strength [4]. Utilization of BF slag as replacement of natural aggregate up to 75% contributes to the strength [5].

The glass fibre mainly consists of silica which does not crystallize after cooled from liquid to solid state [6]. Glass fibres are manufactured in a manner called fiberization in that process melted glass is taken in the form of filaments, through the bottom of platinum tank [7]. Glass fibre has useful properties such as strength, hardness, stiffness, resistance to chemical occurrence [8]. The glass fibre is classified depending on their properties such as low electric conductivity (E-glass), high alkali glass (A-glass), rust resistant glass (ECR-glass), high strength glass (S-, R- and Te-glass), di-electric glass (D-glass), high alkali glass (A-glass), high chemical durability glass (C-glass). To improve the strength of bagasse ash, it is proposed to reinforce it with glass fibres.

2 Characterization of Materials

The sugar cane bagasse ash materials were reinforced with glass fibre which has length 12 mm, BF slag as mix proportion and OPC cement 53-grade cements were used in preparing the materials. The SCBA used in the research had specific gravity of 1.99, the proportions of fine sand 40%, silt 45% and clay 5% obtained from

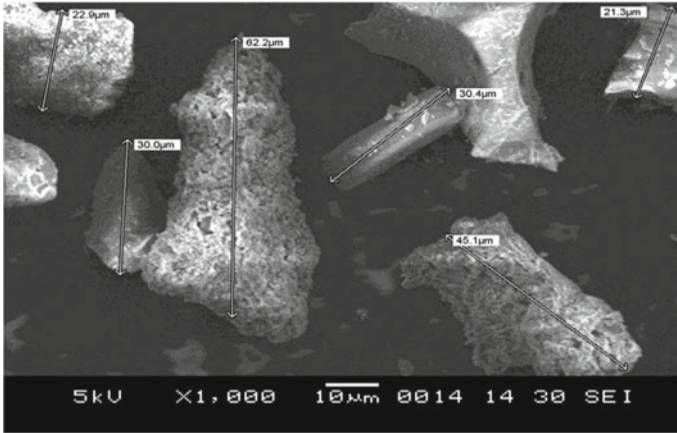


Fig. 1 Scanning electron microscopy (SEM) of sugar cane bagasse ash

hydrometer analysis. After standard proctor test result, maximum dry density (γ_d) of 0.94 g/cc and optimum moisture contain 20%. The BF slag had specific gravity of 2.35, fine modulus 2.89 (IS 383-1970). The X-ray fluorescence test was conducted at Indian bureau mines Nagpur to find the chemical composition of materials. Sugar cane bagasse ash contains maximum percentages of silica 77.23%. Morphological characteristics of SCBA as shown in Fig. 1. X-ray diffraction (XRD) test on SCBA was carried out VNIT Nagpur; it was observed SCBA changes from amorphous (peak) to crystalline nature due to the presence of Cristobalite. As per ASTM c618-12a, it is class F type of materials and contains maximum percentages of quartz. The density of glass fibre was calculated as per ISO 10119 (2002) using Pycnometer method is 780 kg/m³.

3 Experimental Programme

In this investigational work, significance of addition of glass fibre at different mix ratio as reinforcing material on compressive strength, density and stress–strain pattern of materials were found out for curing periods 7 days, 14 days and 28 days

4 Specimen Preparation

In this research work, mix ratio is weight of glass fibre to weight of SCBA. The mix percentage is based on previous [6, 9] literature review. Weight of SCBA is calculated using formula $W_{SCBA} = \gamma_{dm} \times V_{SCBA}$, where γ_{dm} dry unit weight of SCBA and V_{SCBA} . Volume of SCBA, $V_{SCBA} = V - V_{BFslag} - V_{GF}$, V the

Table 1 Mix ratio preparation in the experiment

Mix ratio %	C/SCBA %	W/SCBA %	Mix proportion %
0.2	10, 15, 20	50	10
0.4	10, 15, 20	50	10
0.6	10, 15, 20	50	10
0.8	10, 15, 20	50	10
1.0	10, 15, 20	50	10

total volume to specimen (1000cc), and VBFslag is taken 80cc and volume of VGF glass fibre is taken 2.21 to achieve the mix ratio 0.2% for cube having dimension 10 cm × 10 cm × 10 cm. Mix proportion is defined as weight of BF slag to weight of SCBA (BFslag/SCBA) is taken 10% for the experimental work and cement to weight of SCBA (C/SCBA) is considered 10, 15 and 20%. Water to weight of sugar cane bagasse ash (W/SCBA) is taken 50% weight of bagasse ash. Different mix ratio preparation is shown in Table 1.

5 Test Procedure

The specimen was air dry after curing, and the dimension of specimen was measured. The glass fibre was added after wet mix of sugar cane bagasse ash, BF slag and cement. This was done to avoid lump of glass fibre together [10, 11]. The mass of each specimen is measured using weight balance and has accuracy 0.01 g. The load cell 50 kN capacity and linear variable differential transducer have accuracy 0.01 mm are used to determine the compressive load and deformation in the specimen. The data logger is connected together with load cell, and both are standardized prior to testing. The compressive stress at maximum load and subsequent deformation of specimen was noted. The three samples were taken for each curing phase. Complete 135 samples were tested, and the results were shown in the work.

6 Result and Discussion

6.1 Density

The density is main parameter for prepared materials and was affected by addition of glass fibre, percentages of cement and curing period. Fig. 3a, b shows the density of the materials with respect to mix ratio value. By addition of glass fibre in the mix percentages (0.2–1.0%), the density of specimen was significantly reduced from 1326 to 1150 kg/m³. The percentages of decrease in the density with addition of

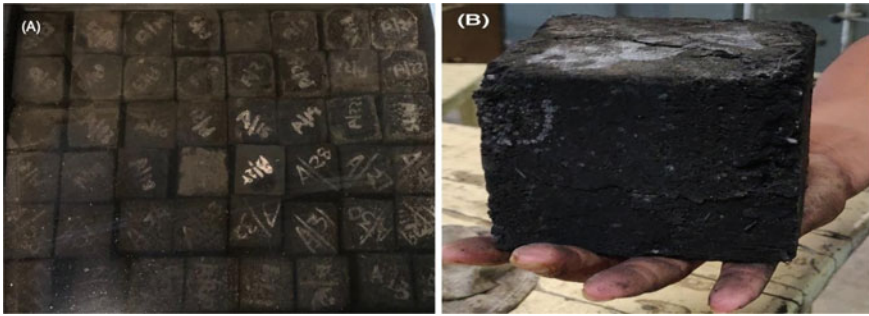


Fig. 2 a Curing of specimen morphology of b crack in cube after testing at deformation rate 1.0 mm/minute

glass fibre for 20% binder 6.1%. The density of materials increases with $C/SCBA$ ratio increased as expected. The density of materials $C/SCBA$ ratio 20% obtained higher value as compared to $C/SCBA$ ratio 10% ratio and 15% ratio. The density of newly prepared materials is lesser than traditional fill materials which are in range from 2100 to 1700 kg/m^3 [12].

6.2 Impact of Mix Ratio Percentages on Compressive Strength

The compressive test on specimen was conducted after curing time 7, 14 and 28 days. Figure 4a, b, c shows the correlation between compressive strength of materials and mix ratio at $W/SCBA$ ratio 50% for all curing periods. The compressive strength of materials linearly increases with $C/SCBA$ ratio 10–20% for all curing periods. The compressive strength for all $C/SCBA$ ratio 10–20% is higher at 0.6% mix ratio after that the strength decrease continuously to mix ratio 0.2%. Compressive strength of materials ranges from 120 kPa to 1060 kPa and from 10 to 20% cement-to- $SCBA$ ratio for curing period 7 to 28 days, respectively. Comparable kind of behaviour was noted by Ram Rathan Lal and Badwaik [13], Ram Rathan Lal and Nawakhare [14], Henry and Lawrence [15]. The percentages of increase in the strength for cement-to-sugar cane bagasse ash ratio 20% ratio and 44.39% at 28 days curing (Fig. 4).

6.3 Stress–Strain Relationship

From the compressive strength test, the stress–strain pattern and stiffness of materials were calculated. Figure 5a–c shows the correlation between compressive stress and strain. $C/SCBA$ ratio 20% shows the higher compressive stress at 0.6% mix ratio for curing period 7-14-28 days. The compressive stress is highly affected by cement to

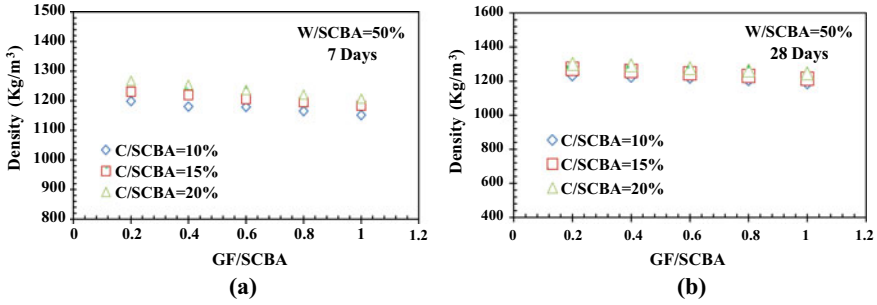


Fig. 3 Impact of mix ratio on density of materials

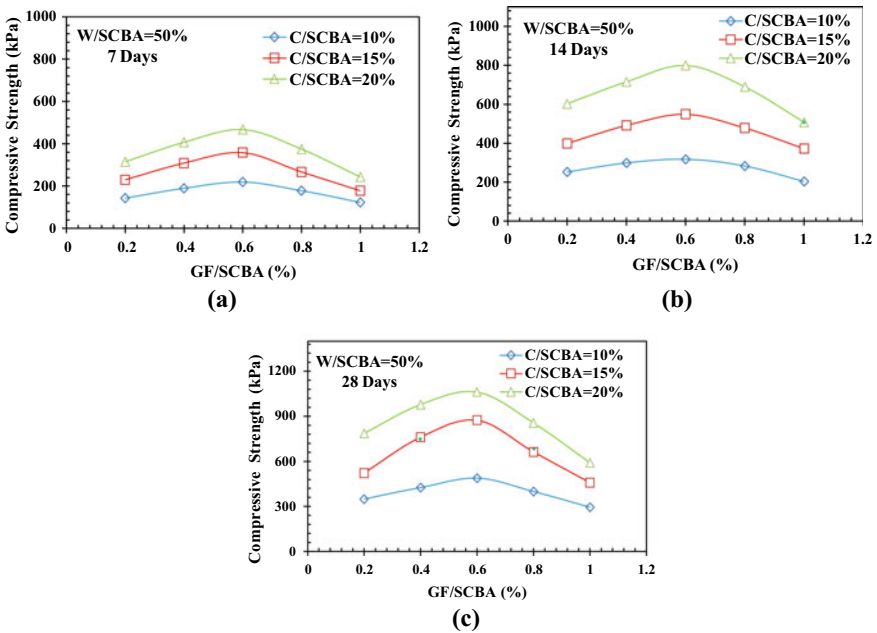


Fig. 4 Relationship between compressive strength of materials for 7, 14 and 28 days with respect to mix value

sugar cane bagasse ash ratio. Nonlinear correlation analysed between compressive stress and strain. Similar behaviour was observed for all mix ratio value.

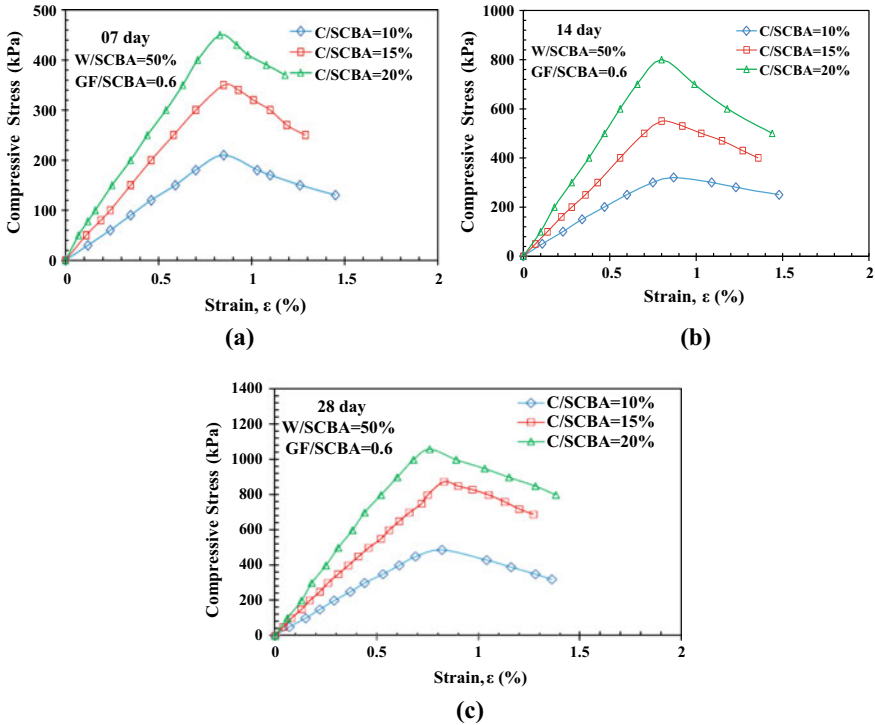


Fig. 5 Variation in stress–strain pattern

7 Conclusion

The experimental study of materials contains sugar cane bagasse ash, blast furnace slag, glass fibre and OPC. Based on the results, conclusion has been drawn.

1. The density of materials was decreased as the percentages of glass fibre. With the accumulation of glass fibre in the between 0.2 and 1.0% mix ratio, the density of materials decreases from 1326 to 1150 kg/m³. Compressive strengths were highly affected by the mix ratio percentages, cement-to-sugar cane bagasse ash ratio and curing periods. Specimen with curing period at 28 days shows higher value than 14 days and 7 days.
2. The compressive strength of materials ranges from 120 to 1060 kPa.
3. The compressive strength of materials using C/SCBA ratio 20% has higher the value than C/SCBA ratio 10 and 15%.
4. Nonlinear correlation was examined amongst compressive stress and strain for each mix ratio and curing times. The specimen fails in the range of 0.5–1.5%.

References

1. Modani PO, Vyawahare MR (2012) Utilization of bagasse ash as a partial replacement of fine aggregate in concrete. In: International conference chemical, civil and mechanical engineering tracks of 3rd Nirma university, pp 25–29
2. Rajakumar C, Yuvaraj S, Meenambal T, Suji S (2014) Experimental study on the utilization of industrial and agricultural wastes to stabilize the expansive soil subgrades. In: 8th International conference on intelligent systems & control (ISCO), pp 368–374
3. ACI Committee 233 (1995) Ground granulated blast-furnace slag as a cementitious constituent in concrete, ACI 233R-95, Report of ACI Committee 233, American Concrete Institute, Detroit, USA
4. Nadeem M, Pofale A (2012) Replacement of natural fine aggregate with granular slag-a waste industrial by-product in cement mortar applications as an alternative construction material. *Int J Eng Res Appl (IJERA)*. ISSN: 2248-9622
5. Hiraskar KG, Patil C (2013) Use of blast furnace slag aggregate in concrete. *Int J Scien Eng Res 4*. ISSN 2229-5518
6. Lyons A (2010) *Materials for architects and builders*, 4th ed. Elsevier, Hong Kong, China, pp 420
7. Wallenberger FT, Watson JC, Li H (2001) Glass fiber. *ASM Handbook* 21:27–34
8. Bentur A, Diamond S (1996) Effect of ageing of glass fiber reinforced cement on the response of an advancing crack on intersecting a glass fibre, strand. *Int J Cement Compos Lightweight Concr* 8(4):213–222
9. Padade AH, Mandal JN (2014) Expanded polystyrene-based geomaterial with fly ash. *Int J Geomech ASCE*:1–7
10. Mandal D, Ram Rathan Lal B (2017) Compressive strength behavior glass fibre reinforced furnace slag-based materials. In: Indian geotechnical conference GeoNEst, IIT 14–16 December, Guwahati, India
11. Ram Rathan Lal B, Hinge VA, Nawkhare SS, Shankar K (2019) Experimental studies on bottom ash and blast furnace slag based geomaterial under compressive loading. In: Geotechnical congress
12. Liu HL, Deng A, Chu J (2016) Effect of different mixing ratios of polystyrenes pre-puff beads and cement on the mechanical behavior of lightweight fills. *Geo-textiles Geomembr* 24:331–338
13. Ram Rathan Lal B, Badwaik VN (2016) Experimental studies on bottom ash and expanded polystyrene beads-based geomaterial. *J Haz Toxic Radioactive Waste* 20(2)
14. Ram Rathan Lal B, Nawakhare SS (2016) Experimental study on plastic strips and EPS beads reinforced bottom ash based materials. *Int J Geosyn Ground Eng*:1–12
15. Henry NM, Lawrence LC (1979) Glass fibre reinforced cement base materials. *Fibre Reinforced Concr* 44(14):247–264

Swelling Behaviour of Expansive Soil Reinforced with Geocell and Jute Fibres



Sanjeev Kumar, Sanjeev Naval, and Anil Kumar Sahu

Abstract To mitigate the effects of the problem created by expansive soils, a number of mitigation techniques are applied. Sand cushioning, chemical stabilization, belled piers, granular pile anchors, and other techniques are only a few examples. It is also possible to reduce the swelling of expansive soil by stabilizing it with randomly distributed fibres. Geosynthetics such as geocells have been utilized as reinforcement in the construction of structures such as foundations, embankments, retaining walls, highways, and so on. This research article discusses the swelling characteristics of reinforced expansive soil. The swelling characteristics of geocell and jute fibre reinforced expansive soil specimens were investigated using one-dimensional swelling experiments in a CBR mould. The geocell reinforced specimen's swell potential and swelling pressure dropped until 0.80% fibre content and then increased at 1.60% fibre content. Swell potential and swelling pressure reduced as fibre length increased, but only until 40 mm, after which they increased for fibre lengths of 50 and 60 mm. The rate of swelling confirms the above observation. In comparison with the unreinforced specimen, the swelling behaviour of geocell–jute fibre reinforced expansive soil specimens improved. The study highlights the use of geocells and jute fibre towards the stabilization of expansive soil.

Keywords Swelling · Expansive soil · Geocell · Jute fibre · Swell potential · Swell pressure

S. Kumar (✉)
IKGPTU, Kapurthala, Punjab, India
e-mail: snjvbansal67@gmail.com

Department of Civil Engineering, Vaish Technical Institute, Rohtak, Haryana 124001, India

S. Naval
Department of Civil Engineering, DAV Institute of Engineering and Technology, Jalandhar, Punjab 144008, India

A. K. Sahu
Department of Civil Engineering, Delhi Technological University, Delhi 110042, India

© The Author(s), under exclusive license to Springer Nature Singapore Pte Ltd. 2023
A. K. Agnihotri et al. (eds.), *Proceedings of Indian Geotechnical and Geoenvironmental Engineering Conference (IGGEC) 2021, Vol. 1*, Lecture Notes in Civil Engineering 280, https://doi.org/10.1007/978-981-19-4739-1_4

1 Introduction

Expansive soil responds to variations in moisture content by experiencing significant volumetric changes. These soils can be found all over the world. In India, the expansive clayey soil is known as black cotton soil because this soil is suitable for the cultivation of cotton plants and it covers around 20% of the country's total land area. Such soils swell when moisture content rises and shrinks as moisture evaporates. As a result, structures such as residential buildings, light-loaded structures, airfields, railway lines, highway pavements, retaining walls, and bridges found over them are exposed to risk and damage. Damage can be minor, requiring just moderate maintenance, but it is usually severe, resulting in serious structural failure. Researchers have developed numerous methods of improving the engineering characteristics of soil through the process known as soil stabilization in response to the problems encountered with expansive soils. To minimize and limit the consequences of the swelling, various soil stabilizing approaches are used. Chemical stabilization and mechanical stabilization are the two different types of stabilization approaches available. Chemical stabilization entails the application of chemicals such as fly ash, lime, cement, polymers, resins, and ionic solutions, among others. Chemical agents interact with soil particles, altering index properties [1–3]. Compaction, together with reinforcement, fibres, or other non-biodegradable elements, is used to stabilize soil in mechanical stabilization. Numerous studies have shown that adding randomly dispersed fibres [4–6] and geosynthetics [7–9] to expansive soils improves their strength and bearing capacity.

Patil [10] described a laboratory approach for evaluating swelling pressure as well as an instrument for testing remoulded or undisturbed soil samples. To measure expansive soil swelling pressure in the laboratory, Basma [11] described the Double odometer swell test and the restrained swell test as procedures. The findings revealed that the constrained swell test yields more accurate results. To classify expansive soils utilizing the free swell ratio and considering the results' comparability with soil clay mineralogy and the odometer free swell test, Sridharan and Prakash [12] developed a procedure which is simple and user-friendly. Vessely and Wu [13] found that geosynthetic inclusion in the expansive soil assisted in limiting the swelling through a soil geosynthetic swell test. While evaluating the effects cement, lime, sarooj, and heat treatment on the swelling capacity of soil, Al-Rawas et al. [14] reported that all stabilizers induce a reduction in swelling potential except sarooj (a pozzolana). When Guney et al. [15] investigated the cyclic soaking and drying influence on the clayey soil swelling behaviour when stabilized with lime, they found that with the completion of the first cycle, in the early phases, the lime stabilization favourable effect vanished. During subsequent cycles, the swelling potential grew even more. Ikizler et al. [16] utilized materials like sand and EPS Geofom as stabilizers and demonstrated that in bentonite; swelling pressure can be decreased using these materials. Viswanadham et al. [17] investigated the effect of tape fibre made of polypropylene on swelling behaviour, finding that, for decreasing swelling, the fibres dispersed randomly and discrete in nature are efficient. Mirzababaei et al. [18]

in expansive soils investigated the polymer's efficacy to reduce swelling and found that free swelling potential had decreased considerably while the furan (a polymer) content had increased. Nagaraj et al. [19] in compacted soils investigated the impact of vertical drains on swelling pressure and on the swell potential. They discovered significant effects. Yazdandoust and Yasrobi [20] investigated the cyclic wetting and drying influence on expansive clay swelling characteristics when stabilized with polymers. In cyclic swelling and shrinkage, with the completion of the first cycle, swelling pressure and swelling potential decreased slowly, and after the fourth cycle, they reached an equilibrium state. Tiwari and Ajmera [21] for key clay minerals and their combinations investigated the swelling and consolidation effects. In the early phases, the liquid limit, void ratio, and plasticity index exhibited a strong correlation with the swelling index and compression. Equations were proposed using the liquid limit for estimating swelling index and compression. Trouzine et al. [22] in composite clayey soils for rubber fibres (extracted from waste tyres) investigated the swelling behaviour. They discovered that for soils with greater swelling potential, the swelling pressure, swelling potential, liquid limit, and time necessary to achieve maximal swelling are all significantly reduced. Malekzadeh and Bilsel [23] in expansive soils when stabilized with fibres made of polypropylene investigated swelling and compressibility and came to the conclusion that to limit swelling potential and compressibility, incorporating fibres made of polypropylene into expansive soils could be an efficient way. Elsharief et al. [24] provided the findings from the experimental investigation to better comprehend the swelling characteristic of two expansive soils. To forecast swelling pressure, they created a few models and concluded that swelling pressure rises as moisture decreases and soil suction rises. With the rise in the liquidity index, it also fell. Phanikumar and Singla [25] concluded that during primary and secondary consolidation, reinforcing expansive soils with nylon fibres is an effective technique to reduce volumetric changes. Through consolidation, swelling pressure, and three-dimensional shrinkage experiments, Jayasree et al. [26] discovered that volume change behaviour was improved when coir waste was incorporated into the expansive soil. Elbadry [27] developed a novel method for predicting the expansive soils' volume change characteristics using the outcomes of certain conventional physical tests. Through the physical and swelling characteristics of soils, Patil et al. [28] developed a relationship between the free swell index and the swelling pressure. Soltani et al. [29] proved that chemical and mechanical stabilization solutions can significantly reduce the swelling problem of expansive soil using unconfined compression tests and free swell tests. Soltani et al. [30] reported the findings of an experimental investigation, concluding that there was a significant reduction in expansive soils' swelling behaviour when fibres were mixed into them. Moghal et al. [31] investigated the fibre treatment effect on the compressibility and swelling properties of expansive soil when stabilized with lime and suggested combining fibres made of polypropylene in lime stabilization as a solution to the swelling and shrinkage problem. Muthukumar et al. [32] investigated the shrinkage and swelling characteristics of expansive soil through varied concentrations of fibres and lime. It was reported that with the increase in fibre content, swelling dropped marginally but

shrinkage decreased significantly. Swelling and shrinking both decreased dramatically as the lime content increased. Tiwari and Satyam [33] investigated the expansion properties and swelling pressure of clayey soil when stabilized with silica fume using polypropylene fibre and discovered a substantial effect. Swelling pressure and expansion are influenced by the matrix's fibre content. Quarry dust is a useful additive for treating expensive soils in wet conditions, according to Onyelowe et al. [34], and its inclusion improved the shrinkage limit and swelling potential of soils consistently. Bekhiti et al. [35] combined fibres consisting of waste tyre rubber with bentonite clayey soil stabilized with cement and found that as the fibre and cement concentration increased, the swelling potential and swelling pressure reduced. Kalkan et al. [36] found that stabilizing expansive soils with quartzite reduces its swelling pressure, swelling potential, and vertical swelling percentage values. Shukla et al. [37] investigated the effect of fibres consisting of waste tyre on expansive soil and found that the soil's swelling pressure and swelling potential are greatly reduced.

In CBR mould, one-dimensional swelling tests on expansive soil from the New Delhi area were carried out in the current experimental investigation. Geocell, reinforcement made of woven geotextile consisting of polypropylene, and jute fibres were used to study the swelling pressure and swell potential for reducing expansive soil swelling. As an agricultural waste, jute provides a low-cost and environmentally acceptable alternative to the expansive soils in this experimental investigation. In comparison with other natural fibres, jute has limited extensibility, elastic modulus, and a high tensile strength. It can also withstand rotting and heat [38].

2 Materials and Methods

2.1 Materials

Soil

A naturally occurring black cotton soil from New Delhi was used as an expansive soil in this experimental study. It was dug to a depth of 1.0 m below the natural ground level. 96% of the collected soil passed through a 75 μ m IS sieve, while 64.5% passed through a 2 μ m IS sieve. Figure 1 depicts a particle distribution curve drawn from sieve and hydrometer study results. Tests were conducted in accordance with Indian Standard IS: 2720 [39] to evaluate index characteristics. The soil was classed as high plasticity clay (CH) by the Bureau of Indian Standard classification. The soil has a high plasticity index (49.68%) and a 72.5% free swell index, as well as an activity of 0.76. A soil with a high plasticity, free swell index, and clay activity is more likely to swell. The result of the X-ray diffraction investigation is shown in Fig. 2. It implies that quartz is the most abundant mineral in the soil, with muscovite and talc being the most abundant minerals. Table 1 lists the soil's index characteristics.

Fig. 1 Soil particle size distribution curve [9]

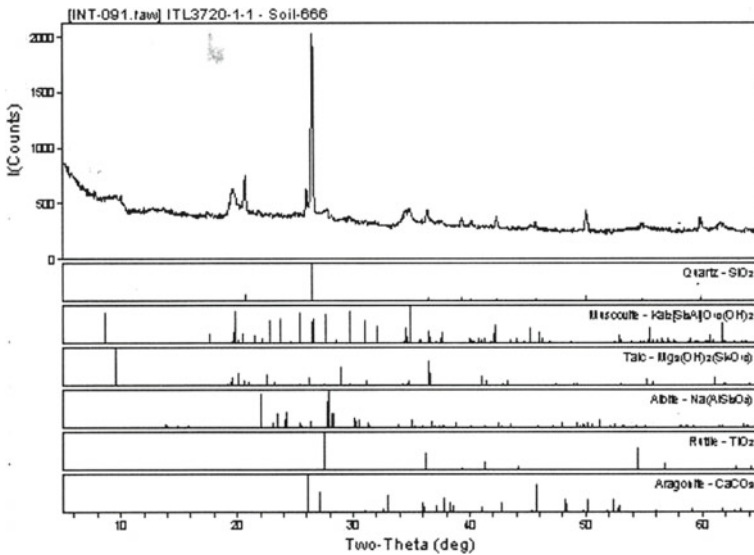
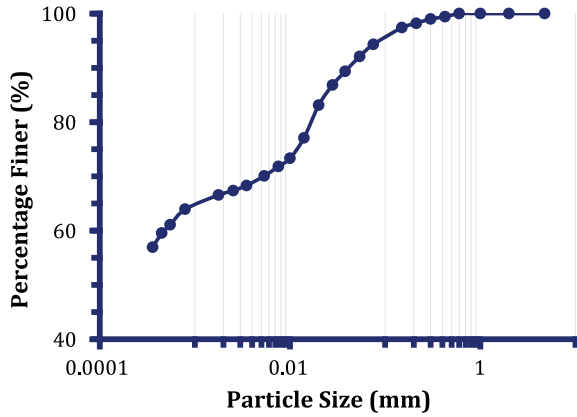


Fig. 2 X-ray diffraction analysis of expansive

2.2 Reinforcing Materials

To limit expansive soil swelling behaviour, two types of reinforcing materials, fibre and geocell, were used in this experimental work.

Fibre

One of the reinforcing materials used in this study was jute fibre. It is a commercially available, multipurpose natural fibre. Among the natural fibres available, it has the highest tensile strength. GoGreen Products in Chennai, Tamil Nadu (India), provided

Table 1 Properties of soil [9]

Parameter	Value	
Specific gravity	2.63	
% Finer than 4.75 mm, %	100.00	
% Finer than 75 μ , %	94	
% Finer than 2 μ , %	64.5	
Liquid limit, %	87.24	
Plastic limit, %	37.56	
Plasticity index, %	49.68	
Free swelling index, %	72.5	
Activity	0.76	
Maximum dry density, kN/m ³	14.85	
Optimum moisture content, %	22.5	
CBR, %	Unsoaked	6.28
	Soaked	1.82
Unconfined compressive strength, kN/m ²	66.54	
Cohesion, kN/m ² (uu test)	33.27	

commercially available jute fibre. It had a diameter of 0.3 mm and a density of 14.00 kN/m³, and it was brown in colour. The findings of numerous experiments conducted at Shree Ram Laboratories in Noida, Uttar Pradesh (India) to determine its properties are listed in Table 2. The fibre length was 10, 20, 30, 40, 50, and 60 mm, while the fibre content was 0.10, 0.20, 0.40, 0.80, 1.60, and 2.40% by dry weight of the soil. Figure 3 depicts jute fibres that have been chopped to the required size.

Geotextile

Filter Fabs, New Delhi (India), supplied a commercially available woven geotextile, PPMF-300, consisting of polypropylene, for fabricating geocells, 3-D confining

Table 2 Properties of jute fibre [6]

Parameter	Value
Diameter, μ m	300
Colour	Brown
Specific area, mm ²	70.65
Density, kN/m ³	14.00
Tensile strength, MPa	518.0
Young modulus, GPa	26.40
Elongation, %	1.60
Water absorption, %	32.00

Fig. 3 Jute fibres cut to size [6]



systems, in a chevron pattern. The woven geotextile is depicted in Fig. 4. Its thickness was measured using IS: 13162 [40], and its mass per unit area was calculated using IS: 14716 [41]. Tensile strength and elongation at break point were determined using the wide width test defined in IS 13162 [42], while joint strength was determined using IS 15060 [43]. Table 3 summarizes the various geotextile properties.

Fig. 4 Woven geotextile [9]



Table 3 Properties of geotextile [9]

Parameter		Value
Thickness, mm		0.8
Weight per unit area, N/m ²		3.4
Wide width tensile strength, kN/m	WARP	80
	WEFT	70
Elongation at break, %	WARP	25
	WEFT	25
Joint strength, kN/m		13.4

2.3 Test Setup

There is no established test procedure for determining the swelling potential of geocell reinforced soil. As a result, the CBR mould was incorporated into the current investigation to evaluate the swelling potential of fibre and geocell reinforced expansive soil. The CBR mould is a rigid cylindrical metallic mould with an interior diameter of 152 mm and a height of 178 mm. To compact the matured dirt in the mould, a 26 N rammer with a drop of 310 mm was used. The compacted soil sample was immersed in a steel tank with a 20-L capacity. To measure swelling, a dial gauge with 50 mm capacity was placed atop the test specimen. The proposed setup is depicted in Fig. 5.

2.4 Sample Preparation

With hand tools, the expansive soil was pulverized and was sieved using a 75-micron IS sieve. All test specimens were prepared to their maximum dry unit weight (MDD) and optimum water content (OMC) as established by standard proctor tests in accordance with IS: 2720 [39]. To achieve maximum dry density, a calculated amount of water was added and thoroughly mixed with the requisite quantity of oven-dried soil. A mixture of homogenous consistency was obtained after kneading it by hand. Before adding water to the reinforced soil sample, fibres were chopped to size and percentages (p), Eq. 1, were dispersed randomly over the moistened soil. The weight of fibres (W_f) to the weight of dry soil (W_s) is expressed mathematically as fibre content (p).

$$p = \frac{W_f}{W_s} \times 100 \quad (1)$$

To prevent fibres from floating, the soil was moistened first with a small amount of predicted water, and then the remaining water was gradually added. After that,

Fig. 5 One-dimensional swelling test setup



moistened reinforced and unreinforced soil was maintained in an airtight container for 24 h to ensure uniform water distribution.

2.5 Test Procedure

A one-dimensional swelling test was performed using CBR mould on soil specimens, unreinforced and geocell reinforced, to evaluate the expansive soil's swell potential. A geocell is a cellular structure. A geocell mattress with a chevron pattern was obtained by cutting the woven geotextile into strips of the desired proportions and placing these in diagonal and transverse directions. Using nylon thread, these strips were stitched together, the lengths and numbers of stitches remaining the same. In 50 mm lifts, the moistened soil was placed in the CBR mould in the unreinforced specimen.

Using the drop hammer, each layer was dynamically compacted to its maximum dry density. Each layer's top surface was scratched before the next one was placed atop it for appropriate bonding. After hitting the desired height in the mould, the

geocell layer was put over the properly levelled surface to prepare the geocell reinforced specimen. The saturated fibre reinforced soil was placed in the geocell pockets. Under a 3 kN/m^2 applied load, the prepared test specimen was submerged in water, Fig. 6, to swell to equilibrium. The swollen specimen was placed in the loading frame, and a compressive load was applied until the test specimen returned to its original volume. The authors in recent past performed an experiment investigation to establish the best geocell and jute fibre reinforcing parameters for a circular foundation lying on expansive soil. A subset of this study's findings was published in a research paper [9]. Experiments were conducted with the test series and parameters listed in Table 4 to determine the efficacy of these ideal parameters in limiting subgrade soil swelling.

Fig. 6 Specimen being immersed in water



Table 4 Details of model test programme

Test series	Reinforcement type	Test parameters
A	Unreinforced expansive soil	Compacted at OMC
B	Geocell	Compacted at OMC
C	Fibre	Compacted at OMC
		Constant parameters: $L = 40 \text{ mm}$, $p = 0.8\%$
D	Geocell and fibre	Variable parameters: $L \text{ (mm)} = 10, 20, 30, 40, 50, 60$
		Constant parameters: $p = 0.8\%$
E	Geocell and fibre	Variable parameters: $p = 0.1\%, 0.2\%, 0.4\%, 0.8\%, 1.6\%, 2.4\%$
		Constant parameters: $L = 40 \text{ mm}$

3 Result and Discussion

On a logarithmic scale, Fig. 7 depicts the change in swelling amount over time, whereas Fig. 8 depicts the change in swelling pressure over time for the test series A through C. These graphs show that, in comparison with the reinforced soil sample, there is greater swelling in the unreinforced soil sample, with maximum swelling pressure and swelling of 137.36 kN/m^2 and 9.04 mm correspondingly. The equilibrium swelling was detected after 4320 min, or 3 days, which is consistent with the findings of [8, 25].

Swelling was decreased when geocell was introduced as reinforcement in the expansive soil. The greatest swelling measured 6.44 mm , indicating a 28.76% reduction. The swell pressure has dropped to 120.41 kN/m^2 . This reduction is mostly due to the creation of resistance caused by friction between geocell pocket walls and soil particles during the soil particle’s upward movement while swelling in a geocell

Fig. 7 Variation of swelling with time for unreinforced, geocell reinforced, fibre reinforced expansive soil

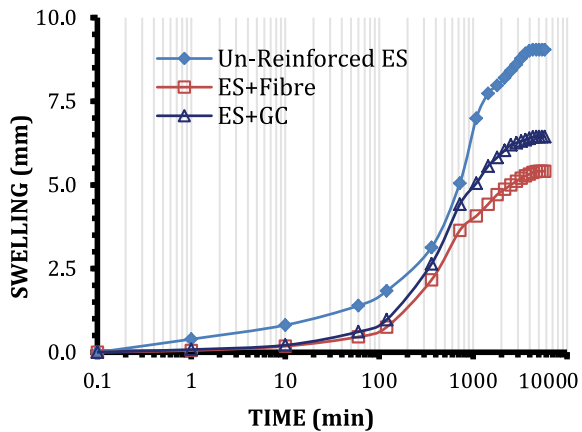
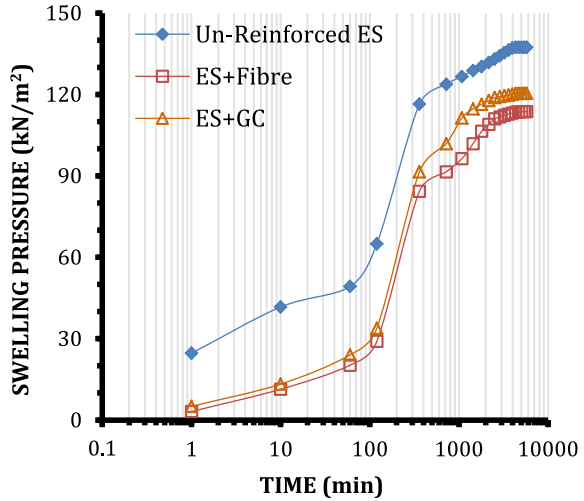


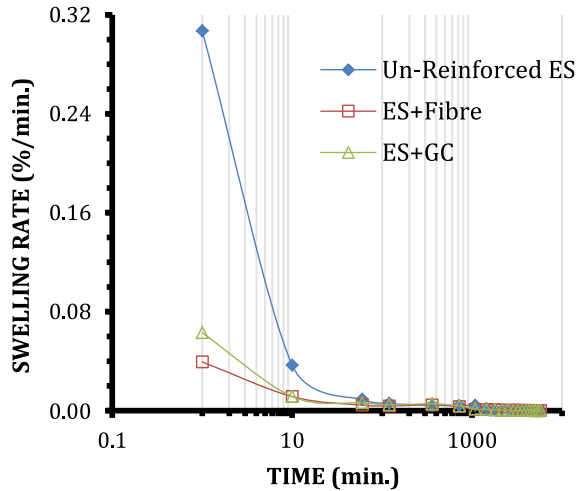
Fig. 8 Variation of swelling pressure with time for unreinforced, geocell reinforced, fibre reinforced expansive soil



reinforced soil sample. Compared to larger pocket-sized geocells, the magnitude of resistive forces is greater with smaller pocket-sized geocells. When 0.8%, 40 mm long fibres were randomly mixed, expansive soil swelling was reduced to 5.41 mm, resulting in a 40.15% decrease in swelling and a 113.70 kN/m² decrease in swelling pressure.

This decrease in soil swelling is described to (i) the replacement of expansive soil particles with non-expansive fibres, which results in a significant reduction in soil swelling potential [8], (ii) the interlocking of soil particles and the fibre [44, 45], and (iii) the creation of resistant tensile stresses in the fibres [25]. The friction between the soil fibre surfaces as a result of substantial swelling forces and fibre stretching generates these resistive tensile stresses. The sum of these forces can significantly reduce expansive soil swelling tendency. Figure 9 shows the rate of swelling of unreinforced and reinforced expansive soil samples in minutes. This graph shows that until 120 min after submerge, the swelling in unreinforced expansive soil is exponential. After that, the swelling rate does not vary significantly. The swelling rate is reduced by adding reinforcement. As a result, the expansive soil does not show the higher rate of swelling change. The expansive soil and reinforcement have air gaps in the early phases, which when filled with water produce pore pressure. As a result, the volume of the expansive soil changes rapidly, but the swelling diminishes as the soil reaches saturation. As a result, it is clear that water gets absorbed by the expansive soil in the initial stages and the change in swelling rate without pressure can be characterized as (1) initial swelling phase, (2) primary swelling phase, and (3) secondary swelling phase when it reaches saturation., these are the phases in which expansive soil swelling occurs [29, 46, 47]. Microstructural rearrangement occurs during the early swelling phase as a result of interlayer swelling and is accountable for a minor volume change, usually under 10% of the overall swell potential. The inter layer swelling persists into the primary swelling phase as well, lasting until

Fig. 9 Variation of swelling rate with time for unreinforced, geocell reinforced, fibre reinforced expansive soil



around 80% of the swell potential is reached. Due to the double layer repulsion, the secondary swelling phase occurs, resulting in minor time-bound volume changes. Swelling of the active clay mineral occurs at the micro-structural level during both the primary and secondary swelling phases. The term swell potential ($S\%$) is used to evaluate the performance of reinforcement, geocell, and fibre in controlling swelling of expansive soil. It is represented in percentage and is computed as the change in height (ΔH) over a specific time interval compared to soil specimen original height (H).

3.1 Fibre Length Effect

On a logarithmic scale, Fig. 10 depicts the change in swelling due to variation in fibre length over time for the test series D. This graph shows that as the fibre length increased, the swelling of the expansive soil decreased. However, until 40 mm of fibre length, there was a reduction in swell potential; beyond that, adding fibres of 50 and 60 mm causes swelling to increase. Swelling resistance of fibre, which is determined by the area of contact between the soil particles and the fibre, is responsible for the reduction of up to 40 mm long fibres. The area of contact between the soil particles and the fibre would be more effective at shorter lengths, while increasing the length resulted in increased contact area and, as a result, improved swelling resistance. A fibre bends and folds when its length exceeds 40 mm, limiting the effective area of contact between the expansive soil particles and the fibre, resulting in less swelling resistance, [8] reported similar findings. As a result, using long fibres of 50 and 60 mm causes increased swelling. Figure 11 depicts the variation in swelling caused

Fig. 10 Variation of swelling with time for different fibre lengths

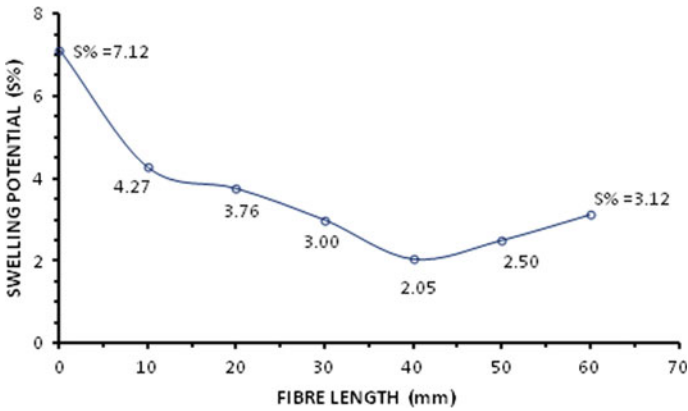
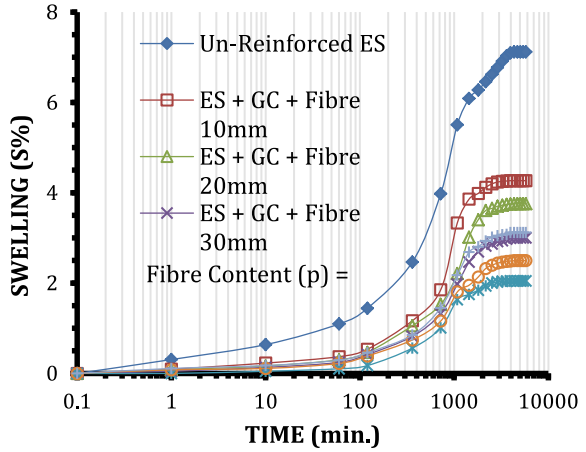


Fig. 11 Variation of swell potential for different fibre lengths

by fibres of varying lengths; the optimum length is 40 mm, after which it increases for 50 and 60 mm fibre lengths.

3.2 Fibre Content Effect

Figure 12 depicts the change in swelling with time, displayed on a logarithmic scale, for experiments performed under test series E. This figure shows that as the amount of fibre content increases, the amount of swelling of the expansive soil decreases. This could be due to the replacement of a bigger amount of the swelling soil by fibres that do not have a tendency to swell. As a result, significant swelling reduction is obtained by increasing the fibre content. Furthermore, the quantity of fibres has

increased as the fibre content in the soil has also increased, resulting in the fibres having a significantly greater resistance due to the fibre interlocking and restricting swelling of the expansive soil. Figure 13 shows that until fibre content was reached at 0.8%, the swelling potential declined, following which it increased as more fibres were added. The reason for this is that at greater fibre levels than the optimum, the fibres are concentrated in the soil mass and generate voids, reducing the effective contact area between the fibre and the expansive soil particles. At higher fibre contents than the optimal, this causes significant swelling. As a result, 0.8% fibre content is considered to be the ideal fibre content. The parameters determined at optimum reinforcement are listed in Table 5.

Fig. 12 Variation of swelling with time for different fibre contents

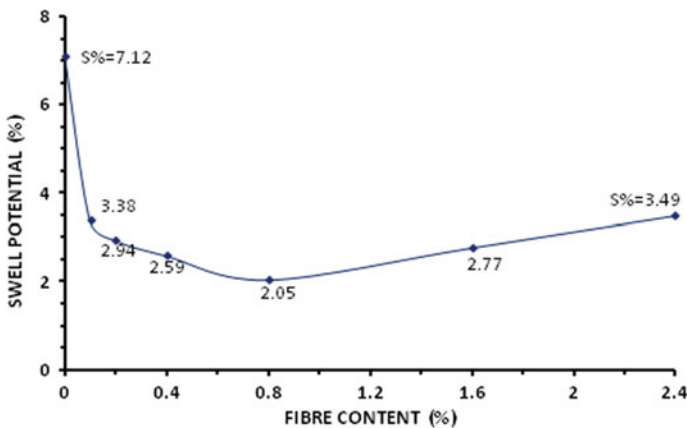
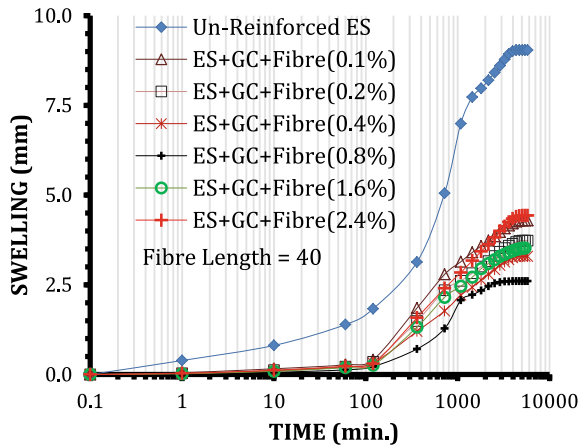


Fig. 13 Variation of swell potential for different fibre contents

Table 5 Summary of results obtained for geocell reinforced expansive soil with fibres of optimal parameters

Parameter	Result
Fibre content, %	0.8
Fibre length, mm	40
Swelling, mm	2.6
Swelling pressure, kN/m ²	80.5
Swell potential, S%	2.05
Reduction in swelling, %	71.24*
Reduction in swelling potential, %	41.40*

*Tiwari et al. [48] reported similar results with polypropylene fibre

4 Conclusion

The experimental investigation on remoulded specimens prepared from expansive soil reinforced with jute fibres that were dispersed randomly and geocells demonstrates that infrastructure construction on expansive soils is a viable option. On expansive soil, the effect of jute fibre and geocell reinforcements on swelling pressure and swell potential has been investigated. The findings reveal that Jute fibres and geocells perform effectively at keeping the expansive soil from swelling. From the present research work, the following particular conclusions are drawn:

- In expansive soils, geocell reinforcement is efficient at reducing swelling. Swelling was reduced by 28.76%, and swelling pressure was reduced by 12.34% when geocell reinforcement was used alone.
- Swelling pressure and swelling potential are both reduced with increasing length of fibre in expansive soil when reinforced with geocells at constant fibre content. The optimal fibre length is 40 mm, after which the fibre lengths of 50 and 60 mm are ineffective in reducing the swelling of expansive soil.
- At constant fibre length, with expansive soil reinforced with geocells, swelling pressure and swelling potential are both reduced as the fibre content increases. This decline was discovered to be limited to 0.8% fibre content, beyond which both swelling pressure and swelling potential began to increase.
- The minimum values for swelling pressure and swelling potential are 80.50 kN/m² and 2.05%, respectively, when optimal parameters ($L = 4$ mm and $p = 0.80\%$) jute fibres along with geocells were used to reinforce the expansive soil, resulting in a reduction in swelling of 71.24% and in swelling pressure of 41.40%.

Declaration

Acknowledgements The experimental study for this article was carried out at the Civil Engineering Department of Vaish Technical Institute in Rohtak, Haryana, India.

Conflicts of Interest The authors declare no conflict of interest.

Funding The authors received no financial support for the research, authorship, and/or publication of this article.

References

1. Çokça E (2001) Use of class C fly ashes for the stabilization of an expansive soil. *J Geotech Geoenviron Eng* 127(7):568–573
2. Kalkan E, Akbulut S (2004) The positive effects of silica fume on the permeability, swelling pressure and compressive strength of natural clay liners. *Eng Geol* 73(1–2):145–156
3. Chittoori BCS, Mishra D, Islam KM (2018) Forensic investigations into recurrent pavement heave from underlying expansive soil deposits. *Transp Res Record: J Transp Res Board* 2672(52):118–128
4. Kumar A, Walia BS, Mohan J (2006) Compressive strength of fiber reinforced highly compressible clay. *Constr Build Mater* 20(10):1063–1068
5. Meena SK, Sahu R, Ayothiraman R (2021) Utilization of waste wheat straw fibers for improving the strength characteristics of clay. *J Nat Fibers* 18(10):1404–1418
6. Kumar S, Sahu AK, Naval S (2020) Influence of jute fibre on CBR value of expansive soil. *Civ Eng J* 6(6):1180–1194
7. Sharma RS, Phanikumar BR (2005) Laboratory study of heave behavior of expansive clay reinforced with geopiles. *J Geotech Geoenviron Eng* 131(4):512–520
8. Viswanadham BVS, Phanikumar BR, Mukherjee RV (2009) Swelling behaviour of a geofiber-reinforced expansive soil. *Geotext Geomembr* 27(1):73–76
9. Kumar S, Sahu AK, Naval S (2019) Performance of circular footing on expansive soil bed reinforced with geocells of chevron pattern. *Civ Eng J* 5(11):2333–2348
10. Patil RM (1953) Determination of swelling pressure of black cotton soil—a method. In: *Proceedings of 3rd international conference on soil mechanics and foundation engineering*, vol 1, pp 170–172
11. Basma AA, Al-Homoud AS, Husein A (1995) Laboratory assessment of swelling pressure of expansive soils. *Appl Clay Sci* 9(5):355–368
12. Sridharan A, Prakash K (2000) Classification procedures for expansive soils. *Proc Inst Civ Eng—Geotech Eng* 143(4):235–240
13. Vessely MJ, Wu JTH (2002) Feasibility of geosynthetic inclusion for reducing swelling of expansive soils. *Transp Res Record: J Transp Res Board* 1787(1):42–52
14. Al-Rawas AA, Hago AW, Al-Sarmi H (2005) Effect of lime, cement and sarooj (artificial pozzolan) on the swelling potential of an expansive soil from Oman. *Build Environ* 40(5):681–687
15. Guney Y, Sari D, Cetin M, Tuncan M (2007) Impact of cyclic wetting–drying on swelling behavior of lime-stabilized soil. *Build Environ* 42(2):681–688
16. Ikizler SB, Aytakin M, Vekli M (2009) Reductions in swelling pressure of expansive soil stabilized using EPS geofoam and sand. *Geosynth Int* 16(3):216–221
17. Viswanadham BVS, Phanikumar BR, Mukherjee RV (2009) Effect of polypropylene tape fibre reinforcement on swelling behaviour of an expansive soil. *Geosynth Int* 16(5):393–401

18. Mirzababaei M, Yasrobi S, Al-Rawas A (2009) Effect of polymers on swelling potential of expansive soils. *Proc Inst Civ Eng—Ground Improvement* 162(3):111–119
19. Nagaraj H, Munnas M, Sridharan A (2010) Swelling behavior of expansive soils. *Int J Geotech Eng* 4(1):99–110
20. Yazdandoust F, Shahaboddin Yasrobi S (2010) Effect of cyclic wetting and drying on swelling behavior of polymer-stabilized expansive clays. *Appl Clay Sci* 50(4):461–468
21. Tiwari B, Ajmera B (2011) Consolidation and swelling behavior of major clay minerals and their mixtures. *Appl Clay Sci* 54(3–4):264–273
22. Trouzine H, Bekhiti M, Asroun A (2012) Effects of scrap tyre rubber fibre on swelling behaviour of two clayey soils in Algeria. *Geosynth Int* 19(2):124–132
23. Malekzadeh M, Bilsel H (2012) Swell and compressibility of fiber reinforced expansive soils. *Int J Adv Technol Civ Eng* 1(2):42–45
24. Elsharief AM, Zumrawi MM, Salam AM (2014) Experimental study of some factors affecting swelling pressure. *Univ Khartoum Eng J* 4(2):1–7
25. Phanikumar BR, Singla R (2016) Swell-consolidation characteristics of fibre-reinforced expansive soils. *Soils Found* 56(1):138–143
26. Jayasree PK, Balan K, Peter L, Nisha KK (2015) Volume change behavior of expansive soil stabilized with coir waste. *J Mater Civ Eng* 27(6):04014195
27. Elbadry H (2017) Simplified reliable prediction method for determining the volume change of expansive soils based on simply physical tests. *HBRC J* 13(3):353–360
28. Patil A, Parkhe D, Shrigriwar R, Panse R (2016) Establishing relationship between swelling pressure and free swell index of soils—a case study. *Int J Adv Sci Eng Technol* 3:4–7
29. Soltani A, Taheri A, Khatibi M, Estabragh AR (2017) Swelling potential of a stabilized expansive soil: a comparative experimental study. *Geotech Geol Eng* 35(4):1717–1744
30. Soltani A, Deng A, Taheri A (2018) Swell–compression characteristics of a fiber–reinforced expansive soil. *Geotext Geomembr* 46(2):183–189
31. Moghal AA, Chittoori BC, Basha BM, Al-Mahbashi AM (2017) Effect of polypropylene fibre reinforcement on the consolidation, swell and shrinkage behaviour of lime-blended expansive soil. *Int J Geotech Eng* 12(5):462–471
32. Muthukumar M, Sekar SK, Shukla SK (2017) Swelling and shrinkage behaviour of expansive soil blended with lime and fibres. In: Shukla S, Guler E (eds) *Advances in reinforced soil structures*. GeoMEast 2017. Sustainable civil infrastructures. Springer, pp 39–48
33. Tiwari N, Satyam N (2019) Experimental study on the influence of polypropylene fiber on the swelling pressure expansion attributes of silica fume stabilized clayey soil. *Geosciences* 9(9):377
34. Onyelowe K, Van DB, Eberemu A, Xuan MN, Bunyamin Salahudeen A, Ezugwu C, Van MN et al (2019) Sorptivity, swelling, shrinkage, compression and durability of quarry dust treated soft soils for moisture bound pavement geotechnics. *J Market Res* 8(4):3529–3538
35. Bekhiti M, Trouzine H, Rabehi M (2019) Influence of waste tire rubber fibers on swelling behavior, unconfined compressive strength and ductility of cement stabilized bentonite clay soil. *Constr Build Mater* 208:304–313
36. Kalkan E, Yarbasi N, Bilici Ö (2020) The effects of quartzite on the swelling behaviors of compacted clayey soils. *Int J Earth Sci Knowl Appl* 2(2):92–101
37. Shukla T, Mistry M, Solanki C, Shukla SK, Shukla S (2020) Influence of randomly distributed waste tire fibres on swelling behaviour of expansive soils. In: *Problematic soils and geoenvironmental concerns*, pp 319–332
38. Wang YX, Guo PP, Ren WX, Yuan BX, Yuan HP, Zhao YL, Shan SB, Cao P (2017) Laboratory investigation on strength characteristics of expansive soil treated with jute fiber reinforcement. *Int J Geomech* 17(11):04017101
39. IS 2720 Methods of test for soils. Bureau of Indian Standard, New Delhi
40. IS 13162 Part 3 (1992) Geotextile-method of test, determination of thickness at specified pressure. Bureau of Indian Standard, New Delhi
41. IS 14716 (1999) Geotextile-determination of mass per unit area. Bureau of Indian Standard, New Delhi

42. IS 13162 Part 5 (1992) Geotextile-method of test, determination of tensile properties using a wide width strip. Bureau of Indian Standard, New Delhi
43. IS 15060 (2001) Geotextile-tensile test for joints/seams by wide-width method. Bureau of Indian Standard, New Delhi
44. Tang C-S, Shi B, Zhao L-Z (2010) Interfacial shear strength of fiber reinforced soil. *Geotext Geomembr* 28(1):54–62
45. Tang C, Shi B, Gao W, Chen F, Cai Y (2007) Strength and mechanical behavior of short polypropylene fiber reinforced and cement stabilized clayey soil. *Geotext Geomembr* 25(3):194–202. <https://doi.org/10.1016/j.geotextmem.2006.11.002>
46. Sridharan A, Gurtug Y (2004) Swelling behaviour of compacted fine-grained soils. *Eng Geol* 72(1–2):9–18
47. Rao SM, Thyagaraj T, Thomas HR (2016) Swelling of compacted clay under osmotic gradients. *Géotechnique* 56(10):707–713
48. Tiwari N, Satyam N, Patva J (2019) Experimental study on the influence of polypropylene fiber on the swelling pressure expansion attributes of clayey soil. In: International conference on geotechnics for high speed corridors, Thiruvananthapuram, India

Stabilization of Black Cotton Soil by Using RBI Grade-81: A Review



Dharmendra Singh  and Vijay Kumar 

Abstract Due to rapid abrupt change in behavior of black cotton (BC) soil, a lot of engineers are worried about construction of durable as well as economical pavements laid on black cotton (BC) soil. Although BC soils are good for agricultural purpose yet these soils are not so perfect for building durable pavements. For any nation to be prosperous and developed, an efficient road network plays a vital role. For constructing a durable and efficient road network in BC soil region, the behavior of such soils should be thoroughly studied. These soils absorb water considerably and show heavy swelling due to presence of a clay mineral ‘montmorillonite’. This may lead to loss in shear strength and increase in compressibility of such soils, subsequently development to cracks in pavement. In the summer season, BC soils show significant shrinkage in its volume, leading to development of cracks. These soils depict extreme hardness and cracks when in dry state. The stability as well as performance of the pavements built on BC soils are highly influenced by the characteristics of sub grade and embankment because they serve as foundation part for the pavement. In this connection, use of a new material ‘RBI grade-81’ is frequently suggested to modify BC soil quality. RBI grade-81 may reduce the use of bitumen and aggregates and thus, it controls over emission of carbon. This may lead to eco-friendly construction practices of road. The use of ‘RBI grade-81’ may impart adequate strength in addition to durability to various layers of pavements. This literature deals with obtaining optimum quantity of the RBI grade-81 to be added with BC soil in order to alter its undesirable properties and providing it better strength. This paper also deals with some main reasons of poor condition of roads over BC soils and measures for improved construction practices with RBI grade-81.

Keywords RBI grade-81 · Black cotton soil · Roads · Bitumen · Bearing capacity

D. Singh (✉) · V. Kumar

Department of Civil Engineering, Motilal Nehru National Institute of Technology Allahabad,
Prayagraj 211004, India

e-mail: dharmendra@mnnit.ac.in

1 Introduction

The presence of expansive soils (ES) in various locations of all over the globe, especially, over the southern as well as a sub-Sahara portion of Africa and Sudan. It covers over a large portion of Australia, South America, the United States, some places of Canada and western as well as the central portion of Indian terrain [1, 2]. Black cotton (BC) soil covers approximately an area of about $8 \times 10^5 \text{ km}^2$, which is nearly equal to 20–25% of the entire available ground part of Indian terrain. BC soil is widely available in the southern part of India (Fig. 1). It extends over various states of India such as Karnataka, Maharashtra, Gujarat, the western and southern area of M.P, the southern part of U.P, the total eastern area of Rajasthan, and in some places in Andhra Pradesh and Odisha, and so on [1–8]. From the ancient time in the field of construction, BC soil has been found as unique of the most problematic soil to use it as soil subgrade for a pavement laying as well as for foundation building over it [5]. There are various difficulties in construction over BC soil that arises because this soil is much susceptible to shrink or swell due to the presence of montmorillonite as a clay mineral. When BC soil comes under contact with moisture, the swelling phenomenon of this soil takes place whereas when BC soil becomes dry due to moisture evaporation, it undergoes high shrinkage [5, 9–12].

As a BC soil stabilizer, Road Building International (RBI) Grade-81 is considered as an inorganic BC soil stabilizer or road pavement material. The use of RBI grade-81 emphasis on saving road construction time as well as natural resources required for pavement construction [1, 13–16]. If we talk about the appearance of RBI grade-81, it looks like a light grayish powdery substance that is insoluble in water (Fig. 2) [17]. It is reported as an inert, environment-friendly, chemically stable, and commercially available additive material. As a construction additive, RBI grade-81 is frequently being used across all over India as well as over world on various projects of roads and highway, railways, military, and even in paramilitary projects too [2]. Field emission scanning electron microscopy of RBI grade-81 is shown in Fig. 3.

Fig. 1 Black cotton soil [12]





Fig. 2 RBI grade-81 [17]

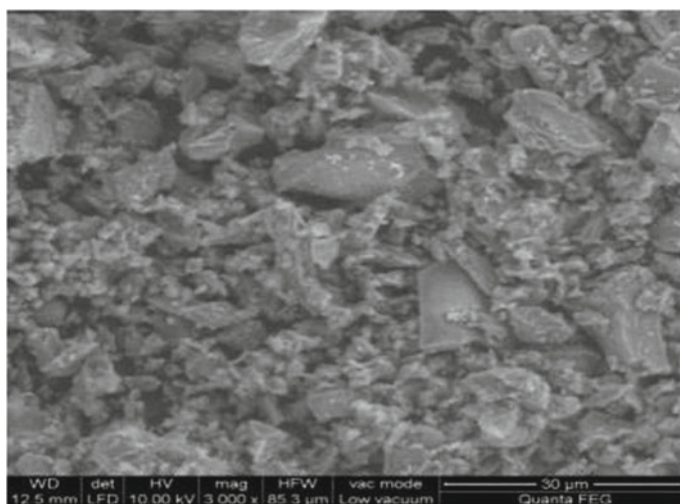


Fig. 3 RBI grade-81 field emission scanning electron microscopy (FESEM) image [1]

1.1 RBI Grade-81 Advantages

Benefits RBI grade-81 are as follows:

1. RBI grade-81 decreases road construction time by 35–40%.
2. The bearing capacity of BC soil enhancement is extremely due to the inclusion of RBI grade-81.
3. It is decreases the pavement in road construction.
4. It is decreases the cost of transportation and earth moving by 50–60%.

5. It decreases the cost of maintenance, aggregate requirement of road construction [1, 2, 5, 13].

1.2 Application of RBI Grade-81

Depending on the soil type, the traffic density and capacity, RBI grade-81 can be effectively used in the different civil engineering areas. These are as

1. High level altitude roads
2. Parking and unbreakable standing
3. Highways and railways
4. Military and paramilitary
5. Unbreakable standing grounds
6. Heliports
7. Progress landing ground [1, 5, 13].

2 Literature Review

Lots of work in the field of BC soil stabilization mixing with RBI grade-81 are concluding. Some important research papers related to BC soil stabilization mixing with RBI grade-81 have been reviewed in this segment of the study.

For most of the soils, RBI grade-81 found to be an effective stabilizer. The extent in modification in CBR value as well as in UCS value depends upon the type of soil to be treated. Due to the addition of RBI grade-81, OMC of soil increases whereas MDD reduces but surprisingly, the strength of the soil does not get adversely affected due to reduction in MDD. Due to the addition of RBI grade-81 with BC soil, the plastic limit of BC soil increases considerably and the liquid limit, as well as the free swell index of BC soil, reduces thus reduction in plasticity index of BC soil takes place [1]. A liquid limit and the plasticity index reduce and the plastic limit enhancement due to the mixing with RBI grade-81 in the BC soil in the following proportions 1, 2, 4, 6, and 8%. The stabilization of BC soil adding with RBI grade-81 in the following proportions 1, 2, 4, and 6%, then CBR value is enhanced [18]. The specific gravity, OMC, and the plastic limit of BC soil increased with an enhancement in the following proportions like 2, 4, 6, and 8%. MDD and liquid limit of BC soil reduced with enhancement in the following percentage like 2, 4, 6, and 8% [4]. With the mixing of RBI grade-81 in BC soil, the liquid limit reduces, and the plastic limit and plasticity index enhance. The MDD of BC soil increases and OMC reduce with the mixing of RBI grade-81 up to 6% by weight of BC soil and an extra increase in RBI grade-81 reduces the MDD and increases the OMC [14]. On mixing RBI grade-81 additives with subgrade soil in the proportion of 4:96, the MDD is reported as 1.46 g/cm³. In addition to this, the variation in MDD is found to be at least whereas a decrease in OMC is found to be considerable [2]. In this literature,

due to an increase in the proportion of RBI grade-81, CBR values are to be increases considerably. On a curing period of 28 days, the increase in CBR values is reported as 19.24% at 5% addition in RBI grade-81 proportion. Results show that up to an increase of 4% of RBI grade-81 proportion with soil, the gain in CBR value of soil is finding to be significant [11].

3 Methodology

The main concern of this research review is to study the geotechnical properties of BC soil and variation in the properties on BC soil stabilization when mixing with RBI grade-81. The following tests were performed as per Bureau of Indian Standards (mentioned below) on expansive soil in different literatures [9, 13, 18, 19]:

Properties	IS standard
Classification of soil	IS: 1498-1970
Liquid limit	IS: 2720 (Part-V)-1985
Plastic limit	IS: 2720 (Part-V)-1985
Natural moisture content	IS: 2720 (Part-VI)-1972
Plasticity index	IS: 2720 (Part-V)-1985
Shrinkage limit	IS: 2720 (Part-VI)-1972
Specific gravity	IS: 2720 (Part-III/Section-II)-1981
Free swell index (FSI)	IS: 2720 (Part-XL)
Grain size analysis	IS: 2720 (Part-IV)-1975
Maximum dry density (MDD)	IS: 2720 (Part-VIII)-1983 Optimum moisture content (OMC)
IS: 2720 (Part-VIII)-1983 California bearing ratio (CBR)	IS: 2720 (Part-XVI)-1987 Unconfined compression strength (UCS)
IS: 2720 (Part-X)-1991 Gravel fraction	IS: 2720 (Part-IV)-1985
Sand fraction	—
Silt fraction	—
Clay fraction	—

3.1 Basic Properties of RBI Grade-81

Physical properties like pH, odor, freezing point, etc., for RBI grade-81 are revealed in Table 1. Similarly, chemicals that are present in RBI grade-81 are presented in Table 2.

Table 1 RBI grade-81 physical properties [5, 11, 13, 17, 18, 20, 21]

S. No.	Physical properties	RBI grade-81
1	pH	12.5
2	Odor	Odorless
3	Freezing point	None
4	Flammability	Non-flammable
5	Life	1 year
6	Storage	Dry storage
7	Bulk density	700 kg/m ³
8	Appearance	Grayish powder
9	Specific gravity	2.5

Table 2 RBI grade-81 chemical properties [9, 10, 12, 13, 15, 16, 18]

S. No.	Chemical properties	% by mass
1	Oxocalcium (CaO)	52–55
2	Silicon dioxide (SiO ₂)	15–19
3	Sulfur trioxide (SO ₃)	9–11
4	Aluminum oxide (Al ₂ O ₃)	5–7
5	Ferric oxide (Fe ₂ O ₃)	0–2
6	Magnesium oxide (MgO)	0–1
7	Synthetic fiber polypropylene (PP)	0–1
8	Other some additives	0–4
9	Manganese, potassium, etc.	0.1–0.3

4 Conclusion

Based on the survey, it has been found that the use of RBI grade-81 as stabilizing for the black cotton soil. The following conclusions are obtained from the literature reviews.

1. With the mixing of RBI grade-81 in BC soil, the liquid limit and plasticity index of BC soil reduce and the plastic limit of BC soil enhancement.
2. Optimum moisture content (OMC) enhancement and maximum dry density (MDD) reduce narrowly due to the mixing of RBI grade-81 in BC soil when compared with BC soil is suitable for subgrade of road construction.
3. Free swell index (FSI) of BC soil reduces with the mixing of RBI grade-81 increases.
4. CBR and UCS values of BC soil enhancement with increase in RBI grade-81.
5. According to some literature reviews, the total cost of pavement reduces instantly after RBI grade-81 is mixed in BC soil to road construction pavement.

References

1. Raghuwanshi N, Kaur S (2016) A review on soil stabilization using RBI grade-81. *Int Res J Eng Technol (IRJET)* 3(7)
2. Dangi DS, Sharma P (2017) Laboratory investigation on expansive soil by using RBI grade-81. *Int J Scien Res Dev (IJSRD)* 5(4). ISSN: 2321-0613
3. Magadi KL, Deepika R (2019) An effect of RBI grade 81 on black cotton soil stabilization. *Int J Eng Sci Comput (IJESC)* 9(4)
4. Singh J, Sharma N (2018) Clay's properties improvement with RBI grade 81 and brick Kiln dust. *Int J Eng Trends Technol (IJETT)* 58(2)
5. Kitture SP, Kshirsagar SA, Garade AA, Auti AL (2019) A review on stabilization of black cotton soil using RBI grade 81, lime, rice husk ash and foundry sand. *Int J Res Appl Scie Eng Technol (IJRASET)* 7(III). ISSN: 2321-9653
6. Tripathi S, Pandey P (2018) A review: stabilization of black cotton soil using RBI grade-81 for pavement construction. *Int J Scien Res Dev (IJSRD)* 6(3). ISSN: 2321-0613
7. Somashekar DPN, Manu A, Murthy KNN, Prajwal KC (2021) Stabilization of black cotton soil using RBI grade 81 and Flyash. *Int J Scien Res Eng Dev* 4(1)
8. Raj S, Gupta N, Sharma L (2017) Comparative study on behaviour of soft soil using various admixtures. *Int J Mod Eng Res (IJMER)* 7(2). ISSN: 2249-6645
9. Venugopal G, Babji CF (2014) Studies on black cotton soil stabilization using RBI grade-81. *Int J Inno Res Sci Eng Technol* 3(12). ISSN: 2319-8753
10. Dhanasekar T, Rajakumar P (2018) Effective utilization of fuzzy logic in stabilize road construction with RBI grade-81. *Int J Civ Eng Technol (IJCIET)* 9(1):41–47
11. Venugopal G, Naagesh S, Gangadhara S (2021) Impact of RBI grade-81 on expansive soil strength characteristic. In: *International conference on advances in materials and manufacturing applications*
12. Aaqib M, Sharma N (2018) Investigation of geotechnical properties of expansive soil using bagasse ash and RBI grade-81. *Int J Eng Sci Res (IJESR)* 8(8):1–10. ISSN 2277-2685
13. Sreedhar A, Mailar G (2016) A study on soil stabilization using RBI grade 81. *IOSR J Mech Civ Eng (IOSR-JMCE)*:72–79. e-ISSN: 2278-1684, p-ISSN: 2320-334X
14. Patil BM, Patil KA (2013) Effect of fly ash and RBI grade 81 on swelling characteristics of clayey soil. *Int J Adv Technol Civ Eng* 2(2). ISSN: 2231-5721
15. Singh T, Riar N (2013) Strengthening of subgrade by using RBI grade-81 a case study. *IOSR J Mech Civ Eng (IOSR-JMCE)* 8(6):101–106. e-ISSN: 2278-1684, p-ISSN: 2320-334X
16. Kumar BV, Teja M, Kumar GK (2015) Comparative studies of black cotton soil with RBI grade 81 and ground granulated blast furnace slag. In: *50th Indian geotechnical conference*
17. John J, Thomas GE, Subair S (2016) A study on the effects of RBI grade 81 on the properties of subgrade soil. *Int J Mod Trends Eng Res (IJMTER)* 3(12). ISSN: 2349-9745
18. Madurwar KV, Dahale PP, Burile AN (2013) Comparative study of black cotton soil stabilization with RBI grade 81 and sodium silicate. *Int J Inno Res Sci Eng Technol* 2(2). ISSN: 2319-8753
19. Nouf N, Naagesh S (2014) Effect of RBI-81 on properties of black cotton soil. *Int J Recent Dev Eng Technol*. ISSN 2347-6435
20. Singh G, Yadav RK (2018) Stabilization of fine grained soil using RBI grade 81. *Int J Res Trends Inno* 3(9). ISSN: 2456-3315
21. Kusuma A, Krishna H (2019) Variations in strength parameters in base layer of pavement with RBI grade 81. *Int J Scien Dev Res (IJSRD)* 4(12). ISSN: 2455-2631

Geotechnical Investigation of Soil for Construction of a Court Building



Nadeem Akhtar, Md. Intekhab Sami, Vaqar Sultan, and Zoha Khairoowala

Abstract This study has been carried out to assess the competence and suitability of the soil stratum so that the foundation and soil underneath can safely bear the incoming load of the court building without the risk of shear failure and undesirable settlements. Standard penetration tests (SPT) were carried out at the proposed site in Sikandra Rao, District Hathras, Uttar Pradesh, and thirty-five soil samples were collected at 1.5 m depth of interval up to 10.5 m depth from the five bore holes and brought to the laboratory for further geotechnical investigations. Laboratory tests conducted on collected disturbed/undisturbed soil samples include sieve analysis, hydrometer analysis, liquid limit and plastic limit, natural moisture content, bulk and dry density, specific gravity and tri-axial shear tests. The soil bearing capacity was determined by settlement and shear criteria according to the procedure laid down by the relevant IS codes. The explorations up to significant depth helped in deciding the minimum depth and type of foundation best suited in the existing situation and the safe bearing capacity of the soil. The investigations also helped in detecting the filled-up stretch or the presence of discontinuities, cavities or zones of weakness beneath the proposed foundation within the zone of pressure bulb. These were taken into account while making recommendations for safe bearing capacity and the type of foundation suitable under the prevailing soil conditions.

Keywords Bore holes · Soil investigation · Safe bearing capacity · Foundation

1 Introduction

Geotechnical investigation is a prior step before constructing any structure. The objective of this investigation is to provide complete information regarding soil, its different strata and water table condition. It involves sampling of soils and its laboratory investigations. After the sampling, the samples are taken to the laboratory for investigations which include sieve analysis, hydrometer analysis, liquid limit and

N. Akhtar (✉) · Md. I. Sami · V. Sultan · Z. Khairoowala
Aligarh Muslim University, Aligarh 202002, India
e-mail: nadeem.akhtar184@gmail.com

© The Author(s), under exclusive license to Springer Nature Singapore Pte Ltd. 2023
A. K. Agnihotri et al. (eds.), *Proceedings of Indian Geotechnical and Geoenvironmental Engineering Conference (IGGEC) 2021, Vol. 1*, Lecture Notes in Civil Engineering 280,
https://doi.org/10.1007/978-981-19-4739-1_6

plastic limit, natural moisture content, bulk and dry density, specific gravity and tri-axial shear tests to estimate different index properties of soil. These investigations helped in determining the bearing capacity of soil and in determining the right size of foundation for the building so as to safely bear the incoming load of structure without excessive settlement. If the surface beneath is of compressible soil, high moisture content soil or organic soil, then it may lead to excessive settlement which in turn will lead to failure of structure. As per IS code specifications, the total permissible settlement on clay for isolated footing is 65 mm and for raft footing is 65–100 mm. Types of foundation are selected keeping in view the incoming structure load and soil condition beneath.

1.1 Description of Site

The proposed site is located at Sikandra Rao, District Hathras, Uttar Pradesh, about 40 km away from AMU Campus, Aligarh. The ground surface at the site was slightly undulated. The plan of proposed site for the construction of court building is shown in Fig. 1.

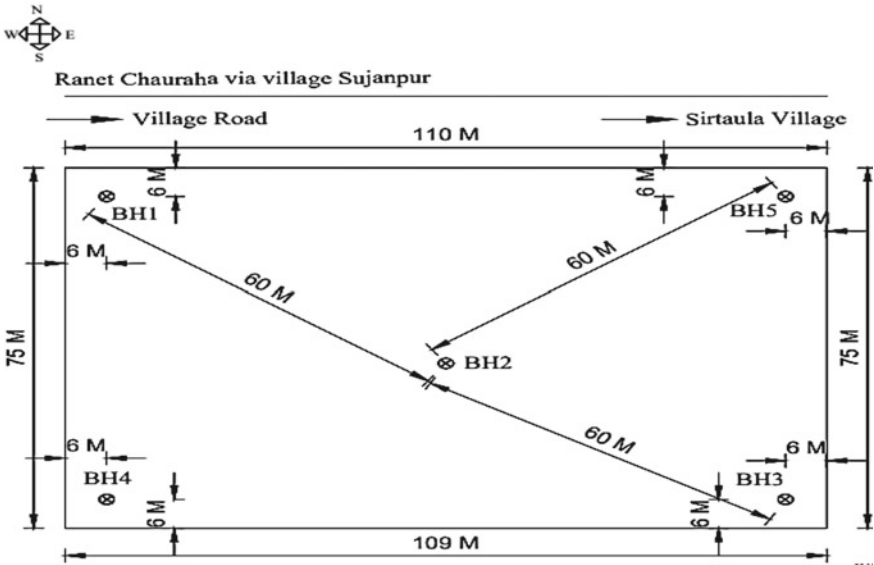


Fig. 1 Site plan (not to scale) of proposed construction of court building at Sikandra Rao, district Hathras, Uttar Pradesh

2 Field Investigations

Necessary equipment and personnel for conducting the requisite field work were mobilized to the site. These were shifted from one test location to another location during execution of the field work and demobilized on satisfactory completion of the entire field work.

2.1 Borings

The in situ inspection of soil samples obtained from five bore holes BH1, BH2, BH3, BH4 and BH5 at depths of 1.5, 3.0, 4.5, 6.0, 7.5, 9.0 and 10.5 m was carried out during the boring operation. The SPT observed N values were recorded for all depths of each bore hole. The soil samples were further identified and classified in the geotechnical engineering laboratory in accordance with the procedure laid down in IS code 1498-2018 “Identification and Classification of Soils for General Engineering Purposes.”

2.2 Standard Penetration Test (IS 2131-1981)

Standard penetration test is widely used field test for engineering purpose related to soil which is relatively quick and simple to perform. This is conducted at the site of project to determine the geotechnical properties of subsurface layers of soil and classification of soil and to obtain the penetration resistance or N value.

The test involves the measurement of the resistance to penetrate the split spoon sampler under dynamic loadings. The test is performed in a cased bore hole of 60–75 mm diameter. A split tube sampler of 50 mm outer diameter and about 650 mm length attached to a string of drill rods is then lowered to the bottom of the hole to take out the undisturbed samples. Subsurface soil conditions are evaluated, and to measure in situ soil resistance at different depths, soil samples are collected at every 1.5 m interval or at depth where there is change in strata. The SPT- N values are obtained for 300 mm sinking of a split spoon sampler into the ground after 150 mm of initial seating drive under the impact of 65 kg hammer having a free fall of 750 mm out simultaneously [1–3]. N values have also been correlated to relative density of cohesionless soil and unconfined compressive strength of cohesive soils [4].

There are two types of corrections generally applied to observe N values (N_{obs}).

1. The overburden correction recommended by Peck et al. [3] given below is being utilized [4, 5].

$$N_{\text{corrected}}(N') = N_{\text{obs}}[0.77 \log_{10}(2000/\sigma')]$$

Table 1 Observed and corrected SPT-N values of 5 bore holes

Depth (m)	Bore hole 1		Bore hole 2		Bore hole 3		Bore hole 4		Bore hole 5	
	N_{obs}	N_c	N_{obs}	N_c	N_{obs}	N_c	N_{obs}	N_c	N_{obs}	N_c
1.5	35	32	34	31	13	17	18	20	31	29
3	14	15	20	19	17	17	15	16	22	20
4.5	19	17	21	18	13	14	17	16	20	18
6	21	17	22	18	20	17	18	16	21	17
7.5	24	18	25	18	19	16	22	17	26	19
9	28	19	26	18	21	16	25	18	30	20
10.5	31	19	28	18	24	19	29	19	36	21

where σ' = effective overburden pressure in kN/m^2 .

$$\sigma' = \gamma' D,$$

where γ' = effective unit weight of soil (kN/m^3) and D = depth of soil in meter.

2. In case of saturated silt and fine sand, the following correction for values after overburden correction, N' greater than 15 is applied [1]:

$$N_{corrected}(N_c) = 15 + \frac{1}{2}(N' - 15)$$

where N_c is the final corrected value of N_{obs} .

Observation

See Table 1.

2.3 Sampling

Representative soil samples were collected from depth at which standard penetration tests were performed (from natural ground surface to 10 m with 1.5 m depth of interval) and also from depths at which change of strata occurred. The bulk unit weights of representative soil samples obtained from split spoon sampler at different depths were also determined.

3 Laboratory Investigations

Following tests were conducted in the laboratory as per relevant IS codes:

- Natural moisture content IS: 2720 (Part II)—2013
- Grain size analysis IS: 2720 (Part IV)—2013
- Atterberg’s limits IS: 2720 (Part V)—2013
- Tri-axial shear tests IS: 2720 (Part XI)—2013
- Soil classification IS: 1498—2013

3.1 Natural Moisture Content

The moisture content of different soil samples obtained from bore hole nos. 1 to 5 in the field was determined by adopting standard oven drying procedure, as per IS: 2720 (Part II)—2013.

3.2 Grain Size Analysis

Sieve analysis tests were conducted on the coarse-grained soil samples obtained from the SPT tests, as per IS: 2720 (Part IV)—2013, and hydrometer analysis is done for fine-grained soils for the purpose of gradation and classification of soils.

Observation

See Fig. 2 and Table 2.

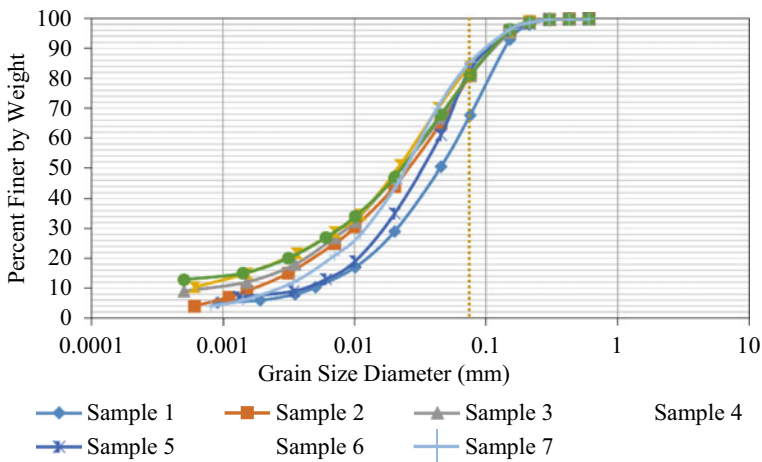


Fig. 2 Particle size analysis (sieve and hydrometer analysis combined)

Table 2 Particle size distribution

Sample No.	1	2	3	4	5	6	7
% clay	6	10	13	18	8	18	9
% silt	62	71	68	66	75	63	77
% Fine sand	32	19	19	16	17	19	14
D_{10}	0.005	0.0015	0.0006	0.0006	0.0032	0.0005	0.0027
D_{30}	0.02	0.01	0.008	0.007	0.018	0.007	0.012
D_{60}	0.06	0.04	0.032	0.03	0.045	0.032	0.03
C_u	12	26.7	53.3	50	14.1	64	11.1
C_c	1.3	1.7	3.3	2.7	2.25	3.06	1.8

D_n = particle size finer than $n\%$, C_u = coefficient of uniformity = D_{60}/D_{10} , C_c = coefficient of curvature = $(D_{30})^2/(D_{60} * D_{10})$

3.3 Atterberg’s Limit Tests

For the purpose of classification of cohesive soils, liquid limits and plastic limits were determined as per IS: 2720 (Part V)—2013 and plasticity index was determined from these tests.

Observation

See Fig. 3 and Table 3.

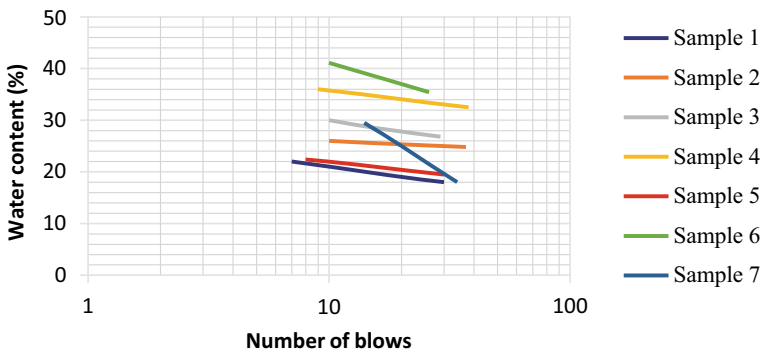


Fig. 3 Flow curve. Water content corresponding to 25 number of blows gives liquid limit of that soil sample

Table 3 Index properties of soil samples

Sample No.	1	2	3	4	5	6	7
Liquid limit W_L	19	25	27	34	20	36	22
Plastic limit W_p	16	19	18	21	15	22	18
Plasticity index I_p	3	6	9	13	5	14	4
Soil classification	ML	CL-ML	CL	CL	CL-ML	CI	ML

$I_p = W_L - W_p$, CL: silty clay (clay of low plasticity), CL-L: silt–clay mixture, CI: clay of intermediate plasticity, ML: low compressible silt

3.4 Tri-axial Shear Tests

The soil samples collected from non-cohesive soil strata were tested in tri-axial apparatus for determining the drained shear strength parameters c and ϕ in order to determine the bearing capacity of the soil strata. The tests were conducted as per IS: 2720 (Part XI)—2013.

Observation

See Table 4.

4 Test Results and Its Interpretation

On the basis of lowest SPT-N values of soil strata, the bore hole no. 3 (BH₃) is considered as the critical bore hole. The properties of soils from natural ground surface to 10.5 m depth with interval of 1.5 m are shown in critical bore hole chart.

The results of lab tests and critical bore hole log chart indicate that the strata from natural ground surface to 10.5 m depth comprise plastic soils like silty clay

Table 4 Comparison of shear strength parameters obtained experimentally and graphically using Mohr’s circle

Sample No.	C			ϕ		
	Analytical	Graphical	Difference (%)	Analytical	Graphical	Difference (%)
1	25	24.9	0.4	15	15.1	0.6
2	30	30.2	0.6	14	13.9	0.7
3	33	33.3	0.9	12.5	12.5	0
4	36.5	36.6	0.3	11.5	11.6	0.8
5	31	31.5	1.6	13	12.8	1.5
6	46	46.5	1.1	8	8	0
7	25	25.2	0.8	15	15.1	0.6

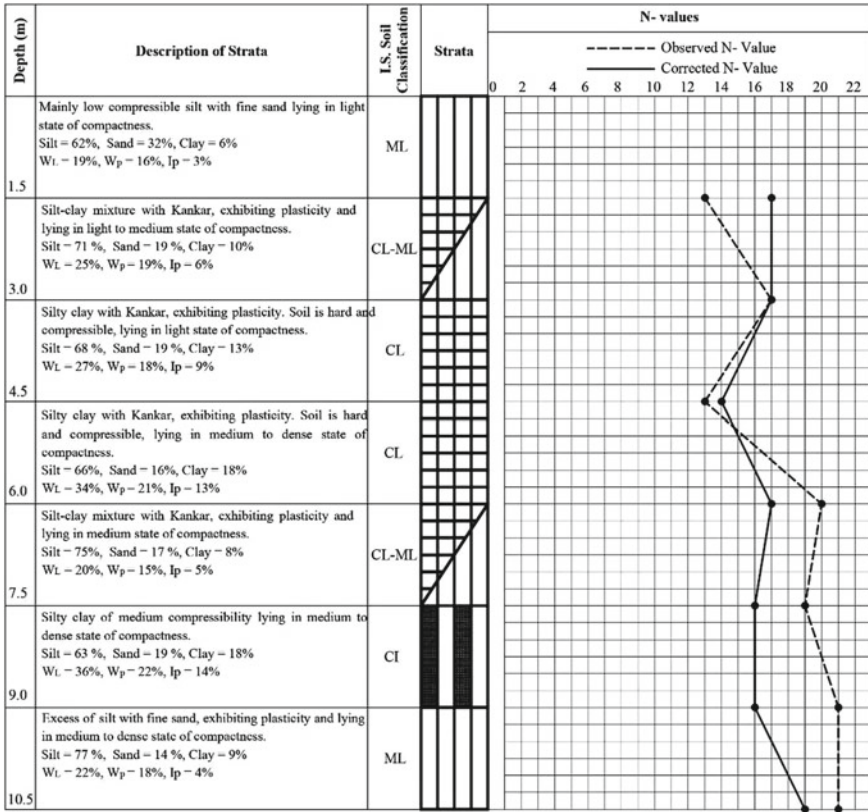


Fig. 4 Bore hole chart for critical bore hole no.3

(CL), mixture of silt and clay (CL-ML), clay of intermediate plasticity (CI) and low compressible silt (ML).

The natural moisture contents of each sample were found to be 1–10% for the critical bore hole up to 10.5 m depth, and the ground water level (GWL) was not encountered up to a depth of 10.5 m below existing natural ground level (N.G.L.). This fact has been taken into account while determining the allowable bearing capacity of the soil foundation system.

The values of shear strength parameters obtained from tri-axial test will be used to compute the bearing capacity of the non-cohesive soils (Fig. 4).

5 Design Considerations

A properly designed foundation should satisfy the following basic requirements:

- Foundation must be safe against shear failure of the supporting soil. A suitable factor of safety (say 3) is applied while assessing the safe bearing capacity.
- The foundation must not settle more than the permissible value.

5.1 Computation of Bearing Capacity

The following procedure was adopted to find out the allowable bearing capacity utilizing shear strength parameters obtained from tri-axial shear strength test and standard penetration test data.

Bearing Capacity from Shear Considerations Using Tri-axial Shear Test Data.

For the proposed construction of court building, footing of 2.0 m width (for calculation purpose) is provided at two depths of 1.5 and 2.0 m below natural ground surface (taking soil data of critical bore hole no. 3). Using equation given below as per IS: 6403-2012 for local shear failure condition “Code of Practice for Determination of Bearing Capacity of Shallow Foundations” [4, 5].

$$q_{ns} = 1/F \left[c_m N'_c S_c d_c i_c + q (N'_q - 1) S_q d_q i_q + \frac{1}{2} g B N'_\gamma S_\gamma d_\gamma i_\gamma R_w \right] \quad (1)$$

where

q_{ns}	net safe bearing capacity
F	factor of safety taken as 3.0
q_s	safe bearing capacity, $q_s = \gamma D_f$
c	unit cohesion
c_m	modified unit cohesion for local shear failure
ϕ	angle of shearing resistance
ϕ_m	modified ϕ for local shear failure
q	surcharge, γD_f (above base of footing)
γ	unit weight of soil
D_f	depth of foundation
B	width of footing
L	length of footing
N'_c, N'_q, N'_γ	modified B.C. factors for ϕ_m (local shear failure)
S_c, S_q, S_γ	shape correction factors
d_c, d_q, d_γ	depth correction factors
i_c, i_q, i_γ	inclination correction factor, $i_c = i_q = i = 1$
R_w	water table correction factor
Inclination factors	$i_c = i_q = \left(1 - \frac{\alpha}{90}\right)^2$ and $i = \left(1 - \frac{\alpha}{\phi}\right)^2$
α	inclination of the load to the vertical in degrees = 0, for vertical loads as in the present case.

Bearing Capacity from Settlement Considerations Using SPT Test Data. The allowable bearing capacity (q_a) has been determined by standard penetration test data. The allowable bearing capacity (q_a) of soil for critical bore hole no. 3 at 1.5 and 2.0 m depths below the existing ground level has been estimated based on average corrected ‘N’ values of effective zone, i.e., $D_f + 1.5 * B$ in accordance with the procedure laid down in IS: 1904—2011, Appendix ‘C’, “Net Allowable Bearing Capacity from settlement considerations is corresponding to 25 mm of settlement of footings on sand.”

6 Conclusion

The bearing capacity of soil has been determined by shear and settlement criterion. The minimum value of bearing capacity at different depths is obtained by shear criteria and recommended as the net safe bearing capacity and safe bearing capacity as shown in Table 5.

The minimum value of bearing capacity at different depths is obtained by shear criteria and recommended as the allowable bearing capacity as shown in Table 6.

The minimum value of bearing capacity out of both the consideration at 2 m depth is considered for design purpose, i.e., 136 kN/m².

The final design and the depth of isolated foundation have been worked out in accordance with IS: 1904—2013 “Code of Practice for Design and Construction of Shallow Foundation in Soils” by the agency who is given the execution of shallow foundation work in consultation with the structural engineer concerned as per actual requirements considering the design load and investigation data results.

Table 5 Recommended value of bearing capacity at different depths

S. No.	Width of footing	Depth of foundation	Net safe bearing capacity (q_{ns})		Safe bearing capacity (q_s)	
	(m)		(m)	kN/m ²	t/m ²	kN/m ²
1	2	1.5	95	9.69	120	12.24
2	2	2	102	10.4	136	13.87

Table 6 Allowable bearing capacity from SPT test [1]

S. No.	Width of footing	Depth of foundation	Allowable bearing capacity	Allowable bearing capacity
	(m)		(m)	kN/m ²
1	2	1.5	160	16.32
2	2	2	160	16.32

References

1. Terzaghi K, Peck RB (1967) Soil mechanics in engineering practice, 2nd edn. Wiley, New York
2. Bowles JE (1984) Physical and geotechnical properties of soils. McGrawHill, Inc., USA
3. Peck RB, Hanson WE, Thornburn TH (1974) Foundation engineering, 2nd edn. Wiley & Sons Inc., New York
4. IS Code 2131 (2012) Method of standard penetration tests for soils. Bureau of Indian Standards, New Delhi
5. Ranjan G, Rao ASR (2007) Basic and applied soil mechanics, Revised 2nd edn. New Age International Pvt. Ltd., India

Application of Electrical Resistivity in Site Investigation at Ground Profile



Swati Ganesh Sonawane, A. B. Saner, Harshal Sarjerao Desale,
and S. R. Joshi

Abstract Exploration geophysics is a branch of geophysics, which deals with physical methods on the surface of earth to determine physical properties of the subsurface along with the something that deviates from what is standard, normal or expected, in those properties. Geophysical methods contain seismic, magnetic, electromagnetic, gravitational and electrical methods. This paper describes about electrical resistivity method. When precise construction is to be executed, soil investigation for knowing geology of the area is done in by using geophysical methods. Basically, in this method, there is determination of nature subsurface strata without excavation we can determine the nature of subsurface using geophysical methods. Electrical sounding method is used for this work as there are variations in subsurface strata with increasing depth at ground profile.

Keywords Resistivity · Electrical resistivity method · Electrical sounding method

1 Introduction

1.1 General

Geophysical method is used for investigation of earth or soil, for knowing the characteristics of soil. It is only used for preliminary observation and when rapid characterization is required. When detailed observations are required, geophysical methods are

S. G. Sonawane (✉) · A. B. Saner · H. S. Desale · S. R. Joshi
Matoshri College of Engineering and Research Centre, Eklahare, India
e-mail: sonawaneswati999@gmail.com

A. B. Saner
e-mail: Amol.Saner@matoshri.edu.in

H. S. Desale
e-mail: harshal.desale28@gmail.com

S. R. Joshi
e-mail: SWAPNIL.joshi@matoshri.edu.in

© The Author(s), under exclusive license to Springer Nature Singapore Pte Ltd. 2023
A. K. Agnihotri et al. (eds.), *Proceedings of Indian Geotechnical and Geoenvironmental Engineering Conference (IGGEC) 2021, Vol. 1*, Lecture Notes in Civil Engineering 280,
https://doi.org/10.1007/978-981-19-4739-1_7

cannot be used. Geophysical method contains electrical, seismic, magnetic and electromagnetic gravity method [1]. Various geophysical methods are applied if primary exploration of subsoil strata is required (Woodward 2007). This method can be used for point of varying strata for a fast evaluation of subsoil properties; at that point, electrical resistivity method is used. Electrical resistivity is a reciprocal of current, resistance of a soil depends upon form of soil, amount of moisture content and dissolved ions concentration (Sheelar and Demiral 2004). Stones, boulders and soil in dry condition have higher resistivity than wet soil clays. Resistivity depends on types of materials as iron have low resistivity than wood; at the same time, water content of materials is responsible for resistivity, as soil contains more water content; its resistivity will be low, and as concentration of dissolved ions is more, it will pass more electric current, as we know salty water is a good conductor of electricity.

1.2 Background

Electrical resistivity test (ERT) was carried out in the premises of STT GLOBAL DATA CENTRE, to ascertain the subsurface geology located at MIDC MAHAPE. Vertical electrical sounding was carried out at 06 locations for an electrode spread of 10 m in 2 directions, namely (east-west and north-south) using Wenner's configuration in order to ascertain subsurface geology.

A. Electrical profiling method/Resistivity mapping method

Electrodes are placed at a constant spacing. To conduct the test, four electrodes of metal pin with higher thickness are driven into the surface. Two no. of current electrodes are placed at corner, and remaining two intermediate electrodes are potential electrodes. Average resistivity of a layer is calculated by giving direct current to electrodes placed at corner and measuring the voltage difference in between the intermediate electrodes [2]. Current of 0.05 to 0.1 A is generally supplied.

Average velocity,

$$\rho = 2\pi av/I$$

where

I = current applied, a = Spacing of electrodes, V = Voltage drop, ρ = Mean electrical resistivity.

The method is useful for establishing boundaries between two different strata and is generally used for locating sand and gravel deposits within a fine grained soil deposits.

B. Electrical Sounding Method

In this method, the electrode system, consisting of four electrodes is expanded about a fixed location say P. The spacing in the first setting is a1 which increased

in a_2 to a_3 in the third setting. The spacing is thus gradually increased to a distance as the equal to a distance equal to the depth of exploration (Baban 2016). As depth of current penetration is equal to electrode spacing, this change in the mean resistivity is correlated to changes in strata at that location (Mostafa 2014).

This method determines:

- (1) Changes in strata with increasing depth at point.
- (2) Can indicate subsurface when hard layer lies over soft.
- (3) It locates water table.

Limitations to Electrical resistivity methods

- (1) Methods are capable of detecting only the strata having different electrical resistivity.
- (2) The service of an expert in the field is needed.

2 Methodology

In Wenner's configuration, observations are made to obtain information on the variation of the physical field in the vertical section at a given location (sounding). The variation in the physical field is interpreted in terms of subsurface in homogeneities which include variation in lithology, quantity and quality of water [3]. The electrical properties of most rocks are primarily dependant on the amount of water in the rock. The higher the porosity of the saturated rock, the lower its resistivity [4]. Saturated rocks have lower resistivity than unsaturated or dry rocks. As the length of probing deepens the resistivity of the earth ranges in between 0.1 to 1.0 Ω . Variation of the resistivity of the soil with depth is more predominant as compared to the variation with vertical distances. Wide variation of resistivity with depth is due to position of earth layers. To design the most provident and technically sound ground in system for large stations, it is necessary to gain the accurate data of the soil resistivity and on its variations at the station side. The resistivity measures at the point will reveal whether the soil homogenous or non-livery. The resistivity of earth varies over a wide range depending upon its humidity content (Soil Survey Investigations Report No. 51, 2004). Wenner's four electrode systems are recommended for these types of field examinations. In these systems, four electrodes driven into the earth along the straight line at equal interval, and the current is passed through the two external electrodes. The voltage difference is observed between the two inner electrodes. The current flowing into the earth produces an electric field commensurable to its viscosity and to the resistivity of the soil. At the named test spots, four electrodes are driven into the earth along a straight line at equal interval. The instrument is placed on a steady roughly position base. Applicable range on the instrument is named to gain clear readings. Wenner's four electrode system is recommended for these of field examinations. In this system, four electrodes are driven into the earth along a straight line at

equal intervals. A current I is passed through the two external electrodes and the earth and the voltage difference V , observed between the two inner electrodes. The current I flowing into the earth produces an electric field commensurable to its viscosity and to resistivity of the soil. The voltage V measured between the inner electrodes is commensurable to the field. Accordingly, the resistivity will be commensurable to the rate of the voltage to current. If the depth of burial of the electrodes in the ground is negligible compared to the distance between the electrodes also,

Average resistivity,

$$\rho = 2\pi aR$$

ρ = Resistivity of soil in ohm cadence

a = Distance between two consecutive electrodes in cadence

R = resistance offered in the system in ohms

RESEARCH GAP

1. In the previous researches, the study was to determine resistivity at higher depths; hence, their results are different from the present study. The present study focuses on determining resistivity at ground profile.
2. Electrical resistivity test is generally carried out on high depth from 30.00–50.00 m. In this case, we are conducting the test on 15 m depth from ground level only.
3. We know resistivity of soil mainly depends on moisture content, and due to the presence of high humidity in surrounding, the resistivity of soil is low, and the site is in MIDC area; therefore, due to pollution, soil properties are already disturbed.
4. This test is time consuming and it does not requires more manpower; it gives instant results and economical too.
5. We get exact details and clear readings because this is a field test on undisturbed samples.

3 Results

The test is carried out in four layers. Results are found in permissible ranges. Top layer is of over burden residual soil at 0.5 m depth. Intermediate layer 1 is consisting of high to moderate weathered and fractured grey basalt at 0.5–6 m depth. Intermediate layer 2 is of moderate to slight weathered greyish basalt at 6–9 m. Bottom layer is found slightly weathered to fresh greyish basalt, i.e. hard strata without cavity, fault, joint and fractures at depth of 9–15 m.

Water table is found on 5–6 m depth.

The average resistivities are given in Tables 1, 2, 3, 4, 5, 6 and 7.

Table 1 Average apparent resistivity values for all six locations

Electrode distance (m)	Average apparent resistivity values					
	ERT-1	ERT-2	ERT-3	ERT-4	ERT-5	ERT-6
1	105.82	280.05	86.97	252.45	224.94	628.31
2	116.43	234.85	102.49	466.60	187.89	1065.71
3	152.88	245.97	111.72	601.93	143.84	942.94
4	194.93	301.44	148.96	802.58	189.27	831.47
6	282.60	401.48	208.55	1154.89	278.27	815.77
8	316.33	535.30	178.08	1539.85	345.64	801.33
10	353.56	640.87	340.69	1924.82	383.20	626.11

Table 2 Electrical resistivity test at location 1

Electrode spacing a (m)	$K = 2a$ (m)	East–West		North–South		Average apparent resistivity
		Resistance R (Ω)	Apparent resistivity $\rho = (K \times R)$ (Ωm)	Resistance R (Ω)	Apparent resistivity $\rho = (K \times R)$ (Ωm)	
1	6.28	18.50	116.18	15.20	95.46	105.82
2.0	12.56	8.90	111.78	9.64	121.08	116.43
3.0	18.84	7.81	147.14	8.42	158.63	152.88
4.0	25.12	7.42	186.39	8.10	203.47	194.93
6.0	37.68	7.42	279.59	7.58	285.61	282.60
8.0	50.24	6.10	306.46	6.49	326.06	316.33
10.0	62.80	5.43	341.00	5.83	366.12	353.56

Table 3 Electrical resistivity test at location 2

Electrode spacing a (m)	$K = 2a$ (m)	East–West		North–South		Average apparent resistivity
		Resistance R (Ω)	Apparent resistivity $\rho = (K \times R)$ (Ωm)	Resistance R (Ω)	Apparent resistivity $\rho = (K \times R)$ (Ωm)	
1	6.28	47.90	300.81	41.30	259.36	280.05
2.0	12.56	17.00	213.52	19.60	246.18	234.85
3.0	18.84	13.70	258.11	12.40	233.62	245.97
4.0	25.12	12.300	308.98	11.70	293.90	301.44
6.0	37.68	11.500	433.32	9.81	369.64	401.48
8.0	50.24	11.500	577.76	9.81	492.85	535.30
10.0	62.80	11.500	722.20	8.91	559.55	640.87

Table 4 Electrical resistivity test at location 3

Electrode spacing a (m)	$K = 2a$ (m)	East–West		North–South		Average apparent resistivity
		Resistance R (Ω)	Apparent resistivity $\rho = (K \times R)$ (Ωm)	Resistance R (Ω)	Apparent resistivity $\rho = (K \times R)$ (Ωm)	
1	6.28	12.90	81.01	14.80	92.94	86.97
2.0	12.56	7.29	91.56	9.03	113.42	102.49
3.0	18.84	5.74	108.14	6.12	115.30	111.72
4.0	25.12	5.74	144.19	6.12	153.73	148.96
6.0	37.68	5.24	197.44	5.83	219.67	208.55
8.0	50.24	5.24	263.26	5.83	292.90	178.08
10.0	62.80	5.240	329.07	5.610	352.31	340.69

Table 5 Electrical resistivity test at location 4

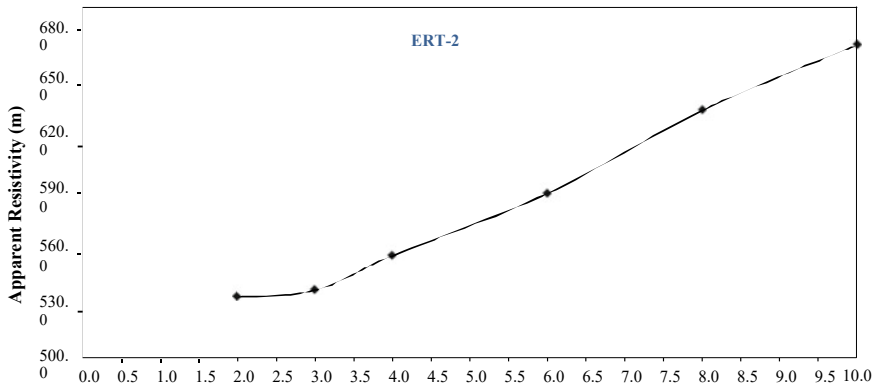
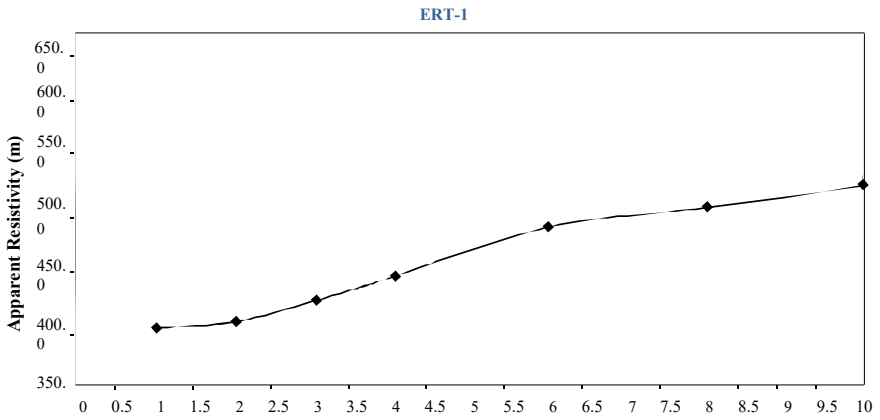
Electrode spacing a (m)	$K = 2a$ (m)	East–West		North–South		Average apparent resistivity
		Resistance R (Ω)	Apparent resistivity $\rho = (K \times R)$ (Ωm)	Resistance R (Ω)	Apparent resistivity $\rho = (K \times R)$ (Ωm)	
1	6.28	39.00	244.92	41.40	259.99	252.45
2.0	12.56	36.20	454.67	38.10	478.54	466.60
3.0	18.84	32.10	604.76	31.80	599.11	601.93
4.0	25.12	32.10	806.35	31.80	798.82	802.58
6.0	37.68	32.10	1209.53	29.20	1100.26	1154.89
8.0	50.24	32.10	1612.70	29.20	1467.01	1539.85
10.0	62.80	32.10	2015.88	29.20	1833.76	1924.82

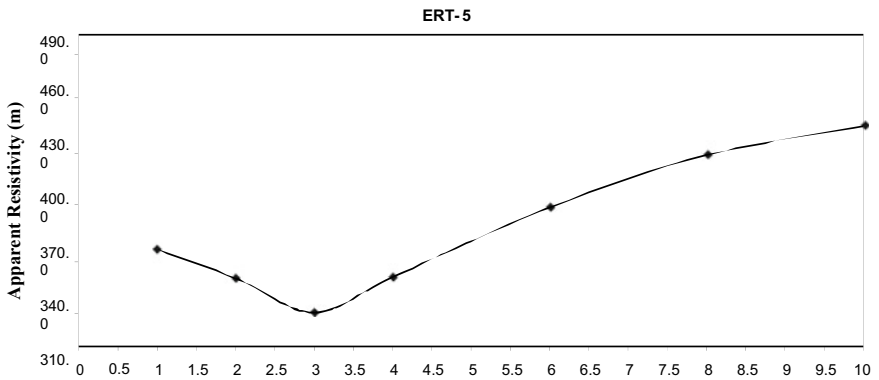
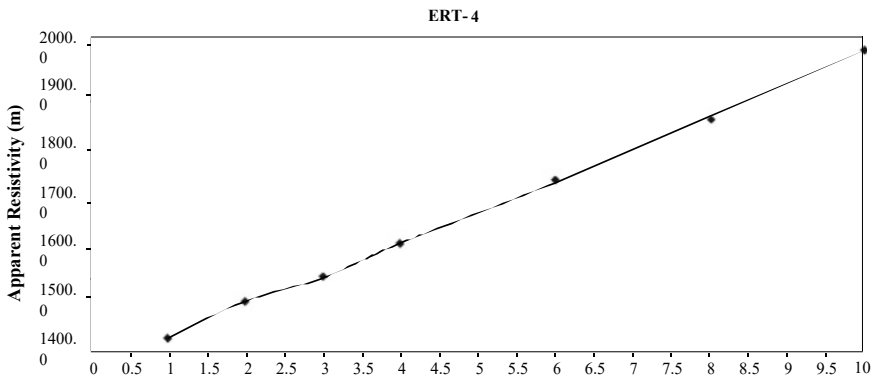
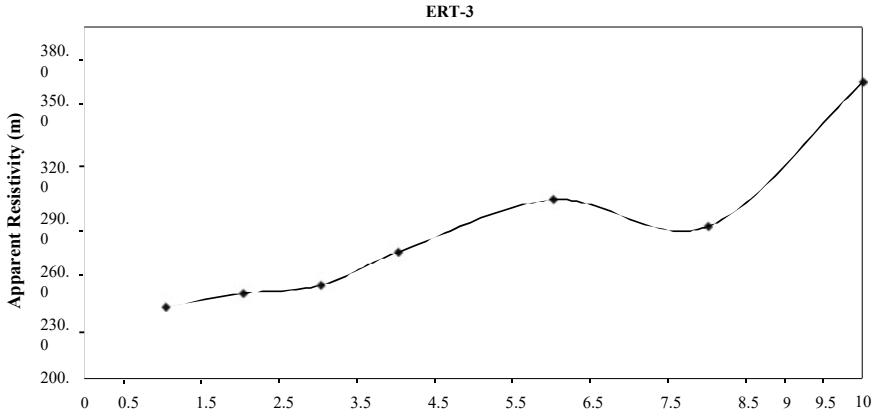
Table 6 Electrical resistivity test at location 5

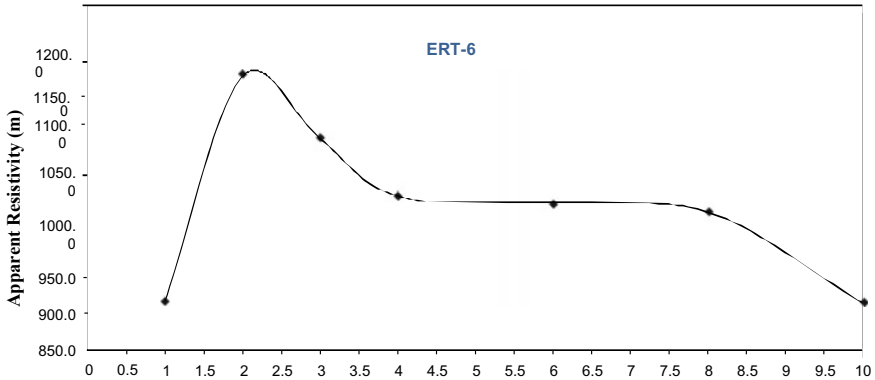
Electrode spacing a (m)	$K = 2a$ (m)	East–West		North–South		Average apparent resistivity
		Resistance R (Ω)	Apparent resistivity $\rho = (K \times R)$ (Ωm)	Resistance R (Ω)	Apparent resistivity $\rho = (K \times R)$ (Ωm)	
1	6.28	35.50	222.94	31.40	197.19	224.94
2.0	12.56	11.90	149.46	14.80	185.89	187.89
3.0	18.84	7.04	132.63	8.23	155.05	143.84
4.0	25.12	7.04	176.84	8.03	201.71	189.27
6.0	37.68	7.54	284.11	7.23	272.43	278.27
8.0	50.24	6.58	330.58	6.84	343.64	345.64
10.0	62.80	5.83	366.12	6.07	381.20	383.20

Table 7 Electrical resistivity test at location 6

Electrode spacing a (m)	$K = 2a$ (m)	East–West		North–South		Average apparent resistivity
		Resistance R (Ω)	Apparent resistivity $\rho = (K \times R)$ (Ωm)	Resistance R (Ω)	Apparent resistivity $\rho = (K \times R)$ (Ωm)	
1	6.28	95.10	597.23	105.00	659.40	628.31
2.0	12.56	81.00	1017.36	88.70	1114.07	1065.71
3.0	18.84	48.80	919.39	51.30	966.49	942.94
4.0	25.12	31.50	791.28	34.70	871.66	831.47
6.0	37.68	21.50	810.12	21.80	821.42	815.77
8.0	50.24	15.70	788.77	16.20	813.89	801.33
10.0	62.80	9.84	617.95	10.10	634.28	626.11







4 Conclusion

1. The major formation in the area is basalt. Secondary porosity is seen developed due to fracturing during deposition. The area has very thin soil cover. The area is productive as it contains large opening in definite pervious horizons, besides being susceptible to weathering.
2. The study area gently slopes in a westerly direction. The lowest point being on the west. The area generally has very thin soil cover below which the original formation is basalt.
3. The system of the study area can be visualized as a multi-layered system. The top most layer consists of thin soil cover. The second layer consists of weathered basalt which then grades into basalt.
4. In this area, groundwater occurs in the pore space of basalt under confined and semi-confined conditions. It also occurs in the secondary porosity formed by weathering of basalt. The groundwater is mainly recharged due to precipitation and seepages.

References

1. Gascoyne JK, Erikson AS (2005) Engineering geology geophysics in encyclopedia of geology. Zetica, Witney, U. K
2. Wightman WE, Jalinoos F, Sirles P, Hanna K (2003) Application of geophysical methods to highway related problems. Federal Highway Administration, Central Federal Lands Highway Division, Lakewood, CO, Publication No. FHWA-IF-04-021, September 2003. <http://www.cflhd.gov/resources/agm/>
3. Binley A (2015) Geophysical methods of soil
4. Lee DK (2016) Electrical properties of soil

5. Woodward Moore R, Highway engineer, Geophysical methods of subsurface exploration applied to materials survey, physical research Branch, Buero of public roads
6. Shelaar JB, Picaut JG, Demirel T, Electrical resistivity of soil-sodium chloride systems, <https://onlinepubs.trb.org/onlinepubs/hrbulletin/349/349-002.pdf>
7. Soil survey investigation report No. 51, (2004)

A Review on Various Geotechnical and Geophysical Investigations for a Dam Rehabilitation Project



Harshit Srivastava , R. P. Tiwari , Vijay Kumar ,
and Dharmendra Singh 

Abstract A dam is a massive hydraulic structure, built across a river to create a reservoir at its upstream for various purposes such as hydropower generation, irrigation, flood control, domestic and municipal supplies, and so on. They are major engineering structures that are designed and constructed with long-life expectancy. In India, most of the large dams are older than 25 years and require proper maintenance. To ensure efficient and safe operation of the dam, rehabilitation of dam is done. Before conducting rehabilitation activities, a detailed investigation of the dam body including surrounding soil is carried out. For embankment dams, appropriate borrow areas are identified, and disturbed and undisturbed samples are extracted. Various laboratories, as well as field tests, are performed on the extracted specimen. For concrete/masonry dams, representative cores are extracted from an existing dam. Various destructive and nondestructive tests are performed on the extracted core for assessing the existing condition of the concrete/masonry dam. For in-depth exploration, various geophysical methods are used to detect hidden defects in the dam bodies and also in surrounding soil too. Ground-penetrating radar (GPR) method is the most suitable technique for detecting cracks in a dam body and also to identifying leakage zones. The main objective of this paper is to review various geotechnical and geophysical investigations carried out for a dam rehabilitation project. In this paper, numerous articles have been reviewed to discuss the various prerequisites for a dam rehabilitation project.

Keywords Dam rehabilitation · Ground-penetrating radar · Nondestructive test

1 Introduction

Dams in general are mega hydraulic structures that are built to facilitate humans in various regards such as irrigation, hydropower generation, flood control, water

H. Srivastava (✉) · R. P. Tiwari · V. Kumar · D. Singh
Department of Civil Engineering, Motilal Nehru National Institute of Technology Allahabad,
Prayagraj 211004, India
e-mail: harshitsrivastava@mnnit.ac.in

© The Author(s), under exclusive license to Springer Nature Singapore Pte Ltd. 2023
A. K. Agnihotri et al. (eds.), *Proceedings of Indian Geotechnical and Geoenvironmental Engineering Conference (IGGEC) 2021, Vol. 1*, Lecture Notes in Civil Engineering 280,
https://doi.org/10.1007/978-981-19-4739-1_8

harvesting, water supply, fisheries purposes, and many more. In the ancient era, dams were mainly built for irrigation purposes [1, 2]. If we talk about the present scenario, India ranks third globally in the case of the maximum number of dams. As per the records of NRLD-2017. In India, at the time of independence, there were only fewer than 300 dams but nowadays, and there are 5254 large dams and about 447 large dam projects under construction. Besides this, there are heaps of smaller dams in India, which have a wider influence on the economic, environmental, cultural, and social growth of the country [3, 4]. However, like all other infrastructure in the world, the service life of a dam is also limited depending upon the type of the dam. After completion of the service life or even in between the service life of the dam, a dam may undergo various defects in its body, surrounding soil as well as various operational defects due to improper maintenance, unprecedented flood, earthquake events, age-related deterioration, construction deficiencies, and so on. This may cause a very severe impact on lives, the economy, and the surrounding environment.

In the case of concrete dams, aging may cause cracking in the dam body, disintegration of the concrete surface, expansion phenomenon, scaling of surface, chances of sulfate attack on the concrete surface. It may also cause crumbling of concrete, seepage through galleries, cavitation phenomenon of the surface, and so on [5]. Typical disintegration of the concrete surface due to aging and sulfate attack is shown in Figs.1 and 2, respectively. The service life of a concrete dam is generally kept at about 100 years. If we talk about dam failure, the majority of failures of dams occurred in the earthen dam due to its high seepage characteristics and high vulnerability. Besides this, a few dam failure was observed in composite and masonry dams too. On analyzing 36 numbers of previous dam failure cases, 30 numbers of dams were earthen dams, 3-3 numbers of dams were composite as well as masonry dams [2, 6]. In India, nowadays, various dams are even older than 25 years from their construction completion time. Several such dams are now subjected to various defects in their bodies as well as in subsoil too. Such dams require proper rehabilitation to ensure safe and efficient operation.



Fig. 1 Disintegration of concrete surface at dam face [5]



Fig. 2 Disintegration of concrete due to sulfate attack [5]

Rehabilitation of dams generally deals with repairing the old and distorted dams to meet our safety standards. Rehabilitation of dam ensures strengthening of weakening location of the dam, reducing seepage and controlling of the piping phenomenon. Detailed investigation of dam body including surrounding soil is carried out before starting repair work. The investigation is generally carried out in two phases. In the first phase, reconnaissance or visual inspection of the dam body is done to ensure the extent of rehabilitation work to be used, whereas, in the second phase, a detailed engineering investigation is carried out [4]. For identifying the existing situation of the underlying soil and dam body, soil samples are extracted out from suitable borrow pit in case of earthen dams and representative cores from suitable location from the dam body in case of a concrete dam, and thereafter various field and laboratory tests are performed over- extracted specimen as well as suitable test locations. Extracting the core by a drilling operation is not preferred as it may damage the homogeneity or intactness of the dam. The typical core extraction process from the concrete dam is shown in Fig. 3. Drilling operation followed by a standard penetration test (SPT) is performed to estimate the strength of foundation as well as strength of joint [7–9]. Besides these tests, some additional geophysical investigation methods may also be useful for the indirect determination of seepage locations, weakened zones, existing soil properties, etc. These methods may include electrical resistivity tomography, seismic refraction method, use of the ground-penetrating radar, etc., for in-depth investigation of dam body as well as surrounding soil [10, 11]. Nowadays, ground-penetrating radar is being frequently used for geophysical investigation purposes for shallow depth of foundation. For the deep foundation case below the water column, the results of the GPR survey may vary significantly due to resolution issues [12].



Fig. 3 Core extraction process from concrete dam [13]

2 Geotechnical and Geophysical Investigations for a Dam Rehabilitation Project

2.1 Geotechnical Investigation

The geotechnical, as well as geological problems associated with a dam body, may be of several types depending upon the soil type, foundation rock features, type of dam, and so on. A dam infrastructure may be subjected to deep weathering of foundation rock, permeable boulder bed, karstic situation, siltation in the reservoir, sliding of slopes, folds, faults, shearing zone in bedrock, uplift pressure, differential settlement, crushing of rocks, excess overburden pressure, and many more. Due to such defects, geological as well as a geotechnical survey before rehabilitation activity has greater importance [14]. Geotechnical investigation for dam rehabilitation generally involves preliminary investigation as well as detailed investigation. The preliminary investigation deals with a visual examination of damaged location in a dam body. It also deals with identifying the extent of treatment to be given at a particular location. All the planning for detailed investigation as well as rehabilitation strategies is made in this stage. The detailed investigation deals with a detailed examination of a distorted dam body. Various records are observed to identify maximum and minimum water levels in the dam, highest past flood records, probable maximum flood, past seismic events, FRL, etc. Detailed sampling/boring is done at a suitable location with the help of different samplers depending upon the underlying soil to extract disturbed as well as undisturbed samples. Various laboratory, as well as field tests, may be performed such as standard penetration test, triaxial shear test, permeability test, proctor compaction test, Atterberg's limit tests, core cutter test, tests for

swelling and shrinkage, chemical analysis of soil, and so on [4, 8, 9, 15, 16]. For concrete dams, the representative core may be extracted out from a suitable location for performing nondestructive as well as destructive tests such as ultrasonic pulse velocity test, compressive and splitting strength test, test for permeability of concrete, etc. Ultrasonic pulse velocity test as a nondestructive test may be useful for assessing the quality of the concrete. Higher ultrasonic pulse velocity indicates the excellent overall quality of the concrete. Besides this, various other non-destructive tests may be useful in the case of gravity of concrete dams such as half-cell potential test, resistivity test, air permeability test, and so on [4, 13]. For an earthen dam, the strength of underlying rock may be obtained empirically by the Hoek–Brown strength criterion [15].

2.2 Geophysical Investigation

Besides the above two stages in investigation, if some of the dam locations are inaccessible and the extent of rehabilitation to be given is high due to considerable damage in the dam body or safety point of view. Geophysical investigations are preferred. Geophysical methods can be easily used for dam safety monitoring. These methods can be used to survey a wider area of dam body thus comparatively cheaper than traditional methods of investigation. These methods are used to identify seepage locations as well as structural discontinuities present in the dam body [10]. Geological survey of underlying rocks as soil strata in addition to electrical resistivity method may be preferable for finding excessive seepage location, structural discontinuities, the existing condition of underlying rocks and subsoil for an earthen dam over ground-penetrating radar method for deep foundation cases [12]. There are various types of geophysical methods available for dam safety monitoring. The type of exploration method to be used depends upon various conditions such as type of dam, type of underlying rocks and subsoil, inaccessibility to take observations, unavailability of direct methods, and so on. Some of the geophysical methods of explorations are as follows:

1. Electromagnetic profiling
2. Ground-penetrating radar profiling
3. Seismic methods
4. Self-potential methods
5. Electrical resistivity tomography
6. Temperature methods [7, 10, 11].

The suitability of the above geophysical methods for dams under steady seepage conditions is discussed in Table 1.

GPR method may be considered as a reflection method as it deals with the emission and receiving of electromagnetic signals through a given structure. The electromagnetic wave reflects when there is a change in material properties. GPR method is suitable for the material whose resistivity is greater than 100 Ω -m [7, 10]. The use

Table 1 Suitability of geophysical methods for impoundment dams under steady seepage condition [10]

Geophysical method	Internal composition	Seepage path identification	Detection requirement intensity of seepage flow	Larger voids	Environmental damage	Location of site (Rural, coastal or urban)
EM profiling	Suitable but only for 1-D mapping	Suitable	Not suitable	Suitable	Suitable but cannot identify solely	Effective in rural as well as in coastal sites but due to metallic disturbance ineffective in urban sites
Electrical resistivity tomography	Suitable	Suitable	Not suitable	Suitable	Suitable	Effective in rural as well as in coastal sites but in urban sites where metallic objects proper care must be adopted
GPR profiling	Suitable but with limitations	Not suitable	Not suitable	Suitable with limitations	Suitable with limitations	Effective in rural as well as in urban sites but may/may not be effective in the coastal sites depending upon the type of soil and saltwater concentration
Seismic methods	Suitable	Not suitable	Not suitable	Suitable	Not suitable	Effective in rural as well as coastal sites but in urban sites, vibrations due to traffic and other factors must be eliminated
Self potential methods	Not suitable	Suitable	Suitable	Not suitable	Not suitable	Effective in rural sites but soil water interaction may disrupt the data in coastal sites and devices may become highly sensitive to electrical perturbation in urban sites
Temperature measurement	Not suitable	Suitable	Suitable but with limitations	Not suitable	Not suitable	Effective in all sites

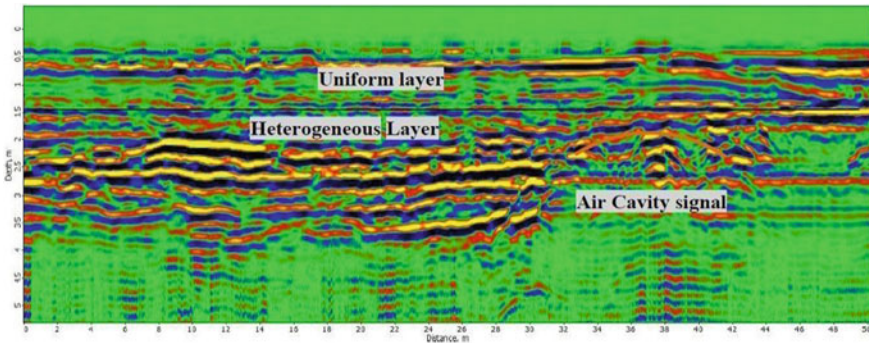


Fig. 4 Typical GPR radargram [7]

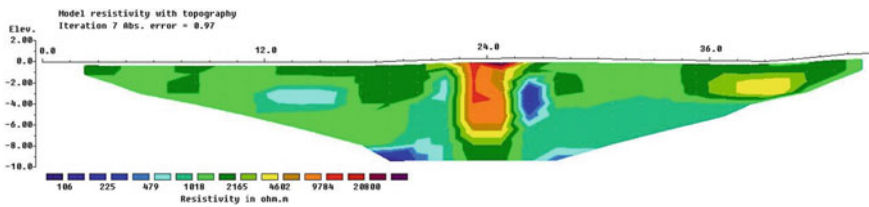


Fig. 5 Typical electrical resistivity tomography [7]

of destructive sources such as heavy hammers, explosives in seismic methods may cause structural discontinuities or loss of strength of an intact dam body making this method unsuitable for exploration at a wider scale. Typical GPR radargram is shown in Fig. 4. As a non-destructive method of exploration, the electrical tomography method may be found as highly suitable for dam monitoring purposes due to its high resolution [12]. For estimating the average value of shear wave velocity, Poisson’s ratio, and other material constants of a dam body, Multichannel Analysis of Surface Wave (MASW) as a seismic method are extensively used over standard penetration test because SPT gives the value of material constants at a certain point where the test is performed [17]. Typical electrical resistivity tomography is shown in Fig. 5.

3 Literature Review

Dams have been played a vital role in the growth of any country. Several dam rehabilitation projects across India, as well as worldwide, have been taken place till now. The majority of such rehabilitation projects of large dams have gone through proper investigation process including geotechnical as well as geophysical investigation.

Tortajada [1] made a general discussion over the necessity of the dams. A wide database is given based on the hydropower capacity and consumption of various countries. Discussions are also made over regional development due to water development projects.

Adamo et al. [5], made a brief discussion over various aging defects in a concrete dam such as cracking, abrasion, cavitation, crumbling of surface, scaling, sulfate attack on concrete, etc., along with various case studies of dams where such defects are found.

Bharti et al. [2], made a general discussion over various components, uses, construction steps along with various failure modes of a dam project. The study also has a wide database of previous dam failure case histories.

Anbazhagan et al. [7], described a general idea of the combined approach of geotechnical as well as geophysical investigation to be used to monitor various defects in a dam body for the further rehabilitation process. Combined field observations, drilling of representative core from dam body along with various geophysical investigation techniques are discussed with their typical results.

Nelson [8], described the investigation of two earthfill dams suffering from leakage phenomenon along with their suitable rehabilitation measures. Geotechnical investigations are performed on two reference sites (RCP2 and RCP5). Investigation showed that there was a shortage of clay in the area immediately after the second reference site. Reconstruction of both the dams had been done in late 2005.

Park [10], made a general discussion about various geophysical investigation techniques, their suitability their merits and demerits, etc., in detail along with suitable examples.

Ghafoori et al. [15], described geological and geotechnical investigations for maintenance of Daroongar Dam site, Iran. 25 boreholes were drilled with a total depth of 980m. The depth of these boreholes varied from 16 to 70m. Core was drilled at a suitable location. Various laboratories, as well as field tests, were performed to obtain various geotechnical as well as geological properties of rock mass and surrounding soil. The strength of rocks was obtained by Hoek–Brown strength criterion. A discontinuity survey was performed to detect structural anomalies if any.

Sissakian et al. [18], described the role of geological investigation regarding Mosul Dam, Iraq, concerning dam silting conditions. They also described various steps in the geological investigation, the negative impact of inadequate geological information on dam silting issues.

Ernesto et al. [16], described the geotechnical investigations carried out for Farneto Del Principe dam, Italy, which is a zoned earthen dam. They also described the field performance of the dam. Various laboratory tests, chemical–physical tests were performed including pressure measurement through piezometers. Results revealed that there was low seepage discharge, no significant change in water characteristics in the dam.

Arora et al. [13], described the importance of the in-situ properties of the construction material of the dam concerning time factor. They also focused on field studies

for a concrete or arch dam for obtaining various in-situ properties of dam material which may be useful for FEM modeling of the dam as well as choosing the appropriate rehabilitation strategy. They also described various nondestructive tests, sampling procedures for concrete and arch dam, and also about mineralogical studies in the dams.

Loperte et al. [19], described the applications of GPR over traditional geotechnical investigation methods for monitoring of Acerenza Dam situated in the southern part of Italy. A two-dimensional GPR survey is carried out for identifying the possible fractures in bedrock, estimating seepage, and the extent of damage present in the dam.

Mathur et al. [20], described the provision of various structural measures for enhancing the safety of an existing dam such as the provision of parapet walls, provision for additional spillway, enhancement in height of the dam, etc., based on revised design flood. They also covered certain case histories of Indian dams with suitable rehabilitation measures.

Raji and Adedoyin [12], described the use of the 2D electrical resistivity technique in addition to the geological mapping of Unilorin Dam, Nigeria, to detect the structural discontinuities present in the dam. The resistivity data obtained was further processed to get the resistivity model of the subsoil around the dam body.

Adamo et al. [11], made a brief discussion over various geophysical methods in addition to their suitability and suitable examples. They also described various case studies where a particular geophysical method was previously used.

4 Conclusion

Dams are such structures that are built for a longer life span because removal of any old built dam is not an easy task. In India, various dams are very old and suffering from various defects in its body as well surrounding soil and operational defects too thus requiring adequate rehabilitation. Before rehabilitation activity, one should conduct proper geotechnical as well as geophysical investigation of the respective dam. From the various kinds of literature, one may conclude:

1. A dam plays a vital role in the economic, social as well cultural growth of any nation. Its positive, as well as negative impact, has a wider influence on society.
2. An old concrete, as well as an earthen dam, may be subjected to various defects such as cracking, spalling of concrete faces, expansion, loss of strength, excessive seepage, differential settlement, efflorescence, cavitation, abrasion, and many more.
3. For a rehabilitation activity to be taken place, engineers must do proper site investigation, a hydrological survey including geotechnical as well as geophysical investigation if required due to inaccessibility in taking observation and lack of availability of direct methods to obtain various parameters for choosing appropriate rehabilitation measures.

4. The geotechnical investigation deals with digging boreholes, extracting disturbed or undisturbed samples of soil, thereafter various laboratories, as well as field tests, are conducted to estimate the current properties of soils. These tests may include SPT, proctor compaction test, test for Atterberg's limits, consolidation test, permeability test, and so on. The type of sampling technique depends upon the type of the soil.
5. In the case of concrete dams, various nondestructive, as well as destructive tests, may be performed such as compressive strength test, ultrasonic pulse velocity test, air permeability test, half-cell potential test, etc. Destructive tests are rarely preferred because the core extracted for such tests may damage the intactness of the dam.
6. In the case of a geophysical investigation, various geophysical techniques may be used depending upon the depth of foundation, depth of the observations to be taken, type of the dam and type of the soil, topographical features, etc. These methods may include electromagnetic profiling, GPR survey, self-potential method, electrical resistivity tomography, seismic methods, etc.
7. Generally, seismic methods are lesser used because they use destructive sources of energy that may cause weakness in the dam bodies or foundation rock. GPR method may be unsuitable for larger depth of foundation due to resolution problems. Generally, electrical resistivity methods are suitable for earthen dams.

References

1. Tortajada C (2014) Dams: an essential component of development. *J Hydrol Eng*:1–9. ISSN: 1084-0699
2. Bharti MK, Sharma M, Islam N (2020) Study on the dam and reservoir and analysis of dam failure: a data base approach. *Int Res J Eng Technol* 7(5):1661–1669. ISSN: 2395-0072
3. Shi H, Chen J, Liu S, Sivakumar B (2019) The role of large dam in promoting economic development under the pressure of population growth. *Sustainability*, MDPI, pp 1–14
4. Manual for rehabilitation of large dams: Government of India, Central Water Commission, Central Dam Safety Organization, New Delhi (2018)
5. Adamo N, Ansari NA, Sissakian V, Laue J, Knutsson S (2020) Dam safety: technical problems of ageing concrete dams. *J Earth Sci Geotech Eng* 10(6):241–279. ISSN: 1792-9040
6. Kolala M, Lungu C, Kambole C (2015) The cause of dam failures—a study of earthen embankment dams on the copperbelt province of Zambia. *Int J Eng Res Technol* 4(2):301–309. ISSN: 2278-0181
7. Anbazhagan P, Rohit D, Prabhakaran A (2016) Investigations existing dam using integrated geotechnical and geophysical methods. In: Second national dam safety conference, 12–13 January, Bengaluru, pp 165–170
8. Nelson EJ (2008) Investigation and repair of a leaking earth fill dam. In: 6th International conference on case histories in geotechnical engineering, 11–16 August, Arlington, pp 1–7
9. Little AL (1969) Geotechnical investigations for embankment dams exploration geotechniques Pour Digues, In: 7th International conference on soil mechanics and foundation engineering. International Society for Soil Mechanics and Geotechnical Engineering, Mexico, pp 301–305
10. Park C (2017) Geophysical methods for reservoir safety investigation. Commissioned by the Environment Agency and British Dam Society, pp 1–37

11. Adamo N, Ansari N, Sissakian V, Laue J, Knutsson S (2020) Geophysical method and their applications in dam safety monitoring. *J Earth Sci Geotech Eng* 11:291–345. ISSN: 1792-9040
12. Raji WO, Adedoyin AD (2019) Dam safety assessment using 2D electrical resistivity geophysical survey and geological mapping. *J King Soud Univ Sci*:1123–1129
13. Arora VV, Singh B, Narayan P (2019) Detailed investigation of large concrete dams in India for finite element analysis and repair strategy. In: International dam safety conference, Bhubaneswar, pp 457–465
14. Gangopadhyay S (1993) Geotechnical problems of dam sites and their solution with reference to the projects of Eastern India. In: 3rd International conference on case histories in geotechnical engineering, June 1–4, St. Louis, Missouri, pp 493–498
15. Ghafoori M, Lashkaripour GR, Azali ST (2011) Investigation of geological and geotechnical characteristics of Daroongar dam, Northeast Iran. *Geotechn Geol Eng Int J*. ISSN: 0960-3182
16. Ernesto A, Giovanni D, Paolo Z (2016) Geotechnical investigation and field performance of a zoned earth dam in Italy. In: International workshop on metrology for geotechnics, 17–18 March Benevento, Italy
17. Chiemek CC (2014) Investigation of dam safety making use of multichannel analysis of surface waves (MASW). *World Acad Sci Eng Technol Int J Environ Earth Sci Eng* 8(1):16251628
18. Sissakian VK, Adamo N, Ansari NA (2019) The role of geological investigation for dam siting: Mosul dam-a case study. *Geotech Geol Eng*
19. Loperte A, Bavusi M, Cerverizzo G, Lapenna V, Soldovieri F (2011) Ground penetrating radar in monitoring: the test case of Acerenza (Southern Italy). *Int J Geophys* 2011:1–9. Article Id-654195
20. Mathur CS, Patra B, Verma VK, Singh V (2019) Major structural measures for dam safety under DRIP from hydrological consideration. In: International dam safety conference, Bhubaneswar, pp 883–892
21. Pillai BRK, Kumar M, Basistha A (2016) Dam safety and climate change: a case study of Hirakud dam. In: Second national safety conference, Bengaluru, pp 28–37
22. Adhikari B, Acharya U, Acharya KK, Ghimire S (2019) Engineering geological investigation of dam site of proposed Sunkoshi-2 hydropower project, Khurkot area, Eastern Nepal. *J Nepal Geol Soc* 58(Special Issue):181–188
23. Camarero PL, Moreira CA (2017) Geophysical investigation of earth dam using the electrical tomography resistivity technique. *REM: Int Eng J Ouro Preto*:4752
24. Adewoye AO, Ajayi PE, Adegbola AA (2015) Geophysical investigation of proposed dam site along river Adunin, Ogbomoso, South-Western Nigeria. *Lautech J Eng Technol*:6–22
25. Brown ET (2016) Reducing risk in the investigation, design and construction of large concrete dams. *J Rock Mech Geotech Eng*:197209
26. Patra B, Schneider W, Dhawan AK (2018) Instrumentation of existing dams. In: International dam safety conference, Kerala, pp 868–878
27. Akinlabi IA, Ayanrinde OS (2018) Geophysical investigation for anomalous seepage in and around an earth dam embankment in Ogbomoso, South-Western Nigeria. *Int J Scien Eng Res* 9(7):1455–1467. ISSN: 2229-5518

Investigation of Geotechnical Factors Affecting Electrical Resistivity of Soil



Suraj Sukhadev Vankamble and Rupa S. Dalvi

Abstract The use of electrical resistivity (ER) in subsurface investigation has increased in recent years. Resistivity imaging (RI) is a non-destructive method and provides a continuous image of the subsurface. However, only, qualitative evaluation of the subsurface can be obtained from RI. The correlations between ER results and geotechnical engineering properties of soils have become important for site investigation using this method. The primary objective of the current study was to determine the geotechnical parameters affecting electrical resistivity of compacted clays. Understanding the influential factors will be helpful in determining the correlations between RI results and geotechnical properties of soil. The geotechnical properties of soil obtained from laboratory tests such as oven dry test and standard proctor compaction test. The effects of moisture content, unit weight, and degree of saturation on soil resistivity were investigated. Resistivity tests were conducted on the actual field on composite soil at varying moisture contents, temperature, and unit weights. The field results reveal that a higher degree of saturation results in a lower electrical resistivity. The electrical resistivity increases gradually with increasing dry unit weight of soil.

Keywords Electrical resistivity · Water content · Degree of saturation · Dry unit weight

1 Introduction

For the accurate design and construction of civil engineering infrastructures, it is necessary to undertake Geotechnical investigation to find out the nature, types, and engineering properties of soils at that site. Such investigations are generally done by digging boreholes at different location at the site extending the same up to the desired depths for collection of soil sample from different depths [1].

S. S. Vankamble (✉) · R. S. Dalvi
Civil Engineering Department, College of Engineering Pune, Pune, India
e-mail: vankambles7@gmail.com

© The Author(s), under exclusive license to Springer Nature Singapore Pte Ltd. 2023
A. K. Agnihotri et al. (eds.), *Proceedings of Indian Geotechnical and Geoenvironmental Engineering Conference (IGGEC) 2021, Vol. 1*, Lecture Notes in Civil Engineering 280, https://doi.org/10.1007/978-981-19-4739-1_9

The different methods used for extending such boreholes are use of trial pits, shafts and headings, boring, augers, hand portable augers, wash borings, rotary drilling. Level and presence of the ground water table is also determined during the boring process.

Alternatively, in-situ tests for geotechnical investigation have also been devised. Commonly used techniques are as follow:

- Plate load test
- Standard penetration test
- Cone penetration test
- Static cone penetration test.

Each of the above tests has their merits and demerits.

The use of electric resistivity(ER) in site investigation has been increasing all over the world. It is a convenient method for evaluating temporal variations of moisture and various geotechnical parameters of subsoil. Geotechnical engineers are able to investigate several parameters using conventional soil test boring methods; however, they can only obtain this information at certain locations and have to conduct interpolations to get area-wide information.

On other hand, ER is able to provide an image of the subsurface, as well as qualitative information of that particular sub soil [2]. Measuring of geotechnical properties has become an important thing for effective use of ER in engineering applications. The correlations of different geotechnical properties with ER will close the gap that currently exists between geophysical testing and geotechnical engineering, and therefore, geotechnical engineers will be able to interpret the geophysical data and utilize the information for their design, therefore making this method more effective for subsurface investigation.

In this study, the different sites are selected at Pune district in Maharashtra. The soil samples are collected from those sites to conduct the test in laboratory and get various geotechnical properties such as moisture content, dry unit weight, and degree of saturation and so on. The geotechnical properties of soil obtained from laboratory tests such as oven dry test and standard Proctor compaction test. The effects of moisture content, unit weight, and degree of saturation on soil resistivity were investigated. Resistivity tests were conducted on the actual field on composite soil at varying moisture contents, temperature, and unit weights [3].

2 Procedure (in Laboratory)

There are different field sites are selected at nearby Pune. From this sites, the soil samples are selected where the electric resistivity test are performed. Sample collected is brought to the laboratory for measuring properties of soil such as different values of water content and dry unit weight of that different soil at different sites.

Table 1 Soil with moisture content

Soil sample	Moisture content (%)
1	48.00
2	10.00

Table 2 Soil with dry unit weight

Soil sample	Dry unit weight (kn/m ³)	Optimum moisture content (percentage)
1	12.00	24.5
2	16.00	23.0

Oven dry test is done to determine the water content in soil by oven drying method as per IS: 2720, Part 2 (1973). Soil sample from site 1 shows the moisture content of 48% and from site 2 shows an moisture content of 10% (Table 1).

The standard Proctor compaction tests were carried out according to the Indian standard method (IS: 2720 Part 7, 1997). Two soil samples are taken from site 1 and site 2 for conducting standard Proctor test, to measure dry unit weight (kn/m³) (Table 2).

3 Procedure (on Field)

For lateral and vertical profiling of soil using resistivity technique, resistance (Ω) is calculated in the field using the Wenner method and Schlumberger method, using instrument electric resistivity imaging (ERI) [4]. In these methods, four electrodes are used in which inner electrodes are potential electrodes and outer electrodes are current electrode. DC (direct current) is applied at the current electrodes, and potential difference is measured at potential electrodes.

Difference between Wenner and Schlumberger method is only about spacing between the electrodes. In Wenner method, the electrodes are equally spaced, but in Schlumberger method, spacing between the current electrodes is three times the spacing between the potential electrodes.

A site selection is also important criteria before conducting the ER test. For taking readings and well set up of ERI instrument, the plain terrain should be there. Such sites are helpful for placing the electrodes with suitable span.

A site at Pune district, Maharashtra is selected for field experimentation. The electrodes are arranged with suitable and constant span and arrangement of acceptor, and electrodes are done carefully. After proper inspection of the setup, the readings are start to collected. Prior of that inputs are set on that ER machine.

Inputs consist following data-

- (a) Name of location
- (b) Latitude and longitude of site

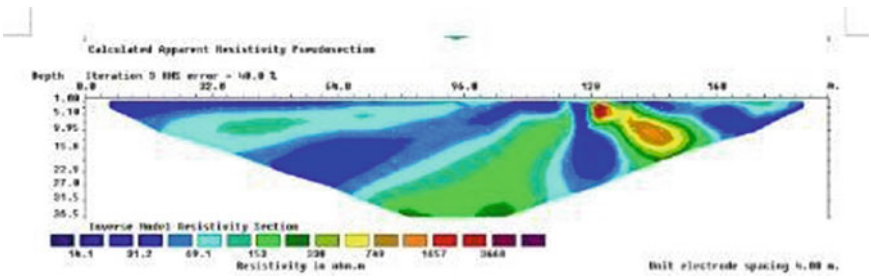
- (c) Nearby locations
- (d) Span between electrodes
- (e) Number of electrodes
- (f) Technique used on site.

The input data are useful for future working of electrical resistivity of same site and store the record of the electrical resistivity values which we get as output.

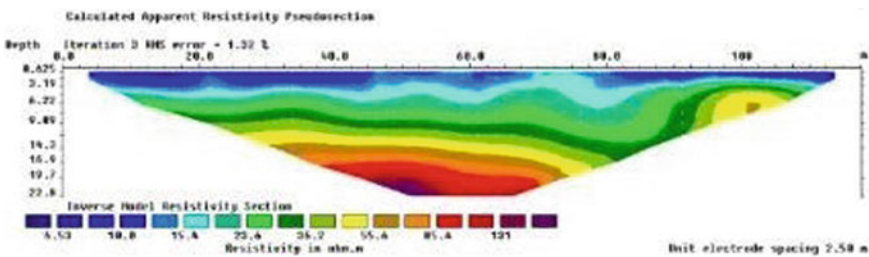
4 Observations and Results

4.1 Soil Profile (Resistivity Pseudo-section)

SITE-1: Calculated apparent resistivity pseudo-section at site 1, Pune district, Maharashtra. The laboratory results obtained from soil sample selected from this site give the moisture content of 48% and dry unit weight of 12.00 kn/m³.



SITE-2: Calculated apparent resistivity pseudo-section at Pune district, Maharashtra. The laboratory results obtained from soil sample selected from this site give the moisture content of 10% and dry unit weight of 16.00 kn/m³.



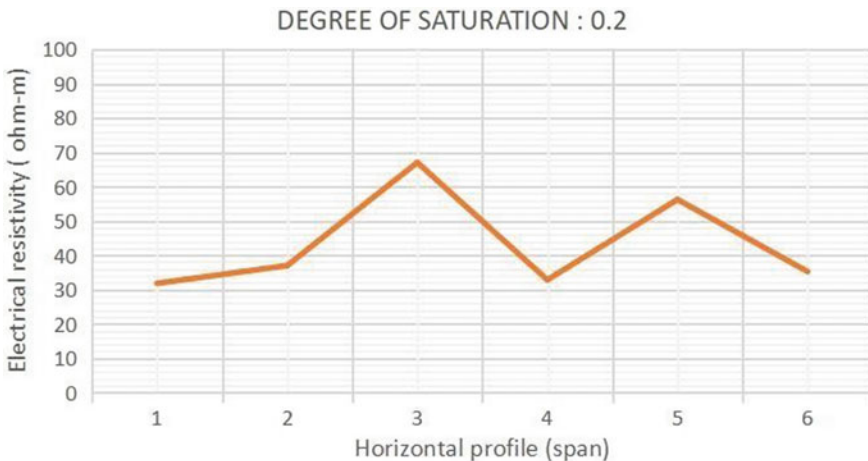
4.2 Relation of Degree of Saturation with ER of Soil

The water content and dry unit weight can be combined to a single geotechnical parameter called degree of saturation. The degree of saturation increases with the increase of water content or dry unit weight. The variations of soil resistivity with the degree of saturation are presented in above figure for the soil Samples 1 and 2. To obtain the degree of saturation, a specific gravity of 2.6 was considered to be constant. Soil resistivity decreased with an increase of degree of saturation. An increase in degree of saturation yields changes in orientation of clay particles. Therefore, soil resistivity decreased with the increase in degree of saturation, as presented in graphical representation of 2 different sites.

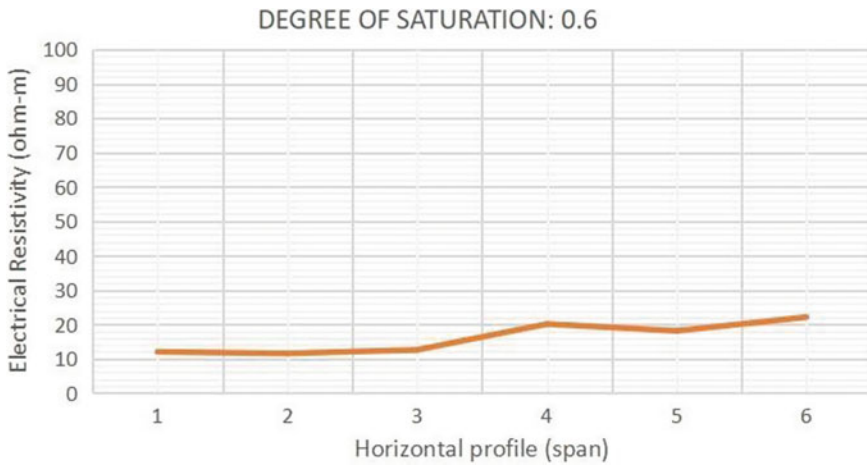
At site 1, the soil sample is taken which gives the value of degree of saturation of 0.2. The graphical representation is showing the relationship of degree of saturation with electric resistivity as *x*-axis representing electrodes span in meter and *y*-axis representing electric resistivity in Ω-m (Graph 1).

At site 2, the soil sample is taken which gives the value of degree of saturation of 0.6. The graphical representation is showing the relationship of degree of saturation with electric resistivity as *x*-axis representing electrodes span in meter and *y*-axis representing electric resistivity in Ω-m (Graph 2).

After the comparing all the graphs of degree of saturation with electrical resistivity, we get that the electric resistivity of soil decreases with increase in degree of saturation of soil, as shown in below figure. With the increase in degree of saturation of soil as 20 and 60%, the soil shows the variation in electrical resistivity as decreasing the values as 42.28 and 12.22 Ω-m. This study shows the inversely proportional relation of degree of saturation and electric resistivity [1].



Graph 1 Relation of degree of saturation with electric resistivity



Graph 2 Relation of degree of saturation with electric resistivity

4.3 Relation of Dry Unit Weight with ER of Soil

To determine the correlation of soil resistivity with dry unit weight, resistivity tests were conducted at different sites having various values of dry unit weights while considering the moisture content constant [1]. Tests were conducted on three sites at Narayan Gaon, Pune. The soil samples are collected from that respective sites and laboratory testing are done as mentioned above to find the properties of soil that are Samples A, Sample B, and Sample C at optimum moisture contents of 24.5, 23.0, and 21.5%, respectively.

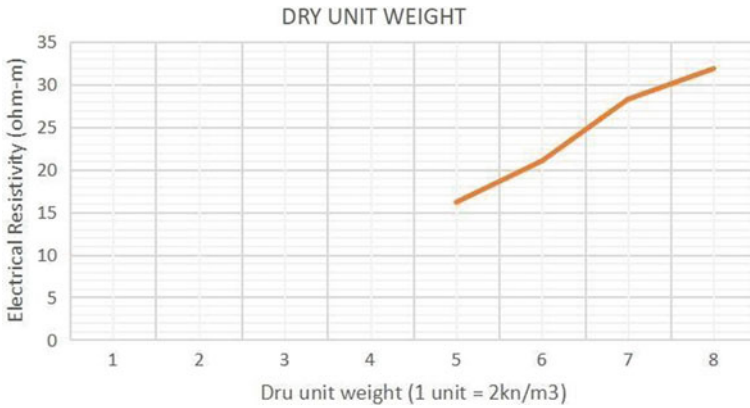
Dry unit weights were varied from site to site, as site 1 and site 2 having the value of dry unit weight of 12.00 and 16.00 kn/m^3 , respectively. Soil resistivity decreased with the increase of unit weight in each condition (Graph 3).

Table 3 shows the soil with dry unit weight and their respective average ER value:

As dry unit weight of soil increases as 12.00 and 16.00 kn/m^3 , the respective electric resistivity values also get increased as 19.18 and 32.32 $\Omega\text{-m}$. This shows that the relation between ER and dry unit weight is directly proportional.

5 Conclusion

- After the complete study of electrical resistivity of soil with different geotechnical parameters such as degree of saturation and dry unit weight of soil, results show the some relation exist between them.
- This relations can useful for further study of the electrical resistivity of soil at different sites.



Graph 3 Relation of dry unit weight with electric resistivity. Graphical representation having dry unit weight (kn/m^3) as x-axis and electrical resistivity ($\Omega\text{-m}$) as y-axis

Table 3 Soil with various properties

Soil	Dry unit weight (kn/m^3)	Electric resistivity ($\Omega\text{-m}$)
Site 1	12.00	20.12
Site 2	16.00	32.32

- Understanding the effects of geotechnical parameters on soil resistivity will help to develop the correlations between ERI results and geotechnical properties.
- With the increase in degree of saturation of soil as 20 and 60%, the soil shows the variation in electrical resistivity as decreasing the values as 42.28 and 12.22 $\Omega\text{-m}$. Inversely proportional relation is existing between the degree of saturation and electric resistivity of soil.
- As dry unit weight of soil increases as 12.00–16.00 kn/m^3 , the respective electric resistivity values also get increased as 20.12–32.32 $\Omega\text{-m}$. This shows that the directly proportional relation exists between dry unit weight and electrical resistivity of soil.
- However, the current study presents the effects of different soil parameters on resistivity. Similar trends are expected to be observed for other sites with different composition of soils.

References

1. Kibria G, Hossain MS (2012) Investigation of geotechnical parameters affecting electrical resistivity of compacted clays. In: ASCE, pp 6–8
2. Ahzegbobor PA (2010) 2D and 3D geoelectrical resistivity imaging: theory and field design. Department of Physics, Covenant University, Ota, Ogun State, Nigeria, pp 4–6

3. Park JH, Kang MG, Lee JS (2014) Properties and variation of electrical resistivity due to temperature change. In: Geo-congress, pp 3–4
4. Kibria G, Hossain MS (2014) Effect of bentonite content on electrical resistivity of soil. In: Congress 2014, pp 2–4
5. Indian Standard (IS: 2720-1997 Part 7): Methods of test for soils part VII Determination of water content-dry density relation using light compaction (second revision) New Delhi 110002
6. Indian Standard (IS: 2720-1973 Part 2): Methods of test for soils part II determination of water content (second revision)

Predicting Compaction Parameters of Silty Soil by Nonlinear Multivariable Approach



Shivani S. Gour, Vijay V. Muthekar, and A. B. Saner

Abstract The compaction parameters viz. optimum moisture content (OMC) and maximum dry density (MDD) plays a vital role in finding solutions for various geotechnical problems. These include amount of compaction energy required in pavement/embankment, strength parameters determination, reduction of soil's susceptibility to settlement, etc. In the present study, an attempt was made to predict compaction parameters of silty soil by nonlinear multivariable approach. For developing the prediction model, various index properties of soil from the available literature were used in the present study. The properties used for the analysis were percent fines, specific gravity (G), liquid limit (LL), and plastic limit (PL). The coefficients of mathematical model were calculated for different combinations of silty soil viz. low plasticity silt, medium plasticity silt, high plasticity. Moreover, the prediction result from all combined silty soil model was found to be more practicable as its regression coefficient was calculated significantly higher for OMC and MDD.

Keywords OMC · MDD · Plasticity · Regression · Nonlinear · Multivariable approach

1 Introduction

Soil is a naturally occurring construction material. The engineering properties of soil play a vital role in construction of foundation of structure, earthen dam, subgrade for

S. S. Gour (✉)

Geotechnical Engineering, Matoshri College of Engineering & Research Centre, Eklahare, Nashik, Maharashtra 422105, India
e-mail: shivinigour391@gmail.com

V. V. Muthekar

Department of Civil Engineering, MIT Academy of Engineering, Alandi, Pune, Maharashtra 412105, India

A. B. Saner

Department of Civil Engineering, Matoshri College of Engineering & Research Centre, Eklahare, Nashik, Maharashtra 422105, India

highways, airfield pavements, etc. [1]. All of these structures require strong and stable soil foundation to ensure stability and long life of structure [2]. Soil compaction is the mechanical stabilization technique by virtue of which soil particles are forced to be packed together by deducing the air voids between them. It is used to achieve the required density of soil particles [3]. The soil compaction investigations paved the path since the 20th century as a method to improve the strength characteristics and decrease the undesirable settlement of structures [1]. Hence, for construction of any structure, it becomes important to assess compaction characteristics as a prime concern.

The laboratory testing such as standard proctor test, modified proctor test, super modified proctor test are used for determination of compaction factors like Optimum Moisture Content (OMC) and Maximum Dry Density (MDD). At the fields, it is determined by using different equipment with variable compaction energies as per requirements. However, either at laboratory or at fields, the testing involves much time and effort [1, 4, 5]. Dire need was felt to have a correlation to reduce the amount of time and effort required for deriving compaction parameters with increased accuracy. An attempt was made in the present study to develop a correlation between index properties and compaction characteristics of silty soil. Many attempts have been made in the past to correlate these parameters through mathematical modelling [1, 2, 6]. It was observed that the liquid limit has a significant contribution for correlation with OMC when compared to other consistency limits [1]. The present study utilizes soil index properties including consistency limits to develop a regression model.

2 Methodology

A total of 61 soil samples were used from the literature in the current work. These samples belong to various sites viz. Penang in Malaysia, Nagaon districts of Assam, Nigde region of Turkey, Bagalkot district of Karnataka, Perganas, Serampore and Hooghly districts of West Bengal, India. Table 1 shows the details of samples used for current analysis.

3 Analysis

The regression analysis was performed on the samples from Table 1. It is useful in determining the effect of independent variables on dependent ones. The regression can be linear or nonlinear depending upon the relationship amongst the dependent and the independent variables.

The basic linear regression equation is in the form of Zain et al. [14]:

$$y = a_0 + a_1x \quad (1)$$

Table 1 Details of soil samples

Sr No	% Fines	G	LL	PL	OMC	MDD	Classification	References
1	54.00	2.55	43.00	27.00	18.00	16.60	MI	[7]
2	91.00	2.57	47.00	30.00	19.50	16.00	MI	[8]
3	34.00	2.56	44.00	28.00	14.00	17.20	MI	
4	75.00	2.54	46.00	29.00	17.00	15.70	MI	
5	44.00	2.55	42.00	26.00	17.00	16.50	MI	
6	44.00	2.58	43.00	28.00	14.50	17.20	MI	
7	34.00	2.60	41.00	26.00	13.50	17.40	MI	
8	60.00	2.72	53.00	29.84	19.40	16.09	MH	
9	59.00	2.73	47.90	28.85	18.00	16.36	MI	
10	74.00	2.72	49.35	28.41	21.95	16.39	MI	
11	53.00	2.74	26.95	2.00	10.40	19.24	ML	
12	90.00	2.78	53.00	28.00	26.40	14.10	MH	[4]
13	72.00	2.78	22.00	16.90	14.50	18.50	ML	Saikia et al. [9]
14	54.90	2.75	20.40	15.40	15.40	18.90	ML	
15	73.30	2.71	20.80	16.90	15.10	18.00	ML	
16	82.70	2.76	23.50	18.90	17.90	18.00	ML	
17	97.00	2.75	47.10	29.00	25.20	15.25	MI	
18	32.25	2.58	43.20	20.30	15.50	19.25	ML	[1]
19	66.70	2.65	34.04	25.75	18.90	15.20	ML	[10]
20	79.00	2.72	59.00	31.00	26.10	14.70	MH	
21	69.00	2.70	26.00	17.00	12.20	18.60	ML	[11]
22	36.00	2.61	22.00	15.00	10.20	19.50	ML	
23	40.00	2.63	21.00	16.00	10.50	19.20	ML	
24	54.00	2.74	30.00	22.00	15.00	17.10	ML	
25	42.00	2.58	30.00	24.00	16.00	17.00	ML	
26	36.00	2.61	22.00	15.00	10.20	19.50	ML	
27	51.00	2.70	22.00	20.00	12.30	16.60	ML	
28	70.00	2.63	28.00	23.00	12.50	18.70	ML	
29	69.00	2.56	26.00	20.00	12.50	19.20	ML	
30	54.50	2.05	27.00	13.04	7.50	17.51	ML	Lakshmi et al. [12]
31	68.00	2.62	36.00	28.00	18.10	16.80	MI	[6]
32	80.00	2.67	44.00	32.00	19.00	16.00	MI	
33	54.00	2.71	52.50	39.50	18.20	16.90	MH	
34	72.85	2.64	28.46	20.24	14.56	16.50	ML	[5]
35	68.71	2.61	34.62	26.65	15.11	17.00	ML	

(continued)

Table 1 (continued)

Sr No	% Fines	G	LL	PL	OMC	MDD	Classification	References
36	68.71	2.69	34.92	27.40	15.20	17.10	ML	
37	69.22	2.74	35.20	27.51	15.35	16.90	MI	
38	58.77	2.69	34.42	27.47	15.62	17.20	ML	
39	62.38	2.67	29.35	23.23	14.39	17.70	ML	
40	63.55	2.68	30.34	23.78	14.92	17.60	ML	
41	70.21	2.64	36.78	28.32	15.82	16.40	MI	
42	68.71	2.61	32.21	25.69	14.42	17.50	ML	
43	74.06	2.71	35.69	28.54	15.62	17.30	MI	
44	71.11	2.71	35.23	27.88	15.52	16.60	MI	
45	69.27	2.49	36.23	28.98	15.62	16.80	MI	
46	69.41	2.60	35.36	28.34	14.65	17.40	MI	
47	63.00	2.64	45.00	25.00	21.05	16.00	MI	[2]
48	92.35	2.70	72.00	39.60	28.00	14.00	MH	[13]
49	94.15	2.72	71.60	41.20	29.00	13.90	MH	
50	93.80	2.71	71.40	38.90	28.00	13.80	MH	
51	79.20	2.72	81.20	44.70	29.00	13.10	MH	
52	92.95	2.71	73.20	41.40	27.50	13.80	MH	
53	94.70	2.72	73.00	40.80	28.00	13.70	MH	
54	85.80	2.71	71.70	37.91	27.00	14.10	MH	
55	81.30	2.69	71.40	40.40	26.00	14.10	MH	
56	76.60	2.62	81.60	43.20	27.50	13.10	MH	
57	92.60	2.70	83.40	46.20	28.50	13.30	MH	
58	92.40	2.70	79.60	45.10	29.00	13.40	MH	[13]
59	81.15	2.68	76.20	40.70	27.50	14.10	MH	
60	94.15	2.70	77.20	46.60	28.00	13.50	MH	
61	70.40	2.65	49.50	30.70	21.00	16.00	MI	

where

- y = dependent variable
- a_0 = y -intercept (constant)
- a_1 = slope of line (constant)
- x = independent variable.

Equation 1 has the limitation to be used only when there is only one independent variable. Since, in cases where there are multiple independent variables, Eq. 1 cannot be used for analysis purpose. In such scenario multilinear regression (MLR) may be adopted in the form of Zain et al. [14]:

$$y = a_0 + a_1x_1 + a_2x_2 + a_3x_3 + \dots + a_nx_n \quad (2)$$

where

a_1, a_2, a_n = regression coefficients
 x_1, x_2, x_n = independent variables.

According to Eq. 2, there is a linear relationship amongst different variables. Since in practical applications, it is not true all the time. This may be due to each one of the independent variable affecting the dependent variable in a unique way as seen in the past studies that highlighted liquid limit as the prime factor affecting OMC. In such cases of dynamic relationships between the variables, the multiple nonlinear regression equation is used. Hence, Eq. 2 is modified by considering logarithmic on both sides.

The resulting equation can be in the form of Zain et al. [14]:

$$\log(y) = \log(a_0) + \log(x_1)a_1 + \log(x_2)a_2 + \dots + \log(x_n)a_n \quad (3)$$

Since, for the prediction of y (dependent variable), the Eq. 3 could be transformed by taking antilogarithm yield of the equation.

$$y = a_0 \cdot x_1^{a_1} \cdot x_2^{a_2} \cdot \dots \cdot x_n^{a_n} \quad (4)$$

The Eq. 4 is termed as a multivariable power equation. This approach has been adopted in the present study to predict OMC and MDD of soil samples, where independent variables x_1, x_2, x_3 , and x_4 are percent fines, specific gravity (G), LL, and PL, respectively. The final form of multivariable Eq. 4 can be derived as:

$$\text{OMC} = a_0 \cdot (\%Fines)^{a_1} \cdot (G)^{a_2} \cdot (LL)^{a_3} \cdot (PL)^{a_4} \quad (5)$$

$$\text{MDD} = a_0 \cdot (\%Fines)^{a_1} \cdot (G)^{a_2} \cdot (LL)^{a_3} \cdot (PL)^{a_4} \quad (6)$$

4 Results and Discussion

A linear approach is preferred in case of linear (incremental or decremental) relationship between the dependent and independent variables. However, in situations where every independent variable affects the dependent variable nonlinearly, it becomes essential to adopt a nonlinear approach. The literature highlighted the varying influence of different index properties of soil on compaction parameters.

Linear effect of individual index property on OMC and MDD was studied. Table 2 shows the coefficient of regression calculated for relation between each index property with compaction parameters.

Table 2 Regression coefficient for Individual index property and compaction parameters

Index properties	OMC	MDD
% Fines	0.572	0.518
Specific gravity	0.169	0.051
Liquid limit	0.854	0.826
Plastic limit	0.751	0.786

Liquid limit and Plastic limit seem to be more influential parameters than other index properties for computing the compaction parameters. Considering only the LL and PL for prediction of compaction parameters may save time, however consideration of nonlinear behaviour of all index properties can increase the accuracy also by seeing the categorized classified silty soil.

Present study used a multivariable nonlinear approach to predict compaction parameters by using Eqs. 5 and 6 as derived in Sect. 3. For the purpose, the soil samples (from Table 1) were separated as low, intermediate, and high plasticity silt. The total samples selected from literature were 61, out of which 24 are low plasticity silt (ML), 20 medium plasticity silt (MI) and 17 as high plasticity silt (MH). Four regression analysis models were developed using a multivariable nonlinear approach. Based on the approach, the values of coefficient of determination (R^2) were calculated. It represents the proportion of variance of predicted properties with respect to actual calculated properties. Closer the value to 1.0, higher is the prediction percentage. Refer Figs. 1, 2, 3, 4, 5, 6, 7 and 8 for the relationship between the experimental and predicted values of OMC and MDD for different models.

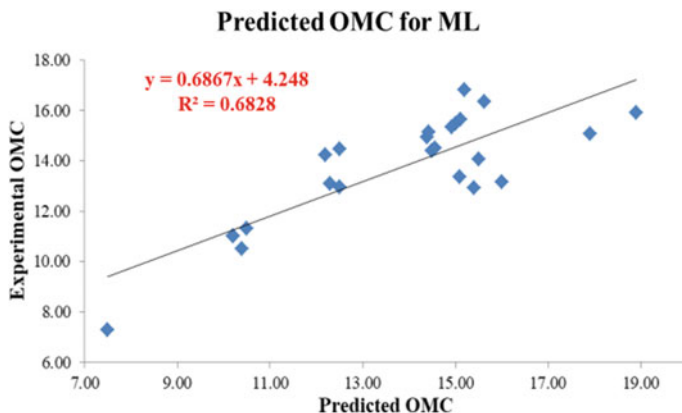


Fig. 1 Predicted OMC for ML

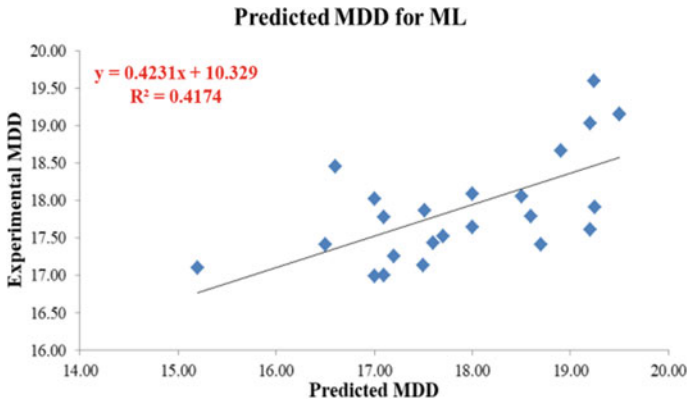


Fig. 2 Predicted MDD for ML

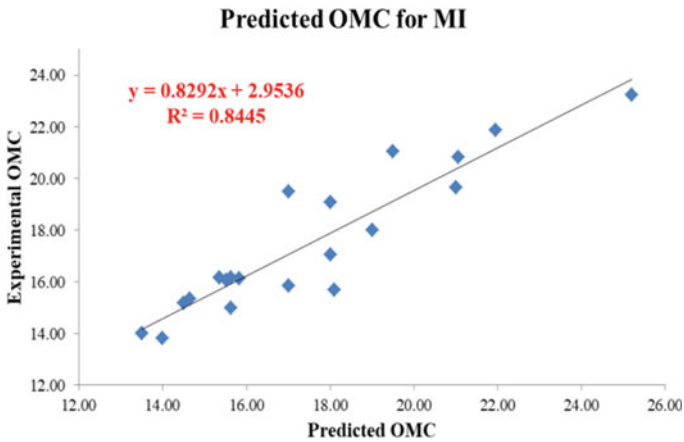


Fig. 3 Predicted MDD for MI

4.1 Model 1—for Low Plasticity Silt (ML)

$$OMC = (-00.7852) \cdot (\%fines)^{0.1591} \cdot (G)^{2.2175} \cdot (LL)^{0.3626} \cdot (PL)^{-0.1438} \quad (7)$$

$$MDD = (1.5549) \cdot (\%fines)^{-0.0866} \cdot (G)^{0.0801} \cdot (LL)^{-0.0963} \cdot (PL)^{-0.0357} \quad (8)$$

Figure 1 and 2 shows the relationship between predicted and experimental values of low plasticity silt.

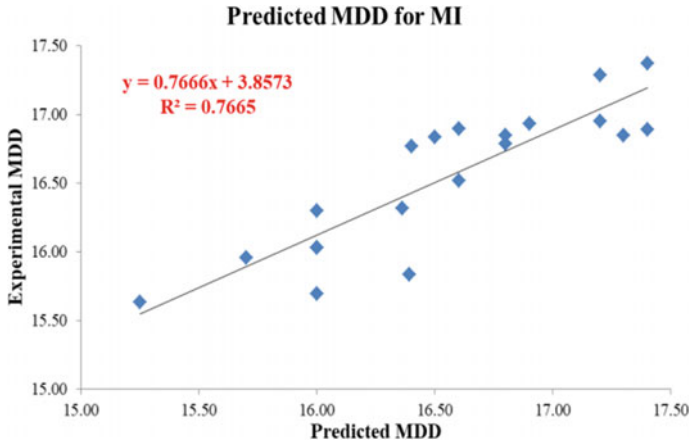


Fig. 4 Predicted OMC for MI

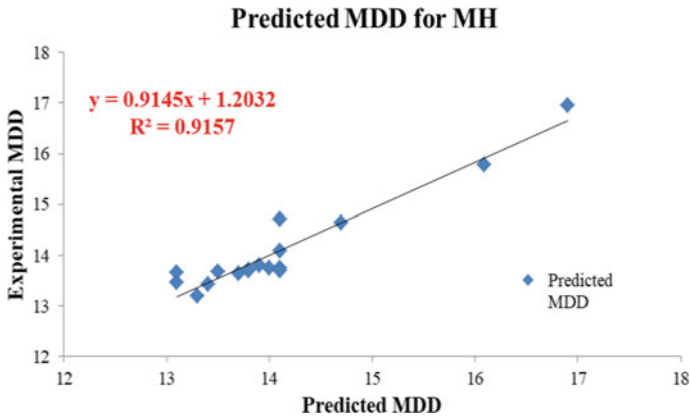


Fig. 5 Predicted OMC for MH

4.2 Model 2—for Intermediate Plasticity Silt (MI)

$$OMC = (0.1285) \cdot (\% \text{ fines})^{0.4302} \cdot (G)^{0.5563} \cdot (LL)^{0.9142} \cdot (PL)^{-0.9511} \quad (9)$$

$$MDD = (1.4533) \cdot (\% \text{ fines})^{-0.0956} \cdot (G)^{-0.1083} \cdot (LL)^{-0.1902} \cdot (PL)^{0.1376} \quad (10)$$

The regression analysis for medium plasticity silt showed slightly better results as compared to low plasticity silt model.

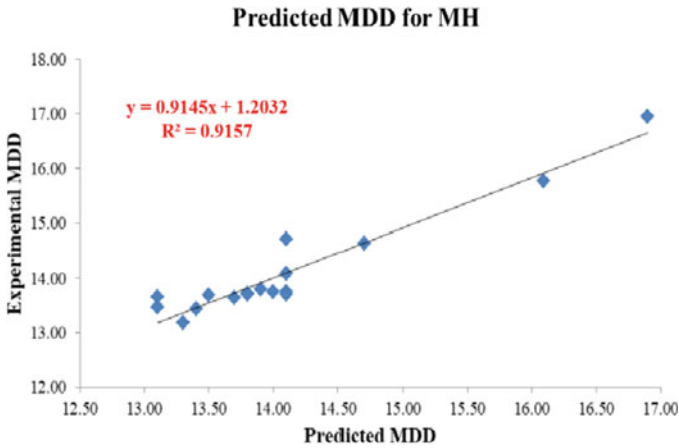


Fig. 6 Predicted MDD for MH

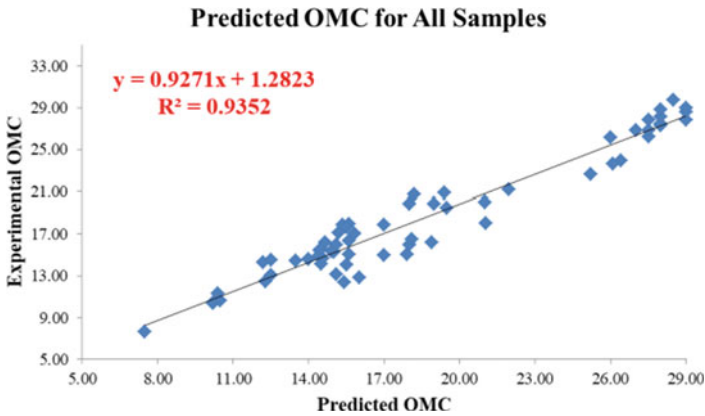


Fig. 7 Predicted OMC for all samples

4.3 Model 3—for High Plasticity Silt (MH)

$$OMC = (-0.6052) \cdot (\%fines)^{0.4297} \cdot (G)^{0.9522} \cdot (LL)^{0.7153} \cdot (PL)^{-0.3317} \quad (11)$$

$$MDD = (2.1693) \cdot (\%fines)^{-0.1145} \cdot (G)^{-0.52} \cdot (LL)^{-0.4769} \cdot (PL)^{0.1903} \quad (12)$$

Figure 5 and 6 are the representation of experimental versus predicted results for MH soils. From the figures, it is clear that coefficient of determination (R^2) is relatively higher but y-intercept is lesser as compared to low and medium plasticity silt models.

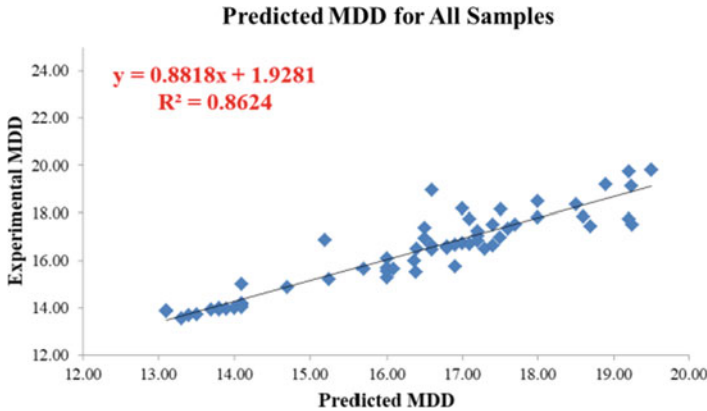


Fig. 8 Predicted MDD for all samples

4.4 Model 4—for All 61 Samples

$$OMC = (-0.9804) \cdot (\%fines)^{0.2453} \cdot (G)^{2.0389} \cdot (LL)^{0.4792} \cdot (PL)^{0.1029} \quad (13)$$

$$MDD = (1.7368) \cdot (\%fines)^{-0.1086} \cdot (G)^{0.0250} \cdot (LL)^{-0.1901} \cdot (PL)^{0.0222} \quad (14)$$

As a result, the regression analysis of medium and high plasticity silt found to be satisfactory and low plasticity silt shows high variance. A combined model was developed considering all the soil sample classification of silt as shown in the Figure 7 and 8.

5 Conclusion

The linear regression coefficients calculated for compaction parameters show varying influence of percentage fines, specific gravity, liquid and plastic limit on OMC and MDD. The regression coefficients for liquid limit and plastic limit found to be more influencing compared to remaining index properties. Considering the effect of all the index properties on compaction properties of the low plasticity soil model it was seen that the values of predicted output are spread out from the line of equality which shows greater variance from the actual results. However, intermediate and high plasticity silt models show lesser variance and considerably high coefficient of regression. The combined model gave significant resemblance to the prediction as 93% of predicted OMC and 86% for predicted MDD lie on the line of equality. Based on the analysis, the proposed correlations using a regression model proved to be satisfactory in predicting OMC and MDD of silty soil samples.

References

1. Hussain A, Atlar C (2019) Estimation of compaction characteristics of soil using Atterberg limits. *Mater Sci Eng (IOP Publishing Ltd)* 800
2. Shirur N, Dandin S, Patil V (2017) Establishing relationship between CBR value and physical properties of soil. *Int J Eng Res Mecha Civil Eng (Adv Trans Syst Infrast Dev Developing India)*
3. Sridharan A, Nagaraj HB (2004) Plastic limit and compaction characteristics of fine grained soils. *Ground Improvement* 9(1):17–22
4. Gurtug Y, Sridharan A, Ikizler SB (2018) Simplified method to predict compaction curves and characteristics of soil. *Iranian J Sci Technol Trans Civil Eng* 42(6)
5. Talukdar DK (2014) A study of correlation between California bearing ratio (CBR) value with other properties of soil. *Int J Emerg Technol Adv Eng* 4(1):559–562
6. Nagaraj HB, Reesha B, Sravan MV, Suresh MR (2014) Correlation of compaction characteristics of natural soils with modified plastic limits. *Trans Geotech (ELSEVIER)* 2:65–67
7. NG KS, Chew YM, Osman MH, Mohammad Ghazali SK (2015) Estimating maximum dry density and optimum moisture content of compacted soils. *Int Conf Adv Civil Environ Eng Pulau Pinang*
8. Gunaydin O (2009) Estimation of soil compaction parameters by using statistical analyses and artificial neural networks. *Environ Geol* 57:203–215
9. Saikia A, Baruah D, Das K et al (2017) Predicting compaction characteristics of fine-grained soils in terms of atterberg limits. *Int J Geosynthetics Ground Eng* 3:18. <https://doi.org/10.1007/s40891-017-0096-4>
10. Ramasubbarao GV, Sankar SG (2013) Predicting soaked CBR values of fine grained soils using index and compaction characteristics. *Jordan J Civil Eng* 7(3):354–360
11. Araujo W, Ruiz G (2000) Correlation equations of CBR with index properties of soil in the city of Piura. *Eng Innov Global Sustain*
12. Lakshmi SM, Subramaniyan S, Lalithambikhai MP, Vela MA, Ashni M (2016) Evaluation of soaked and unsoaked CBR value of soil based on the compaction characteristics. *Malays J Civil Eng* 28(2):172–182
13. Miryala P, Rao NB, Komu S (2017) Prediction of soaked CBR values with index properties of black cotton soils of Sangareddy region. *J Civil Eng* 7(1)
14. Zain M, Suhad MF, Abd M, Sopian K, Jamil M, Che-Ani AI (2008) Mathematical regression model for the prediction of concrete strength. *Math Methods Comput Tech Nonlinear Syst Intell Syst (Research Gate)* 396–402

Study of Arch Formation in Basalt Rock—A Case Study



Tejal K. Khule and Rupa S. Dalvi

Abstract The arching effect is the most universal phenomenon which exist in an underground engineering due to excavation, encountered by Terzaghi in 1943. The arch theory was widely used in the underground tunnel. A numerical investigations were performed using 3D finite element method (MIDAS GTS NX) to study the formation of arches above the tunnel roof in rock mass. In this case study, a 5-km-long-circular twin tunnel between Range hill and Swargate is being excavated by tunnel boring machine (TBM) to improve traffic system of Pune city, Maharashtra, India is consider. Rock types encountered during tunnelling are amygdaloidal basalt, vesicular basalt and compact basalt. In this study, numerical analysis is performed for prediction of arching action. Arch action is studied with the help of transfer of stresses around tunnel. Various model tests are carried out to analyse the differences of the arch action above tunnel face between dry rock mass and saturated rock mass with varying overburden depth (2D, 2.5D, 3D, 3.5D, 4D, 4.5D, 5D) “D” is diameter of the tunnel. 14 numerical models are studied in which 7 are for dry rock mass and 7 for saturated rock mass. Analysis shows that forming process of arch. Furthermore, factors affecting formation of pressure arch, i.e. overburden depth and water table effect on arch formation, are defined. Overburden depth factor has less influence on the arching action. Test results show that the arching coefficient can be decreased 10–15% by groundwater. The results obtained from this study will increase the ability to deal with similar ground conditions during tunnelling using TBM.

Keywords Pressure arch · Roof stability · Water table · TBM tunnelling

T. K. Khule

Geotechnical Engineering, College of Engineering Pune, Pune, India
e-mail: khuletk19.civil@coep.ac.in

R. S. Dalvi (✉)

Department of Civil Engineering, College of Engineering Pune, Pune, India
e-mail: rsd.civil@coep.ac.in

1 Introduction

The collapse of roof of underground cavities is a problem which arises in shallow tunnels and also in deep buried tunnels. After a tunnel being excavated, the form of stress of the surrounding rock in the excavation face changes from three-dimensional to two-dimensional stress form. The stress form is continuously arranged by rock itself to resist the irregular deformation of the surrounding rock, and finally, the stress concentration area forms in the surrounding rock, which is known as the pressure arch.

Recently, deeper and longer tunnels are under construction in India. Pune metro network is one of the significant public tasks in India. Its objective is to solve the severe traffic problems in Pune by providing an elevated and underground transportation system. In this research, a case study of 5-km-long underground Pune metro tunnel is consider. Depth of the tunnel is varying from 12 m to 30 m. Tunnel has 84 m stretch below river Mutha. The underground line includes 5 underground stations which are Shivajinagar, Civil court, Budhwar Peth, Mandai, and Swargate.

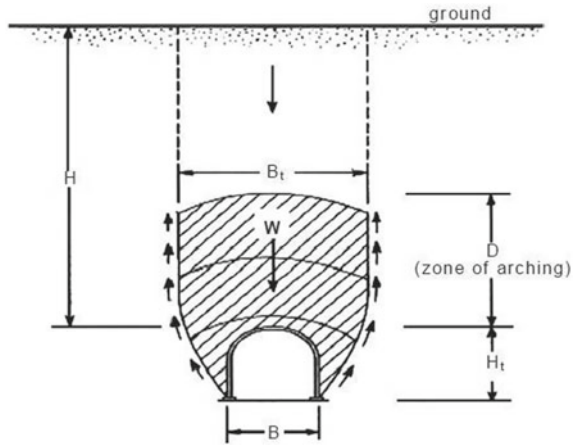
In this research work, series of numerical experiments are performed to understand the arching mechanism of rock structures after excavation. By using finite element method, the formation of arch is determined by analysing the stress distribution around tunnel; furthermore, factors affecting arch formation are analysed and discussed.

2 Literature Study

Terzaghi conducted experimental and theoretical investigations of arching. The study of the arching effect can help to understand the stability of excavation face and surface ground. Theory of surrounding rock pressure includes Terzaghi theory, Platts theory, Bill Bowman theory, theory of whole soil column and Xie Ji Xiaoxiao theory. Roof arch was defined by Terzaghi that transfer of forces between a yielding mass of geomaterial and adjoining stationary members (Fig. 1).

Analysed soil arch effect of shield tunnel in dry sandy ground. This effect was studied with different depth/diameter ratios of the tunnel by using Model box test. As the support force on the tunnel face decreases, the stress distribution around the tunnel face can be changed. Redistribution of soil stress can induce effect of arch near the tunnel face (Anagnostou 2012) [2, 3]. Wang (2016) analysed the forming process, lateral pressure coefficients varied from small to large, distributional pattern and evolution characteristics of the pressure arch of the highway tunnel under different stress forms. The failure mechanism of the stratified rock roof of the tunnel was studied. Discontinuous deformation analysis is used to investigate pressure arch formation; the distribution characteristics of the pressure arch in the horizontal stratified rocks are analysed using FLAC 3D software (He 2014; Wang 2015) [3]. Song et al. [4] effect of ground water on soil arch is determined in sand by experimental

Fig. 1 Zone of loosened ground developed in response to tunnel construction [1]



study; the test system is designed, including glass box, tunnelling model and measure system.

3 Case Study

Pune metro is aimed to tackle growing traffic congestion from the increasing population and fast urbanisation and provide comfortable and convenient commute in the city. Metro rail will act as the back bone to the public transport system of the Smart City Project. Total stretch is 54.5 km from which 16.59 km line 1 is elevated between PCMC Bhawan and Range hill, from range hill 5 km is underground and line 2 is elevated between Vanaz to Ramwadi. In this study, arch formation around 5-km-long underground tunnel is analysed. The tunnel for Pune Metro line has a circular cross-section of 5.8 m internal diameter that consists of a precast segmental lining thickness of 275 mm. There are two construction methods used in tunnelling New Austrian tunnelling method and tunnel boring machine.

3.1 Geology and Hydrology of the Area

The project alignment is set in the stratigraphic domain of an approximately 250-m-thick Pahoehoe flow, Karla Formation. Based on the drilling information from the boreholes, from existing ground level to about 2.0 m (below ground level) is assumed as made ground/filled-up material. Underlying the filled material layer, the residual soil stratum is primarily composed of sand, clay and silt with presence of gravel. The bed rock identified with the Deccan basalt flows are vesicular basalt (VB), amygdaloidal basalts (AB) and compact basalts (CB). No major geological

structure like folds, faults and any large shear zones and dykes are reported. The records of ground water levels published for city suggest its depth in range of 2.5–7.5 m from ground level measured during the monsoonal months of June, July and August. This could drop down to about another 2.5 m during pre-monsoon seasons. The permeability of rock mass is a largely a function of intensity of fracturing and jointing whilst that of the soil by its grain size distribution. For the variably fractured rock mass in the project area, the coefficient of permeability k is found to vary between 10 and 7 m/sec in more persistent and open jointed conditions and to 10–8 m/sec in more massive rock. It must be however noted that the permeability/water ingress from local—persistent open joints or fracture/weak zones can be substantially high, e.g. red bole layers, especially below the river and deeply weathered and fractured basalt.

4 Arch Mechanism in Rock

In order to improve understanding of the arching phenomenon in general and specifically the stress distribution around tunnels, experimental investigations were made by Kienzl in Terzaghi's laboratory in Vienna (Terzaghi 1936). From these results, the theories of arching were derived in 1943. Terzaghi (1943) described the arching effect as “the transfer of pressure from a yielding mass of soil onto adjoining stationary parts,” and the soil is said to “arch over the yielding part of the support”.

Due to gravity, all the rock in area is under pressure before excavation of tunnel. Any curve line in surrounding rock shows compression state in all three directions. After excavation of tunnel, the stress in the surrounding rock changes. With different tensile stresses, the surrounding rock is in the tensile state. The stress distribution after excavation of tunnel is consider as a method to determine the arch zone.

5 The Computational Model

The excavation diameter of the tunnel by TBM is 6.650 m. By using MIDAS GTS NX software, 14 computational models of tunnel were built with varying depth of 12–30 m under the hydrostatic stress state. The model is divided into many elements. To know the effect of overburden depth, height-to-width ratio is considered, i.e. (H/D). Total 14 models are constructed from which 7 for dry rock strata and 7 for saturated rock strata.

For the analysis, some assumptions are made

- (1) The material is assumed to be elasto-plastic.
- (2) Along the tunnel length, geometry is same.
- (3) The rock mass surrounding the tunnel is homogenous, isotropic in all directions.
- (4) Rock mass should follow the Hoek–Brown failure criteria.

Fig. 2 Numerical mesh

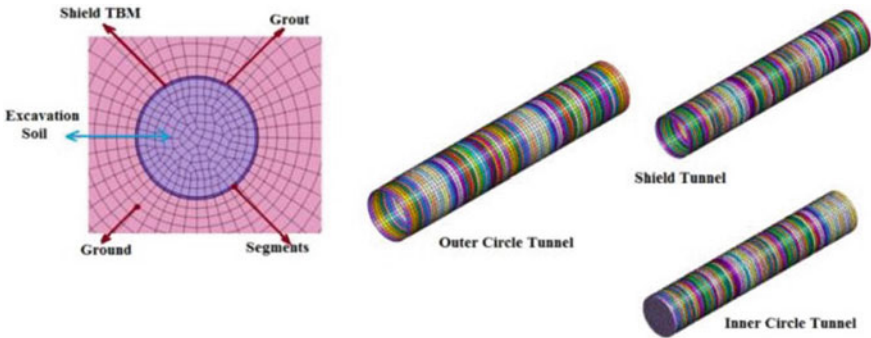
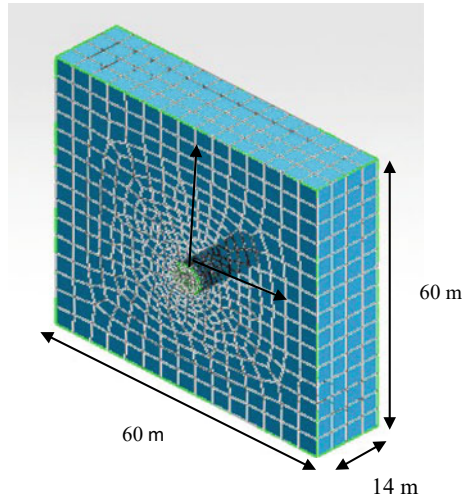


Fig. 3 Schematic diagram of the numerical mode

(5) Full face excavation is considered (Fig. 2).

Numerical mesh having size $60\text{ m} \times 60\text{ m} \times 14\text{ m}$ is constructed with varying overburden depth (2D, 2.5D, 3D, 3.5D, 4.5D, 5D); mesh size is 4 m. Outer diameter of the tunnel is 6.35 m, and internal diameter is 5.8 m. Tunnel is supported with precast segmental lining having thickness 275 mm and length equal to 1.4 m (Fig. 3).

6 Design Parameters

Figure 4 shows design parameters of shield tunnel. Face pressure and grouting pressure are determined according to [5]. Other than this, Jack thrust force is considered for design (Table 1).

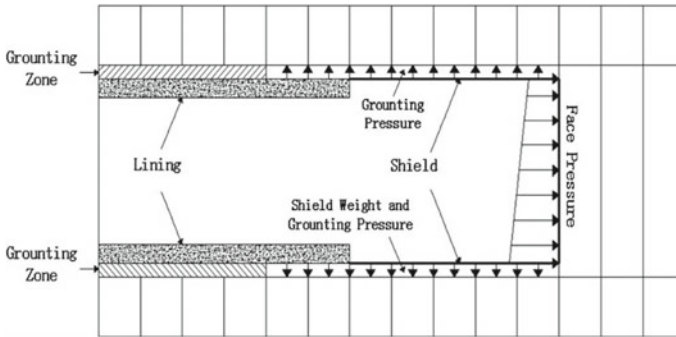


Fig. 4 Design forces

Table 1 Soil and rock properties

	Unit wt. of overburden (MN/m ³)	Young's modulus (Mpa)	Poisson's ratio	Peak tensile strength (Mpa)	Peak cohesion (Mpa)	Friction angle (Degree)
<i>Soil properties</i>						
Made ground	16	1.5	0.3	–	0	25
Sandy clay to silty clay	18	3.5	0.3	2	0.09	30
<i>Rock properties</i>						
HW	25	4500	0.3	0.001	0.06	30
MW	25	7500	0.3	0.01	0.16	47
SW	25	14,000	0.3	0.3	1	60

7 Results and Discussion

Figure 5 shows the vertical stress contours around tunnel face. The formation of the soil arch is clearly visible. The graph of vertical stresses versus construction stages is drawn for both dry and saturated rock mass for all the depth factors 2D, 2.5D, 3D, 3.5D, 4.5D, 5D (Figs. 6, 7, 8, 9, 10, 11, 12). Stresses are calculated at the crown of the tunnel and plotted on Y- axis and construction stages plotted on X-axis. At first stage of construction, excavation is not carried out; from stage 2 to stage 4, excavation is done by TBM, and at stage 5, segments are provided as a support of tunnel.

Graph (Figs. 7, 8, and 9) shows that at initial stage, overburden (vertical) stress value is high, and after excavation is started, value is decreasing suddenly. This sudden changes in values of vertical stress show distribution of stresses above tunnel, according to Terzaghi's theory presence of arch action is detected. Also, graph shows very slightly changes in values of vertical stress after installation of support segments. Graph for saturated rock zone shows similar trend as of dry rock zone, but due to uplift pressure created by water, the value of vertical stress at initial stage is different.

Fig. 5 Vertical stress contours around the tunnel face

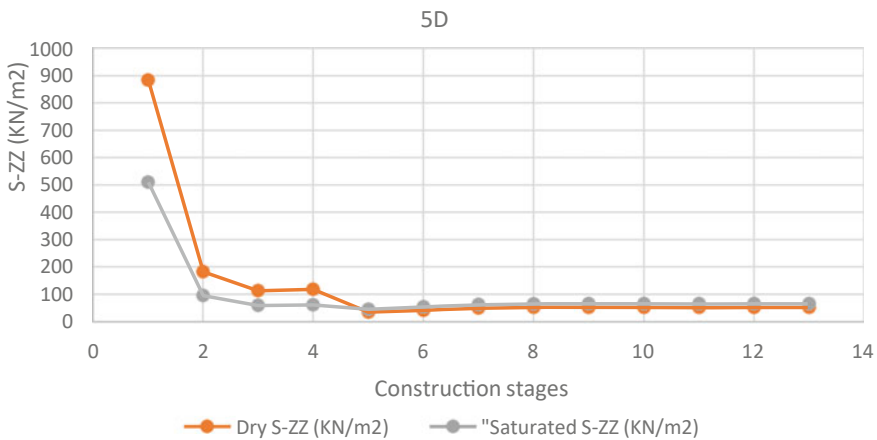
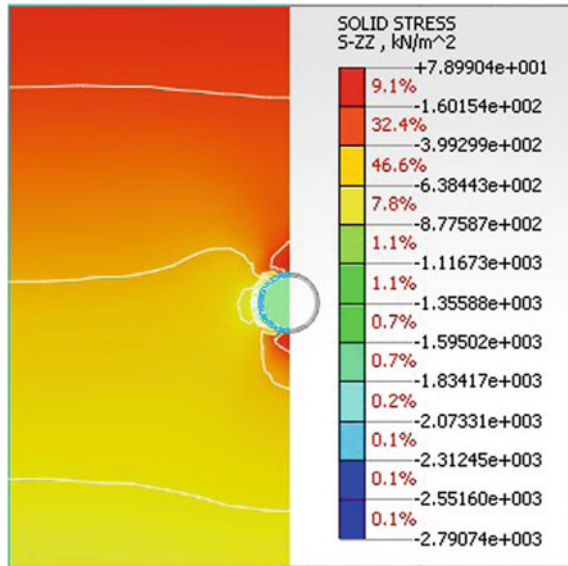


Fig. 6 Vertical stresses versus construction stages at depth 5D

Figure 13 and 14 show graph of vertical stress versus overburden depth for dry and saturated rock mass condition. For dry condition, the actual deformation (vertical stress) before construction shows increasing trend as depth increases overburden stress increases. Deformed overburden stress shows opposite nature to actual vertical stress. This is because of the shear stresses acting in the upward direction to reduce the overburden stress acting at crown of the tunnel. The graph of saturated rock mass condition is similar to dry rock mass condition.

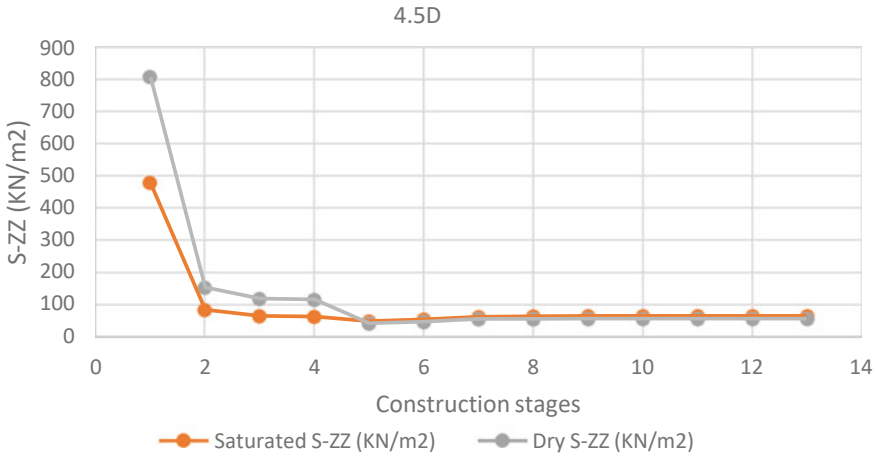


Fig. 7 Vertical stresses versus construction stages at depth 4.5D

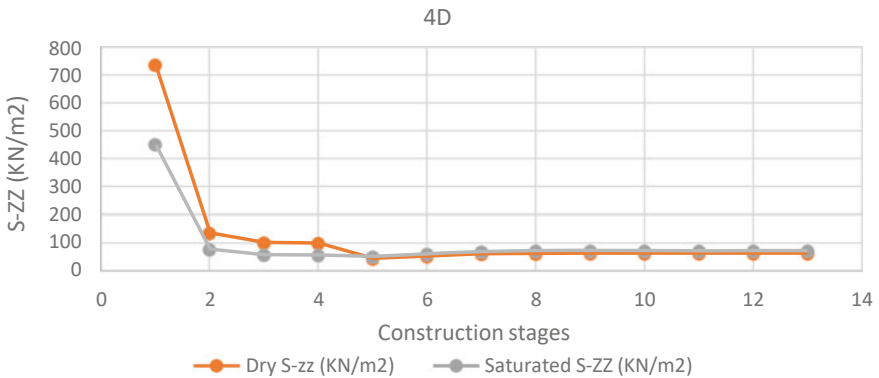


Fig. 8 Vertical stresses versus construction stages at depth 4D

To show relation between dry and saturated condition of rock mass, one factor called stress coefficient of arching is introduced. Percentage (%) of arching occurring at particular depth of tunnel can be calculate from this factor.

$$\text{Stress Coefficient of Arching} = \frac{\sigma - \sigma'}{\sigma} * 100$$

σ = Actual overburden stress

σ' = Deformed overburden stress.

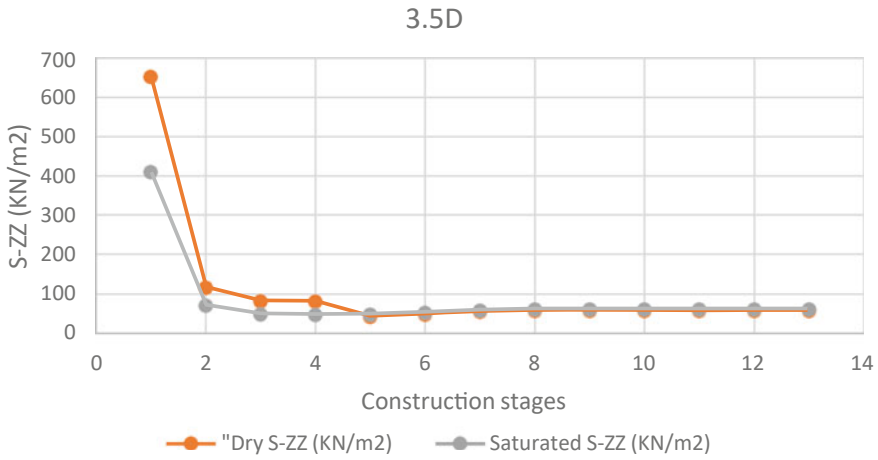


Fig. 9 Vertical stresses versus construction stages at depth 3.5D

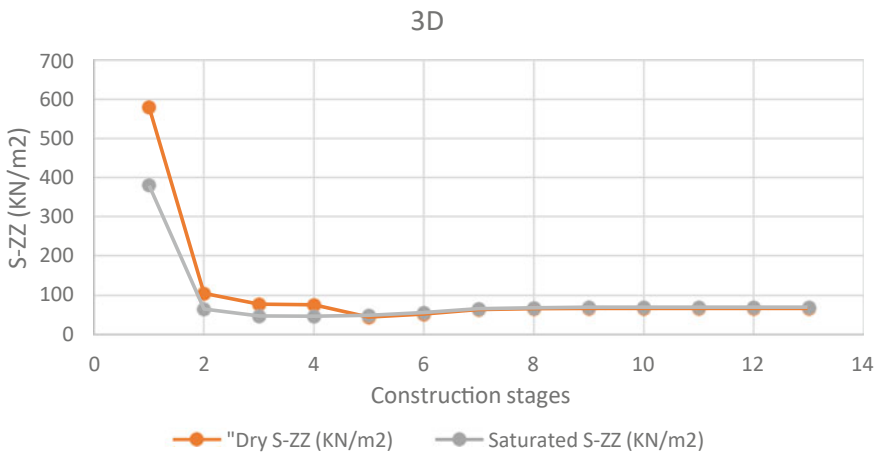


Fig. 10 Vertical stresses versus construction stages at depth 3D

Figure 15 shows graph of stress coefficient of arching versus H/D ratio (H is overburden height, and D is diameter of tunnel), as tunnel depth-to-width ratio increases arching coefficient increases for both dry and saturated condition of rock mass.

Figure 15 shows that stress coefficient of arch for saturated rock mass is smaller than dry rock mass. From this it is clear that ground water is affecting arch action; the buoyant force on rock strata can change the effective stress coming at crown of the tunnel.

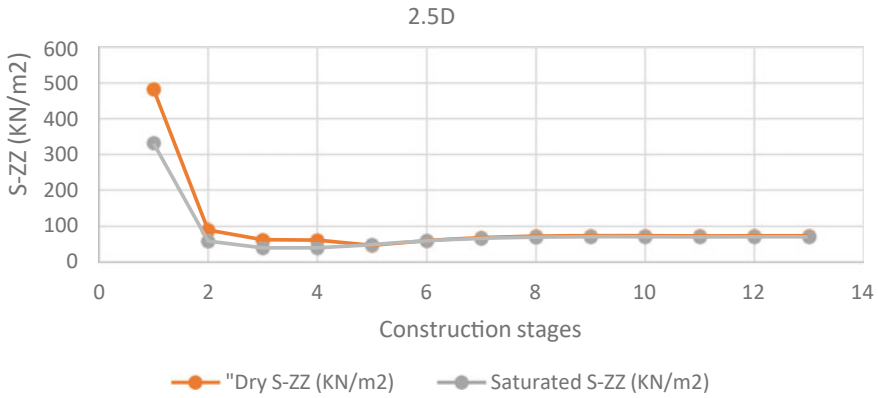


Fig. 11 Vertical stresses versus construction stages at depth 2.5D

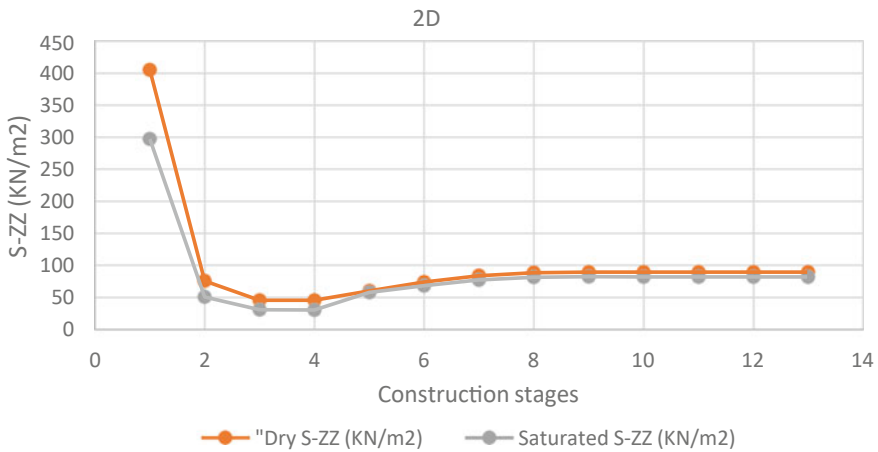


Fig. 12 Vertical stresses versus construction stages at depth 2D

8 Conclusion

In this paper, series of numerical model tests are carried out to analyse arch action and also differences of arch between dry sand and saturated rock mass. The following conclusions can be drawn from test results

1. Presence of arch action in basalt rock is identified at Pune metro site. The stress observed at crown of the tunnel is different after excavation of tunnel.
2. As basalt rock is defined as a hard rock, arch action will not affect stability of tunnel. Overburden depth (D) factor has less influence on the arching action.
3. Underground water is one of the most important destabilising factor for underground structures.

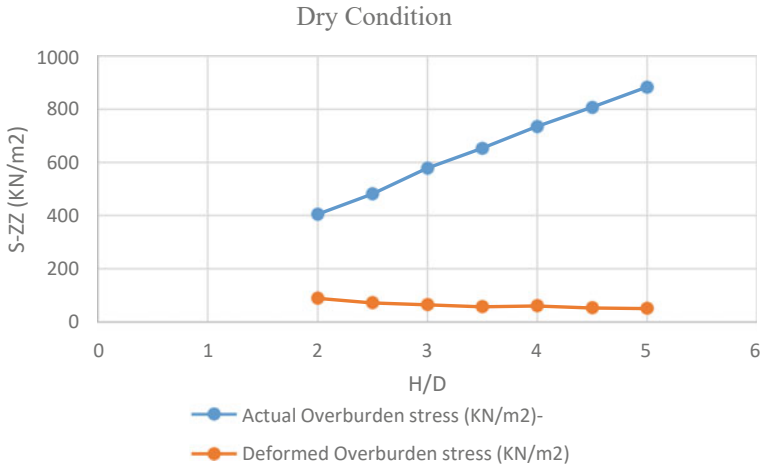


Fig. 13 Vertical stresses versus *H/D* ratio

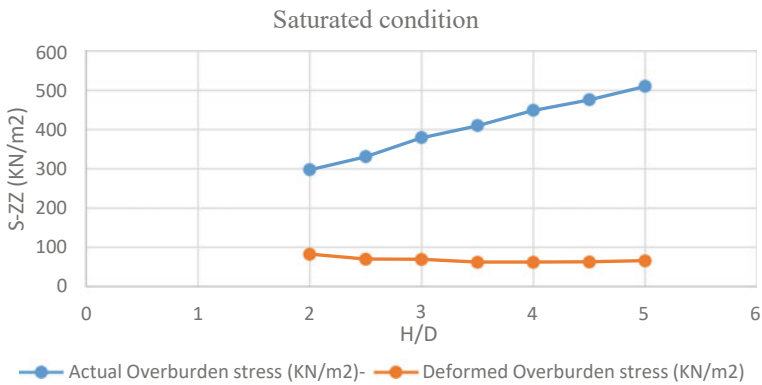


Fig. 14 Vertical stresses versus *H/D* ratio

4. Test results show that the stress coefficient of arching can be decreased 10–15% by groundwater.
5. The results obtained from this study will increase the ability to deal with similar ground conditions during tunnelling using TBM.

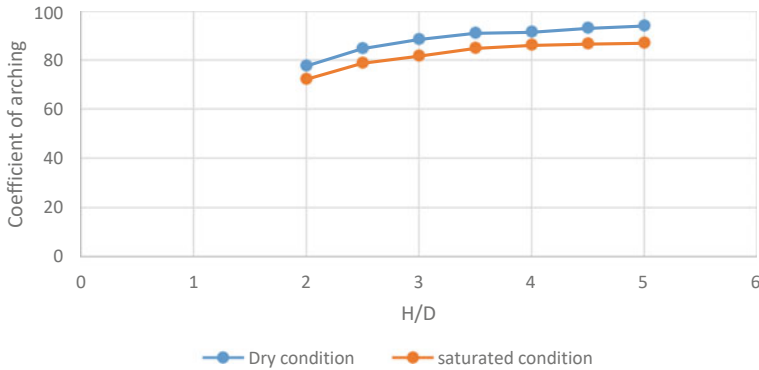


Fig. 15 Arching coefficient versus H/D ratio

References

1. Terzaghi K (1946) In: Proctor RV, White T (eds) Rock defects and load on tunnel supports rock tunneling with steel supports. Commercial Shearing and stamping Co, Youngstown, Ohio, pp 15–99
2. Lee CJ, Wu BR, Chen HT, Chiang KH (2006) Tunnel stability and arching effects during tunneling in soft clayey soil. *Tunn Undergr Space Technol* 21:119–132
3. Chen CN, Huang WY, Tseng CT (2011) Stress redistribution and ground arch development during tunnelling. *Tunn Undergr Space Technol* 26(1):228–235
4. Song J, Gao Y, Liu S (2018) Analysis of the effect of groundwater on soil arch in shield tunneling. *Arab J Geosci* 11:534. <https://doi.org/10.1007/s12517-018-3829-3>
5. Anagnostou G, Kovari K (1996) Face stability conditions with earth-pressure-balanced shields's. *Tunn Undergr Space Technol* 11(2):165–173
6. Mohammed (2017) Numerical modelling for circle tunnel under static and dynamic loads for different depth. *Res J Min* 1(1):1–11
7. Zhang ZX, Xu Y, Kulatilake PHSW, Huang X (2012) Physical model test and numerical analysis on the behaviour of stratified rock masses during underground excavation. *Int J Rock Mech Min Sci* 49:134–147. <https://doi.org/10.1016/j.ijrmms.2011.11.001>
8. Jia P, Tang CA, Wang SH (2006) Destroy mechanism of tunnel with stratified roof. *J Chin Coal Soc* 31(1):11–15
9. He L, An XM, Zhao ZY, Zhao J (2015) Development of a unified rock bolt model in discontinuous deformation analysis. *Int J Rock Mech Min Sci* (in preparation)
10. Wang SR, Li N, Li CL, Cao C (2015) Distribution characteristics analysis of pressure-arch in horizontal stratified rocks under coal mining conditions. *Int J Rock Mech Min Sci* ISSN 1330-365
11. Wang SR, Li N, Li CL, Hagan P (2014) Mechanics evolution characteristics analysis of pressure-arch in fully mechanized mining field. *J Eng Sci Technol Rev* 7(4):40–45

Consolidation of Layered Soils with Variable Compressibility



Deepak Kumar Singh , Chitranshu Kumawat, and Siddharth Mehndiratta

Abstract The distribution of consolidating load in any soil is related directly to the distribution of pore water pressure. Terzaghi's consolidation theory that is used to define this distribution is based on some certain linearized assumptions that may or may not be reasonable in practice. The linearized equation surely may have some mathematical benefits; however, they are of slight importance when working on non-homogeneous soils. In the following study, a numerical method is developed. A finite difference approach for computing 1D consolidation in analysing consolidation problem is presented. Most software applications utilize an explicit finite difference evaluation method. While using this approach, the solution space in the problem is discretized in time and space. The same problem may also be solved implicitly, so that the excess pore pressures at all nodes are solved together at the selected time. A nonlinear formulation, involving variations of compressibility, indicated in the results is deemed essential for the behaviour that is observed. Critical investigation may be done to investigate the nature of these variations.

Keywords Terzaghi's theory · Finite difference method · Consolidation

1 Introduction

Tiny solid particles form soil, and these particles are not bonded together, with the exception of the force of cohesion, internal friction, minor van der Waals forces and adsorbed double-layer water. Whenever a load is experienced by a soil mass, the elastic deformation undergone by the solid particles is quite small when compared

D. K. Singh (✉) · C. Kumawat · S. Mehndiratta
MNIT Jaipur, Jaipur, India
e-mail: 2020rce9526@mnit.ac.in

C. Kumawat
e-mail: 2020pct5254@mnit.ac.in

S. Mehndiratta
e-mail: siddharth.ce@mnit.ac.in

with the deformation that is due to variation in the relative position of distinct soil particles, and this following reduction in the soil mass' volume is due to reduction in volume of voids. If the voids are occupied by only air, rapid compression of soil takes place, since air can easily escape from the voids. When soil is saturated and its voids are occupied with water that is incompressible, any volume reduction or compression may only take place once water is ousted from the voids. This phenomenon occurs due to an extended period of static load, and the resulting expulsion of pore water is called consolidation. Also, we can conclude that consolidation is a natural phenomenon because it is due to the very long-term static load.

According to Terzaghi, 'every process involving a decrease in the water content of a saturated soil without the replacement of water by air is a process of consolidation'.

Xie et al. [1] presented a solution for 1D consolidation that was entirely explicit analytical. In their study, a double-layered soil with partly drained boundaries was taken. The results were indicative that the boundary drainage conditions and the soils' layered characteristics also impact the consolidation behaviour.

Conte and Troncone [2] analysed consolidation problem regarding time-dependent loading on thin clay. A modest solution to nonlinear 1D theory of consolidation that utilized certain analytical expressions in combination with Fourier series was forwarded.

Liu and Lei [3] presented a universal analytical solution that was explicit for one-dimensional consolidation of layered soil problems. An applicable computer code was written, and the results for some examples were conveyed. According to these results, a thorough study pertaining to one-dimensional consolidation behaviour of layered soil system was conducted.

2 Objectives

In the application of Terzaghi's theory, many significant shortcomings were pointed out in later researches arising due to the limitations of the assumptions in the theory, especially those involving soft clays, and, in his theory, the constant value of coefficient of consolidation is one of the major limitations. The objective of the present study is to obtain results between pore water pressure and time by varying different parameters.

3 Methodology

According to Terzaghi's theory, the value of C_v (coefficient of consolidation) is assumed constant. For the purpose of this study, a 1D nonlinear partial differentiation equation derived by Abbasi et al. [4] for estimation of consolidation characteristics of

clays is utilized. To approach towards the solution of the above-mentioned nonlinear equation, a finite difference methodology is selected.

On the basis of Terzaghi's fundamental equation and in view of the point that every variation in pore pressure equals a variation in the effective stress, we have

$$\frac{\partial^2 u}{\partial z^2} = \frac{\partial^2 \sigma'}{\partial z^2} \quad (1)$$

For homogeneous soils:

$$\frac{\partial k}{\partial z} = 0 \quad (2)$$

When the applied total stress is constant, the equation for continuity for 1D consolidation is given as follows:

$$\left(\frac{1}{1 + e_0} \right) \frac{\partial e}{\partial t} = - \frac{k}{\gamma_w} \frac{\partial^2 \sigma'}{\partial z^2} \quad (3)$$

For soft soil/clays:

$$e = a - C_c \text{Log } \sigma' \quad (4)$$

e and k relationship:

$$e = b + M \text{Log}(k) \quad (5)$$

where

' a ' and ' b ' are intercepts of slope line.

A = void ratio of unit effective stress.

b = void ratio of unit coefficient of permeability, ($k = 1$).

On combining both equations:

$$k = 10^{(a-b)/M} (\sigma')^{-C_c/M} \quad (6)$$

Differentiate Eq. 4 with respect to t :

$$\frac{\partial e}{\partial t} = \frac{-2.3 C_c}{\sigma'} \frac{\partial \sigma'}{\partial t} \quad (7)$$

Substituting Eqs. 6 and 7 in Eq. 3.

$$\frac{\partial \sigma'}{\partial t} = \frac{2.3(1 + e_0)}{C_c \gamma_w} 10^{(a-b)/M} (\sigma')^{(1 - \frac{C_c}{M})} \frac{\partial^2 \sigma'}{\partial z^2} \quad (8)$$

Assuming

$$\alpha = 1 - \frac{C_c}{M} \quad (9)$$

and

$$C_n = \frac{2.3(1 + e_0)}{C_c \gamma_w} 10^{(a-b)/M} \quad (10)$$

So

$$\frac{\partial \sigma'}{\partial t} = C_n (\sigma')^\alpha \frac{\partial^2 \sigma'}{\partial z^2} \quad (11)$$

Assuming linear relationship for $e - \text{Log}(\sigma')$ and $e - \text{Log}(k)$, Equation 11 can be reworked in terms of the excess pore water pressure, (u) seeing that $\sigma' = \sigma_t - u$

$$\frac{\partial u}{\partial t} = C_n (\sigma_t - u)^\alpha \frac{\partial^2 u}{\partial z^2} \quad (12)$$

$$C_n (\sigma_t - u)^\alpha = C_v \quad (13)$$

According to Eq. 12, the coefficient of consolidation, C_v , fluctuates during consolidation when the surplus pore water pressure, u , varies. It is clearly observed here that coefficient of consolidation is associated nonlinearly with effective stress. α is a dimensionless factor that relies upon compressibility and permeability characteristics (from Eq. 9 (M and C_c) of the soil, and C_n , a coefficient, can be ascertained using Eq. 10 and is dependent on permeability and compressibility characteristics (M , b , C_c , a), initial void ratio (e) and the unit weight of water (γ_w). In the present study, the coefficients C_n and α will be labelled as basic coefficient of consolidation and nonlinearity factor, respectively. For special cases, i.e. $\alpha = 0$ (or $C_c/M = 1$), C_v will remain constant, equivalent to C_n , and Eq. 12 will diminish to Terzaghi's theory.

$$\frac{\partial u}{\partial t} = C_v \frac{\partial^2 u}{\partial z^2} \quad (14)$$

Table 1 Characteristics of samples

Sample number	Coefficient of consolidation C_v (m ² /sec)	Applied pressure (kPa)	α
1	8.44×10^{-7}	15	0.34
2	1.25×10^{-5}	60	-0.14

4 Single-Layered Profile: Parametric Study

4.1 Problem Statement

The problem undertaken in the paper involves weightless soil (depth = 12 cm) where water table is at the ground surface. Two soil samples having different coefficient of consolidation and applied pressure are considered (Table 1). At time zero, excessive pore water pressure is equivalent to applied pressure at all nodes except at the drainage boundaries. It is found that successive application of finite difference equation soon leads to absurd values of pore water pressures (is divergent) if $\beta = C_v \Delta t / (\Delta z^2)$ exceeds 0.5. In the present study, β is forced to remain less than 0.5. The accuracy of the solution is improved by using a small spacing of node points in the z direction.

4.2 Effect of Parameter A

In the analysis, applied pressure is taken as 100 kPa and initial coefficient of consolidation is considered as 8.44×10^{-7} m²/sec.

Figure 1 illustrates the consequence of α on $U-t$ curve profile. Regarding negative α values, the $U-t$ curve is located under the curve projected by Terzaghi's solution, i.e. (constant C_v , or $\alpha = 0$). Indicating that values of α that are negative, the consolidation will be at a slower rate than expected with respect to Terzaghi's solution and consolidation gets slower when the value of α decreases. Alternatively, for positive α values, consolidation is quicker than anticipated by Terzaghi's solution, and with increase in the value of α , the rate of consolidation increases.

As presented earlier that during consolidation, the coefficient of consolidation varies as effective stress (or pore pressure) varies in both spatial and temporal directions. Figures 2 and 3 display distinctive deviations of C_v with time and depth, respectively. The effect that α has on C_v is depicted in Fig. 3. This figure displays that the coefficient of consolidation, C_v , has increasing and decreasing tendencies with respect to time for positive and negative α values, respectively. The permeability of soil declines at a rate faster when likened to decrease in compressibility when α is larger than 0. Thus, as the consolidation advances, an increase in the coefficient of consolidation can be observed. Alternatively, when the value α is below 0, during consolidation, the coefficient of consolidation reduces. It can also be observed that

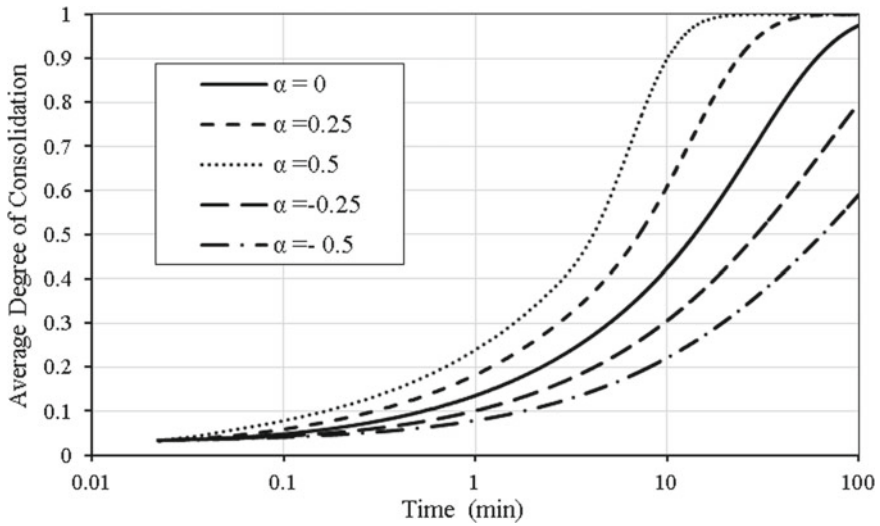


Fig. 1 Average degree of consolidation versus time curve for different value of α

the coefficient of consolidation is unchanged, and finally when α is equal to zero, the outcomes are identical to Terzaghi's solution.

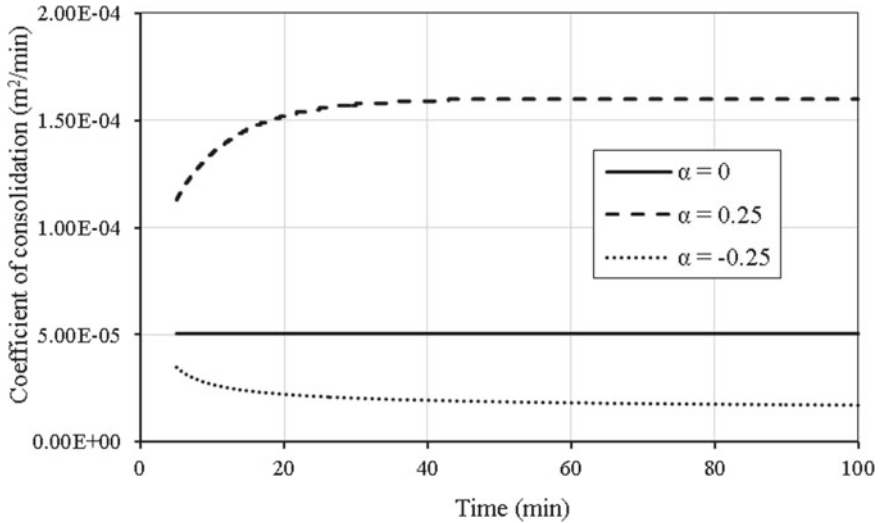


Fig. 2 Coefficient of consolidation (C_v in m^2/min) versus time factor curve for various values of α

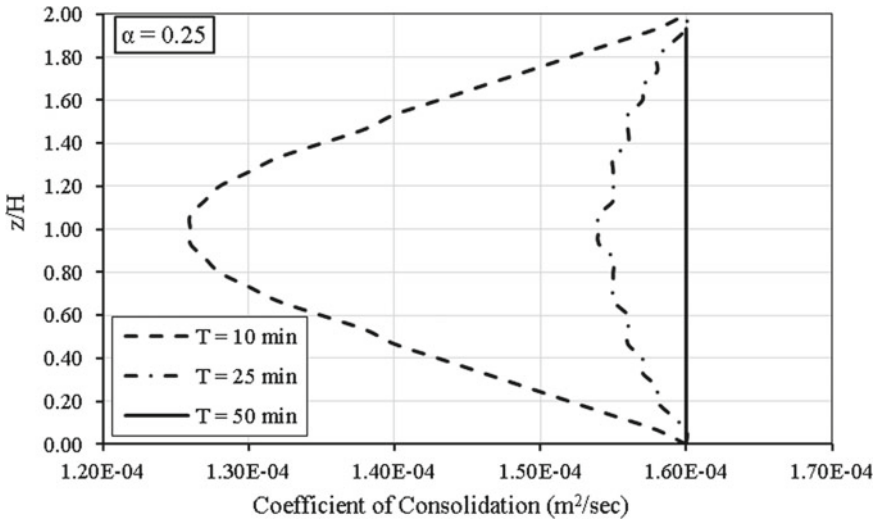


Fig. 3 Average degree of consolidation versus time factor curve for differing values of Δz

4.3 Effect of Applied Pressure

Figure 4 displays the outcome of applied pressure on the $U-t$ curve shape ($\alpha = 0.25$). It can be clearly observed that increasing applied pressure increases the consolidation rate. The surcharge pressures have a great influence on consolidation characteristics.

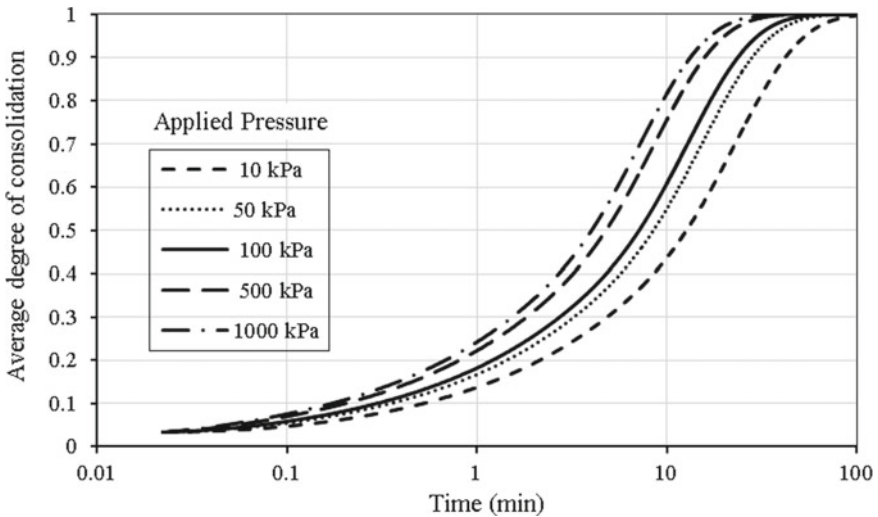
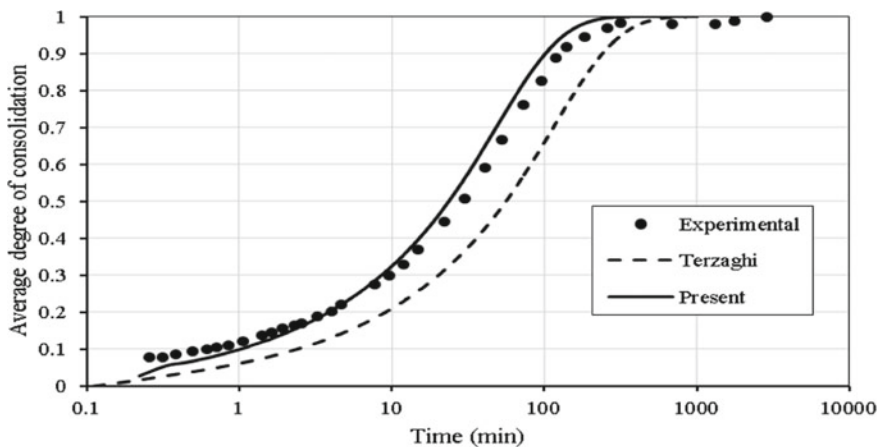


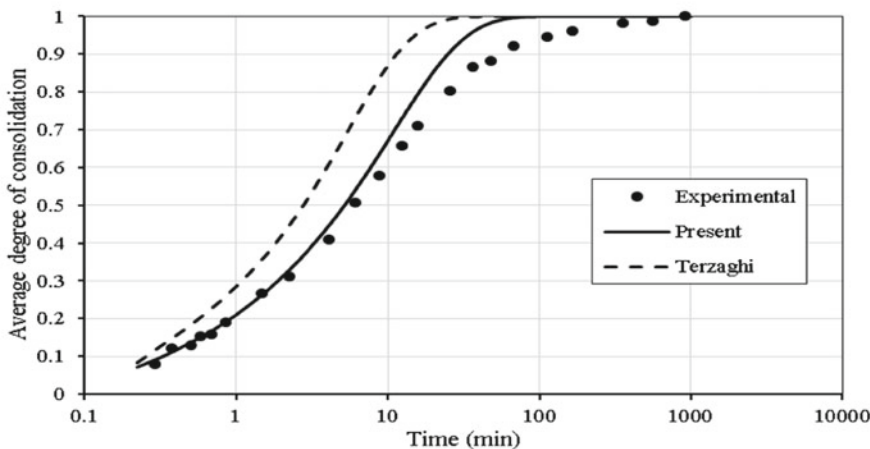
Fig. 4 Variation of average degree of consolidation with time at different applied pressure

5 Validation

The experimental results of Abbasi et al. [4] and from Terzaghi's theory are compared with the results that were achieved through numerical solution using nonlinear equations. It is observed from Fig. 5 that the results achieved using nonlinear theory are similar to the results obtained experimentally when compared with the results achieved by Terzaghi's linear theory. Additionally, for the soil samples 1 having positive values of α (Fig. 5a), consolidation occurs quicker than anticipated by Terzaghi's theory. For samples 2 and 3 that comprise α values that are negative (Fig. 5b), consolidation occurs at a rate slower than anticipated by Terzaghi's theory.



(a) Sample 1



(b) Sample 2

Fig. 5 Change in average degree of consolidation with time

6 Double-Layered Profile

Laplace equation for two-dimensional seepages is written as follows:

$$k_x \frac{\partial^2 h}{\partial x^2} + k_z \frac{\partial^2 h}{\partial z^2} = 0 \tag{15}$$

In the case of flow through the boundary of a homogenous soil layer to another, the equation is modified (Das [5]).

Referring to Fig. 6, flow area is situated half in soil 1 and has a permeability coefficient k_1 and the other part in soil 2 having a permeability coefficient, k_2 , we say that:

$$k_{avg} = \frac{1}{2}(k_1 + k_2) \tag{16}$$

If soil 1 and soil 2 are swapped, the replaced (soil 1) evidently has a hydraulic head of h'_4 instead of h_4 .

Having equal velocity,

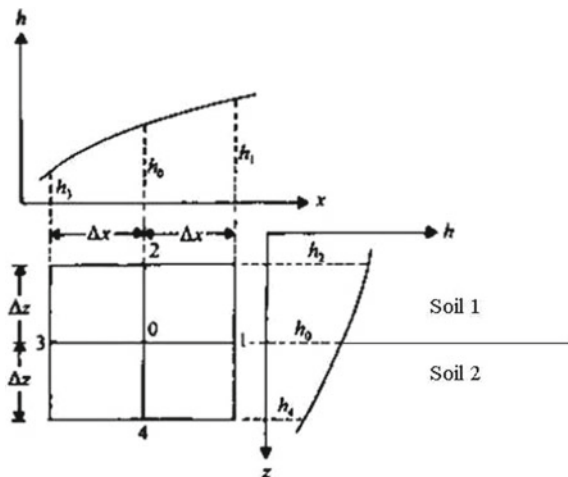
$$k_1 \cdot \frac{h'_4 - h_0}{\Delta z} = k_2 \cdot \frac{h_4 - h_0}{\Delta z} \tag{17}$$

or

$$h'_4 = \frac{k_2}{k_1} \cdot (h_4 - h_0) + h_0 \tag{18}$$

Therefore, from Eq. 15

Fig. 6 Hydraulic heads for flow in a region (Das [5])



$$\frac{k_1 + k_2}{2} \frac{h_1 + h_3 - 2h_0}{(\Delta x)^2} + k_1 \frac{h_2 + h'_4 - 2h_0}{(\Delta z)^2} = 0 \quad (19)$$

Taking $\Delta x = \Delta z$ and substituting the value of h'_4 in above equation,

$$h_0 = \frac{1}{4} \left(h_1 + \frac{2k_1}{k_1 + k_2} h_2 + h_3 + \frac{2k_2}{k_1 + k_2} h_4 \right) \quad (20)$$

6.1 Finite Difference Formulation 1D Consolidation for Layered Soil

Every time it may not be feasible to formulate a sealed-form result for consolidation in layered soils. Many a time, numerous variables are involved like the thickness of layers, different coefficients of permeability and differing coefficient of consolidation. Hence, numerical solutions are said to be a prudent method. If evaluation of surplus pore water pressure at the boundary of two dissimilar types (i.e. varying values of C_v) of clayey soils is involved, finite difference equations are altered to some degree. According to Terzaghi's consolidation theory:

$$\frac{k}{c_v} \frac{\partial u}{\partial t} = k \frac{\partial^2 u}{\partial z^2} \quad (21)$$

where

$$\begin{aligned} k \frac{\partial^2 h}{\partial z^2} &= k_1 \left[\frac{h_1 + h'_4 - 2h_0}{(\Delta z)^2} \right] \\ &= \frac{k_1}{(\Delta z)^2} \left[h_2 + \frac{k_2}{k_1} (h_4 - h_0) + h_0 - 2h_0 \right] \end{aligned}$$

On dividing and multiplying above equation with 2 and taking $(k_1 + k_2)$ common, then

$$k \frac{\partial^2 u}{\partial z^2} = \frac{1}{2} \left(\frac{k_1 + k_2}{(\Delta z)^2} \right) \left[\frac{2k_1}{k_1 + k_2} u_{1,t} + \frac{2k_2}{k_1 + k_2} u_{3,t} - 2u_{0,t} \right] \quad (22)$$

For the boundary element, average change in volume is

$$\frac{k}{C_v} \frac{\partial u}{\partial t} = \frac{1}{2} \left[\frac{k_1}{C_{v1}} + \frac{k_2}{C_{v2}} \right] \frac{1}{\Delta t} [u_{0,t+\Delta t} - u_{0,t}] \quad (23)$$

Therefore, from Eqs. 21, 22 and 23

$$\therefore u_{0,t+\Delta t} = \frac{\Delta t}{\Delta z^2} (k_1 + k_2) \left[\frac{2k_1}{k_1 + k_2} u_{1,t} + \frac{2k_2}{k_1 + k_2} u_{3,t} - 2u_{0,t} \right] + u_{0,t} \quad (24)$$

From the above equation, at the interface of two dissimilar types of soil at any $(t + \Delta t)$ time, we can calculate pore water pressure.

6.2 Problem Statement

The diagram shown in Fig. 7 depicts one-dimensional, nonlinear consolidation of double-layered clayey soil. In the same figure, $h_i =$ thickness of the clay layer i ($i = 1, 2$); $H = h_1 + h_2$, the total thickness of two clay layers; $q(t) =$ load applied on the top surface of the soil that is uniformly distributed. In the present study, h_1 and h_2 are considered as 4 m. The amount of the instant load over the top surface is equal to 100 kPa. Material properties used in the analysis are reported in Table 2.

Fig. 7 Double-layered soil system

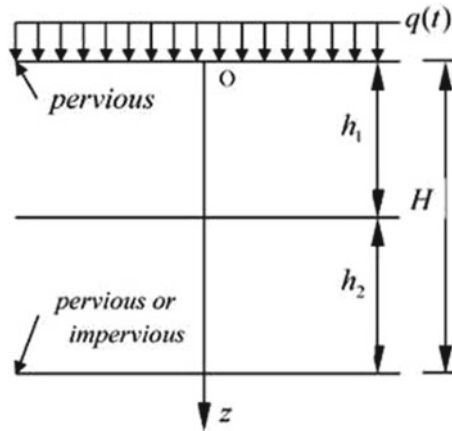


Table 2 Material properties

Layer	Depth (m)	Coefficient of permeability, k (m/sec)	Coefficient of consolidation, C_v (m ² /sec)	α
1	4.0	0.28×10^{-6}	7.25×10^{-5}	0.1
2	4.0	0.20×10^{-9}	8.44×10^{-9}	0.34

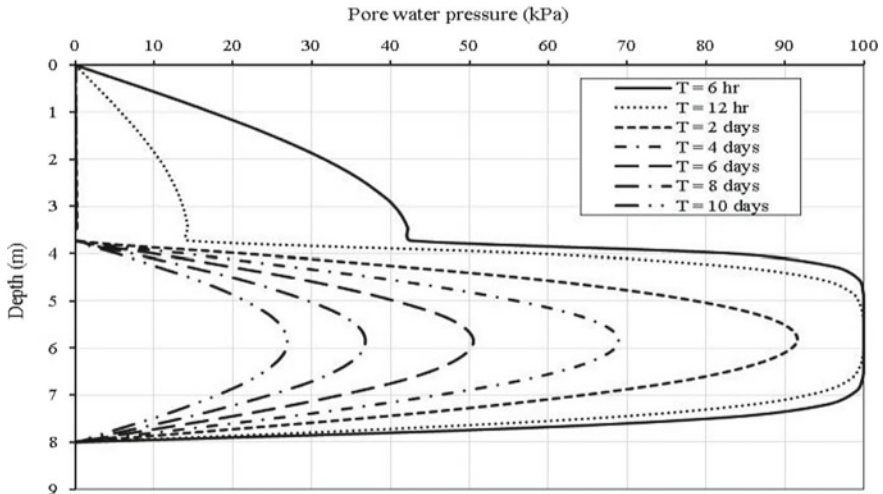


Fig. 8 Variation of pore water pressure with depth at various time

6.3 Variation of Pore Water Pressure and Coefficient of Consolidation C_v Temporally and Spatially

Figure 7 shows the variation of PWP with depth at various time. Layer 1 is sand (as its permeability is high) and Layer 2 is clay (due to low permeability in comparison with above layer). Top surface of Layer 1 is pervious and bottom surface of Layer 2 is pervious so it is the case of double drainage. From Fig. 8, it is clearly seen that Layer 1 pore water pressure dissipates rapidly due to high value of coefficient of permeability, but Layer 2 will take time to dissipate pore water pressure. It is observed from Fig. 8 that after 2 days Layer 1 is completely drained and pore water pressure along the depth is zero, but for Layer 2 as it is clay it takes large time to drain completely.

Figure 9 shows that C_v in Layer 1 is constant along the depth at various time, but at the interface of two soils (transition from Layer 1 to Layer 2), there is a sudden increase in the value of coefficient of consolidation (C_v). This is because at the interface of two soils, water from the Layer 2 at the top moves towards Layer 2, and when water reaches to a particular depth, it simply drains out from the top of Layer 1. In the Layer 2, pore water pressure is maximum at centre and decreases with time. As proved earlier, the coefficient of consolidation is inversely proportional to the pore water pressure; hence, C_v is minimum at the center, and it increases with time.

Figure 10 shows that in Layer 1 (Depth = 2.67 m), C_v is constant at any time, but for Layer 2 (Depth = 5.34 m) there is increment in C_v with increment in the time of consolidation. This is because the pore water pressure decreases with increase in time. Thus, C_v increases.

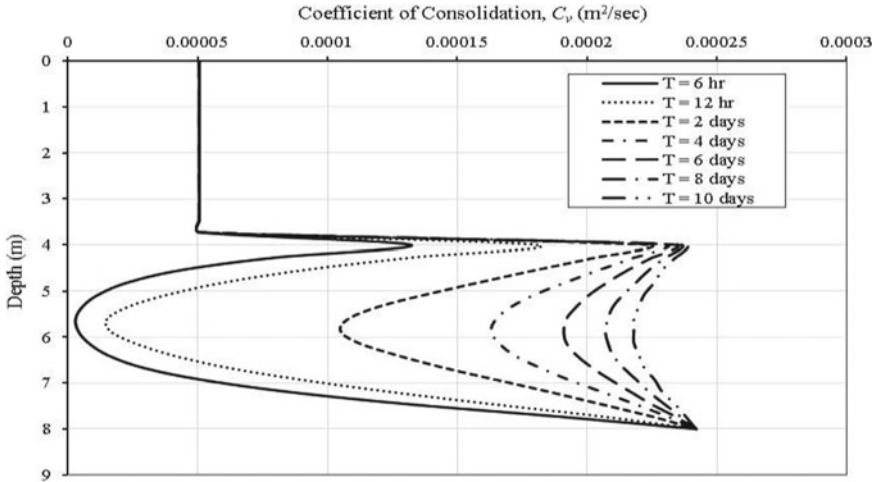


Fig. 9 Change in of coefficient of consolidation (C_v) with depth at different time period

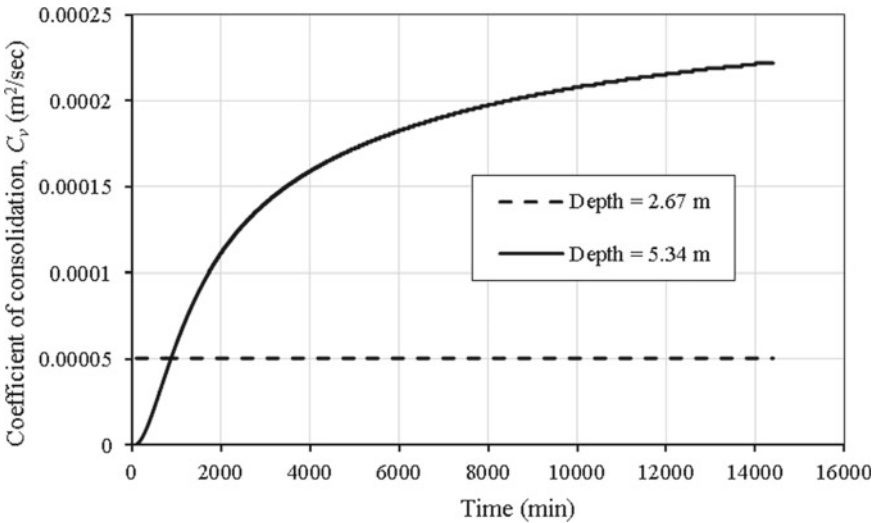


Fig. 10 Variation of coefficient of consolidation with time at various depths

7 Conclusion

The nonlinear theory specified by Abbasi et al. [4] for consolidation of soil while permitting for differences in coefficient of consolidation with time and space has been utilized in the present study. A finite difference approach that follows an iterative

technique to arrive at the result for the developed nonlinear principal equation was utilized. According to the results attained, the subsequent inferences are drawn:

- (a) At different times, all the consolidation characteristics of soil, i.e. degree of consolidation, pore pressure, coefficient of consolidation and time factor, can be simply evaluated at desired depth (and the average over depths) while using the numerical model.
- (b) For negative α values, consolidation is slower when compared with Terzaghi's solution, and for positive α values, consolidation is faster than anticipated from Terzaghi's solution.
- (c) As C_v increases, pore water pressure along the depth decreases.
- (d) As the value of C_v increases, time required for consolidation decreases because as we know from mathematical equation of C_v , it is directly related to coefficient of permeability (k).
- (e) For the selected relative C_v values, the reduction in the thickness of the lower layer (clay) has greater effect than decrease in the thickness of the upper layer (sand).
- (f) As the applied pressure increases, value of coefficient of consolidation increases at various depths.

References

1. Xie KH, Qi T, Dong YQ (2006) Nonlinear analytical solution for one-dimensional consolidation of soft soil under cyclic loading. *J Zhejiang University-Sci A* 7(8):1358–1364
2. Conte E, Troncone A (2006) One-dimensional consolidation under general time-dependent loading. *Can Geotech J* 43(11):1107–1116
3. Liu JC, Lei GH (2013) One-dimensional consolidation of layered soils with exponentially time-growing drainage boundaries. *Comput Geotech* 54:202–209
4. Abbasi N, Rahimi H, Javadi AA, Fagher A (2007) Finite difference approach for consolidation with variable compressibility and permeability. *Comput Geotech* 34(1):41–52
5. Das BM (2019) *Advanced soil mechanics*. CRC Press

1D Consolidation of Silty Clay Subject to Different Ramp Loadings



Sumanta Roy and Sibapriya Mukherjee

Abstract In engineering projects, soils are subjected to pre-loading and radial drainage to accelerate the process of consolidation. A comparative study for consolidation of silty clay under time-dependent ramp loadings is presented in this paper. The distribution of pore water pressure across the depth of a soil sample at various time intervals is computed numerically in MATLAB considering various ramp loadings. Finite difference method has been adopted for the analysis. Further, the characteristics of the consolidation under instantaneous loading and time-dependent loading are discussed. The results of this study present the magnitude of average of degree of consolidation of the soil at various time intervals for the respective time variant loading conditions. All of these are compared with a standard invariable load of same magnitude at those respective time intervals. Hence, the most effective loading procedure can be chosen from the results of this study which would result in the most efficacious consolidation in shortest time.

Keywords Consolidation · Isochrones · Pore pressure · Pre-loading

1 Introduction

The phenomenon of consolidation is one of the most fundamental aspects of geotechnical engineering and, if not dealt properly, might lead to catastrophic infrastructure failures due to abnormally large settlements. Consolidation is predominant in fine-grained soils. To accelerate the settlements, the commonly adopted engineering practices include the usage of vertical drains and pre-loading the soil and are often used in unison. In most projects, the surcharge loading is not applied instantaneously, instead gradually increased to the final load. This type of loading has been termed

S. Roy (✉) · S. Mukherjee
Jadavpur University, Kolkata 700032, India
e-mail: roysumanta47@gmail.com

S. Mukherjee
e-mail: sibapriya.mukherjee@jadavpuruniversity.in

as ramp loading. Pre-loading using sand bags is the most common example of this. Some studies for one-dimensional consolidation under time-dependent loading were reported by Darrag and El Tawil [2], Tang and Onitsuka [6], Conte and Troncone [1], Olson [3], Zhu and Yin [9], Rao and Raju [4], Vaziri and Christian [7], Wang et. al. [8], and Sun et al. [5]. This paper presents a numerical comparison between possible time-dependent ramp loadings, and from the results of this study, the most effective loading mechanism can be chosen which would result in the fastest consolidation.

Terzaghi's one-dimensional consolidation theory gives a quantitative relation between time t and excess pore water pressure u at any location within a saturated clay deposit subject to an initial excess pore water pressure u_0 due to some instantaneous load. This relationship is written as follows:

$$\frac{\partial u}{\partial t} = c_v \frac{\partial^2 u}{\partial z^2} \quad (1)$$

Equation (1) is a simple partial differential equation that relates the variation of pore water pressure along the depth of soil and across various time intervals. However, if the loading is not instantaneous, the partial differential equation to be considered is difficult to solve analytically. If sand drains are also introduced, then the equation would get more and more complex.

2 Problem Statement

The soil sample used in this study is fully saturated, homogeneous, and isotropic and represents silty clay behavior. The height of the soil sample is 4 m. It has coefficient of permeability $k = 1.5 \times 10^{-7}$ m/s and coefficient of consolidation $c_v = 0.1$ m²/month. A time varying load $q(t)$ acts on it, and it is singly drained (see Fig. 1).

The aim of soil pre-loading is to make it overconsolidated. It is a well-known fact that the closer we move to the ground surface, the higher the pre-consolidation pressure we get. This is because the top surface of the soil is almost always subjected to physical and chemical changes due to weathering and erosion and they tend to 'feel' less loaded compared to what they felt some thousand years ago. Hence, the soil sample used in the study shows characteristics found in soils very close to ground

Fig. 1 Soil specimen used for the study

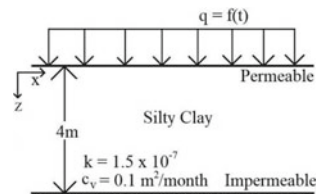


Fig. 2 Typical variation of effective stress and pre-consolidation pressure with depth below ground surface

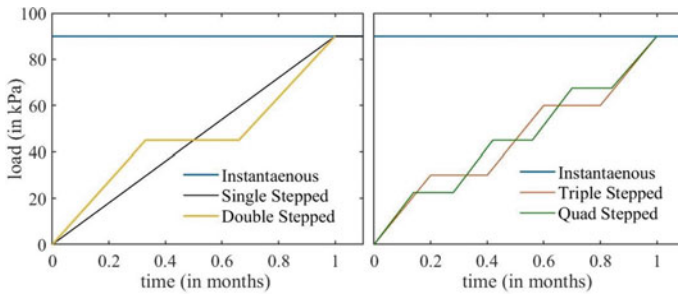
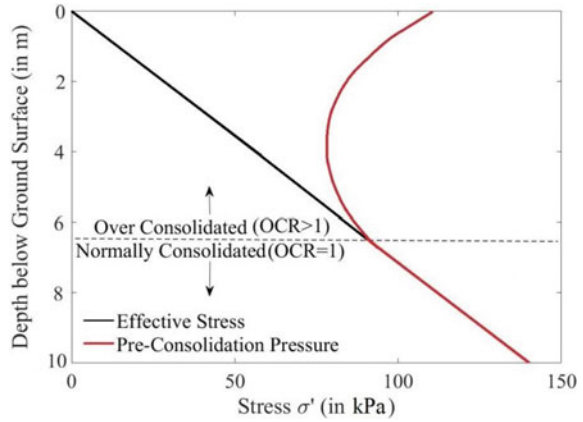


Fig. 3 Load versus time curves for the loading conditions used

surface and reflects overconsolidated behavior. This was done in order to mimic the effect of the pre-loading (see Fig. 2).

Four types of time-dependent loadings were used in this study. The first is a single stepped ramp loading where the load increases linearly from 0 to 90 kPa and then remains constant. The second is a double stepped ramp loading, where the load increases from 0 to 45 kPa, remains constant at 45 kPa for a time period, then increases linearly to 90 kPa, and remains constant after that. Two more types of ramp loading were also used where the load increased from 0 to 90 kPa in three and four steps, respectively (See Fig. 3).

3 Mathematical Solution

The non-homogenous partial differential equation used to solve the non-instantaneous loading is given below:

$$\frac{\partial(u - \sigma)}{\partial t} = c_v \frac{\partial^2 u}{\partial z^2} \quad (2)$$

where u = pore water pressure at a distance z from bottom and time t ; σ = surcharge at time t ; c_v = coefficient of consolidation (assumed constant over time); and z = distance from bottom of sample. The domain of u was discretized in two dimensions consisting of 36 rows and 1001 columns indexed by i and j , respectively, with i denoting the time axis having an interval of Δt and j denoting the depth axis having an interval of Δz . The finite difference approximations were plugged in Eq. (2), and equation obtained is shown below:

$$u_{i,j} = \frac{2c_v \Delta t}{\Delta z^2} (u_{i+1,j} + u_{i-1,j} - 2u_{i,j}) + u_{i,j} + \sigma_{j+1} - \sigma_j$$

The bottom layer is impervious; hence applying no flow boundary condition at the bottom layer ($u_{i+1,j} = u_{i-1,j}$), we get:

$$u_{i,j} = \frac{4c_v \Delta t}{\Delta z^2} (u_{i-1,j} - u_{i,j}) + u_{i,j} + \sigma_{j+1} - \sigma_j \quad (3)$$

The boundary conditions are as follows:

- $u_{0,j} = 0$, as the uppermost layer is in contact with the permeable surface; hence, any water molecule at this layer drains immediately.
- $u_{i+1,j} = u_{i-1,j}$ at the bottommost impermeable layer, as already discussed above, and Eq. (3) has to be used while iterating this layer.

The program was run on MATLAB, and the function was iterated till the solution converged within the tolerance limit of 10^{-4} . The results were stored in the u matrix. Each cell in the u matrix represents the value of pore water pressure at a depth (given by the row) and a time (given by the column). The vector corresponding to the last column of the u matrix gives the distribution of remaining excess pore pressures with depth at the time t used for that particular time analysis. Hence, a plot between remaining excess pore pressure versus depth can be drawn. This is done for time intervals: 1, 3, 6, 9, 12, 18, 24, 32, and 42 months, respectively. Each line is called an isochrone. Hence, a set of nine isochrones for the nine time intervals were plotted for each of the four loading conditions. The average degree of consolidation conforming to each isochrone, i.e., for each time interval, was calculated by numerically integrating the pore pressure vector via the Simpson's rule using the SIMPS function in MATLAB. This gave the area enclosed by the isochrone under the depth axis. Subtracting this area from the area enclosed by the isochrone at $t = 0$, taking a ratio of this value over the area enclosed by the isochrone at $t = 0$, and expressing it as a percentage, the average degree of consolidation was obtained. This is illustrated in the equation:

$$U(\%) = \frac{\int_{z=0}^{z=4} u(z)_{t=0} dz - \int_{z=0}^{z=4} u(z)_t dz}{\int_{z=0}^{z=4} u(z)_{t=0} dz} \times 100 \quad (4)$$

The terms used in Eq. (4) are $U(\%)$ = average consolidation at time t expressed as percentage and $u(z)_t$ = pore pressure at depth z at time t . This variation of average degree of consolidation with time was formulated and also presented in a tabular manner. It is to be noted that as time goes, the soil consolidates, the effective stresses increase, and the pore pressures as well as the soil voids decrease. Hence in reality, the coefficient of consolidation, permeability of soil, and some other soil properties changes. But, as the surcharge load applied is just 90 kPa and there is no radial drainage, the effect of the variability of soil parameters in this study would be inappreciable and hence neglected, and c_v and k have been assumed to remain constant.

4 Results and Inferences

Based on the methodology described in the previous section, Figs. 4, 5, 6, 7 and 8 show the nine isochrones in different colored lines in depth versus pore water pressure plots for instantaneous, single stepped, double stepped, triple stepped and quad stepped ramp loadings, respectively. As the soil sample taken is a single drained system, the layers immediately close to the topmost permeable layer (depth = 0) attain a value of zero pore water pressure immediately while the layers farther from the topmost permeable surface take more time to consolidate. For the sake of illustration, three particular time intervals are chosen from the nine isochrones, namely for 1, 24, and 32 months and have been tabulated in Tables 1, 2, and 3, respectively. The columns in these tables are nothing but the isochrones for each loading condition and for each time interval. It is very evident from the plots that introduction of ramp loading has a significant effect on the overall picture of consolidation. From the isochrones (in Figs. 4, 5, 6, 7 and 8), it is visible that, after 48 months, the pore pressure at the farthest point ($z = 4$) changes from 58.64 kPa to 55.45 kPa to 54.87 kPa to 54.12 kPa as one increases the ramp loading from one to four steps compared to a staggering 60 kPa for an instantaneous loading. Hence, introduction of ramp loading significantly accelerates the consolidation of the layer furthest away from the permeable boundary. However, with the increase of steps of the ramp loading, this improvement gets less pronounced.

There are some important features to be noted from the results. First, being the layers immediately close to the permeable boundary seems to consolidate better in case of an instantaneous loading compared to if it is done in steps. In fact, increasing the number of steps makes the soil layers close to the ground surface consolidate lesser and lesser. This is understood from Tables 1, 2, and 3. This is observed till a depth of 2 m, i.e., till the mid-point of the stratum. The only exception in this trend is the case of quad stepped loading, where the values suddenly decrease corresponding

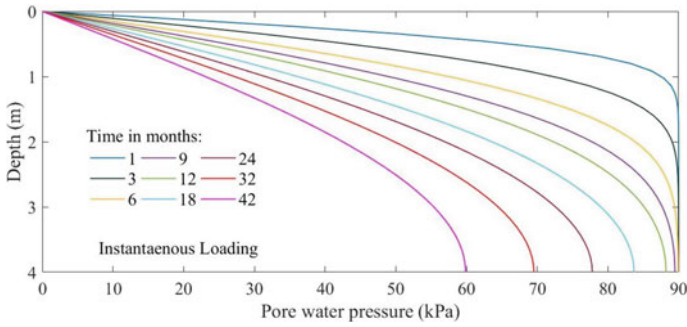


Fig. 4 Pore water pressure isochrones for an instantaneous loading

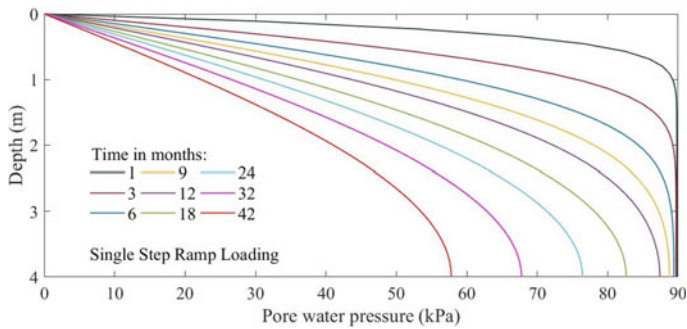


Fig. 5 Pore water pressure isochrones for a single stepped ramp loading

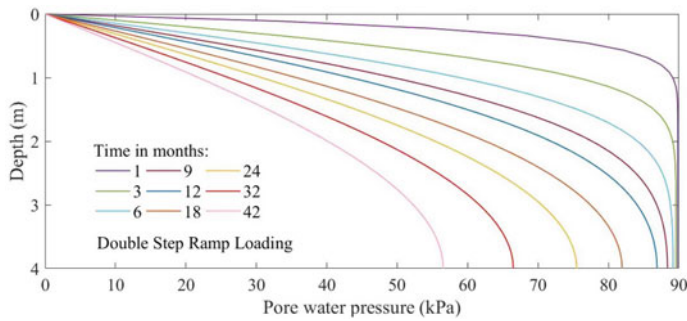


Fig. 6 Pore water pressure isochrones for a double stepped ramp loading

to depths less than 2 m, but this exception is visible only during the initial phases of consolidation, and as time goes on, usual trend is restored. The second most interesting observation is not only instantaneous loading consolidates soils better than ramped loadings at positions relatively close to the permeable layer, but a similar kind of nature is observed in the average degree of consolidation trend too (see

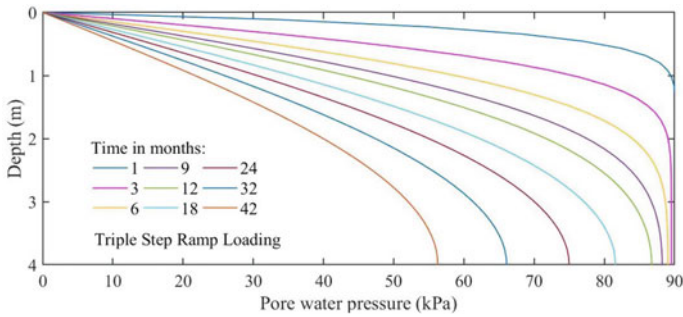


Fig. 7 Pore water pressure isochrones for a triple stepped ramp loading

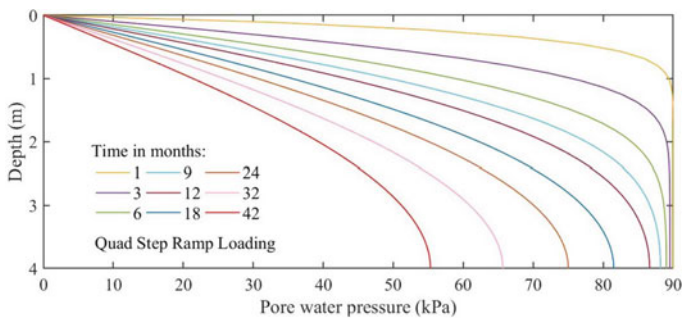


Fig. 8 Pore water pressure isochrones for a quad stepped ramp loading

Table 1 Depth (in m) versus pore pressure (in kPa) variation after 1 month

Depth Z (in m)	Single step	Double step	Triple step	Quad step	Instantaneous
0.5	76.72642	76.92326	76.98322	76.81455	62.40126
1	89.34822	89.25754	89.58732	89.45919	87.94371
1.5	89.80469	89.84317	90.12892	89.98012	89.89504
2	89.82009	89.86514	90.14987	89.99987	89.99909
2.5	89.82018	89.86527	90.0000	90.00000	89.99999
3	89.82018	89.86527	90.0000	90.00000	90.00000
3.5	89.82018	89.86527	90.0000	90.00000	90.00000
4	89.82018	89.86527	90.0000	90.00000	90.00000

Fig. 9). At initial stages, the average degree of consolidation is greater in case of instantaneous loadings compared to other ramp loadings. But this trend quickly disappears approximately after 6 months and the ramp loadings take over. This is a very striking feature and may be attributed to the effect of ‘effective stress lock-ins’ in the initial stages because of the impulsive nature of instantaneous loading. This is

Table 2 Depth (in m) versus pore pressure (in kPa) variation after 24 months

Depth Z (in m)	Single step	Double step	Triple step	Quad step	Instantaneous
0.5	14.64266	14.45815	14.35759	14.36579	14.23758
1	31.95194	31.54990	31.33168	31.34870	31.39391
1.5	44.31327	43.75669	43.45612	43.47824	43.95465
2	57.23059	56.51370	56.12951	56.15520	56.11389
2.5	65.24825	64.43272	63.99840	64.02504	66.30613
3	72.23256	71.33182	70.85532	70.88171	73.46295
3.5	75.39808	74.45900	73.96392	73.98981	76.71432
4	76.44777	75.49601	74.99487	75.02052	77.79368

Table 3 Depth (in m) versus pore pressure (in kPa) variation after 32 months

Depth Z (in m)	Single step	Double step	Triple step	Quad step	Instantaneous
0.5	12.42444	12.18662	12.11335	12.03944	10.76775
1	27.25763	26.73638	26.57572	26.41278	23.67954
1.5	38.05319	37.32634	37.10222	36.87338	33.15450
2	49.63144	48.68507	48.39308	48.09195	43.42897
2.5	57.03557	55.9495	55.61427	55.26575	58.48198
3	63.66865	62.45802	62.08415	61.69225	65.30262
3.5	66.74399	65.47582	65.08409	64.67172	68.46727
4	67.77463	66.48721	66.08949	65.67021	69.52820

a very interesting finding from this study and opens up a lot of scope for research. The average degree of consolidation for ramp loadings gets significantly larger than instantaneous loading as time goes on; however, this trend is not so pronounced when compared between the ramp loadings. Still, a slight inference that can be drawn from the curves is that the variation between two, three, and quad stepped ramp loadings is quite insignificant, but together they vary quite appreciably compared to single stepped ramp loading.

5 Conclusions

The following conclusions may be drawn from the present study:

1. Instantaneous loading consolidates soil better than ramp loading at depths close to the permeable layer. In fact, increasing the number of steps in ramp loading makes the soil layers close to the ground surface consolidate lesser and lesser.

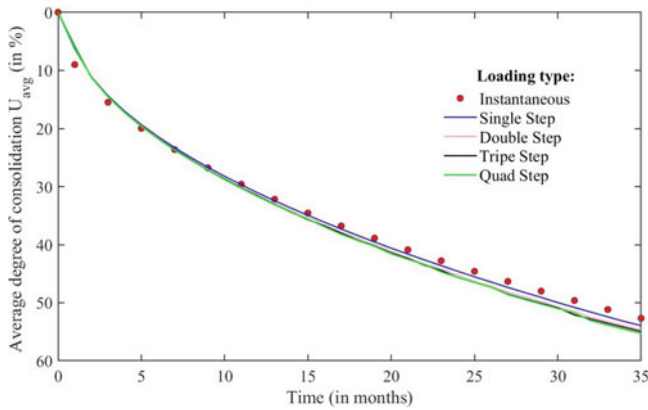


Fig. 9 Average degree of consolidation of the soil specimen U_{avg} (in %) versus time (in months) for the loading envelopes

The only exception in this trend is the case of quad stepped loading, where the pore pressure values suddenly decrease corresponding to depths less than 2 m, but this exception is visible only during the initial phases of consolidation, and time goes on, usual trend is restored.

2. At depths far away from the permeable layer, ramp loading consolidates soil significantly better than instantaneous loading, and among the ramp loadings, increasing the number of steps in ramps further improves the consolidation. But this difference gets less pronounced as the number of steps is increased more and more.
3. At initial stages of consolidation, particularly in this case up to six months, the average degree of consolidation for instantaneous loading is greater compared to ramp loadings. This is one of the most interesting findings from the study and opens up scope for a lot of research.
4. The average degree of consolidation for ramp loadings gets significantly larger than instantaneous loading as time goes on; however, this trend is not so pronounced when compared between the ramp loadings but overall, the highest efficiency is displayed by quad stepped ramp loading at any time beyond six months.

References

1. Conte E, Troncone A (2009) Radial consolidation with vertical drains and general time-dependent loading. *Can Geotech J* 46(1):25–36
2. Darrag A, El Tawil M (1993) The consolidation of soils under stochastic initial excess pore pressure. *Appl Math Model* 17(11):609–612
3. Olson R (1977) Consolidation under time dependent loading. *J Geotech Eng Div* 103(1):55–60

4. Rao K, Raju M (1990) One-dimensional consolidation with three-dimensional flow for time-dependent loading. *J Geotech Eng* 116(10):1576–1580
5. Sun M, Zong M, Ma S, Wu W, Liang R (2018) Analytical solution for one-dimensional consolidation of soil with exponentially time-growing drainage boundary under a ramp load. *Math Probl Eng* 2018:1–10
6. Tang X, Onitsuka K (2000) Consolidation by vertical drains under time-dependent loading. *Int J Numer Anal Meth Geomech* 24(9):739–751
7. Vaziri H, Christian H (1994) Application of Terzaghi's consolidation theory to nearly saturated soils. *Can Geotech J* 31(2):311–317
8. Xie K, Wang K, Chen G, Hu A (2008) One-dimensional consolidation of over-consolidated soil under time-dependent loading. *Front Archit Civil Eng China* 2(1):67–72
9. Zhu G, Yin J (1998) Consolidation of soil under depth-dependent ramp load. *Can Geotech J* 35(2):344–350

Assessment of Effective Shear Strength Parameters in Triaxial CU Shear Test



Suresh Maurya

Abstract Test condition and shear strength parameters should be chosen to represent the field conditions as closely as possible. To stimulate the field condition, triaxial shear test was conducted with consolidated-undrained (CU) method on MI (inorganic silt of medium plasticity) type of soil. Laboratory specimens were remoulded at 98% of maximum dry density (MDD) at varying water content. Remoulded specimens were further saturated without any volume change with the help of back pressure system in the triaxial machine. The deviator stress vs. strain graphs and pore water pressure vs. strain graphs are plotted at incremental confining pressures (σ_3) and analysed at different remoulded water content (w). The difference in deviator stress and pore water pressure obtained between the specimens at respective confining pressures seems to be very less, which suggests that difference in the water deficiency between the specimens and the consequent pore water tension is greatly reduced after saturation. The maximum stresses obtained are also employed to understand modified failure envelopes and shear strength parameters with respect to total and effective stress measurement. The total angle of internal friction (ϕ) obtained is lower than the effective angle (ϕ'), whereas cohesion (c) obtained is higher than effective cohesion (c'). The difference in the results suggests that effective stress analysis should be preferred, as it is more rational. This study helps to compare the results of total and effective stress analysis and how pore water pressure (u) plays an important role in effective stress analysis.

Keywords Water content · Shear strength · Effective · Deviator stress

1 Introduction

Shear strength is the basic strength properties of soil which controls the stability of a soil mass under loads. Strength may decrease significantly under rainfall conditions, surface water infiltration or groundwater rising. All the problems of soil engineering

S. Maurya (✉)
CSMRS, M/o Jal Shakti, D/o WR, RD & GR, New Delhi, India
e-mail: maurya_suresh@yahoo.co.in

© The Author(s), under exclusive license to Springer Nature Singapore Pte Ltd. 2023
A. K. Agnihotri et al. (eds.), *Proceedings of Indian Geotechnical and Geoenvironmental Engineering Conference (IGGEC) 2021, Vol. 1*, Lecture Notes in Civil Engineering 280,
https://doi.org/10.1007/978-981-19-4739-1_14

151

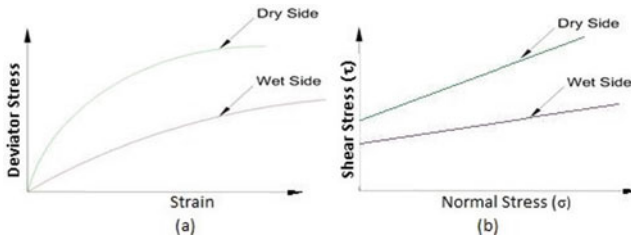


Fig. 1 Typical deviator stress–strain curves and failure envelopes [1]

are related in one way or the other to shear strength of the soil. The shear strength is influenced by soil density, mineralogy, grain size, shape of particle and drainage condition. If the density of sample is more, the shear strength also increases. When clay is dominant in soil mass, the maximum shear strength is taken by cohesive force ‘ c ’, and when sand is dominant in soil mass, then the maximum shear strength is taken by angle of internal friction (ϕ). The test results may vary and depend largely on the drainage condition, and therefore, adopting or simulating the field drainage condition in laboratory can yield better results. The water content at which the soil is compacted in the field is controlled by the value of the optimum moisture content (OMC) determined by the laboratory compaction test. The soils compacted dry of the optimum have a steeper deviator stress–strain curve than those on the wet side (see Fig. 1a). The modulus of elasticity for the soils is therefore high. Such soils have brittle failure like dense sands or over-consolidated clays. The soils compacted wet of the optimum have relatively flatter stress–strain curve and lower value of modulus of elasticity. The failure in this occurs at a large strain and is of plastic type [1].

1.1 Shear Strength at Moulded Water Content

When two samples are compacted to the same dry density (one dry of optimum and other wet of the optimum) and tested for shear strength, the soils compacted dry of the optimum have a higher shear strength at low strains. Figure 1b shows the Mohr–Coulomb strength failure envelopes. However, at large strains, the flocculated structure for the soils on the dry side is broken and the ultimate strength is approximately equal for both the samples. On the wet side, compaction induces large shear strains, and the shear strength is further reduced due to greater orientation towards a dispersed structure. To avoid large expansion and swelling pressure, cohesive nature of soils in such cases is generally compacted at a water content more than the OMC with the resulting dry density less than the MDD. The clayey soil in the impervious core of an earth dam is also compacted on the wet side of the optimum to reduce swelling pressure. Likewise, the soil in the outer shells of earth dams is compacted dry of the optimum to obtain high shear strength, high permeability and low pore pressure.

1.2 Shear Strength After Saturation

Two samples are compacted to the same dry density, one dry of the optimum and the other wet of the optimum, and then soaked in water, without any volume change, to have full saturation. The samples compacted dry of the optimum will show greater strength. However, the difference in the strength of the two samples will be much smaller than that prior to saturation. The difference in the water deficiency of the two samples and the consequent pore water tension is greatly reduced after saturation. If swelling is permitted during saturation, the difference in strength of the two samples is further reduced. As it is difficult to determine accurately the effective stresses in partially saturated soil, it is common practice to draw the failure envelope in terms of total stresses. When initial degree of saturation is increased, the shear stress to cause failure is decreased as shown in Fig. 2. For a fully saturated soil, the total stress failure envelope is horizontal. The triaxial tests are conducted simulating the field conditions. However, an actual soil deposit in field may not remain unsaturated if it has an access to water. For such a case, the soil sample is saturated in the laboratory, and undrained shear strength in saturated conditions should be determined [2].

2 Use of Mohr–Coulomb Failure Theory in the Study

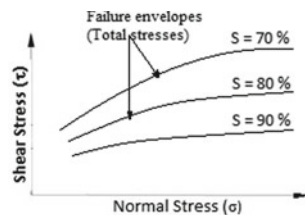
Mohr–Coulomb failure theory is a valuable function in analysis of the shear strength. Failure criterion is written in terms of principal stresses (σ_1 and σ_3). According to Mohr, the failure is caused by a critical combination of the normal and shear stress. Figure 3 shows Mohr’s graphical representation of stresses when a soil element is subjected to principal stresses (σ_1 and σ_3).

Mohr–Coulomb failure envelope is represented by a straight line. It represents shearing resistance of soil linearly related to ‘ σ ’. Here ‘ c ’ equals to the intercept on r -axis, and ‘ ϕ ’ is the angle that the envelope makes with the σ -axis.

$$\text{Total shear strength, } \tau = c + \sigma \tan \phi \tag{1}$$

Effective stress state. The total shear strength parameters, i.e. c and ϕ , represent the failure condition for a particular soil under given conditions. These parameters indicate the intercept and slope of the failure envelope, respectively. The actual

Fig. 2 Failure envelopes for different degree of saturation (S) [2]



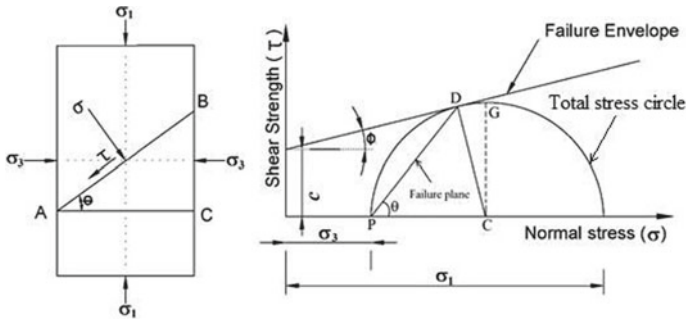


Fig. 3 Mohr's graphical representation of stresses [3]

stresses which control the shear strength of a soil are the effective stresses. Thus, Eq. (1) is modified and represented in terms of effective stresses in Eq. (2) and is known as revised Mohr–Coulomb equation for the shear strength of the soil. It is one of the most important equations of soil engineering [1].

$$\tau' = c' + \sigma' \tan \phi' \quad (2)$$

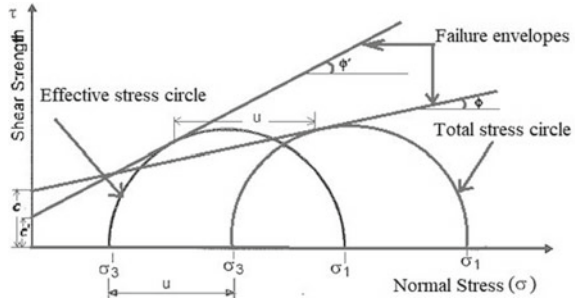
where c' and ϕ' are the effective shear strength parameters (also called the effective cohesion and effective angle of shearing resistance, respectively); σ' is the effective normal stress, written as ($\sigma' = \sigma - u$). The stress state can be defined in terms of effective stress where pore water pressure (u) can be estimated. Considering the principal stresses σ_3 and σ_1 and pore pressure in the soil, the stress circle and failure envelopes in terms of total and effective stresses are shown in Fig. 4. Based on Fig. 4, one can emphasize two points:

- The effective stress circle is moved to the left, relative to the total stress circle of a value equal to the pore pressure, i.e. pore pressure acting hydrostatically, and reduces normal stresses equally in all planes. In case of negative pore pressures, the circle moves to the right.
- The shear stresses on any plane are independent of pore pressure, because the water does not transmit shear stress. The shear stresses are due only to the difference between the principal stresses, and this difference is the same in both total and effective stress.

3 Choice of Test Conditions and Scope of Study

Test conditions should be chosen to represent the field conditions as closely as possible. In case of fine-grained soils, drainage takes place very slowly, and there is chance of pore water to develop during loading. Immediately after the application of the load, undrained conditions are suitable. Consolidated-undrained (CU) tests are

Fig. 4 Pore water pressure (u) effect on stress state of soil [1]



required for the cases when the soil gets consolidated under a certain loading, and then additional load is applied; for example, in the case of earth dams, wherein the soil gets consolidated under self-weight before the reservoir is filled and the water pressure causes additional stresses. Laboratory study to assess the shear strength of the compacted soil remoulded at 98% MDD under varying water content and further allowing remoulded soil to undergo saturation with the help of back pressure may represent the similar behaviour of earth dam, wherein the soil gets consolidated and undergoes additional stresses.

To realize the effect of saturation, consolidation and additional stresses on the soil, field conditions are simulated in triaxial shear test with consolidated-undrained (CU) method on MI type of soil. The deviator stress (σ_d)–strain (ϵ) graphs and pore water pressure, PWP (u)–strain (ϵ) graphs are plotted at incremental confining pressures (σ_3) and analysed at different remoulded water content (w). This paper discusses the results of modified failure envelope and shear strength parameters with respect to total and effective stress measurement.

4 Experimental Work

The basic physical and mechanical properties of soil are presented in Table 1. To study the variation between total and effective shear strength parameters, two samples with different water content were prepared from same type of soil. Samples were prepared with the water content as given in Table 2.

Four identical specimens from each samples having varying water content (see Table 2) were remoulded in a standard sample mould at 98 % of standard proctor density for a set of tests. The specimen is prepared into a cylindrical shape with a diameter of 38 mm and height of 76 mm by means of mould. Height-to-diameter ratio of 2 is maintained for all sample specimen as per IS code [4]. It is also ensured that ratio of diameter of specimen to maximum particle size should not be less than 5. Pictures of standard sample mould and specimen are shown in Fig. 5. Cylindrical specimen along with filter paper and porous stone is placed between rigid caps,

Table 1 Basic physical and mechanical properties of soil

Physical properties						Value
BIS classification						MI
Atterberg limits (LL, PL, PI)						(42.8, 29.2, 13.6)
Specific gravity (G)						2.73
Maximum dry density (MDD/ $\gamma_d(\max)$)						1.65 g/cc
Optimum moisture content (OMC)						20.4%
<i>Mechanical analysis</i>						
Clay: 0.002 mm and less	Silt: 0.002 to 0.075 mm	Fine sand: 0.075 to 0.425	Medium sand: 0.424 to 2.0 mm	Coarse sand: 2.0 to 4.75 mm	Gravel: 4.75 mm & above	
28.8%	49.6%	5.6%	8.8%	7.2%	0%	

Table 2 Water content of samples

Sample No.	Water content of samples, w (%)
1	23.62
2	25.18

covered with latex membrane and secured with rubber O-ring. Transparent perspex cylinder is then secured on a triaxial cell apparatus which is filled with water.

All the remoulded specimens were measured for their initial degree of saturation in the triaxial cell. On measurement, specimens exhibited B-factor less than 0.9. To cover up deficiency in saturation without disturbing any volume change, specimens were further fully saturated in a controlled manner with the help of back pressure system.

Importance of back pressure and measurement of B-factor. It becomes a difficult task to force the air out beyond OMC and also at the same time remould the sample between OMC and SMC with respect to maximum dry density. At OMC, the air voids attain approximately a constant volume. With further increase in water content, the air voids do not decrease, but the total voids (air plus water) increase and dry density may decrease. Back pressure plays an important role in increasing degree



Fig. 5 Specimen preparation

of saturation without disturbing internal structure of soil. B-factor is defined as the ratio of increase in pore water pressure to the increase in cell pressure.

Specimens exhibiting B-factor less than 0.9 imply that pore space contains some air which on further application of load to the specimen compresses and causes volume change in the specimen, thereby damaging the internal structure of soil. By steady application of back pressure in the triaxial machine, the air gets compressed and dissolved in pore water smoothly, and one can ensure that the soil is fully saturated. This can be tested by measuring the B-factor of the soil. Back pressure may be continued to be increased until B-factor exhibits the value of 1.0 preferably but not less than 0.9 as per IS 2720-Part 12 [4]. Back pressure should be applied in small steps of about 0.5 kg/cm^2 so as to avoid creating stress concentration in soil specimen.

Pore water pressure measurement. Pore water pressure measurement is made with the help of pressure gauge which should have a least count of at least 0.1 kg/cm^2 . The crucial requirement for the pore water pressure measuring system is that it shall be able to measure the pore water pressure under undrained condition; that is, water should neither flow out of the soil sample nor flow into it during the process of measurement. This is ensured by completely de-airing the drainage and back pressure line, the pore pressure measurement line, the tubing (non-expansive annealed tube) and the connectors.

5 Testing Machine and Methodology of Test

To study the variation between total and effective shear strength parameters, series of triaxial tests were conducted as per IS 2720-Part 12 [4] in semi-automatic triaxial compression machine. In doing so, consolidated-undrained (CU) test was carried out at incremental confining pressures (σ_3) of 1 kg/cm^2 , 2 kg/cm^2 , 3 kg/cm^2 and 4 kg/cm^2 to obtain failure envelopes in terms of total stress and effective stresses.

5.1 Testing Machine

Semi-automatic triaxial compression machine consists of a strain-controlled loading frame, a triaxial cell set-up and pressure chambers. Machine is attached with read-out devices like load cell, LVDT and pressure transducer for measuring load, strain and stress, respectively. All the three read-outs devices are connected to the data acquisition system (DAS) which is interfaced with a computer system. Figure 6 shows the semi-automatic triaxial machine set-up in CSMRS, New Delhi. Triaxial laboratory consists of four machines in one row to test the specimens at four different confining pressures.

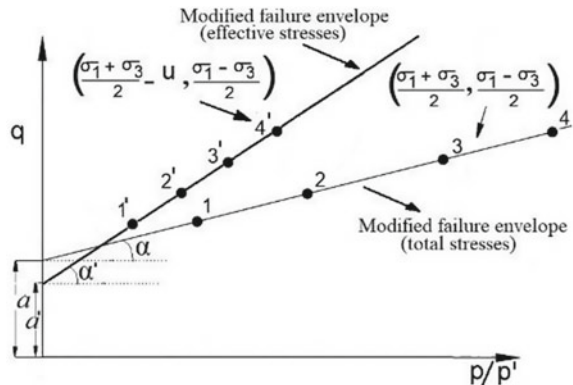
Fig. 6 Semi-automatic triaxial machine in CSMRS, New Delhi



5.2 Methodology of Test

Laboratory specimens were remoulded at 98 % of MDD at varying water content. Due to the measurement of B-factor value less than 0.9, remoulded specimens were further saturated with the help of back pressure system in the triaxial machine. After the specimen is saturated exhibiting B-factor greater than 0.9, it is tested in two stages in triaxial CU test, i.e. consolidation stage and shear stage. Four different confining pressures (σ_3) at 1 kg/cm², 2 kg/cm², 3 kg/cm² and 4 kg/cm² were applied to specimens to accomplish 95 % consolidation. In the shear stage, when the deviator stress attained a peak value, it is considered that the specimen has failed. We get peak stress and respective pore water pressure (u) for all the samples tested at incremental confining pressures (σ_3). Results are plotted, and total shear strength parameters (c and ϕ) and effective shear strength parameters (c' and ϕ') are determined from the best fit line of respective modified failure envelopes of total and effective stresses (see Fig. 7).

Fig. 7 Modified failure envelopes, (p/p' - q plot)



In case of total stress analysis, the coordinates of the top points of the Mohr circle correspond to the maximum stresses and are represented as p and q which are greater than the shear stresses on the failure plane. The failure envelope (Mohr envelope) gives the shear stresses on the failure planes, which are represented by the point of tangency, whereas modified failure envelope joins the point of maximum shear stresses at failure.

$$\text{where } p = \frac{(\sigma_1 + \sigma_3)}{2} \text{ and } q = \frac{(\sigma_1 - \sigma_3)}{2} \quad (3)$$

Line drawn through points 1, 2, 3 and 4 (see Fig. 7) makes an angle α with the p -axis and an intercept a on the q -axis and has the line equations as $q = a + p \tan \alpha$. Comparing with the Coulomb equation of $r = c + \sigma \tan \phi$, the values of shear strength parameters c and ϕ are obtained from the intercept a and the slope α , using below equations.

$$c = \frac{a}{\cos \phi} \text{ and } \phi = \sin^{-1}(\tan \alpha) \quad (4)$$

In case of effective stress analysis, normal stress ($p' = p - u$) is reduced by pore water pressure and shear stress is independent of pore pressure, and therefore, modified failure envelope for effective stresses gets shifted by an amount, u (see Sect. 3). The coordinates of these new top points of the Mohr circle are represented as p' and q . Top points (i.e. 1', 2', 3' and 4') are joined to get angle α' and intercept a'

$$\text{Where } p' = \frac{(\sigma_1 + \sigma_3)}{2} - \mu \text{ and } q = \frac{(\sigma_1 - \sigma_3)}{2} \quad (5)$$

The values of parameters c' and ϕ' are obtained from the intercept a' and the slope α' , using below equations.

$$c' = \frac{a'}{\cos \phi'} \text{ and } \phi' = \sin^{-1}(\tan \alpha') \quad (6)$$

6 Results and Discussion

Deviator stress vs. strain graphs and pore water pressure vs. strain graph obtained from experimental work for incremental confining pressures (σ_3) at different water content, w , (%) are shown in Figure 8. Each sample is tested at four different confining pressures of 1 kg/cm², 2 kg/cm², 3 kg/cm² and 4 kg/cm². Because of relative complexity of the test, inconsistent graphs were omitted, and minimum three readings [5] of different confining pressures were considered to plot the failure envelopes.

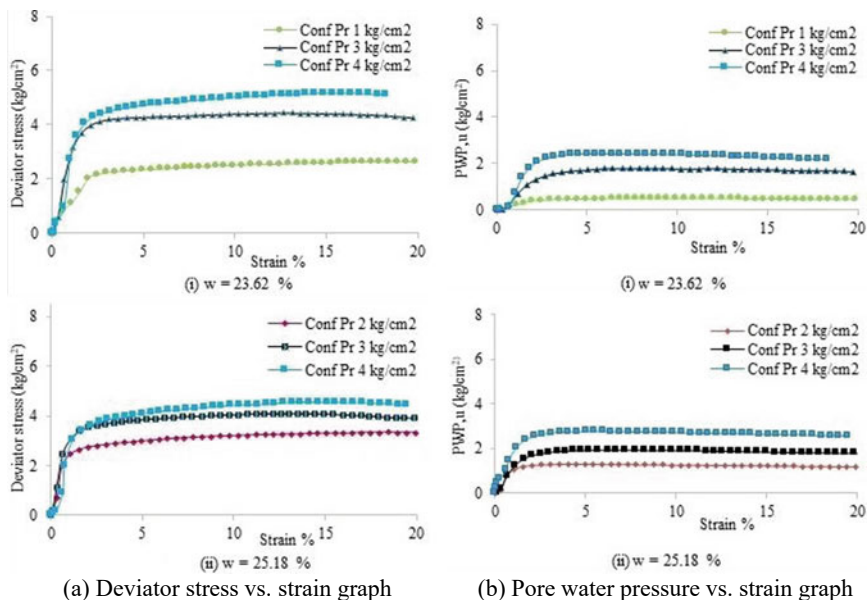


Fig. 8 Deviator stress versus strain graph and pore water pressure versus strain graph obtained for experimental work at varying moisture content (i) 23.62% and (ii) 25.18%

At confining pressure of 1 kg/cm², the deviator stress to cause failure is in the range of 2.4–2.6 kg/cm² and pore water pressure exerted is in the range of 0.44–0.47 kg/cm². At higher confining pressure of 4 kg/cm², the deviator stress to cause failure is in the range of 4.5–5.1 kg/cm² and pore water pressure exerted is in the range of 2.23–2.67 kg/cm². The difference in the deviator stress between the specimens seems to be less in respective cases of confining pressure, which suggests that difference in the water deficiency between the specimens and the consequent pore water tension is greatly reduced after saturation.

Maximum normal stress (p/p') and maximum shear stress (q) values are calculated using Eqs. (3) and (5), and modified failure envelopes for total and effective stresses are plotted as shown in Figure 9.

Shear strength parameters are obtained from the intercept and slope of modified failure envelopes using Eqs. (4) and (6) and are given in Table 3. It is observed that the total angle of internal friction (ϕ) obtained is much lower than the effective angle (ϕ'), whereas cohesion (c) obtained is higher than effective cohesion (c').

7 Conclusions

The maximum stresses obtained for MI type of soil are employed to understand modified failure envelopes and shear strength parameters with respect to total and

Fig. 9 p/p' - q plot

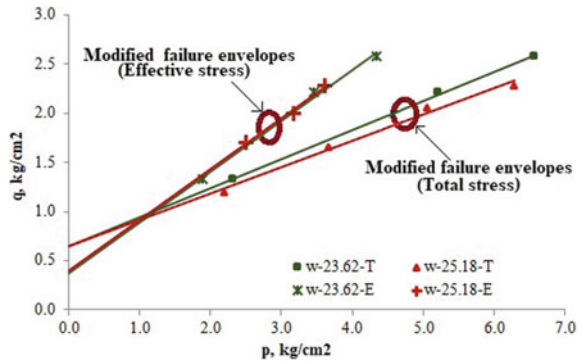


Table 3 Shear strength parameters

Sample No.	Moisture content, w (%)	Stress analysis	c (kg/cm ²)	ϕ (Deg)
1	23.62	Total stress	0.67	17
2	25.18		06.7	15
1	23.62	Effective stress	c' (kg/cm ²)	ϕ' (Deg)
2	25.18		0.44	31
			0.46	31

effective stress measurement. The study helps in comparing the results of total and effective stress analysis. From the results, it is observed that the total angle of internal friction (ϕ) obtained is lower than the effective angle (ϕ'), whereas cohesion (c) obtained is higher than effective cohesion (c'). The difference in the results suggests that effective stress analysis should be preferred, as it is more rational and it gives the closer indication to achieve real factor of safety. The difference in deviator stress and pore water pressure obtained between the specimens at respective confining pressures is much smaller. This implies that difference in the water deficiency between the specimens and the consequent pore water tension is greatly reduced after saturation. Achievement of full saturation by the normal procedure is not always necessary or not desirable. Soils are nominally saturated initially, the degree of saturation should be checked as a standard practice, and further saturation is to be applied in a controlled manner with the help of back pressure [3].

It may be emphasized that shear strength parameters do not have unique values for a given soil. These parameters are meaningless unless drainage conditions, type of strength envelope, normal stress range, etc., are considered. Selection of these parameters will depend upon the field conditions and the type of analysis.

Disclaimer

MI type of soil is selected in the study as illustration to explain total and effective stress analysis. Tests are conducted on limited samples. More experiments are required to be done to establish the results.

References

1. Punmia BC, Jain AK, Jain AK (2017) soil mechanics and foundation, 17th edn. Laxmi Publication, New Delhi
2. Arora KR (2003) Soil mechanics and Founsation engineering, 6th edn. Standard Publisher, New Delhi
3. Head KH (1998) Manual of soil laboratory testing volume 3: effective stress tests, 2 ed. Published by John Wiley & Sons Ltd, England
4. IS 2720-Part 12: Determination of shear strength parameters of soil from consolidated undrained triaxial compression test with measurement of pore water pressure. Bureau of Indian Standards, New Delhi (2016)
5. Head KH (1994) Manual of soil laboratory testing volume 2: permeability, shear strength and compressibility tests, 2 ed. Halsted Press: an imprint of John Wiley & Sons, Inc., New York-Toronto

Geotechnical Properties of Copper Slag, Rice Husk Ash Blended with Lime, Cement and Geopolymer—A Comparative Study



Kuldeep Sharma and Arvind Kumar

Abstract A total of 98 experimental test results have been compared on different mixes of Copper Slag (CS), Rice Husk Ash (RHA), Lime (L), Cement (C), and Alkali Activator (AA) in order to evaluate Specific Gravity (SG) and compaction properties of these mixes. Hydrated lime, ordinary Portland cement of 43—Grade were used in this study. Sodium Silicate (SS) and Sodium Hydroxide (SH) solutions were used as activators with alkali activator ratio of 2.5 SS/SH and concentration of SH 10 M (morality) solution. The SG and compaction tests have been performed using a Pycnometer and Modified Proctor Compaction (MPC) tests. Based on the experimental results mathematical models have been constructed to estimate predicted values of SG, Maximum Dry Density (MDD), and Optimum Moisture Content (OMC). SPSS software and Microsoft Excel were used to develop mathematical models and to analyze the data. The maximum value of SG obtained was 3.37 for the combination of 95% CS + 5% RHA; the minimum SG value was obtained as 2.17 for the mix proportion of 56% CS + 35% RHA + 9% AA. Compared to all the combinations the mix with 93% of copper slag, 5% of rice husk ash, 1% of lime, and 1% of cement has shown the highest value of MDD and OMC of about 2.64 g/cc and 9.86%, respectively. These combinations may be used in highway construction, as earth filling material, construction of embankments, etc. as per Indian road congress (IRC) guidelines.

Keywords Compaction · Specific gravity · Lime · Cement · Alkali activator · MLRA

K. Sharma (✉) · A. Kumar
Department of Civil Engineering, Dr. B. R. Ambedkar National Institute of Technology,
Jalandhar, Punjab 144011, India
e-mail: kuldeepsha333@gmail.com

A. Kumar
e-mail: agnihotriak@nitj.ac.in

© The Author(s), under exclusive license to Springer Nature Singapore Pte Ltd. 2023
A. K. Agnihotri et al. (eds.), *Proceedings of Indian Geotechnical and Geoenvironmental Engineering Conference (IGGEC) 2021, Vol. 1*, Lecture Notes in Civil Engineering 280,
https://doi.org/10.1007/978-981-19-4739-1_15

Abbreviations

AA	Alkali activator
C	Cement
CS	Copper slag
FA	Fly ash
IRC	Indian road congress
L	Lime
M	Molarity
MDD	Maximum dry density
MPC	Modified Proctor compaction
Ms	Activator modulus ratio
OMC	Optimum moisture content
PA	Pond ash
RHA	Rice husk ash
S	Sodium silicate
SG	Specific gravity
SH	Sodium hydroxide
SPSS	Statistical package for the social sciences

1 Introduction

Many industries are generating huge amounts of waste. According to Maximize Market Research Pvt. Ltd., the metal mining market rapidly increasing every year as shown in Figure 1. Metallic wastes are generated from various types of metal industries globally, i.e., Steel industry, copper industry, aluminum industry, lead industry, zinc industry, and other industries. Further, thermal power plants, sugar mills, paddy mills, etc. generates fly ash, sugar cane bagasse, and rice husk ash. Proper utilization and disposal of this industrial waste have become a big challenge around the globe. Various industrial wastes have been used to enhance the properties of materials. Various researchers have used these types of industrial waste to improve the strength, durability, workability, maximum dry density, CBR, UCS, etc. of the mixes [1–7].

Copper industries generate copper slag after the smelting process of copper [8]. Nearly about 40 million tons of copper slag is produced annually around the world [9]. Roughly 2.2 tons of copper slag produces after one ton of copper [10]. The copper slag is utilized in various fields such as development of pavement, production of cement, embankment construction, and in the production of concrete [11, 12] because the physiochemical properties of copper slag are similar to those of coarse and fine sand and thus can be.

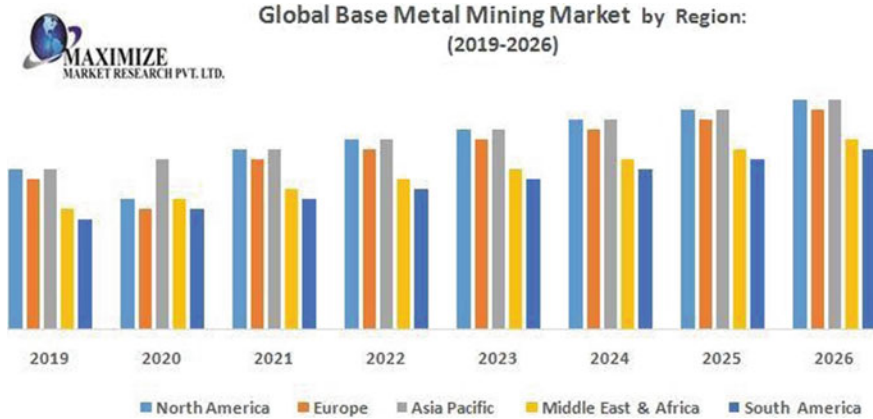


Fig. 1 Global base metal mining market by region (source <https://www.maximizemarketresearch.com/market-report/global-base-metal-mining-market/34133/>)

Rice mills produce RHA after the burning of RH (rice husk) with temperature range 500 °C–1200 °C. Forty kilograms (40 kg) of RHA is generated after the burning of 200 kg of rice husk [13]. It consists high amount of silica [14, 15]. RHA has been used to stabilize the soil and in production of cement [16–18]. Moreover, for soil stabilization geopolymer and alkali activator have been used [5, 19–23].

This comparative study is to recognize the effect of specific gravity and compaction behavior of CS blended with various percentages of RHA, L, C, and AA. Additionally, based on the experimental data different mathematical models have been constructed to estimate predicted values of SG, MDD, and OMC.

2 Materials

In the present study CS, RHA mixed with L, C, and AA has been considered. The physiochemical properties of the CS and RHA are same as discussed in previous research by Sharma and Kumar [2].

2.1 Copper Slag

CS was a cohesion-less material and the particle size similar to sand. CS was procured from Hindustan Copper Limited, Bharuch Gujarat, India. The main chemical compounds found in CS are Fe₂O₃ = 40.77%, SiO₂ = 35.22, CaO = 6.79, Al₂O₃ = 2.80, MgO = 1.75. CS having SG, OMC, and MDD of 3.50, 11%, and 2.232 g/cc, respectively.

2.2 Rice Husk Ash

RHA was collected from the Jackpot rice mill in Jalandhar. The physical appearance of RHA was black in color and cohesion-less material. The main chemical compound of RHA consists $\text{Fe}_2\text{O}_3 = 1.70\%$, $\text{SiO}_2 = 91.90\%$, $\text{Al}_2\text{O}_3 = 1.38\%$, $\text{K}_2\text{O} = 1.35\%$. The observed SG, OMC, and MDD values are 1.43, 53%, and 0.861 g/cc, respectively.

2.3 Lime

Hydrated lime procured from a local market (Kartarpur), Jalandhar. XRF technique has been used to quantifying the chemical compounds. XRF results were received from Institute Instrumentation Center (IIC) Roorkee. The main chemical compounds such as $\text{CaO} = 70.38\%$, $\text{Fe}_2\text{O}_3 = 0.41\%$, $\text{MgO} = 0.32\%$ were observed. The specific gravity of the hydrated lime is determined 2.15 in the previous research.

2.4 Cement (OPC-43)

Ordinary Portland cement grade of 43 was used in the present comparative study and it was procured from a Shree Cement supplier in Jalandhar. The physicochemical properties of OPC-43 are considered from the foregoing study [2]. The SG of the cement was found to be 3.15.

2.5 Alkali Activator

In this study, SH and SS as alkali activator was used. AA was procured from Garg Chemicals in Jalandhar. The sodium hydroxide was procured in flakes form with 98% purity, whereas sodium silicate was procured in liquid form with activator modulus ratio (M_s) = 3.3. The SS solution was prepared by using silicon dioxide = 26.5%, sodium oxide = 8% and dihydrogen monoxide = 65.5% (by weight) [24]. SH solution 10M (molarity) has been used. The SG of SH and SS were found to be 1.31 and 1.54, respectively.

3 Testing Methods

In the present comparative study the testing methodology, procedure, and preparation of samples have been utilized as elaborated in the previous research [2].

3.1 Specific Gravity Test

The SG tests on CS, RHA mixed with L, C, and AA were conducted as per ASTM D854—14 [25].

3.2 Compaction Test

MPC tests have been performed using an automatic compaction machine. The compaction tests on CS, RHA, L, C, and AA were conducted as per ASTM D1557—09 [26].

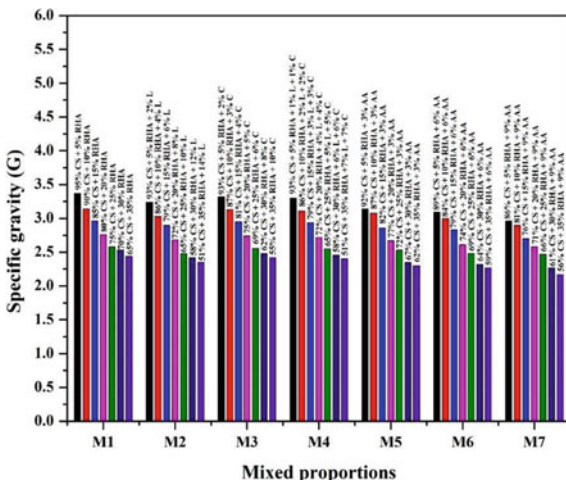
4 Results and Discussion

The results of CS, RHA treated with L, C, and AA on their compaction and SG properties are compared. The comparison of geotechnical properties of CS and RHA treated with various additive materials (L, C, and AA) are discussed in the following sections.

4.1 Specific Gravity

The SG tests have been compared for different mixes of copper slag, rice husk ash, lime, cement, and AA presented in Figure 2. The SG tests of various combinations copper slag + rice husk ash (CS + RHA); copper slag + rice husk ash + lime (CS + RHA + L); copper slag + rice husk ash + cement (CS + RHA + C); copper slag + rice husk ash + lime + cement (CS + RHA + L + C); copper slag + rice husk ash + alkali activator (CS + RHA + AA) are compared. It can be observed that the content of rice husk ash, lime, cement, lime with cement, and alkali activator to copper slag becomes reduced the value of SG for all the mixes. The maximum value of SG obtained was 3.37 for the mix proportion of 95% CS + 5% RHA; the minimum SG value was obtained as 2.17 for the combination 56% CS + 35% RHA + 9% AA. The SG of various mixes mainly decreases due to the lower SG of other materials that were mixed to CS. Moreover, the SG of rice husk ash, lime, cement, sodium hydroxide, and sodium silicate are 1.43, 2.15, 3.15, 1.31, and 1.54, respectively. CS has the highest SG as compared to other materials. Further, the agglomeration of delicate particles of rice husk ash, lime, cement, and lighter density of AA to the coarser particles of copper slag is also responsible for reduced the value of SG of different mixes [2].

Fig. 2 Specific gravity of various mixed proportions (lime, cement, and AA)



4.2 Compaction Test

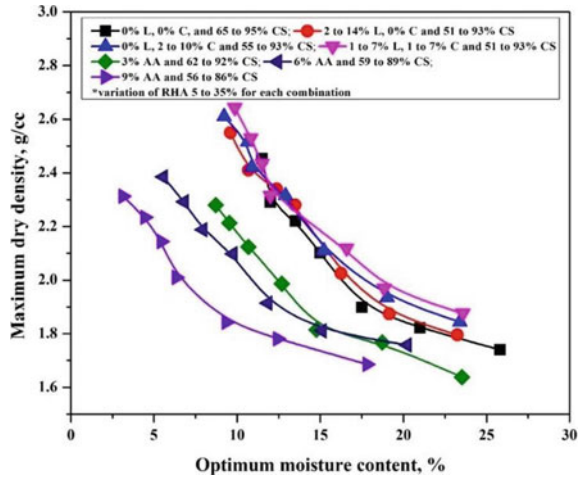
Figure 3 presents the effect on maximum dry density and optimum moisture content of various combinations. The compaction tests results of various combinations copper slag + rice husk ash (CS + RHA); copper slag + rice husk ash + lime (CS + RHA + L); copper slag + rice husk ash + cement (CS + RHA + C); copper slag + rice husk ash + lime + cement (CS + RHA + L + C); copper slag + rice husk ash + alkali activator (CS + RHA + AA) are compared. The test results clearly indicate that the MDD values have been found to decrease and optimum moisture content has been observed to increase, respectively with the increased content of rice husk ash ranging from 5 to 35%, content of lime ranging from 1 to 14%, percentage of C in the range of 1 to 10%. Moreover, the MDD has been increased with the increased percentage of AA up to 6%, thereafter addition of AA above 6% MDD values have been found to be decreased. Further, OMC has been found to decrease with the increased percentage of AA. Similar patterns observed in soil stabilization using RHA, L, FA, C, PA, etc. as reported in the previous investigation [2, 16–18, 27–31].

The highest MDD and OMC have been observed for the mix of copper slag and rice husk ash (without L, C, and AA) of about 2.45 g/cc and 11.50%, respectively. These maximum values were found in case mix composition of 95% of CS and 5% of RHA.

CS–RHA treated with L (without C and AA) in various percentages have been subjected to compaction tests, in which the highest MDD and OMC have been obtained as 2.55 g/cc and 9.60%, respectively for the mix of 93% of CS, 5% of RHA, and 2% of L.

MPC tests have been performed for CS–RHA treated with C (without L and AA). The optimum mix was with 93% of CS, 5% of RHA, and 2% of C for which the highest MDD and OMC have been achieved of about 2.61 g/cc and 9.22%, respectively.

Fig. 3 MDD and OMC of various mix proportions (lime, cement and AA)



For the case of copper slag–rice husk ash (CS–RHA) treated with lime and cement (without AA) the optimum results of compaction test were obtained with highest MDD of 2.64 gm/cc and OMC of about 9.86% for the combination with 93% of CS, 5% of CS, 1% of L, and 1% of C.

Further, in case of CS–RHA treated with AA (without L and C) in various percentages such as 92%, 89%, 86% of CS, 5% of RHA, and 3%, 6%, 9% of AA have been tested for compaction behavior in which the highest MDD and OMC values have been obtained of about 2.28 g/cc, 2.39 g/cc, 2.31 g/cc, and 8.72%, 5.56%, 3.14%, respectively.

Out of all the compaction test results as discussed above for all the combinations studied in the current comparative study the highest value of MDD and OMC observed were of about 2.64 g/cc and 9.86%, respectively corresponding to the mix consisting of 93% of copper slag, 5% of rice husk ash, 1% of lime, and 1% of cement.

The reduction observed in maximum dry density value on enhancing contents of rice husk ash, lime, cement, and AA (after 6%) may be attributed to the lower SG of rice husk ash, lime, cement, and alkali activator as compared to that of copper slag. The comparatively lesser SG values of rice husk ash, pond ash, and fly ash (lightweight materials) might be the cause for abatement in maximum dry density [2, 17, 27, 32]. These combinations may be used in highway construction, earth filling materials, and construction of embankments as per Indian road congress (IRC) guidelines.

5 Mathematical Modeling

It is the mathematical model (Multiple Linear Regression Analysis—MLRA) to establish relation between dependent variables and more than two independent variables. SPSS software has been used for MLRA. This mathematical technique has been used by many investigators to verify laboratory data [2, 3, 18]. The basic equation of multiple linear regression analysis is as follows:

$$Y = \beta_o + \beta_1 X_1 + \dots + \beta_n X_n + e \quad (1)$$

where

Y = Predict variable

X_i = Observed variable, $i = 1, 2, 3 \dots$

β_1 = observed variable coefficient

β_o = Intercept constant

e = error (if any).

The mathematical model has been constructed to fit the best connection between different variables such as contents of copper slag, rice husk ash, lime, cement, and AA as independent variables with dependents variables SG, OMC, and MDD to predicted values of SG, OMC, and MDD.

The equations developed through MLRA to predict the SG, OMC, and MDD values are as follows:

$$\begin{aligned} (\text{SG})_p &= 3.403 - (0.000048 * CS) - (0.0298 * \text{RHA}) - (0.00759 * L) \\ &\quad - (0.000212 * C) - (0.0254 * AA) \end{aligned} \quad (2)$$

$$\begin{aligned} (\text{OMC})_p &= -18.60 + (0.251 * CS) + (0.737 * \text{RHA}) + (0.1095 * L) \\ &\quad + (0.00053 * C) - (0.611 * AA) \end{aligned} \quad (3)$$

$$\begin{aligned} (\text{MDD})_p &= 4.912 - (0.0228 * CS) - (0.0494 * \text{RHA}) - (0.014 * L) \\ &\quad - (0.00141 * C) - (0.0348 * AA) \end{aligned} \quad (4)$$

For Eqs. (2), (3), and (4) the R^2 (coefficient of determination) values are found to be 0.97, 0.93, and 0.98, respectively. The predicted values of SG, OMC, and MDD have been calculated by using equations (2), (3), and (4). The linear scatter diagrams constructed between the observed values and predicted values are as shown in Figures 4, 5, and 6, respectively. The regression plot of forecast (predicted) and laboratory experimental values lies acceptably within the 95% confidence interval.

Fig. 4 Graphical representation of predicted SG versus observed SG

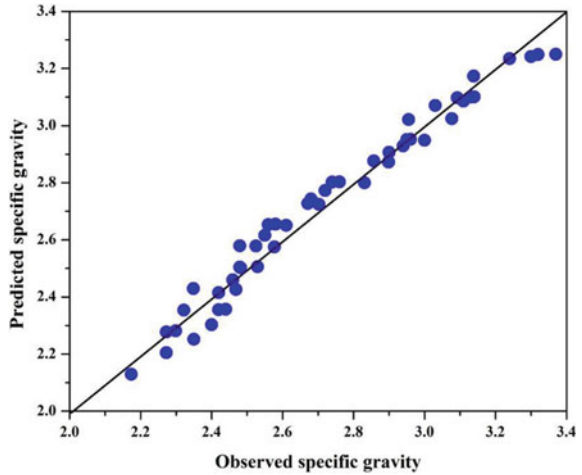
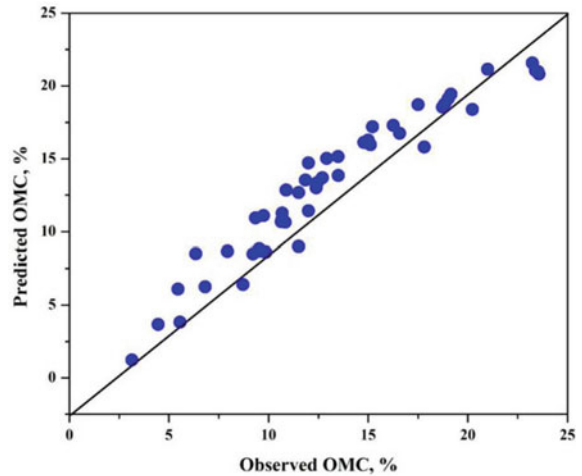


Fig. 5 Graphical representation of predicted OMC versus observed OMC

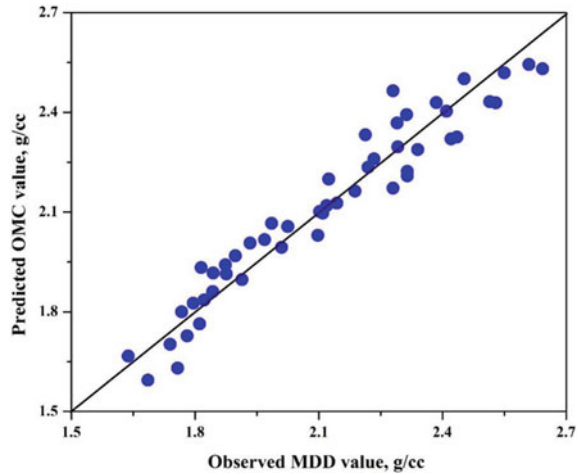


6 Conclusions

Following remarkable outcomes can be observed from the exhibit comparative study:

- The highest value of SG obtained was 3.37 for the combination of 95% CS + 5% RHA; the minimum SG value was obtained as 2.17 for the combination of 56% CS + 35% RHA + 9% AA.
- The highest value of MDD with OMC has been obtained 2.64 g/cc and 9.86%, respectively. This mix consists of 93% of CS, 5% of RHA, 1% of lime, and 1% of cement.

Fig. 6 Graphical representation of predicted MDD versus observed MDD



- The mathematical models generated by using MLRA technique have been found to predict the dependent variables with a good agreement between observed values of SG, OMC, and MDD.
- These combinations may be used in highway construction, earth filling materials, and construction of embankments as per Indian Road Congress (IRC) guidelines.

References

1. Yoobanpot N, Jamsawang P (2014) Effect of cement replacement by rice husk ash on soft soil stabilization. *Kasetsart J Nat Sci* 48(2):323–332
2. Sharma K, Kumar A (2021) Influence of rice husk ash, lime and cement on compaction and strength properties of copper slag. *Transp Geotech* 27:1–16. <https://doi.org/10.1016/j.trgeo.2020.100464>
3. Gupta D, Kumar A (2016) Strength characterization of cement stabilized and fiber reinforced clay-pond ash mixes. *Int J Geosynth Gr Eng*. <https://doi.org/10.1007/s40891-016-0069-z>
4. Yu J, Chen Y, Chen G, Wang L (2020) Experimental study of the feasibility of using anhydrous sodium metasilicate as a geopolymer activator for soil stabilization. *Eng Geol* 264:1–12. <https://doi.org/10.1016/j.enggeo.2019.105316>
5. Sukprasert S, Hoy M, Horpibulsuk S, Arulrajah A, Rashid SA, Nazir R (2019) Fly ash based geopolymer stabilisation of silty clay/blast furnace slag for subgrade applications. *Road Mater Pavement Des* 1–15. <https://doi.org/10.1080/14680629.2019.1621190>
6. Shahiri J, Ghasemi M (2017) Utilization of soil stabilization with cement and copper slag as subgrade materials in road embankment construction utilization of soil stabilization with cement and copper slag as subgrade materials ...
7. Nasiri M, Lotfalian M, Modarres A, Wu W (2016) Optimum utilization of rice husk ash for stabilization of sub-base materials in construction and repair projects of forest roads
8. Schlesinger ME, King MJ, Sole KC, Davenport WG (2011) Extractive metallurgy of copper
9. Shi C, Meyer C, Behnood A (2008) Utilization of copper slag in cement and concrete. *Resour Conserv Recycl* 52(10):1115–1120. <https://doi.org/10.1016/j.resconrec.2008.06.008>

10. Dhir OBE RK, de Brito J, Mangabhai R, Lye CQ (2016) Sustainable construction materials: copper slag
11. Ma Q et al (2018) Performance of copper slag contained mortars after exposure to elevated temperatures. *Constr Build Mater* 172:378–386. <https://doi.org/10.1016/j.conbuildmat.2018.03.261>
12. Jia Q et al (2016) Effects of fine content, binder type and porosity on mechanical properties of cemented paste backfill with co-deposition of tailings sand and smelter slag. *Electron J Geotech Eng* 21(22):7017–7032
13. P. K. (1986). Mehta, *Concrete structure properties and materials*. 1986.
14. Celik F, Canakci H (2015) An investigation of rheological properties of cement-based grout mixed with rice husk ash (RHA). *Constr Build Mater* 91:187–194. <https://doi.org/10.1016/j.conbuildmat.2015.05.025>
15. Della VP, Kühn I, Hotza D, Rice husk ash as an alternate source for active silica production
16. Rahman MA (1987) Effects of cement-rice husk ash mixtures on geotechnical properties of lateritic soils. *Japanese Soc Soil Mech Found Eng* 27(2):61–65
17. Ali FH, Adnan A, Choy CK (1992) Geotechnical properties of a chemically stabilized soil from Malaysia with rice husk ash as an additive. *Geotech Geol Eng* 10(2):117–134. <https://doi.org/10.1007/BF00881147>
18. Gupta D, Kumar A (2017) Performance evaluation of cement-stabilized pond ash-rice husk ash-clay mixture as a highway construction material. *J Rock Mech Geotech Eng* 9(1):159–169. <https://doi.org/10.1016/j.jrmge.2016.05.010>
19. Abdullah HH, Shahin MA, Sarker P (2019) Use of fly-ash geopolymer incorporating ground granulated slag for stabilisation of kaolin clay cured at ambient temperature. *Geotech Geol Eng* 37(2):721–740. <https://doi.org/10.1007/s10706-018-0644-2>
20. Ghadir P, Ranjbar N (2018) Clayey soil stabilization using geopolymer and Portland cement. *Constr Build Mater* 188:361–371. <https://doi.org/10.1016/j.conbuildmat.2018.07.207>
21. Salimi M, Ghorbani A (2020) Mechanical and compressibility characteristics of a soft clay stabilized by slag-based mixtures and geopolymers. *Appl Clay Sci* 184:1–15. <https://doi.org/10.1016/j.clay.2019.105390>
22. Sreelakshmi SG, Kumar K, Krishnaiah E (2017) Strength and durability of geopolymer stabilized soil. In: *Indian Geotechnical conference 2017 GeoNEst*, pp 1–4
23. Phummiphon I, Horpibulsuk S, Rachan R, Arulrajah A, Shen SL, Chindapasirt P (2018) High calcium fly ash geopolymer stabilized lateritic soil and granulated blast furnace slag blends as a pavement base material. *J Hazard Mater* 341:257–267. <https://doi.org/10.1016/j.jhazmat.2017.07.067>
24. Singh J, Singh SP (2019) Development of Alkali-activated cementitious material using copper slag. *Constr Build Mater* 211:73–79. <https://doi.org/10.1016/j.conbuildmat.2019.03.233>
25. ASTM International (2002) ASTM D 854—02 standard test methods for of soil specific gravity solids by water pycnometer
26. ASTM International (2002) Standard test methods for laboratory compaction characteristics of soil using modified effort
27. Kumar A, Gupta D (2016) Behavior of cement-stabilized fiber-reinforced pond ash, rice husk ash-soil mixtures. *Geotext Geomembranes* 44(3):466–474. <https://doi.org/10.1016/j.geotextmem.2015.07.010>
28. Kaniraj SR, Havanagi VG (1999) Geotechnical characteristics of fly ash-soil mixtures. *Geotech Eng* 30(2):129–147
29. Al-Rawas AA, Hago AW, Al-Sarmi H (2005) Effect of lime, cement and Sarooj (artificial pozzolan) on the swelling potential of an expansive soil from Oman. *Build Environ* 40(5):681–687. <https://doi.org/10.1016/j.buildenv.2004.08.028>

30. Kolas S, Kasselouri-Rigopoulou V, Karahalios A (2005) Stabilisation of clayey soils with high calcium fly ash and cement. *Cem Concr Compos* 27(2):301–313. <https://doi.org/10.1016/j.cemconcomp.2004.02.019>
31. Mir BA, Sridharan A (2013) Physical and compaction behaviour of clay soil-fly ash mixtures. *Geotech Geol Eng* 31(4):1059–1072. <https://doi.org/10.1007/s10706-013-9632-8>
32. Jha JN, Gill KS (2006) Effect of rice husk ash on lime stabilization of soil. *J Inst Eng Civ Eng Div* 87:33–39

Effect of Addition of Slag on Engineering Properties of Clayey Soil



Aditya D. Ahirwar and H. S. Chore

Abstract Rapid urbanization has resulted in huge number of infrastructure projects across the country. Amid this urbanization and industrialization, consumption of steel has increased enormously. India is currently the second largest producer of the steel. For every tonne of steel produced, an integrated steel plant produces 2–4 tonnes of slag. Disposal of the enormous magnitude of waste in an economically feasible and environment-friendly manner has become a challenging task. This study looks into the efficient use of steelmaking slag as a highway construction material. Locally available soft clay was stabilized with steel slag fines, and experimental investigations were carried out to evaluate consistency limits, compaction characteristics and strength characteristics of different combination of mixes. The strength of clay is found to increase with the addition of steel slag and also with the curing period.

Keywords Problematic soft clay · Steel making slag · Environmental impact

1 Introduction

Rapid urbanization has resulted in huge number of infrastructure projects across the country. Thus demand of steel products has increased enormously. India is second largest producer of steel, just trailing China. Mainly, there are two types of steel manufacturers in India. Integrated/major steel plants provide facilities to convert the iron ore and raw material into the hot metal through blast furnace (BF)-basic oxygen furnace (BOF) route and eventually convert it into finished products like slabs, coils and bars.

A. D. Ahirwar (✉) · H. S. Chore
Department of Civil Engineering, Dr.B.R. Ambedkar National Institute of Technology, 144011,
Jalandhar, India
e-mail: ahirwarad.ce.19@nitj.ac.in

H. S. Chore
e-mail: chorehs@nitj.ac.in

© The Author(s), under exclusive license to Springer Nature Singapore Pte Ltd. 2023
A. K. Agnihotri et al. (eds.), *Proceedings of Indian Geotechnical and Geoenvironmental Engineering Conference (IGGEC) 2021, Vol. 1*, Lecture Notes in Civil Engineering 280,
https://doi.org/10.1007/978-981-19-4739-1_16

175

Secondary or MSME steel producers convert steel scrap and sponge iron into finished products through electric arc furnace route (EAF) or induction furnace route (IF). During the refining process, 2–4 tonnes of steel slag is generated for every tonne of steel produced. Disposal of the huge quantum of waste in an environment-friendly manner has become a challenging task.

Shi [1] reviewed the manufacturing, processing and properties of steel slag, as well as its use in cement and concrete production. Horii et al. [2] emphasized on material characteristics of iron and steel making slag. Oluwasola et al. [3] reviewed the properties of the slag. They pointed out that presence of dicalcium silicate, tricalcium silicate and tetra-calcium alumina ferrite in steel slag qualifies it as cementitious material. Akinwumi et al. [4] concluded that steel slag can be effectively utilized for stabilization of weak soil so as to meet requirement set by Nigerian standards for utilization of various component layers of the pavements.

Aldeeky et al. [5] examined the efficacy of steel slag in the context of highly plastic soil and noticed improvement in geotechnical properties of such soil from utilization in subgrade of the pavement. Rao et al. [6] pointed out that addition of steel slag reduced optimum moisture content, liquid limit and plastic limit and increased workability, maximum dry density, California bearing ratio and shear strength characteristics like cohesion and angle of friction.

Wua et al. [7] evaluated the engineering properties to understand behaviour of expansive soil modified with steel slag. Poh et al. [8], Goodarzi and Salimi [9] identified that low adsorption capacity, pozzolanic action and cation exchange between soil and slag particle are indicative of steel slag being excellent soil modification agent.

After identifying some of the gaps in available literature and identifying the problems related to utilization of problematic soft clay and disposal of waste by-products, experimental investigations were conducted to evaluate the compaction and strength properties of soft clay after addition of steel slag as the stabilizer.

2 Material and Method

In the current study, the problematic soft clay was mixed with the different proportions of steel slag (5%, 10%, 15%, 20% and 25%). The soil used for the project was brought from local supplier. The geotechnical properties of different combinations of mixes were found out. The geotechnical investigations involved the determination of plasticity characteristics, compaction characteristics and strength of clay-slag composite mix. Table 1 shows particulars of clay-slag mixes, considered in the present study.

Table 1 Different combination of mixes

Sr. No	Property	Value
1	PC (plain clayey soil)	100% Clay
2	C5S	Clay +5% steel slag fines
3	C10S	Clay +10% steel slag fines
4	C15S	Clay +15% steel slag fines
5	C20S	Clay +20% steel slag fines
6	C25S	Clay + 25% steel slag fines

3 Discussion of Results

The experimental programme comprises conducting the preliminary tests to attain the index properties of soft clay. Table 2 shows geotechnical properties of the soft clay considered in the study.

In the present study, consistency limits of various combinations of mixes were evaluated using Atterberg's limit test. Figure 1 illustrates the variation in index properties such as LL, PL and PI of various mixes.

From Fig. 1, it can be observed that the LL, PL and PI reduce after addition of steel slag. The reduction in consistency limits can be linked with the addition of steel slag, which has a high specific gravity but low water retention capacity. Because of the non-plastic nature of slag, affinity for water decreases, making composite mix more workable. The reduction in the PI is an indication of an improvement of soil property. The MDD and OMC are the two most important factors for determining geotechnical properties of soil. The focus of the present study is on studying the effect of addition of slag on compaction properties (MDD and OMC) of different combinations. With increase in steel slag contents while MDD of the composite mix increases, OMC decreases (Fig. 2).

The experimental study was extended to evaluate the effect of addition of steel slag on unconfined compressive strength (UCS) of various combinations of clay-slag composite mixes. The investigations were further extended to study the effect of curing period on strength properties of such composite mixes.

Table 2 Geotechnical properties

Sr. No	Property	Value
1	Liquid limit (LL) (%)	32.68
2	Plastic limit (PL) (%)	24.51
3	Specific gravity	2.64
4	Optimum moisture content (OMC) (%)	17.41
5	Maximum dry density (MDD) (gm/cc)	1.78
6	California bearing ratio (CBR) (%)	8.02

Fig. 1 Effect of addition of steel slag on LL, PL and PI

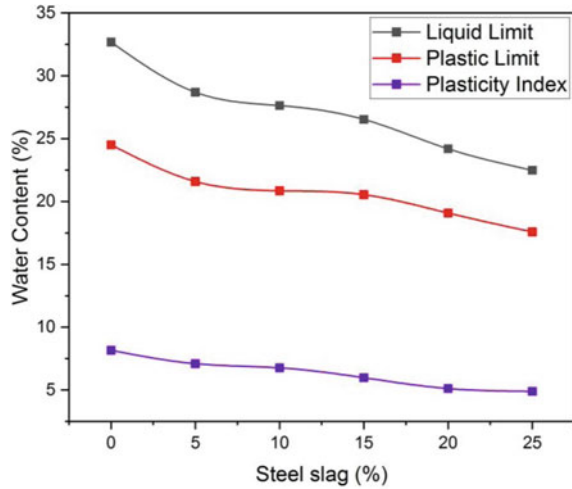
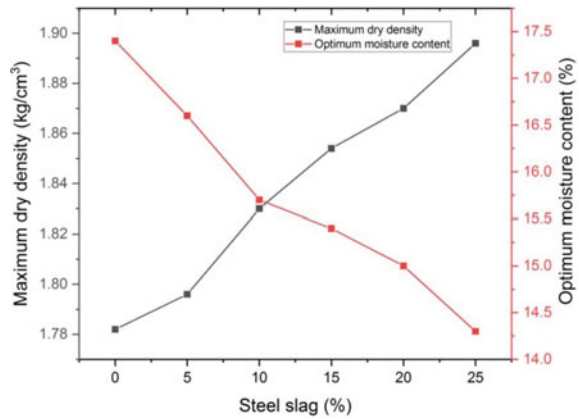


Fig. 2 Effect of addition of steel slag on MDD and OMC of soil-slag composite mix



It is observed from Fig. 3 that the UCS of composite mix increases with steel slag contents up to 20%. It is also observed that the UCS of different combination of mixes improves significantly with curing period.

The study was further extended to study the effect of addition of steel slag on California bearing ratio (CBR) of different combination of mixes. Figure 4 shows the variation in CBR of soil-slag composite mix which indicates enhancement in CBR of composite mixes with the addition of steel slag.

Fig. 3 Variation in UCS of composite mix for 0 and 7 days curing

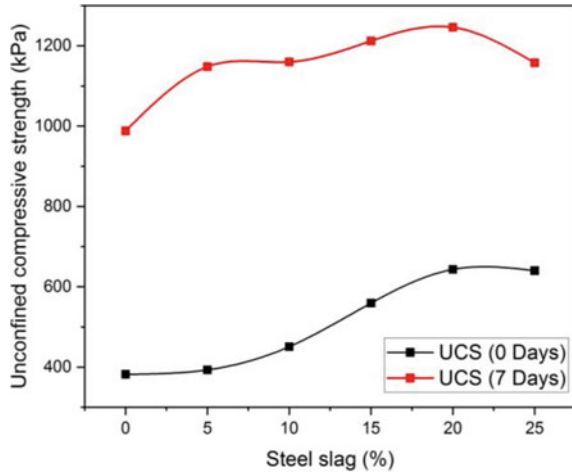
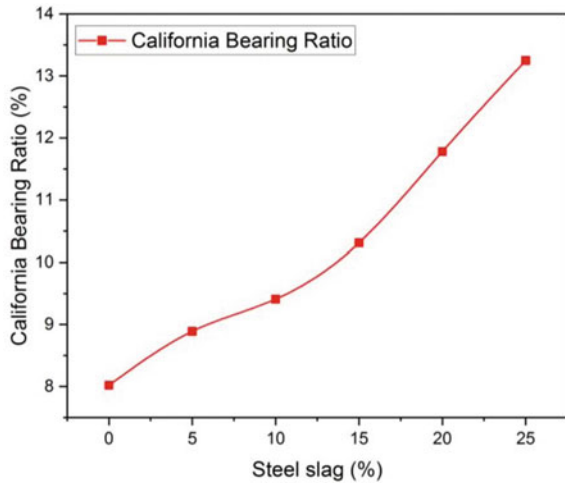


Fig. 4 Effect of addition of steel slag on CBR



4 Summary and Conclusion

Following conclusions can be deduced from the laboratory investigations conducted on clay samples stabilized with steel slag:

1. The values of the index properties (LL, PL and PI) of composite mix decrease after addition of slag, thereby making the composite mix more workable.
2. Addition of slag increases MDD of composite mix and reduces OMC.
3. The UCS of the composite mixes increases with addition of steel slag up to 20%.
4. The UCS of the composite mix increases significantly with curing period.
5. With addition of slag, CBR of the composite mix increases.

Thus, industrial waste materials such as steel slag can prove as the sustainable road construction material to stabilize clayey soil. This will not only provide an alternate solution for safe disposal of the waste by-product, but will also provide suitable alternative to raw materials which would have been used in highway construction.

References

1. Shi C (2004) Steel slag—its production, processing, characteristics, and cementitious properties. *J Mater Civ Eng* 16(3):230–236
2. Horii K, Tsutsumi N, Kitano Y, Kato T (2013) Processing and reusing technologies for steelmaking slag. *Nippon Steel Tech Rep* 104(104):123–129
3. Oluwasola EA, Hainin MR, Aziz MMA (2014) Characteristics and utilization of steel slag in road construction. *Jurnal Teknologi* 70(7)
4. Akinwumi II, Adeyeri JB, Ejohwomu OA (2013) Effects of steel slag addition on the plasticity, strength, and permeability of lateritic soil. In: *ICSDEC 2012: developing the frontier of sustainable design, engineering, and construction*, pp 457–464
5. Aldeeky H, Al Hattamleh O (2017) Experimental study on the utilization of fine steel slag on stabilizing high plastic subgrade soil. *Adv Civil Eng*
6. Rao DK, Sravani G, Bharath NA (2014) Laboratory study on the effect of steel slag for improving the properties of marine clay for foundation beds. *Int J Sci Eng Res* 5(7)
7. Wu J, Liu Q, Deng Y, Yu X, Feng Q, Yan C (2019) Expansive soil modified by waste steel slag and its application in subbase layer of highways. *Soils Found* 59(4):955–965
8. Poh HY, Ghataora GS, Ghazireh N (2006) Soil stabilization using basic oxygen steel slag fines. *J Mater Civ Eng* 18(2):229–240
9. Goodarzi AR, Salimi M (2015) Stabilization treatment of a dispersive clayey soil using granulated blast furnace slag and basic oxygen furnace slag. *Appl Clay Sci* 108:61–69

Analysis of Bearing Capacity and Settlement from Cone Penetration Test Results at an Irrigation Project



J. Sumalatha and J. Suresh Babu

Abstract A cut-off wall was constructed as part of a multipurpose irrigation project located in East Godavari district of Andhra Pradesh state in India. As the soil strength is a major concern in the design of substructures in soils, it is proposed to study the soil conditions at the site. The cone penetration test results were collected from the water resources department to analyze the bearing capacity and settlement of the soil at different locations. The analysis was carried out using GEO5 software tool considering pile foundations of diameter 1 m and depth of 10 m. From the analyses, it was observed that the bearing capacity of the pile at selected locations was in the range of 2752–4940 kN and the estimated settlements were within the allowable limits.

Keywords Bearing capacity · Settlement · Cone resistance · Pile foundation

1 Introduction

The value of bearing capacity varies with the soil properties, location of water table, type of foundation, depth of foundation, etc. The bearing capacity of soil can be estimated by various methods such as analytical methods, plate load tests and penetration tests. There are various analytical methods available to estimate the bearing capacity. The penetration tests such as Standard Penetration Test (SPT) and Cone Penetration Test (CPT) give more accurate values of bearing capacity compared to analytical methods. The pile behaviour and bearing capacity can be estimated using several theoretical and experimental procedures depending on the type of soil and pile [1, 2].

J. Sumalatha (✉)

Department of Civil Engineering, M S Ramaiah Institute of Technology, Bangalore, India
e-mail: sumalatha@msrit.edu

J. S. Babu

Water Resources Department, PIPRC Division, Kovvur, Andhra Pradesh, India

The design engineers generally use SPT and CPT test results to estimate the load-bearing capacity of piles and then to apply a suitable safety factor in the design process to attain a firm foundation [3]. The bearing capacity analysis based on CPT values was studied by several researchers [4–8]. The bearing capacity is calculated by measuring the cone resistance (q_c) and shaft friction (f_s) from the CPT test [9, 10]. Many researchers have used artificial intelligence in the form of artificial neural networks (ANN) and Genetic programming (GP) for solving engineering problems such as predicting pile capacity [11, 12]. The comparative studies to correlate SPT and CPT values that were carried by several researchers [3, 13–15] indicated that for the same case, the capacity predictions vary with the method adopted.

Heidarie et al. [14] have studied the SPT-based and CPT-based methods to estimate the bearing capacity and found that the CPT-based methods are more reliable than SPT-based methods. The load-settlement behaviour of the piles was also studied using artificial intelligence and CPT data [15–19].

In the present study, the CPT results of the study area were collected to analyze the load-carrying capacity and settlement behaviour with respect an assumed size of pile foundation. Since the CPT data gives more reliable values of bearing capacity, the test results collected from the water resources department are taken as input to the GEO5 software and the analyses were conducted for different locations of the study area. The factors of safety with respect to the assumed loading conditions were also estimated.

2 Materials and Methods

2.1 Cone Penetration Test Details

The cone penetration test results of five locations (CPT1, CPT2, CPT3, CPT4 and CPT5) were considered to analyze the bearing capacity and settlement. The spacing of these locations is around 500 m. The cone resistance values corresponding to different depths were taken for the analysis which are shown in Table 1.

2.2 GEO5 Analysis

The bearing capacity of the soil with respect to a pile foundation was analyzed using GEO5 software tool. The CPT results corresponding to different depths were given as input to the software to obtain the soil classification and the load-carrying capacity. The settlement analysis was also conducted using the same software tool corresponding to the selected locations. The diameter and length of the pile were taken as 1 m and 10 m, respectively. The vertical load on the pile was assumed as 1000 kN. The depth of water table at the selected location is 2 m below ground level.

Table 1 CPT results of five locations at the study area

Location	Depth (m)	Cone resistance (qc) in MPa	Local friction (fs) in KPa	Pore pressure (u2) in KPa
CPT1	2	4.52	5.0	0
	4	1.35	57.8	116.8
	6	2.21	88.2	32.0
	8	3.23	115.8	439.8
	10	3.18	111.7	36.5
	12	3.07	83.5	-59.0
	14	1.24	20.4	-41.2
	16	1.53	34.8	7.4
	17	6.84	109.6	-59.3
CPT2	2	7.50	14.4	-2.1
	4	6.59	10.5	12.8
	6	1.71	48.7	33.6
	8	2.48	67.5	-67.5
	10	2.99	83.1	-66.0
	12	3.09	79.1	-64.3
	14	2.39	72.3	-81.8
	16	1.89	55.4	-80.6
	18	2.52	64.9	-79.3
CPT3	2	6.44	8.4	-2.5
	4	6.12	9.4	15.7
	6	2.17	85.6	-41.5
	8	2.56	90.6	-45.2
	10	3.08	108.4	-48.9
	12	3.39	104	-46.2
	14	3.38	96.1	-44.0
	16	3.19	92.0	-41.6
	18	3.33	87.5	-37.6
CPT4	2	6.44	9.9	1.6
	4	1.51	0.4	20.4
	6	2.39	70.0	93.9
	8	2.75	81.9	45
	10	2.81	76.9	-16.3
	12	3.7	92.2	-50.9

(continued)

Table 1 (continued)

Location	Depth (m)	Cone resistance (qc) in MPa	Local friction (fs) in KPa	Pore pressure (u2) in KPa
	14	3.46	93.9	-47.7
	16	3.19	84.5	-45.0
	18	3.24	69.3	-41.0
	20	3.71	88.5	-38.7
CPT5	2	8.69	15.1	-2.4
	4	7.04	11.2	13.6
	6	8.45	20.6	34.5
	8	3.66	83.6	87.0
	10	3.86	92.4	133.8
	12	3.65	90.1	170.1
	14	3.33	95.6	190.6
	16	3.39	77.3	120.1
	18	3.23	85.2	42.0
	20	2.77	75.9	35.8

3 Results and Discussions

The soil classification based on the CPT values corresponding to location CPT1 is shown in Fig. 1. From this figure, it can be observed that the soil type is varying from clean sand to sandy silt to silty clay. Considering a pile foundation of 1 m diameter and 10 m length, the bearing capacity is estimated as 2752.67 kN (Fig. 2). The estimated factor of safety corresponding to a vertical load of 1000 kN is 2.75. The load-settlement curve obtained from the CPT results (Fig. 2) shows that the settlement corresponding to 1000 kN is less than 5 mm.

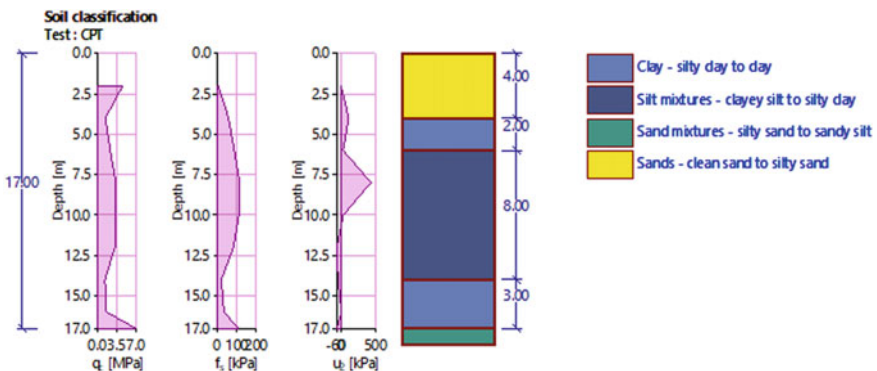


Fig. 1 CPT values and soil classification at location 'CPT1'

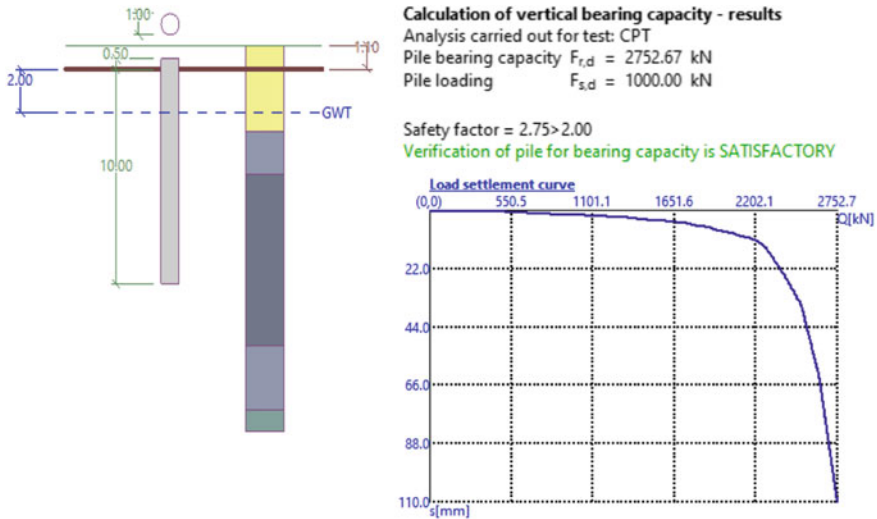


Fig. 2 Bearing capacity analysis and load-settlement curve at location ‘CPT1’

The similar analyses were conducted at the other locations using GEO5 software and the results are shown in Figs. 3, 4, 5, 6, 7, 8, 9 and 10. The bearing capacities corresponding to locations CPT2, CPT3, CPT4 and CPT5, respectively are 2985.58 kN, 3555.19 kN, 4867.01 kN and 4941.1 kN. The estimated factors of safety for these locations are ranging between 2.9 and 4.9. The type of soil at these locations is varying from clean sand to sandy silt to silty clay. From the load-settlement curves of these test locations, it can be observed that the settlement corresponding to 1000 kN are less than 5 mm. From these analyses, it can be observed that the soil is having sufficient bearing capacity and the settlements are within the allowable range.

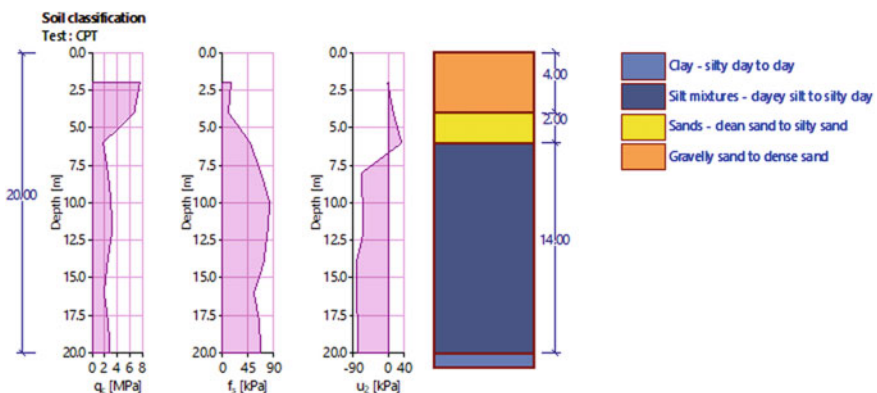


Fig. 3 CPT values and soil classification at location ‘CPT2’

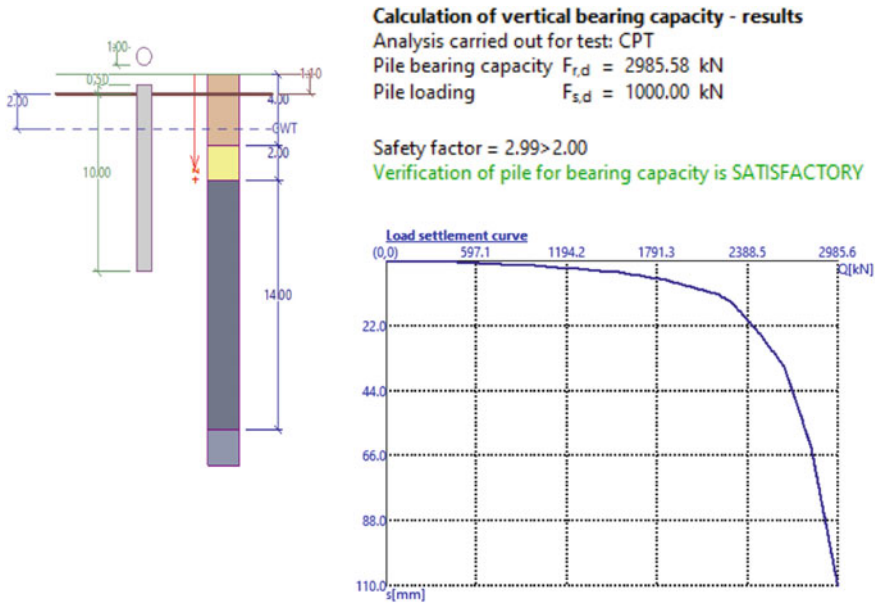


Fig. 4 Bearing capacity analysis and load-settlement curve at location 'CPT2'

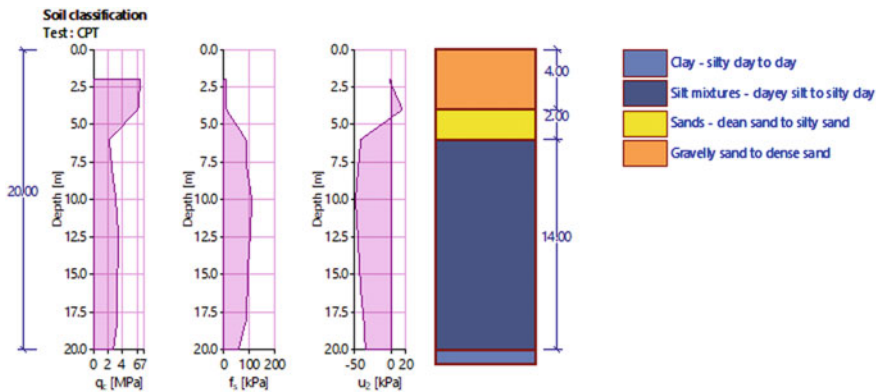


Fig. 5 CPT values and soil classification at location 'CPT3'

4 Conclusions

The soil properties at an irrigation project were studied through the results of Cone Penetration Tests conducted at the study area. The CPT results were taken as input to the software tool and the analyses were conducted for load-carrying capacity and settlement. The CPT values corresponding to different depths were analyzed and

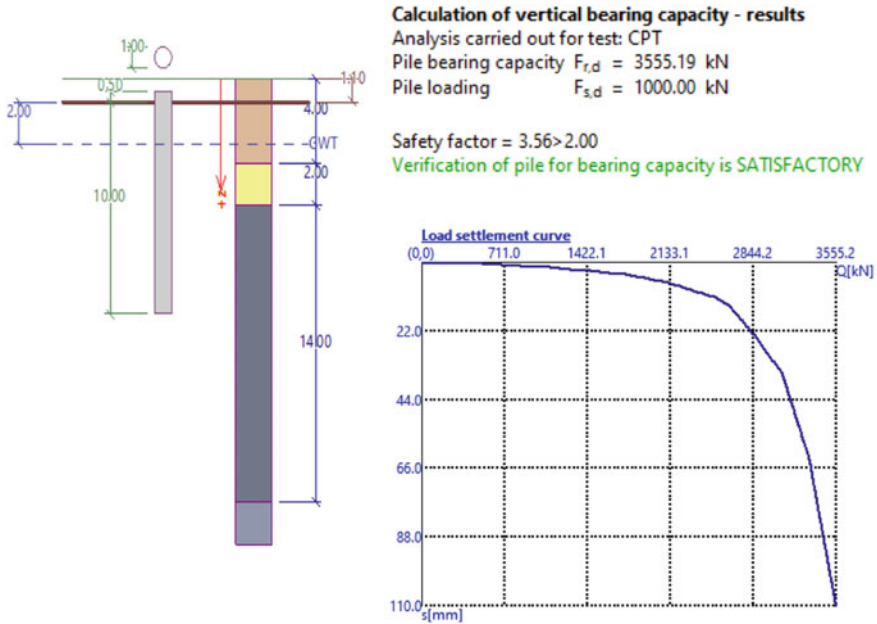


Fig. 6 Bearing capacity analysis and load-settlement curve at location ‘CPT3’

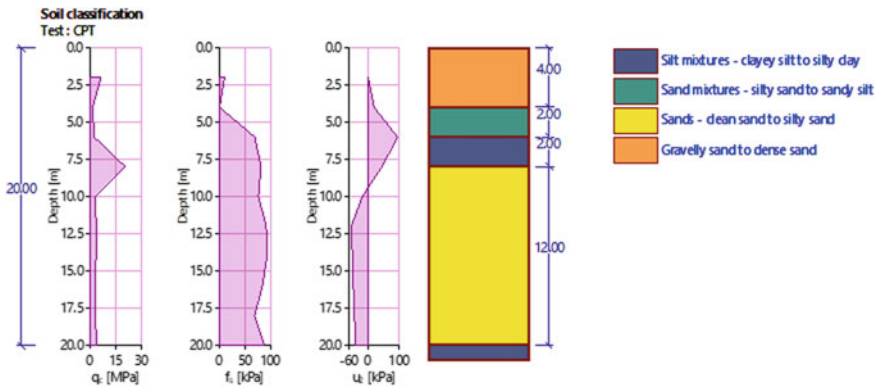


Fig. 7 CPT values and soil classification at location ‘CPT3’

the soil classification obtained with respect to five locations of the study area was reported.

The pile foundation was assumed and the size is maintained constant for all the locations. The bearing capacity estimated at selected locations was in the range of 2752–4940 kN and the settlements estimated from the load-settlement curves were less than 5 mm.

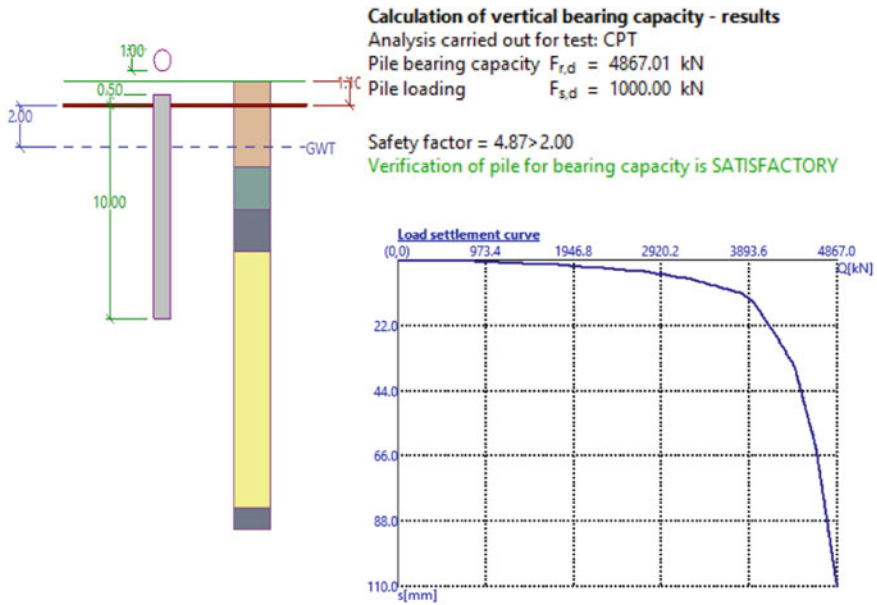


Fig. 8 Bearing capacity analysis and load-settlement curve at location ‘CPT4’

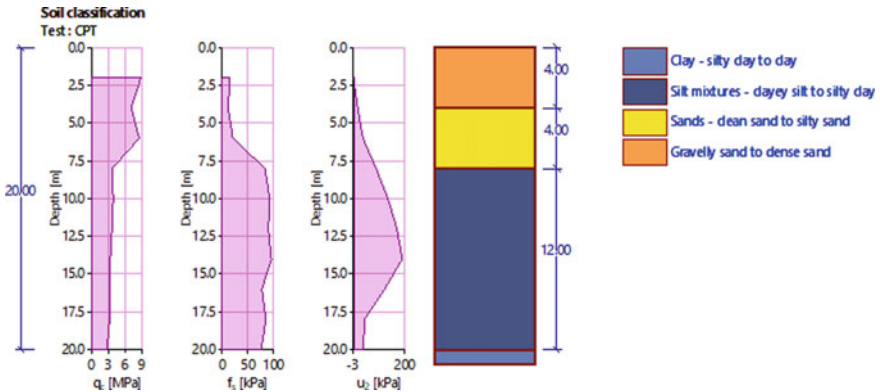


Fig. 9 CPT values and soil classification at location ‘CPT5’

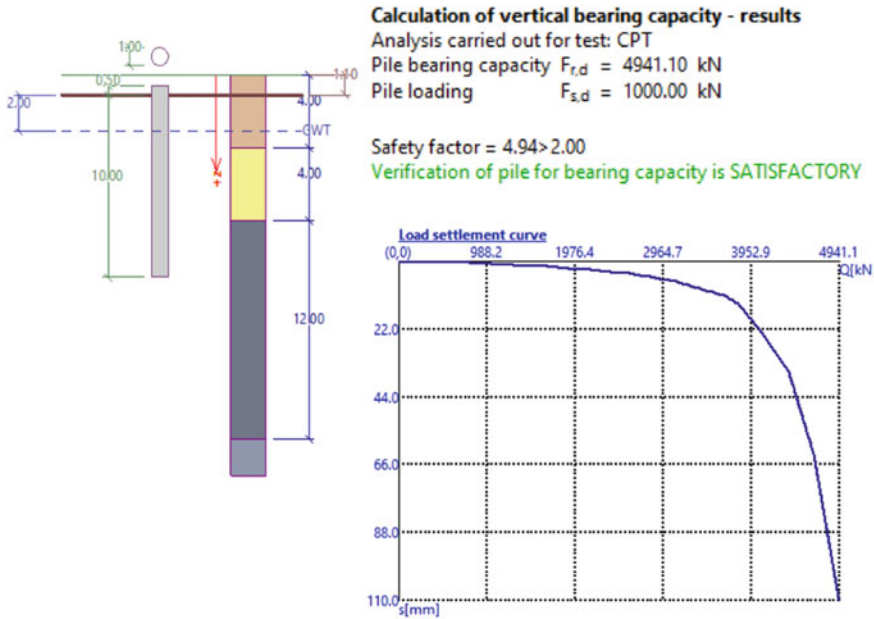


Fig. 10 Bearing capacity analysis and load-settlement curve at location 'CPT5'

References

- Alkroosh IS, Bahadori M, Nikraz H, Bahadori A (2015) Regressive approach for predicting bearing capacity of bored piles from cone penetration test data. *J Rock Mech Geotech Eng* 7(5):584–592
- Shahin MA (2010) Intelligent computing for modeling axial capacity of pile foundations. *Can Geotech J* 47(2):230–243
- Abu-Farsakh MY, Titi HH (2004) Assessment of direct cone penetration test methods for predicting the ultimate capacity of friction driven piles. *J Geotech Geoenviron Eng* 130(9):935–944
- Krasiński ADAM (2012) Proposal for calculating the bearing capacity of screw displacement piles in non-cohesive soils based on CPT results. *Studia Geotechnica et Mechanica* 34(4):41–51
- Wrana B (2015) Pile load capacity—calculation methods. *Studia Geotechnica et Mechanica* 37(4)
- Heidari P, Ghazavi M (2021) Statistical evaluation of CPT and CPTu based methods for prediction of axial bearing capacity of piles. *Geotech Geol Eng* 39(2):1259–1287
- Sirait B, Sarah D (2021) Bearing capacity prediction of mine hauling road using cone penetration testing (CPT). In: *IOP conference series: earth and environmental science*, vol 789, No. 1. IOP Publishing, p 012071
- Xu DS, Liu ZW, Chen B, Xu XY (2020) Bearing capacity analysis of offshore pipe piles with CPTs by considering uncertainly. *Comput Geotech* 126:103731
- Ardalan H, Eslami A, Nariman-Zadeh N (2009) Piles shaft capacity from CPT and CPTu data by polynomial neural networks and genetic algorithms. *Comput Geotech* 36(4):616–625
- Eslami A, Fellenius BH (1997) Pile capacity by direct CPT and CPTu methods applied to 102 case histories. *Can Geotech J* 34(6):886–904
- Pal M, Deswal S (2008) Modeling pile capacity using support vector machines and generalized regression neural network. *J Geotech Geoenviron Eng* 134(7):1021–1024

12. Moayedi H, Bui DT, Thi Ngo PT (2019) Neural computing improvement using four meta-heuristic optimizers in bearing capacity analysis of footings settled on two-layer soils. *Appl Sci* 9(23):5264
13. Cai G, Liu S, Tong L, Du G (2009) Assessment of direct CPT and CPTU methods for predicting the ultimate bearing capacity of single piles. *Eng Geol* 104(3–4):211–222
14. Heidarie Golafzani S, Jamshidi Chenari R, Eslami A (2020) Reliability based assessment of axial pile bearing capacity: static analysis, SPT and CPT-based methods. *Georisk: Assess Manage Risk Engineered Syst Geohazards* 14(3):216–230
15. Nejad FP, Jaksza MB (2017) Load-settlement behavior modeling of single piles using artificial neural networks and CPT data. *Comput Geotech* 89:9–21
16. Shahin MA (2014) Load–settlement modeling of axially loaded steel driven piles using CPT-based recurrent neural networks. *Soils Found* 54(3):515–522
17. Alkroosh I, Nikraz H (2011) Simulating pile load-settlement behavior from CPT data using intelligent computing. *Central Eur J Eng* 1(3):295–305
18. Baziar MH, Azizkandi AS, Kashkooli A (2015) Prediction of pile settlement based on cone penetration test results: an ANN approach. *KSCE J Civil Eng* 19(1):98–106
19. Gwizdala K (2020) Polish design methods for single axially loaded piles. In: *Design of Axially Loaded Piles European Practice*. CRC Press, pp 291–306

**Soil-Structure Interaction, Earthquake
Engineering and Computational
Geo-mechanics**

Influence of Burial Depth of Soil on Reinforced Concrete Tunnel Against the Impact and Blast Loading



K. Senthil, Keshav Saini, and Manish Kumar

Abstract Underground Tunnels are a necessary segment of the present infrastructure system. The tunnel system has become an important part of the present infrastructure all over the world. With increasing use and popularity, the underground tunnels are always prone to natural and man-made attacks. Therefore, an attempt has been made to study the response of underground tunnels against impact loading as well as blast loading for different burial depths 5, 10, and 15 cm of soil. This paper highlights the influence of burial depth over the tunnel against impact loading with the mass of impactor 104 kg. Also, the paper highlights the influence of burial depth over the tunnel against blast loading of varying masses of TNT. The experiments were performed on the underground tunnels with different burial depths 5, 10, and 15 cm of soil and measured in terms of the impact force as well as deformed profile. The simulations were conducted on a semi-circular shaped reinforced concrete tunnel with 0.5 m center to center diameter, 1.2 m of length, and 0.05 m of thickness using ABAQUS/CAE Explicit software. The constitutive behavior of concrete, steel reinforcement, and soil element are defined by using the Concrete Damaged Plasticity model, Johnson–Cook Plasticity model, and Drucker-Prager model, respectively. The simulation findings were compared to the experimental results and they were found in good agreement. The major conclusions were drawn based on the impact as well as blast loading on the underground tunnels with varying burial depths.

Keywords Underground tunnels · Burial depth · Blast loading · Impact loading · Experiment · Simulations

K. Senthil (✉) · K. Saini · M. Kumar

Department of Civil Engineering, Dr. B R Ambedkar National Institute of Technology, G.T. Road, Amritsar Bypass, Jalandhar, Punjab 144011, India

e-mail: kasilingams@nitj.ac.in

1 Introduction

Tunneling has become a critical component of today's infrastructure systems all around the world. As a result, it's become critical to ensure the tunnels' safety against any form of man-made blasting activity or any unintentional blasting events as a result, previous research on the dynamic behavior of these structures in the face of surface blast and impact loads should be investigated. The research was based on small-diameter single-track tunnels, which are more vulnerable to internal blast stress and are typical in New York City, and used the Finite Element Method. The lining Theme: Soil-Structure Interaction, Earthquake Engineering, and Computational Geo-mechanics surface was subjected to blast pressure from the explosion, which was applied using a triangle pressure-time diagram, with the elastoplasticity of the ground and lining, as well as their nonlinear interaction, taken into account in the numerical model [1]. The damage was caused by a surface explosion of a sedan, van, small delivery truck (SDT), and container carrying 227, 454, 1814, and 4536 kg of TNT charge weight, respectively, on an underground box frame tube. To simulate and monitor the propagation of the blast pressure waves into the soil, the Arbitrary Lagrangian-Eulerian (ALE) technique was used. The research should be carried out using the ANSYS/LS-DYNA program [2]. The dynamic responses of the buried tunnel at depths of 3.5, 7, 10.5, and 14 m for the surface detonation of a 1000 kg TNT charge in sandy soil. To evaluate and compare semi-ellipse, circular, and horseshoe form tunnels, the Kobe box shape sub-way tunnel was chosen as an example. The finite element software LS-DYNA was utilized to simulate and assess the project's outcome, with the second interaction due to explosion being precisely modeled [3]. Using the widely used explicit dynamic nonlinear finite element program ANSYS/LS-DYNA, analyze the dynamic responses of the operational metro tunnel in soft soil. The blast-induced wave propagation in the soil and tunnel, as well as the von Mises effective stress and acceleration of the tunnel lining, were presented, and the tunnel lining's safety was assessed using the failure criterion and a TNT charge on the ground of no more than 500 kg, and the selection of soil parameters should be given more attention to conduct a more precise analysis [4]. Drop hammer testing is used to test the deformation behavior of tunnels in rock subjected to impact loading. To establish important factors governing fracture and deformations in structural integrity, a thorough examination is conducted. The effect of cover depth and impact energy on the shallow tunnels' settlement. The study is also carried out for various rock masses of varied strength, and tunnel collapse is calculated along the tunnel length [5]. Crack speeds are not constant during crack propagation, and cracks may temporarily stop for a length of time; the greatest arrest period in this study is 227.52 s; propagation toughness is proportional to crack speeds, and arrest toughness is lower than initiation toughness. To simulate crack propagation behavior and path, numerical models were created using the finite-difference code AUTODYN. The dynamic stress intensity factors (SIFS) were calculated using the finite element code ABAQUS [6].

Based on the detailed literature review, it was observed that the investigation on the impact of TNT mass on tunnels subjected to external blast loading AND impact loading is limited. The study was focused to analyze the behavior of reinforced concrete tunnels and its constitutive modeling based on different models is discussed in Sect. 2, while detailed finite element modeling using ABAQUS software is presented in Sect. 3. Then, the impact of external blast loading for different TNT masses placing at 1 m from the top of the soil AND impact loading on the tunnel is studied in Sect. 4, followed by conclusions in Sect. 5.

2 Constitutive Modeling

The concrete damage plasticity model was used to accommodate the tunnel’s constitutive behavior, which includes compressive and tensile activity. The Johnson-cook model has been used to incorporate the elastic and plastic behavior of steel reinforcement bars, which includes the effects of state of stress, temperature, and strain rate, and is discussed in this section.

2.1 Johnson–Cook Model for Reinforcement

In the modeling of the finite element available in ABAQUS, the action of the steel deformation was computed using the Johnson-Cook model. According to strain hardening, strain rate hardening, and thermal softening, the Johnson-Cook model is a function of von Mises tensile flow stress. The Johnson-cook model is represented by Eq. (1):

$$\bar{\sigma} = \left[A + B(\bar{\epsilon}^{pl})^2 \right] \left[1 + C \ln \left(\frac{\dot{\epsilon}^{pl}}{\dot{\epsilon}_0} \right) \right] \left(1 - \hat{\theta}^m \right) \tag{1}$$

where A , B , C , m , and n are material parameters, $\bar{\epsilon}^{pl}$ is equivalent plastic strain, $\dot{\epsilon}^{pl}$ is corresponding plastic strain rate, $\dot{\epsilon}_0$ is a reference strain rate, and $\hat{\theta}^m$ is non-dimensional temperature. The material parameter at melting temperature 1800 K, transition temperature 293 K, reference strain 0.0005, and others are shown in Table 1.

Table 1 Johnson–cook model parameters for steel Fe420

A (Mpa)	B (Mpa)	C	n	m
493	383	0.0114	0.45	0.94

Table 2 Response of concrete to uniaxial loading in **a** compression, **b** tension

Concrete compression damage		Concrete tension damage	
Damage parameter	Inelastic strain	Damage parameter	Cracking strain
0	0	0	0
0.2	0.0011	0.5	0.003
0.5	0.004	0.55	0.005
–	–	0.61	0.007
–	–	0.67	0.01

2.2 Concrete Damaged Plasticity Model

The concrete damage model is a continuum, plasticity-based model. Tensile cracking and compressive crushing of the concrete material are assumed to be the two main failure causes. As indicated in Table 2, the model assumes that the uniaxial tensile and compressive response of concrete is defined by damaged plasticity.

The stress–strain response under uniaxial tension follows a linear elastic relationship until the failure stress, σ_{t0} is achieved. The development of micro-cracking in the concrete material corresponds to the failure stress. The production of micro-cracks is reflected macroscopically by a softening stress–strain response, which promotes strain localization in the concrete structure, in addition to the failure stress. The response to uniaxial compression is linear until the initial yield value, σ_{c0} , the response in the plastic regime is usually characterized by stress hardening followed by strain softening beyond the ultimate stress, σ_{cu} . This representation, although somewhat simplified, captures the main features of the response of concrete.

If E_0 is the material’s initial (unaffected) elastic stiffness, the stress-strain relationships under uniaxial tension and compression loading are:

$$\sigma_t = (1 - d_t)E_0(\varepsilon_t - \tilde{\varepsilon}_t^{pi}) \tag{2}$$

$$\sigma_c = (1 - d_c)E_0(\varepsilon_c - \tilde{\varepsilon}_c^{pi}) \tag{3}$$

where the tension and compression damage variables are denoted by d_t and d_c , respectively. The concrete material properties for the M25 grade were taken from Keshav Saini [7]. As shown in Table 3.

2.3 Finite Element Modeling

The reinforced concrete tunnel and soil finite element model were completed by ABAQUS. The dimension of the semi-cylindrical tunnel is taken as the length of the tunnel is 1.2 m, center to center diameter of 0.5 m, and thickness of 0.05 m in concrete

Table 3 Material constants for concrete material

Density (kg/m ³)	2400
Young’s Modulus (N/m ²)	2.66×10^{10}
Poisson’s ratio	0.2
Dilation angle	30
Eccentricity(m)	1
<i>K</i>	0.66
fb0/fc0	1.16

tunnel modeling as shown in Fig. 1a. A layer of 6 mm in diameter longitudinal and transverse steel reinforcement mounted at 60 mm center to center gap as shown in Fig. 1b. The geometry of the concrete tunnel, soil, and reinforcing steel was modeled correspondingly as solid deformable and deformable wire. The crater for the external blast is located 1 m above the top of the soil. The exterior boundary of the soil element was defined by an acoustic medium with a bulk density of 1500 MPa and a density of 110 Kg/m³. The CONWEP model with the AIR BLAST concept is used to describe the origin of TNT blast load.

At the crown of the tunnel, the stress concentration was high, so fine meshing of size 0.0075 m was used whereas in the rest parts of the tunnel, global seeding of size 0.01 m was introduced. The meshing of soil was done using global seeding of size 0.05 m, mesh size of 0.02 m was provided for both longitudinal and transverse reinforcement. The acceleration due to the gravity of 9.81 m/s² was applied to the whole element except acoustic medium where for skin, the boundary condition is fixed in all directions.

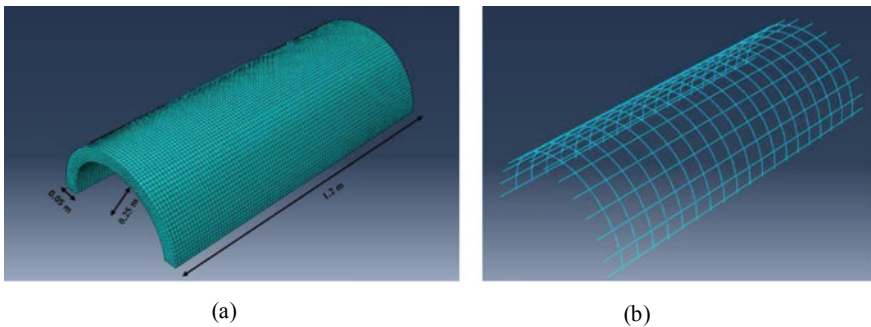


Fig. 1 Mesh modeling of **a** tunnel and **b** reinforcement

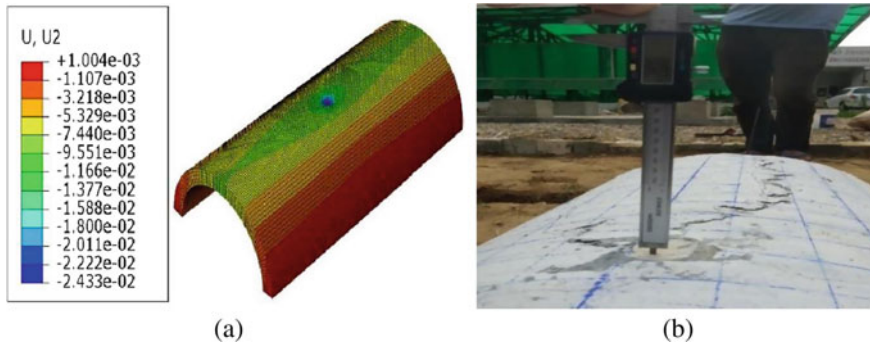


Fig. 2 Downward displacement obtained by **a** numerical simulation and **b** experimentally

2.4 Finite Element Results Validation

The experiment was carried out in a tunnel with a semi-circular cross-section with 1.2 m length, 0.5 m center to center diameter, and 0.05 m lining thickness, by falling a 104 kg hemispherical impactor from a height of 2.4 m over the tunnel [8]. The results have been recorded in terms of down-wards displacement, tension, and compression damage zone on the tunnel based on the experimental observations, as shown in Fig. 2. Overall, the numerical results accurately anticipated the region of tension and compression damage on the tunnel throughout the time step and were shown to be in good agreement with the actual results.

It was observed that a maximum deviation of 15% has been observed between the values of actual displacement and the foreseen displacement. Hence, the considered finite element model is accurate and effective.

3 Results and Discussions

The simulations were carried out for different masses of TNT placed 1 m above the center of burial soil at different burial depths of the tunnel. The tunnel was analyzed by placing TNT at 1 m from the top of the soil.

3.1 Von Mises Stresses for 0.05 m of Burial Depth

The stresses observed in the tunnel, having TNT 1 kg, were 8.5 MPa, 7.8 MPa, and 7.8 MPa at a time of 0.02, 0.035, and 0.05 s, respectively. Similarly, for 5 kg of TNT, at the same times as that for 1 kg were 15 MPa, 16.2 MPa, and 15.2 MPa, respectively, and that for 10 kg of TNT, were 17.7 MPa, 17.4 MPa, and 16.5 MPa, respectively. It

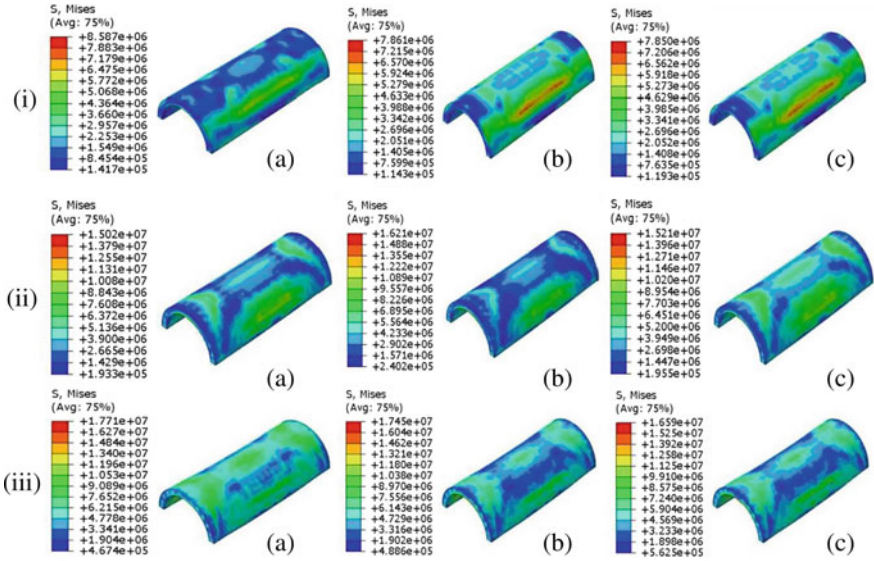


Fig. 3 Von Mises stresses for (i) 1 kg, (ii) 5 kg, (iii) 10 kg and (a) 0.02 s, (b) 0.035 s and (c) 0.05 s with 0.05 m burial depth

was seen that the stresses developed in the tunnel were increasing with the increase in the mass of TNT. For the rest times, comparatively higher stresses were developed when 10 kg TNT was used. Contour plots for different masses of TNT are presented in Fig. 3.

3.2 Von Mises Stresses for 0.1 m of Burial Depth

The stresses observed in the tunnel, having TNT 1 kg, were 7.9 MPa, 7.6 MPa, and 7.4 MPa at a time of 0.02, 0.035, and 0.05 s, respectively. Similarly, for 5 kg of TNT, at the same times as that for 1 kg were 14.5 MPa, 14.4 MPa, and 14.4 MPa, respectively, and that for 10 kg of TNT, were 18.2 MPa, 17.9 MPa, and 17.3 MPa, respectively. It was seen that the stresses developed in the tunnel were increasing with the increase in the mass of TNT. For the rest times, comparatively higher stresses were developed when 10 kg TNT was used. Contour plots for different masses of TNT are presented in Fig. 4.

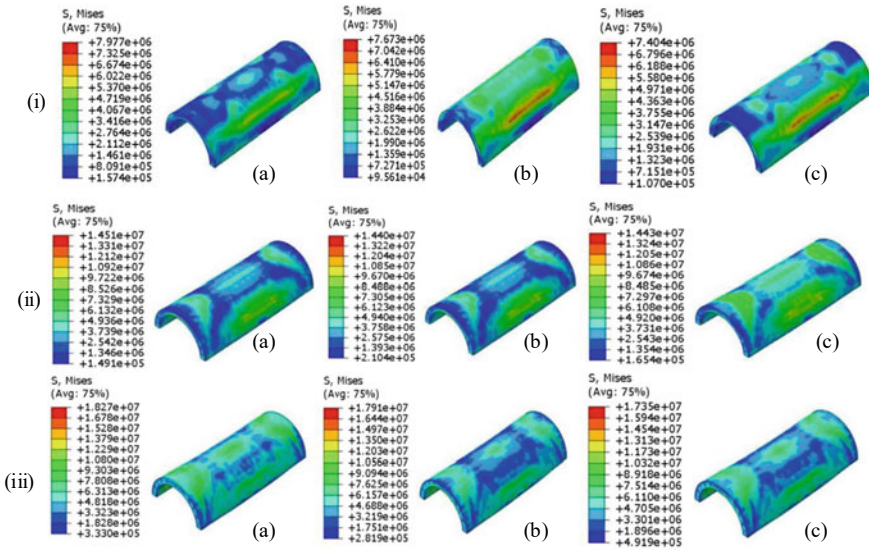


Fig. 4 Von Mises stresses for (i) 1 kg, (ii) 5 kg, (iii) 10 kg and (a) 0.02 s, (b) 0.035 s and (c) 0.05 s with 0.1 m burial depth

3.3 Von Mises Stresses for 0.15 m of Burial Depth

The stresses observed in the tunnel, having TNT 1 kg, were 7.6 MPa, 6.9 MPa, and 7.3 MPa at a time of 0.02, 0.035, and 0.05 s, respectively. Similarly, for 5 kg of TNT, at the same times as that for 1 kg were 15 MPa, 15 MPa, and 15.1 MPa, respectively, and that for 10 kg of TNT, were 17.6 MPa, 17.5 MPa, and 17.5 MPa, respectively. It was seen that the stresses developed in the tunnel were increasing with the increase in the mass of TNT. For the rest times, comparatively higher stresses were developed when 10 kg TNT was used. Contour plots for different masses of TNT are presented in Fig. 5.

3.4 Von Mises Stresses for Impact Loading of 104 kg

The stresses observed in the tunnel, having the weight of 104 kg of impactor at a burial depth of 0.05 m, were 25.5 MPa, 14.6 MPa, and 15.17 MPa at a time of 0.02, 0.035, and 0.05 s, respectively. Similarly, for 0.1 m of burial depth, at the same times as that for 5 cm, burial depth was 73.2 MPa, 18.9 MPa, and 19.4 MPa, respectively, and that for 0.15 m burial depth, were 19 MPa, 72.7 MPa, and 75.9 MPa, respectively. It was seen that the stresses developed in the tunnel were increasing with increase burial depth. Contour plots for different burial depths are presented in Fig. 6.

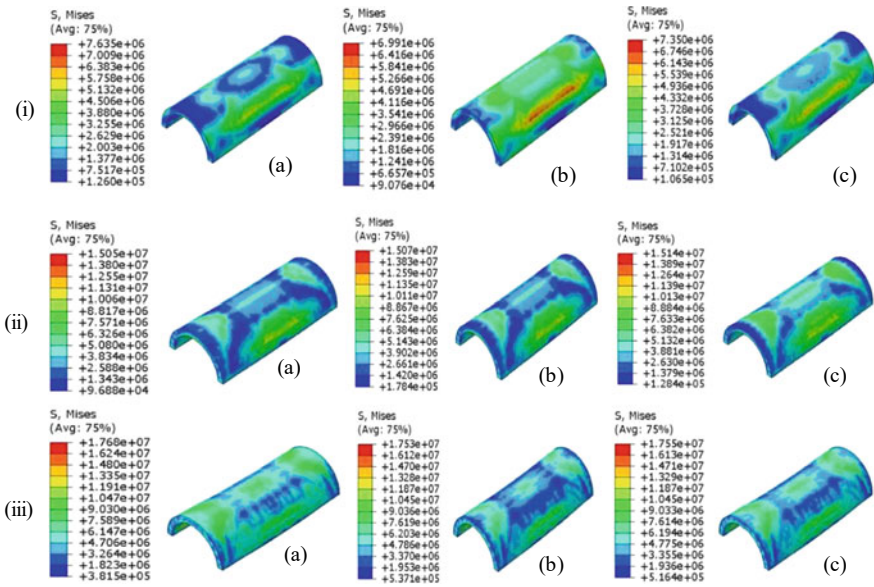


Fig. 5 Von Mises stresses for (i) 1 kg, (ii) 5 kg, (iii) 10 kg and (a) 0.02 s, (b) 0.035 s and (c) 0.05 s with 0.15 m burial depth

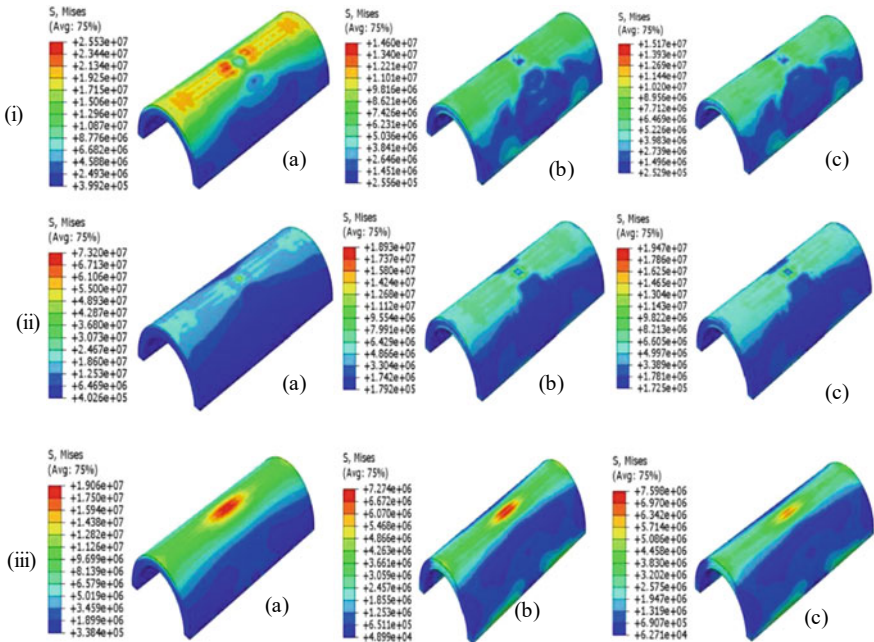


Fig. 6 Von Mises stresses for (i) 5 cm, (ii) 10 cm, (iii) 15 cm and (a) 0.02 s, (b) 0.035 s and (c) 0.05 s against 104 kg mass of impactor

4 Displacement

The displacement observed in the tunnel, at Burial Depth (BD) 0.05 m having TNT 1 kg, was maximum displacement 3.26 mm, respectively. Similarly, for 5 kg were 14.703 mm, and that for 10 kg of TNT, were 23.684 mm, respectively. It was seen that the displacement in the tunnel was increasing with the increase in the mass of TNT. For the rest times, comparatively higher displacement was developed when 10 kg TNT was used. Graph plots for different masses of TNT are presented in Fig. 7a.

The displacement observed in the tunnel, at Burial Depth (BD) 0.1 m having TNT 1 kg, was maximum displacement of 3.087 mm, respectively. Similarly, for 5 kg were 18.858 mm, and that for 10 kg of TNT, was 34.9 mm, respectively. It was seen that the displacement in the tunnel was increasing with the increase in the mass of TNT. For the rest times, comparatively higher displacement was developed when 10 kg TNT was used. Graph plots for different masses of TNT are presented in Fig. 7b.

The displacement observed in the tunnel, at Burial Depth (BD) 0.15 m having TNT 1 kg, was maximum displacement 3.05 mm, respectively. Similarly, for 5 kg

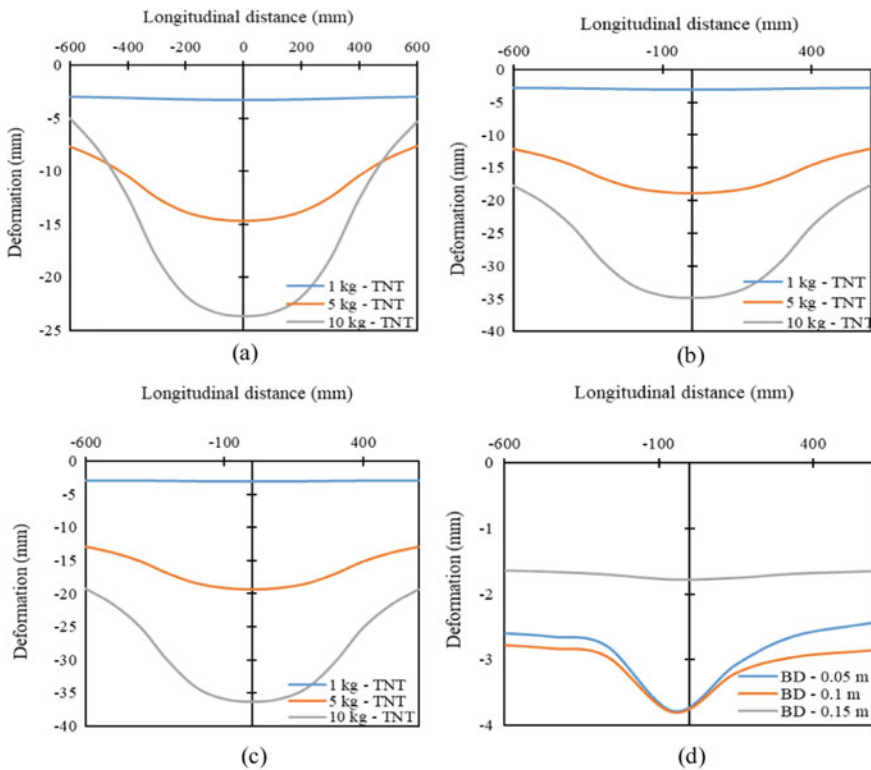


Fig. 7 Vertical downward displacements for burial depth (a) 0.05 m (b) 0.1 m (c) 0.15 m at different TNT masses and (d) impact load at different burial depth

were 19.403 mm, and that for 10 kg of TNT, were 36.332 mm, respectively. It was seen that the displacement in the tunnel was increasing with the increase in the mass of TNT. For the rest times, comparatively higher displacement was developed when 10 kg TNT was used. Graph plots for different masses of TNT are presented in Fig. 7c.

The displacement observed in the tunnel, having the weight of 104 kg of impactor at a burial depth of 0.05 m, was a maximum displacement of 3.79 mm. Similarly, for 10 cm of burial depth were 3.81 mm, respectively, and that for 15 cm burial depth, were 1.79 mm, respectively. It was seen that the displacement in the tunnel was decreased with increase burial depth. Contour plots for different burial depths are presented in Fig. 7d.

The displacement observed in the tunnel at the center node, at Burial Depth (BD) 0.05 m having TNT 1 kg, were maximum displacement 5.284 mm, respectively. Similarly, for 5 kg was 27.927 mm, and that for 10 kg of TNT, were 57.359 mm, respectively. It was seen that the displacement in the tunnel was increasing with the increase in the mass of TNT. For the rest times, comparatively higher displacement was developed when 10 kg TNT was used. Graph plots for different masses of TNT are presented in Fig. 8a.

The displacement observed in the tunnel at the center node, at Burial Depth (BD) 0.1 m having TNT 1 kg, were maximum displacement 5.086 mm, respectively. Similarly, for 5 kg were 26.7 mm, and that for 10 kg of TNT, were 53.7855 mm, respectively. It was seen that the displacement in the tunnel was increasing with the increase in the mass of TNT. For the rest times, comparatively higher displacement was developed when 10 kg TNT was used. Graph plots for different masses of TNT are presented in Fig. 8b.

The displacement observed in the tunnel at the center node, at Burial Depth (BD) 0.15 m having TNT 1 kg, were maximum displacement 4.995 mm, respectively. Similarly, for 5 kg were 26.46 mm, and that for 10 kg of TNT, was 53.64 mm, respectively. It was seen that the displacement in the tunnel was increasing with the increase in the mass of TNT. For the rest times, comparatively higher displacement was developed when 10 kg TNT was used. Graph plots for different masses of TNT are presented in Fig. 8c.

The displacement observed in the tunnel at the center node, having the weight of 104 kg of impactor at a burial depth of 0.05 m, was a maximum displacement of 12.923 mm. Similarly, for 0.1 m of burial depth were 13.669 mm, respectively, and that for 0.15 m burial depth, were 5.964 mm, respectively. It was seen that the displacement in the tunnel was decreased with increase burial depth. Contour plots for different burial depths are presented in Fig. 8d.

5 Acceleration

The acceleration observed at the center node in the tunnel having burial depth of 0.05 m, having TNT 1 kg, was maximum acceleration of 5774.82 m/s², respectively.

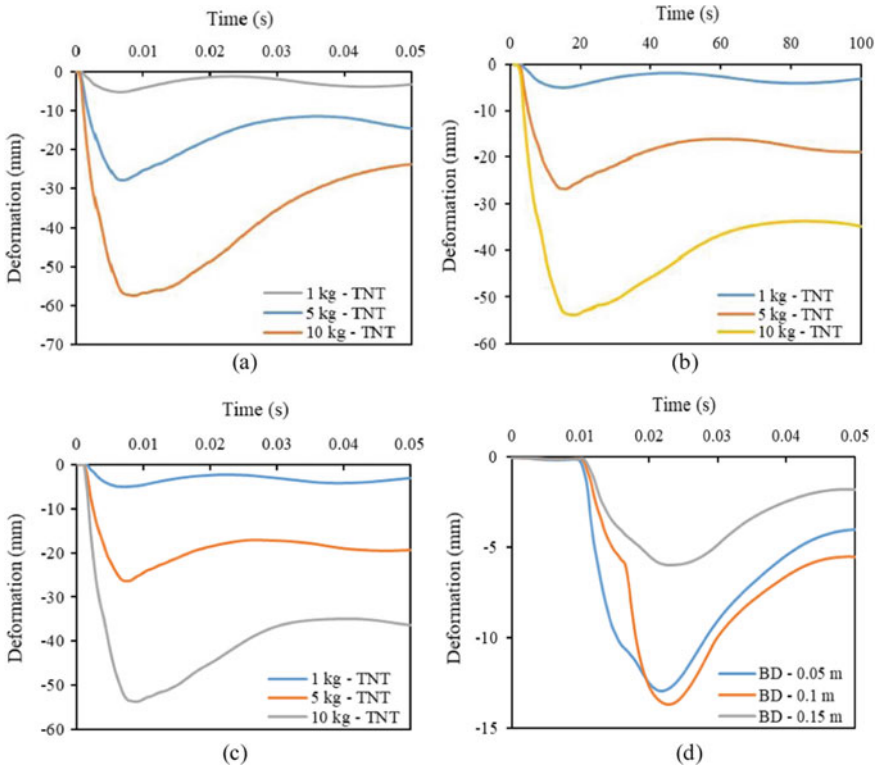


Fig. 8 Vertical downward displacements at center node for burial depth **a** 0.05 cm **b** 0.1 cm **c** 0.15 m at different TNT masses and **d** impact load at different burial depths

Similarly, 5 kg of TNT was a maximum of 15659.7 m/s^2 , and that for 10 kg of TNT, was a maximum of 42149 m/s^2 , respectively. It was seen that the acceleration in the tunnel was increasing with the increase in the mass of TNT. For the rest times, comparatively maximum acceleration was developed when 10 Kg TNT was used. Graph plots between time versus acceleration are presented in Fig. 9a. The acceleration observed at the center node in the tunnel having burial depth of 0.1 m, having TNT 1 kg, was maximum acceleration of 7644.69 m/s^2 , respectively. Similarly, 5 kg of TNT were maximum 35142.7 m/s^2 and that for 10 kg of TNT, were maximum 55039.7 m/s^2 , respectively. It was seen that the acceleration in the tunnel was increasing with the increase in the mass of TNT. For the rest times, comparatively maximum acceleration was developed when 10 kg TNT was used. Graph plots between time versus acceleration are presented in Fig. 9b.

The acceleration observed at the center node in the tunnel having burial depth of 0.15 m, having TNT 1 kg, was maximum acceleration 7461.64 m/s^2 , respectively. Similarly, 5 kg of TNT was a maximum of 6994.83 m/s^2 , and that for 10 kg of TNT, was a maximum of 18559.9 m/s^2 , respectively. It was seen that the acceleration in the tunnel was increasing with the increase in the mass of TNT. For the rest

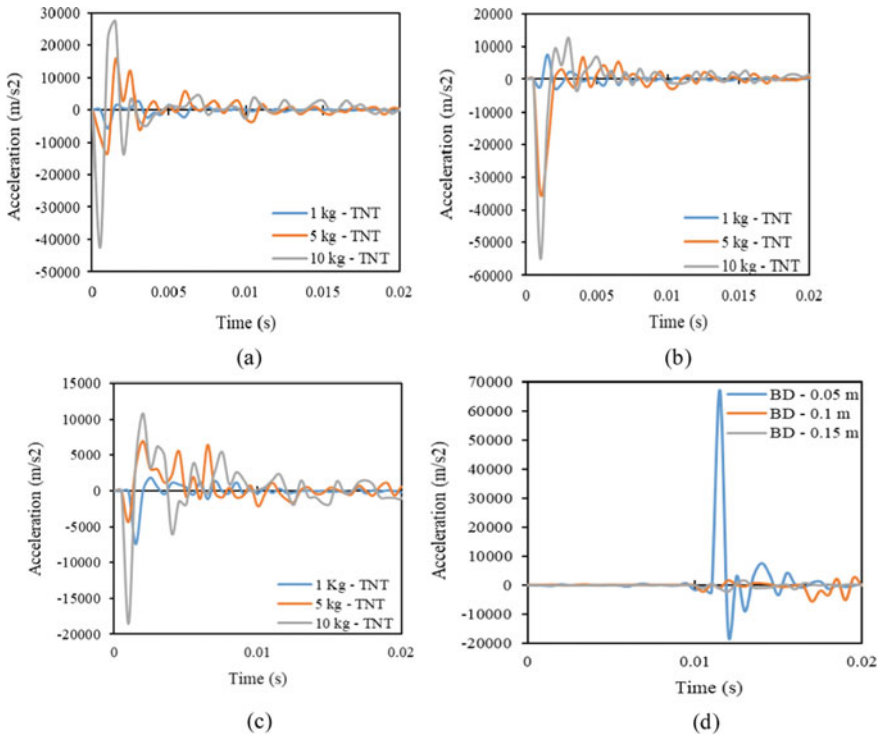


Fig. 9 Vertical accelerations at center node for burial depth (a) 0.05 m (b) 0.1 m (c) 0.15 m at different TNT masses and (d) impact load at different burial depth

times, comparatively maximum acceleration was developed when 10 kg TNT was used. Graph plots between time versus acceleration are presented in Fig. 9c. The acceleration observed at the center node in the tunnel, having the weight of 104 kg of impactor at a burial depth of 0.05 m, was maximum acceleration 67021.2 m/s², respectively. Similarly, for burial depth 0.1 m were maximum 17393.3 m/s², and that for burial depth 0.15 m, were maximum 2102.45 m/s², respectively. It was seen that the acceleration in the tunnel was decreased with an increase in the burial depth of soil. For the rest times, comparatively maximum acceleration was developed at a 0.05 m burial depth graph plots between time versus acceleration are presented in Fig. 9d.

Longitudinal, node deformation and acceleration in the tunnel increase with increase mass of TNT for a burial depth. Longitudinal, node deformation and acceleration in the tunnel decrease with an increase in burial depth for impact loading shown in Table 4.

Table 4 Peak longitudinal, node displacement and acceleration on the tunnel with varying burial depth

Specimen no		Peak displacement		Peak acceleration (m/s ²)
		Longitudinal deformation (mm)	Node deformation (mm)	
BD-0.05 m	1 kg-TNT	3.26	5.284	5774.82
	5 kg-TNT	14.703	27.927	15,659.7
	10 kg-TNT	23.684	57.359	42,149
BD-0.10 m	1 kg-TNT	3.087	5.086	7644.69
	5 kg-TNT	18.858	26.7	35,142.7
	10 kg-TNT	34.9	53.7855	55,039.7
BD-0.15 m	1 kg-TNT	3.05	4.995	7461.64
	5 kg-TNT	19.403	26.46	6994.83
	10 kg-TNT	36.332	53.64	18,559.9
Impact loading	BD-0.05 m	3.79	12.923	67,021.2
	BD-0.1 m	3.81	13.669	17,393.3
	BD-0.15 m	1.79	5.9644	2102.45

6 Conclusion

The following conclusions were obtained based on the extensive investigations:

- It was observed that the Von Mises stresses developed in the tunnel increase with increase mass of TNT for a burial depth and decrease with increase with burial depth for a TNT mass.
- The longitudinal deformation in the tunnel increase with increase mass of TNT for a burial depth, and node deformation also increases with increase mass of TNT for a burial depth.
- It was concluded that the acceleration in the tunnel increase with increase mass of TNT for a burial depth.
- It was also concluded that the deformation in the tunnel decrease with an increase in burial depth for impact loading.
- The acceleration in the tunnel decrease with an increase in burial depth for impact loading.

References

1. Liu H (2009) Dynamic analysis of subway structures under blast loading. *Geotech Geol Eng* 27(6):699–711
2. Zaid M (2021) Preliminary study to understand the effect of impact loading and rock weathering in tunnel constructed in quartzite. *Geot Geol Eng*

3. Tiwari R, Chakraborty T, Matsagar V (2017) Dynamic analysis of tunnel in soil subjected to internal blast loading. *Geotech Geol Eng* 35(4):1491–1512
4. Xiang Y, Yang Y (2017) Spatial dynamic response of submerged floating tunnel under impact load. *Mar Struct* 53:20–31
5. Gahoi, Zaid M, Mishra S, Rao KS (2017) Numerical analysis of the tunnels subjected to impact loading
6. Zhou L, Zhu Z, Wang M, Ying P, Dong Y (2018) Dynamic propagation behavior of cracks emanating from tunnel edges under impact loads. *Soil Dyn Earthq Eng* (August 2017)
7. Saini K (2021) MTech Thesis, National Institute of Technology, Jalandhar
8. Hafezolzghorani M, Hejazi F, Vaghei R, Jaafar MSB, Karimzade K (2017) Simplified damage plasticity model for concrete. *Struct Eng Int*

Plate Load Tests on the Ring and Circular Footings



Vaibhav Sharma and Arvind Kumar

Abstract Ring foundations are suitable for axi-symmetrical structures, like tall towers, chimneys, overhead tanks, etc. It is a common practice that designers often adopt circular footing for these structures as foundations because of limited amount of studies conducted on ring footings. However, a ring footing can be employed in place of a circular footing because of its two advantages. Firstly, ring footing behaves in a similar way as that of a circular footing, which profoundly depends on the radius-ratio (ratio of inner radius to the outer radius of the footing) of ring footing under consideration. Secondly, the ring footing will act as an economical solution because of the lesser consumption of material to produce it. Therefore, the aim of this paper is to conduct the plate load tests on surface ring and circular footings resting on sand by varying radius-ratios from 0.00, 0.30, 0.40, 0.50 and 0.60. Here, radius-ratio of 0.00 signifies a circular footing. Moreover, a comparison between the behavior of circular and ring footings is done. From the experimental results, it was discovered that the ring footing with a radius-ratio in the range of 0.30–0.40 proved to be the better option out of the used footings, when compared with the circular footing.

Keywords Ring footing · Plate load test · Sand · Bearing capacity factor · Settlement factor

V. Sharma (✉)

School of Civil Engineering, Lovely Professional University, Punjab 144411, India

e-mail: civil.vaibhav.sharma@gmail.com

A. Kumar

Department of Civil Engineering, Dr. B R Ambedkar National Institute of Technology, Jalandhar 144011, India

e-mail: agnihotriak@nitj.ac.in

1 Introduction

Ring footings are an ideal choice for axi-symmetrical structures, like tall towers, silos, chimneys, etc. [1–4]. However, the designers often opt circular footings instead of ring footings because there is limited proof available that it can perform better than circular footing.

At present, no universally accepted bearing capacity formula pertaining to the ring footing is available. Moreover, majority of studies conducted on ring footings were based on the assumption of plain-strain condition [5–18].

Although the plain-strain condition simulates the approximate behavior of ring footing, but for its true behavior it needs to be considered as a three-dimensional body, which can only be achieved through model testing or using any three-dimensional (3D) analytical or numerical approach. Therefore, few researchers had conducted studies on ring footing using model tests [19–23], analytical methods [7, 10] and numerical modeling [9, 18, 24].

From the literature, it has been observed that there is a need to conduct studies on ring footings using any of the aforementioned 3D approaches to explore the true behavior of ring footings. Moreover, a comparative study is also required between ring and circular footings. Therefore, the present study is undertaken to study the effect of ring footing resting on sand stratum. Moreover, a comparison with the circular footing is done. Furthermore, results obtained from this study were compared with the literature. Four ring footings with different radius-ratios (ratio of inner radius to the outer radius) of 0.30, 0.40, 0.50 and 0.60 were used. One circular footing was used in the study with outer diameter of 300 mm. The outer diameter of ring and circular footings was kept constant throughout the study.

2 Soil

The soil used in the study was river sand, which was classified as poorly graded sand, SP, according to the unified soil classification system (ASTM D2487, [25]). The sand has a specific gravity of 2.65. The maximum and minimum dry unit weights were observed as 16.8 kN/m³ and 13.6 kN/m³, respectively. The minimum and maximum void ratios were 0.56 and 0.93, respectively. The grain-size distribution data revealed that the sand has a coefficient of curvature (C_c) of 0.97, a coefficient of uniformity (C_u) of 2.20, an effective size (D_{10}) of 0.15 mm and a mean size (D_{50}) of 0.22 mm. The angle of internal friction, ϕ , obtained for drained tri-axial test was 36.30°.

3 Footings

Five different footings were used in the study, that is, one circular footing and four ring footings. All of these footings were made from mild steel and were corrected to the desired size and thickness. The diameter of the circular footing was 300 mm, which is also the external diameter of ring footing. Ring footings with different radius-ratio were used. The thickness of all of the footings was kept constant at 25 mm. The outer radius of the ring footing was kept constant throughout the study, and only the inner radius of the ring footing was varied to produce different ring footings with the radius-ratios of 0.30, 0.40, 0.50 and 0.60. To make the footings rough, sand layer was pasted to the underside of the footings with the help of epoxy glue.

4 Testing Setup, Sample Preparation and Testing Procedure

Plate load test was performed in a testing-cum-loading frame assembly. The testing tank was made with inner dimensions of 1500 mm long, 1500 mm wide and 1000 mm deep. A loading frame was installed in such a manner that the tank was located at its center. Loading frame was used to apply load on the prepared soil bed through a hydraulic jack. Figure 1 shows the testing assembly used in the study to carry plate load test. The testing tank was filled with dry sand using sand pluviation technique to achieve a dry unit weight of 15.40 kN/m^3 with a void ratio of 0.71. In this technique, sand is poured in the tank from a constant height so as to maintain uniformity of density in the tank. However, to verify the uniformity of denseness of sand different cans of known volume were placed in the four corners of the tank and at different depths. The difference in density observed at these locations was observed to be less than 1.00%. Moreover, its coefficient of variation was found to be less than 0.81%.



Fig. 1 Testing assembly; a testing-cum-loading assembly; b close view of testing arrangement

Fig. 2 Loading platform

After filling the tank up to the desired level, footing was placed centrally and carefully. It was, perhaps, impossible to place the hydraulic jack directly on the ring footing because it will slip through the hole of the ring footing. This problem was, however, simplified by using a loading platform (Fig. 2). It was, only after placing the hydraulic jack, made possible to apply load on the footing. The hydraulic jack was placed centrally on the footing to avoid any eccentricity. Thereafter, spacer blocks were used to make the connection between the hydraulic jack and the reaction frame's beam. Then, two 0.01 mm sensitive dial gauges were placed on the opposite sides of the footing to measure its settlement corresponding to each load increment. The dial gauges were resting on steel datum bars which were supported on the tank edges which are stable and cannot undergo any kind of deformation during the testing procedure.

Then, load was applied through a manually operated hydraulic jack and the load increment was done until the footing fails (a small load increment produces excessive settlement) or the piston of the hydraulic jack gets fully extended. The application of load was maintained until the rate of settlement ceases or reduces to a value of 0.02 mm/min.

5 Results and Discussions

Plate load tests were carried out on circular and ring footings resting on sand bed. The results are presented in the form of ultimate bearing capacity (UBC), ultimate settlement, bearing capacity factor (BCF) and settlement factor (SF). The BCF compares the ultimate bearing capacity of ring footings with circular footing, and its expression

is given in Eq. (1).

$$BCR = \frac{UBC \text{ of ring footing}}{UBC \text{ of circular footing}} \tag{1}$$

The SF compares the settlement corresponding to the UBC of ring footings with settlement corresponding to the UBC of circular footing, and its expression is given in Eq. (2).

$$SF = \frac{\text{Ultimate settlement of ring footing}}{\text{Ultimate settlement of circular footing}} \tag{2}$$

Figure 3 shows the pressure-settlement curves obtained from the plate load tests conducted on ring and circular footings. To obtain the UBC, tangent intersection method was adopted owing to the non-availability of clear failure point on the curve. In this method, initial and the final straight part of the respective pressure-settlement curve is extended to meet at a point. The pressure and settlement corresponding to this point are taken as UBC and ultimate settlement, respectively. It can be inferred from Fig. 3 that the pressure-settlement curves of ring footings with radius-ratio of 0.30 and 0.40 lie above the circular footing. However, the curves for ring footings, pertaining to radius-ratio of 0.50 and 0.60, lie below the circular footing. This shows that the ring footing behaves in a better way than the circular footing provided the radius-ratio of the ring footing lies in the range of 0.30 and 0.40.

Figure 4 shows the variation of UBC and ultimate settlement with the radius-ratio. It can be seen that as the radius-ratio increases, UBC increases until radius-ratio reaches 0.40 and on further increasing the radius-ratio, that is, beyond 0.40, UBC starts decreasing and reaches an asymptotic state when radius-ratio achieves a value of 0.60. Similarly, on increasing the radius-ratio the ultimate settlement starts decreasing until the radius-ratio reaches a value of 0.40, and on further increasing

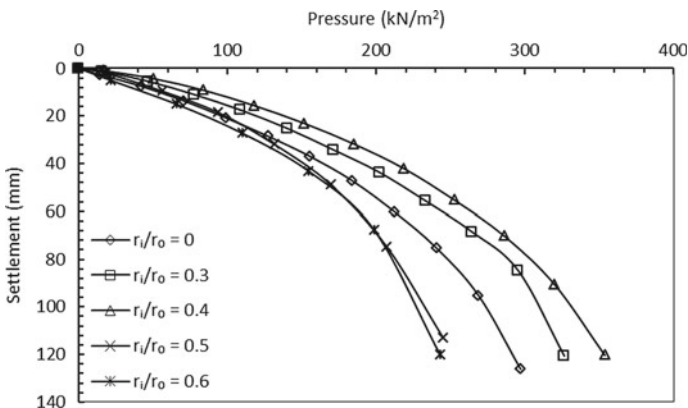


Fig. 3 Pressure-settlement curves obtained from plate load test

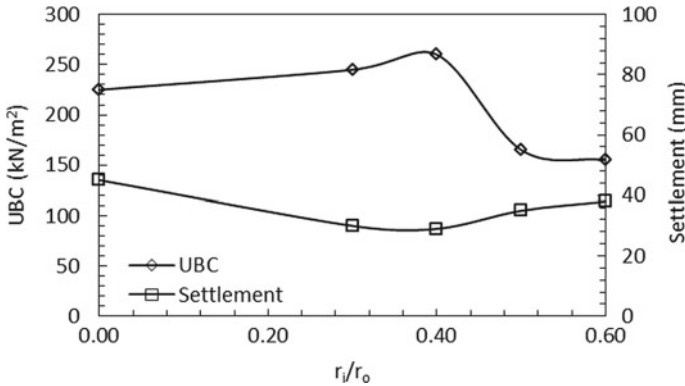


Fig. 4 UBC and settlement obtained from plate load test

the radius-ratio, the ultimate settlement starts increasing and reaches an asymptotic state at a radius-ratio of 0.60. The percentage improvement in UBC of ring footings, having radius-ratio of 0.30 and 0.50, compared to circular footing is 9% and 15.55%, respectively, whereas, a reduction of UBC of ring footing (radius-ratio, 0.50 and 0.60) compared to circular footing is of the order of 26.67% and 31.11%, respectively. Moreover, the percentage reduction in ultimate settlement of ring footing with radius-ratio of 0.30 and 0.40 is 33.33% and 35.55%, respectively. On contrary to this, the reduction in settlement of ring footing (radius-ratio, 0.50 and 0.60) in comparison with circular footing is of the order 22.22% and 15.55%, respectively.

Figure 5 shows the variation of BCF and SF with radius-ratio. It can be seen that as the radius-ratio increases, the BCF increases and reaches a maximum value of 1.15 when radius-ratio reaches 0.4. However, beyond this the radius-ratio decreases and reaches an asymptotic state with a value of 0.69 when radius-ratio is 0.60. Similar trend was observed by Boushehrian and Hataf [22]. In their study, the soil used was well-graded sand, SW, with an angle of internal friction, ϕ , 38° , maximum dry unit weight, γ_{\max} , 17 kN/m^3 , minimum dry unit weight, γ_{\min} , 14.10 kN/m^3 , coefficient of uniformity, C_u , 1.07 and coefficient of curvature, C_c , 8.40. The comparison shows a good agreement when radius-ratio is in the range of 0.00–0.40; however, some variation can be observed in the BCF values when radius-ratio goes beyond 0.40. This variation is due to many factors which can affect the BCF values, like footing size, footing material and soil properties. On the bright side, the trend is, somewhat, similar in both the studies. The reason that ring footing behaves better both in the context of UBC and ultimate settlement is because of the phenomenon called soil arching [1–4, 22]. Moreover, it can be seen from Fig. 5 that the SF keeps on decreasing until the radius-ratio reaches a value of 0.40 and beyond this the SF value starts increasing. The SF value reaches a minimum value of 0.64 at radius-ratio of 0.40 and reaches an asymptotic state when radius-ratio reaches a value of 0.60.

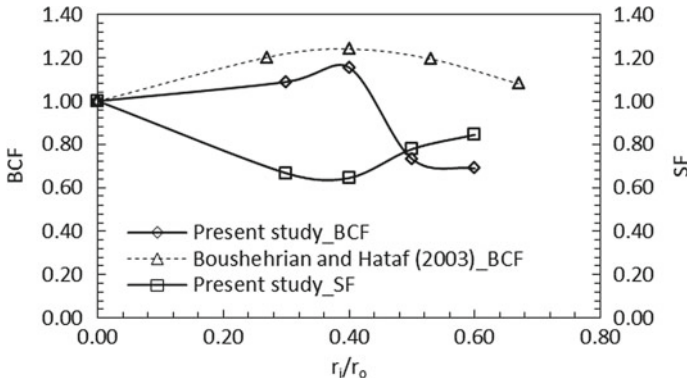


Fig. 5 BCF and SF obtained from plate load test and comparison with Boushehrian and Hataf [22]

6 Conclusions

Plate load tests were conducted on ring and circular footings resting on poorly graded sand stratum. The test results were presented in the form of UBC, ultimate settlement, UBF and SF. Moreover, a comparison of the test results of this study had been done with the one in literature. From the test results, the following conclusions were drawn.

- (a) Ring footings can behave better than a circular footing provided the right type of radius-ratio is chosen. For better performance of ring footing, the optimum range of radius-ratio is 0.30–0.40.
- (b) The percent increase in the UBC of ring footing with radius-ratio in the range of 0.3–0.4 in comparison with circular footing having same outer diameter is in the range of 9–15.55%. Similarly, the ultimate settlement reduction is in the range of 26.67–31.11%.
- (c) The BCF reaches a maximum value of 1.15 when radius-ratio is 0.40. Similarly, the SF value reaches a minimum value of 0.64 when radius-ratio is 0.40.
- (d) The UBC, ultimate settlement, BCF and SF values reach an asymptotic state when radius-ratio reaches 0.60.
- (e) The test results were found to be in good agreement with the literature.

References

1. Sharma V, Kumar A (2019) Numerical study of ring and circular foundations resting on fibre-reinforced soil. *Int J Geotech Eng* 1–13. <https://doi.org/10.1080/19386362.2019.1603680>
2. Sharma V, Kumar A (2019) Influence of relative density of soil on performance of fiber-reinforced soil foundations. *Geotext Geomembr* 45(5):499–507. <https://doi.org/10.1016/j.geotextmem.2017.06.004>

3. Sharma V, Kumar A (2018) Behavior of ring footing resting on reinforced sand subjected to eccentric-inclined loading. *J Rock Mech Geotech Eng* 10(2):347–357. <https://doi.org/10.1016/j.jrmge.2017.11.005>
4. Sharma V, Kumar A (2017) Strength and bearing capacity of ring footings resting on fibre-reinforced sand. *Int J Geosynthetics Ground Eng* 3:1–17. <https://doi.org/10.1007/s40891-017-0086-6>
5. Prasad SD, Chakraborty M (2021) Bearing capacity of ring footing resting on two layered soil. *Comput Geotech* 134:104088. <https://doi.org/10.1016/j.compgeo.2021.104088>
6. Benmebarek S, Remadna MS, Benmebarek N, Belounar L (2012) Numerical evaluation of the bearing capacity factor N_y of ring footings. *Comput Geotech* 44:132–138. <https://doi.org/10.1016/j.compgeo.2012.04.004>
7. Kumar J, Chakraborty M (2015) Bearing capacity factors for ring foundations. *J Geotech Geoenviron Eng* 141(10):06015007. [https://doi.org/10.1061/\(ASCE\)GT.1943-5606.0001345](https://doi.org/10.1061/(ASCE)GT.1943-5606.0001345)
8. Naseri M, Hosseininia ES (2015) Elastic settlement of ring foundations. *Soils Found* 55(2):284–295. <https://doi.org/10.1016/j.sandf.2015.02.005>
9. Sargazi O, Hosseininia ES (2017) Bearing capacity of ring footings on cohesionless soil under eccentric load. *Comput Geotech* 92:169–178. <https://doi.org/10.1016/j.compgeo.2017.08.003>
10. Kumar J, Ghosh P (2005) Bearing capacity factor N_y for ring footings using the method of characteristics. *Can Geotech J* 42(5):1474–1484. <https://doi.org/10.1139/T05-051>
11. Zhao L, Wang JH (2008) Vertical bearing capacity for ring footings. *Comput Geotech* 35:292–304. <https://doi.org/10.1016/j.compgeo.2007.05.005>
12. Choobbasti AJ, Heshami S, Najafi A, Pirzadeh S, Farrokhzad F, Zahmatkesh A (2010) Numerical evaluation of bearing capacity and settlement of ring footing—case study of kazeroon cooling towers. *Int J Res Rev Appl Sci* 4(2):263–271
13. Seyedi HE (2016) Bearing capacity factors of ring footings. *Iran J Sci Technol Trans Civil Eng* 40(2):121–132. <https://doi.org/10.1007/s40996-016-0003-6>
14. Kumar J, Chakraborty M (2015) Bearing capacity factors for ring foundations. *J Geotech Geoenviron Eng* 141(10):1–7. [https://doi.org/10.1061/\(ASCE\)GT.1943-5606.0001345](https://doi.org/10.1061/(ASCE)GT.1943-5606.0001345)
15. Tang C, Phoon K (2018) Prediction of bearing capacity of ring foundation on dense sand with regard to stress level effect. *Int J Geomech* 18(11):1–12. [https://doi.org/10.1061/\(ASCE\)GM.1943-5622.0001312](https://doi.org/10.1061/(ASCE)GM.1943-5622.0001312)
16. Vali R, Beygi M, Saberian M, Li J (2019) Bearing capacity of ring foundation due to various loading positions by finite element limit analysis. *Comput Geotech* 110:94–113. <https://doi.org/10.1016/j.compgeo.2019.02.020>
17. Kadhum MQ, Albusoda BS (2021) Behaviours of ring and circular footings subjected to eccentric loading: a comparative study. In: *IOP conference series: materials science and engineering* 2021. IOP Publishing; vol 1067, pp 12056. <https://doi.org/10.1088/1757-899x/1067/1/012056>
18. Keshavarz A, Kumar J (2017) Bearing capacity computation for a ring foundation using the stress characteristics method. *Comput Geotech* 89:33–42. <https://doi.org/10.1016/j.compgeo.2017.04.006>
19. Karaulov AM (2006) Experimental and theoretical research on the bearing capacity of ring-foundation beds. *Soil Mech Found Eng* 43(2):37–40
20. Ismael NF (1996) Loading tests on circular and ring plates in very dense cemented sands. *J Geotech Eng* 122(4):281–287
21. Naderi E, Hataf N (2014) Model testing and numerical investigation of interference effect of closely spaced ring and circular footings on reinforced sand. *Geotext Geomembr* 42(3):191–200. <https://doi.org/10.1016/j.geotexmem.2013.12.010>
22. Boushehrian JH, Hataf N (2003) Experimental and numerical investigation of the bearing capacity of model circular and ring footings on reinforced sand. *J Geotext Geomembr* 21(4):241–256. [https://doi.org/10.1016/S0266-1144\(03\)00029-3](https://doi.org/10.1016/S0266-1144(03)00029-3)
23. El SM, Nazir A (2012) Behavior of eccentrically loaded small-scale ring footings resting on reinforced layered soil. *J Geotech Geoenviron Eng* 138(3):376–384. [https://doi.org/10.1061/\(ASCE\)GT.1943-5606.0000593](https://doi.org/10.1061/(ASCE)GT.1943-5606.0000593)

24. Laman M, Yildiz A (2007) Numerical studies of ring foundations on geogrid-reinforced sand. *Geosynth Int* 14(2):52–64. <https://doi.org/10.1680/gein.2007.14.2.52>
25. ASTM D2487: Standard practice for classification of soils for engineering purposes (Unified Soil Classification System) 2017. <https://doi.org/10.1520/D2487-11>

Analytical Study on Soil-Structure Interaction of Framed Structure with Isolated Footing Resting on Silty Sand



R. Chaitra, R. Sridhar, and B. M. Ramesh

Abstract The traditional analysis does not consider any interaction between the soil and foundation element. It is very vital to assess the mechanism of the soil-structure interaction. Also, in usual method of analysis, the analysis of the framed structures is expected to rest on unyielding supports. The present study emphasis on the soil-structure interaction importance of three bay, three-storey RC frame and evaluated the displacement and stresses in frame and soil (the point of contact). The frame was modelled as linear elastic and the ground was modelled as linear elastic and non-linear elastic–plastic. The foundation settlement was analysed for the soils which have low stiffness, which leads to excessive settlement.

Keywords Soil-structure interaction · Framed structure · Isolated footing · Displacement · Stress intensities

1 Introduction

The essentials of substructures have a direct contact with the ground. When these substructures were exposed to lateral forces, the structure dislocated horizontally and lost contact with the soil. The procedure wherein the reaction between soil-structure and the displacement of the structure influences the response of the soil is named as soil-structure interaction (SSI). The concern is about learning and the plan of the different structures, therefore multi-storied structures, towers, stacks, industrial structures, reactors and covered structures. The plan of these structures represents one of the most difficult specialised parts of structural building practice, as it requires a structural and geotechnical examination. Soil-Structure Interaction is an interdisciplinary field of undertaking which lies at the convergence of soil and structural mechanics, computational and numerical techniques and assorted other specialised controls.

R. Chaitra · R. Sridhar (✉) · B. M. Ramesh
Department of Civil Engineering, SJB Institute of Technology, Bengaluru, India
e-mail: sridharrajagopal@gmail.com

© The Author(s), under exclusive license to Springer Nature Singapore Pte Ltd. 2023
A. K. Agnihotri et al. (eds.), *Proceedings of Indian Geotechnical and Geoenvironmental Engineering Conference (IGGEC) 2021, Vol. 1*, Lecture Notes in Civil Engineering 280,
https://doi.org/10.1007/978-981-19-4739-1_20

219

Vivek and Hora [1], analysed about three bay, three-storey 3D RCC frame and laying on homogeneous soil and exposed to gravity loading was analysed and examined the interaction behaviour using FE method and reported that the linear elastic is considered for frame, foundation and soil mass resulted by comparing between the without interaction and with interaction analysis and act as an alone compatible structural element for more realistic analysis. Thangaraj and Ilamparuthi [2], analysed the quarter raft and the situation of the sections of three \times five bay, five stories and about the non-linear response of soil is analysed through multi-linear isotropic model. They have reported that the size of the contact pressure was higher at the extreme edge of raft. Milind and Gaurav [3], considered about three \times three bay three-storey RCC building subjected to the gravity loading on which was placed on medium hard clay soil and the computational modelling of ground is analysed by FEM. They have reported that in elastic medium the soil stiffness is induced in frame and in elastic-plastic medium the stiffness decreases and it offers only settlement. Gaurav [4], investigated on three bay, 10-storey structure. Soil was modelled as linear elastic; they have reported that the displacement of soil on mat shows lower value in the first layer. Ismail [5], investigated the impact of SSI on essential dynamic attributes of RC structures with spread footing and raft foundation. The impact of soil elasticity on the vibration induces on stiff structural framework is laying on it. Authors described that the elasticity of the soil elongating of the lateral fundamental time period of the structural framework because of overall change in lateral stiffness. Chaudhari and Kadam [6], investigated on the effect of pile span setups on the behaviour of RC structures were evaluated under seismic loading and resulted that the moment of soft clay is higher than the soft soils. The settlements of foundations are less influenced by soft soils. Eldin and Arafa [7], carried out a study on the elastic-plastic finite element analysis was done by the 15-node wedge element in 3-dimensional PLAXIS programme and they reported that raft with mid, edge and corner opening positions the settlement of soil and moment increases when it compared with different types of soil. Kalyanshetti et al. [8], researchers investigated on the SSI, considering two models, therefore one was substituting soil by spring of comparable stiffness and in the second type, the entire soil is assumed as elastic continuum and due to that, the stiffness of foundation increases which confirms the vulnerability and the structural performance [9].

Several investigators have analysed the linear soil-structure interaction. Various investigators have proposed different methodologies for arrangement of interaction issues from time to time [10]. The settlement, bending moment and contact pressure is analysed but they have not investigated for different foundations and soil properties for non-linear behaviour. Hence in the present paper, the displacement and stresses for frame, soil and foundation for different soil properties and foundations are evaluated.

2 Objectives

The objective of the present study is to evaluate the behaviour of isolated and mat foundations on a single layer. The structure is analysed and compared with non-interaction analysis.

To know the behaviour of elastic and elasto-plastic soil mass on silty sand.

To know the performance of soil and structure model by vertical and horizontal displacement and stresses.

3 Modelling and Analysis

3.1 General

The model frame of three bay and three storey was established and analysed using ANSYS 18.1. All the beams and columns are analysed as beam elements and column elements and the element was characterised by eight nodes. The three models NIA, IAE and IAEP was analysed for isolated and mat foundation and considered rigidly fixed. The properties of beam, column and footing has been presented in Table 1.

Where,

NIA= Non-Interaction Analysis

IAE= Interaction Analysis–Elastic

IAEP= Interaction Analysis–Elastic-plastic.

3.2 Loads

Self-weight and Live load were considered from IS 456-2000 as shown in Table 1. The Dead wall loads are calculated and factored for the beams. On the basis of IS 1893-2002, the lateral loading is considered for ordinary moment resisting frames.

3.3 FE Modelling

The SSI analysis is done using ANSYS 18.1 software. In the model, the horizontal displacements were restrained as boundary conditions. For cases 1, 2 and 3 the soil is isotropic, homogeneous. The element (PLANE 82) is considered for each node (U_x and U_y). In case 1 the foundation is considered as a rigid base, case 2 considers elastic analysis and case 3 considers elasto-plastic (Drucker–Prager criteria). The contact interface between the foundation and soils was achieved using CONTA172

Table 1 Geometric and material properties of structural elements, foundation and soil mass

Sl. No	Structure	Component	Details
		Number of storeys	3
		Number of bays in <i>X</i> -direction	3 m
		Number of bays in <i>Y</i> -direction	3 m
		Storey height	3 m
1	Frame	Plinth height	2.5 m
		Bay width in <i>X</i> -direction	4 m
		Bay width in <i>Y</i> -direction	4 m
		Beam size	(0.23 × 0.3) m
		Columns—(A) C1, C13, C4, C16	(0.23 × 0.3) m
		Columns—(B) C2, C14, C3, C15, C5, C9, C8, C12	(0.38 × 0.23)m
		Thickness of slabs	0.15 m
2	Isolated footing	Footing under Columns C1, C13, C4, C16 (F1)	(1.5 × 1.5 × 0.35) m
		Footing under Columns C2, C14, C3, C15, C5, C9, C8, C12 (F2)	(1.8 × 1.8 × 0.4) m
3	Concrete	Young's Modulus of concrete for (M20)	22,360 × 10 ⁶ N/m ²
		μ_c	0.15
		Density	2500 kg/m ³
		Acceleration due to gravity (<i>g</i>)	9.81 m/s ²
4	Soil Mass	Soil mass	30 m × 15.0 m
5	Silty Sand	Young's modulus	205 × 10 ⁶ N/m ²
		μ_s	0.3
		Density	2100 kg/m ³
		Cohesion	100 × 10 ³ N/m ²
		Friction angle	36
		Safe Bearing Capacity (SBC)	200 kN/m ²
6	Load	Slab and live load	3 kN/m ²
		Floor finish	1.25 kN/m ²

and TARGE169 elements. The mesh size of 0.1 × 0.1 m is used to discretised for the frame, foundation and soil.

4 Results and Discussion

The study emphasis on the displacements on superstructure and soil, stresses in soil and frames for Isolated Footing and Mat Foundation on silty sand with three cases with results are discussed in this section.

4.1 Vertical Displacement

The vertical displacement in silty sand for isolated footing at elastic and elasto-plastic conditions in comparison is done with respect to Non-Interaction Analysis (NIA) along the length of the terrace floor.

As discussed before, the vertical displacement of the terrace floor is maximum, so here the comparison is done for the terrace floor beams.

As far as stress intensities due to bending and settlement are concerned, stresses are increasing rapidly and also slight change in all cases. This is due to, soil offers resistance in IAE and IAEP. Also, in IAE displacement is due to deflection and settlement both but in IAEP displacement is due to settlement only and soil shows perfect plastic behaviour in IAEP. Thus, stress intensities are compared for IAE and IAEP, respectively and are presented in the bar chart as shown, in Figs. 1, 2, 3 for Silty Sand.

Therefore, displacement in IAEP and stresses in IAE are important from design consideration. The frame shows the maximum vertical displacement as total load acts towards C.G. of structure due to flexible support conditions thus soil stiffness is reduced and displacement increases.

As stress in IAE and IAEP for frames are almost same hence it was concluded that soil behaves as plastic and hence stress in IAE is important from design consideration. But the vertical displacement in IAEP is maximum hence displacements in IAEP must

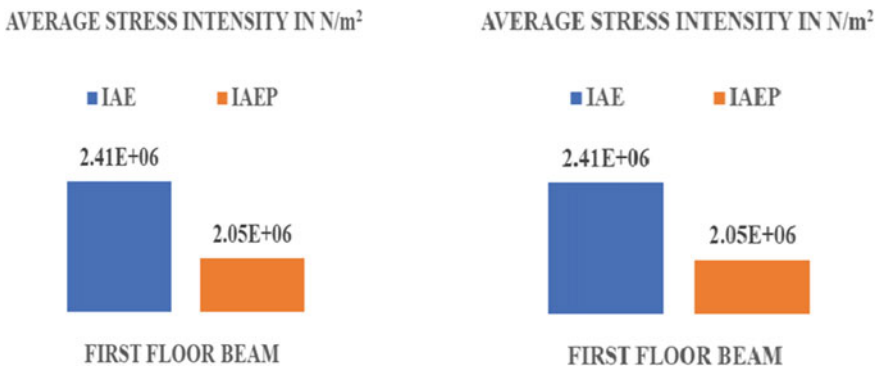


Fig. 1 Variation of stresses in beams for silty sand in isolated footing

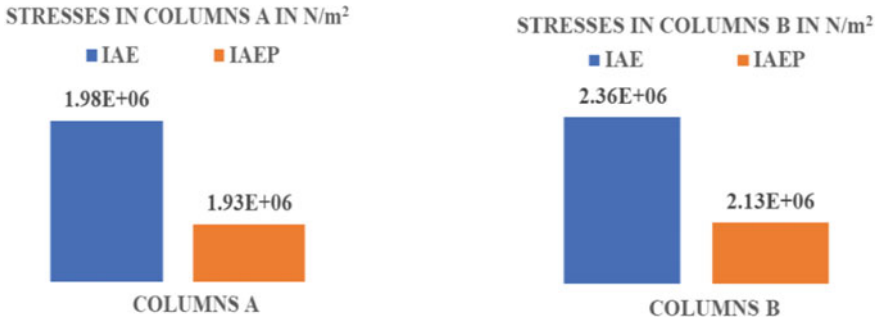


Fig. 2 Variation of stresses in columns for silty sand in isolated footing

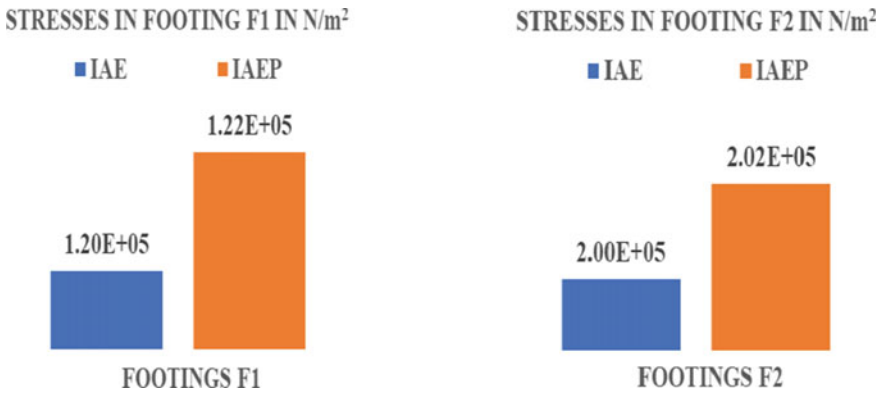


Fig. 3 Variation of stresses in footings for silty sand in isolated footing

be considered while designing. Therefore, in soil model behaviour, the displacement approach and stress approach are considered. In the present study, the outcome of soil models for elastic-plastic soil properties on 3D frames is discussed.

4.2 Displacement Approach

The models considered for IAE and IAEP analysis the vertical displacement of the soil mass is examined and discussed. While modelling the soil mass, two types of geometries were adopted in mentioned models. Therefore, to analyse the behaviour of the variation of displacements, vertical displacement is compared along the depth of soil. The displacement along the depth of mid-width is plotted for soil continuum.

The soil mass is assumed as 15 m depth, the translations movement is restrained in bottom boundary for both X and Y directions and hence regardless of soil material stiffness, at 15 m depth displacement must be zero. Practically wrong to assume the

depth that there should not be substantial settlement and shear stress below this depth. Hence, for the model of SSI analysis, the shear wave velocity should be considered to arrive at exact volume of soil mass. As in the considered models, soil shifted towards end footing due to uplifting the maximum displacement of soil mass.

In soil mass, depth of 15 m and elastic and elastic-plastic soil properties are considered, In elastic and elasto-plastic soil mass, displacement was decreased and similar variation was observed in IAE model.

The stress in soil as well as in buildings represented by the stress analysis. But the stress in soil mass was shown by contours of same colour, perceptibly the motive behind is the stress value is much less than the stress value of frame. The graphs are shown the stress variation in soil along the width.

The width of soil mass at $1/3 \times (5\text{ m})$ depth and $2/3 \times (10\text{ m})$ depth is chosen for all the models. Thus, the stress is plotted for specified locations for IAE and IAEP in all models as shown in Figs. 4 and 5.

Thus, from Figs. 4 and 5, the following points are drawn.

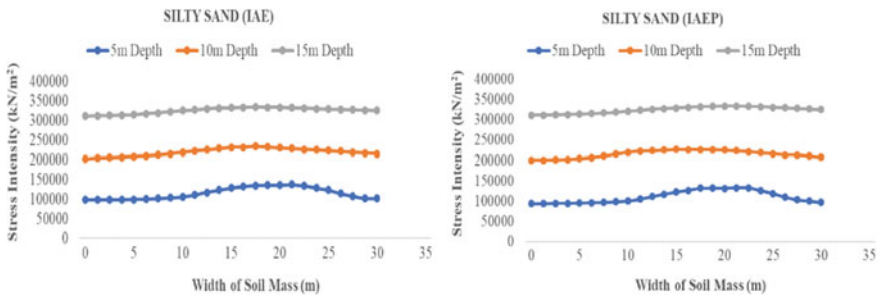


Fig. 4 Comparison of stress along width for soil for isolated footing of silty sand

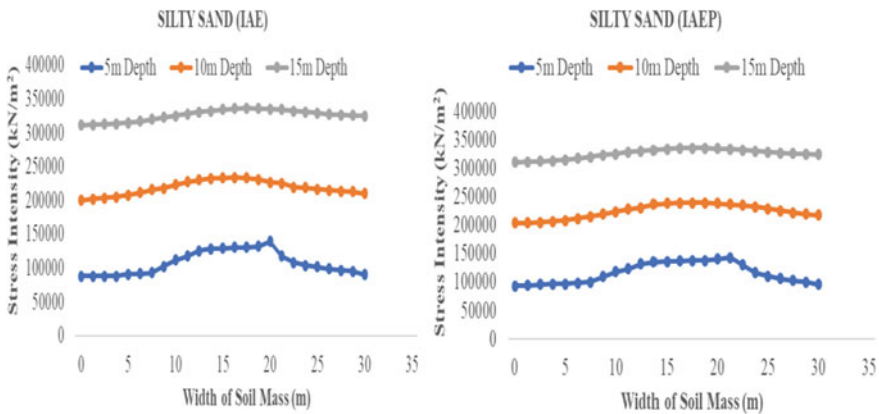


Fig. 5 Comparison of stress along width for soil for mat foundation of silty sand

It indicates that the stress is spread all along the soil mass. Accordingly, it illustrates that the stress is distributing and get extinct after the appropriate depth, obviously such depth is implemented in all models, as it is noticed that if the depth is 15 m then the stress intensity is enhanced more than the actual depth.

If stress is compared between IAE and IAEP, then it indicates that the stress value is almost same but for all the models, the response of soil changes from IAE to IAEP. Therefore, soil act as plastic showing the stress value approximately same but major change occurred after the loading. That's why for the precise analysis, plasticity of soil must be considered.

5 Conclusions

The following specific conclusions are drawn from the present work.

1. The maximum displacement in frame is safe in silty sand.
2. The frame shows the maximum vertical displacement as total load act towards C.G. of structure due to flexible support condition if the soil stiffness reduces displacement increases.
3. It has been intended to demonstrate that soil behaves as plastic and hence stresses in frames increases from IAEP to IAE. In some frames are almost same and vertical displacement increases from IAE to IAEP, accordingly it tends to be concluded that stresses in IAE and vertical displacement in IAEP are significant.
4. In NIA, because of fixed support conditions the displacement in footings is zero but soil does not offer such fixity due to stiffness.
5. Value of maximum stress at 15 m depth of soil mass is more than 100 mm in soft clay, therefore it can be determined that for proper distribution of stress the appropriate depth must be considered.
6. The stress underneath the footings is more to such a level that soil fails its strength and that is the cause of enhancing the vertical displacement.

References

1. Garg V, Hora MS (2012) Interaction effect of space frame—strap footing—soil system on forces in superstructure. *ARPN J Eng Appl Sci* 7(11). ISSN 1819-6608
2. Daniel Thangaraj D, Ilamparuthi K (2012) Interaction analysis of mat foundation and space frame for the non-linear behaviour of the soil. *Bonfring Int J Ind Eng Manag Sci* 2(4)
3. Mohod MV, Dhadse GD (2014) Importance of soil structure interaction for framed structure
4. Dhadse GD (2017) Response of flexible base with different shapes of raft footing: a soil structure interaction analysis
5. Ismail A (2014) Effect of soil flexibility on seismic performance of 3-D frames. *IOSR J Mech Civil Eng (IOSR-JMCE)* 11(4), e-ISSN: 2278-1684, p-ISSN: 2320-334X
6. Chaudhari RR, Kadam KN (2013) Effect of piled raft design on high—rise building considering soil structure interaction. *Int J Sci Technol Res* 2(6). ISSN 2277-8616

7. Eldin MS, El-Helloty A (2014) Effect of opening on behaviour of raft foundations resting on different types of sand soil. *Int J Comput Appl* (0975–8887) 94(7)
8. Kalyanshetti MG, Halkude SA, Mhamane YC (2015) Seismic response of R.C. building frames with strap footing considering soil structure interaction. *Int J Res Eng Technol* eISSN: 2319-1163 | pISSN: 2321-7308
9. ElSideek MAB (2014) Effect of overlap stress as well as tie beam length and width on settlement of isolated footing using finite element. Civil Engineering Department, Al-Azhar University, Cairo, Egypt
10. Yesane PM, Ghugal YM, Wankhade RL (2016) Study on soil structure interaction: a review. *Int J Eng Res* 5(3):737–741

Simulation of Load Bearing Capacity of a Single Pile in a Multi-layered Soil



Pratyusha Bandaru and Hemaraju Pollayi

Abstract This paper deals with the modelling of load-deformation behaviour of a circular footing on sandy stratum in a two-layered soil system. The main goal of this study is to evaluate the settlement and bearing capacity of a circular pile supported by a sandy soil multilayer constructed on a soft clay foundation. This article discusses the main principles of pile capacity calculations with the help of Abaqus software. Two traditional methods are used for determining pile load capacity: (1) the α method and (2) β method. The alpha technique determines the short-term load capacity of piles in cohesive soils. In contrast, the beta method determines the long-term load capacity of piles in both cohesive and cohesionless soils. A model generated using finite element software is utilised for numerical analysis. The findings for load settlement diagrams and bearing capacity obtained from numerical results are similar with those obtained from finite element analysis.

Keywords Bearing capacity · Circular footing · Numerical analysis · α method and β method · Finite element method

1 Introduction

Pile foundations function as the most significant structural components in designing and constructing offshore and onshore structures such as oil-rig platforms, jetties and naval bases. Usually, the vertical loading of the pile is predominant. For instance, in certain situations, piles supporting offshore wind energy foundations or conductors, the vertical load is complemented by a lateral load.

P. Bandaru (✉) · H. Pollayi
Department of Civil Engineering, GITAM University, Hyderabad, Telangana 502329, India
e-mail: pbandaru2@gitam.edu

© The Author(s), under exclusive license to Springer Nature Singapore Pte Ltd. 2023
A. K. Agnihotri et al. (eds.), *Proceedings of Indian Geotechnical and Geoenvironmental Engineering Conference (IGGEC) 2021, Vol. 1*, Lecture Notes in Civil Engineering 280,
https://doi.org/10.1007/978-981-19-4739-1_21

229

Current design practice includes a separate study of vertical piles and lateral responses and does not address the interaction between the various load directions. Several findings of studies on the behaviour of piles exposed to inclined loads have been published in the literature [1–3]. According to these findings, a vertical load has only a marginal effect on a pile's horizontal reaction, whilst lateral loads substantially impact a pile's vertical response. However, there has been no clear and understandable presentation of critical characteristics and quantification of interaction effects [4–6]. This article provides the result of a three-dimensional finite element analysis in ABAQUS to examine the behaviour of vertical piles embedded in multi-layered cohesionless soil under varied vertical loads.

2 Modelling

To better understand the bearing capacity behaviour of piles under combined loading conditions, numerical techniques utilising the finite element method (FEM) have recently become widely used. This is due to the rapid advancement of computing technology [7]. With numerical analysis, the complex soil layers with a soil-structure interaction may be addressed precisely [8, 9]. We use ABAQUS to analyse reaction piles embedded in non-cohesive soil under vertical loading in this present study. The soil is divided into two layers. The top layer is the NC clay layer (Normally consolidated), which is 10 m thick, and the bottom layer is the OC clay layer (Over-consolidated). The pile is constructed of concrete and has a diameter of 0.6 m and an embedded length of 16 m.

3 Numerical Analysis

With ABAQUS, the correctness of the numerical model of a single pile's behaviour under vertical loading was confirmed by looking at an example like [10]. Figure 1 depicts the schematic diagram for a single pile subjected to a vertical load. The pile dimensions are 0.6-m-diameter concrete pile of 16 m long is considered in a two-layered soil. Table 1 displays the pile and soil properties.

For this reason, Fig. 2 depicts the finite element mesh used in this model for half of the pile and surrounding soil. The current model's single pile and soil were modelled to have the same dimensions and boundary conditions as the real thing.

In this work, symmetry is used to examine half of the pile. When the pile and soil interact, a penalty-type interface is used to understand such interaction. The frictional interaction between the pile surface and the soil in contact may be described using this interface type. It took experimenting with different mesh densities, void ratios and boundary positions before arriving at a numerical solution that worked.

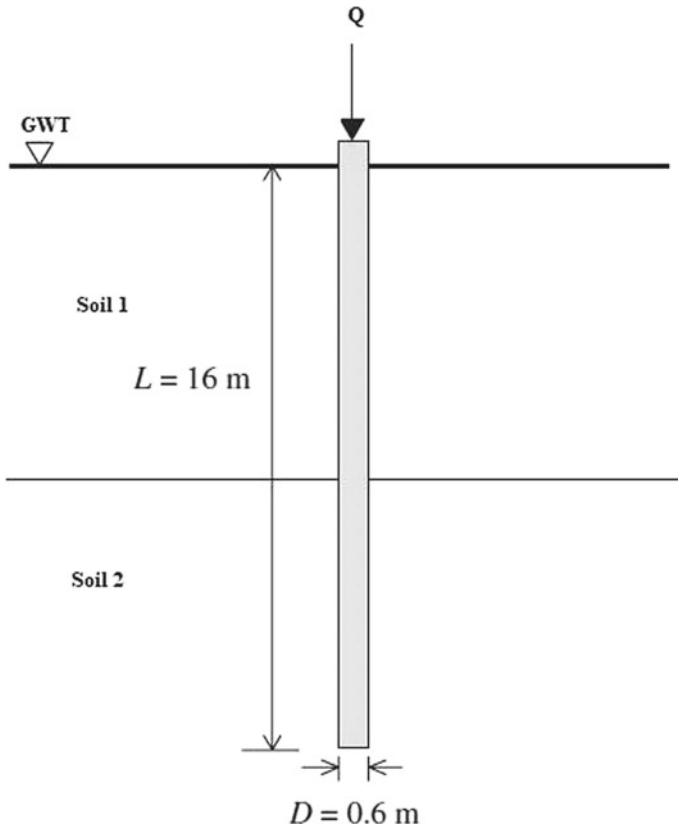


Fig. 1 Single pile subjected to vertical loading

Table 1 Material properties

Material	Young's modulus (MPa)	Poisson's ratio	Friction angle (°)	Void ratio
Pile	30	0.2	25	0.1
Soil 1	1.44	0.3	30	1.5
Soil 2	1.44	0.35	50.2	1.5

4 Numerical Analysis Results

4.1 Vertical Load–displacement Response

Graph 1 depicts the vertical displacement of the pile head against the applied vertical load (Q). This figure shows that the vertical force required to move a pile vertically

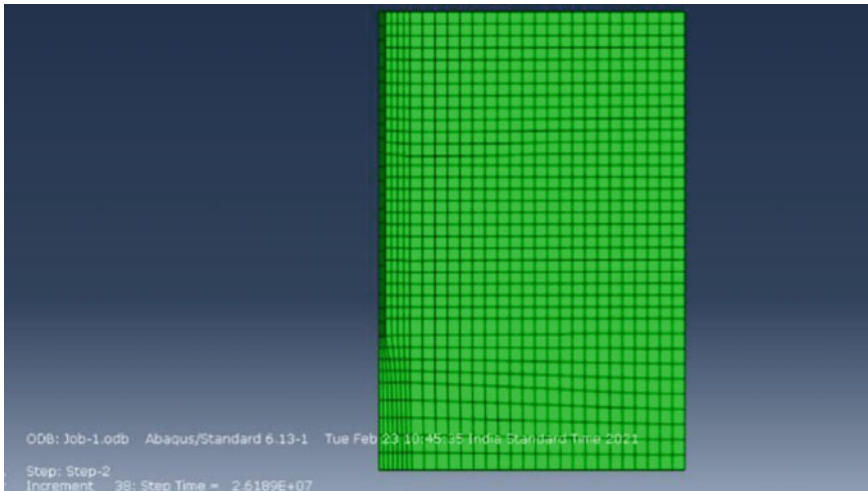


Fig. 2 Meshed pile in a multi-layered soil

decreases as the inclination angle decreases. This implies that the horizontal load has a major impact since it results in softer vertical behaviour.

A penalty-based interface element with the friction coefficient of 0.385 between both the soil and the pile is often used to represent the column and ground interactions [1]. The abrasive contact between both the pile face as well as the topsoil by which it comes into direct contact can be expressed through this device.

The “body-force” method is being used to generate the clay material’s tare. The “geostatic” programme is being used in key point to assure that homeostasis is ensured inside the clay layer. The geostatic command confirms that the original stress condition in any portion of the soft clay is restricted within the capping model’s initial elastic limit. A maximum load frequency is suggested by such an undrained state even though a low loading being reflected by a drained condition.

The upper part of the soft clay is also permeable, enabling pore pressure to dissipate. The proposed scenario likewise particularly includes reduced design loads, revealing that the specimen should really be loaded gently to avoid the development of excessive pore water pressure within the finite element model.

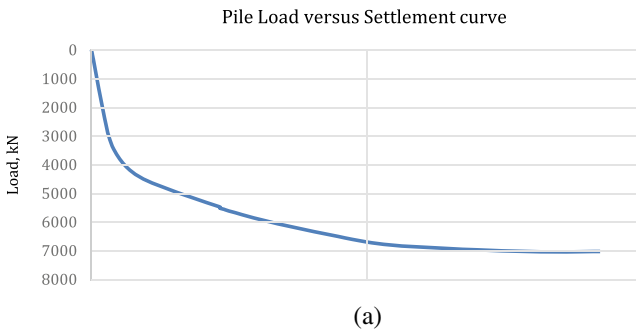
As a response, in step 2, the pile load applied whilst using maximum vertical failure criterion, allowing the upper portion of the pile to drop downward 30 cm at a quite modest steady rate of $3 \times 10^{-13} \frac{\text{cm}}{\text{sec}}$ [4]. The soil can adapt in a depleted manner resulting in low applied load. Under loading, the residual excess pore pressure within those sections seems to be almost quasi, indicating that perhaps the pressure is efficiently evacuated. Additionally, since its mass is raised, the settlement initially increases actually closer to 400 kN piling load, where at moment a pile movement of around 1.10 cm is attained. The pile subsequently commences to dramatically

collapse, proving that certain pile’s stress distribution (530 kN) is being exceeded. It can be emphasised that certain method’s capacity forecasting would be around 15% fairly low than the finite element assessment of pile load capacity.

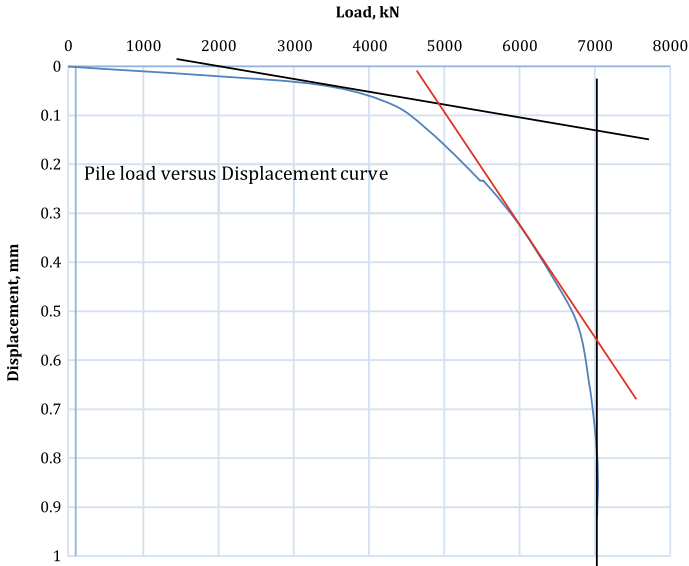
5 Conclusion

Due to the use of finite element models in this study, the response of the pile to vertical loads could be investigated. This study makes use of an ABAQUS software-built 3D numerical model. It compares typical methods for analysing single piles subjected to vertical loads, which is provided by this research study. There were three different inclinations tested on the piles, with being measured from the horizontal direction. As a result of this research, the following conclusions may be drawn.

The stiffness of the pile is heavily influenced by the behaviour of the pile when it is combined with other piles. The vertical loading of the pile significantly effects the displacement of the pile in lateral direction; from Graph 1a, b, we could conclude that the loading and inclination extensively effect the piles position. Additional horizontal piles reduce the pile’s maximum vertical capacity.



Graph 1 Pile load versus settlement curve



Graph 1 (continued)

References

1. Prandtl L (1920) Über die Härte plastischer Körper. Nachr. Ges. Wiss. Goettingen. Math-Phys Kl, 74–85.dtl, L. (1920)
2. Reissner H (1924) Zum Erddruckproblem. In: Biezeno CB, Burgers JM (eds) Proceedings of the 1st international congress for applied mechanics, Delft, The Netherlands, pp 295–311
3. Terzaghi K (1943) Theoretical soil mechanics. John Wiley and Sons, New York. ISBN 0-471-85305
4. Meyerhof GG (1953) The bearing capacity of foundations under eccentric and inclined loads. In: Proceedings of the III international conference on soil mechanics and foundation engineering, Zürich, Switzerland, 1, pp 440–445
5. Meyerhof GG (1963) Some recent research on the bearing capacity of foundations. Can Geotech J 1(1):16–26
6. Caquot A, Kerisel J (1953) Sur le terme de surface dans le calcul des fondations en milieu pulvérulent. In: Proceedings of the third international conference on soil mechanics and foundation engineering, Zurich, Switzerland, 16–27 August 1953, vol 1, pp 336–337
7. Brinch Hansen JA (1970) Revised and extended formula for bearing capacity, Bulletin no. 28. Danish Geotechnical Institute Copenhagen, pp 5–11
8. Vesic AS (1967) A study of bearing capacity of deep foundations (Final Report Project B-189). Georgia Institute of Technology, Atlanta, pp 231–236
9. Vesic AS (1973) Analysis of ultimate loads of shallow foundations. J Soil Mech Found Div 99(1):45–76
10. Johnson K, Lemcke P, Karunasena W, and Nagaratnam S (2006) Modelling the load–deformation response of deep foundations under oblique loading. Environ Modell Softw 21:1375–1380. <https://doi.org/10.1016/j.envsoft.2005.04.015>

Studies on Evaluation of Effect of Sloping Ground on Lateral Pile Response: A Brief Review



Nitesh Thakur and Hemant Chore

Abstract The foundations of a structure constructed in the close vicinity of the hill slope cause concern for the engineers dealing with the design of such structures since the stability of the slope is the most important factor under such circumstances. The structures constructed near slopes are mostly supported by deep foundation (pile). The presence of slope on one side lowers the passive resistance of soil which is bound to decrease the capacity of the foundation. Moreover, the problem of laterally loaded pile foundation is more complicated as compared to the axially loaded piles. The pile foundation encountered near the slope renders the problem of laterally loaded piles. On this backdrop, the present paper reviews the various research work (experimental, theoretical and analytical) undertaken by the researchers up till pertaining to the behavior of pile foundation constructed in the close vicinity of embankment or hill slope.

Keywords Sloping ground · Laterally loaded pile

1 Introduction

Deep foundations are chosen when there are substantial horizontal forces acting on it or when loads are to be transmitted into the deep. The sources of resultant lateral forces can vary depending on the superstructure supported by the pile foundation. Water currents, waves, earthquakes and wind gusts are all important contributors to the creation of lateral forces. The vertical component of inertia force is less than the horizontal component in case of earthquake. If the horizontal forces are not correctly accounted for in the design, it is possible for the design to fail. The primary generators of horizontal force in bridge abutments and piers are vehicle and wind movement. The horizontal forces are transferred by water pressure onto the supporting piles

N. Thakur (✉) · H. Chore

Department of Civil Engineering, Dr. B.R. Ambedkar National Institute of Technology, Jalandhar, India

e-mail: nitesht.ce.19@nitj.ac.in

of dam structure. The buildup of lateral force acting on supporting structures is the cause of major failure in all of these cases.

The design of pile involves considerations of unusually large ratios of lateral to vertical loads, particularly in the areas subjected to severe storms. While the analysis of foundation for the vertical load follows conventional procedures, the lateral load analysis poses a more complex problem. Since combined flexural and axial stresses are usually the major factor, bending moments in the pile must be reliably predicted. This requires interaction between the structure and the foundation elements, be rationally analyzed.

When the pile is laterally loaded, it is important to have an appropriate evaluation of pile-soil interaction. The important parameters to be considered in design of pile subjected to lateral loading are maximum bending moment and top displacement. Many computational and experimental researches have already been done to study laterally loaded pile response in level ground. A variety of different methods for predicting the laterally loaded pile behavior in level ground were developed in recent years. Linear subgrade reaction, nonlinear subgrade reaction (p - y) approach, elastic continuum approach and 3D finite element analysis are some of the approaches.

The subgrade reaction approach is based on Winkler's hypothesis, as per which the soil is treated as infinite number of closely spaced independent and elastic springs [1]. In the elastic continuum approach, pile is idealized as an infinitely thin linearly elastic strip embedded in the elastic soil media. Shear stresses developed at the interface of the soil pile are not considered [2]. The finite element method allows for a more precise results than the above two methods; since the pile is modeled more accurately, the heterogeneous soil conditions are also modeled easily and correctly [3]. The successful application of a rational method of lateral load analysis depends on the availability of detailed information concerning soil properties. It is especially important to have accurate soil information concerning soil surface, at a depth less than 10–20 pile diameters.

In hilly areas, there are a number of situations when houses or other superstructures have to be constructed close to the slope. If a shallow foundation is used in these kinds of conditions, the weight carried by the footing will serve as a surcharge. For such circumstances, stability of slope is more important. The slope geometric properties (slope angle and height) as well as soil material properties (unit cohesion, unit weight and angle of internal friction) determine slope stability. Though various approaches have been proposed in the past to assess slope stability, the most accurate methodology is slope monitoring with proper instruments.

Deep foundations are always preferred over shallow foundations for transmitting load from superstructure to hard strata below slip surface. This is essential as per the stability of slope is concerned. There are several instances when piles are provided near slopes (Fig. 1). Buildings near slopes in many hilly areas are supported by the deep foundations. Presence of slope on one side lowers the soil passive resistance. Under such circumstances, the foundation's capacity in the direction of the slope is dramatically decreased. This is also dependent on the pile's position with respect to the slope.

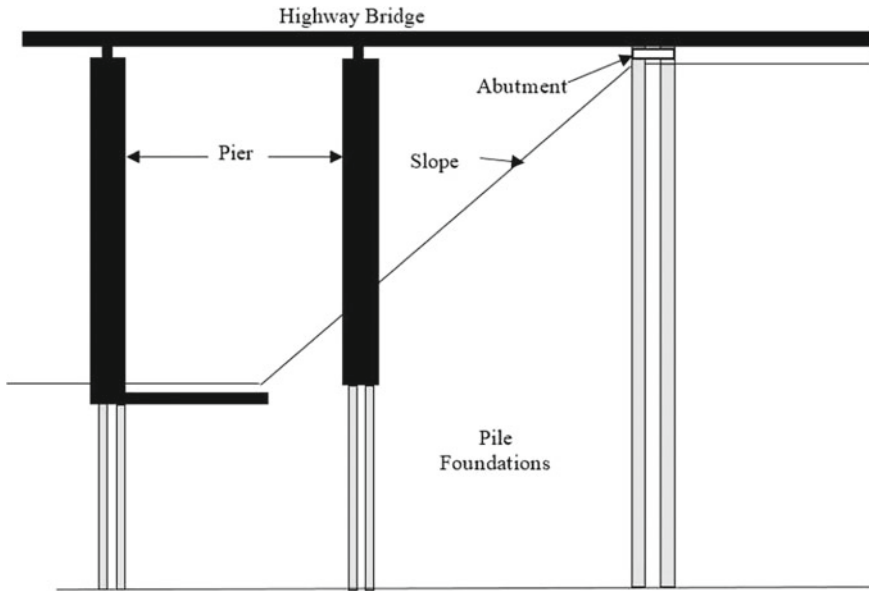


Fig. 1 Pile foundations provided near slope for support of highway bridge

2 Brief Review of Literature

Despite the fact that the reaction of piles in horizontal ground conditions has been extensively studied, the impact of neighboring slope on pile behavior is not well established. Behavior of pile is widely known to be highly reliant on the relative stiffness of soil and pile. In case of sloping ground, evaluation of the relative stiffness is very difficult. The resistance provided by the sloping ground to pile differs significantly from the level ground condition. Currently, there is no approach for the assessment of the relative stiffness in a sloping ground condition. Out of the above approaches of pile analysis in the level ground, only finite element analysis can be employed for piles in the sloping ground. For piles in sloping ground, p - y or elastic continuum analyses cannot be readily extended. The elastic continuum analysis is based on modeling soil boundary by Mindlin's equation which is valid for horizontal semi-infinite soil media. Hence, it cannot be extended to piles near slope. The available p - y relationships so far are also derived for horizontal ground conditions and hence cannot be directly used for sloping ground condition. However, with modifications in p - y relationships, piles in sloping ground can be analyzed. This requires extensive experimental investigations on piles near slope to develop p - y relationships in the sloping ground. It is essential to study effect of slope angle and edge distance on p - y relationships of piles in slopes. Although many research works are studied, only few prominent works are reported in the subsequent paragraph.

Few experimental researches have been conducted to examine single pile and pile group response on sloping ground when subjected to lateral load. A very few studies have considered the influence of distance between slope crest and pile. Mezazigh and Levacher [4] found out experimentally the distance from slope crest at which the pile response approaches the horizontal ground response. $8D$ was the reported edge distance, where D being pile diameter, for 1 in 2 slope and $12D$ for 2 in 3 slopes, regardless of the soil relative density. Muthukkumaran et al. [5, 6] investigated the influence of surcharge loads on pile reaction for changing relative density and slope angle, and p - y relationship was drawn out from analyzed results for different ground conditions. Muthukumaran [7] investigated the influence of direction of the lateral load and slope geometry in cohesionless soil. Further effect of distance from slope crest for varying properties of soil has also been examined. Muthukumaran and Begum [8] carried out a series of studies to see how relative density, embedment length and slope influence pile response. The data were presented as p - y relationships.

There are plenty of studies available in the literature in the context of the experimental, theoretical and numerical research on the analysis of single pile and pile group thereof with respect to the level ground. However, very little experimental and numerical researches are available in the literature on the single pile response when the piles near the ground slope are considered. The experimental investigations on laterally loaded single pile reported in [4, 7–13] and some numerical investigations have been reported with respect to the analysis of a single pile [6, 14–20]. Further, some numerical studies were carried out with respect to the pile group [21–27]. Hardly, any experimental researches are done on the pile group behavior located near the ground slope.

3 Summarized Findings from the Literature Survey

Extensive literature survey is carried out in the context of analysis of single pile or group of piles thereof near sloping ground. For the sake of brevity, work reported by the various researchers with respect to the theme of the proposed research work is not elaborated. It is observed from the literature review that in order to examine the sloping angle effects on pile lateral capacity using analytical, scaled laboratory models and the numerical models, very few studies are conducted.

Although the elastic continuum method and p - y approach have been utilized for determining the pile capacity to carry the lateral loads in the horizontal ground, only latter approach can be put to use for sloping ground with improved relationship to account for slope. Majority experimental investigations are carried out to quantify the slope effect on the laterally loaded piles embedded in sand. Very few experimental studies are available for clayey soil or pozzolanic waste materials. Very few studies are reported on the analysis of the group of piles near sloping ground though relatively more studies are carried out with respect to the single pile.

References

1. Matlock H, Reese LC (1962) Generalized solutions for laterally loaded piles. *Trans Am Soc Civil Eng ASCE* 127(1):1220–1247
2. Poulos HG (1971) Behavior of laterally loaded piles: I-Single piles. *J Soil Mech Found Div ASCE* 97(5):711–731
3. Desai CS, Appel GC (1976) 3D analysis of laterally loaded structures. In: *Proceedings of 2nd international conference on numerical methods in geomechanics*, Blacksburg, 1, 405–518
4. Mezazigh S, Levacher D (1998) Laterally loaded piles in sand: slope effect on p - y reaction curves. *Can Geotech J* 35(3):433–441
5. Muthukumar K, Sundaravadivelu R, Gandhi SR (2004) Effect of sloping ground on single pile load deflection behaviour under lateral soil movement. In: *Proceedings of 13th world conference on earthquake engineering*, Vancouver, BC, Canada, Paper Id 2147 (1–6)
6. Begum NA, Muthukumar K (2008) Numerical modeling for laterally loaded piles on a sloping ground. In: *Proceedings of 12th international conference of IACMAG*, Goa, India, 1–6
7. Muthukumar K (2014) Effect of slope and loading direction on laterally loaded piles in cohesionless soil. *Int J Geomech ASCE* 14(1):1–7
8. Muthukumar K, Begum NA (2015) Experimental investigation of single model pile subjected to lateral load in sloping ground. *Geotech Geol Eng* 33(4):935–946
9. Sivapriya SV, Gandhi SR (2011) Behaviour of single pile in sloping ground under static lateral load. In: *Proceedings of Indian geotechnical conference (IGC2011)*, Kochi, India, 199–202
10. Rathod D, Muthukumar K, Sitharam TG (2016) Response of laterally loaded pile in soft clay on sloping ground. *Int J Geotech Eng* 10(1):10–22
11. Rathod D, Muthukumar K, Sitharam TG (2017) Development of non-dimension p - y curves for laterally loaded piles in sloping ground. *Indian Geotech J* 47(1):47–56
12. Yin P, He W, Yang ZJ (2018) A simplified nonlinear method for a laterally loaded pile in sloping ground. In: *Advances in Civil Engineering*, Hindawi, Article Id 5438618 (1–9)
13. Khati BS, Sawant VA (2018) Variation in lateral load capacity of pile embedded near slope with ground inclination and edge distance. *Int J Geotech Eng*. <https://doi.org/10.1080/19386362.2018.1541149>
14. Ng CWW, Zhang LM, Ho KKS (2001) Influence of laterally loaded sleeved piles and pile groups on slope stability. *Can Geotech J* 38(3):553–566
15. Georgiadis K, Georgiadis M (2010) Undrained lateral pile response in sloping ground. *J Geotech Geoenviron Eng ASCE* 136(11):1489–1500
16. Sawant VA, Shukla SK (2012) Finite element analysis for laterally loaded piles in sloping ground. *Coupled Syst Mech Int J* 1(1):59–78
17. Sawant VA, Shukla SK (2012) Three-dimensional finite element analysis of laterally loaded piles in sloping ground. *Indian Geotech J* 42(4):278–286
18. Sawant VA, Shukla SK (2014) Effect of edge distance from the slope crest on the response of a laterally loaded pile in sloping ground. *Geotech Geol Eng* 32(1):197–204
19. Jebur AA, Atherton W, Alkhadar RM, Loffill E (2017) Nonlinear analysis of single model piles subjected to lateral load in sloping ground. *Procedia Eng* 196(2017):52–59
20. Chandaluri VK, Sawant VA (2018) Influence of sloping ground on lateral load capacity of single piles in clayey soil. *Int J Geotech Eng* 1–8. <https://doi.org/10.1080/19386362.2017.1419538>
21. Stewart DP, Jewell RJ, Randolph MF (1993) Numerical modelling of piled bridge abutments on soft ground. *Comput Geotech* 15(1993):21–46
22. Ng CWW, Zhang LM, Ho KKS (2011) Influence of laterally loaded sleeved piles and pile groups on slope stability. *Can Geotech J* 38(3):553–566
23. Chae KS, Ugai K, Wakai A (2004) Lateral resistance of short single piles and pile groups located near slopes. *Int J Geomech ASCE* 4(2):93–103
24. Martin GR, Chen CY (2005) Response of piles due to lateral slope movement. *Comput Struct* 83(2005):588–598
25. Pourkhosravani A, Asakereh A (2013) Behavior of laterally loaded piles in cohesive soil slopes. *Int J Sci Eng Invest* 2(23):52–55

26. Rathod D, Muthukkumaran K, Sitharam TG (2015) Response of laterally loaded pile groups in sloping ground. In: Proceedings of Indian geotechnical conference (IGC2015), Pune, India
27. Rathod D, Muthukkumaran K, Sitharam TG (2018) Analysis of laterally loaded group of piles located on sloping ground. *Int J Geotech Eng.* <https://doi.org/10.1080/19386362.2018.1448521>

Numerical Modelling of Coal Mine Overburden Dump Slopes: Developments and Current State-of-the-Art



Madhumita Mohanty, Rajib Sarkar, Sarat Kumar Das,
and Krishna R. Reddy

Abstract With the rapid increase in the accumulation rate of coal mine overburden (OB) dumps, the geoenvironmental hazards due to their failures have taken a toll. A major segment of the standard Indian regulations laid down for the overall geometry of the OB dump is based on limit equilibrium method (LEM) without any information about the displacement of the failed slope, confining stresses, stress–strain behaviour of slope material, time factor and heterogeneity (shape and size). This paper highlights the various methodologies used in the stability analysis of coal mine OB dumps. The problem domain in continuum approaches is considered as a single continuous body, so they are unable to model the discrete particle failure in the OB dump mass, whereas in the discontinuum approaches (like discrete element method (DEM)) it is treated as an assembly of independent particles giving a better realistic representation. Using DEM, the studies on slope stability analysis of OB dumps considering the aspects of heterogeneity of particles, site and environmental factors are very limited. Though OB dump consists of heterogeneous material, the previous literature is silent on the aspect of reliability analysis. The work presented here sheds light on all the above aspects from past literature and is believed to serve as a significant contribution in knowing the shortcomings, challenges and moving towards the feasible solutions utilizing the most appropriate computational technique.

Keywords Coal mine overburden · Continuum · Discontinuum · Discrete element method · Numerical modelling · Slope stability analysis

M. Mohanty (✉) · R. Sarkar · S. K. Das
Indian Institute of Technology (Indian School of Mines), Dhanbad, India
e-mail: madhumita.iitism@gmail.com

R. Sarkar
e-mail: rajib@iitism.ac.in

S. K. Das
e-mail: saratdas@iitism.ac.in

K. R. Reddy
University of Illinois at Chicago, 842 West Taylor Street, Chicago, IL 60607, USA
e-mail: kreddy@uic.edu

1 Introduction

India has an immense desire to switch over to renewable sources of energy due to their multifarious benefits, but coal is immensely used due to its low cost. To reach the useful coal reserves, the overlying waste materials in an open cast coal mine have to be removed, these wastes when dumped nearby form the coal mine OB dump [1]. The formation of OB dumps causes the pollution of air, water, soil and landscape [2]. To prevent the dangerous consequences due to OB dump failure, its proper management is very important [3, 4]. Some of the significant dump failures in coal mines have been enlisted along with their catastrophic impacts in Table 1.

In India, Coal Mines Regulations, 2017 [10] has laid down the standard design guidelines for the overall geometry of the spoil banks and dumps amongst which the significant ones include: a spoil bank shall have a maximum slope of 37.5° from the horizontal, still a steeper slope may be permitted by the regional inspector having an expertise in slope stability; no bench shall exceed a height of 30 m; the overall slope shall not exceed 1 vertical to 1.5 horizontal; adequate precautions shall be taken to prevent failure of slopes of the spoil banks or dumps and the toe of a spoil bank shall not be extended to any point within 100 m of a mine opening, railway or other public works, public road or building or other permanent structure not belonging to the owner. The acute scarcity of adequate disposal area binds the hands of the coal mine producers in following the aforesaid guidelines. Thus, adopting a steeper slope becomes the last resort leading to frequent dump failures, their consequent geoenvironmental problems, loss of economy and human lives [10]. Thus, the importance of slope stability analysis of OB dumps knows no bounds.

Dump failures are initiated due to the disruption of the delicate balance of OB dump slopes by anthropogenic activities or natural agents. For slope stability analysis,

Table 1 Slope failure in coal mine OB dump

Year	Location	Cause	Impact	Reference
1982	Poker Flats (coal) mining area, Central Alaska	OB dump failure	Interruption in production	[5]
2001	Central Anatolia, Turkey	Large scale spoil pile failure due to unexpected rainfall	Spoil material moved 600 m	[6]
2012	Pha Me coalmine dump site, Vietnam	Deep-seated landslide in OB dump	Buried many houses and 7 persons	[7]
2013	Mugla lignite province, Turkey	OB dump failure	Interruption in production	[8]
2012	Muara Enim open pit lignite mine, Indonesia	OB dump failure	Disruption of mining operation, environmental problems and a high cost of remediation	[9]

the 2D limit equilibrium method (LEM) is widely used due to its simplicity and ease of application, but the escalating advances in computing technology in the past decades has brought forth the extensive use of continuum and discontinuum methods. Each of these methods has its own inherent advantages and disadvantages, none being perfectly ideal. Thus, bringing on a single platform, the comparative study of the various methods of coal mine OB dump slope stability analysis and their considerable development, the present work will unfold a way for the selection of the most appropriate method in analyzing the slope stability of a particular coal mine OB dump. In the end, an effort is made to put in a nutshell, the important research gaps and key shortcomings of the aforesaid methods.

The failure of OB dumps is a crucial issue for the overall safety of mines, since a myriad of parameters work in a combined manner to influence its stability. Slope stability analysis with its different aspects has a wide spectrum, thus in this review, emphasis has been given to the application of LEM, continuum modelling [finite difference method (FDM), finite element method (FEM)] and discontinuum modelling. The following sections discuss the abovesaid methodologies used to assess the slope stability of coal mine OB dumps.

2 Limit Equilibrium Method

Various commercial software have been used in the successful estimation of the factor of safety (FOS) using different LEM methods which vary mostly in terms of the satisfaction of force and/or moment equilibrium equations and other assumptions.

With back analysis of a dump failure by the program Slope 8, the probable causes of instability were shown as (i) infiltration due to one-month prior rainfall with the subsequent increase in pore water pressure and (ii) groundwater flow due to floor geometry [6]. It was seen from SLIDE software that layerwise dumping process was conducive in the compaction which could drain out the moisture contained in the weak swamp layer at the dump base [11]. Stability analysis by Slope/W found that the overburden load of the coal mine wastes were very high in comparison to the shear strength of the residual soils and this resulted in a deep-seated landslide [7]. The back analysis of an OB dump by SLIDE program gave the approximate value of FOS as 1. The sensitivity study also showed that stability was more affected by the changes in friction angle of black cotton soil foundation rather than its cohesion [4]. The variation of FOS with the slope height and slope angle of various saturated dump slopes was analyzed by SLIDE and preventive measures were suggested [12]. The results revealed by using SLIDE software for the back analysis of the instabilities of the OB at a lignite pit were: sliding surfaces are circular and composite; during failure, pore pressure ratio was between 0.3 and 0.4 and the residual shear strength was critical [8]. The intricacies of the past studies have been summarized in Table 2.

Table 2 Summary of the details used in the past studies based on LEM

Study area	Parameter	Software	Type of failure	Reference
Turkey	1. Groundwater and rainfall	Slope 8	Combined failure—a circular surface through dump and a planar surface along dump-floor interface	[6]
	2. Gravity loading			
Indonesia	1. Weak swamp layer at dump base	SLIDE	Composite failure (having plane and circular failure)	[11]
	2. Gravity loading			
Vietnam	1. Gravity loading	Slope/W	Base failure	[7]
India	1. Gravity loading	SLIDE	Toe failure	[4]
India	1. A tension crack	SLIDE	Toe failure	[12]
	2. Gravity loading			
	3. Rainfall infiltration			
Turkey	1. Groundwater condition	SLIDE	Slope failure Toe failure (Circular and composite sliding surfaces)	[8]

3 Continuum Modelling

Continuum modelling can simulate complex mechanisms, but its use is challenged with certain limitations: needs experienced users; lack of sufficient input data and sensitivity analysis is restricted due to constraints in run time [13]. The past studies on slope stability of coal mine OB dump utilizing FDM and FEM are discussed in the upcoming subsections.

3.1 Finite Difference Method

On examining the FOS of a vegetated OB dump slope of a coal mine by FLAC 2D, it was seen that the FOS increased with the age of tree [14]. Residual friction angle was found as the most influential factor affecting stability when the back analysis of the OB dump of an Indian colliery was done by FLAC 2D [4]. FLAC/Slope used to analyze a 60 m high combined slope [OB waste + 20% fly ash] found the slope to be critically stable at 36° and an optimum slope of 32° was enough to accommodate the mine dump for its long-term stability [15]. The mechanism of accumulation of dump slope was simulated numerically by FLAC 3D and FOS was assessed [16]. Table 3 summarizes the usage of FDM in OB dump slope stability analysis.

Table 3 Summary of the details used in the past studies based on FDM

Study area	Parameter	Software	Type of failure	Reference
India	1. Gravity loading	FLAC 2D	Slope failure (without vegetation)	[14]
	2. Biological stabilization		Toe failure (with vegetation)	
India	1. Gravity loading	FLAC 2D	Toe failure	[4]
–	1. Gravity loading	FLAC/Slope	Toe failure	[15]
	2. Effect of flyash			
Tibet	1. Gravity loading (simulation of stacking process)	FLAC 3D	Combined sliding mode (circular sliding in upper side and broken line sliding into bottom layer)	[16]

3.2 Finite Element Method

It was investigated by Plaxis 2D that the dump had a compound sliding failure mechanism and the practice of movement monitoring studies were ascertained for long-term safety [6]. The parametric study was done to study the failure mechanism of an 80 m high internal dump slope with Plaxis 2D by varying the bench height and the number of benches keeping a constant slope angle [17]. The settlement properties of spoil dumps during and after construction stage were analyzed with Plaxis 2D [18]. The optimization of the volumetric capacity of a coal mine OB dump by Phase2 showed an increase in 14% in the storage capacity with a FOS of 1.3 [19]. Numerical models of Phase2 were used to study the effect of heavy rainfall on coal mine OB dump stabilized with fly ash [20]. Table 4 enlists the above-mentioned approaches using FEM.

4 Discontinuum Modelling

Along with the inherent advantages of continuum modelling, the discontinuum modelling allows deformation of blocks and relative movement of blocks; can combine material and discontinuity behaviour along with hydro-mechanical and dynamic analysis [13]. Apart from other limitations of continuum modelling, it requires the geometry of the discontinuity to be provided and the data about the joint properties is inadequate [13].

The values of FOS for four different orientations of joint plane of a coal mine OB slope were known by LEM and the failure behaviour of equivalent PFC 2D models were assessed [21]. The static stability characteristics due to gravity load on an OB dump slope model were assessed by PFC 2D and then seismic forces were monitored by applying local damping to understand the dynamic characteristics [22].

Table 4 Summary of the details used in the past studies based on FEM

Study area	Parameter	Software	Type of failure	Reference
Turkey	1. Groundwater and rainfall	Plaxis 2D	Combined failure—a circular surface through dump and a planar surface along dump-floor interface	[6]
	2. Gravity loading			
India	1. Gravity loading	Plaxis 2D	Slope failure	[17]
India	1. Gravity loading	Plaxis 2D	–	[18]
	2. Compaction			
India	1. Gravity loading	Phase2	Compound failure (circular failure at top, planar failure at dump-floor interface)	[19]
–	1. Rainfall infiltration	Phase2	–	[20]
	2. Horizontal layers of fly ash			

Table 5 Summary of the details used in the past studies based on DEM

Study area	Parameter	Software	Type of failure	Reference
–	1. Gravity loading	PFC 2D	Irregular potential failure surface in dump slope	[21]
	2. Effect of a joint			
India	1. Gravity loading	PFC 2D	Slope failure (4 sets of joints)	[22]
	2. Seismic forces			
	3. Effect of joints		Progressive failure (earthquake excitation)	
–	1. Gravity loading	PFC 2D	Crack at corner of coal rib	[23]

The analysis of an internal dragline OB dump by PFC 2D revealed: dump was found to be unstable at 38° and stable at 34° and there was an increase in load bearing capacity of rib pillar with increase in coal rib thickness [23]. The numerical analyses carried out with DEM have been briefly mentioned in Table 5.

5 Conclusion

The above discussion clearly reveals that there has been substantial application of LEM, FDM and FEM in simulating the real-life coal mine OB dumps under various loading conditions, whereas the review affirms limited research being conducted using DEM. Therefore, a gap is affirmed in the current state-of-the-art in relation to the slope stability assessment of coal mine OB dumps by DEM, meshless methods and hybrid (or, coupled) methods. It was further seen that there have been negligible studies dealing with reliability and sensitivity analysis on the above subject which

are left to be explored. Also, there lies a wide scope for studying the stability of coal mine OB dump considering spatial heterogeneity of its constituent particles.

References

1. Prasad MNV (2015) *Bioremediation and bioeconomy*, 1st edn. Elsevier
2. Gupta AK, Paul B (2015) Ecorestoration of coal mine overburden dump to prevent environmental degradation: a review. *Res J Environ Sci* 9(7):307–319
3. Kainthola A, Verma D, Gupte SS, Singh TN (2011) A coal mine dump stability analysis—A case study. *Geomaterials* 01(01):1–13
4. Poulsen B, Khanal M, Rao AM, Adhikary D, Balusu R (2014) Mine overburden dump failure: a case study. *Geotech Geol Eng* 32(2):297–309
5. Speck RC, Huang SL, Kroeger EB (1993) Large-scale slope movements and their affect on spoil-pile stability in Interior Alaska. *Int J Surf Min Reclam Environ* 7(4):161–166
6. Kasmer O, Ulusay R, Gokceoglu C (2006) Spoil pile instabilities with reference to a strip coal mine in Turkey: mechanisms and assessment of deformations. *Environ Geol* 49(4):570–585
7. Duc DM, Hieu NM, Sassa K, Hamasaki E, Khang DQ, Miyagi T (2014) Analysis of a deep-seated landslide in the Phan Me coal mining dump site, Thai Nguyen Province, Vietnam. *Proceedings of World Landslide Forum 3*, 2–6 June 2014, Beijing, 1. In: Sassa K, Canuti P, Yin Y (eds) *Landslide Science for a Safer Geoenvironment*. Springer, Cham
8. Solak KC, Tuncay E, Ulusay R (2017) An investigation on the mechanisms of instabilities and safe design of the south slope at a lignite pit (SW Turkey) based on a sensitivity approach. *Bull Eng Geol Env* 76:1321–1341
9. Wang J, Chen C (2017) Stability analysis of slope at a disused waste dump by two-wedge model. *Int J Min Reclam Environ* 31(8):575–588
10. Director General of Mines Safety (DGMS): Coal Mines Regulations, Notification, New Delhi, dated 27.11.2017. Ministry of Labor and Employment, Directorate General of Mines Safety (2017)
11. Sulistianto B, Karian T, Kardiansyah, Hidayatullah S, Widhy S (2013) Optimalization of output dump at Asam-Asam open pit coal mine, PT Arutmin Indonesia. *J Novel Carbon Res Sci* 7:53–59
12. Behera PK, Sarkar K, Singh AK, Verma AK, Singh TN (2016) Dump slope stability analysis—a case study. *J Geol Soc India* 88(6):725–735
13. Coggan JS, Stead D, Eyre J (1998) Evaluation of techniques for quarry slope stability assessment. *Trans Inst Min Metall Sect B Appl Earth Sci* 107:B139–B147
14. Rai R, Shrivastva BK (2011) Biological stabilization of mine dumps: Shear strength and numerical simulation approach with special reference to Sisam tree. *Environ Earth Sci* 63(1):177–188
15. Pradhan SP, Vishal V, Singh TN, Singh VK (2014) Optimisation of dump slope geometry vis-à-vis flyash utilisation using numerical simulation. *Am J Min Metall* 2(1):1–7
16. Zou P, Zhao X, Meng Z, Li A, Liu Z, Hu W (2018) Sample rocks tests and slope stability analysis of a mine waste dump. *Adv Civil Eng* 1–17
17. Verma D, Kainthola A, Gupte SS, Singh TN (2013) A finite element approach of stability analysis of internal dump slope in Wardha Valley coal field, India, Maharashtra. *Am J Min Metall* 1(1):1–6
18. Bishwal RM, Sen P, Jawed M (2016) A study on the need of assessment of settlement properties of coal mine waste dumps. *Recent Adv Rock Eng (RARE 2016)* 133–136
19. Narwal S, Mandal J, Gupte SS (2017) Optimisation of overburden dump capacity using limit equilibrium and finite element techniques. *Int J Eng Res Technol* 6(5):1079–1089
20. Gupta T, Singh TN (2018) Geo-hydrological stability analysis of fly ash stabilised overburden dump slopes in opencast coal mines using finite element analysis. *Int J Adv Sci Eng Inf Technol* 8(2):405–410

21. Koner R, Chakravarty D (2010) Discrete element approach for mine dump stability analysis. *Min Sci Technol* 20(6):809–813
22. Koner R, Chakravarty D (2010) Stability study of the mine overburden dumps slope: a micromechanical approach. *Studia Geotechnica et Mechanica* 32(1):35–57
23. Kumar T, Garg P, Rai R, Shrivastva BK (2015) Stability analysis of internal dragline dump: Distinct modeling. *ISRM Regional Symposium EUROCK 2015—Future Development of Rock Mechanics* October 7–10, 2015, Salzburg, Austria, 1027–1032 (2015)

Slope Stability Analysis of Highway Embankment by Using GEO5 Software



Dharmendra Singh  and Vijay Kumar 

Abstract In order to prevent the change in the level required by the terrain, generally, embankments are formed using compacted soil (i.e., generally clay or rock based) are used to sustain roads, railways or even canals built over it. The following study focuses on slope failure analysis which is primarily based on site investigations and lab testing. Design analysis completed on GEO5 software that requires geotechnical properties. Slope stability analysis using GEO5 software deals with various techniques such as Bishop's changed technique, Spencer's method, Morgenstern-Price method, Janbu's simplified method, and so on. Parameters such as cohesion of soil, angle of internal friction, and unit weight of soil on which slope stability analysis depends are determined in the laboratory. Geotechnical properties of soil including grain size, optimum moisture content (OMC), maximum dry density (MDD), and shear strength parameters are taken into consideration for designing and construction of high embankment up to 20 m. In the present study, the optimization aspect of slope stability with required FOS as per IRC guidelines is discussed. Highway embankment was taken and settlement analyzed for different combinations of soil stratum. The numerical modeling finished the usage of GEO5 geotechnical software for discovering the FOS. The geotechnical parameters varied for specific slope and the FOS computed.

Keywords Slope stability · Angle of internal friction · Cohesion · Factor of safety · GEO5

D. Singh (✉) · V. Kumar
Department of Civil Engineering, Motilal Nehru National Institute of Technology Allahabad,
Prayagraj 211004, India
e-mail: dharmendra@mnnit.ac.in

© The Author(s), under exclusive license to Springer Nature Singapore Pte Ltd. 2023
A. K. Agnihotri et al. (eds.), *Proceedings of Indian Geotechnical and Geoenvironmental Engineering Conference (IGGEC) 2021, Vol. 1*, Lecture Notes in Civil Engineering 280,
https://doi.org/10.1007/978-981-19-4739-1_24

249

1 Introduction

Earth slopes shaped for highway embankments, railway formations, earth dams, canals, and works, and at many extra locations. The slope may be ground level as embankments or underground degrees as cuttings [1, 2]. Slopes can be natural or man-made [1, 2, 3, 4]. Slope failure is linked to the following reasons—the geometry of slope, water content, specific gravity, soil properties in slope and vibrations due to the shakings [5, 6]. Slopes may either occur naturally or may be constructed by humans for various purposes. The problems of slope stability (SS) were also faced in the past when men or nature had disturbed the balance of the natural soil slopes. Stability-related issues in natural slopes are common challenges for researchers and professionals [7, 8]. A slope may be either supported or unsupported or have an inclined surface of soil mass [4, 9]. Variability may result due to an increase in the groundwater table, rainfall, and change in stress conditions in the slope [10]. Natural slopes may remain unchanged for decades. Rapid failure of slopes may occur due to outside forces, change in geometry, and loss of shear strength. Estimating the stability of slopes is an interesting task of civil engineering. Slope instability is a geo-dynamic phenomenon that may naturally reshape the geomorphology of the earth's crust [11]. The main objective of the SS analysis is to estimate the FOS below static and dynamic load. The failure of slopes frequently revenues place due to the act of seepage force, gravity force, seismic force within the body of the slope [4, 12]. SS analysis is a very significant discussion in the design and embankments, retaining walls, and various other civil engineering structures [9, 13]. A slope may be failed in its construction area due to an increase in the groundwater table, rainfall, and change in stress condition [3]. With slopes, the angle of internal friction increases, thus decreasing the FOS of the slopes and the extent of the additional destruction described by the slopes. Rising groundwater level increases the failure risk of slopes to some extent [12, 14]. Calculating the FOS, a natural slope or a man-made highway embankment based on forces. Use GEO5 software program to calculate the value of stability and safety factor of highway embankment [3, 15, 16].

1.1 *GEO5 Software*

Slopes considered are checked for stability by finite element method-based (FEM) software called GEO5. Geotechnical engineering methods applied in GEO5 are used all around the world [1, 5, 17]. GEO5 contains integrated segments such as SS, rock stability, reinforced slopes, spread footing, abutment, plates, gravity wall, sheeting design, and settlement [15, 16, 18]. The GEO5 consists of two types of analysis, namely all methods and optimized methods [11].

Table 1 Factor of safety guidelines for slopes [21]

Factor of safety (FOS)	Details of slope	Factor of safety (FOS)
<1.0	Considered to be unsafe	<1.0
1.0–1.25	Considered to be questionable for safety	1.0–1.25
1.25–1.40	Considered to be satisfactory for routine cuts and fills but may be questionable for dams, or where failure would be catastrophic	1.25–1.40
>1.40	Considered to be satisfactory for the dams	>1.40

1.2 Factor of Safety (FOS)

SS depends upon several parameters, like the physical features and mechanical capabilities of the soil. Physical functions of the soil are described as water content, material present within the soil mass, the texture of the soil. At the same time, mechanical features of the soil are described as shear energy, described by cohesion and corresponding inner friction [3, 19, 20]. Factor of safety guidelines for slopes is show in Table 1. FOS is thus given by:

Simply, FOS is the ratio of resisting force to driving force, i.e., $FOS = S/r$

1.3 Types of Slope Failure

There are various types of failures that may happen in a given slope such as planar failure, wedge failure, circular failure, toppling failure, two-block failure.

1.4 Angle of Internal Friction

The angle formed between the resultant force and the normal force after the occurrence of complete failure due to shearing stress is termed as the angle of internal friction [5, 17]. The material should be capable of withstanding any amount of shear stress. Factors are responsible for particle roundness, particle size, and amount of quartz content in the soil. It predicts that the slope will be greater [7, 13].

1.5 Cohesion

The material of rock resists deformation or cracking against forces. In a similar way, cohesion occurs due to electrostatic forces between surrounding soils or through pore water pressure, usually due to negative capillary tension and loading systems. Slopes

with low concurrent forces tend to be less in constant [13, 17]. Parameters that may affect cohesive force are friction, particles viscosity, cementation of grains by calcite or silica, man-made reinforcement, water content, etc.

1.6 Factors Affecting Slope Stability

Following factors have an effect on slope stability are slope geometry, dynamic forces, cohesion, angle of internal friction, lithology, groundwater, etc. [13].

2 Literature Review

A lot of work has been completed till now in the field of slope stability evaluation of the highway embankments. Slope stability analysis is one of the most challenging parts of the field of soil settlement calculation. Some critical research articles related to the embankment stability evaluation are reviewed in this section.

Slope failure is one of the most common happenings in the field of geotechnical engineering. Nowadays, the GEO5 software has become one of the most consumer-friendly tools for developing models for slope stability analysis. The evaluation of stability for homogeneous finite slopes under static loading conditions may be executed by this software [1]. This study also describes that the use of such anchors in the homogeneous soil slope may improve the safety aspect. From the analysis of the result, active forces were found to be 576.51 kN and passive force as 964.50 kN, whereas the sliding moment and factor of safety were found to be 4730.66 kN-m and 1.5, respectively [2]. This paper describes a sequence of experiments in addition to finite detail method with/without model checking, as well as protected reinforcement, provided inside the soil, and also comparative evaluation between the values. One may conclude that provision of such reinforcement in the soil may lead to enhancement in the bearing capacity of the soil [5]. Soil samples may be extracted from different locations of the slope. These samples may be tested in the laboratory for obtaining their geotechnical properties. These properties may include grain size, Proctor density, direct shear strength, and so on. Some of the results obtained in this paper include—grain size (gravel—34%, sand—35%, silt—29% and clay—2%), optimum moisture content—18%, maximum dry density—1.74 gm/cc, cohesion—0.02 to 0.11 kg/cm², and friction angle—40° to 46° [22]. The stability of slopes in waterfront structures such as dams, embankments, and natural riverside slopes may be affected due to the significant change in water level. The geometric model is analyzed using GEO5 software. This software has the tool for analyzing both the limit equilibrium method (LEM) and finite element method (FEM) that is based on slope stability problems. Methods such as Bishop's modified method, Spencer method, Morgenstern-Price method, Janbu's simplified method, Fellenius method, and other

Table 2 Geotechnical properties of various soil samples [23]

Condition	Sample	Water content (%)	Bulk density (kN/m ³)	Cohesion 'c' (kN/m ²)	Angle of internal friction (φ°)
1	1	14.29	19.414	2.6	8.2
	2	8.60	18.740	4.5	26.8
	3	6.80	17.088	5.1	24.9
	4	10.0	17.629	6.8	22.4
	5	4.71	16.363	4.8	25.4
2	1	7.36	18.639	3.8	21.4
	2	8.50	19.52	2.6	26.1
	3	4.65	21.042	6.4	20.2
	4	9.80	22.28	1.8	2.1
	5	6.09	20.05	1.6	4.5

methods are based on LEM whereas Mohr–Coulomb criteria model is based on the FEM approach [15].

2.1 Objectives

The first aim of this study is to assess the stability of the slope of an embankment for clayey soil; the next objective is to check the slope stability of a given embankment for sandy soil. Another aim of this study is to evaluate the slope stability of an embankment for silty soil in Table 2.

3 Analysis and Results

The problem is defined in terms of embankment fill properties, soil stratigraphy, soil properties, and embankment geometry. In Fig. 1, the total height of the embankment is 9.2 m on the higher side and 5 m on the lower side. The slope of the embankment is 1:1.84; the total length of the embankment is 30 m.

In condition 1, the thickness of soil (depth) is assumed 5 m, and the water table is 1 m below the ground surface. Figure 2 depicts the geometry and stratigraphy of the embankment according to condition 1. The fill material used to fill the embankment is clay, and the soil assumed clay with low of medium plasticity. The properties of fill material and clay are shown in Table 3.

In the next condition, assume that there are 3 types of soil; the first layer of soil is clayey sand (SC) which is 2 m thick followed by the second layer, clay with low or medium plasticity (CL, CI) which is 2.2 m thick, and third layer is silty gravel (GM)

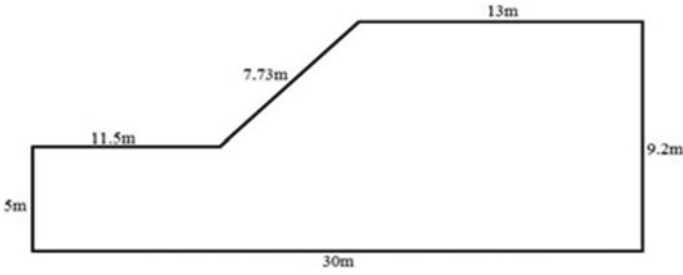


Fig. 1 Embankment size

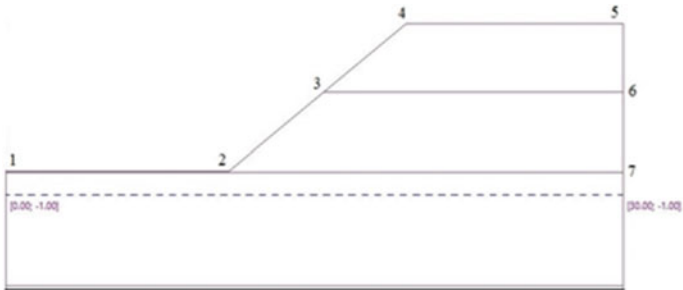


Fig. 2 Embankment geometry and soil stratigraphy with a water table

Table 3 Soil properties for condition 1

Parameters	Clay sand (SC)	Clay with low or medium plasticity (CL, CI)
Unit weight, (kN/m ³)	18.5	21.0
Saturated unit weight, (kN/m ³)	20.0	21.5
Angle of internal friction, (°)	27.0	19.0
Cohesion (kPa)	8.0	12.0
Stress state	Effective	Effective

which is 5 m thick. The water table lies below 1 m from the ground surface. Figure 3 represents the geometry and stratigraphy of the embankment as per the mentioned situation.

The fill material used to fill the embankment is clayey sand (SC), clay with low or medium plasticity (CL, CI) and silty gravel (GM). The properties of fill material and clay are presented in Table 4. Models developed as per the condition 1 & 2 are run through GEO5 geotechnical software. Results obtained are illustrated in Table 5. Factor of safety for both the conditions is acceptable because FOS in both the conditions is greater than 1.5.

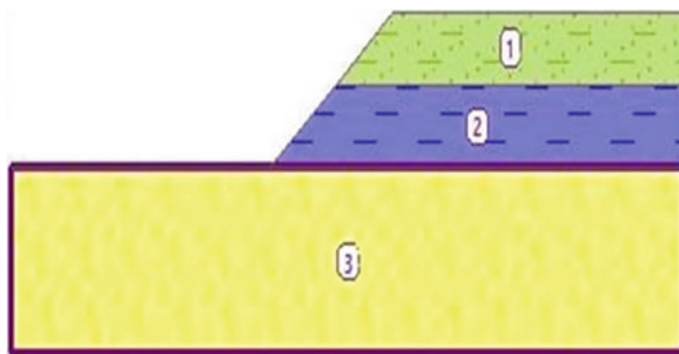


Fig. 3 Embankment geometry and soil stratigraphy

Table 4 Soil properties for condition 2

Parameters	Clay sand (SC)	Clay with low or medium plasticity (CL, CI)	Silty gravel (GM)
Unit weight, (kN/m ³)	18.5	21.0	19.00
Saturated unit weight, (kN/m ³)	20.0	21.5	19.50
Angle of internal friction, (°)	27.0	19.0	32.50
Cohesion of soil (kPa)	8.0	12.0	4.00
Stress state	Effective	Effective	Effective

Table 5 Results depicted in different conditions

	Result from condition 1	Result from condition 2
Sum of active forces, Fa	66.87 kN/m	99.27 kN/m
Sum of passive forces, Fp	134.94 kN/m	161.22 kN/m
Sliding moment, Ma	385.21 kN-m/m	644.26 kN-m/m
Resisting moment, Mp	777.29 kN-m/m	1046.29 kN-m/m
Factor of safety, FOS	2.02	1.62
Slope stability	Acceptable	Acceptable

4 Conclusions

There are two different conditions which have been taken for slope stability analysis by Bishop's method. This study leads to the following conclusions:

1. From the results of stability analysis, sum of active forces, sum of passive forces, sliding moment, resisting moment, and FOS for condition no. 1 are

obtained as 66.87 kN/m, 134.94 kN/m, 385.21 kN-m/m, 777.29 kN-m/m, and 2.02, respectively.

2. For condition no. 2, sum of active forces, sum of passive forces, sliding moment, resisting moment, and FOS are obtained as 99.27 kN/m, 161.22 kN/m, 644.26 kN-m/m, 1046.29 kN-m/m, and 1.62, respectively.
3. From the stability analysis of given slopes at condition one and two by Bishop's method, the slope was found to be stable, as the factor of safety for both the conditions is greater than 1.5.
4. This study highlights that condition 1 is good for embankment because of more factor of safety of soil stratum after the construction of embankment.

References

1. Arun KU, Jisna P, Simon R, Mathews OA, Anju EM (2020) A comparison study on stability of kuranchery slopes using GEO5 and PLAXIS 2D software. *Int J Res Eng Sci Manag* 3(3)
2. Deepika T (2018) Slope stability analysis for proposed footing construction seated on sloppy ground. *Int J Eng Technol* 7(3.35):30–31
3. Harabinova S, Panulinova E (2017) Assessment of slope stability. *MATEC Web Conf* 107:00031
4. Kumar P, Premalatha K (2018) Stability analysis of slopes during monsoon in nilgiris", Indian geotechnical conference. Indian Institute of science, Bengaluru, 13–15 December
5. Farshidfar N, Nayeri A (2015) Slope stability analysis by shear strength reduction method. *J Civil Eng Urbanism* 5(1):35–37
6. GEO5 Engineering Manuals.
7. Halder S, Imam MO, Basir MS (2016) A detailed analysis of slope stability using finite element method (FEM). In: 3rd International conference on advances in civil engineering, 21–23 December 2016, CUET, Chittagong, Bangladesh
8. Iravanian A, Shlash A (2020) A comparative study of critical failure surface determination in slope stability assessment. In: 5th International conference on new advances in civil engineering ICNACE
9. Keskin I (2017) Stability analysis of a high stone retaining wall: a case of Eskipazar/Turkey. *Int J Adv Res Eng IJARE* 3(2)
10. Suroshe P, Gondage S, Kasture K, Lamb R, Mahajan P, Bhagat S (2020) Design of tunnel by using GEO5 Software. *Int Res J Eng Technol (IRJET)* 07(06)
11. Santosh N, Borole ST, Sagar M, Kale S (2019) Slope stability analysis with GEO5 software for Malin landslide in Pune (Maharashtra). *Global J Eng Sci Res. ISSN 2348-8034*
12. Janták V (2017) Stability analysis of landslide on the R1 expressway by limit equilibrium and finite element methods. *World Multidisciplinary Earth Sciences Symposium*. In: IOP Conference Series: Earth and Environmental Science 95
13. Krishnan A, Kolathayar S (2020) Stability analysis of dike to impound freshwater in brackish water estuarine environment. *Open Constr Build Technol J*
14. Madhusudhan C, Rajeswari K, Fayaz S (2018) Slope stability analysis using Geo-studio software. *J Emerg Technol Innov Res (JETIR)* 5(7)
15. Sazzad MM, Hie ABKMA, Hossain MS (2016) Stability analysis of reinforcement slope using FEM. *Int J Adv Struct Geotech Eng* 05(03). ISSN 2319-5347
16. Sharma P (2017) Evaluation and comparison of classical earth pressure theories for cohesionless (φ) backfill using professional softwares. *Int J Creative Res Thoughts (IJCRT)* 5(4)
17. GEO5, Fine Spol. S. R. O.: Settlement Program. Demo version. Czech Republic

18. Saranaathan SE (2015) Different research techniques and models in rock mass rating and slope stability analysis. *J Chem Pharm Res* 7(7):160–168
19. Goliya HS, Gour P (2014) Slope stability analysis for high embankment with metacoputing technique “a case study of natrax high speed track”. *Int J Core Eng Manag (IJCEM)* 1(2)
20. Nugroho CP, Suryo EA, Setyowulan D (2019) Software analysis on slope stability of Gunung Banyak in Batu City. *Int Res J Adv Eng Sci* 4(1):56–58
21. Varghese DA, Isaac DS (2020) FEM analysis of slopes in idukki using GEO5. *Int Res J Eng Technol (IRJET)* 07(08)
22. Ghosh A, Sarkar S, Kanungo DP, Jain SK, Kumar D, Kalura AS, Kumar S (2009) Slope instability and risk assessment of an unstable slope at Agrakhal, Uttarakhand. *Indian Geotechnical Conference* 16–19 December 2009 Guntur, Andhra Pradesh
23. Sharma RK, Kumar V, Sharma N, Rathore A (2012) Slope stability analysis using software GEO5 and C programming. In: *International conference on chemical, ecology and environmental sciences (ICEES'2012)*, Bangkok

Prediction of Unconfined Compressive Strength of Clayey Soil Stabilized with Steel Slag and Cement



Aditya D. Ahirwar and H. S. Chore

Abstract Rapid urbanization has resulted in huge increase in number of infrastructure projects across the country. Availability of suitable material for construction of infrastructure projects is of utmost importance for completing the projects within time and budget. This is putting a lot of pressure on naturally available resources. Demand of steel has also increased enormously due to these global processes. India is producing steel through blast furnace–basic oxygen furnace route as well as electric furnace or induction furnace route. During steel refining process, 2000–4000 kg of steel slag is generated for every tonne of steel produced. Geotechnical properties of the soil can be boosted by addition of steel slag. Unconfined compressive strength (UCS) is important parameter which is widely used to determine the strength of the subgrade soil. Laboratory investigation using UCS is complex and time-consuming process. Experimental and analytical study aims at developing the equation based on multiple linear regression for evaluating the strength of the soil-slag and soil-slag-cement composite mix. Equations so developed showed better prediction capacity based on coefficient of determination.

Keywords Unconfined compressive strength · Regression analysis

1 Introduction

Demand of steel has increased exponentially over last few decades due to increase in infrastructure projects. India is second largest producer of steel, just trailing China. Mainly, there are two types of steel manufacturers in India: integrated/major steel plants and secondary or MSME steel producers. During steel refining process, waste

A. D. Ahirwar (✉) · H. S. Chore
Department of Civil Engineering, Dr. B. R. Ambedkar National Institute of Technology,
Jalandhar 144011, India
e-mail: ahirwarad.ce.19@nitj.ac.in

H. S. Chore
e-mail: chorehs@nitj.ac.in

by-product, i.e., steel slag, is generated. Disposal of the massive quantity of waste in an environment-friendly manner has become a challenging task.

Oluwasola et al. [1] reviewed the properties of the slag and pointed out that presence of dicalcium silicate, tricalcium silicate and tetra-calcium alumina ferrite in steel slag qualifies it as cementitious material. Poh et al. [2], Goodarzi and Salimi [3] identified that low adsorption capacity, pozzolanic action and cation exchange between soil and slag particle are indicative of steel slag being excellent soil modification agent. Akinwumi et al. [4], Aldeeky et al. [5], Rao et al. [6] and Wu et al. [7] concluded that steel slag can be effectively utilized for stabilization of weak soil so as to be used in various component layers of the pavements.

Unconfined compressive strength is the important parameter that determines the strength of the soil or composite mix. Laboratory experimentation is tedious and time-consuming process which also includes curing period. Anagnostopoulos et al. [8] and Sharma and Singh [9] gave statistical model for determination of compressive strength of modified soil. Das et al. [10] and Suman et al. [11] developed prediction model to determine UCS of stabilized soil using artificial intelligence techniques.

Analytical study aims at developing the equations using multiple regression technique based on statistical approach. Intention of the study is to reduce the time-consuming process used for determination of UCS for varying curing period.

2 Material and Method

Material used in present investigation involves marine clay, steel slag and cement. In the current study, the marine clay was mixed with 5, 10, 15, 20 and 25% steel slag and 4, 6 and 8% cement. The strength characteristics like unconfined compressive strength of different combinations of mixes were evaluated from laboratory investigation. Study also involves determination of UCS for 7 days and 28 days curing period. Samples were also tested for soaked and unsoaked conditions.

Multiple regression technique was used to derive the equations from the data obtained during laboratory testing. Data was divided in two parts, dependent and independent variables. Steel slag content and cement content are considered as independent variables, whereas unconfined compressive strength is considered as dependent variable in current study. After deriving the regression equation for evaluation of UCS, predicted values were compared with the laboratory test results to check the precision of the model equations.

3 Discussion of Results

The experimental program comprises primary tests to get the index properties of marine clay. Table 1 shows geotechnical characteristics of the clayey soil considered in the study.

Table 1 Geotechnical properties

Sr. No.	Property	Value
i	Liquid limit (LL) (%)	68.10
ii	Plastic limit (PL) (%)	32.80
iii	Specific gravity	2.45
iv	Maximum dry density (MDD) (gm/cc)	1.46
v	Optimum moisture content (OMC) (%)	27.50
vi	Unconfined compressive strength (kPa)	118.60

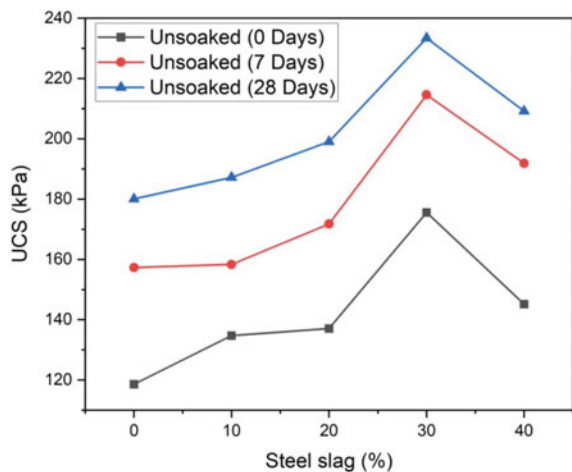
In the current study, unconfined compressive strength of different combination of mixes containing soil and steel slag was evaluated. Figure 1 illustrates the variation in unsoaked UCS of various mixes.

From Fig. 1, it can be noted that the unsoaked UCS of the soil-steel slag composite mix increases with increase in proportion of steel slag up to 30%; thereafter, reduction in UCS is observed. Same pattern can be seen in case of 7 and 28 days of curing period. Also, it can be seen that unsoaked UCS of the mix increases with curing period.

Study involves analyzing the effect of addition of steel slag (10, 20, 30 and 40%) in conjunction with cement (4, 6 and 8%). From Figs. 2 and 3, it can be concluded that unsoaked and soaked UCS of soil-steel slag-cement composite mix increases with increase in cement content.

Laboratory experimentation is also conducted to identify the effect of curing on UCS of soil-steel slag-cement composite mix. Cylindrical samples were prepared and cured for 7 and 28 days. Test was conducted in unsoaked and soaked conditions. For implementing test in soaked condition, samples were soaked in water for 8 h before testing. Figure 2 suggests the variation in unsoaked UCS of the various combination

Fig. 1 Effect of steel slag on unsoaked UCS for 0, 7 and 28 days of curing



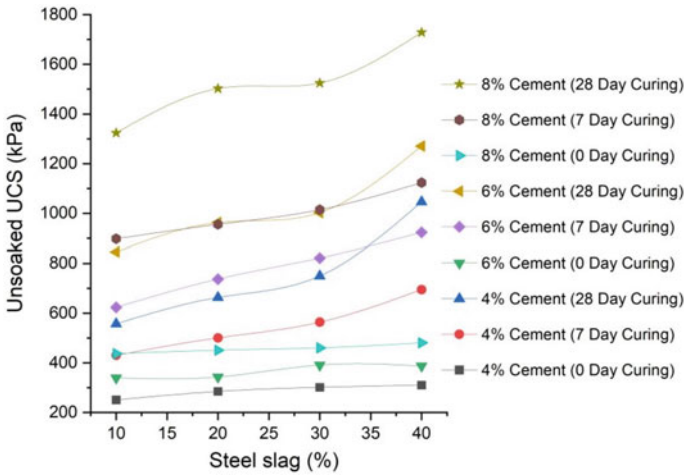


Fig. 2 Variation in UCS (unsoaked) with variation in steel slag and cement for different curing period

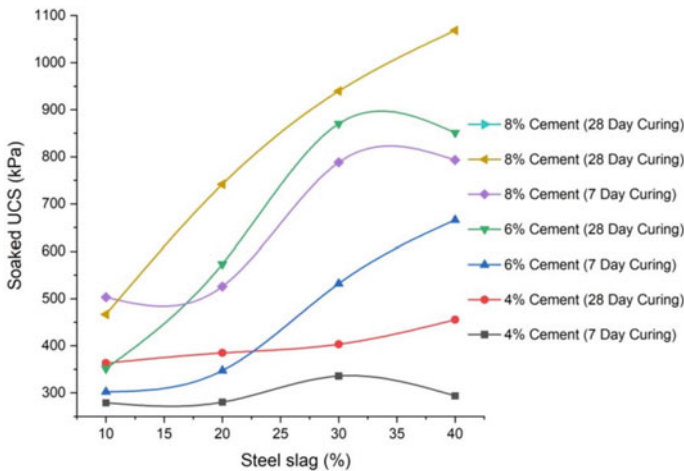


Fig. 3 Variation in UCS (soaked) with variation in steel slag and cement for different curing period

of mixes for 0, 7 and 28 days of curing period, whereas Fig. 3 depicts the effect of curing period on soaked UCS of various composition of mixes. From Figs. 2 and 3, it can be observed that with increase in curing period, unsoaked and soaked UCS of the composite mix increases. It can also be established that soaking reduces the UCS of the composite mix.

After extensive laboratory investigation, data so obtained is used to derive the equation to determine the UCS of various combination of mixes. Independent and dependent variables were identified. Proportion of steel slag and cement is considered

Table 2 Equations developed to evaluate UCS

Details of various mixes considered in Current study			
Mix	Curing period	Equation	R^2
I	Soil + Steel slag (Unsoaked condition)		
A	0 days	$0.94 \text{ SS} + 123.42$	0.5017
B	7 days	$1.2539 \text{ SS} + 153.69$	0.6603
C	28 days	$1.0443 \text{ SS} + 180.88$	0.6249
II	Soil + Steel slag + Cement (Unsoaked condition)		
A	0 Days	$1.7530 \text{ SS} + 42.602 \text{ C} + 70.360$	0.9859
B	7 days	$8.591 \text{ SS} + 112.57 \text{ C} - 116.255$	0.9929
C	28 days	$13.688 \text{ SS} + 191.46 \text{ C} - 392.69$	0.9561
III	Soil + Steel slag + Cement (Soaked condition)		
B	7 days	$8.360 \text{ SS} + 88.86 \text{ C} - 271.67$	0.8573
C	28 days	$13.644 \text{ SS} + 100.61 \text{ C} - 322.44$	0.8296

as independent parameter, whereas unsoaked UCS and soaked UCS are considered as dependent variable. Multiple regression analysis is used to determine the coefficient which helps in determining the UCS of various combination of mixes for different curing period. Table 2 enlists the equations derived from statistical analysis for prediction of unconfined compressive strength in soaked and unsoaked conditions.

Values of soaked and unsoaked UCS of various composition of mixes were evaluated using above regression equation. Figure 4 shows the comparison between the predicted value of UCS obtained from equation and actual UCS value obtained from laboratory experimentation work. Accuracy of the equation is evaluated in terms of coefficient of determination (R^2), value of which ranges from 0 to 1. $R^2 = 0$ indicates that dependent variable cannot be predicted from dependent variable, whereas $R^2 = 1$ reflects that dependent variable can be predicted without any error. Coefficient of determination for various equation ranges from 0.5017 to 0.9929. This suggests that UCS of the different combination of mixes for varying curing period can be predicted with more accuracy.

Figure 4 depicts the comparison between UCS predicted from equation and UCS value obtained from experimental investigation for varying curing period. It can be noted from the values of coefficient of determination that predicted values and observed values are in close proximity to each other.

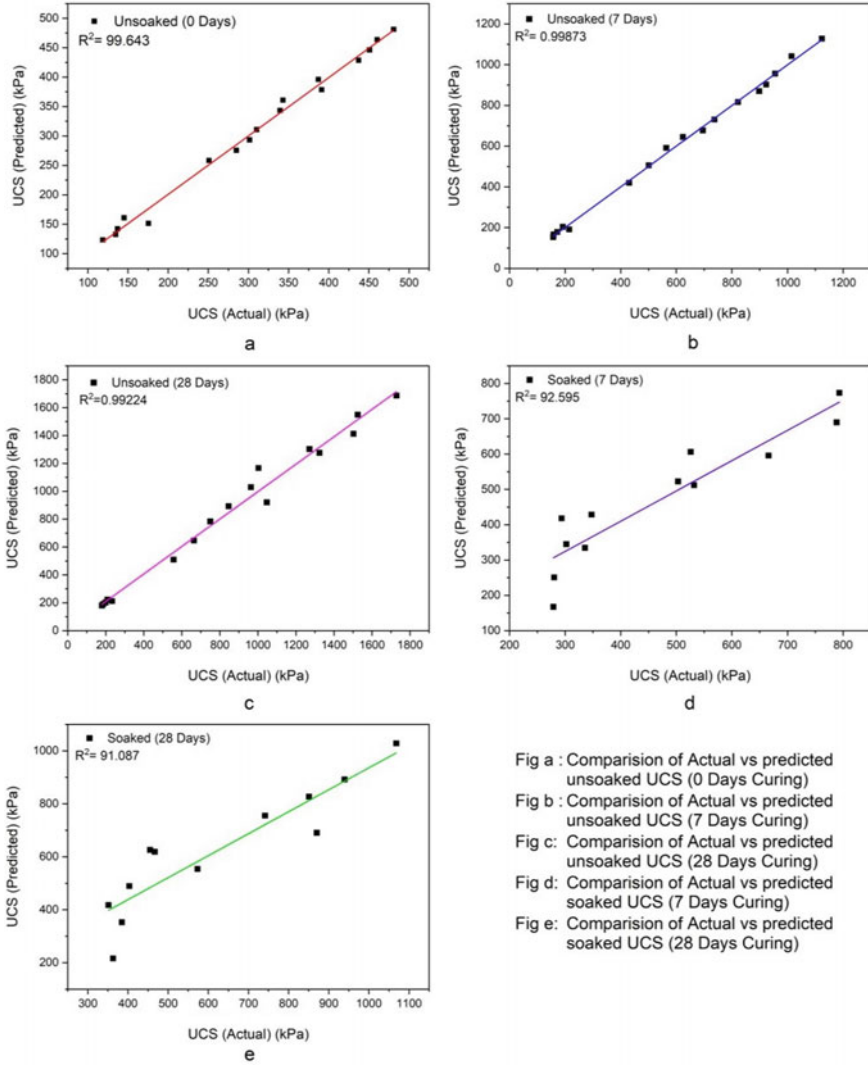


Fig a : Comparison of Actual vs predicted unsoaked UCS (0 Days Curing)
Fig b : Comparison of Actual vs predicted unsoaked UCS (7 Days Curing)
Fig c : Comparison of Actual vs predicted unsoaked UCS (28 Days Curing)
Fig d : Comparison of Actual vs predicted soaked UCS (7 Days Curing)
Fig e : Comparison of Actual vs predicted soaked UCS (28 Days Curing)

Fig. 4 Comparison of actual versus predicted unconfined compressive strength (unsoaked and soaked) for 0, 7 and 28 days of curing

4 Summary and Conclusion

Following inferences can be drawn from the laboratory and analytical investigations conducted to estimate the strength characteristics of clay stabilized with steel slag and cement:

1. The unsoaked UCS of the soil-steel slag composite mix increases with increase in steel slag content up to 30%. Thereafter, reduction in strength is observed.
2. Unsoaked UCS of the soil-steel slag composite mix increases with curing period.
3. UCS (soaked and unsoaked) of the soil-steel slag-cement composite mix increases with increase in cement content.
4. Strength (soaked and unsoaked) of the soil-steel slag-cement composite mix increases with curing period.
5. Soaking reduces the UCS of the composite mix.
6. Equations developed by performing statistical analysis gave satisfactory results. Coefficient of determination suggests that predicted values are in agreement with actual values obtained from extensive laboratory investigation.

Thus, based on the laboratory findings, we can conclude that industrial waste materials such as steel slag can be used as a sustainable road construction material to improve the strength of clayey soil when used in conjunction with cement. Unconfined compressive strength test is time-consuming process, which includes the curing period. Equations so derived from analytical study prove to be beneficial in terms of its time-saving potential as it gives an idea about strength characteristics at 7 and 28 days of curing period.

References

1. Oluwasola EA, Hainin MR, Aziz MMA (2014) Characteristics and utilization of steel slag in road construction. *Jurnal Teknologi* 70(7)
2. Poh HY, Ghataora GS, Ghazireh N (2006) Soil stabilization using basic oxygen steel slag fines. *J Mater Civ Eng* 18(2):229–240
3. Goodarzi AR, Salimi M (2015) Stabilization treatment of a dispersive clayey soil using granulated blast furnace slag and basic oxygen furnace slag. *Appl Clay Sci* 108:61–69
4. Akinwumi II, Adeyeri JB, Ejohwomu OA (2013) Effects of steel slag addition on the plasticity, strength, and permeability of lateritic soil. In: *ICSDEC 2012: developing the frontier of sustainable design, engineering, and construction*, pp 457–464
5. Aldeeky H, Al Hattamleh O (2017) Experimental study on the utilization of fine steel slag on stabilizing high plastic subgrade soil. *Advances in Civil Engineering* 2017:1
6. Rao DK, Sravani G, Bharath NA (2014) Laboratory study on the effect of steel slag for improving the properties of marine clay for foundation beds. *Int J Sci Eng Res* 5(7)
7. Wu J, Liu Q, Deng Y, Yu X, Feng Q, Yan C (2019) Expansive soil modified by waste steel slag and its application in subbase layer of highways. *Soils Found* 59(4):955–965
8. Anagnostopoulos CA, Chatziangelou M (2008) Compressive strength of cement stabilized soils. A new statistical model. *Electron J Geotech Eng* 13:1–10
9. Sharma LK, Singh TN (2018) Regression-based models for the prediction of unconfined compressive strength of artificially structured soil. *Engineering with Computers* 34(1):175–186

10. Das SK, Samui P, Sabat AK (2011) Application of artificial intelligence to maximum dry density and unconfined compressive strength of cement stabilized soil. *Geotech Geol Eng* 29(3):329–342
11. Suman S, Mahamaya M, Das SK (2016) Prediction of maximum dry density and unconfined compressive strength of cement stabilised soil using artificial intelligence techniques. *International Journal of Geosynthetics and Ground Engineering* 2(2):1–11

Experimental and Analytic Study of the Uplift Capacity of a Horizontal Plate Anchor Embedded in Geo-Reinforced Sand



K. B. Akbar Husain and Samirsinh P. Parmar

Abstract The foundation systems under uplift loads, in particular, should be designed in accordance with the factors that influence uplift capability. Anchor systems have recently been used successfully in structures that have been subjected to uplift force. These anchor systems are affected by soil properties, loading conditions, embedment ratio and anchor group configuration. Model tests in the laboratory were used to investigate the uplift behaviour of plate anchors embedded in cohesion-less soil media with and without geosynthetic. Many factors, including the type of geosynthetic, the area of the anchor plate, relative density, the depth of embedment, the type of soil and the area of geosynthetic inclusion, have significantly influenced plate anchor uplift behaviour. The present paper describes the methodology and experimentation on model horizontal plate anchors embedded in geosynthetic reinforced cohesion-less soil beds. Also, the analytical investigation was carried out and the results were compared. It is observed those plate anchors embedded in reinforced soil exhibit 1.4 times more uplift capacity than the anchors embedded in unreinforced soil. Inclusion of geosynthetic layer increases the effective area of anchorage.

Keywords Plate anchors · Uplift capacity · Reinforced soil · Model study

Abbreviations

γ	In situ dry density
γ_{\max}	Maximum dry density
γ_{\min}	Minimum dry density
ϕ	Angle of internal friction
Cu	Uniformity coefficient
Cg	Unit cohesion between soil and geogrid.
Tg	Frictional force due to soil geogrid system

K. B. A. Husain · S. P. Parmar (✉)
Department of Civil Engineering, Dharmasinh Desai University, Nadiad, India
e-mail: spp.cl@ddu.ac.in

© The Author(s), under exclusive license to Springer Nature Singapore Pte Ltd. 2023
A. K. Agnihotri et al. (eds.), *Proceedings of Indian Geotechnical and Geoenvironmental Engineering Conference (IGGEC) 2021, Vol. 1*, Lecture Notes in Civil Engineering 280,
https://doi.org/10.1007/978-981-19-4739-1_26

θ_g	Angle of Interface between soil and geogrid
σ_n	Normal stress over geogrid surface
A_g	Effective area of geogrid
B'	Width of equivalent anchor at geogrid level
C_c	Coefficient of curvature
G_s	Specific Gravity of sand
D_{10}	Size of particle at 10% finer on the gradation curve
D_{30}	Size of particle at 30% finer on the gradation curve
D_{60}	Size of particle at 60% finer on the gradation curve
D_R	Relative density
Q_u	Ultimate uplift capacity
N_q	Breakout factor
δ	Displacement
H/B	Embedment ratio

1 Introduction

Tall engineering structures such as chimneys, offshore and onshore wind turbines, transmission towers and communication facility towers, etc. are subjected to wind load and hence uplift forces exerted on their foundations. To resist uplift forces, ground anchors are required. Depending on the subsoil conditions and the magnitude of loading, anchor dimensions, embedment depth and orientation of the anchor plate are selected. Horizontal plate anchors are commonly used to resist uplift load in vertical or inclined directions.

Installations of anchors in problematic soil is difficult as well as it offers minimum uplift resistance hence the subsoil conditions need to be improved. On the other hand, due to the global meteorological uncertainties, there is increase in frequency of cyclones per year. These situations force geotechnical engineers to improve or reinforce the plate anchors so that it can offer more uplift resistance. The use of geosynthetic inclusions is a well-established approach for enhancing soil strength, in which the soil's strength is improved by interaction with the strong, flexible, tensile reinforcement.

2 Brief Review

Balla was the first to report on a study of the pull-out resistance of horizontal plate anchors. Since then, there has been a significant amount of research in this field. Many analytical and experimental studies in this area of research have been reported by several investigators, including Meyerhof and Adams, Vesic, Hanna et al., Meyerhof, Neely et al., Vesic, Das and Seeley, Basset, Davie and Sutherland, Das, Saran et al.,

Dickin. Loading on various structures necessarily requires the uplift resistance of anchors, such as free-standing towers, wind turbines, submerged pipelines, chimneys, suspension bridges and roofs. Anchors are commonly embedded within nearby soil in these applications to provide stability and transmit tensile forces to a competent medium. Anchors, which are commonly found in the form of plate anchors, helical anchors, Deadman anchors, pile anchors and drag anchors, are the most common means of resisting these loads. A buried anchor's uplift capacity is mainly composed of the weight of soil within the failure zone as well as frictional and/or cohesive resistance along the realized failure surface. The uplift capacity of anchors can be increased by increasing the size and embedment depth of the anchor or improving backfill strength and density.

Geosynthetics have become increasingly popular in recent years due to their cost-effectiveness in reinforcement applications. Geosynthetics are typically manufactured in planar form (geotextiles, geogrids, geonets, geomembranes, strips). However, limited research has been made to improve geosynthetic anchor capacities—which are almost exclusively limited to the use of planar inclusions in dry sands, reinforced by geotextiles and geogrid types. The uplift capacity of a small-scale anchor plate embedded into dry sand with and without geosynthetics has been examined by Krishna and Parashar (1994) and the results indicate that the reinforcements can significantly enhance the uplift capacity.

Main objectives of the existing investigation are to study:

- i. The effects of geosynthetics inclusion on the uplift behaviour of plate anchors.
- ii. The effect of location of geosynthetic inclusion for enhancing the ultimate uplift capacity of plate anchors.
- iii. The effect of the soil density on the uplift capacity.

3 Experimental Programme

To analyze the effect of reinforcement in pull-out capacity of the embedded anchor, model testing on square anchor plate was carried out which is 10 mm thick and 0.15 m \times 0.15 m in size, anchored from the centre by rod of the same material. The size of anchor plate is selected in such a way that the width of anchor plate ($B = 0.15$ m) is less than 1.2 m the width of test tank. (i.e. $5B < 1.2$ m). Two relative density 70 and 85% were selected to understand the effect of relative density on pull-out capacity of the model reinforced anchor. Table 1 outlines the total experiments to be carried out for mentioned objectives. Total of 48 tests had been carryout out for uplift load measurement.

The embedment ratio is defined as the ratio of depth of footing below ground surface to the size of plate anchor. Embedment ratio is the dimension to place the reinforcement at different depths from the anchor plate the embedment ratio was 2, 3 and 4 (i.e. 0.15 (anchor plate size) \times 2 = 0.3 m and, respectively). As the analysis has been developed only for shallow anchors, testing of model anchors with large embedment ratios has not been attempted. In all the tests anchor plates were kept

Table 1 Experimental programme

Sr. No	Plate size	Relative density	Embedment ratio (H)	Reinforcement position
	$L * B$			
1	0.15 m * 0.15 m (square plate)	70%	2, 3 and 4	(1) Without reinforcement
				(2) At top of anchor plate
				(3) At 0.25B
				(4) At 0.5B
2		85%	2, 3 and 4	(1) Without reinforcement
				(2) At top of anchor plate
				(3) At 0.25B
				(4) At 0.5B

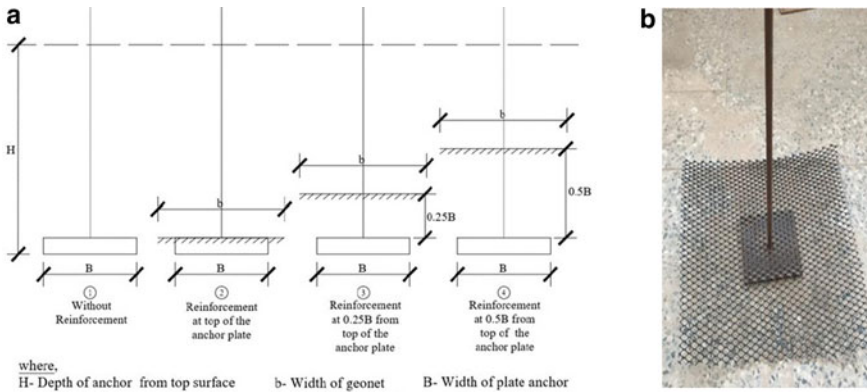


Fig. 1 **a** Placement of geosynthetic inclusions and Embedment depth. **b** Reinforcement at top of anchor plate ($0*B$)

horizontal and shaft vertical. Figure 1a indicates the location of reinforcement and Fig. 1b is the actual model anchor plate along with geogrid reinforcement.

3.1 Loading Frame and Loading Mechanism

Loading Frame is designed for more than 50 kN load capacity. Chain pulley block with 3 t capacity is hung on frame for apply uplift load. The schematic diagram of the experimental set-up is shown in Fig. 2 and the actual loading device and plaxiglass tank is shown in Fig. 3. It is made of C-channel section with angle section bracing. The

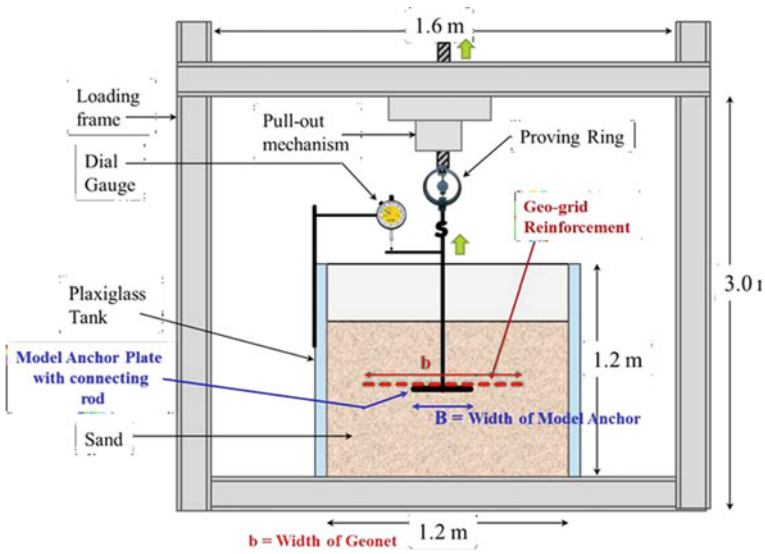


Fig. 2 Schematic diagram of model test set-up

stiffness of the loading frame was analyzed in *Staad* software and found relatively rigid compared to applied loads in pull-out testing. Figure 4 indicates modelling of the loading frame in *Staad* software.

Plaxiglass tank is arranged to generate ground condition by filling sand. Dimension of the tank is 1.2 m * 1.2 m * 1.2 m. Base of the tank is made of iron steel plate and side of the tank is made of plaxiglass sheet with support of angle section.

Anchor plate with rod is made of Mild steel material. It is designed for 30 kN loading conditions. Dimension of the anchor plate is 0.15 m * 0.15 m. Anchor Rod is 1.2 m in length and 12 mm in diameter. Proving ring with 5 t capacity (5.55 kg/div) is used to measure the load. It is connected between chain pulley block's hook and anchor rod. Dial gauge with 0.01 mm least count is used to measure the anchor plate's vertical displacement.

3.2 Engineering Properties of Geotextiles

This was used as reinforcement in the form of HDPE geonets in the experimental work. This was locally available and was manufactured by Maharshi Geomembrane (India) Pvt. Ltd. The properties of this material are shown in Table 2. The size of geosynthetics used as three times the size of anchor plate with hole at centre for anchor shaft.

Table 2 Properties of geonet used in experiment

Sr No	Properties	Value
1	Form	Roll
2	Colour	Black
3	Apparent opening size	20 mm * 10 mm
3	Thickness of material	≥ 5 mm
	EN ISO-9863	
4	Wide width tensile strength MD-EN ISO 10319	≥ 13.5 kN/m
5	CBR puncture resistance—EN ISO 12236	≥ 2.2 kN
6	Mass per unit area—EN ISO 9864	≥ 830 g/m ²
7	In plane permeability—EN ISO 12958	
	Hydraulic gradient (<i>i</i> = 1)	
	@ 100 kPa	≥ 0.6 l/ms
	@ 200 kPa	≥ 0.55 l/ms

3.3 Sand Properties and Bed Preparation

The soil for both backfills and infill used in the experimental series was consistent throughout all of the physical experiments—poorly graded sand (SP in the Unified Soil Classification System, ASTM D 2487-11, $G_s = 2.66$). There is a significant quantity of medium sand (65.17%) and very little coarse sand (<5%), as shown in the grain size distribution (Fig. 5).

Relative density test (confirming IS:) was conducted. The maximum dry density γ_{max} is 1.83 gm/cc and minimum dry density γ_{min} is 1.67 gm/cc. The relative density was carried out at 70% and 85% which was reported as 1.78 gm/cc and 1.80 gm/cc, respectively. Direct shear test also carried out at the two relative densities and the angle of internal friction (ϕ) was derived, 37.15° for 70% Rd. and 40° for 85% Rd.

Fig. 5 Grain size distribution curve of sand

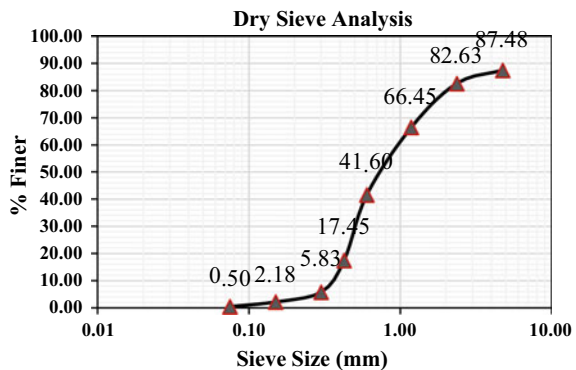


Table 3 Results of sieve analysis

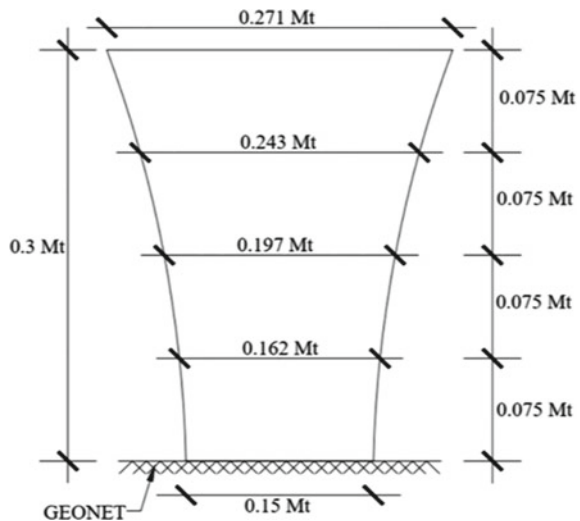
Sr. No.	Granulometry parameters	Value
1	Percentage of coarse sand (%)	4.85
2	Percentage of medium sand (%)	65.17
3	Percentage of fine sand (%)	17.45
4	Effective grain size, D_{10} (mm)	0.37
5	D_{30} (mm)	0.50
6	D_{60} (mm)	0.96
7	Coefficient of uniformity, C_u	2.53
8	Coefficient of curvature, C_c	0.70
9	Classification of sand	SP

All the pull-out experiment was conducted at both 70% and 85% relative density (Table 3).

4 Analytical Method

The excel spreadsheet was used to analyze the analytical results for various embedment depths, locations of reinforcement and soil density. Model calculation is shown here for the reference. The following data has been used in analysis for computing the value of pull-out capacity with reinforcement at the top of the anchor plate. Shape of plate = Square, $\phi_i = 36^\circ$, $D_r = 70\%$, Embedment depth = 0.3 m, $\gamma = 17.799 \text{ kN/m}^3$, $\phi = 37.15^\circ$, Diameter of failure zone at the top = 0.271 m (Fig. 6).

Fig. 6 Total weight of soil in the failure wedge: Weight of soil in strip 1 = $\pi/4 * 0.257^2 * 0.075 * 17.799 = 0.06924 \text{ kN}$; Weight of soil in strip 2 = $\pi/4 * 0.22^2 * 0.075 * 17.799 = 0.05074 \text{ kN}$; Weight of soil in strip 3 = $\pi/4 * 0.1795^2 * 0.075 * 17.799 = 0.03378 \text{ kN}$; Weight of soil in strip 4 = $\pi/4 * 0.156^2 * 0.075 * 17.799 = 0.025515 \text{ kN}$; Total weight of soil in the failure zone (W) = 0.17929 kN



4.1 Shearing Resistance

The variation of the shape factor coefficient m with the soil friction angle \emptyset as suggested by Meyerhof and Adams is as follows:

From Table 4 for $\emptyset = 37.15^\circ$, $m = 0.293$

$$S_f = 1 + m \left(\frac{D}{B} \right)$$

$$S_f = 1 + 0.293 * \left(\frac{0.3}{0.15} \right) = 1.586$$

$$P = 2\gamma H^2 S_f B K \tan \emptyset$$

$$= 2 * 17.799 * (0.3)^2 * 1.586 * 0.15 * 1 * \tan(37.15)$$

$$= 0.5774 \text{ kN}$$

Frictional force due to reinforcement:

$$(t_g)_{\text{ver}} = \{C_g + \gamma(H - H')k \sin \emptyset i \tan \emptyset i\} \sin \emptyset i$$

$$= \{0 + 17.799(0.3 - 0) * 1 * \sin 36 * \tan 36\} \sin 36$$

$$= 1.5940 \text{ kN/m}^2$$

For square plate: A_g (Effective area) = $18B^2 - 2B'^2$

$$= 18 * 0.15^2 - 2 * 0.15^2$$

$$= 0.36 \text{ m}^2$$

$$T_g = (t_g)_{\text{ver}} * A_g$$

$$= 1.5940 * 0.36$$

$$= 0.5738 \text{ kN}$$

Predicted pull-out capacity = $W + P + T_g$

$$= 0.17929 + 0.5774 + 0.5738$$

Table 4 Variation of the shape factor coefficient m with the soil friction angle \emptyset

Soil friction angle (\emptyset), ($^\circ$)	Shape factor coefficient, (m)
30	0.15
35	0.25
40	0.35
45	0.5

Table 5 Predicted pull-out capacity for reinforcement at the top of anchor plate case

Sr No.	Relative density (%)	Embedment depth (m)	Predicted pull- out capacity (kg)
		0.3	135.67
1	70	0.45	286.49
		0.6	514.44
		0.3	149.83
2	85	0.45	323.97
		0.6	607.99

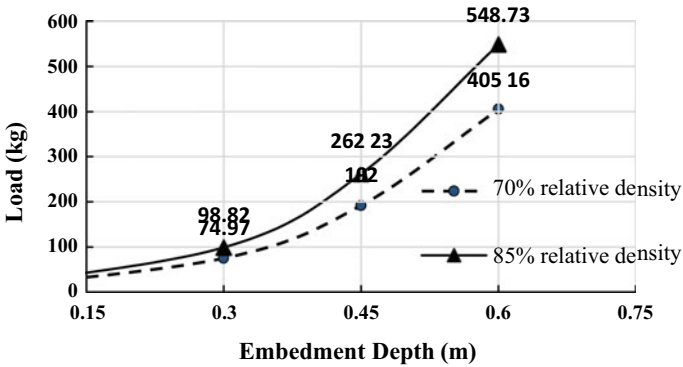


Fig. 7 Without reinforcement

$$= 1.330 \text{ kN}$$

Similarly, predicted pull-out capacity using analytical calculation are carried out for embedment depth 0.3, 0.45, 0.6 and relative density 70 and 85% as shown in Table 5.

Analysis by analytical Method: (Figs. 7, 8, 9, 10 and 11).

4.2 Experiments on Model Anchor Embedded in Reinforced Soil

See Figs. 12 and 13.

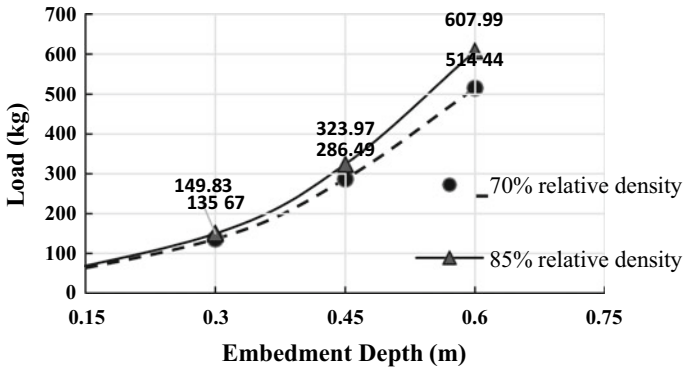


Fig. 8 Reinforcement at top of the anchor plate

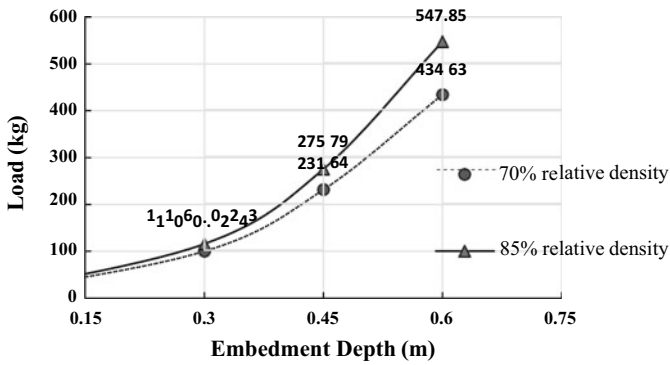


Fig. 9 Reinforcement at 0.5b from top of the anchor plate

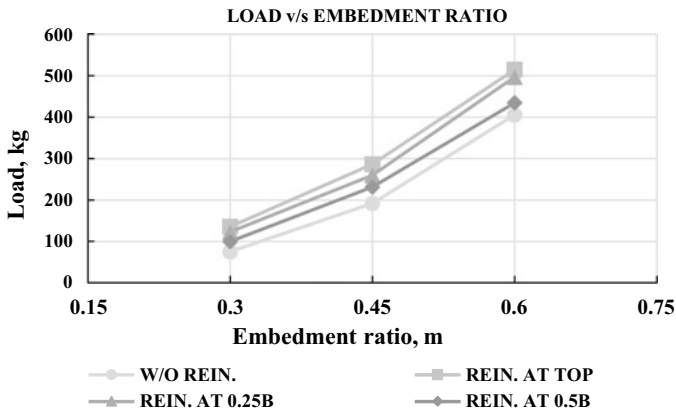


Fig. 10 Analytical uplift capacity comparison for 70% relative density

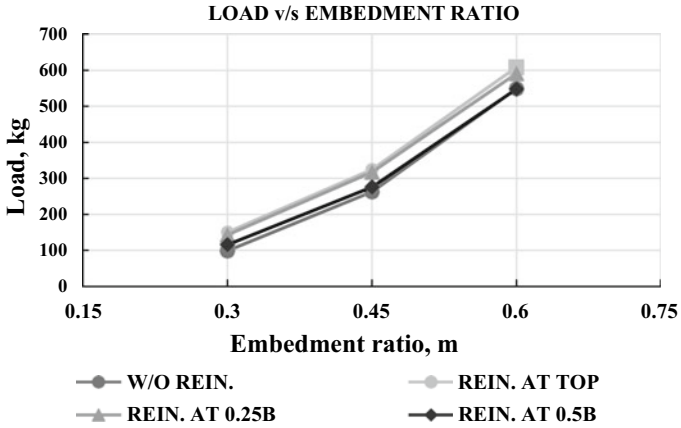


Fig. 11 Analytical uplift capacity comparison for 85% relative density

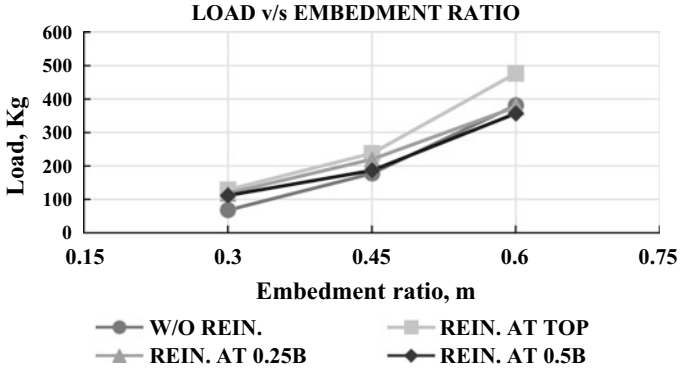


Fig. 12 Experimental uplift capacity comparison for 70% relative density

4.3 Load Versus Displacement for Different Densities of Soil, Embedment Ratio and Place of Reinforcement

4.3.1 Without Reinforcement

See Figs. 14, 15 and 16.

4.3.2 Reinforcement at the Top of Reinforcement

See Figs. 17, 18 and 19.

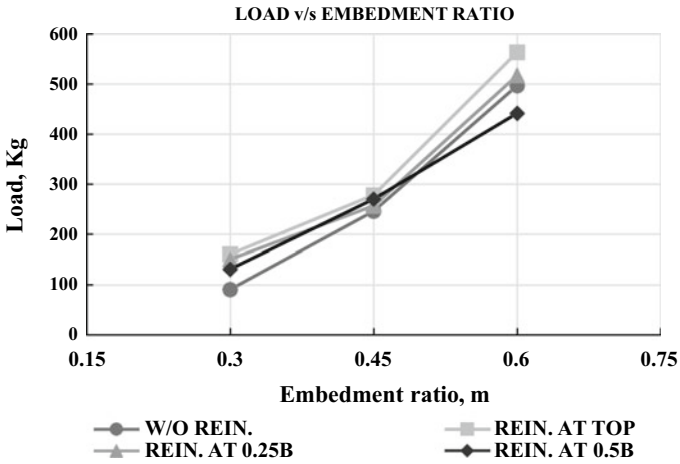


Fig. 13 Experimental uplift capacity comparison for 85% relative density

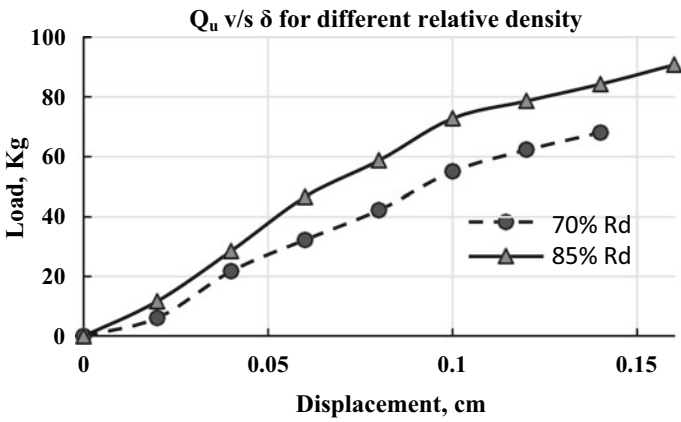


Fig. 14 Embedment depth = 0.3 m, without reinforcement

4.3.3 Reinforcement at 0.25B of the Reinforcement

See Figs. 20, 21 and 22.

4.3.4 Reinforcement at 0.5B of Reinforcement

See Figs. 23, 24 and 25.

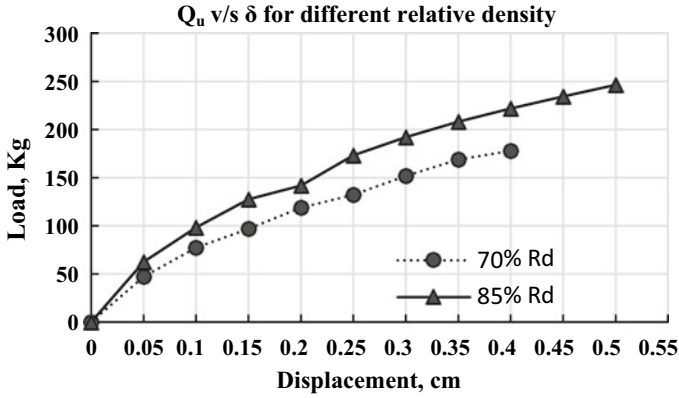


Fig. 15 Embedment depth = 0.45 m, without reinforcement

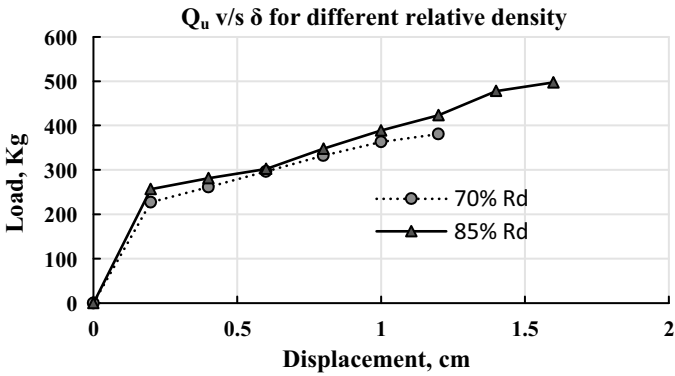


Fig. 16 Embedment depth = 0.6 m, without reinforcement

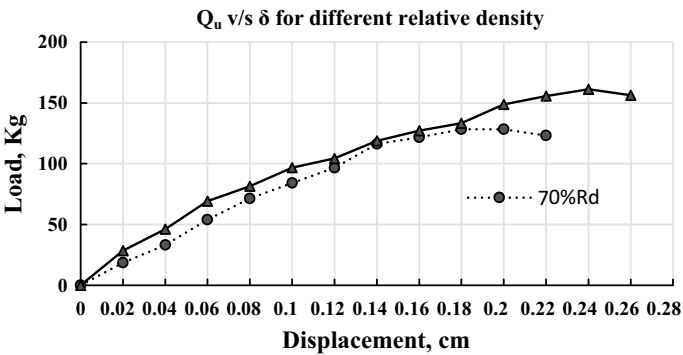


Fig. 17 Embedment depth = 0.3 m, Rein. At top of the anchor plate

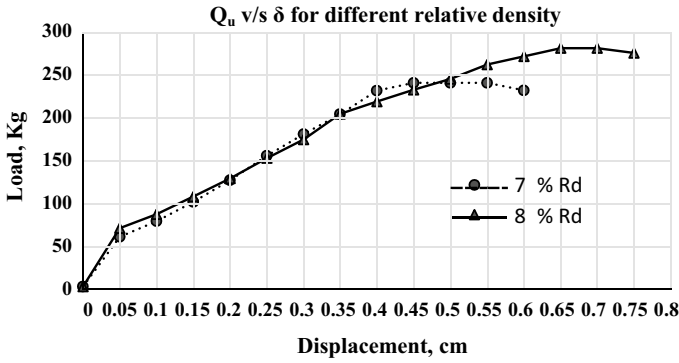


Fig. 18 Embedment depth = 0.45 m, Rein. At top of the anchor plate

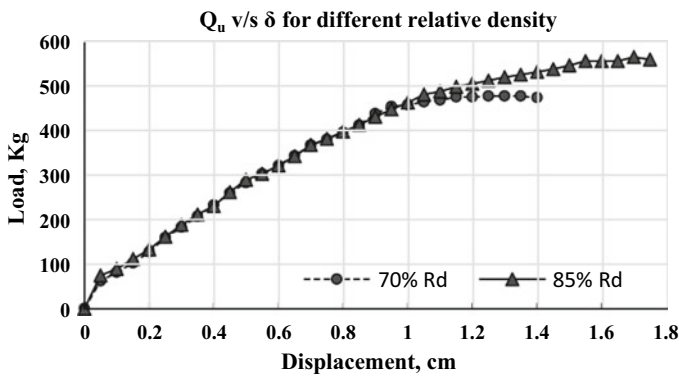


Fig. 19 Embedment depth = 0.6 m, Rein. At top of the anchor plate

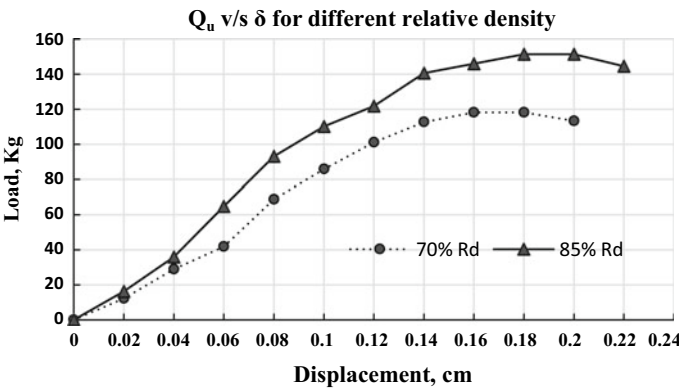


Fig. 20 Embedment depth = 0.3 m, Rein. At 0.25B from top of the anchor plate

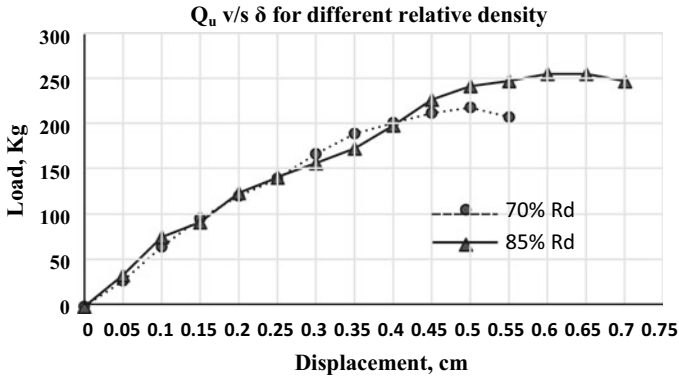


Fig. 21 Embedment depth = 0.45 m, Rein. At 0.25B from top of the anchor plate

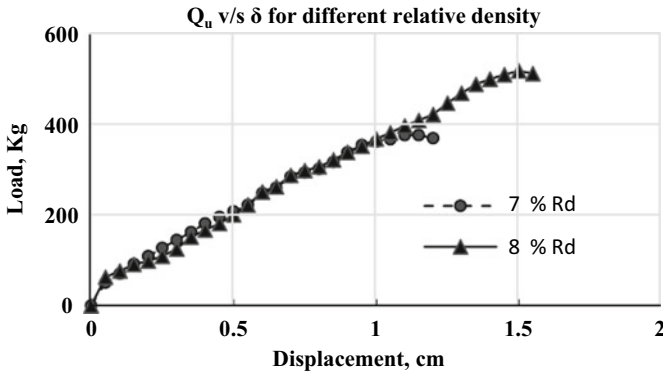


Fig. 22 Embedment depth = 0.6 m, Rein. At 0.25B from top of the anchor plate

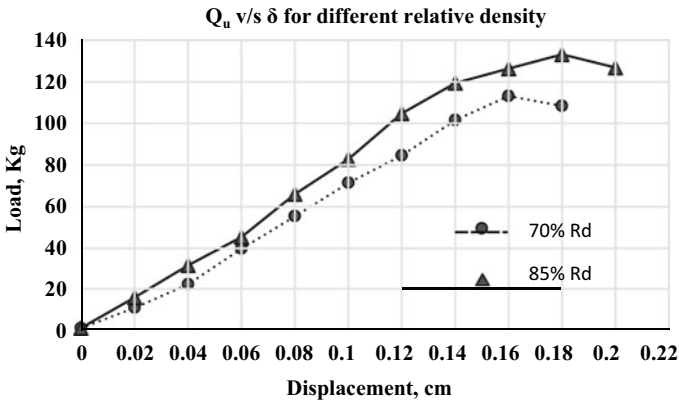


Fig. 23 Embedment depth = 0.3 m, Rein. At 0.5B from top of the anchor plate

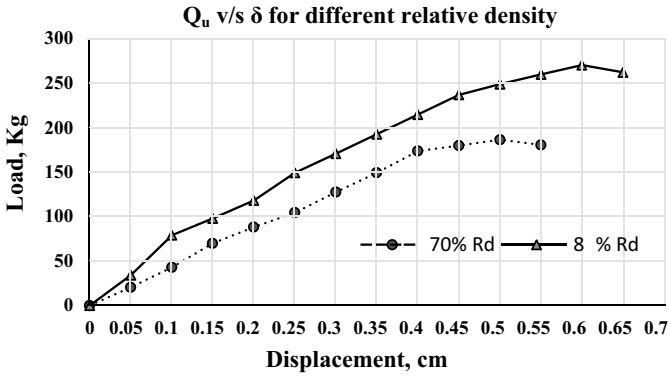


Fig.24 Embedment depth = 0.45 m, Rein. At 0.5B from top of the anchor plate

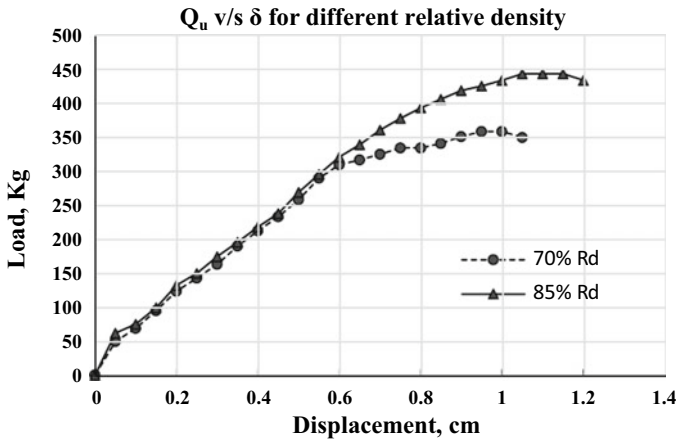


Fig. 25 Embedment depth = 0.6 m, Rein. At 0.5B from top of the anchor plate

5 Comparison of the Results Obtained by Analytical Method and Experiments

Predicted versus observed pull-out capacity (Tables 6, 7; Figs. 26 and 27):

6 Observations and Discussion

A. Observations During Filling Tank

To achieve dense condition ($D_r = 70\%$) in tank free fall & compaction (at every 15 cm) is required. To achieve very dense condition ($D_r = 85\%$) in tank

Table 6 Experimental and analytical uplift capacity for 70% relative density

Reinforcement position	Relative density = 70%							
	Embedment ratio (m)							
	2		3		4		4	
	Analytical (kg)	Experimental (kg)	Analytical (kg)	Experimental (kg)	Analytical (kg)	Experimental (kg)	Analytical (kg)	Experimental (kg)
Without reinforcement	74.97	68.09	192	177.82	405.16	381.09		
Rein. at the top of the anchor plate	135.67	128.32	286.49	237.96	514.44	476.32		
Rein. at 0.25 b from the top of the anchor plate	123.05	118.22	259.81	219.72	497.13	375.92		
Rein. at 0.5 b from the top of the anchor plate	100.24	111.42	231.64	186.33	434.63	356.84		

Table 7 Experimental and analytical uplift capacity for 85% relative density

Reinforcement position	Relative density = 85%							
	Embedment ratio (m)							
	2		3		4		4	
	Analytical (kg)	Experimental (kg)	Analytical (kg)	Experimental (kg)	Analytical (kg)	Experimental (kg)	Analytical (kg)	Experimental (kg)
Without reinforcement	98.82	90.82	262.23	246.32	548.73	497.29		
Rein. at the top of the anchor plate	149.83	161.23	323.97	278.34	607.99	563.98		
Rein. at 0.25 b from the top of the anchor plate	143.06	151.29	317.46	257.11	590.76	517.47		
Rein. at 0.5 b from the top of the anchor plate	116.02	131.32	275.79	270.11	547.85	441.78		

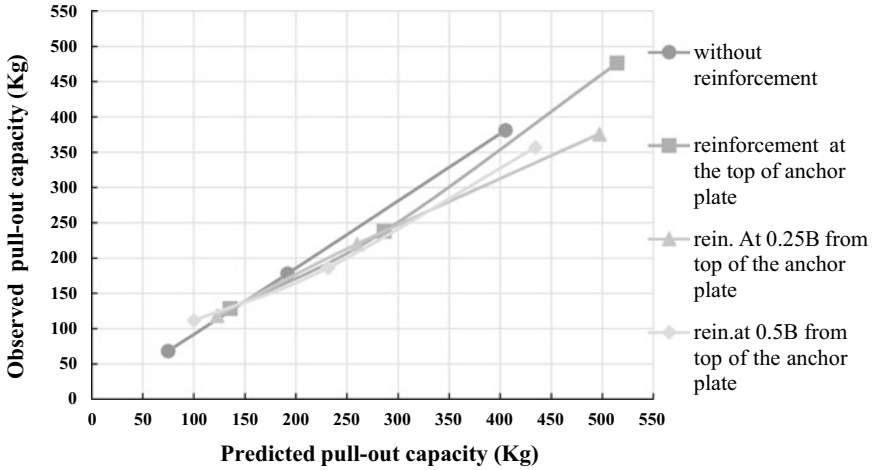


Fig. 26 Predicted pull-out capacity versus observed pull-out capacity (70%Rd)

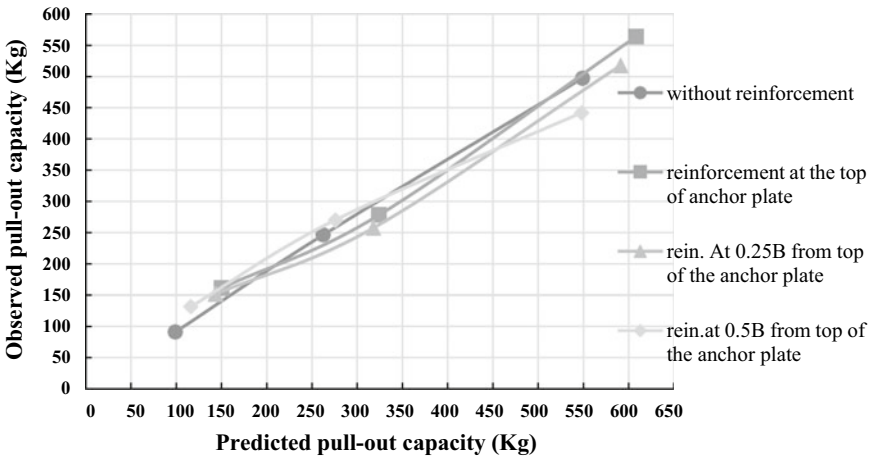


Fig. 27 Predicted pull-out capacity versus observed pull-out capacity for 85%Rd

free fall and compaction (at every 5–10 cm) is required. Proper care should be taken to achieve uniform density throughout the tank. Top-level of sand in tank should be properly levelled so that during applying uplift load proper heave (failure formation) is clearly visible.

B. Observations During Fixing Square Anchor Plate

At the time of fixing the plate with proving ring, it should be properly fixed. At the time filling new layers of sand care must be taken that the plate is exactly at its position. The plate should be exactly placed at the centre of the tank above the first 15 cm layer of sand.

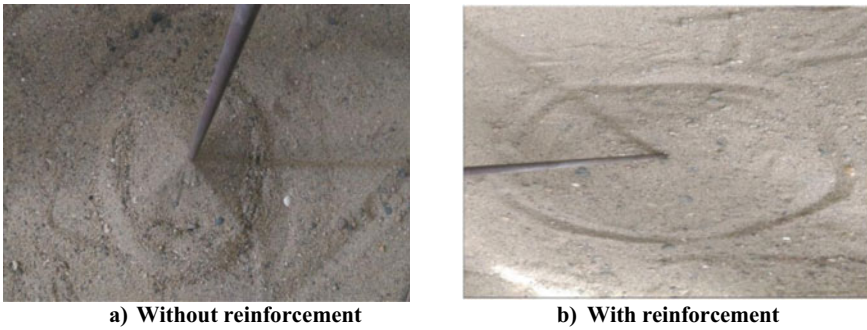


Fig. 28 Heave formed on top surface of sand after failure

C. Observations During Fixing Proving ring and Dial Gauge

Proving ring should be properly attached to chain pulley block by mechanical arrangements. Dial gauge should be fixed properly to the rod connecting both side of tank. It should properly touch to the arrangement made in anchor rod connected to plate so that it can measure the displacement accurately.

D. Observations During Applying Uplift Load

Loading must be applied at uniform rate. During failure, load in proving ring may be decreasing or constant.

E. Observations After Failure

Heave formed on the top surface of the sand after failure is circular in shape and its diameter of failure is depend on embedment depth and location of reinforcement. Figure 28 shows the different heave formation for different reinforcement locations.

7 Conclusions

The ultimate uplift capacity of plate anchors can be increased significantly by the use of geonets. Based on test results, it is observed that using geonets reinforcement the uplift carrying capacity of the square plate anchor can be significantly increased 1.4 times than that of unreinforced case.

Four different configurations of geosynthetic inclusion, as shown in Fig. 1a, were employed during model test to determine the optimum location of the geosynthetic inclusion for achieving the maximum increase in the uplift capacity. The configuration illustrated by case 2 in Fig. 1a, where the geosynthetic inclusion was resting directly on the top of the anchor plate, proved to be the best location for achieving the maximum increase in ultimate uplift capacity.

The increase in soil density results in a higher ultimate uplift capacity of anchors both with and without geosynthetic inclusion. As the soil density increased, the load–displacement curves exhibit a clear well-defined peak. According to test results, the

uplift capacity of plate anchor increases with the increase in embedment ratio. This increase can be explained that the thickness of homogenous zone between anchor and soil surface is efficient and the uplift capacity increase with increase of thickness of this zone.

Diameter of failure surface is increased from unreinforced plate anchor to reinforced plate anchor. Predicted value of uplift capacity of reinforced square plate anchor show very encouraging agreement with experimental value. Inclusion of geosynthetic layer increases the effective area of anchorage. A clear and distinct upheaval of soil was observed during peak resistance conditions. Maximum upheaval occurred near the shaft.

Acknowledgements The authors would like to gratefully acknowledge Dr. H.M. Desai, Vice Chancellor, Dharmasinh Desai University, Nadiad, Gujarat to allow tests under geotechnical laboratory of civil engineering department.

References

1. AASHTO (2007) LRFD bridge design specifications, 4th edn. AASHTO, Washington DC
2. Ali MS (1969) Pull-out resistance of anchor plates and anchor piles in soft bentonite clay. Duke University, Durham
3. Allen TM, Nowak AS, Bathurst RJ (2005) Calibration to determine load and resistance factors for geotechnical and structural design. Transportation Research Board, Washington, DC
4. Bathurst RJ, Allen TM, Nowak AS (2008) Calibration concepts for load and resistance factor design (LRFD) of reinforced soil walls. *Can Geotech J* 45:1377–1392
5. Clemence SP (1983) The uplift and bearing capacity of helix anchors in soil. Syracuse University, Syracuse, Department of Civil Engineering
6. Clemence SP, Hoyt RM (1989) Uplift capacity of helical anchors in soil. AB Chance Company
7. Das BM (2007) Theoretical foundation engineering. J. Ross Publishing, Fort Lauderdale (Reprint c1987)
8. Das, BM (2007) Earth anchors. J. Ross Publishing, Fort Lauderdale (Reprint c1990).
9. Davis RK (1982) The behavior of anchor plates in clay. *Geotechnique* 32:9–23
10. Francis & Lewis International, L. (2012) FLI structures site services. Retrieved from FLI Structures Screw Pile Foundations. <http://www.fliscrewpiiles.co.uk/site-services.php>
11. Handojo H (1997) Uplift capacity of helical anchors. Oregon State University, Corvallis
12. Hoyt RM, Clemence SP (1989) Uplift capacity of helical anchors in soil. A.B. Chance Company, Centralia
13. Hubbel I (2012) Helical pile walkway report. Retrieved from AB Chance Civil Construction. <http://www.abchance.com/resources/case-histories/04-0701.pdf>
14. Kondner R (1963) Hyperbolic stress strain response: cohesive soils. *Journal of the Soil Mechanics and Foundations Division* 89(SMI):115–144
15. Lutenegeger AJ (2003) Helical screw piles and screw anchors—an historical prospective and introduction. In: Proceedings of the helical foundations and tie-backs seminar, Unpublished
16. Lutenegeger AJ (2009) Cylindrical shear or plate bearing? Uplift behavior if multi-helix screw anchors in clay. International Foundation Congress and Equipment Expo 456–463
17. Magnum Piering I (2012) Magnum helical pile system. Retrieved from Magnum Piering, Rock Solid. http://www.magnumpiering.com/commercial/helical_pier_system.aspx
18. Merifield RS (2011) Ultimate uplift capacity of multiplate helical type anchors in clay. *Journal of Geotechnical and Geoenvironmental Engineering* 704–716

19. Mooney JS (1985) Uplift capacity of helical anchors in clay and silt. Uplift Behavior of Anchor Foundations in Soil. American Society of Civil Engineers, Detroit, pp 48–72
20. Mooney JS, Adamczak S, Clemence SP (1985) Uplift capacity of helical anchors in clay and silt. Uplift Behavior of Anchor Foundations in Soil. American Society of Civil Engineers, Detroit, pp 48–72
21. Pack JS (2000) Design of helical piles for heavily loaded structures. New Technological and Design Developments in Deep Foundations (GSP 100). American Society of Civil Engineers, Denver, pp 353–367
22. Pack JS (2006) Performance of square shaft helical pier foundations in swelling soils. Geovolution 76–85
23. Perko HA (2000) Energy method for predicting installation torque of helical foundations and anchors. New Technological and Design Developments in Deep Foundations (GSP 100). American Society of Civil Engineers, Denver, pp 342–352
24. Perko HA (2009) Helical piles, a practical guide to design and installation. Wiley, Hoboken
25. Prasad Y, Rao S (1996) Lateral capacity of helical piles in clays. Journal of Geotechnical Engineering 938–941
26. Rao S, Prasad Y (1993) Estimation of uplift capacity of helical anchors in clays. Journal of Geotechnical Engineering 352–357
27. Rao S, Prasad Y, Shetty M (1991) The behavior of model screw piles in cohesive soils. Soils Found 31:35–50
28. Rao S, Prasad Y, Veeresh C (1993) Behavior of embedded model screw anchors in soft clays. Geotechnique 43:605–614
29. Sakr M (2009) Performance of helical piles in oil sand. Can Geotech J 46:1046–1061
30. Shipton BA (1997) The effect of uplift, compressive, and repeated loads on helical anchors. Oregon State University, Corvallis
31. Strahler AW (2012) Bearing capacity and immediate settlement of shallow foundations on clay. Oregon State University, Corvallis
32. Structures F (2012) Screw pile foundations—site services. Retrieved from FLI Structures Screw Pile Foundations. <http://www.fliscrew piles.co.uk/site-services.php>
33. Stuedlein AW (2008) Bearing capacity and displacements of spread footings on aggregate pier reinforced clay. University of Washington, Civil and Environmental Engineering, Seattle

Finite Element Analysis (FEA) of Geocell Reinforced Pavement in Hilly Terrain



Aman Kashyap, Vijayasri Thanikella, G. Bharat, and Kranthi Kumar Kuna

Abstract The dissertation aims to perform finite element analysis (FEA) of geocell reinforced pavement using with OPENSEES software. The study uses marginal material found in Himalayan regions and StrataWeb® SW 356-150 geocell and StrataWeb® SW 356-200 geocell. Calibration data for finite element model (FEM) and material characteristics can be obtained from the literature. Additionally, triaxial test must be performed to obtain layer moduli and Poisson's ratio. The study attempts to model cylindrical test tank consisting of subgrade, geocell reinforced base layer and base cover tested for cyclic loading. The cyclic loading represents total number of wheel passes for pavement to fail. The whole tank is modelled rather than a quarter model to improve accuracy of result. The geocell is modelled considering honeycomb structure rather than simple rhomboidal structure—the honeycomb structure needs to be solved after performing regression analysis. The soil materials either coarse sand or clay are modelled using PressureDependMultiYield02 model or PressureIn-dependMultiYield model, respectively. The elements, soil and geocell are modelled using brickUP elements and ShellMITC4 elements. The model takes into account pore water pressure, pressure dependence, strain rate, etc. The results clearly indicate that geocell reinforced test section has better performance than that of unreinforced test section. This is evident by rut depth reduction factor. The values of velocity and acceleration were also compared, and it was evident that they were greater for geocell reinforced test sections.

A. Kashyap
IIT Kharagpur, Kharagpur, West Bengal 721302, India

V. Thanikella (✉)
MVSr Engineering College, Nadargul, Hyderabad 500097, India
e-mail: vijjuthanikella@gmail.com

G. Bharat
CRRl, Delhi-Mathura Road, New Delhi 110 025, India

K. K. Kuna
IIT Kharagpur, Kharagpur, West Bengal 721302, India

Keywords FEA · Geocell · OpenSees · FEM · Cyclic loading · PressureDependMultiYield02 · PressureIndependent MultiYield · brickUP · And ShellMITC4

1 Introduction

India has over 5.9 million kilometres of roads as of 31 March 2019 and has second largest road network in the world. Out of which over 0.16 million km roads extend in hilly regions. Indian hilly roads are especially facing the problems due to poor subgrade condition, deprived quality of aggregates and badly maintained drainage conditions. Generally due to these reasons, the pavements (rigid/flexible) fail well before the design period. Transportation is a basic need for people. Ideally, transportation system must offer desirable accessibility and mobility, but is it always? Let's consider pavement system on a hilly terrain. It lacks good quality pavement material; thus, pavement material is sourced from far distances which add expense. Also, regular pavement construction on a hilly terrain is difficult due to changed topography. Thus, an alternate pavement which uses locally available marginal materials and less expertise workforce where regional people may contribute to pavement construction is desired. Geocell reinforced pavement is one such alternative which satisfy the above-mentioned requirement and has a lower life cycle cost than conventional pavement. Geocell is a cellular confinement system. It has three-dimensional honeycomb structure with compacted infill [3]. The soil–geocell composite acts as a stiff layer. It distributes the traffic load over subgrade soil, increasing its bearing capacity. Many studies have been conducted to study the mechanism of improved bearing capacity [2, 6, 7, 13, 15], but it has not been well understood. Finite element analysis (FEA) of geocell reinforced pavement using commercially available software like LS Dyna was carried out to understand exact mechanism for pavement improvement [1, 11]. The results are promising but need further refinement to match hoop stress in geocell; also, one doesn't exactly understand how the inbuilt model works. Based on the above-mentioned studies, the present study focuses on developing a robust FE model of geocell reinforced pavement and assessing its performance during the cyclic load. Advanced fluid–solid coupled materials are used in the analysis, for coupling of soil and pore. Particular emphasis is given to the FEM analysis of geocell pavement in terms of acceleration amplification, horizontal and vertical displacement profile, nonlinear stress–strain behaviour, rut depth reduction factor.

2 Experimental Studies

Mehar [5] performed the laboratory test for geocell reinforced pavement with an aim to evaluate MIF with varying infill material. The major components of the test are discussed in proceeding subsections.

Table 1 Marginal materials and associated property [6]

Marginal material	Soil classification	Specific gravity	Compaction characteristics	
			MDD (g/cc)	OMC (%)
	IS 1498	IS 2720-3	IS 2720-8	
Landslide soil	GP-GM	2.63	2.25	6
Nagpur soil	CH	2.50	1.77	17

2.1 Infill Material

The soil infill material is marginal in nature, such as tunnel muck, landslide soil, Nagpur soil, reclaimed asphalt material. Table 1 describes the marginal material tested for soil classification, specific gravity and compaction characteristics for this study.

2.2 Material Property of Geocell

Geocell manufactured by StrataWeb® SW 356-150 or equivalent is preferred. When placed with infill and compacted, the geocell gets curved. Properties of StrataWeb® SW 356-150 geocell used for modelling are summarised in Table 2. The geocell consists rhomboidal texture which helps increase friction with soil infill [12].

The domain of tank diameter 1 m and height 1 m to simulate in Numerical modelling. The test section or domain consisted of:

- subgrade and subbase for sections without reinforcement
- subgrade, geocell placed above subgrade, infill material (subbase soil) in geocell, soil (subbase) cover. The test considered CRRI soil for subgrade uses as additional materials. The properties of CRRI soil and RAP material are mentioned in Table 3.

Also, laboratory test was performed to find cohesion value for landslide soil. The cohesion was found to be 40°.

Table 2 Property of StrataWeb® SW 356-150 geocell (Source StrataWeb® 356 data)

Material: HDPE (Density—g/cc)	0.935 – 0.965		ASTM D 1505
Minimum sheet wall thickness (mm)	1.65		ASTM D 5199
Dimensions			
Depth (mm)	150 + 3%		
	Width (mm)	Length (mm)	Area (sq. cm)
Cell	259 ± 3%	224 ± 3%	289 ± 3%
Section	2590 ± 3%	6500 ± 3%	168,000 ± 3%

Table 3 Properties of CRR I soil

Marginal material	Soil classification	Specific gravity	Compaction characteristics	
			MDD (g/cc)	OMC (%)
	IS 1498	IS 2720-3	IS 2720-8	
CRR I soil	CL	2.63	2.04	11

3 Numerical Modelling

3.1 Geometry of the Domain

The domain consists heterogeneous layers of subgrade and subbase. 500 mm of subgrade was chosen, and 225 mm of subbase was chosen. In case of geocell reinforcement, geocell was placed above subgrade, over which 225 mm of subbase soil was placed. The layout of test domain is represented in Fig. 1.

The domain was made up of various combination of soil in subgrade and subbase layers. The subgrade was formed using Nagpur soil, whereas the subbase was formed using landslide soil. The test cases are summarized in Table 4

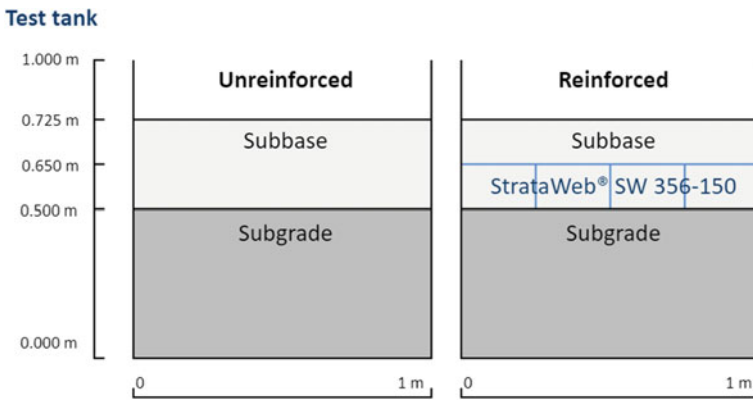


Fig. 1 Layout for test domain

Table 4 Test cases considered for analysis

Case	Subgrade	Subbase	Reinforcement
1	Nagpur soil	Landslide soil	No
2	Nagpur soil	Landslide soil	StrataWeb® SW 356–150

4 Methodology

4.1 Modelling

The robust nonlinear FE Model is prepared by Opensees [4]. Thus, two tcl codes are written case 1 without reinforcement case 2 with geocell reinforcement and the geometry, i.e. nodes and elements for test section are as follows: Figs. 2 and 3 show the display of nodes and elements in unreinforced FEM.

4.1.1 Geometry of Unreinforced FEM

The unreinforced or without geocell FEM considered:

- Five layers in subgrade of 100 mm depth.
- Three layers in subbase of 75 mm depth.
- The periphery is approximated by polygon of 20 sides. Hegde et al. [2] talk about edge effect neglect; i.e. settlement is negligible for radial distance of six times radius of the loading plate. Thus, the circular periphery can be approximated by a polygon such that the farthest point on polygon. Precisely, the polygon must edges more than seven.
- About central symmetric axis 20 angular division of 18 degree each.
- Five divisions along radius, i.e. from central axis to the periphery having radial distances of 75, 175, 300, 400 and 500 mm.

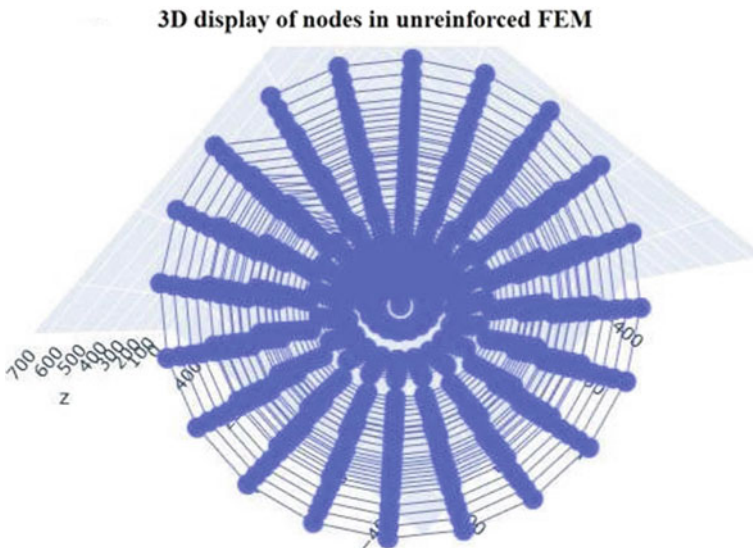


Fig. 2 3D display of nodes in unreinforced FE

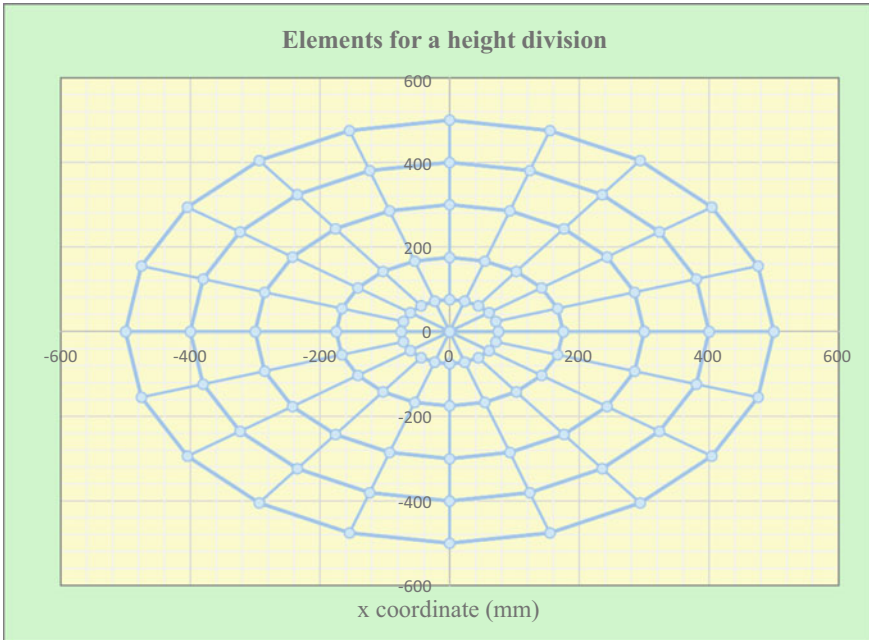


Fig. 3 Number of elements for a height division in unreinforced FEM

- Number of nodes for a given z-coordinate equals: 101

$$1 + \text{No. of radial divisions} \times \text{No. of angular divisions} = 1 + 5 \times 20$$

- Total number of nodes equals: 909

$$\text{No. of nodes for given } z \text{ - coordinate} \times \text{No. of } z \text{ - coordinates} = 101 \times (8 + 1)$$

- Number of elements for a height division equals: 90

$$\begin{aligned} &\text{No. of angular divisions}/2 \\ &+ \text{No. of angular divisions} \times (\text{No. of radial divisions} - 1) \\ &= 20/2 + 20 \times (5 - 1) \end{aligned}$$

Total number of elements: 720

$$\text{No. of elements for height divisions} \times \text{No. of height divisions} = 90 \times 8$$

4.1.2 Geometry of Geocell Reinforced FEM

- Five layers in subgrade of 100 mm depth.
- Two layers in geocell of 75 mm depth.
- Two layers in subbase cover of 37.5 mm depth.
- The periphery is approximated by polygon of 28 sides.
- The geocell is placed symmetrically.
- In geocell layers, extra nodes are created at same coordinates that of soil.
- The soil–geocell are connected by intermediate dummy nodes. The dummy nodes are joined to geocell nodes using zero length element [14]. The soil nodes and geocell nodes are joined by master–slave equal degree of freedom. This allows for sliding at interface of soil and geocell as shown in Figs. 4 and 5.

The soil model includes Mohr–Coulomb model, von Mises model and Drucker–Prager model. The concept of flow is explained using Mohr–Coulomb model. The soil was represented using pressure dependent and pressure independent model [8, 9]. Two sets of geometrical models are created—one for unreinforced condition and other for geocell reinforced condition. The elements were chosen—eight-node brickUP element and four-node ShellMITC4 element. The boundary condition, i.e. nodes on bottom of tank and at the tank surface, is fixed. Damping conditions of Lysmer dashpot are applied at these boundary nodes. The connections between

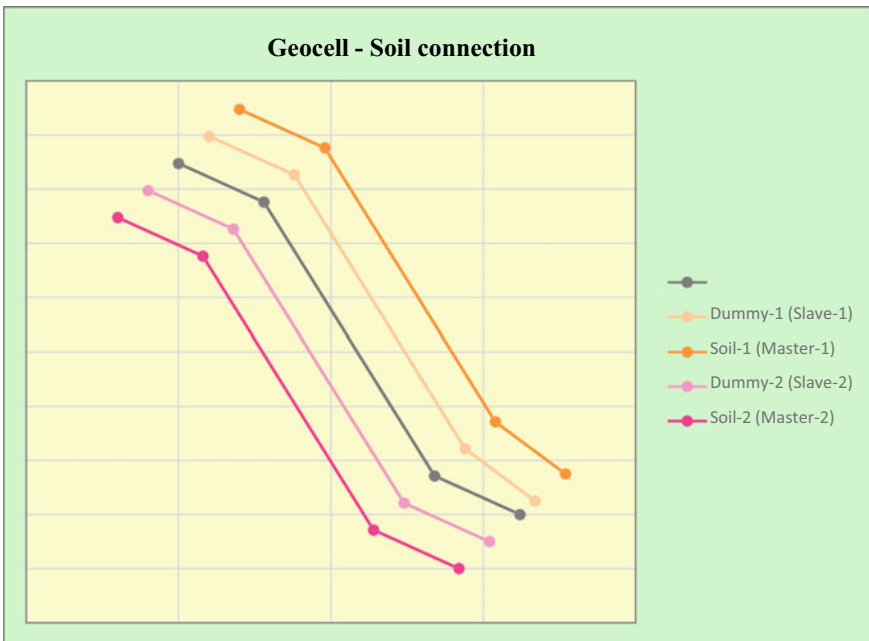


Fig. 4 Soil–geocell connection (Note: Black Line: Geocell, Light Magenta and orange are Dummy nodes)

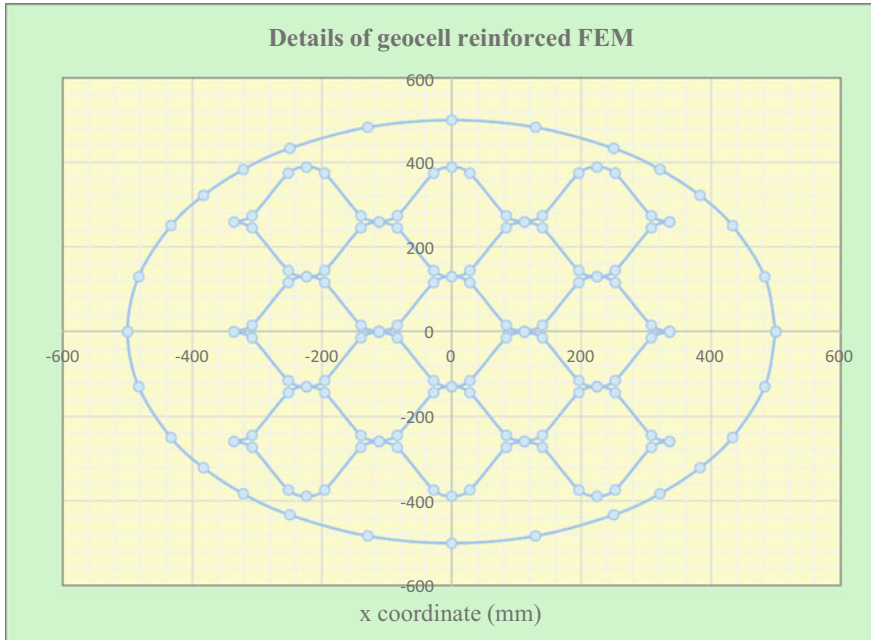


Fig. 5 Number of elements for a height division in reinforced FEM

geocell and soil nodes are made using set of dummy nodes on both sides of geocell. The dummy nodes and geocell nodes have zero length elements, whereas soil nodes and dummy nodes have master–slave equal degree of freedom. Load pattern is applied as surface pressure over elements joining the topmost centrally situated top node.

Input motion: Repeated cyclic load step motion considered for this analysis (Fig. 6).

5 Results and Discussions

FEM results were obtained corresponding to the 2 cases. It should be noted that the FEM results presented here are at offset of distance greater than plate radius (75 mm). The central readings were considerably high owing to incomplete details of various parameters required in model such as permeability, porosity and cohesion. The results obtained are presented as cases shown in Table 5. The cases are similar to the cases described in Table 4.

The above results are represented in Fig. 7. The FEM predicts lower settlement for geocell reinforced test section. This result is qualitatively in accordance with existing literature.

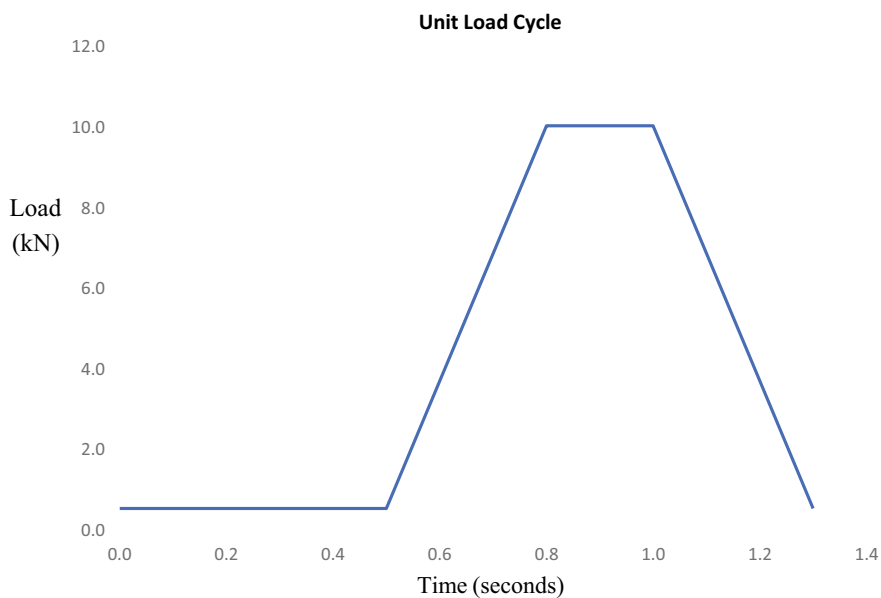


Fig. 6 Cyclic load applied over circular test section

Table 5 FEM results with respect to settlement

No. of cycles	Settlement (mm)	
	Case 1 and 2	
	Without reinforcement	With reinforcement
1	1.091	0.382
2	2.309	0.894
3	3.486	1.600
4	4.576	2.617
5	5.778	4.110
6	7.010	–
7	8.252	–
8	9.521	–
9	10.706	–
10	12.022	–

5.1 Rut Depth Reduction

It is the ratio of the difference between cumulative permanent deformations of the unreinforced section and the geocell reinforced section to that of the unreinforced section at a specific numbers of load cycle [10]. From Table 6, it is observed that the

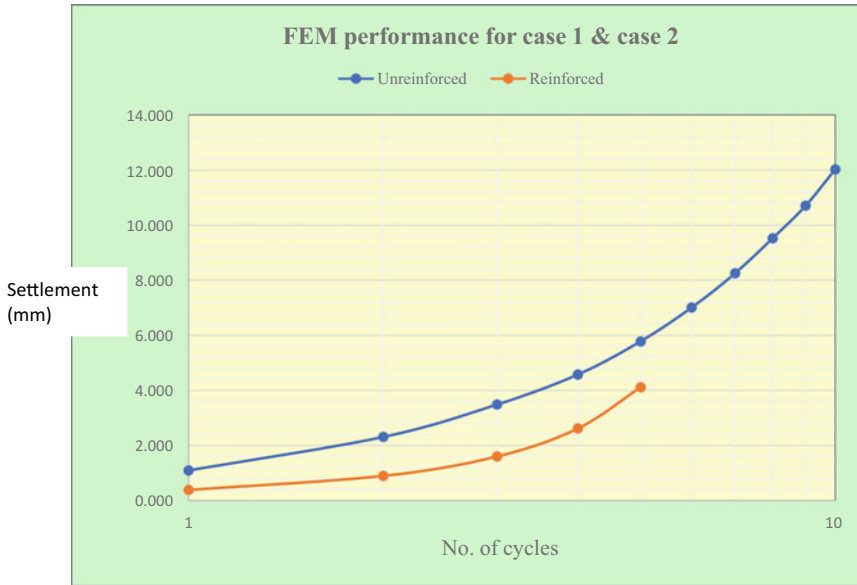


Fig. 7 FEM settlement performance with varying number of cycles for case 1 and case 2

Table 6 Comparison of RDR for laboratory results and FEM results—cases 1 and 2

No. of cycles	Rut depth reduction	
	FEM results	
	Reduction	RDR (%)
1	0.709	65
2	1.415	61
3	1.886	54
4	1.959	43
5	1.668	29

results show up to 5 cycles. But in the real analysis run the code up to 100 cycles. The mean rut depth reduction factor was observed be 45%. From the rut depth reduction factor, the geocell reinforced pavement gives better performance than unreinforced pavement section.

5.2 FEM Results—Velocity and Acceleration

The FEM model has also evaluated velocity and acceleration for the topmost node. Velocity and acceleration are calculated by differentiation of displacement profiles

with and without reinforcement by using MATLAB code. The value for these variables as a function of time is represented in Table 7, and the comparison of velocity is demonstrated in Fig. 8, respectively.

Firstly, it can be seen that for given number of load cycles the velocity and acceleration are higher for unreinforced test section. Further, number of load cycles must be observed to explain the observed trend (curvature).

The broad objective of present study was to compare the performance of domain with and without geocell reinforcement subject to cyclic traffic load. This was aimed to be evaluated using FEM.

Table 7 FEM results for velocity and acceleration—case 1 and case 2

No. of cycles	Velocity (mm/s)		Acceleration (m/s ²)	
	With reinforcement	Without reinforcement	With reinforcement	Without reinforcement
1	1.161	1.713	1.032	2.152
2	1.370	1.998	2.284	2.533
3	1.218	2.284	1.636	4.051
4	1.149	2.616	1.189	1.468
5	1.271	2.654	1.325	3.581

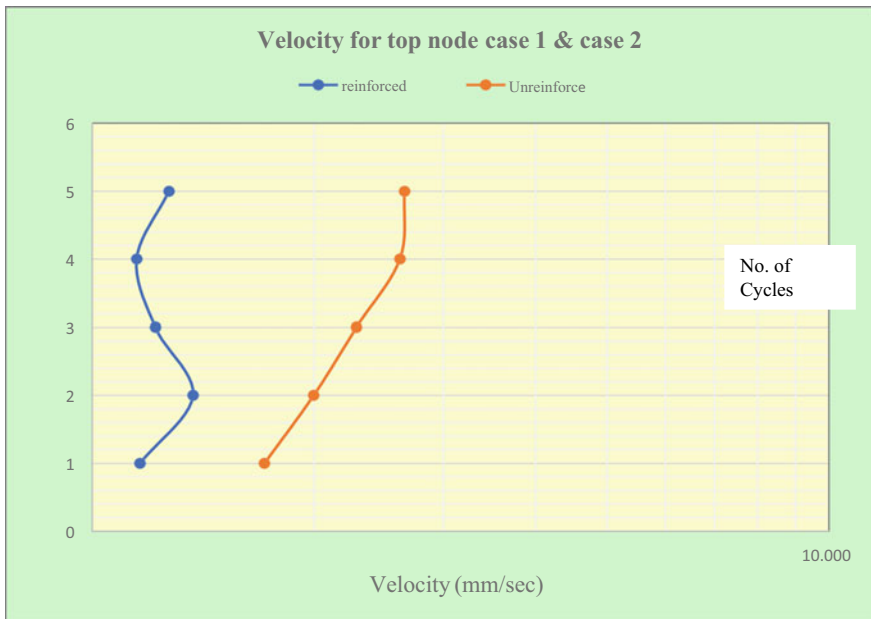


Fig. 8 Comparison of velocity (mm/s) with number of cycles for case 1 and case 2

6 Conclusions

The present work concludes that:

- Geocell reinforced test section performs better than unreinforced test section in terms of settlement observed for the topmost point.
- Thus, rut depth reduction (RDR) factor is observed for the cases having either Nagpur soil or CRRI soil as subgrade and landslide soil as subbase.
- The results for settlement obtained from laboratory results approach the results obtained by literature.
- The velocity and acceleration values for topmost node are lower for geocell reinforced test domain.

References

1. Arias JL, Inti S, Tandon V (2020) Influence of geocell reinforcement on bearing capacity of low, vol roads. Springer, Berlin
2. Hegde A, Sitharam TG (2016) Behaviour of geocell reinforced soft clay bed subjected to incremental cyclic loading. Geomechanics and Engineering
3. IRC SP-59 (2019) Guidelines for use of geosynthetics in road pavements and associated work, Indian Road Congress (IRC), New Delhi
4. Mazzoni S, McKenna F, Scott MH, Fenves GL (2006) OpenSees command language manual. University of California, Berkeley
5. Mehar B (2020) Development modulus of improvement factors for pavement layer with geocell. M.Tech thesis, IIT Kharagpur
6. Pokharel SK (2009) Experimental study on geocell-reinforced bases under static and dynamic loading. Doctoral thesis, University of Kansas
7. Pokharel SK (2010) Experimental study on geocell-reinforced bases under static and dynamic loading. Doctoral thesis, University of Kansas
8. Pressure Independent multi yield soil model: https://opensees.berkeley.edu/wiki/index.php/PressureIndependentMultiYield_Material. Accessed on 29 April 2021
9. Pressure Dependent multi yield soilmodel: https://opensees.berkeley.edu/wiki/index.php/PressureDependMultiYield02_Material. Accessed on 29 April 2021
10. Saride S, Rayabharapu VK, Vedpathak S (2015) Evaluation of rutting behaviour of geocell reinforced sand subgrades under repeated loading. Indian Geotechnical Journal
11. Sharma M, Inti S, Tirado C, Tandon V (2016) Evaluating the benefits of geocell reinforcement of the base course in flexible pavement structures using 3-D finite element modeling. ASCE
12. StrataWeb® 356 Data. https://cdn.glenraven.net/geogrid/pdf/en_us/StrataWeb356.pdf. Accessed on 26 April 2021
13. Thakur JK, Han J, Parsons RL (2016). Factors influencing deformations of geocell-reinforced recycled asphalt pavement bases under cyclic loading. J Mater Civ Eng. [https://doi.org/10.1061/\(ASCE\)MT.1943-5533.0001760](https://doi.org/10.1061/(ASCE)MT.1943-5533.0001760)
14. Vijayasri T, Raychowdhury P, Patra NR (2018) Dynamic behavior of a geotextile-reinforced pond ash embankment. Journal of Earthquake Engineering
15. Yoo C, Kim SB (2009) Numerical modeling of geosynthetic-encased stone column-reinforced ground. Geosynthetics International

Plaxis 2D Numerical Analysis of Encased Stone Column in Soft Clay



Sanket S. Mudekar, Vidya N. Patil, Hemant S. Chore,
and Vishwas A. Sawant

Abstract Strengthening soft soil ground with different techniques requires several tries with available material and properties of the same. Widely accepted soft ground strengthening technique is ordinary stone column (OSC), and it is encased with geosynthetic material, known as Geosynthetic Encased Stone Column (GESC). In this paper, different stone column (SC) parameters are tested with finite element method in Plaxis 2D software Version 8.6 and analyzed with load settlement observations. SC use with or without encasement is found more effective and sustainable as it provided strengthening feature. Three models of soft clay, baseline clay model, OSC and GESC, were tested with some constant variables like loading in center with same plate and water table at 300 mm from top of model. Result of increase in bearing capacity and decrease in settlement with these three axisymmetric models was compared. The selected property geosynthetic geotextile material is found suitable to encase the SC as it laterally confined SC with avoidance of bulging and improved load settlement curve nature.

Keywords Finite element · Soft soil improvement techniques · Stone column · Numerical analysis · Geosynthetic

S. S. Mudekar · V. N. Patil (✉)

Department of Civil Engineering, All India Shri Shivaji Memorial Society's College of Engineering, Kennedy Road, Pune, Maharashtra, India

e-mail: vidya_patil55@rediffmail.com

H. S. Chore

Department of Civil Engineering, Dr. B. R. Ambedkar National Institute of Technology Jalandhar (NITJ), Jalandhar, Punjab, India

e-mail: chorehs@nitj.ac.in

V. A. Sawant

Department of Civil Engineering, Indian Institute of Technology Roorkee (IITR), Roorkee, Uttarakhand 247667, India

e-mail: sawntfce@iitr.ac.in

1 Introduction

The embankment supporting on the soft soils like clay with high groundwater level is extremely challenging and often requires prior analysis. The causes of soil failure in the road result in either large settlement or sliding due to inadequate shear strength. This happens because of soft soil properties like less bearing capacity and higher compressibility. In pavements, the soft soil movement results in differential settlements, surface cracking furthermore creating difficult driving conditions and costly rehabilitation and maintenance for the highways.

This causes more appeal toward research in ground improvement techniques. To resolve this difficult situation, acceptability of available material can be strengthened with emerging SC to strengthen soil strength. The objective behind this expected is increase in the bearing capacity and reducing the settlement with slope stability improvement. Also, the liquefaction resistance is required in many of the cases. Many soft ground improvement stabilization techniques are in practice, like deep mixing, well compaction, SC, etc. Many times, SC are selected to improve the soft clay as it is providing inclusion of a firmer column material such as crushed stones or granules in clay. During the installation of SC, the densification is surrounding of clay take place and this column itself creates the vertical drainage path in clay.

Instead of going with expensive and time-consuming experimental testing, numerical modeling by finite element analysis techniques would be definite option. Different software are made available like GEO5, ABACUS and Plaxis for numerical evaluation and comparison with different models. Few researchers used commercial software like Plaxis 2D and compared experimental results with software results on constant as well as variable parameters. Numerical analysis with Plaxis 2D is found suitable for SC design as per properties of soil as compared to an experimental investigation. It is more flexible, as well as efficient in terms of cost and time. With different cases, understanding of ground improvement analysis with software has been achieved.

In this paper, numerical analysis on three cases is compared: baseline clay model, OSC and GES. This is the plane strain numerical model of axisymmetric SC in soft clay with the groundwater level at 300 mm from top.

2 Literature Review

The SC is being used as soft ground improvement elements since they act as reinforcing inclusions with water drain path. On the other hand, due to the lack of sufficient lateral confinement for the OSC, this technique is not applicable for the improvement of grounds that consist of very soft soils. With lateral confinement and increase in the load bearing capacity of SC installed in very soft clay soils, encasement with suitable geosynthetic materials is found effective. Several researchers developed studies related to numerical, experimental and field evaluation of SC [1–5].

Researchers conducted experimental, numerical studies and stated effectiveness of study on the load settlement analysis. Also, researchers compared single or grouped at the same time encased or OSC by varying parameters like the area replacement ratio, shear strength of soft clay, column stiffness, etc. The simulation and analysis of SC ground improvement which are a complex modeling of the soil reinforcement system are needed [1, 4].

Many researcher studied different approaches to the modeling of GESC in soil, with special emphasis on homogeneous techniques using the composite parameter and improving the homogeneous soil with SC [6–12]. They concluded that the axisymmetric model which is “unit cell” comprised only one column in surrounding soil. In case of embankment which sustain under long load studied under plane strain model, where the cylindrical column is are modeled as stone trenches [1, 7]. Axial symmetrical techniques are used by few researchers, where stone ring is modeled and not considered cylindrical shape of columns. This condition is tried to imitate the columns under circular loads such as tanks [8]. Also, another option of the effect of applied pressure in all directions with 3D model was done and stated that it was the most complex approach [11, 12]. Initially, the comparison of pressure settlement analysis in unit cell and plain strain was done and found effective in both of the cases [1, 6, 7]. They studied single as well as group end bearing SC in soft clay with 2D finite element method and found some impacted factors, i.e., the settlement improvement factor and excess pore water pressure in the unit cell and plain strain model.

The effect of varying length and diameter of SC encasement was studied in 3D numerical approach [13]. The geosynthetic encasement with different elasticity modulus along with angle of friction and its effect calibrated in reclamation of field as it was related to the determination of settlement and lateral deformations (bulging), and the results indicated that encasing only the outer columns of the SC group is sufficient in providing an optimal design [13]. Also, these results confirmed increasing stiffness of the encasement with increasing ratio of the soft soil replaced by the SC (i.e., the area replacement ratio). Furthermore, the change in modulus of elasticity of the column material resulted with small effects whereas comparatively less sensitive to the internal friction angle change [13].

The failure stress on end bearing single as well as group of SC was studied with different encasements [14]. Geogrid reinforcement is found effective as compared to natural geosynthetic encasement to encase SC as it avoided cutting because of stone angular sharp edges [14]. This geosynthetic encased granular column was analyzed by using FLAC 3D prototype scale in three-dimensional numerical models. Two different diameters of granular column (50 and 100) with three different pattern reinforcements were used (single, triangular and square) in direct shear box to examine the effect of group confinement. The various pressures were applied at four series (i.e., 15, 30, 45 and 75) kPa in numerical simulations. With these parameters, the tensile forces were mobilized in both vertical and circumferential direction as effect of the encasement [15].

Numerical studies with 2D, 3D, single column, group of SC, varying length to diameter ratio, different encasement lengths, different types of encasements and filling material of column by means of strengthening soft soil resulted in load bearing capacity and lateral encasement increase [16–21]. Performance enhancement of encased SC with conductive natural geotextile under k_0 stress condition was done and stated its positive effect in strength improvement with sustainable solution remark [16]. A numerical investigation tried with pressure settlement behavior of embankment on GESG installed soft ground [17]. Numerical modeling of geosynthetic encased granular columns was compared with experimental results and found with slight variations [18]. Furthermore, numerical and analytical evaluations with behavior of GESG in soft clay were satisfied [19]. Numerical study with Plaxis 2D was done on ground improvement for liquefaction mitigation using SC encased with geosynthetics, and efficacy with result improvements was discussed [21].

3 Stone Column Ground Improvement Techniques

Heights of compacted gravel or crushed stone installed in soft soil below the foundation are known as SC. It provides vertical support for load transferred from the structure above and also reduces drainage of the soil. Also, it provides resistance to horizontal or inclined shear like normal piles. SC is providing the passive resistance to the soft soil that can be mobilized to withstand radial bulging and by the friction angle of the compacted material in the column. The required minimum depth of the column in soft soil can be estimated based on the shearing strength along the sides and the end bearing capacity. The soft clay model is tested with OSC and GESG inclusions for comparison with FEM numerical evaluations.

3.1 Ordinary Stone Column

OSC inclusion involves adding vertical columns of stone into the soft soil ground. This is tried with cylindrical holes in soil by vibrating probe penetrating in jet method with the help of casing pipes; simultaneously, soil is compacted in layers. Length and diameter of SC can be varied. In some of the cases, single stone column or group of stone column is tried.

3.2 Encased Stone Column

SC is vertically covered as encasement for lateral confinement of stones. Different encasement materials are available for this. Geosynthetic geotextile is found suitable for strength increase and lateral confinement decrease by researchers as well as case

studies. Also, natural geotextile like coir and jute is tested by many of the researchers and used in practice. GESC was used in ordinary clay model, and geosynthetic material taken in this study was geotextile.

4 Numerical Analysis with Plaxis 2D

The FEM analyses were done using the two-dimensional model in which clay material, stone material and geosynthetic material were represented by polyhedral elements as in Plaxis. In this, the variables were assigned at discrete locations and the zones behaved independently. The load settlement curves achieved with different load applications and shown different parameters like vertical as well as total displacement, stresses in all directions in addition to plastic points highlighting the stress distribution after application of load. The model shows different vertical settlements and got failed when ultimate load got applied. In this, the finite elements moved, took new positions and deformed in incremental displacements resulting in final collapse results.

4.1 *Plaxis 2D Model*

The axisymmetric model was taken in numerical analysis with size 0.8 m diameter and 1 m height. The soft clay with geotechnical properties is considered as shown in Table 1. This is termed as baseline clay model. The SC of size 10 cm diameter in center was used to strengthen the baseline clay model and termed OSC. Length of SC is considered 40 cm from top as shown in Fig. 1 by considering required length to diameter ratio ($L/D = 4$). OSC remedy was done with compacted crushed stone, and in Plaxis, the material known as deep sand is considered for the same. In case of GESC, the OSC was covered with geotextile encasement around full length of OSC and used to strengthen the baseline clay model.

4.2 *Material Properties with Model Generation*

The finite element model (FEM) is created by Plaxis 2D, Version 8.6 software. The general setting with size of model of 1 m diameter and 0.8 m depth was simulated by plane strain model, using Plaxis 2D where the 2D models for baseline clay model, OSC baseline clay model and GESC baseline clay model. The performance related to load settlement curve, bearing capacity and settlement changes with the same was evaluated with the selected material properties. The 2D-axisymmetric model with 15-node triangular elements was built. The phreatic level was set at half length, i.e., 0.4 m below the top surface. The cross sections of the three models used in the

Table 1 Properties of sub-soils used in FE analysis

Properties	Soft clay	Deep sand	Unit
Type of behavior	Undrained	Drained	
γ_{unsat}	16.00	17.000	kN/m ³
γ_{sat}	18.00	21.000	kN/m ³
k_x	1.000E-03	0.500	m/day
k_y	1.000E-03	0.500	m/day
E_{ref}	1.000E+04	1.200E+05	kN/m ²
ν	0.350	0.300	–
c_{ref}	5.000	1.000	kN/m ²
ϕ	25.000	33.000	Degree
ψ	0.000	3.000	Degree
Material model	Mohr–Coulomb (MCM)		–

analysis with a finite element mesh and boundary conditions are shown in Fig. 1. The drainage boundaries were assumed to be at the ground surface, i.e., at the bottom of model (the excess pore pressure at the nodes along the boundaries was set to zero), and the lateral boundaries of the models were closed (impervious). The soil element was replaced by SC after the generation of the initial stress and pore water pressure. The criterion adopted for all the material element failure was Mohr–Coulomb failure.

The properties of the soft clay, stone grains and geosynthetic geotextile material are as per Table 1. The soft clay was taken in undrained condition, and the OSC and GESC behavior was taken in drained condition. With input parameters of the Mohr–Coulomb model as per Table 1, the stiffness modulus (E), drained cohesion (c), internal friction angle (ϕ), dilation angle (ψ), Poisson's ratio (ν) and unit weight (γ) were entered in Plaxis 2D. The clay is assumed to be fully saturated.

In this, a consolidation analysis was done to investigate the baseline clay model and clay strengthened with OSC and ESC. Also, the dissipation of excess pore water pressure is considered in the analysis. This numerical modeling was divided into three major steps: (a) initializing the stress field and hydrostatic pore water pressure distribution (the calculations were taken until the excess pore pressure had dissipated to a residual value of 1 kPa to determine the final consolidation settlement for 25 days); (b) the simulation of the model was done with the plate element placed at top of the model and (c) applying UDL on center of model (Fig. 1) covering full top of SC and partially clay surface. The baseline clay model was tested till collapse of model with Plaxis and recorded with load settlement curve as shown in Figs. 1d and 2d. The vertical load was simulated by applying different uniformly distributed loads (15, 17.5 and 20 for OSC and 15, 22.5 and 25 for GESC) kPa on the center of the model top and the outputs were compared in terms of load settlement curve (Figs. 1d and 2d). The consolidation period taken in this is 25 days.

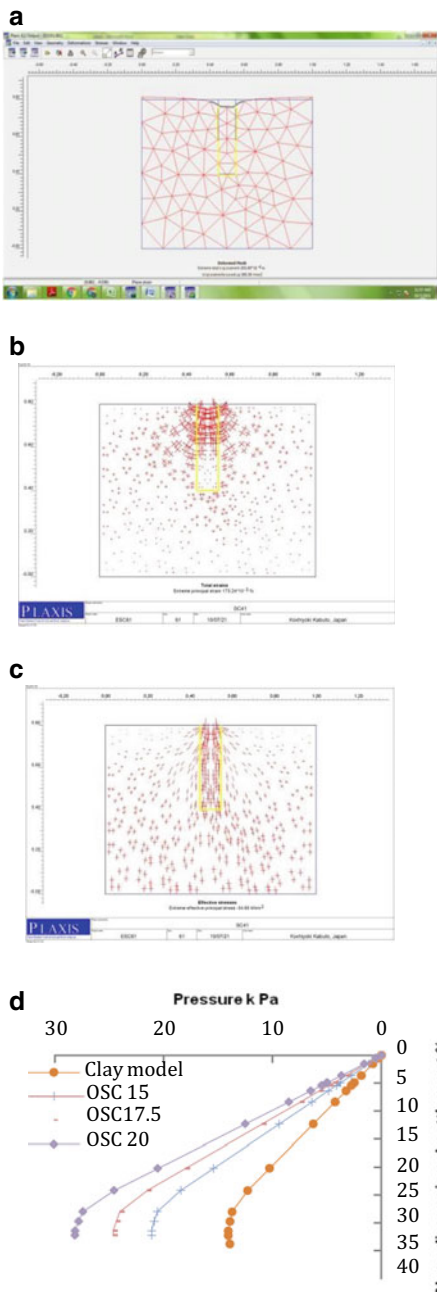


Fig. 1 a Deformed mesh of OSC. b Extreme principal strain output of clay model with OSC. c Effective stresses output of clay model with OSC. d Load settlement curve for baseline clay model and OSC clay model

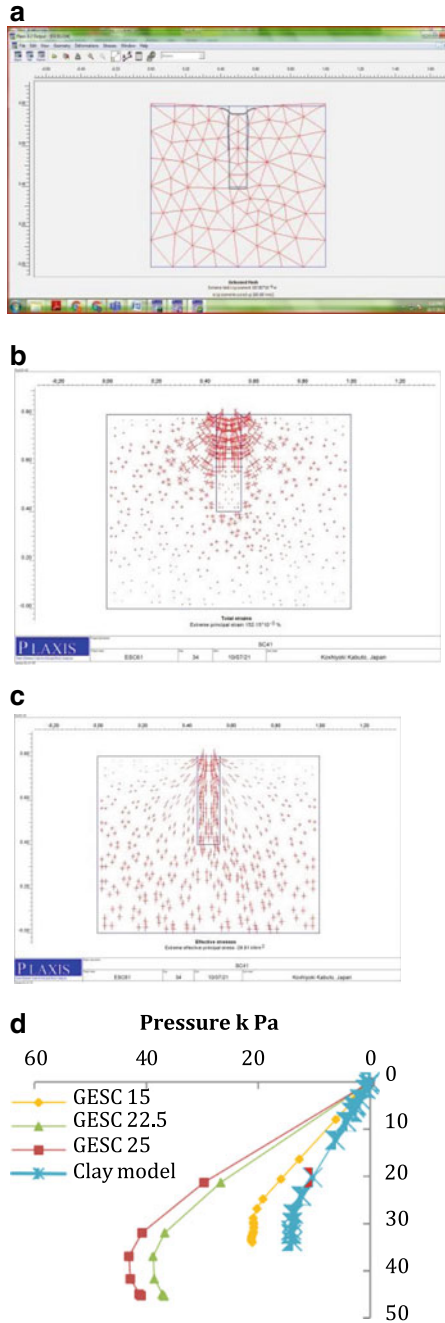


Fig. 2 a Deformed mesh of GESC. b Extreme principal strain output of clay model with GESC. c Effective stresses output of clay model with OSC. d Load settlement curve for baseline clay model and GESC clay model

Table 3 Parameters

Model made up with size	Model height (mm)	Model diameter (mm)	SC diameter (mm)	SC length (mm)	Encased SC length (mm)
Baseline clay	800	1000	–	–	–
OSC	800	1000	100	400	–
GESC	800	1000	100	400	400

The two vertical boundaries are assumed to be x -direction. The initial condition is the zone of saturation at the depth of 0.3 m below the ground level. It can pass water from all boundaries of embankment as well as water pressure will be distributed in all direction.

4.3 Initial Conditions and Boundary Conditions:

In the initial condition, water unit weight is set to 10 kN/m^3 . This pressure is based on saturation level zone or phreatic line, and this pressure is fully saturated. Boundary cognition for consolidation analysis can be additional input. The consolidation line needs to be selected in vertical direction; it means vertical boundaries are close to horizontal flow of groundwater. Then, this is restrained. Hence, no any type of outflow is their boundary. In that analysis, constant groundwater level has been considered.

4.4 Different Parameters Considered in Plaxis 2D Model

Numerical analysis with parameters to evaluate the behavior of the soft clay was done with parameters as explained in Table 3. In all cases, the number of consolidation days taken is 25 days and pore pressure is 10 kN/m^2 . Strengthening of clay with the ordinary SC and geosynthetic ESC is compared with different simulation key factors.

5 Result and Discussion

The model of soft clay in the company of improvement technique was simulated with FEM in Plaxis 2D software. With every model, water table was selected at 3.0 m from top of the clay fill and cavitation stress taken 10 kN/m^2 . Baseline clay model, OSC and GESC were evaluated with different magnitudes, and load settlement observations are compared with graph in Figs. 1d and 2d. These results were normalized against

the Plaxis 2D outputs of deformed FE mesh, plastic points, vertical displacement and vertical stresses. The vertical uniformly distributed load was applied at center of model and varied with different phase iterations. The baseline clay model was failed and expressed load settlement curve as shown in Figs. 1d and 2d. OSC inclusion improved the bearing capacity of clay, and settlement was decreased considerably (Figs. 1d and 2d). The ultimate bearing capacity was improved by 11.2% with OSC and 16.2% with GESC. GESC confined mode shows less bulging mode resulting in higher bearing capacity and lesser settlement as compared to plain clay and OSC models.

With comparison of the resulting deformed mesh after load application on models (OSC and GESC) are illustrated with Figs. 1 and 2. With this, it is well clear that the bulging of SC got reduced and confined with use of geosynthetic encasement. The settlement of OSC clay model and GESC clay model was compared, and it was found that applied load produced total displacement on the failure condition, 0.205 mm, 0.197 mm, respectively, after collapse. The OSC clay model with deep sand material column produced small improvement in settlement reduction, whereas the GESC clay model with encased deep sand material column produced considerable improvement in settlement reduction (Figs. 1a–d and 2a–d).

6 Conclusion

The numerical study presented the case of baseline model of soft clay protected by geotextile encased SC. The settlement with depths excess pore water pressure and lateral movement of the soft clay foundation were analyzed. The resulting output curve and output images are compared with baseline OSC and GESC clay model. Some analyses reveal the following conclusions:

- The load settlement curve shown with output curve shows increase in ultimate bearing capacity with inclusion of OSC and more with GESC.
- A settlement is measured below the test model and found that the use of encased SC reduced the settlement considerably.
- The geosynthetic material geotextile covering SC provided a confinement effect to the SC, and the more settlement reduction.
- This is indicating that the use of a geotextile could reduce the deviator and shear strain as well as increase the effective stress of the clay contributing to the consolidation of the clay.

References

1. Ng KS, Tan SA (2015) Stress transfer mechanism in 2D and 3D unit cell models for stone column improved ground. *International Journal of Geosynthetics and Ground Engineering* 1–15
2. Greenwood DA (1970) Mechanical improvement of soils below ground surfaces. In: *Proceedings of the ground engineering conference, (GEC '70)*, Institution of Civil Engineers, London, pp 11–22
3. Ambily AP, Gandhi SR (2016) Behavior of stone columns based on experimental and FEM analysis. *ASCE J Geotech Geoenviron Eng* 133:405–415
4. Lo SR, Zhang R, Mak J (2010) Geosynthetic encased stone columns in soft clay: a numerical study. *Geotextiles Geomembranes* 28:292–302
5. Golait YS, Padade AH (2017) Analytical and experimental studies on cemented stone columns for soft clay ground improvement. *Int J Geomech* 17(4):1–21
6. Pengpeng N, Yaolin Y, Songyu L (2010) Bearing capacity optimization of T-shaped soil-cement column-improved soft ground under soft fill. *Soils Found* 61:416–428
7. Dheerendra Babu MR, Nayak S, Shivashankar R (2013) A critical review of construction, analysis and behaviour of stone columns. *J Geotech Geol Eng* 31:1–22
8. Balaam NP, Booker IR (1981) Analysis of rigid rafts supported by granular piles. *Int J Numerical Analytical Meth Geomechan* 5:379–403
9. Van Impe WY, De Beer E (1983) Improvement of settlement behavior of soft layers by means of stone columns. In: *Proceedings of the 8th international conference on SMFE, (SMFE '83)*, Helsinki, pp 309–312
10. Elshazly HA, Hafez DA, Mossaad ME (2008) Reliability of conventional settlement evaluation for circular foundations on stone columns. *J Geotech Geol Eng* 26:323–334
11. Jellali B, Bouassida M, Buhan PD (2005) A homogenization method for estimating the bearing capacity of soils reinforced by columns. *Int J Numerical Analytical Meth Geomech* 29:989–1004
12. Abdelkrim M, Buhan PD (2007) An elastoplastic homogenization procedure for predicting the settlement of a foundation on a soil reinforced by columns. *Eur J Mechan A/Solids* 26:736–757
13. Weber TM, Springman SM, Gab M, Racansky V, Schweiger HF (2008) Numerical modelling of stone columns in soft clay under an embankment. In: *Karstunen M, Leoni M (eds) Geotechnics of soft soils-focus on ground improvement*. Taylor and Francis, London, pp 305–311
14. Keykhosropur L, Soroush A, Imam R (2012) 3D numerical analyses of geosynthetic encased stone columns. *Geotext Geomembr* 35:61–68
15. Almeida M, Hosseinpous I, Riccio M, Alexiew D (2015) Behaviour of geotextile encased granular columns supporting test embankment on soft deposit. *ASCE Geotech Geoenviron Eng* 141(3)
16. Mohapatra SR, Rajagopal K, Sharma J (2017) 3-Dimensional numerical modeling of geosynthetic encased granular columns. *Geotext Geomembr* 45:131–141
17. Pandey BK, Rajesh S, Chandra S (2018) Performance enhancement of encased stone column with conductive natural geotextile under k_0 stress condition. *Geotext and Geomembr* 49:1095–1106
18. Chungsik Y (2015) Settlement behavior of embankment on geosynthetic-encased stone column installed soft ground e a numerical investigation. *Geotext Geomembr* 43:484–492
19. Ambily AP, Gandhi SR (2007) Behavior of stone columns based on experimental and FEM analysis. *ASCE J Geotech Geoenviron Eng* 133:405–415

20. Alkhorshid NR, Araujo GL, Palmeira EM (2018) Behavior of geosynthetic encased stone columns in soft clay: numerical and analytical evaluations. *Soils Rocks* 41(3):333–343
21. Tang L, Shengyi C, Xianzhang L, Jinchi L, Ahmed E (2015) Numerical study on ground improvement for liquefaction mitigation using stone columns encased with geosynthetics. *Geotext Geomemb* 43:190–195

Multiple Linear Regression Analysis for Predicting Unconfined Compressive Strength of Fiber Reinforced Fly Ash Stabilized Lateritic Soil



Hemant S. Chore, Swati Yede, Bhupati Kannur, and Rakesh Kumar

Abstract The importance of the prediction models for any of the engineering properties is due to time saving and material conservation which or else will take a lot of material and longer periods of time to determine the same through the laboratory experiments. The lateritic soil stabilized with fly ash (FA) and reinforced with glass fiber might be an effective alternative construction material in application to the geotechnical structures such as embankments, pavement sub-bases, retaining walls and structural landfills. This paper deals with the multiple linear regression (MLR) analysis to develop the prediction models for unconfined compressive strength (UCS) of lateritic soil stabilized with fly ash and reinforced with glass fibers. The lateritic soil replaced with 10, 20, 30 and 40% fly ash and added with glass fiber contents such as 0.1, 0.2 and 0.3% is varied by weight of lateritic soil. In total, 17 combinations were tested for UCS at curing period of 7 days in un-soaked condition. The results obtained in the experimental investigation are used for developing the regression model using MLR analysis technique. The models thus developed were found to predict the UCS in fair to better agreement with the experimental values obtained through laboratory trials. The values of R^2 range from 0.963 to 0.973 indicating the good co-relation between the UCS as dependent variable and contents of fly ash and glass fiber as independent variables.

Keywords Lateritic soil · Fly ash (FA) · Glass fibers · UCS · Multiple linear regression analysis

H. S. Chore · B. Kannur (✉)

Department of Civil Engineering, Dr. B. R. Ambedkar National Institute of Technology, Jalandhar, Punjab, India

e-mail: bhupati.kmt@gmail.com

S. Yede

Department of Civil Engineering, Datta Meghe College of Engineering Airoli, Navi Mumbai, Maharashtra, India

R. Kumar

Department of Industrial and Production Engineering, Dr. B. R. Ambedkar National Institute of Technology, Jalandhar, Punjab, India

1 Introduction

Prediction modeling is a vital tool in engineering field as it helps in decision-making and selection of optimum material compositions. Further, the models developed help in knowing effects of different ingredients on the important engineering characteristics of their mixes in terms of strength and durability. UCS is an important strength characteristics of any geotechnical material which measures the compressive strength of the material or mix of different materials. Nowadays, a lot of waste from different industries is being disposed into water bodies or in open lands. This causes the health issues due to air, water and land pollution. Fly ash is one of the hugely produced industrial wastes by coal combustion in thermal power plants. On other hand, there is scarcity in the locality of the quality construction materials for different geotechnical applications such as road subgrade, sub-bases, road embankments and structural fills. Thus, utilization of waste materials to stabilize the problematic soils will solve both the issues of waste disposal and non-availability of construction materials. Thus, in the present study one such technique to stabilize lateritic soil with fly ash along with glass fibers is discussed. More specifically, the strength of lateritic soil-fly ash-glass fiber system in terms of UCS at curing period of 7 days has been tested by in laboratory experimental program and using the results of the same different prediction models for the same have been established. Further, the efficiency of the developed models through MLR has been validated by plotting the predicted UCS values with the actual experimental UCS values.

2 Literature Review

There are studies on lime and fly ash used in stabilization of soil [1–3]. Mitchell and Katti [1] studied the state-of-the-art report on the stabilization of soil. The physio-chemical reactions involved in lime stabilizations of soil-fly ash or soil mixes have been reported extensively by many researchers [4–6]. Chakraborty and Dasgupta [7] studied the triaxial test results to reveal the effect of polymer fibers in plain fly ash. Dhariwal [8] studied fly ash with woven geo fibers and jute fiber system. Kaniraj and Gayatri [9] evaluated the geotechnical properties of fly ash reinforced with fibers oriented in random fashion. Few studies evaluated the performance of clay-fiber system [10, 11].

Chore et al. [12] studied the polypropylene (PP) fiber-sand-fly ash system and its performance with varying contents of FA, sand and PP fibers. Singh and Goswami [13] carried out research on compaction properties of lateritic soil along with lime and low calcium fly ash. Singh and Kalita [14] evaluated the CBR of a fine-grained residual lateritic soil. Lekha et al. [15] stabilized the lateritic soil in application to pavements by chemical stabilization.

The engineering characteristics of soil and other geotechnical materials along with pozzolanic and stabilizing materials vary significantly and are uncertain as the

formation process of these materials is imprecise and complex. Thus, it is important to investigate the effect of different ingredients on the overall performance of the conglomerate in precise manner. The simple laboratory experimental program through numbers of repeated trials is not justified as it consumes time and resources. Thus, in today's soft computing era many researches are going on to use different software and data analyzing techniques such as linear regression analysis (LAR), artificial intelligence (AI), Internet of Things (IoT), algorithms, artificial neural networks (ANN) and many more [16–23]. The use of multiple linear regression (MLR) analysis for the prediction of different engineering properties of civil engineering materials is reported in few studies [24–28].

Thus, this paper discussed the development of prediction models by relating the dependent variable UCS to the independent variables such as contents of fly ash and glass fiber. The study aimed at evaluating the effect of varying percentages of fly ash ranging from 10 to 40% in conjunction with glass fibers ranging from 0.1 to 0.3% on the strength of lateritic soil and to develop the regression model using multiple linear regressions technique based on the statistical approach and to compare the UCS observed experimentally and predicted using the model so developed.

3 Materials and Methodology

3.1 Materials

The lateritic soil from the Devgad (Ratnagiri) of state of Maharashtra was used. The soil was red in color. The properties of lateritic soil were tested in the laboratory and are mentioned in Table 1.

The FA was procured from Nasik which was a waste material produced in thermal power plant, Nashik. The physical characteristics of the FA as found in laboratory are shown in Table 2.

The properties of glass fibers by the supplier's data sheet are as given in Table 3.

Table 1 Index properties of soil

Property	Value [29]
Liquid limit	21.79% [29]
Plastic limit	19.43%
Specific gravity	3.1 [30]
Optimum moisture content	1.932 [30]
Maximum dry density	13.45

Table 2 Physical properties of fly ash

Specific gravity	2.12
Liquid limit	20
Plastic limit	29
Loss of ignition	2.5
Moisture	0.21

Table 3 Properties of glass fibers

Property	Value	Property	Value
Length	6 mm	Tensile strength	1700 Mpa
Diameter	14 μm	Modulus of elasticity	72 Gpa
Nature	Inert	Softening point	860 °C
Material	Alkali resistant	Moisture	0.30%
Density	2.68 g/cm ³	Loss of ignition	0.55%

3.2 Multiple Linear Regression (MLR) Analysis

The MLR analysis is useful in modeling the relationship between two or more variables independent in nature to one variable dependent on others by generating an equation with linear fitting of the data provided. The general form of MLR model is

$$y = (c + a_1x_1 + a_2x_2 + \dots + a_nx_n)$$

where c, ai = regression constants, xi are independent variables, and y is the dependent variable. The best fitting model has been generated for the experimental values of UCS test result data by reducing the sum of squares of the deviation of each data point to the regression formula. The software SPSS version 20 has been utilized for regression analysis in which equations were formed by substituting the different input parameters.

4 Results and Discussion

4.1 Formulae Derived from the Analysis

Utilizing the laboratory experimental results as per IS: 2720 Part 10 [31] and SPSS v20 statistical program, MLR model was developed which correlates the varying contents of soil, fly ash, cement and glass fibers with the dependent variable, UCS.

The formula derived from the multiple regression analysis in respect of various soil stabilized mixes comprising different combinations of the ingredients and having been cured for 7 days is given below.

Combination I—Soil + Fly Ash

$$7\text{days' UCS} = 0.850 + (0.009 \times \text{Fly Ash}) \tag{1}$$

Combination II—Soil + Fly Ash + Glass Fibers

$$7\text{days' UCS} = 0.892 + (0.056 \times \text{Fly Ash}) + (4.363 \times \text{Fiber}) \tag{2}$$

The plot of the experimental UCS values and the UCS values obtained by prediction models for 4 trial mixes similar to combination I after curing for 7 days is as in Fig. 1. From Fig. 2, it can be observed that the model overestimated the UCS by 2.58% in one of the trial mixes. However, in case of other 3 trial mixes the UCS predicted was found to be lower than the experimental UCS values by 0.91% on an average.

The graphical plot between the actual values obtained through laboratory tests and the predicted strength with help of the model generated for 12 trial mixes similar in nature to the combination II for curing period of 7 days is as shown in Fig. 2. From Fig. 2, it can be observed that for six trial mixes out of 12, the model overestimated the UCS values by 3.27% on an average compared to the actual UCS values obtained by laboratory tests. However, in other 6 trials the model underestimated the actual strength values by 4.68% on an average.

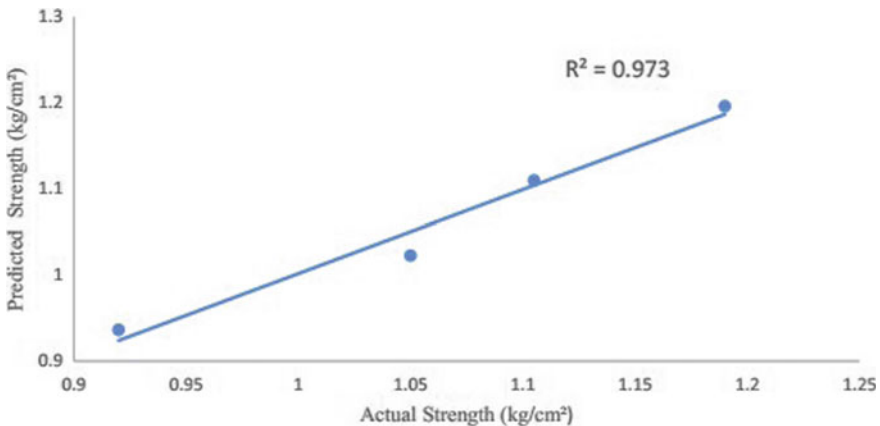


Fig. 1 Actual v/c predicted values of UCS, for combination I after 7 days' curing

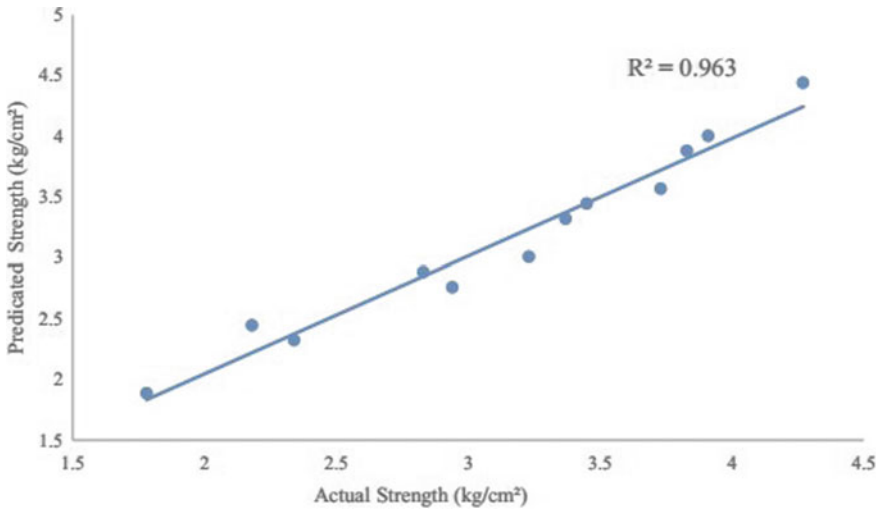


Fig. 2 Actual v/c predicted values of UCS, for combination II after 7 days' curing

5 Conclusion

Based on the laboratory experimental work and the regression analysis carried out to formulate the prediction models for the UCS values of soil-FA-glass fiber system, following conclusions are drawn:

- (i) The multiple regression analysis by SPSS software is an effective tool in formulation of prediction models for engineering properties of such complex construction materials with various combinations of ingredients.
- (ii) The UCS prediction models generated in the present study for combination I and combination II of lateritic soil-FA-glass fiber system for curing period of 7 days can be effectively used in prediction of UCS of the said combinations.
- (iii) The strength prediction models were found to estimate the UCS values in fair to better agreement with those of actual laboratory experimental values.

References

1. Mitchell JN, Katti RK (1981) Soil improvement: state-of-the art report. In: Proceedings of 10th international conference on soil mechanics and foundation engineering. International Society of Soil Mechanics and Foundation Engineering, London, pp 261–317
2. Maher MH, Butziger JM, DiSalvo DL, Oweis IS (1993) Lime sludge amended fly ash for utilization as an engineering material. Fly Ash for Soil Improvement: Geotech, Special Publication no. 36, ASCE, New York, p 88
3. Consoli NC, Prietto PDM, Carraro JAH, Heinech KS (2001) Behavior of compacted Soil-fly ash-carbide lime mixtures. *J Geotech Geoenviron Eng* 127(9):774–782

4. Ingles OG, Metcalf JB (1972) Soil stabilization principles and practice. Butterworth, Sydney
5. Brown RW (1996) Practical foundation engineering handbook. Mc-Graw hill, New York
6. Edil TB, Acosta HA, Benson CH (2006) Stabilizing soft fine grained soils with fly ash. *J Mater Civ Eng* 18(2):283–294
7. Chakraborty TK, Dasgupta SP (1996) Randomly reinforced fly ash foundation Material. In: Proceedings of Indian geotechnical conference, Madras, India, pp 231–235
8. Dhariwal A (2003) Performance studies on California bearing ratio values of fly ash reinforced with jute and non-woven geo fibres. *Advances in Construction Materials* 45–51
9. Kaniraj SR, Gayathri V (2003) Geotechnical behavior of fly ash with randomly oriented fiber inclusions. *Journal of Geotextiles and Geomembranes* 21:123–140
10. Kumar S, Tabor E (2003) Strength characteristics of silty clay reinforced with randomly oriented nylon fibers. *Electronic Journal of Geotechnical Engineering*
11. Kumar A, Walia BS, Mohan J (2005) Compressive strength of fiber reinforced highly compressible clay. *Construction Building Materials* 20(10):1063–1068
12. Chore HS et al (2011) Performance evaluation of polypropylene fibers on sand-fly ash mixtures in highways. *Journal of Civil Engineering (IEB)* 39(1):91–102
13. Singh B, Goswami RK (2012) Compaction characteristics of lateritic soil mixed with fly ash and lime. *Int J Geotech Eng* 6:437–444
14. Singh B, Kalita A (2013) Influence of fly ash and cement on CBR behaviour of lateritic soil and sand. *Int J Geotech Eng* 7(2):173–177
15. Lekha BM, Ravi Shankar AU, Sarang G (2013) Fatigue and engineering properties of chemically stabilized soil for Pavements. *Journal of Geotechnical Engineering* 43(1):96–104
16. Goh ATC (1995) Modelling soil correlations using neural networks. *ASCE J Comput Civil Eng* 9(4):275–278
17. Penumadu D, Zhao R (1999) Triaxial compression behaviour of sand and gravel using artificial neural networks (ANN). *Comput Geotech* 24(3):207–230
18. Kurup PU, Dudani NK (2002) Neural networks for profiling stress history of clays from PCPT data. *ASCE J Geotech Geoenviron Eng* 128(7):569–579
19. Javadi AA, Rezaei M (2009) Applications of artificial intelligence and data mining techniques in soil modeling. *Geomechanics and Engineering* 1(1):53–74. <https://doi.org/10.12989/GAE.2009.1.1.053>
20. Alavi AH, Gandomi AH, Mollahassani A, Heshmati AA, Rashed A (2010) Modeling of maximum dry density and optimum moisture contents of stabilized soil using artificial neural networks. *J Plant Nutr Soil Sci* 173(3):368–379
21. Das SK, Samui P, Sabat AK (2011) Application of artificial intelligence to maximum dry density and unconfined compressive strength of cement stabilized soil. *Geotech Geol Eng* 29(3):329–342
22. Spandana K, Pabboju S (2019) Applications of IoT for soil quality. In: ICICCT 2019—system reliability, quality control, safety, maintenance and management, pp 277–286. https://doi.org/10.1007/978-981-13-8461-5_31
23. John K et al (2020) Using machine learning algorithms to estimate soil organic carbon variability with environmental variables and soil nutrient indicators in an alluvial soil. *Land* 9:487. <https://doi.org/10.3390/land9120487>
24. Yoon GL, Kim BT (2004) Regression analysis of compression index for Kwangyang marine clay. *KSCE J Civil Eng* 10(6):415–418
25. Yildirim B, Gunaydin O (2011) Estimation of California bearing ratio by using soft computing systems. *Exp Syst Appl* 38(5):6381–6391
26. Abasi N, Javadi AA, Bahramloo R (2012) Prediction of compression behaviour of normally consolidated fine grained soils. *World Appl Sci J* 18(1):6–14
27. Akayuli CFA, Ofosu B (2013) Empirical model for estimating compression index from physical properties of weathered Birimian phyllites. *E J Geotech Eng* 18(Z):6135–6144
28. Viji VK, Lissy KF, Shobha C, Benny MA (2013) Predictions on compaction characteristics of fly ashes using regression analysis and artificial neural network analysis. *J Geotech Eng* 7(3):282–292

29. IS: 2720 Part 5–1970, Determination of liquid limit and plastic limit. Bureau of Indian Standards (BIS), New Delhi
30. IS: 2720 Part 7–1983, Determination of water content—dry density relation using light compaction. Bureau of Indian Standards (BIS), New Delhi
31. IS: 2720 Part 10–1973, Determination of unconfined compressive strength. Bureau of Indian Standards (BIS), New Delhi

Prediction of Unconfined Compressive Strength of Fly Ash–Soil–Lime–Fiber System Using Multiple Regression Analysis



Hemant S. Chore, Swati Yede, Bhupati Kannur, and Rakesh Kumar

Abstract This study reports the development of the prediction models using multiple regression analysis for predicting the unconfined compressive strength (UCS) of fly ash–soil–lime system reinforced with polypropylene fibers. The results obtained through laboratory UCS tests on different combinations of the fly ash–soil–lime–fiber system are utilized for the development of the models using SPSS software. The mixes of fly ash stabilized with 15 and 25% of soil, 10, 15 and 20% of lime contents and polypropylene fibers having 0.1, 0.2 and 0.4% were prepared and tested for their strength at curing periods of 7 days and 28 days. Six prediction models are developed. Further, the developed models are validated by using 12 laboratory trial mixes. The UCS values predicted by using these models are found to be in fair to better agreement with the actual values of UCS obtained by the laboratory results.

Keywords Soil · Fly ash · Lime · Polypropylene fibers · Multiple regression analysis

1 Introduction

The industrialization is necessary for the development of the country, but the environmental pollution due to by-products or waste materials of the industries is unavoidable. The solution is to reuse such materials in the construction industry which also saves the original materials and proves to be economic option. Fly ash is one such

H. S. Chore · B. Kannur (✉)

Department of Civil Engineering, Dr. B. R. Ambedkar National Institute of Technology, Jalandhar, Punjab, India
e-mail: bhupati.kmt@gmail.com

S. Yede

Department of Civil Engineering, Datta Meghe College of Engineering Airoli, Navi Mumbai, Maharashtra, India

R. Kumar

Department of Industrial and Production Engineering, Dr. B. R. Ambedkar National Institute of Technology, Jalandhar, Punjab, India

industrial waste which has the potential in improving the strength of soil. Further, there might be scarcity of locally available quality materials nearby construction sites and procuring the materials from long distances increases the project cost. The tonnes of fly ash being generated by thermal power plants can be promisingly utilized in the geotechnical constructions like structural landfills, road sub-base, embankments, etc., as a substitute to the conventional weak earth material. On the other hand, the use of fibers renders the reinforcing effect. The utilization of the fly ash–soil–fiber system along with cementitious material solves both the problems of elimination of solid waste, firstly, and provision of a huge amount of needed construction material, secondly.

The most important geotechnical property of any geotechnical construction material is its strength. The strength is generally determined by using UCS test by rigorous laboratory experimental program. This process involves preparation of many samples, curing them for different and longer periods before laboratory testing. The experimental evaluation of strength is a tedious process owing the lengthy curing period. In view of this, it would be convenient if the strength parameters could be predicted on the basis of the results of the laboratory tests without going in for actual curing.

2 Brief Literature Survey

There are many studies on the fly ash–soil reinforced with fibers. Kaniraj and Gayatri [1] reported improvement in strength of the raw fly ash mix due to inclusion of fibers as reinforcement. Kumar et al. [2] studied fly ash embankments with randomly distributed polypropylene fibers. Kumar and Singh [3] studied the UCS, CBR, shear strength and modulus of elasticity of fly ash with polypropylene fibers. There are ample studies on randomly distributed and discrete fibers [4–6]. Kar and Pradhan [7] studied the UCS of soil reinforced with randomly distributed fibers. Singh and Goswami [8] studied the compaction properties of lateritic soil with low calcium fly ash and lime. Singh and Kalita [9] studied the California bearing ratio (CBR) behavior of fine-grained lateritic soil. Khan [10] studied the swelling pressure of clayey soil–fly ash system. Chore and Vaidya [11] studied the strength behavior of cement–fly ash mixes reinforced with fibers.

Prediction models for the compression index with variables such as void ratio, water content and liquid limit were proposed adopting the regression analysis by Yoon et al. [12]. Yildirim and Gunaydin [13] employed regression analysis for the prediction of CBR values. The empirical equations were developed using the regression analysis technique by Akayuli and Ofosu [14] to arrive upon the compression index depending upon physical properties of the Birimian Phyllites in weathered condition. The prediction models for the fly ash compaction characteristics with the help of regression analysis were established by Viji et al. [15]. Along similar lines, many other studies reported regression analysis for developing the prediction models for important properties of engineering materials [16, 17]. Chore and Magar [18] used

Table 1 Physical and chemical properties of fly ash

Physical properties	
Specific gravity	2.13
Liquid limit	21
Shrinkage limit	29
Loss on ignition	1.06
Moisture (%)	0.21
Chemical composition	
Silica (SiO ₂)	58.04
Alumina (Al ₂ O ₃)	25.71
Ferric oxide (Fe ₂ O ₃)	5.31
Sulfur trioxide (SO ₃)	0.676
Calcium oxide (CaO)	5.60
Magnesium oxide (MgO)	1.589

the multiple regression analysis and artificial neural networks for the development of prediction models for the UCS and Brazilian tensile strength of cement stabilized fly ash reinforced with fibers.

Literature survey finds relatively less research on the prediction of UCS values of the fly ash–soil–lime system reinforced with polypropylene fibers using soft computing tools. On this backdrop, the present study is aimed at deriving the UCS values with multiple regression analysis technique by using fly ash (FA), soil (S), lime (L) and fiber (F) contents as variables for curing periods of 7 and 28 days in both the soaked and unsoaked conditions.

3 Materials

Fly ash was procured from thermal power plant, Nashik. The physio-chemical properties of the same are presented in Table 1. The polypropylene fibers were supplied by Build Core Chemicals, Andheri, Mumbai. The fibers were of length 12 mm and diameter 34 μm with density about 0.91 g/cm^3 . The lime used in the study was purchased from the local vendor. The soil used in this study was brought from Ratnagiri. The properties of the fly ash are presented in Table 1 while that of soil in Table 2.

4 Experimental Program

The present study entailed a series of tests on various materials for their physical, chemical and geotechnical properties along with the tests for evaluating the strength

Table 2 Index properties of soil

Liquid limit	63.8%
Plastic limit	33.36%
Shrinkage limit	25%
OMC	36.31%
MDD (gm/cm ³)	1.396
Specific gravity	2.7

of the system. In total, 18 combinations were prepared of fly ash stabilized with 15 and 25% of soil, lime of about 10, 15 and 20% and polypropylene contents of about 0.1, 0.2 and 0.4%. The index properties have been determined as per IS: 2720 Part 5-1965 [19]. Standard Proctor tests were conducted to evaluate the maximum dry density (MDD) and optimum moisture content (OMC) as per IS: 2720-1983 [20]. Unconfined compression strength (UCS) test on all the combinations in both soaked and unsoaked conditions was performed as per IS: 2720-1973 [21].

4.1 Unconfined Compression Strength

Sample preparation

A cylindrical mold of 38.1 mm diameter and height of 76.2 mm was used for preparing the samples. The prepared samples were then cured for 7 days and 28 days. In order to simulate the possible field inundation of the stabilized fly ash to assess the effect of soaking, tests were conducted in both soaked and unsoaked conditions on the samples compacted at OMC. For soaked tests, the samples of the stabilized system were kept immersed into the water for 8–10 h after required curing period.

Testing of samples

The UCS testing machine with a proving ring of capacity of 2–30 kN was used for the UCS test. For each combination, three samples were prepared, one was kept for soaked condition, and other two specimens were used for unsoaked condition. All the specimens were tested after curing for 7 days and 28 days.

5 Results and Discussion

In the present study, a multiple regression analysis (MRA) technique was used to formulate the equations and predict the strength of various fly ash–soil–lime stabilized mixes with fiber reinforcements based on the results obtained in the laboratory investigations. The SPSS (Version 16) software was made use of for performing the

regression analysis. Different formulae were formed in the multiple regression analysis by varying the input parameters to arrive upon the strength of such stabilized mixes for 7 and 28 days of curing.

The model considered four independent variables as fly ash (FA), lime (L), soil (S) and fibers (F) and a dependent variable as unconfined compressive strength (UCS). The formulae developed are given below.

$$UCS_{7(S)lime} = 4.246 - 98.031 FA + 176.098 S + 139.678 L \tag{1}$$

$$UCS_{7(US)lime} = 1.049 - 54.695 FA + 220.618 S + 209.722 L \tag{2}$$

$$UCS_{7(US)fiber} = -215.210 + 2420 FA - 148.821 S + 31.50 F \tag{3}$$

$$UCS_{28(S)lime} = -27.058 + 291.649 FA + 421.423 S + 1000.921 L \tag{4}$$

$$UCS_{28(US)lime} = -56.842 + 614.901 FA + 854.268 S + 1032.064 L \tag{5}$$

$$UCS_{28(US)fiber} = 548.428 - 6175 FA + 535.821 S - 4950 F \tag{6}$$

Further, the developed models are validated by the trial mixes. These formulae (Eqs. 1–6) are applied on twelve trial mixes for predicting UCS values. The experimental values and the predicted values by using the models developed for both 7 days and 28 days of curing periods are compared as shown in Figs. 1, 2, 3, 4, 5, 6.

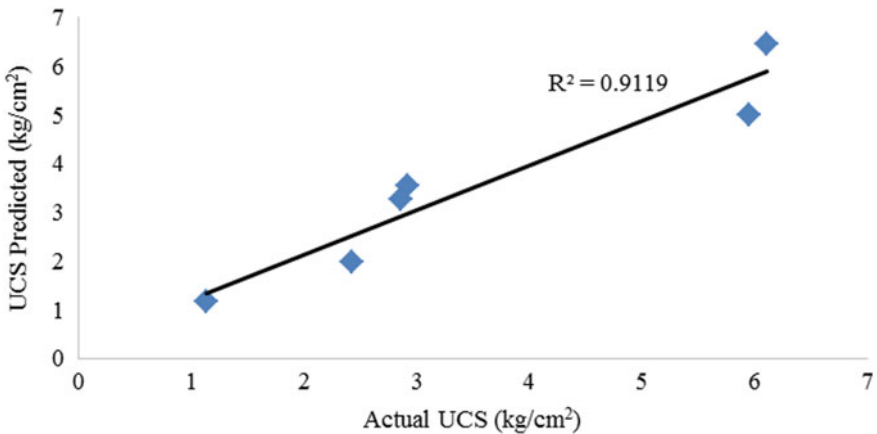


Fig. 1 Actual and predicted values of UCS for (FA + soil + lime) combination (soaked) for 7 days of curing

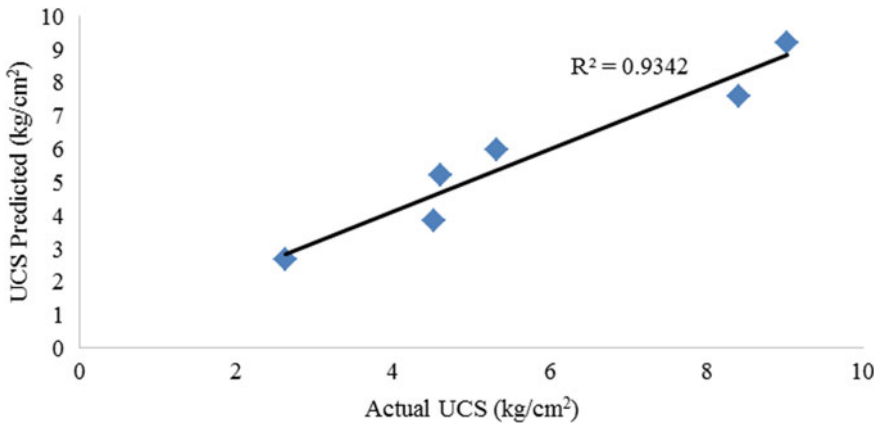


Fig. 2 Actual and predicted values of UCS for (FA + soil + lime) combination (unsoaked) for 7 days of curing

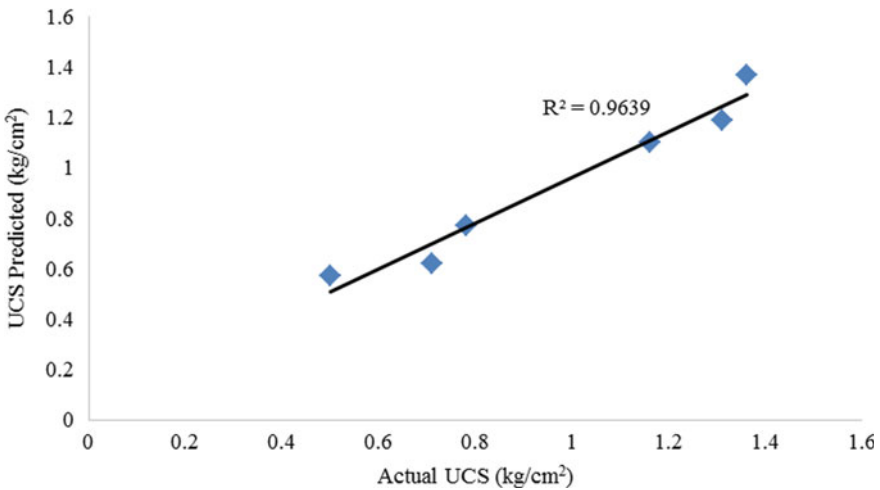


Fig. 3 Actual and predicted values of UCS for (FA + soil + fiber) combination (unsoaked) for 7 days of curing

The value of R^2 is in the range of 0.82–0.96. This clearly indicates the fair to better agreement in the actual and predicted strength of the different mixes considered in the study. In respect of the mixes corresponding to seven days of curing, predicted UCS is found to overestimate the actual strength in six trial mixes by 8.76% on an average. However, in nine trials it seems to underestimate the actual strength by 7.52% on an average. Similarly, for the 28 days of strength values, predicted strength was found to be 9.75% more as compared to the actual strengths on an average in respect of five trials. However, in case of seven trial mixes, actual strength is found to

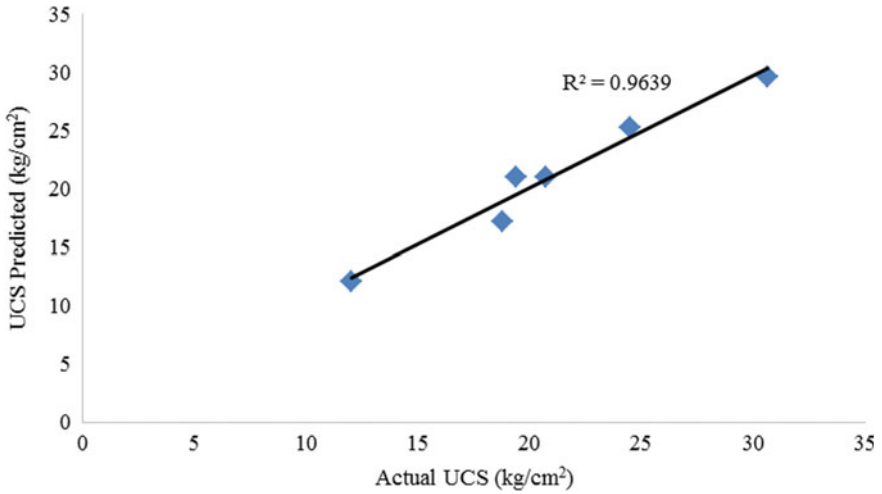


Fig. 4 Actual and predicted values of UCS for (FA + soil + lime) combination (soaked) for 28 days of curing

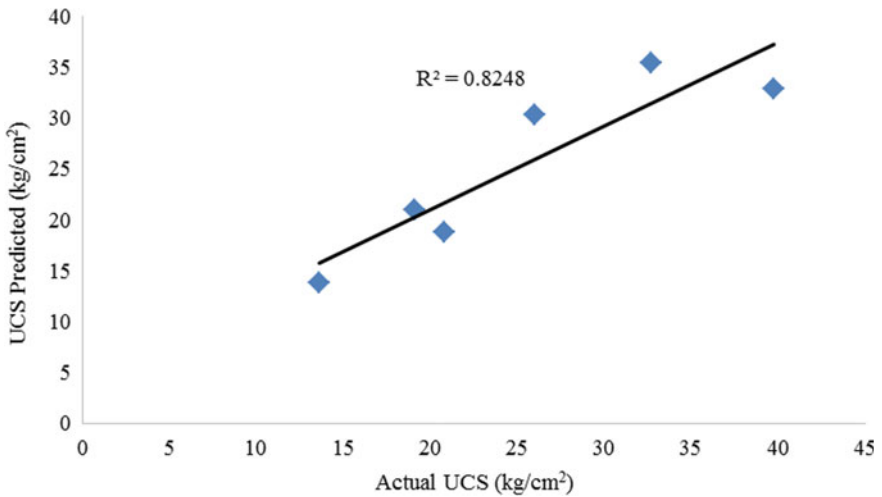


Fig. 5 Actual and predicted values of UCS for (FA + soil + lime) combination (unsoaked) for 28 days of curing

be 14.96% more than that of the predicted strength. This variation may be attributed to the material variability within the stabilized mixes.

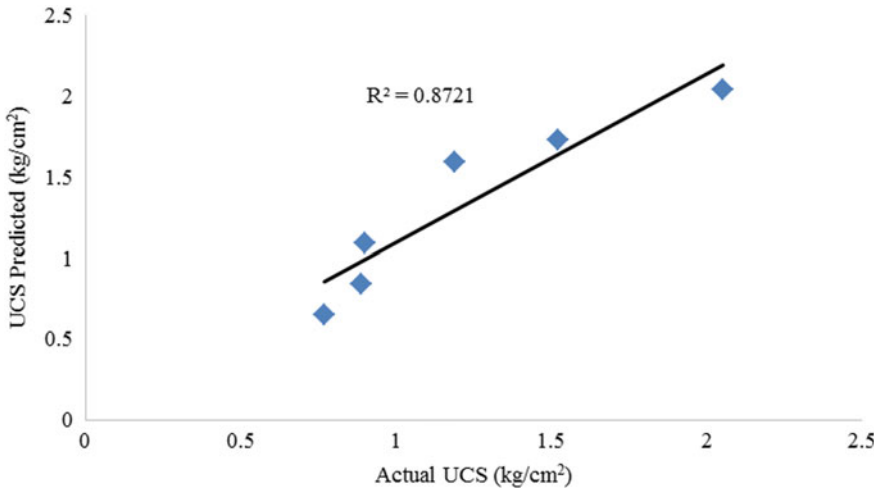


Fig. 6 Actual and predicted values of UCS for (FA + soil + fiber) combination (unsoaked) for 28 days of curing

6 Conclusion

The statistical models for prediction of UCS of fly ash–soil–lime–fiber system are developed by using multiple linear regression analysis. Fair to close agreement is seen in the actual and predicted values of the strength. The models developed in the present study can be used for predicting the strength of such mixes without waiting for the actual experimental work.

References

1. Kaniraj SR, Gayatri V (2003) Geotechnical behavior of fly ash with randomly oriented fiber inclusions. *J Geotext Geomembr* 21:123–140
2. Kumar A, Walia BS, Mohan J (2005) Compressive strength of fiber reinforced highly compressible clay. *Construct Build Mater*
3. Kumar P, Singh SP (2008) Fiber reinforced fly ash sub-bases in rural roads. *J Transp Eng ASCE* 134(4):171–180
4. Chauhan MS, Mittal S, Mohanty B (2008) Performance evaluation of silty sand and sub grade reinforced with fly ash and fiber. *J Geotext Geomembr*
5. Sadek S, Najjar SS, Freiha F (2010) Shear strength of fiber reinforced sand. *J Geotech Eng Geomech ASCE* 136(3):490–499
6. Chore HS et al (2011) Performance evaluation of polypropylene fibers on sand-fly ash mixtures in highways. *J Civ Eng (IEB)* 39(1):91–102
7. Kar R, Pradhan P (2011) Strength and compressibility characteristics of randomly distributed fiber-reinforced soil. *Int J Geotech Eng IJGE* 5:235–243
8. Singh B, Goswami RK (2012) Compaction characteristics of lateritic soil mixed with fly ash and lime. *Int J Geotech Eng IJGE* 6:437–444

9. Singh B, Kalita A (2013) Influence of fly ash and cement on CBR behaviour of lateritic soil and sand. *Int J Geotech Eng IJGE* 7(2):173–177
10. Khan MA (2013) A CBR based study evaluating subgrade strength of flexible pavements having soil fly ash interface. *Int J Civ Eng Trans B: Geotech Eng* 11(1):1–18
11. Chore HS, Vaidya MK (2015) Strength characterisation of fibre reinforced cement-fly ash mixes. *Int J Geosynth Ground Eng* 1(30):1–8
12. Yoon GL, Kim BT, Jeon SS (2004) Empirical correlations of compression index for marine clay from regression analysis. *Can Geotech J* 41(6):1213–1221
13. Yildirim B, Gunaydin O (2011) Estimation of California bearing ratio by using soft computing systems. *Exp Syst Appl* 38(5):6381–6391
14. Akayuli CFA, Ofosu B (2013) Empirical model for estimating compression index from physical properties of weathered Birimianphyllites. *E J Geotech Eng* 18(Z):6135–6144
15. Viji VK, Lissy KF, Shobha C, Benny MA (2013) Predictions on compaction characteristics of fly ashes using regression analysis and artificial neural network analysis. *J Geotech Eng* 7(3):282–292
16. Borowiec A, Wilk K (2014) Prediction of consistency parameters of fen soils by neural networks. *Comput Assist Meth Eng Sci* 21(1):67–75
17. Bhatt S, Jain PK (2014) Prediction of California bearing ratio of soils using artificial neural networks. *Am J Res Sci Technol Eng Math* 8(2):156–161
18. Chore HS, Magar RB (2017) Prediction of unconfined compressive and Brazilian tensile strength of fiber reinforced cement stabilized fly ash mixes using multiple linear regression and artificial neural network. *Advances in Computational Design* 2(3):225–240. <https://doi.org/10.12989/ACD.2017.2.3.225>
19. IS: 2720 Part 5-1965, Determination of liquid limit and plastic limit. Bureau of Indian Standards (BIS), New Delhi
20. IS: 2720 Part 7-1983, Determination of water content—dry density relation using light compaction. Bureau of Indian Standards (BIS), New Delhi
21. IS: 2720 Part 10-1973, Determination of unconfined compressive strength. Bureau of Indian Standards (BIS), New Delhi

ANN Model for Prediction of Compressive and Tensile Strength of Bacterial Concrete



S. Varadharajan , S. V. Kirthanashri , Mohammad Shahban ,
Bishnu Kant Shukla , and Gaurav Bharti 

Abstract Concrete is a popular construction material in developing nations like India. Parameters like compressive, split tensile, and flexural strength are used to assess concrete's quality. Marble is widely used in India as a construction material. Processing of marble wastes around 30% of this stone. The marble waste powder can be disposed by utilizing it in concrete as a substitute of fine aggregate. Concrete post cracking behaviour has been improved by inclusion of marble and bacterial solution. Experimental data have been collected and used to suggest formulae for estimating concrete strength. The suggested equations correlated well with the experimental findings, demonstrating their accuracy.

Keywords Seismic response · Marble dust · Bacterial concrete

1 Introduction

Concrete manufacturing has risen dramatically in the last decade, resulting in increasing CO₂ emissions. Also, solid effluents like marble powder (WMP) pollute the environment [1–3, 7–14]. About 30% of marble is lost during its processing. Its fineness may block soil pores, preventing air and water flow. It can cause land infertility and will prevent ground water recharging. To address this problem, WMP was utilized to substitute fine aggregate in concrete up to 30%, and a bacterial solution was employed to improve post-cracking behaviour. Inclusion of WMP in concrete resulted in reduction of strength according to Costa et al. [7]. Arel [2] found increased strength and economy when fine aggregate were replaced 50% of WMP. Corinaldesi et al. [6] found that replacing 10% of WMP by fine aggregate increased cement

S. Varadharajan · M. Shahban · B. Kant Shukla · G. Bharti
JSS Academy of Technical Education, Noida, India
e-mail: gauravbharti@jssaten.ac.in

S. V. Kirthanashri (✉)
AIMMSCR, AmityUniversity, Noida, India
e-mail: kirthanasy@gmail.com

mortar strength Ulubeyli et al. [14] found that substituting 20% WMP for fine aggregate in concrete increased strength and durability. Kabeer and Vyas [9] reported similar findings. The inclusion of WMP in concrete increased fire resistance [10].

2 Experimental Programme and Discussion of Results

Ordinary portland cement was utilized as a binder in the current research [4, 5]. The material characteristics for OPC have been evaluated experimentally (Table 1). In this research work, crushed gravels of 20 and 10 mm in size were used as coarse aggregates. Table 2 lists the chemical properties of cement and WMP. Natural sand conforming to Zone 2 of BS 383 (Table 3) has been used as Fine aggregate. Figure 1 shows the sieve analysis findings for aggregates and WMP. WMP contains mostly dolomite, with minor amounts of calcium carbonate and silicon dioxide. Following earlier study, ureolytic bacteria were employed to improve post-cracking behaviour of concrete [13, 14]. To improve the characteristics of concrete, hooked end steel fibres were utilized. The mix design of concrete was based on IS 10262:2009 [5] as shown in Table 4. The compressive strength was determined experimentally by casting and breaking $150 \times 150 \times 150$ mm samples in a universal testing machine. The findings of the experiments show that the compressive strength of A1, A2, and A3 mixes increases by 12.12%, 14.24%, and 17.34% compared to reference mix (In which no WMP and bacterial solution was used). The equivalent rise in 28 day strength was 13.34%, 14.74%, and 16.35% (Fig. 2). Concrete cylinders were used to test split tensile strength. The samples are placed in the curing tank for 7 and 28 days. The findings of the experiment indicate that WMP increases compressive strength by 11.21%, 13.40%, and 17.45% for A1, A2, and A3 mixes, respectively. The equivalent increases in 28 day split tensile strength were 14.11%, 18.23%, and 21.34% (Fig. 3). An ANN model was used to estimate compressive and split tensile strength (Fig. 4). The bacterial solution increases the total strength by 7.93%, proving its effectiveness (as observed from results of B1, B2 & B3 mixes). The equations to estimate compressive and split tensile strength may be developed based on regression analysis of experimental data as shown below

$$f_c = 0.613 t + 265.45 s + 15.11 m + 15.45 \quad (1)$$

$$f_{sts} = 0.0431 t + 18.64 s + 3.89 m + 1.754 \quad (2)$$

where f_c is compressive strength, t is number of days, s is percentage of steel fibres, and m is percentage of WMP.

Experiment findings show excellent correlation with the suggested equation for estimating compressive and split tensile strength (Figs. 5 and 6; Table 5).

Table 1 OPC test results

Tests	Experimental value	Standards as per is 8112-1980
Normal consistency	28%	–
Initial setting time (min)	124	Not less than 30 min
Final setting time (min)	278	Not greater than 600 min
Fineness (m ² /kg)	249.89	
Specific gravity	3.14	–
<i>Compressive strength in Mpa</i>		
3 days	31.23	27
7 days	43.12	41
28 days	48.34	43

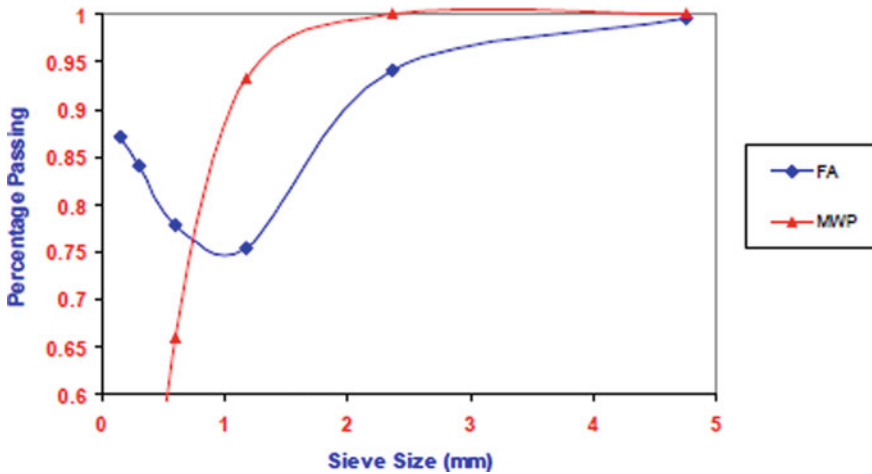


Fig. 1 Properties of FA and MWP

Table 2 Chemical composition of cement and MWP

Chemical composition	Cement	MWP
Calcium oxide	65.2	41.65
Silicon di oxide	22.16	5.98
Aluminium oxide	6.03	0.50
Iron oxide	2.67	0.86
Sulphur trioxide	0.86	0.15
Magnesium oxide	0.82	15.51
Potassium oxide	0.40	0.070
Sodium oxide	0.95	0.065

Table 3 Property of fine aggregate

Property	Coarse aggregates		Fine aggregates	
	20 mm	10 mm		
Specific gravity	2.69	2.75	2.54	2.63
Water absorption	0.88	0.94	1.62	1.82
Fineness modulus	6.87	6.45	2.53	2.43

Table 4 Details of mixes

Mix number	MWP (%)	Bacterial concentration
A1	10	Not present
A2	20	Not present
A3	30	Not present
B1	10	10 ⁶ per 'ml'
B2	20	10 ⁶ per 'ml'
B3	30	10 ⁶ per 'ml'

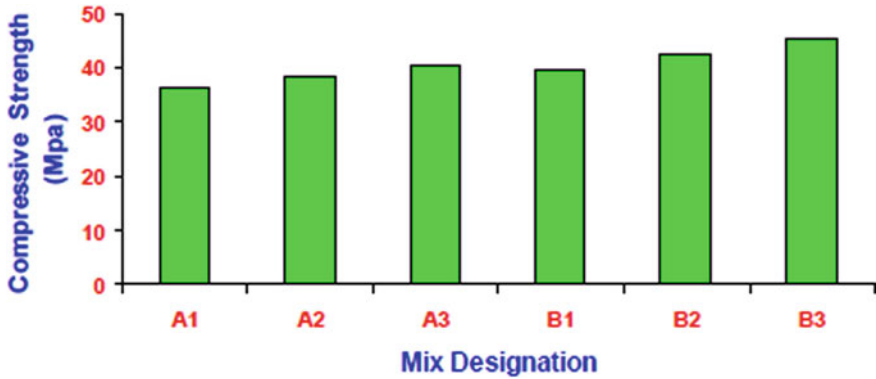


Fig. 2 Mean compressive strength results

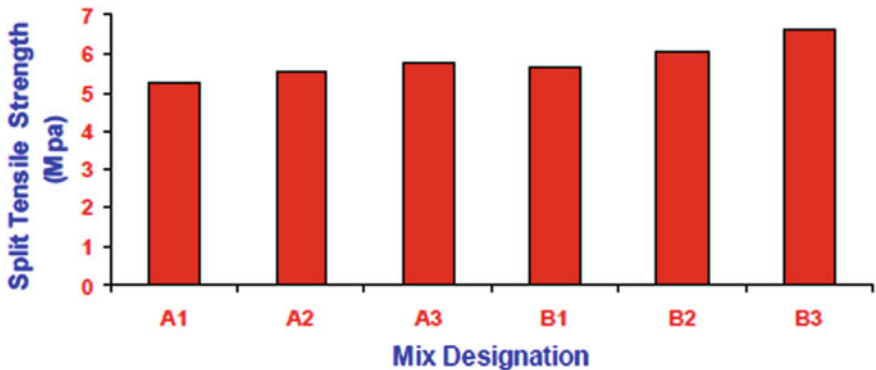


Fig. 3 Mean split tensile strength results

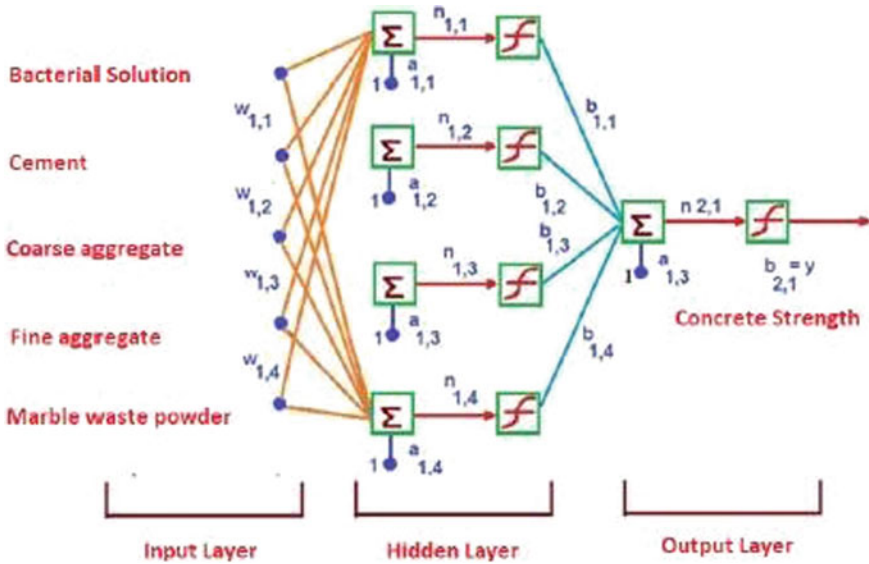


Fig.4 ANN model adopted

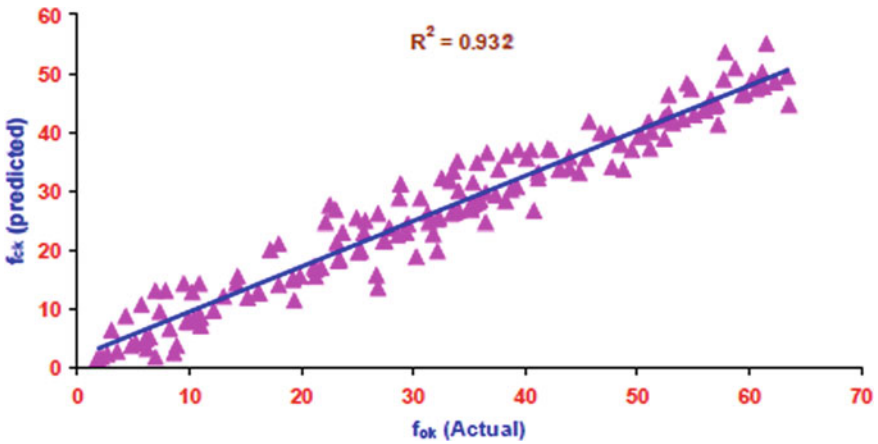


Fig. 5 Comparison between actual and predicted compressive strength

3 Conclusions

This study aims to utilize byproducts as WMP into concrete to make it more cost-effective and eco-friendly. Concrete strength has been enhanced with ureolytic bacteria and hooked steel fibres. To forecast compressive and split tensile strength, an ANN model is used on the experimental data to propose new equations. The

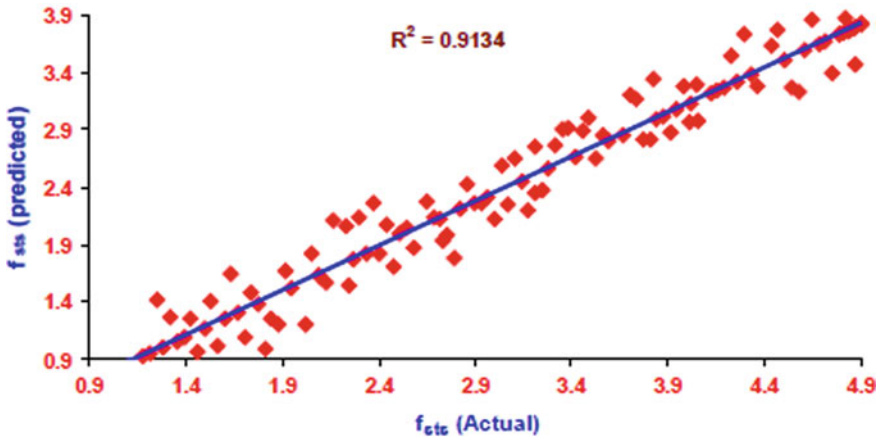


Fig. 6 Comparison between actual and predicted split tensile strength

Table 5 Correlation percentage for proposed equations of compressive and split tensile strength

Type of frame	Experimental result	Data from previous research works
Compressive strength predicting equation	0.9321	0.63435
Split tensile strength predicting equation	0.9134	0.63767

inclusion of WMP improves the mechanical strength of concrete. The addition of bacterial solution and steel fibres also enhance strength characteristics. The ANN model equations presented had good correlation with experimental findings and may be used to forecast concrete strength characteristics.

References

1. André A, de Brito J, Rosa A, Pedro D (2014) Durability performance of concrete incorporating coarse aggregates from marble industry waste. *J Cleaner Prod* 15(65):389–396
2. Arel HŞ (2016) Recyclability of waste marble in concrete production. *J Cleaner Prod* 10(131):179–188
3. Ashish DK (2018) Feasibility of waste marble powder in concrete as partial substitution of cement and sand amalgam for sustainable growth. *J Build Eng* 15:236–242
4. BIS 8112 (2013) Ordinary Portland cement, 43 grade-specification. Bureau of Indian Standards, New Delhi
5. BIS-10262 Guidelines for concrete mix proportioning. Bureau of Indian Standards, New Delhi.
6. Corinaldesi V, Moriconi G, Naik TR (2010) Characterization of marble powder for its use in mortar and concrete. *Constr Build Mater* 24(1):113–117

7. Costa J, Pinelo C, Rodriguez A (1991) Characterization of the Estremoz, Borba and Vila Viçosa region marble quarrying dump ins NPR/GERO. Natl Lab Civ Eng Lisbon Port
8. Gameiro F, De Brito J, da Silva DC (2014) Durability performance of structural concrete containing fine aggregates from waste generated by marble quarrying industry. *EngStruct* 1(59):654–662
9. Kabeer KS, Vyas AK (2018) Utilization of marble powder as fine aggregate in mortar mixes. *Constr Build Mater* 20(165):321–332
10. Keleştemur O, Arıcı E, Yıldız S, Gökçer B (2014) Performance evaluation of cement mortars containing marble dust and glass fiber exposed to high temperature by using Taguchi method. *Constr Build Mater* 16(60):17–24
11. Mishra A, Pandey A, Maheshwari P, Chouhan A, Suresh S, Das S (2013) Green cement for sustainable concrete using marble dust. *Int J ChemTech Res, CODEN (USA): IJCRGG*. ISSN: 0974–4290
12. Rodrigues RD, De Brito J, Sardinha M (2015) Mechanical properties of structural concrete containing very fine aggregates from marble cutting sludge. *Constr Build Mater* 77:349–356
13. Siddique R, Kaur G (2016) Strength and permeation properties of self-compacting concrete containing fly ash and hooked steel fibres. *Constr Build Mater* 103:15–22
14. Ulubeyli GC, Bilir T, Artir R (2016) Durability properties of concrete produced by marblewaste as aggregate or mineral additives. *Procedia Eng* 1(161):543–548

Ring Foundation—A Review



Prince Karandeep Singh and Arvind Kumar

Abstract Ring foundations support different types of onshore and offshore structures like towers, chimneys, windmills, OHSRs, etc. Numerous experimental, analytical and numerical studies were performed to determine parameters like bearing capacity factors and bearing capacity equation for ring footing and to understand the behavior of ring footing and behavior of soil under application of applied load. The main aim of the present study is to gather the information regarding behavior of ring footing under the influence of various factors like variation of inside diameter with respect to the outside diameter, stiffness of soil and ring footing, the effect of soil reinforcement and inclined and eccentric load. Furthermore, more weightage is given to numerical modeling of soil media and ring footing and comparison of experimental, analytical and numerical studies used to compute ring footings' behavior and bearing capacity factors.

Keywords Ring footing · Bearing capacity factors · Elastic analysis · Soil structure interaction analysis

1 Introduction

As India is a developing economy, residential complexes and industrial units are increasing day by day, leading to an increase in construction of more OHSRs, chimneys, towers, etc. There are various government norms related to the height of the chimney, towers, etc., and for example, as per the government of India, specification height of the thermal power plant chimney should not be less than 275 m. For such a round type of structure, ring foundation may serve the purpose. Moreover, a ring foundation also saves the material as compared to a circular foundation. The geometry of ring footing gives more uniform contact pressure and soil reactions. Several

P. K. Singh (✉) · A. Kumar
NIT, Jalandhar, India
e-mail: princekss.ce.18@nitj.ac.in

© The Author(s), under exclusive license to Springer Nature Singapore Pte Ltd. 2023
A. K. Agnihotri et al. (eds.), *Proceedings of Indian Geotechnical and Geoenvironmental Engineering Conference (IGGEC) 2021, Vol. 1*, Lecture Notes in Civil Engineering 280,
https://doi.org/10.1007/978-981-19-4739-1_32

341

investigators [1–2] performed laboratory as well as in situ tests and numerical analysis to study the behavior of ring footings supported by unreinforced and reinforced soil under vertical, inclined and eccentric loads.

Majority of studies reveal that the bearing capacity of ring foundation is function of soil stiffness, radii ratio (r_i/r_o) and degree of eccentricity, embedment ratio, angle of internal friction, angle of dilatancy, base roughness of ring footing, degree of heterogeneity, etc. Various attempts have been made to derive equations, design charts and tables for bearing capacity factors [1, 3, 4, 5–6] of smooth and rough ring footing by different methods such as stress characteristics method (SCM), finite element method (FEM) and finite difference method (FDM) and with the help of various software like Flac Model, Plaxis, Abaqus and Matlab. In the present study, an attempt has been made to collect the relevant information regarding ring footing to help the researchers choose suitable study and design.

Table 1 shows different researchers' findings with title, author's name, methods of investigation, soil type and description of work.

2 Experimental Investigations

An attempt has been made by various authors [29, 27, 13–18, 28] to establish the relation between BCR/bearing capacity and radii ratio of r_i/r_o for cohesionless and cohesive soils. Effect of eccentricity, number of reinforcement layers and reinforcing the soil with fiber reinforcement on the behavior of ring footing were also studied. BCR_{UR} (bearing capacity ratio) for unreinforced soil is defined as under:

$$\frac{\text{Bearing capacity of ring footing resting on unreinforced soil}}{\text{Bearing capacity of circular footing resting on unreinforced soil}}$$

or

BCR_R (bearing capacity ratio) for reinforced soil is defined as under:

$$\frac{\text{Bearing capacity of ring footing resting on reinforced soil}}{\text{Bearing capacity of ring footing resting on unreinforced soil}}$$

Following factors have been considered during experimental investigation by different researchers.

2.1 Radii Ratio (r_i/r_o)

Hataf and Razavi [29] found that maximum ultimate bearing capacity of ring footing does not occur at defined value of r_i/r_o but in a range of 0.2–0.04. Demir et al. [16] tried to establish the relation between bearing capacity of cohesive soil and r_i/r_o .

Table 1 Findings of different researcher

S./No.	Author	Methods of investigation	Soil type	Discussion
1	Becker [7]	Experimental investigation	Clay	Carried out the case study of 22 m high concrete silo supported by a ring footing of external diameter 9 m resting on clay. The main aim of this study was to measure pore pressure, pressure distribution and settlement of ring footing during the construction process. It was observed that stresses developed below ring footing were linear up to one-third height of the silo, and after that, increase in stress was at rapid rate. During the construction process, significant dissipation of pore pressure was observed, and the rate of dissipation was also rapid after construction
2	Madhav [1]	Elastic analysis	Sand	Developed the settlement equation and allowable pressure for ring footing with an assumption of ring footing supported by semi-infinite elastic space
3	Hasan et al. [8]	Experimental investigation	Sand	A series of plate load tests were conducted on very dense calcareous sand for the construction of a 370 m high tower antenna and a 61 m high telecommunication building. For plate load test, radii ratio of ring plate was kept equal to the actual ring footing and the three different sizes of circular plates were used. The main aim of these tests was to find out the soil modulus so that settlement of these structures can be predicted. Various factors like ground wetting and size of loading area were considered

(continued)

Table 1 (continued)

S./No.	Author	Methods of investigation	Soil type	Discussion
4	Ismael [9]	Experimental investigation	Sand	Plate load test was carried out on 0.6 m outer diameter of ring and circular footing resting on dense cemented sand at depth of 0.4 m. Ring footing of different radii ratios was used. It was observed that settlement of ring footing was smaller than the circular footing under applied pressure
5	Hajjani and Hataf [5]	Experimental and numerical investigation	Sand	Both laboratory and numerical studies were carried out to evaluate the performance of ring and circular footing resting on sand, reinforced with biaxial geogrid. Parameters for the study include number of reinforcement layer (N), depth of first layer (a), spacing between the reinforcement and effect of increasing stiffness of reinforcement
6	Saran et al. [10]	Indian geotechnical journal	Sand	Proposed an analytical procedure for the prediction of tilt and vertical settlement of smooth ring footing resting on sand under the application of eccentric and inclined load by using nonlinear constitutive approach. Model tests were also performed to validate the same. Proposed an analytical procedure using nonlinear constitutive law for the calculation of pressure-settlement and pressure tilt of ring footing resting on cohesionless soil subjected to eccentric and inclined loading

(continued)

Table 1 (continued)

S./No.	Author	Methods of investigation	Soil type	Discussion
7	Kumar and Ghosh [11]	Numerical investigation	C- ϕ soil	Value of N_p was determined for ring footing with smooth and rough base by using method of stress characteristics with an assumption of angle of friction (δ) at interface of base of rough ring footing and cohesionless soil, where value of δ gradually increases from zero at axis of symmetry to value of ϕ at outer edge of ring footing
8	Laman and Yildiz [12]	Numerical investigation	Sand	Numerical modeling was done to understand the behavior of ring footing resting on sand with/without geogrid reinforcement. Hardening soil model was adopted. The factors like depth of first layer (u), number of layer and size of reinforcement were studied
9	Zhao and Wang [13]	Numerical investigation	C- ϕ soil	Value of N_p was determined for ring footing with smooth and rough bases resting on cohesionless soil. The soil was assumed as an elastic–plastic material and follows Mohr–Coulomb model and an associative flow rule

(continued)

Table 1 (continued)

S./No.	Author	Methods of investigation	Soil type	Discussion
10	Choobbasti et al. [14]	Numerical investigation	Clay	Numerical analysis was carried out to find bearing capacity and bearing capacity factors of ring footing resting on cohesive soil using Plaxis software. The Mohr–Coulomb model was followed. Bearing capacity was calculated for depth of 200 m
11	Sawwaf and Nazir [15]	Experimental investigation	Sand	The effects of partial replacement of weak soil with soil compacted at different relative densities. Ring footing was subjected to both vertical and lateral loading. Configuration like number of geogrid layer in compacted soil, stiffness of geogrid and different radii ratios was studied
12	Demir et al. [16]	Filed tests	Clay	Field tests were conducted on natural clay using rigid ring footing for different radii ratios. Outer diameter of ring footing was fixed at 200 mm, and different inner diameters of ring foundation were used to evaluate the effect of changing radii ratio of ring footing on load carrying capacity of soil
13	Benmebarek et al. [17]	Numerical investigation	Soil	The value of N_y was calculated for rough and smooth ring footings for low and high friction soils that follow associated and non-associated flow rule. Effect of dilatancy angle on the N_y was also taken in account

(continued)

Table 1 (continued)

S./No.	Author	Methods of investigation	Soil type	Discussion
14	Moayed et al. [3]	Numerical investigation	Clay	Numerical analysis was performed to analyze the behavior of ring footing resting on soft clay overlays a cohesionless soil. Effects of cohesive layer thickness and radii ratio were considered. It was found that ultimate bearing capacity of ring footing reduces with increase in radii ratio and thickness of clay layer
15	Naderi and Hataf [18]	Experimental and numerical investigation	Sand	Numerical and experimental study was done to evaluate the interference effect of two closely spaced circular and two closely spaced ring footings supported by soil reinforced with single geogrid layer. The effect such as interference, shapes of footing, horizontal spacing between footings and depth geogrid layer was evaluated. Mohr–Coulomb model was followed for the numerical study
16	Naseri and Hosseiniia [19]	Elastic analysis	Soil	Numerical investigation was carried out using finite differential method to analyze the settlement of ring footing resting supported by elastic half space. Displacement influence factors were introduced to calculate the settlement of ring footing. The influence factors used in this study mainly address the stiffness of footing, geometry of ring, soil non-homogeneity and footing embedment, and it was assumed that elastic modulus of soil exhibits linear relation with depth. A proposed a formula that can predict the elastic settlement of flexible and rigid ring footing resting on cohesive and cohesionless soils
17	Kumar and Chakraborty [4]	Numerical investigation	C- ϕ soil	Bearing capacity factors were computed by considering the components of cohesion, unit weight and surcharge for ring footing with both rough and smooth bases for combinations of radii ratio between 0 and 1 and for different angle of friction by using lower and upper bound theorems limit analysis in concurrence with limit optimization and finite elements

(continued)

Table 1 (continued)

S./No.	Author	Methods of investigation	Soil type	Discussion
18	Hosseiniinia [20]	Numerical investigation	C- ϕ soil	Bearing capacity factors were determined using finite differential method (FDM) with an assumption of rough and smooth base underneath the ring footing
19	Lee et al. [21]	Numerical investigation	Clay	The value N_c (bearing capacity factor) was evaluated for rough ring footing by taking the effect of radii ratio, soil heterogeneity and embedment ratio. Numerical solution for bearing capacity factor was established using small strain finite element method
20	Lee et al. [22]	Numerical investigation	Clay	Small displacement finite element analysis was used to evaluate the undrained bearing capacity of two-layered soil for both homogenous and linearly increasing shear strength. Ratio of the shear strength of topsoil to bottom soil (sut/sub) varied from 0.25 to 5; ratio of depth of top layer soil to outer diameter of ring footing (H/D) varied from 0.25 to 5. The degree of soil non-homogeneity varied from 0 to 4
21	Remadna et al. [23]	Numerical investigation	C- ϕ soil	Attempt was made to determine value of N_c for ring footing with smooth and rough bases for both low and high friction associated and non-associated soils that follow Mohr–Coulomb model
22	Sharma and Kumar [24]	Experimental investigation	Sand	Laboratory model plate test was performed on ring and circular footing supported by randomly distributed fiber reinforced sand (RDFS) layer underlain by loose sand to evaluate the effect of variation in relative density on top and bottom layer. Effect of variation in radii ratio of ring footing, thickness of fiber reinforced layer and percentage of fiber in fiber reinforced layer were studied

(continued)

Table 1 (continued)

S./No.	Author	Methods of investigation	Soil type	Discussion
23	Sargazi and Hosseininia [25]	Numerical investigation	Sand	Using FDM, numerical study was performed to evaluate the bearing capacity of ring footing with rough base footing subjected to eccentric load resting on cohesionless soil. Reduction method factor was applied to evaluate the effect of eccentric loading. Mohr–Coulomb criteria were followed
24	Gholami and Seyed [6]	Numerical investigation	$C-\phi$ soil	Bearing capacity factors for ring foundation were developed by writing codes using stress characteristics method. Soil was considered as frictional-cohesive and follows Mohr–Coulomb criteria, and moreover, the effect of unit weight and surcharge was also considered
25	Sharma and Kumar [26]	Experimental investigation	Sand	Shear parameters were determined by conducting the laboratory large shear box and triaxial test for sand that was reinforced with different percentage of fiber reinforcement. These shear parameters were used to calculate the ultimate bearing capacity of ring footing by modifying the already available equation of ultimate bearing capacity of ring footing given by kakroo (1985)
26	Keshava and Kumar [27]	Numerical investigation	$C-\phi$ soil	Bearing capacity factors for ring footing with smooth and rough base were computed with help of stress characteristics method (SCM) by simulating stress singularities at inner and outer edge of ring footing. Computer code was written in Matlab for determining the bearing capacity factors. Prandtl type of failure mechanism for smooth ring footing and curvilinear non-plastic wedge mechanism for rough ring footing was employed

(continued)

Table 1 (continued)

S./No.	Author	Methods of investigation	Soil type	Discussion
27	Sharma and Kumar [2]	Numerical investigation	Sand	Numerical analysis was carried out for ring footing supported by two-layered soil. Only top layer of soil was reinforced with fiber. Parameters included for the study were shape of footing (circular or ring), thickness of top reinforced layer, variation of relative densities between top and bottom sand layers and scale effect. It was found that bearing capacity increases as the radii ratio of ring footing increased from 0 to 0.4
28	Chavda and Doddegoudar [28]			Bearing capacity factors of ring footings were examined from asymmetric to the plain strain solutions using finite element analysis. Based from findings of finite element results, some guidelines were provided regarding (a) the proper choice of the equation for ultimate bearing capacity of ring footing, (b) the effect of Poisson's ratio and Young's modulus on the ultimate bearing capacity and (c) the dependency of bearing capacity factor N_{γ} on the width of ring footing. A equation was proposed for calculating the ultimate bearing capacity of ring footing

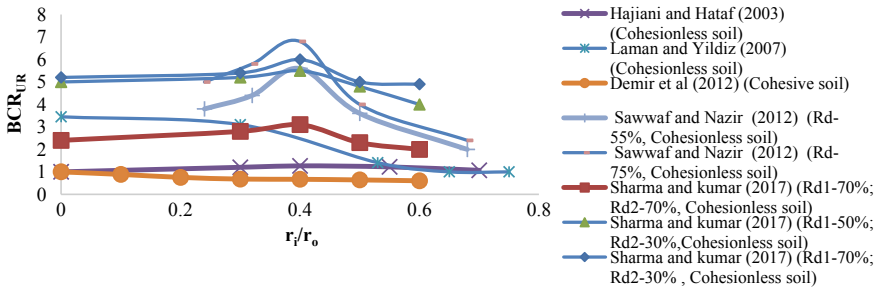


Fig. 1 BCR versus r_i/r_o

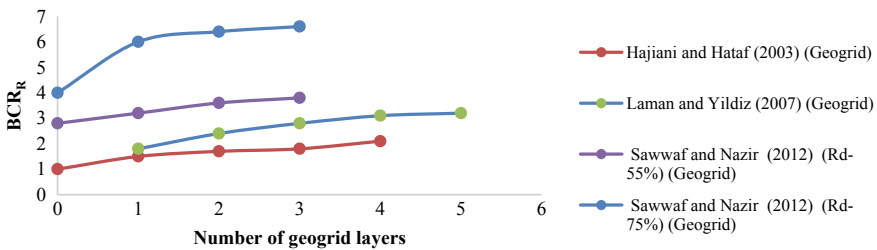


Fig. 2 BCR versus number of geogrid layers

Figure 1 clearly states that as r_i/r_o (r_i and r_o are inner and outer radius of ring footing) increases to 0.4, significant drop in bearing capacity of clay was observed but this trend became steady as the radii ratio r_i/r_o increased beyond 0.4. It was recommended that optimum value of r_i/r_o equal to 0.4 can be used for clays.

Figure 1a shows that as the radii ratio (r_i/r_o) increases to 0.35–0.4, BCR_{UR} of cohesionless soil increases irrespective of relative density of soil.

2.2 Number of Reinforcement Layers

Figure 2 shows that as the number of geogrid reinforcement layers increases in range between 3 and 4, BCR_R of ring footing increases [29, 13, 16].

2.3 Depth of First Layer of Reinforcement (U)

Figure 3 shows that placing the first layer of reinforcement approximately at depth of 0.15–0.3 times D_o (outer diameter of ring footing) results maximum benefits in terms of bearing capacity and placing the first layer of reinforcement beyond 0.5

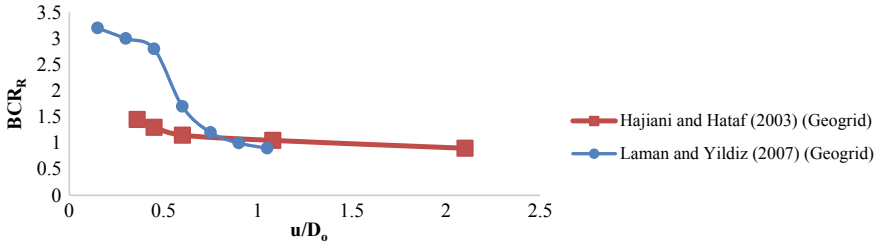


Fig. 3 BCR versus depth of first layer of reinforcement (u)

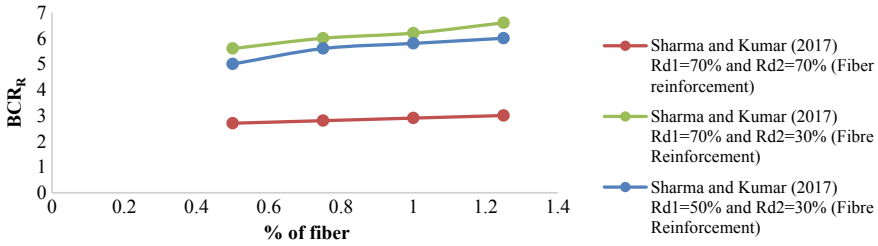


Fig. 4 BCR versus percentage of fiber reinforcement

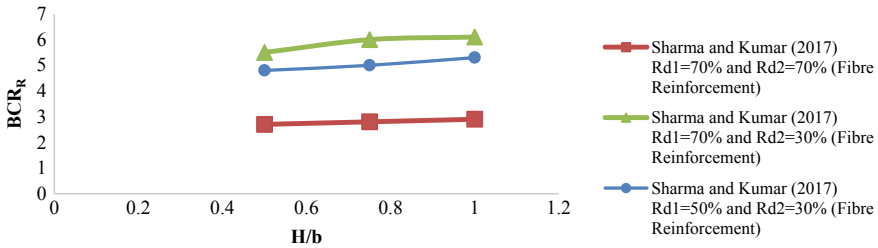


Fig. 5 BCR versus depth fiber reinforced layer (RDFS) (H)

D_o has no significant effect on bearing capacity ratio [29, 13]. With the placing of reinforcement layer in range between 0.45 and $0.75 D_o$, BCR_R reduces significantly as shown in Figs. 3, 4 and 5.

2.4 Eccentric Load

Figure 6 shows the two different views; first, bearing capacity ratio of ring footing increases with increase in eccentricity up to $0.1 D_o$ and beyond $0.1 D_o$ BCR_R becomes nearly constant [16]; and second, ultimate load of loose sand decreases more as

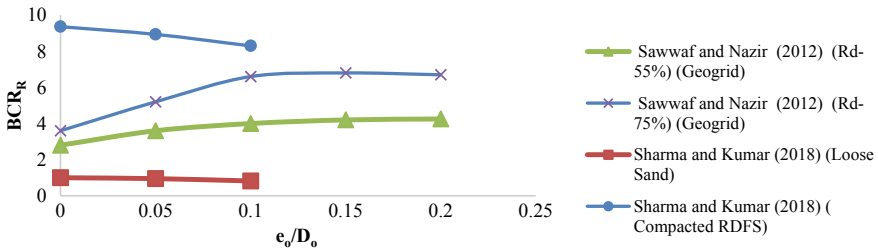


Fig. 6 BCR versus effect of eccentricity on ring footing

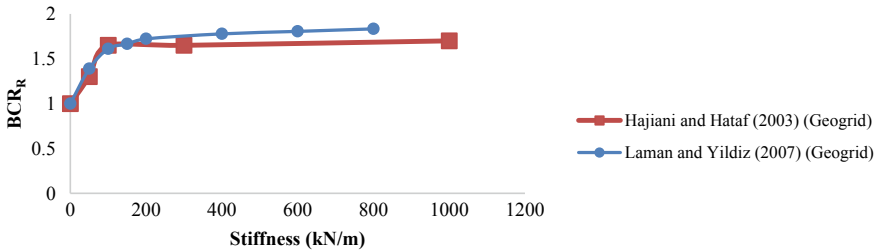


Fig. 7 BCR versus stiffness of geogrid

compared to compacted fiber reinforced sand underlain by loose sand with increase in eccentricity [28].

2.5 Stiffness of Reinforcement Layer

Figure 7 shows that bearing capacity ratio (BCR_R) increases with increase in the stiffness of reinforcement up to critical and beyond critical it becomes constant [29, 13].

3 Bearing Capacity Factor

3.1 General

The bearing capacity of ring footing theoretically is being calculated by means of bearing capacity factors N_c , N_q and N_γ by using the conventional Teragazhi's equation. Nowadays, numerical method along with analytical methods is being employed to solve the more complex problems such as ultimate bearing capacities of ring footing.

Figure 8a, b shows the variation of N_y w.r.t r_i/r_o , and Fig. 8c, d shows variation of N_c w.r.t r_i/r_o for different φ values for both smooth and rough ring footing. Figure 8a–d also shows different software techniques and soil conditions (i.e., c - φ , clay and sand) used by different researchers to compute the bearing capacity factors. It was found that most of researchers gave different values of bearing capacity factors at same radii ratio r_i/r_o .

Following variables have been included in calculating value of bearing capacity factors by various authors.

3.2 Angle of Friction and r_i/r_o

Figure 8a, b shows that bearing capacity factors N_y for ring footing with smooth base [3, 14, 6] and rough base [3, 30, 14, 6] decrease with increase in radii ratio r_i/r_o . Some researchers [30, 20, 21] found that change in value of N_y for smooth ring and rough ring footing [2, 20] with respect to variation of radii ratio depends upon angle of internal friction (φ). For some degree of φ , its value may increase, and for another degree of φ , its value may decrease with increase in radii ratios. Figure 8c, d [20, 6, 26] shows that value of N_c for smooth and rough base ring footing decreases with increase in radii ratios. Variation in value of N_c for smooth ring footing [22, 24] and rough ring footing [26] with respect to change in radii ratio is function of angle of internal friction. Some authors [22, 24] observed that value of N_c for rough ring footing first increases with increase in value of radii ratio up to some certain range; after that, it decreases with increase in radii ratio. Most of authors [3, 30, 14, 21, 24, 23, 26] concluded that value of bearing capacity factors N_c and N_y for both smooth and rough base ring footing increases with increase in angle of internal friction.

3.3 Footing Roughness

Kumar and Ghosh [11] assumed following three distributions for calculation of δ .

1. Parabolic concave
2. Linear
3. Parabolic convex.

Maximum value of N_φ was for parabolic convex distribution of δ (angle of dilation), and minimum value of N_y was for parabolic concave distribution of δ . The pressure distribution is maximum for axis of symmetry and is lowest at outer edge of ring footing.

For rough ring footing, bearing capacity factors become maximum for radii ratio of 0.2 [23]. On increasing the internal radius of ring footing up to r_i/r_o of 0.2, collapse load does not show any reduction for a given value of r_o for rough bases but in case of smooth bases, magnitude collapse load decreases continuously with increase in

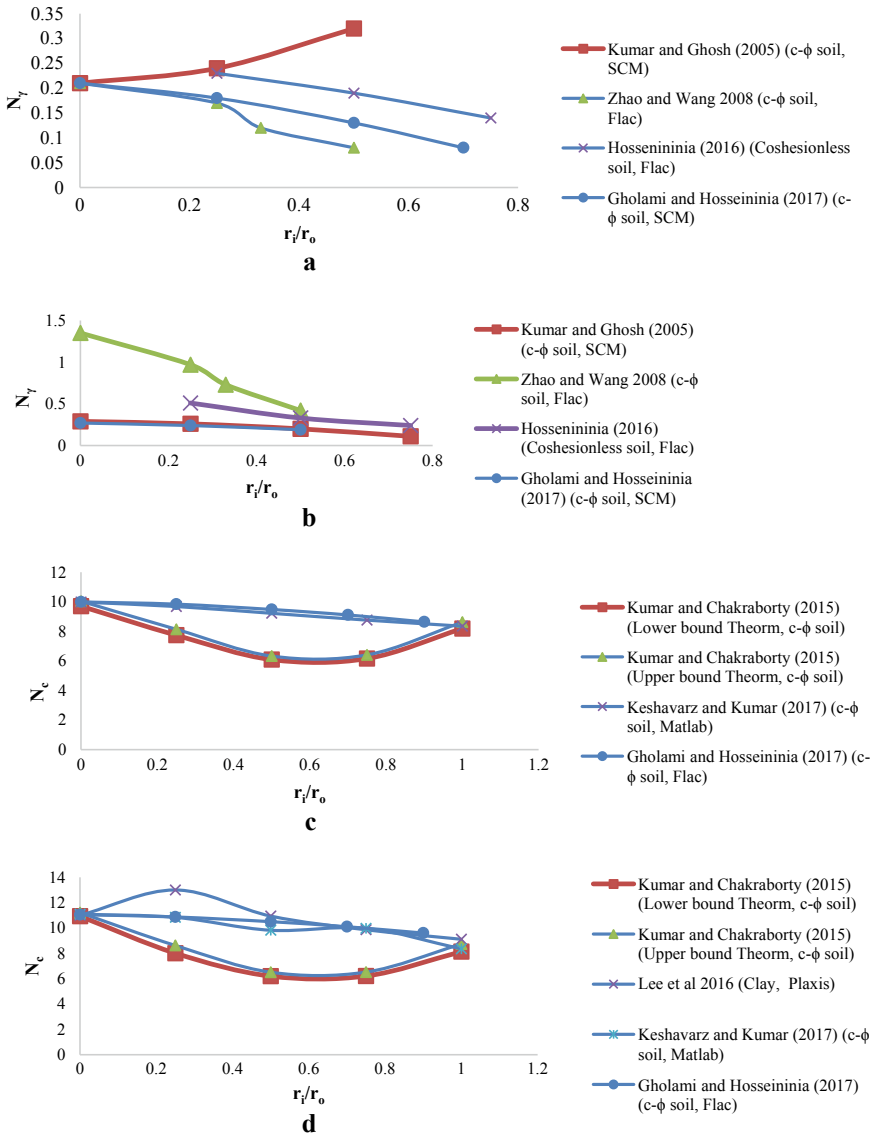


Fig. 8 **a** N_γ versus r_i/r_o for smooth ring footing ($\varphi = 10^\circ$), **b** N_γ versus r_i/r_o for rough ring footing ($\varphi = 10^\circ$), **c** N_c versus r_i/r_o for smooth ring footing ($\varphi = 10^\circ$), **d** N_c versus r_i/r_o for rough ring footing ($\varphi = 10^\circ$)

radii ratio [20]. It means instead of full circular footing, a ring footing with rough bases can be employed by keeping the radii ratio up to r_i/r_o 0.2 [20].

Value of N_c is highly influenced by angle of dilation for soil that exhibits high non-associativity for higher range of φ [24]. For low friction soil, optimum value of N_c was obtained at r_i/r_o equal to 0.26, and for medium and high friction soil, N_c reaches the optimum value at r_i/r_o equal to 0.33 and 0.46, respectively [24]. Dilation angle does not affect the optimized value of r_i/r_o except for low friction soil; for low friction soil, optimized value of r_i/r_o decreases with increase in dilation angle [24].

For rough footing, maximum value of N_c and N_y lies in the range of radii ratio 0.1–0.5 [26]. As the value of radii ratio is reduced from 1 to 0, failure mechanism becomes asymmetrical [26].

The values of N_y for smooth ring computed by Gholami and Seyedi [6] were nearly close to the values given by Kumar and Ghosh [11] and Zaho and Wang [13] but in case of rough footing conditions, there is a considerable difference between the values of N_y .

3.4 Degree of Soil Heterogeneity and Embedment Ratio

The degree of soil heterogeneity is described by the non-dimensional factor kB/S_{um} (k is the strength gradient, S_{um} is undrained strength at surface, and B is width of footing) [23]. At lower value of embedment ratio D/B (D is the depth of footing), N_c values are higher and N_c increases with increase in kB/S_{um} [23]. Finite element displacement diagram shows that with decrease in radii ratio, plastic zone increases and with increase in embedment ratio (D/B), surface failure transforms into cavity mode failure [23]. Moreover, effect of φ on N_c is more prominent at lower value of r_i/r_o and at higher value of D/B and kB/S_{um} [6].

3.5 Strength Ratio

The value N_c increases with decrease in strength ratio, and effect is more significant in higher range of r_i/r_o but independent of H/D (H is the thickness of topsoil layer) [22]. For strength ratio (s_{u0-t}/s_{u0-b}) less than unity, value of N_c reduces for $H/D < 0.25$ and this effect is more prominent for small value of r_i/r_o . If strength ratio is greater than unity, N_c value increases with increase in H/D ratio, and effect is more prominent for small value of r_i/r_o .

3.6 Eccentricity

In order to obtain effect of eccentric load on ultimate bearing capacity of footing, a reduction factor was introduced which is multiplied to the ultimate bearing capacity obtained under vertical loading to get the ultimate bearing capacity under eccentric loading [6]. Reduction factor is defined as

$$R_f = 1 - \exp[0.4(1 - n)(e^o/D_o)^{0.5}] \quad (1)$$

Moreover, the reduction factor only depends upon the radii ratio of ring footing, where n is the radii ratio.

4 Critical Appraisal

More emphasis has been given to understanding the behavior of ring footings resting on cohesionless soil. More work needs to be done to comprehend the behavior of ring footings under the effect of different loading conditions. Very little work has been done to understand the response of ring footing resting on clay under the application of vertical load. The behavior of ring footing under eccentric and inclined load supported by the clay bed still needs to be understood.

A little emphasis has been given to knowing the effect of depth of ring footing, effect of angle of inclination of load, shape factor, bearing capacity factor N_q and formation of stress pressure bulb underneath the ring footing.

Moreover, bearing capacity factors such as N_c and N_γ calculated by various authors seem to be not so reliable because various authors used different methods to calculate bearing capacity factors. As each author has given different values of these factors at the same radii ratio, it is difficult to generalize any author's findings, so calculating the theoretical ultimate bearing capacity for ring footing becomes difficult. Few researchers considered the effect of dilatancy and eccentricity for ring footing while calculating the values of bearing capacity factor N_γ . Effect of soil heterogeneity, embedment ratio, strength ratio, etc., have not been taken in account for calculating the value of N_γ . In the case of N_c , the effect of eccentricity has not been explored yet.

5 Conclusions

The main conclusion of the review is as follows:

- Most laboratory model tests indicate that load carrying capacity of ring footing resting on cohesionless soil increases with an increase in radii ratio in a range of 0.3–0.4. Beyond 0.3–0.4 radii ratio, bearing capacity decreases.

- The bearing capacity factors increase with the increase in the angle of soil but decrease with an increase in radii ratios.
- The N_c , N_q and N_γ for ring footing with a rough base are higher than with a smooth base.
- As mentioned earlier, different authors gave different values of N_c , N_q and N_γ at the same radii ratios, so it becomes challenging to calculate the bearing capacity for the ring raft.
- More emphasis was given to calculating the N_γ and N_c under different soil and loading conditions. On the other hand, very little work has been done in the case of N_q .

References

1. Madhav MR (1980) Settlement and allowable pressures for ring or annular footings. *Ind Geotech J* 10(3):267–271
2. Sharma, V, Kumar A (2018) Behavior of ring footing resting on reinforced sand subjected to eccentric-inclined loading. *J Rock Mech Geotech Eng* 2018:1–11. <https://doi.org/10.1016/j.jrmge.2017.11.005>
3. Moayed ZM, Rashidian V, Ehsan I (2018) Evaluation on bearing capacity of ring foundations on two-layered soil. *World Acad Sci Eng Technol* 61:1108–1112
4. Kumar J, Chakraborty M (2015) Upper-bound axisymmetric limit analysis using the Mohr-Coulomb yield criterion, finite elements, and linear optimization. *J Eng Mech* 140(12):1–8. [https://doi.org/10.1061/\(ASCE\)EM.1943-7889.0000820](https://doi.org/10.1061/(ASCE)EM.1943-7889.0000820)
5. Hajiani J, Hataf N (2003) Experimental and numerical investigation of the bearing capacity of model circular and ring footings on reinforced sand. *Geotext Geomembr* 21(4):241–256. [https://doi.org/10.1016/S0266-1144\(03\)00029-3](https://doi.org/10.1016/S0266-1144(03)00029-3)
6. Gholami H, Seyedi E (2017) Bearing capacity factors of ring footings by using the method of characteristics. *Geotech Geol Eng*. <https://doi.org/10.1007/s10706-017-0233-9>
7. Becker DE (1979) Pore-pressure response beneath a ring foundation on clay. *Can Geotech J* 16:551–566
8. Hasan A, Al-Sanad INF, Brenner RP (1993) Settlement of circular and ring plates in very dense calcareous sands. *J Geotech Eng* 119(4):622–638
9. Ismael NF (1996) Loading tests on circular and ring plates in very dense. *J Geotech Eng* 122:281–287. [https://doi.org/10.1061/\(ASCE\)1090-0241\(1997\)123:10\(990\)](https://doi.org/10.1061/(ASCE)1090-0241(1997)123:10(990))
10. Saran S, Bhandari NM, Al-Smadi MMA (2003) Analysis of eccentrically–obliquely loaded ring footings on sand. *Indian Geotech J* 33(4):422–446
11. Kumar J, Ghosh P (2005) Bearing capacity factor N_γ for ring footings using the method of characteristics. *Can Geotech J* 42(5):1474–1484. <https://doi.org/10.1139/t05-051>
12. Laman M, Yildiz A (2007). Numerical studies of ring foundations on geogrid-reinforced sand. *Geosynthetics Int* 14(2):52–64. <https://doi.org/10.1680/gein.2007.14.2.52>
13. Zhao L, Wang JH (2008) Vertical bearing capacity for ring footings. *Comput Geotech* 35(2):292–304. <https://doi.org/10.1016/j.compgeo.2007.05.005>
14. Choobbasti AJ, Najafi A, Pirzadeh S, Farrokhzad F, Zahmatkesh A (2010) Numerical evaluation of bearing capacity and settlement of ring footing :case study of Kazeroon cooling towers. *Int J Res Rev Appl Sci* 4:263–271
15. SawwafEl M, Nazir A (2012) Behavior of eccentrically loaded small-scale ring footings resting on reinforced layered soil. *J Geotech Geoenviron Eng* 138(3):376–384. [https://doi.org/10.1061/\(ASCE\)GT.1943-5606.0000593](https://doi.org/10.1061/(ASCE)GT.1943-5606.0000593)

16. Demir A, Örnek M, Laman M, Yıldız A (2012) Analysis of ring footings using field test results. In: 3rd international conference on new developments in soil mechanics and geotechnical engineering, 28–30 June 2012, Near East University, Nicosia, North Cyprus
17. Benmebarek S, Remadna MS, Benmebarek N, Belounar L (2012) Numerical evaluation of the bearing capacity factor N_{γ} of ring footings. *Comput Geotech* 44:132–138. <https://doi.org/10.1016/j.compgeo.2012.04.004>
18. Naderi E, Hataf N (2014) Model testing and numerical investigation of interference effect of closely spaced ring and circular footings on reinforced sand. *Geotext Geomembr* 42(3):191–200. <https://doi.org/10.1016/j.geotextmem.2013.12.010>
19. Naseri M, Ehsan SH (2015) Elastic settlement of ring foundations. 55(2):284–295. <https://doi.org/10.1016/j.sandf.2015.02.005>
20. Hosseininia ES (2016) Bearing capacity factors of ring footings. *Iran J Sci Technol Trans Civ Eng Eng*. <https://doi.org/10.1007/s40996-016-0003-6>
21. Lee JK, Jeong S, Lee S (2016) Undrained bearing capacity factors for ring footings in heterogeneous soil. *Comput Geotech* 75:103–111. <https://doi.org/10.1016/j.compgeo.2016.01.021>
22. Lee JK, Jeong S, Shang JQ (2016) Undrained bearing capacity of ring foundations on two-layered clays. *Ocean Eng* 119:47–57. <https://doi.org/10.1016/j.oceaneng.2016.04.019>
23. Remadna MS, Benmebarek S, Benmebarek N (2016) Numerical evaluation of the bearing capacity factor N_c of circular and ring footings. *Geomech Geoeng* 12(1):1–13. <https://doi.org/10.1080/17486025.2016.1153729>
24. Sharma V, Kumar A (2017) Influence of relative density of soil on performance of fiber-reinforced soil foundations. *Geotext Geomembr* 1–9. <https://doi.org/10.1016/j.geotextmem.2017.06.004>
25. Sargazi O, Hosseininia ES (2017) Bearing capacity of ring footings on cohesionless soil under eccentric load. *Comput Geotech* 92:169–178. <https://doi.org/10.1016/j.compgeo.2017.08.003>
26. Sharma V, Kumar A (2017) Strength and bearing capacity of ring footings resting on fibre-reinforced sand. *Int J Geosynthetics Ground Eng* 2017:3–17. <https://doi.org/10.1007/s40891-017-0086-6>
27. Keshavarz A, Kumar J (2017) Bearing capacity computation for a ring foundation using the stress characteristics method. *Comput Geotech*. 89:33–42. <https://doi.org/10.1016/j.compgeo.2017.04.006>
28. Chavda Jitesh T, Dodagoudar GR (2019) On vertical bearing capacity of ring footings: finite element analysis, observations and recommendations. *Int J Geotech Eng*. <https://doi.org/10.1080/19386362.2019.1648737>
29. Hataf N, Razavi MR (2003) Behavior of ring footing on sand. *Iran J Sci Technol Trans B* 27:47–56
30. Noorzaei J, Naghshineh A, Kadir MRA, Thanoon WA, Jaafar MS (2006) Nonlinear interactive analysis of cooling tower foundation soil interaction under unsymmetrical wind load. *Thin-Walled Struct* 44:997–1005. <https://doi.org/10.1016/j.tws.2006.08.019>

Seismic Site Response and Liquefaction Potential for Proposed Underground Parking Site in Saharanpur (U.P.)



Manish Bhutani and Sanjeev Naval

Abstract Ground response analysis has a significant role in planning and designing of reinforced cement concrete structures in high seismic zone as sever conditions at the surface may occur due to the amplification of seismic design coefficient as compared to the value of bedrock level. The present study focuses on ground response analysis of underground parking site proposed in Saharanpur (U.P.). One-dimensional equivalent linear ground response analysis has been conducted using DEEPSOIL (one of the techniques for ground response analysis) by using Sikkim 2011 and Uttarkashi 1999 earthquake motion. Shear modulus (G) was evaluated from SPT-N values based on available correlations. The Peak Ground Acceleration (PGA) was calculated, and it has been observed that the PGA values at the ground surface are found to be more than the values mentioned in the relevant code. It has also been found that site is susceptible to liquefaction. Hence, special care must be taken in designing the multistoreyed building in the region of Saharanpur (U.P.)

Keywords Ground response analysis · Liquefaction · Peak ground acceleration · Saharanpur (U.P.)

1 Introduction

The Indian subcontinent has a history of earthquakes. The reason for the intensity and high frequency of earthquakes is the Indian plate driving into Asia at a rate of approximately 49 mm/year. The damage pattern of most of the recent earthquakes around the world has demonstrated that site-specific ground response analysis plays an major role [1]. Local site conditions have profound influence on all the important characteristics, i.e. amplitude, frequency content and duration of strong ground

M. Bhutani (✉)
IK Gujral Punjab Technical University, Kapurthala, India
e-mail: manish_0220@yahoo.com

S. Naval
Department of Civil Engineering, DAV Institute of Engineering and Technology, Jalandhar,
Punjab 144008, India

© The Author(s), under exclusive license to Springer Nature Singapore Pte Ltd. 2023
A. K. Agnihotri et al. (eds.), *Proceedings of Indian Geotechnical and Geoenvironmental Engineering Conference (IGGEC) 2021, Vol. 1*, Lecture Notes in Civil Engineering 280,
https://doi.org/10.1007/978-981-19-4739-1_33

361

motions. The extent of influence depends upon the thickness and properties of the soil layers, site topography and on the characteristics of the input motion itself. Therefore, identification of soil layers susceptible to ground motion amplification is an important task for accurate assessment of seismic hazard in earthquake prone areas. Adequate safety of structures under seismic condition can only be achieved with the knowledge of a proper site response. The regions which belong to higher potential of seismic hazard are given prime importance for determining the site response. Soil's potential against liquefaction for 45 locations of Jalandhar region (Punjab, India) has been carried out by Bhutani and Naval [2], and it has been observed that eighteen sites out of forty-five are found to be susceptible to liquefaction. In order to help structural designers and geotechnical engineers for the preparation of realistic plan towards disaster risk reduction for the region, Peak Ground Acceleration contour map of obtained results and liquefaction hazard maps for earthquake of magnitude 6.0 and 7.0 have been prepared on geographical information system (GIS) platform using QGIS software.

Seismic waves generally travel several kilometres in rock but a few metres in soil, yet the soil plays a very important role in determining the characteristics of ground motion and its analysis. The local soil conditions have a profound influence on the ground response during an earthquake. Also, the topography, nature of bedrock and the nature and the geometry of the deposits are the primary factors that influence the local modification of the wave motion between the bedrock and soil outcrop. Hence, local site effects play a key role in earthquake-resistant design and must be accounted for on a case-by-case basis. Ground response analysis can be done by using one-dimensional, two-dimensional and three-dimensional methods. Ground response analysis is used to predict ground surface motions for development of design response spectra, to evaluate dynamic stress and strain for evaluation of liquefaction hazards and to determine the earthquake-induced forces that can lead to instability of earth or earth retaining structure [3]. In north India, Deterministic Seismic Hazard Analysis of Jalandhar revealed the variation of Peak Ground Acceleration values from 0.14 g to 0.454 g that was found to be much higher values as compared to the values published in IS 1893 by Bureau of Indian Standards [4]. According to National Centre for Seismology (NCS), Ludhiana featured among other 29 cities highly vulnerable to earthquakes. After carrying out Deterministic Seismic Hazard Analysis of Ludhiana city by dividing whole city into $0.025^\circ \times 0.025^\circ$ grids and using ground motion equation developed by National Disaster Management Authority (NDMA), the Peak Ground Acceleration obtained ranged from 0.1 g to 0.392 g. Seismic Hazard Analysis helps in determining Peak Ground Acceleration for rock sites based upon different tectonic features present in the region but the soil overlying the rocks can modify the ground motion parameters on surface like Peak Ground Acceleration, Peak Ground Velocity and Peak Ground Displacement. To analyse the effect of local soil conditions on input ground motion, site-specific ground response analysis is must to accurately get Peak Ground Acceleration on surface which can be used by structural engineers to design safe earthquake-resistant structures.

The response of soil due to seismic hazards producing a significant amount of cumulative deformation or liquefaction has been one of the major concerns for

geotechnical engineers working in the seismically active regions. Liquefaction can occur in moderate to major earthquakes, which can cause severe damage to structure. The pressure generated by seismic wave vibrations will cause the groundwater to flow up and out. When this occurs, the sand grains lose its effective shear strength and will behave more like a fluid. The liquefaction potential of soil is either estimated from laboratory tests or field tests. Liquefaction is controlled by grain size of soil, durations of earthquake and amplitude and frequency of shaking, distance from epicentre, location of water table, cohesiveness of the soil and permeability of the layer. The rate majority of liquefaction hazard are associated with saturated sandy and silty soils of low plasticity and density. Among the field in situ tests, the SPT test has been widely used for this purpose. Rao and Nath evaluated liquefaction potential for Delhi through exhaustive studies based on extensive field SPT data and shear wave velocity survey using different modes.

Most of the state of Uttar Pradesh lies in the Gangetic Plain and has a population of 166,198,000 according to 2001 census and has an area of 240,928 km². There are 71 districts, 312 tehsils, 820 blocks and 107,452 villages. The state has population density of 690 per sq. km. (as against the national average of 312). Uttar Pradesh is bounded by Nepal and Uttarakhand on the north, Himachal Pradesh on the northwest, Haryana on the west, Rajasthan on the southwest, Madhya Pradesh on the south and southwest, Bihar on the east and Jharkhand on the southeast. Situated between 23°52'N and 30°25'N latitudes and 77°3' and 84°39'E longitudes, this is the fourth largest state in the country. According to GSHAP data, the state of Uttar Pradesh falls in a region of moderate to high seismic hazard and Saharanpur city falls in the high seismic hazard zone as shown in Fig. 1.

1.1 Equivalent Ground Response Analysis

In the present study, 1-D equivalent ground response analysis for the **Proposed Underground Parking Site** in Saharanpur (UP) region subjected to different earthquake ground motions has been carried out using DEEPSOIL Software.

DEEPSOIL is a one-dimensional site response analysis program that can perform: (a) 1-D nonlinear time domain analyses with and without pore water pressure generation and (b) 1-D equivalent linear frequency domain analyses including convolution and deconvolution. DEEPSOIL was developed under the direction of Prof. Youssef M.A. Hashash in collaboration with several graduate and undergraduate students including Duhee Park, Chi-Chin Tsai, Camilo Phillips, David R. Groholski, Daniel Turner, Michael Musgrove, Byungmin Kim and Joseph Harmon at the University of Illinois at Urbana-Champaign.

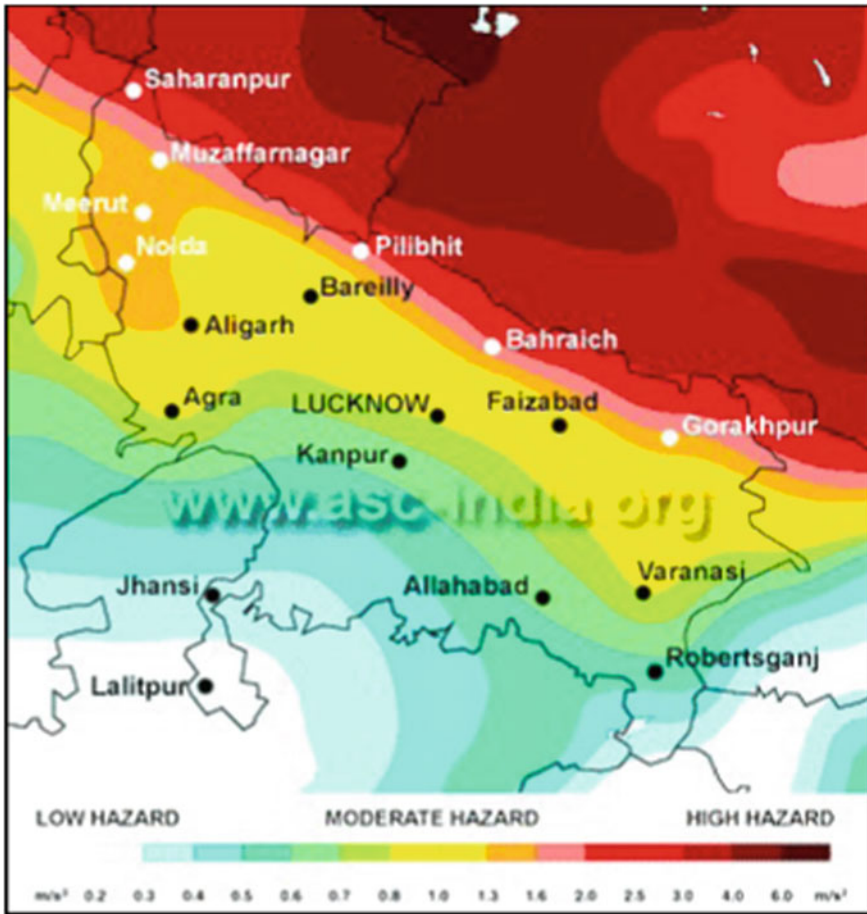


Fig. 1 Earthquake hazard map of Uttar Pradesh (www.asc.india.org)

2 Study Region

Saharanpur district is the northernmost of the districts of Uttar Pradesh state, India. Bordering the states of Haryana, Himachal Pradesh and Uttarakhand, and close to the foothills of Shivalik range, it lies in the northern part of the Doab region. It is primarily an agricultural area. The district headquarters are Saharanpur city, and it belongs to Saharanpur Division. Other principal towns are Behat, Deoband, Gangoh and Rampur Maniharan. Saharanpur is located at $29.97^{\circ}N$, $77.55^{\circ}E$, about 130 km (81 mi) south-southeast from Chandigarh and 170 km north-northeast from Delhi. It has an average elevation of 284 m (Fig. 2).

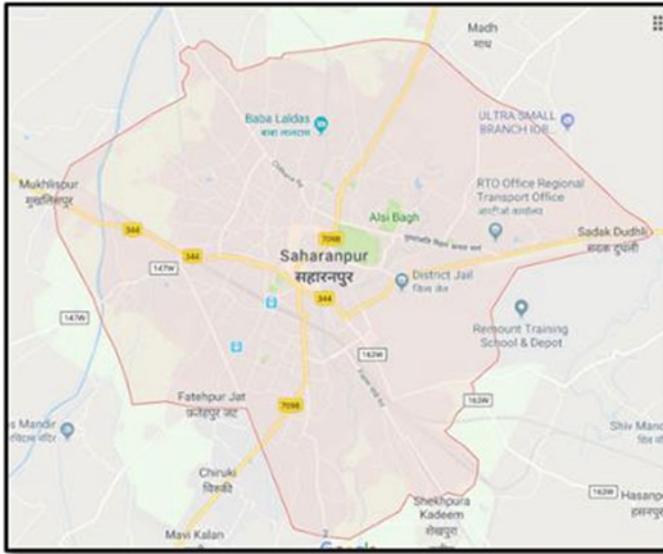


Fig. 2 Saharanpur region map

2.1 Site Characterization

In the present study, one-dimensional equivalent linear ground response analysis of four borehole drilled at Proposed Underground Parking Site is carried out. The field borehole data of the sites were collected from Saharanpur Smart City Office to access the soil properties (thickness of subsoil strata, standard penetration test (SPT) values, index properties) and groundwater conditions (Fig. 3).

The locations of the sites selected for ground response analysis have been shown in Table 1 and Fig. 4.

The SPT-N values are obtained at 1.5–2 m intervals up to the bottom of the borehole. The geologic strata comprise mostly sand, sandy silt, silty sand and small pockets of clay having low compressibility at shallow depths. The water table was found in all four boreholes (SRE-1 to SRE-4) at a uniform depth of 7.30 m from NGL.

Site effects that represent seismic ground response characteristics are usually incorporated as amplification factors in seismic codal provisions (e.g. NEHRP 2001, UBC 97, IBC 2000 and EC8 2003). So, that site effects can be accounted for while designing. These factors are based on average shear wave velocity of top 30m of the soil profile (V_{s30}). It is a general recommendation to use the actual shear wave velocity of the bedrock in site classification [1]. However, due to non-availability of V_s profiles, sites have been classified using N_{30} values as per the recommendations of NEHRP [1]. The current NEHRP provisions categorize soils into the classes A, B, C, D, E and F based on average N value of the profile. Average N value (N_{30}) for



Fig. 3 Soil survey at Jubilee Park

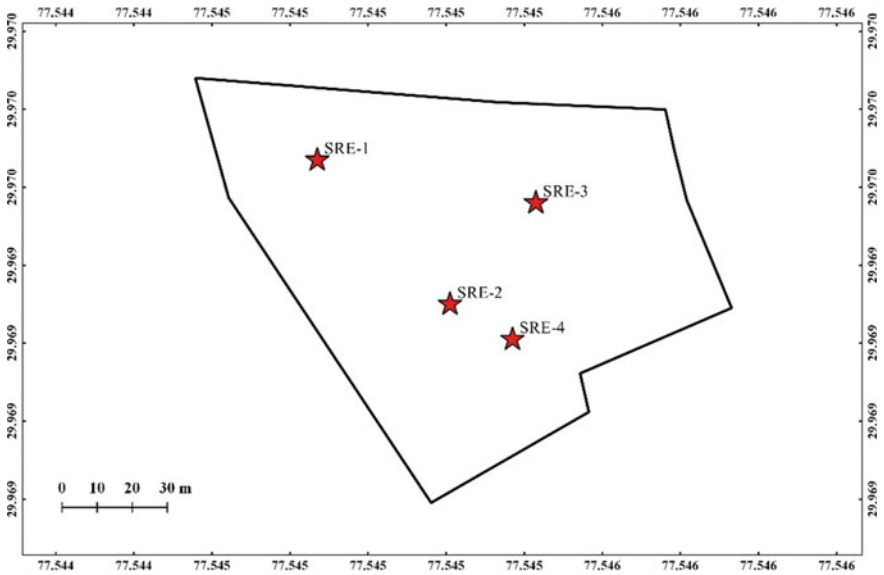


Fig. 4 Location of borehole in Saharanpur region

Table 1 Location detail of selected sites for ground response analysis

Site code	Area	Latitude	Longitude
SRE-1	Saharanpur	29°58'10.80"	77°32'41.54"
SRE-2	Saharanpur	29°58'9.48"	77°32'42.76"
SRE-3	Saharanpur	29°58'10.40"	77°32'43.54"
SRE-4	Saharanpur	29°58'9.16"	77°32'43.32"

Table 2 Site class as per NEHRP

Site code	Area	Avg. <i>N</i> Value (<i>N</i> ₃₀)	Site class as per NEHRP
SRE-1	Saharanpur	16.37	D
SRE-2	Saharanpur	13.87	D
SRE-3	Saharanpur	15.73	D
SRE-4	Saharanpur	8.61	E

the soil profile can be calculated using the Eq. 1.

$$N_{30} = \frac{\sum_{i=1}^n di}{\sum_{i=1}^n \frac{di}{Ni}} \tag{1}$$

where *N*₃₀ = average SPT-*N* value for 30 m depth, *N_i* = SPT-*N* value of any layer and *d_i* = thickness of any layer. It has been observed that out of 04 selected sites, 03 sites come under class D and 01 sites come under class E with the average *N* value for the profiles ranging from 8.61 to 16.37 with minimum and maximum values observed at SRE-01 and SRE-04 sites, respectively. The thickness of the layers is so adjusted that the maximum frequency that a layer can propagate is always above 25 Hz. The engineering bedrock is generally assumed to be the uppermost layer, having a shear wave velocity (*V_s*) ≥ 760 m/s of the soil column in accordance with NEHRP provisions [5].

Therefore, in this study, engineering bedrock has been assumed at refusal, i.e. for *N* > 50 for 15 cm penetration or *N* > 100 for 30 cm penetration of SPT split-spoon sampler. Hence, the boreholes drilled up to refusal have been considered for the analysis. Bedrock has been modelled as an elastic half space with 2% damping, density of 2.5 g/cc and shear wave velocity (*V_s*) of 760 m/s. The average *N* value and site class of selected boreholes have been presented in Table 2 and shown in Fig. 5.

2.2 Dynamic Properties of Soil

Shear modulus (*G_{max}*) is one of the most important input parameters to represent the stiffness of the soil layers. It also plays a vital role in seismic ground response studies. The ground motion parameters at the surface are generally obtained by conducting

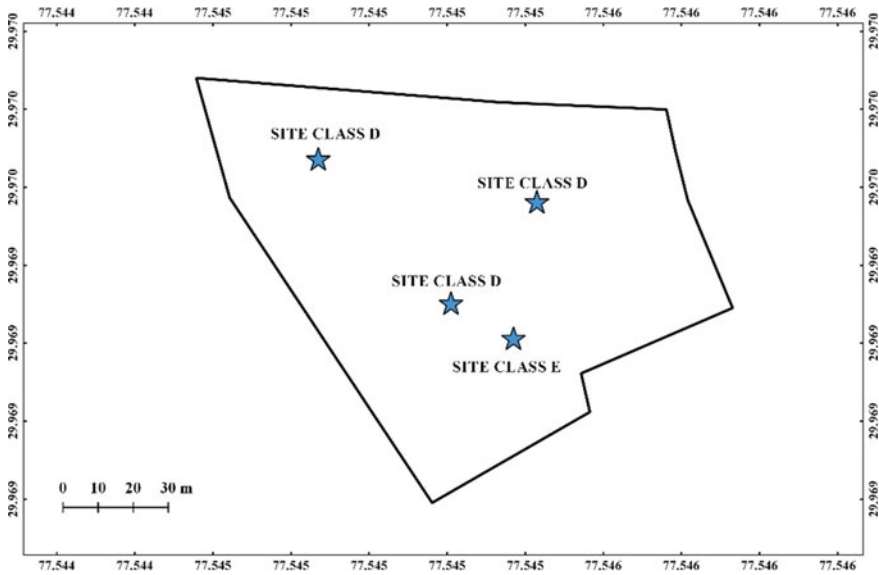


Fig. 5 Site class for selected sites of Saharanpur region as per NEHRP

Table 3 Correlations for calculation of shear modulus

Correlations	Soil type	Author(s) name
$G = 1220N^{0.62}$	Clay	Ohba and Toriunmi
$G = 650$	Sand	Ohsaki and Iwasaki
$G = 1182$	Other soils	Ohsaki and Iwasaki
$G = 82.5$	Gravel	Imai and Tonouchi

one-dimensional ground response analysis considering only the upward propagation of shear wave.

As shear modulus for study region is not available, it has been calculated using available correlations of SPT-N value and shear modulus (G) for different soil types. Correlations can be selected based on the soil type and value of correlation coefficient (R). In the present study, correlations given in Table 3 have been selected as per the recommendations of Anbzahagan et al.

2.3 Input Motion

Ground response analysis involves in generating the suitable input motion based on PGA, magnitude of controlling earthquake, source to site distance and site class, which is compatible with the maximum dynamic loading expected at the site of interest. For present analysis, PGA values for rock sites given in IS: 1893-2016 are

Table 4 Strong motion characteristics considered in this study

S.No.	Strong motion parameter	Sikkim Eq	Uttarkashi Eq
1	Date of occurrence	18-09-2011	19-10-1991
2	Magnitude, Mw	6.8	7.0
3	Location of epicentre	27.723 N 88.064 E	30.837 N 78.984 E
4	Distance from the source	68 km	34 km
5	Recording station	Gangtok	Uttarkashi
6	PGA (g)	0.152	0.253

used for the selection of acceleration time histories. Sikkim earthquake motion (2011) and Uttarkashi earthquake motion (1991) have been applied at the bedrock level to study the soil effects. The earthquake characteristics of these motions like date of occurrence, recording station, distance from the source, magnitude and maximum horizontal acceleration are presented in Table 4.

3 Results and Discussion

3.1 Assessment of PGA and Amplification

Equivalent linear (EL) ground response analysis has been carried out to study the effect of local ground conditions for the sites of Saharanpur region using DEEPSOIL v6.1 software. The ground surface acceleration with time history was computed at all four locations of Saharanpur region in response to the 1999 Uttarkashi and 2011 Sikkim earthquake applied at the bedrock, and the results are given in Tables 5 and 6.

It has been observed that under the influence of Sikkim (2011) earthquake, PGA values for the sites of Saharanpur region vary from 0.287 to 0.321 g. Similarly, PGA values ranging from 0.317 to 0.376 g were observed during the ground response

Table 5 Results of ground response analysis for the sites of Saharanpur region with Sikkim earthquake (2011) input motion

Site code	Area	PGA rock (g) as per IS: 1893	PGA soil (g)	AF
SRE-1	Saharanpur	0.24	0.293	1.22
SRE-2	Saharanpur	0.24	0.312	1.30
SRE-3	Saharanpur	0.24	0.287	1.19
SRE-4	Saharanpur	0.24	0.321	1.33

Table 6 Results of ground response analysis for the sites of Saharanpur region with Uttarkashi earthquake (1999) input motion

Site code	Area	PGA Rock (g) as per IS: 1893	PGA soil (g)	AF
SRE-1	Saharanpur	0.24	0.321	1.33
SRE-2	Saharanpur	0.24	0.365	1.52
SRE-3	Saharanpur	0.24	0.317	1.32
SRE-4	Saharanpur	0.24	0.376	1.56

analysis conducted on sites of Saharanpur region by selecting Uttarkashi (1999) earthquake motion. The effect of local soil conditions in amplifying earthquake ground motion has been observed at all the sites of Saharanpur region as amplification factor (AF) varies from 1.19 to 1.33 using Sikkim (2011) motion and 1.32 to 1.56 using Uttarkashi (1991) motion.

3.2 Assessment of Liquefaction Potential

Liquefaction potential assessment has been done using simplified procedure given in IS 1893 (Part 1):2016. Due to the difficulties in obtaining and testing undisturbed representative samples from potentially liquefiable sites, in situ testing is the approach preferred widely for evaluating the liquefaction potential of a soil deposit. The most common procedure used in engineering practice for the assessment of liquefaction potential of sands and silts is the simplified procedure. The procedure may be used with either standard penetration test (SPT) blow count or cone penetration test (CPT) tip resistance or shear wave velocity (V_s).

Two parameters are required for the assessment of liquefaction susceptibility of soils, i.e. cyclic stress ratio (CSR) which implies the cyclic stress induced by the earthquake and cyclic resistance ratio (CRR) of the soil which implies the resistance of soils towards liquefaction. The ratio of CRR to CSR gives the factor of safety (FOS). Generally, if the FOS value is less than 1, the site is considered to be liquefiable and if it is greater than 1, the site is considered to be non-liquefiable. However, soil that has a FOS slightly greater than 1.0 may still liquefy during an earthquake. For example, if a lower layer liquefies, then the upward flow of water could induce liquefaction of the layer that has a factor of safety slightly greater than 1.0. After site response analysis, using amplification factor and rock PGA, soil PGA for all the sites has been calculated and used for the assessment of liquefaction potential. The magnitude of an earthquake is taken as 7.0. Soil PGA obtained from equivalent linear analysis is used for assessment.

For general understanding, the susceptibility level can be related to factor of safety as per Table 7 as proposed by Sitharam et al.

In view of the above table, the susceptibility level of liquefaction hazard for various sites of Saharanpur region is reported in Table 8.

Table 7 Susceptibility index of liquefaction hazard

S.No.	Factor of safety range	Severity index
1	FS < 1	High
2	FS 1 to 2	Moderate
3	FS 2 to 3	Low
4	FS > 3	Nil
5	Non-liquefiable (NL)	Nil

Table 8 Liquefaction potential of various sites in Saharanpur region

Site code	Region	Min. FOS	Severity index
SRE-1	Saharanpur	1.23	Moderate
SRE-2	Saharanpur	1.61	Moderate
SRE-3	Saharanpur	1.47	Moderate
SRE-4	Saharanpur	1.49	Moderate

4 Conclusion

Equivalent linear (EL) ground response analysis has been carried out to study the effect of local ground conditions and evaluation of liquefaction potential for the 04 sites of Saharanpur region. The following conclusions are obtained after the analysis of results:

1. As per the provisions of NEHRP (2003), out of 04 selected sites, 03 sites come under class D and 01 site comes under class E with the average N value for the profiles ranging from 8.61 to 16.37 with minimum and maximum values observed at SRE-01 and SRE-04 sites, respectively.
2. All the sites of Saharanpur region get amplified by both Sikkim (2011) and Uttarkashi (1991) Eq. motion with maximum observed amplification value of 1.56 for site SRE-04, respectively.
3. The maximum and minimum PGA has been observed to be 0.376 g and 0.287 g for site SRE-04 and SRE-01, respectively.
4. The IS 1893 (Part1): (2016) codal specifications for Zone IV are found to be unsuitable as we got the higher value of PGA at all sites, when the sites of Saharanpur regions were analysed by both Sikkim (2011) and Uttarkashi (1991) Eq. motion.
5. After evaluating the factor of safety against liquefaction for all sites of Saharanpur region, it was found that FS of all sites lies between 1 and 2 and moderate level against liquefaction hazard is found for all sites.

It can be concluded from the above that site-specific ground response analysis must be undertaken to ascertain the design coefficients for the respective sites. Furthermore, any geotechnical investigation carried out in liquefiable susceptible zones identified above needs to incorporate special considerations in design of foundation.

So that the liquefiable sites (if any) may be given due consideration before the actual construction is undertaken.

References

1. Desai SS, Choudhury D (2015) Non-linear site specific ground response analysis for port site in Mumbai, India. *Jpn Geotech Soc.* <https://doi.org/10.3208/Jgssp.IND-22>
2. Bhutani M, Naval S (2021) Assessment of seismic site response and liquefaction potential for some sites using Borelog data. *Civil Eng J* (6)11:2103–2119
3. Kramer SL (1996) *Geotechnical earthquake engineering*, vol 653. Prentice Hall, New Jersey
4. Naval S, Deep G, Puri N (2016) Deterministic seismic/hazard analysis for proposed smart city Jalandhar. In: *International geotechnical engineering conference on sustainability in geotechnical engineering practices and related urban issues*
5. Hashash Y, Park D, Tsai CC, Philips C, Groholski DR (2016) DEEPSOIL—1-D wave propagation analysis program, version 6.1, Tutorial and User Manual, University of Illinois at Urbana, Campaign
6. Anbazhagan P, Sitharam TG (2008) Seismic microzonation of Bangalore, India. *J Earth Syst Sci* 117(S2):833–852
7. Anbazhagan P, Manohar DR, Sayed SRM, Nassif SNA (2016) Selection of shear modulus correlation for SPT N values based on site response analysis. *J Eng Res* 4(3):18–42
8. Basu D (2016) Comparative 1D ground response analysis of homogeneous sandy stratum using linear, equivalent linear and non-linear meshing approach. *Indian Geotechnical Society, Kolkata*
9. BSSC NEHRP (2003) Recommended provisions for seismic regulations for new buildings and other structures, part1: provisions, FEMA 368, Federal Emergency Management Agency, Washington, D.C.
10. Choudhury D, Savoikar P (2009) Equivalent-linear seismic analyses of MSW landfills using DEEPSOIL. *Eng Geol* 107(3–4):98–108
11. Choudhury D, Shukla J (2011) Probability of occurrence and study of earthquake recurrence models for Gujarat state in India. *Disaster Adv* 4(2):47–59
12. Dipendra G, Deepak C (2016) Ground response analysis of soft sediments of Kathmandu valley. In: *14th national convention of Nepal engineers' association.* <https://doi.org/10.13140/RG.2.1.4696.2325>
13. Datta UJ (2015) Ground response analysis: a comprehensive review. In: *50th Indian Geotechnical Conference*
14. Govinda Raju L, Ramana GV, HanumantaRao C, Sitharam TG (2004) Site specific ground response analysis. *Curr Sci* 87(10):1354–1362
15. Idriss IM, Boulanger RW (2006) Semi-empirical procedures for evaluating liquefaction potential during earthquakes. *Soil Dyn Earthq Eng* 26:115–130
16. IS 1893 (Part1) (2016) Criteria for earthquake resistant design of structure. Bureau of Indian Standards, New Delhi
17. Siddhartha S, Joseph TM, Puri N, Jain A (2014) Deterministic seismic hazard analysis of Chandigarh city. In: *Sixth Indian young geotechnical engineers conference 6IYGEC2017*
18. Mahmood K, Khan SA, Iqbal S (2020) Equivalent linear and nonlinear site-specific ground response analysis of Pashto Culture Museum Peshawar, Pakistan. *Irranian J Sci Technol Trans Civil Eng* 1–13. <https://doi.org/10.1007/s440996-020-00346-4>
19. Phanikanth VS, Choudhury D, Rami Reddy G (2011) Equivalent-linear seismic ground response analysis of some typical sites in Mumbai. *J Geotech Geol Eng.* <https://doi.org/10.1007/s10706-011-9443-8>
20. Youd TL, Idriss IM, Andrus RD, Arango I (2001) Liquefaction resistance of soils: summary report from the 1996 NCEER and 1998 NCEER/NSF workshops on evaluation of liquefaction resistance of soils

ANN Model for Evaluation of Seismic Behavior of Irregular Steel Building Frames



S. Varadharajan , S. V. Kirthanashri , Mrityunjai Govind Rao , Animesh Jaiswal , and Bishnu Kant Shukla 

Abstract The past decade has seen a surge in finding seismic behavior of buildings due to the significant number of building failures during the past earthquakes. Seismic design codes presume stiff beam-column connections, which is untrue. A stiff beam-column connection may also lead to erroneous seismic response data. This study attempts to address the flexibility of beam-column connections and suggest simpler equations for estimating fundamental time period. From analytical study it was concluded that the proposed equations findings matched the dynamic analysis closely.

Keywords ANN · Steel buildings · Fundamental time period · Sensitivity analysis · Artificial neural network

1 Introduction

Previous study has demonstrated that moment resistant steel frames are preferred in seismic prone areas as it transfers seismic forces. In reality, all connections are semi-rigid due to their inherent degree of elasticity. Code proposed equations for estimating fundamental time period are shown in Table 1. The fundamental time period (T) is an important parameter that reflects seismic behavior and may be utilized to simplify the seismic design process [1–8]. There are three types of beam-column connections in India namely: Rigid, semi-rigid, and flexible. Semi-rigid connections transfer partial moments to columns in comparison to full moment transfer in case of rigid connections. The Indian Standard assumes all connections to be rigid which is unrealistic as every connection possess some degree of flexibility. Therefore, connection flexibility should be incorporated in equations to determine T . To achieve this,

S. Varadharajan (✉) · M. G. Rao · B. K. Shukla
JSS Academy of Technical Education, Noida, India
e-mail: svrajan82@gmail.com

S. V. Kirthanashri · A. Jaiswal
Amity University Noida, Noida, India

Table 1 T as per different building codes [18–22]

Code	Fundamental time period
IS 1893	$0.9 h/D^{0.5}$
EC 8	$0.075 h^{0.75}$
ASCE 7:2005	$0.075 h^{0.75}$
NBCC 2005	$0.01 N$
UBC 97	$0.075 h^{0.75}$

Where h is building height, D is minimum lateral dimension of building, N is no. of stories

several building models with varying connection flexibility have been modeled and examined. Then, using the findings of the investigation, new equations for estimating T were proposed. The proposed equations should be compared to the code equations to assess their correctness and validity.

2 Details of Building Models Used

The building models employed in this study are symmetrical in both transverse directions. Using the E-Tabs V 9.0 program [9], the degree of flexibility of connections was changed from 0 to 100%. ISMB 350 and ISHB 450 sections have been used for modeling of beams and columns, as per Indian Standard rules. The number of storeys in the building were adopted as 5, 10, 15 and 20 with a story height of 3.5 m. The dead and live load have been adopted as 3 kN/m² and 4 kN/m² in accordance with provisions of IS 875 Part 3 [10]. The input data adopted was based on previous study [11–14]. Artificial neural networks (ANNs) are widely employed in engineering, according to previous literature review. The ANN model is made up of highly sensitive and interconnected neurons. After creating and training an ANN model, a feed-forward computing network was used to determine the error. The accuracy of ANN models in predicting steel connection behavior has been shown [15–17]. The current study's ANN model is shown in Fig. 1, with the Logsig function in conjunction with Levenberg–Marquardt algorithm. In the output layer, a single neuron forecasts the parameter T . The seismic response was computed using E-Tabs V 9.0 [9].

3 Discussion of Analysis Results

In this section it is analyzed how altering an input parameter impacts an output parameter. It compares mean – variance with mean + variance. This is confirmed by the sensitivity analysis Fig. 2. Variable input parameters impacts fundamental time period as seen from Figs. 3, 4 and 5. Building height and connection flexibility affects

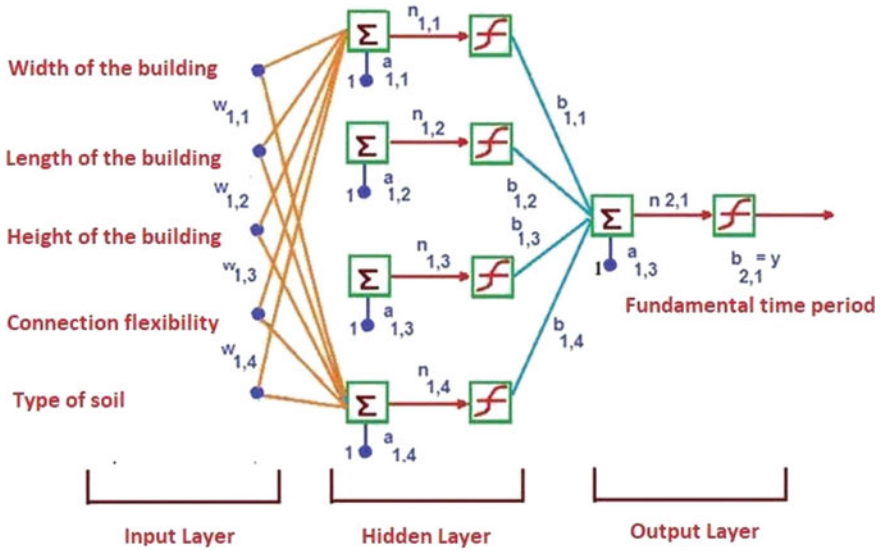


Fig. 1 Used ANN model for analytical study

the fundamental time period to greatest extent in comparison to other parameters and following equations to estimate parameter T as

$$T = 0.8128 + 0.00180H - 0.0001669B + 0.0003171L \tag{1}$$

$$T = 0.8489 + 0.002837H - 0.0001960B + 0.000393L \tag{2}$$

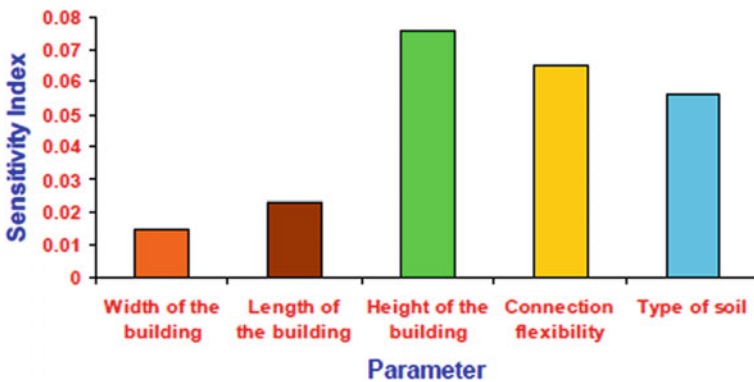


Fig. 2 Parametric sensitivity results

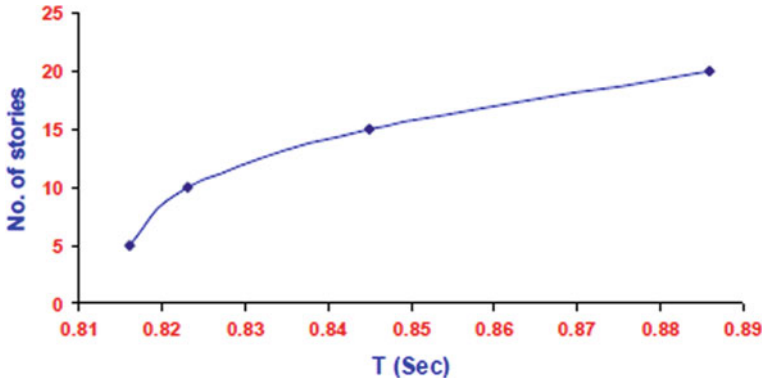


Fig. 3 Variation of T with no. of stories

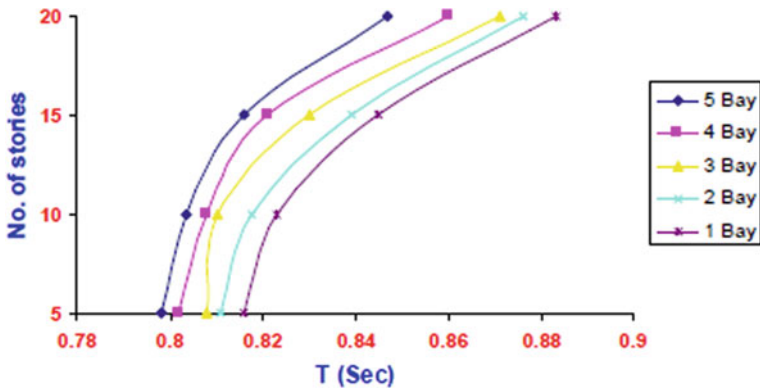


Fig. 4 Impact of number of bays on T

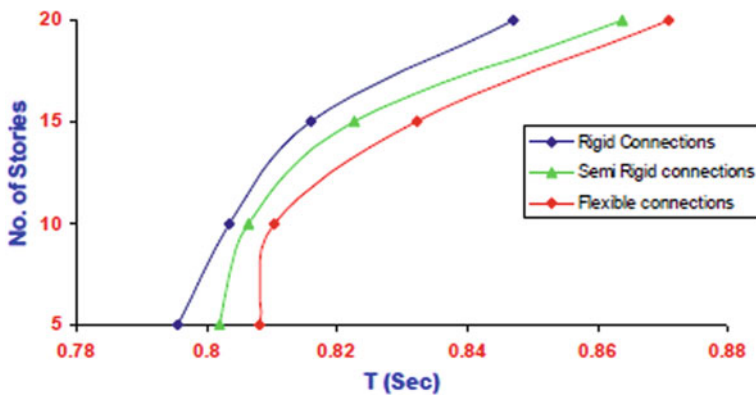


Fig. 5 Impact of connection flexibility on T

Using the sensitivity analysis findings, removing unimportant parameters like B and L from the above equations become as follows

$$T = 0.8128 + 0.00180H \tag{3}$$

$$T = 0.8489 + 0.002837H \tag{4}$$

The earlier research work [12, 14] have proposed equations to estimate period-height relationship. The analytical study shows that the Author proposed equation's results are in close correlation with dynamic analysis results (Fig. 6). A removal of unnecessary factors reduces the accuracy of the proposed equations but still proposed equations outperform code proposed equations (Fig. 7). The recommended equations are dependent on input data, thus they should be checked for accuracy. However, the investigation demonstrates that the recommended equations have a stronger correlation than the code expressions (Fig. 8).

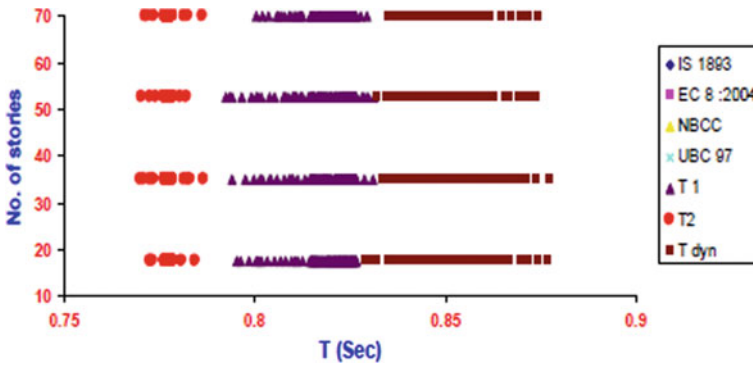


Fig. 6 Estimation of parameter T as per different methods

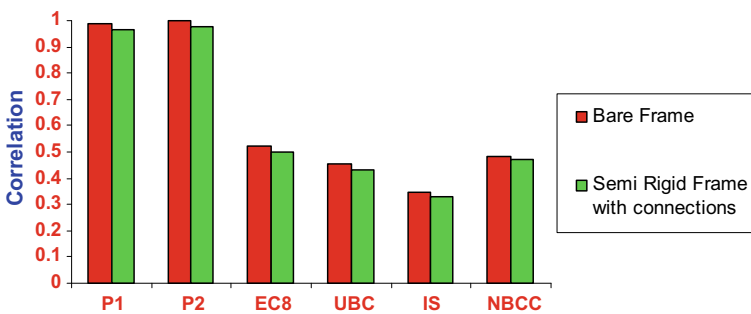


Fig. 7 Correlation of building models considered in analytical study

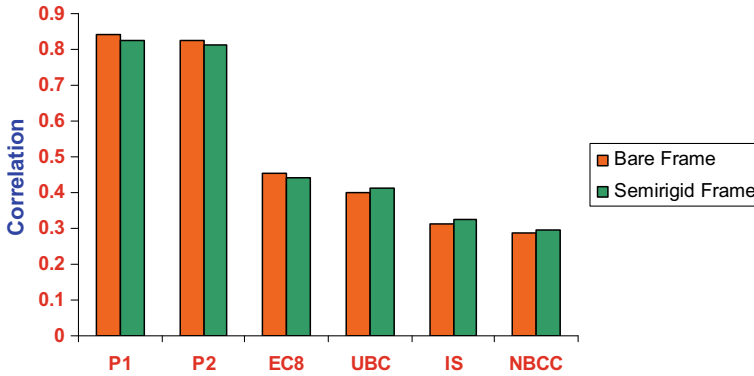


Fig. 8 Correlation results of building models considered in analytical study

4 Conclusions

The code proposed equations to calculate period-height relationship are based on Rayleigh's assumptions which are unrealistic. Moreover, connection flexibility aspect has been ignored in previous research studies to estimate seismic behavior. Therefore, there was a necessity of an alternative equation to estimate seismic response for addressing these issues. This was done by analyzing 315 models with varied beam—column connections and compiling the analysis data. The sensitivity analysis of the building models shows that height impacts period—height relationship to the greatest extent. The recommended equations and the dynamic analysis demonstrate good correlation. Although, the accuracy of the proposed equation reduces after removing insignificant parameters but still the proposed equations exhibit better performance in comparison to the code proposed equations.

References

1. Crowley H, Pinho R (2006) Simplified equations for estimating the period of vibration of existing buildings. In: Proceedings of first European conference on earthquake engineering and seismology 2006, paper no. 1122, Geneva, Switzerland
2. Dym OL, Williams HE (2003) Estimating fundamental frequencies of tall buildings. *J Struct Eng* 133:1–5
3. Asteris PG, Repapis CC, Cavaleri L, Sarhosis V, Athanasopoulou A (2015) On the fundamental period of infilled RC frame buildings. *Struct Eng Mech* 54(6):1175–1200
4. Xiong W, Jiang LZ, Li YZ (2016) Influence of soil–structure interaction (structure-to-soil relative stiffness and mass ratio) on the fundamental period of buildings: experimental observation and analytical verification. *Bull Earthq Eng* 14(1):139–160
5. Goel RK, Chopra AK (1997) Period formulas for moment-resisting frame buildings. *J Struct Eng* 123:1454–1461
6. Hong H, Hwang (2000) Empirical formula for fundamental periods of vibration for reinforced concrete buildings in Taiwan. *Earthq Eng Struct Dyn* 29:327–337

7. Kose MM (2008) Parameters affecting the fundamental time period of RC buildings with infill walls. *Eng Struct* 31:93–102
8. Ricci P, Verderame GM, Manfredi G (2011) Analytical investigation of elastic period of infilled RC MRF buildings. *Eng Struct* 33:308–319
9. E-Tabs (2009) Integrated software for structural analysis and design. Version 9.0. Berkeley (California), Computers & Structures, Inc.; 2007
10. IS 875 (Part-3) (1987) Code of practice for design loads (other than earthquake) for buildings and structures—part 3 wind loads, Bureau of Indian Standards, Manak Bhawan, New Delhi, Section 7, p 47
11. Karavasilis TL, Bazeos N, Beskos DE (2008) Estimation of seismic inelastic deformation demands in plane steel MRF with vertical mass irregularities. *Eng Struct* 30:3265–3275
12. Varadharajan, Sehgal VK, Saini B (2014) Seismic response of multistory reinforced concrete frame with vertical mass and stiffness irregularities. *Struct Des Tall Spec Build* 23:362–389
13. Varadharajan, Sehgal VK, Saini B (2012) Review of different structural irregularities in buildings. *J Struct Eng* 39:393–418
14. Varadharajan, Sehgal VK, Saini B (2015) Fundamental time period of RC setback buildings. *Concrete Res Lett* 5:901–935, 2014b
15. Nguyen T-H, Tran N-L, Nguyen D-D (2021) Prediction of critical buckling load of web tapered I-section steel columns using artificial neural networks. *Int J Steel Struct* 1(23)
16. Zarringol M, Thai H-T, Naser MZ (2021) Application of machine learning models for designing CFCFST columns. *J Constr Steel Res* 185:1056–1066
17. Faridmehr, Iman et al Hybrid Krill Herd-ANN model for prediction strength and stiffness of bolted connections. *Buildings* 11(6):229
18. NBCC (2005) National building code of Canada 1995, National Research Council of Canada, Ottawa, Ontario 1995
19. UBC (1997) International conference of building officials (ICBO), Uniform Building code, Whittier, California
20. EC8 (2004) Design of structures for earthquake resistance. General rules seismic actions and rules for buildings (EN 1998-1:2004), European committee for Standardization, Brussels
21. IS (2002) IS 1893 (Part 1)-2002: Indian standard criteria for earthquake resistant design of structures, part 1—general provisions and buildings (fifth revision), Bureau of Indian Standards, New Delhi
22. ASCE (2005) Minimum design loads for building and other structures (ASCE/SEI 7-05), American Society of Civil Engineers, New York, USA

Deterministic Seismic Hazard Analysis for Amritsar, Punjab, India



Nikhil Bhatti, Sanjeev Naval, and Gagan Deep

Abstract The concept of smart city is destined to give improved personal satisfaction to residents and make their lives more secure than ever. Safety of the smart citizens cannot be confirmed without safe structures. Careful designing, planning, and execution can enhance the life span of any structure. Zone factor (Z) is one of the vital parameters analyzing the earthquake-resistant structures and can be calculated via seismic hazard analysis. In this paper, Deterministic Seismic Hazard Analysis (DSHA) for a proposed smart city, Amritsar is done by using earthquake data of size (M_w) ≥ 5 for the past 516 years. Peak ground acceleration value at bedrock level, considering the grid of size $0.025^\circ \times 0.025^\circ$ and using ground motion parameter equation (GMPE) by National Disaster Management Authority (NDMA) is found out to be 0.414 g which is on higher side as compared to 0.24 g recommended by IS 1893-2016 part 1. The present study shows the importance of carrying out site-specific seismic hazard analysis for proposed smart cities.

Keywords DHSA · SHA · Deterministic seismic hazard analysis

1 Introduction

Countless hazardous earthquakes occurred in India, and it has been assessed that greater than 50% of the nation's territory region remains powerless against seismic tremors. Especially the North India, which is parallel with Eurasian plate, is quite dynamic in terms of seismicity. Even the moment in the northeastern plate of India has already caused misshaping in the range of Himalayas, Tibet, and in the northeast

N. Bhatti (✉)

DAV Institute of Engineering and Technology, Jalandhar, India

e-mail: bhatti.nikhil269@gmail.com

S. Naval

Department of Civil Engineering, DAV Institute of Engineering and Technology, Jalandhar, India

G. Deep

Lyallpur Khalsa College Technical Campus, Jalandhar, India

of India. The belt of Himalayas, plates of Indian and Eurasian ones are combining yearly at the degree of 50 mm/year [1–3]. Seismic risk is characterized as an actual marvel as it assists in assessing ground trembling which might be related with a tremor causing unfriendly impact on human exercises. The seismic hazard analysis (SHA) is even capable of measuring tremors which have the potential of causing harm and misfortune in near future. It includes quantitative assessment of ground trembling peril at a specific location. The principle factors influencing seismic peril in an area are magnitude of earthquake, source-to-spot distance, span of ground trembling, and return period. SHA can be utilized to create territorial full scale or miniature drafting maps which are valuable for the improvement of seismic tremor safe structure plan and development, land use arranging, crisis plan, and assessment of financial misfortune. Seismic hazard for any region can be assessed by two methods: (1) Deterministic Seismic Hazard Analysis (DSHA) and probabilistic seismic hazard analysis (PSHA) [4].

Gupta [5] stated that the PSHA utilizes information of previous occasions, viz. earthquake magnitude, place, and time of happening around that specific region while deterministic methodology utilizes land records that can be utilized for modeling a worst-case scenario earthquake. The necessity of complete past quake information is fundamental for probabilistic seismic hazard evaluation method, and in certain remote areas, it turns to be troublesome task to acquire the required information. Such conditions (DSHA) is the most straightforward, simplest, and much faster technique for conducting seismic hazard examination. For the direst outcome imaginable, DSHA is more helpful and it is essential to develop quake safe plan for future structures or for assessing the well-being of a current construction of significance, similar to dams, thermal energy stations, long-length spans, tall structures, and so on. Hence, deterministic seismic hazard analysis of Amritsar (Punjab) has been selected over probabilistic seismic hazard analysis. To assess the seismic risks by utilizing DSHA for a location, all potential faults of seismic action should be recognized and their possibility for creating future solid ground movement should be assessed. The most recent variant of seismic drafting guide of India [6] recommends four zones which define seismic intensity for the whole India. The fundamental downside of seismic zonation code of India [6] is that it is in view of the historical tectonic activities and not founded on a thorough logical seismic risk examination. A study [7] has shown that the risk esteems given by [6] should be overhauled. The primary endeavor to assess the seismic risk of Indian subcontinent by [8] depended upon deterministic procedures. This analysis considered 40 seismogenic sources in India and groups were dependent upon seismicity, tectonics, and geodynamics. The PGA esteems were accounted for four regions in south India, and the most extreme PGA esteem announced was 0.08 g. The SHA of Bangalore, India, was assessed by [9] in view of deterministic methodology utilizing the connection proposed by [10] and deduced the PGA_{max} value of 0.159 g. [11] presented a paper on DSHA for proposed smart city Jalandhar, India, and concluded the value of PGA to be 0.42 g. Similarly, [12] followed the DSHA for the State of Haryana, India, and reported the maximum PGA value of 0.514 g. Likewise, [13] used the deterministic approach and concluded the value of PGA for Ludhiana, India, to be 0.392 g. Equally, [14] calculated the PGA

for active neotectonic faults in Chennai based on the correlation and found the most extreme value for PGA to be 0.176 times g.

Careful analysis and design of structural components play a vital role in serviceability and strength of structures [15, 16]. So far the focal point of the smart city plan is by all accounts style and not primarily about safety. A large number of the structures in the clogged neighborhoods of Amritsar are profoundly defenseless. It won't take an enormous earthquake to harm these structures. Detailed literature reveals that none of the researchers have performed any analysis regarding the seismic hazard on proposed smart city Amritsar. To overcome this gap, authors present the Deterministic Seismic Hazard Analysis on Amritsar. In the current examination, 14 active sources have been distinguished in the seismic investigation region. The most extreme extent has been relegated to each active fault considering provincial burst character. For this reason, seismic information has been gathered for a time of 516 years from IMD and a tremor inventory is prepared based on data collected. Ground Motion Predictive Equation (GMPE) developed by [17] for Indo-Gangetic district has been utilized for the expectation of strong motion characteristics.

2 Seismic Study Area

Amritsar, a city of state Punjab, lies in northwestern part of India. It happens to fall about 15 miles (25 km) east of the LOC that shares border with Pakistan. It is the greatest and most huge city in Punjab and is a critical business, social, and transportation focus. The study territory lies between scope of latitude 30° N to 33° N and longitude 74° E to 77° E. It falls in the Zone IV of seismic drafting guide [6] (Figs. 1 and 2).

3 Methodology

The technique developed for DSHA for SSA Amritsar is in view of the accompanying advances:

1. Guide diagrams on sheet numbers 4 and 5 of Seism tectonic Atlas of India and its Environs by [18] have been examined and converged to set up a solitary guide for the outline of the investigation area and its structural arrangement. Total of 121 points in the grid size $0.025^{\circ} \times 0.025^{\circ}$ are selected which enclosed the seismic study area (SSA) as demonstrated in Fig. 3.
2. Quake information has been gathered from Indian Meteorological Department, Delhi, and a seismic tremor index as shown in Table 1 for the investigation area has been created for a period between January 1505 and February 2021 that is 516 years. An Epicenter map depicted in Fig. 4 has been formed utilizing the pre-arranged list.

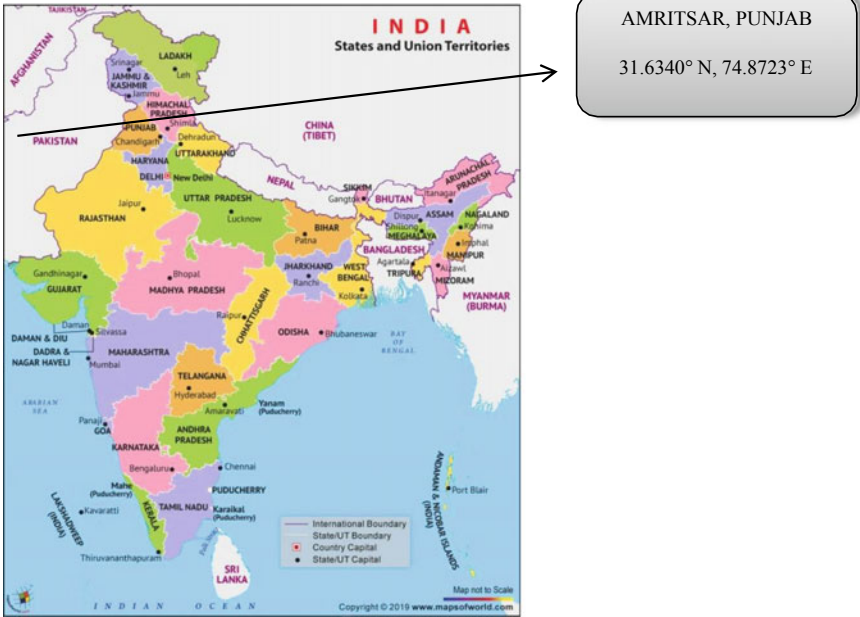


Fig. 1 Seismic study area depicted in the map of India. Source www.mapsofindia.com/

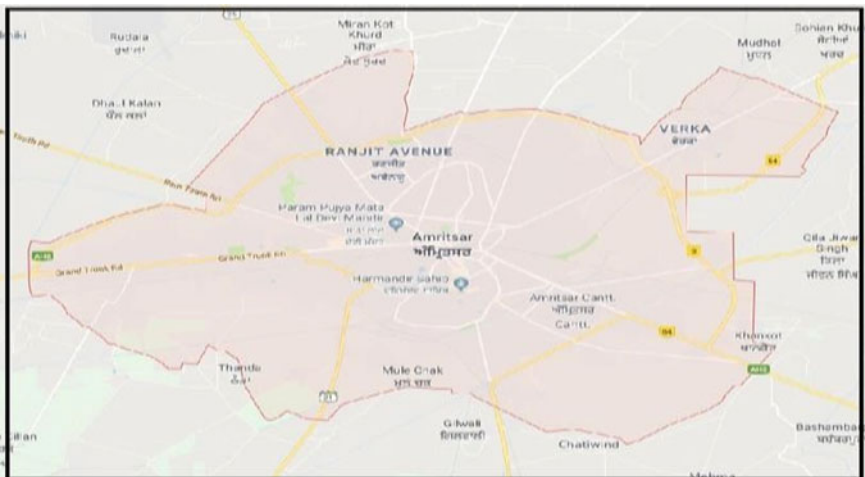


Fig. 2 Map of Amritsar (Punjab), India. Source Google Maps

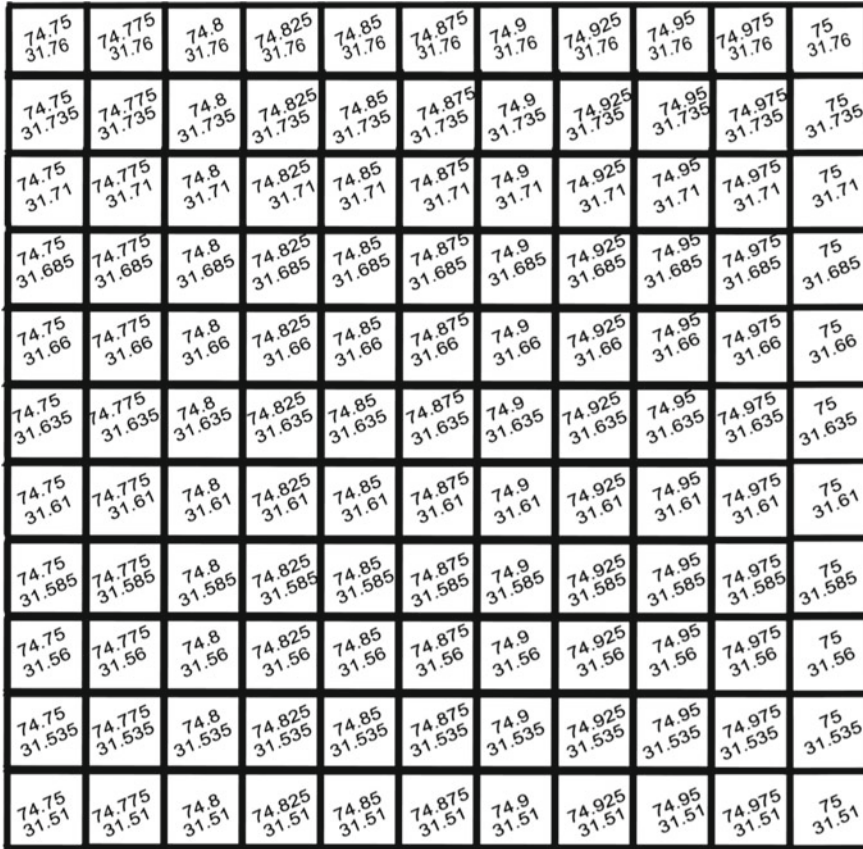


Fig. 3 Grid with size $0.025^\circ \times 0.025^\circ$ consisting of 121 points

1. Every one of the structural fault liable to create huge ground movements in the examination region has been recognized by superimposing epicentral map on tectonic plot. There exist 14 structural highlights in the seismic investigation region out of which 07 faults have been chosen as possible seismogenic sources. Figure 5 shows the tectonic map near Amritsar (Punjab).
2. The most extreme capability of seismogenic sources that is M_{max} has been assessed utilizing the findings proposed by [19].
3. The hypocentral distance of network highlight from each seismogenic source has been figured out using “geodatsource.com” taking the depth of focus equal to 15 km.
4. Parameters of the Ground Motion are computed by using GMPE, i.e., Ground Motion Parameter Equation developed by [17].
5. Ground Motion parameters have been figured out concerning different seismic faults for the calculation of SHA at a point and the sources which cause the most extreme movement at the focal point have been distinguished. For the network

Table 1 List of all the earthquakes occurring near seismic study area (IMD, Delhi)

S.no.	Year	Month	Day	Origin Time			Latitude (°N)	Longitude (°E)	Depth (km)	Magnitude M_w
				Hr.	Min	Sec				
1	1720	07	15	00	00	00	29.37	77.10	–	6.5
2	1827	09	06	00	00	00	32.50	76.00	–	5.5
3	1828	06	24	00	00	00	31.60	74.40	–	6.5
4	1842	03	05	00	00	00	30.00	78.00	–	5.5
5	1851	01	21	00	00	00	32.00	74.00	–	5.0
6	1856	04	07	00	00	00	31.00	77.00	–	5.0
7	1903	05	11	11	30	36.0	32.70	77.40	–	5.5
8	1905	04	04	0	50	0	32.30	76.25	–	8.0
9	1906	02	28	0	0	0	32.00	77.00	–	7.0
10	1945	06	22	18	0	51	32.60	75.90	–	6.5
11	1947	07	10	10	10	19	32.60	75.90	–	6.2
12	1950	08	12	03	59	6.0	32.60	75.90	–	5.5
13	1952	12	27	18	45	37.0	31.20	74.80	–	5.5
14	1962	09	15	12	35	8.0	31.90	76.20	–	5.5
15	1963	04	22	14	51	9.0	31.50	74.00	–	5.5
16	1975	12	11	10	09	50.2	33.00	76.10	42	5.0
17	1976	01	07	13	24	52.9	32.97	76.12	40	5.3
18	1978	06	14	16	12	4.8	32.24	76.61	6	5.0
19	1980	08	23	21	36	49	32.95	76.10	5	5.3
20	1980	08	23	21	50	1.2	32.90	75.80	12	5.2
21	1981	03	03	08	43	29.1	31.36	73.22	47	5.0
22	1986	04	26	07	35	16.2	32.15	76.40	33	5.5
23	1996	04	01	08	08	02	31.50	73.50	27	5.6
24	2012	03	05	13	11	04	28.70	76.59	14	5.0
25	2012	10	02	14	04	52	32.42	76.27	10	5.0
26	2014	08	21	13	41	16	32.25	76.8	10	5.1
27	2020	02	26	20	34	13	32.95	76.28	8	5.5
28	2021	02	12	22	34	40	31.57	75.09	10	6.1

point under thought, the greatest size capability of seismogenic source has been considered as the controlling quake.

4 Assessment of M_{\max}

The M_{\max} of any area depicts the capability of seismic strain which is relied upon to be delivered in the area. M_{\max} is for the most part assessed utilizing two methodologies

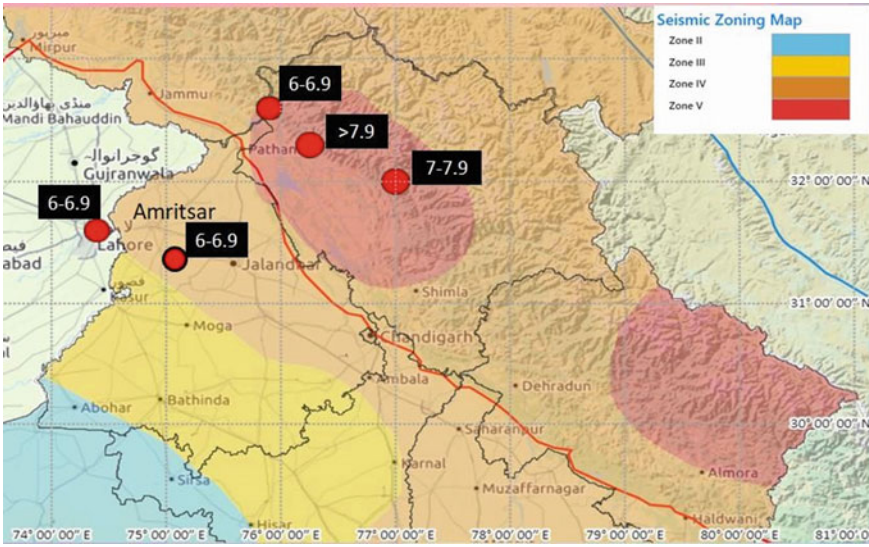


Fig. 4 Epicentral map

in particular deterministic and probabilistic strategies. The estimation of the M_{max} is done deterministically, for instance, adding an addition esteem to the greatest size noticed (i.e., to M^0) in the area. This technique is basic and can be applied to any seismotectonic setting. Earthquakes of extent (M_w) of 5 or more have been considered for M_{max} estimation. Sub-surface crack lengths (RLD) have been assessed as 1/3rd to 1/2th of the Total Fault Length (TFL) based on the worldwide data [20]. TFL of different sources in examination area has been taken from accessible writing [12, 21]. M_{max} for the potential seismogenic sources has been determined utilizing the all-around perceived connection through equation suggested by [19], i.e.,

$$\text{Log(RLD)} = 0.59M_w - 2.44 \tag{1}$$

This Eq. (1) isn't pertinent to seismogenic sources having deficiency length in excess of 350 km. Consequently, the upsides of M_{max} for such sources have been assessed by adding an addition 0.5 to maximum observed magnitude [5]. The upsides of Maximum observed magnitude (M_{obs}) for different seismogenic sources have been accounted for in Table 2. The M_{max} esteems as far as second extent assessed for the seismic investigation region go from 5.94 to 8.5 and have been accounted in Table 3.

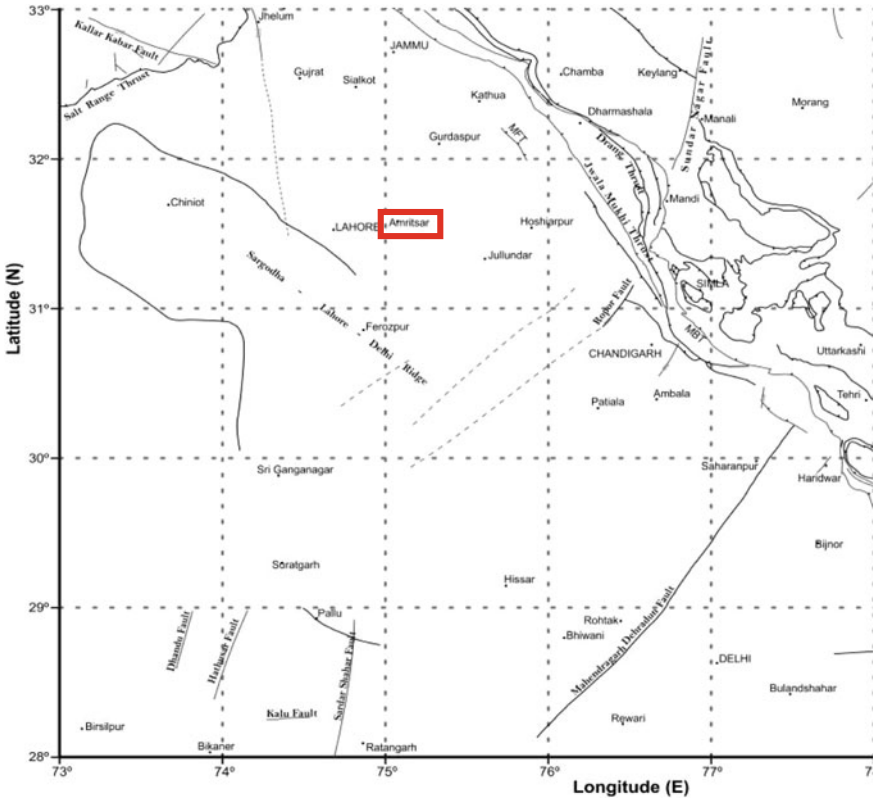


Fig. 5 Tectonic map of SSA [11]

Fig. 6 Hypocentral distance (r)

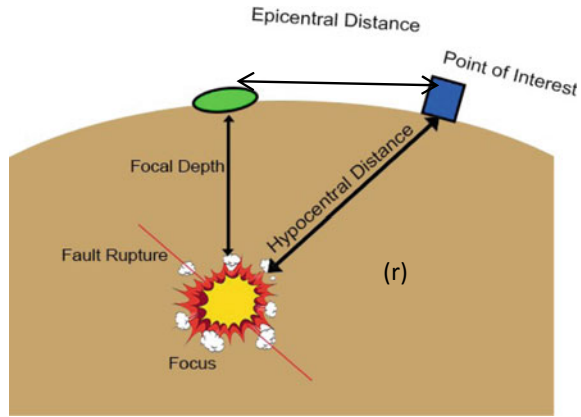


Table 2 List of all the active tectonic faults lying in SSA [11]

S.no.	Seismogenic source	M_{obs}
1	Sargodha-Lahore-Delhi-ridge (SLDR)	6.5
2	Main boundary thrust (MBT)	8
3	Main frontal thrust (MFT)	2.9
4	Jwalamukhi thrust (JMT)	5.5
5	Ropar fault (RF)	3.6
6	Lineament 1 (L1)	2.6
7	Lineament 2 (L2)	3.0

Table 3 Maximum magnitude potential for various seismic sources [11]

S.No.	Source	Fault type	Length (L_o)	Rupture length	M_{max}
1	SLDR	Neotectonic fault	605	201.66	7
2	MBT	Neotectonic thrust fault	450	150	8.5
3	MFT	Neotectonic thrust fault	35	11.66	5.94
4	JFT	Neotectonic thrust fault	277	92.33	7.47
5	RF	Neotectonic fault	35	11.66	5.94
6	L1	Minor lineament	87	29	6.61
7	L2	Minor lineament	159	53	7.06

5 Estimation of Seismic Hazard

The motivation behind SHA is to evaluate likely harm and misfortune because of forthcoming earthquakes. It includes measurable assessment of ground trembling hazard at a specific site. SHA can be used to plan provincial full scale or miniature drafting maps which are valuable for the improvement of quake safe structure plan and development, land use arranging, crisis plan, and assessment of conceivable monetary misfortune. In this investigation, ground movement model created by [17] is being utilized for assessing seismic hazard for City of Amritsar. The relationship is given by Eq. (2).

$$\ln\left(\frac{S_a}{g}\right) = C_1 + C_2M + C_3M^2 + C_4r + C_5 \ln(r + C_6e^{C_7M}) + C_8 \log(r) f_0 + \ln(\epsilon) \tag{2}$$

where $f_0 = m(\ln(r/100), 0)$

Spectral acceleration is written as ‘‘Sa’’, ‘‘M’’ represents the moment magnitude, and ‘‘r’’ is the hypocentral distance in kilometers and has been illustrated in Fig. 7. The coefficients C_1 to C_8 in the attenuation relation for Indo-Gangetic region.

$$C_1 = -3.1373, C_2 = 0.9365, C_3 = 0.0258, C_4 = -0.0076, C_5 = -1.4326,$$

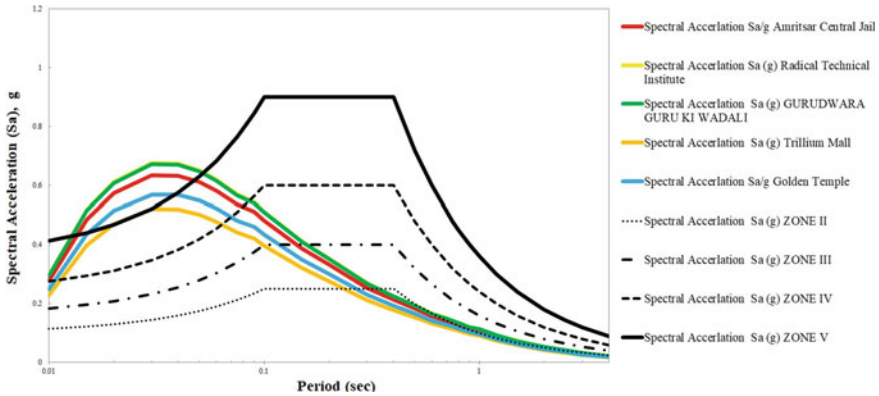


Fig. 7 DSHA-based response spectrum versus codal response spectra

$$C_6 = 0.0183, C_7 = 1.0198, C_8 = 0.1047, \sigma(\varepsilon) = 0.4095$$

where “*M*” is the moment magnitude, “*r*” is the hypocentral distance (shown in Fig. 7) in kilometer. The value of “*r*,” i.e., Epicentral distances as shown in Fig. 8 between source and site, has been determined using online site “GEODATASOURCE.” The focal depth has been accepted as 15 km since the recorded profundities of seismic tremors in this area fall in scope of 10 km to 20 km. For computing the values of spectral acceleration, site coefficients (C_1 to C_8) in the constriction connection are made available from NDMA report as announced in case of Indo-Gangetic area.

6 Results and Discussion

The PGA_{max} value at bedrock level for all network points sorts from 0.006 g to 0.414 g. As it is clear from Fig. 6, the Sargodha-Lahore-Delhi-Ridge (SLDR) is the fault which is active and lies closest to the seismic study area. Any tectonic activity in this neotonic fault will have major influence on Amritsar, thus causing the major threat to its important structures. Table 4 demonstrates the maxed out PGA values for all the active seismic faults lying in the seismic study area. Spectral acceleration which is demonstrated in Fig. 8 has additionally been created for the locales with the most extreme peril expectation to help tremor safe plan around there. Figure 8 shows correlation between plan reaction range for different zones according to Indian Seismic Code and DSHA reaction spectra produced for Amritsar.

Observation has been made that codal standards [6] disparage the peril for City of Amritsar. The spectra introduced are for rock destinations, and subsequently, it is important to complete ground reaction investigation for the locales underlain by soils to process most extreme flat ground speed increase needed for the plan of quake safe constructions.

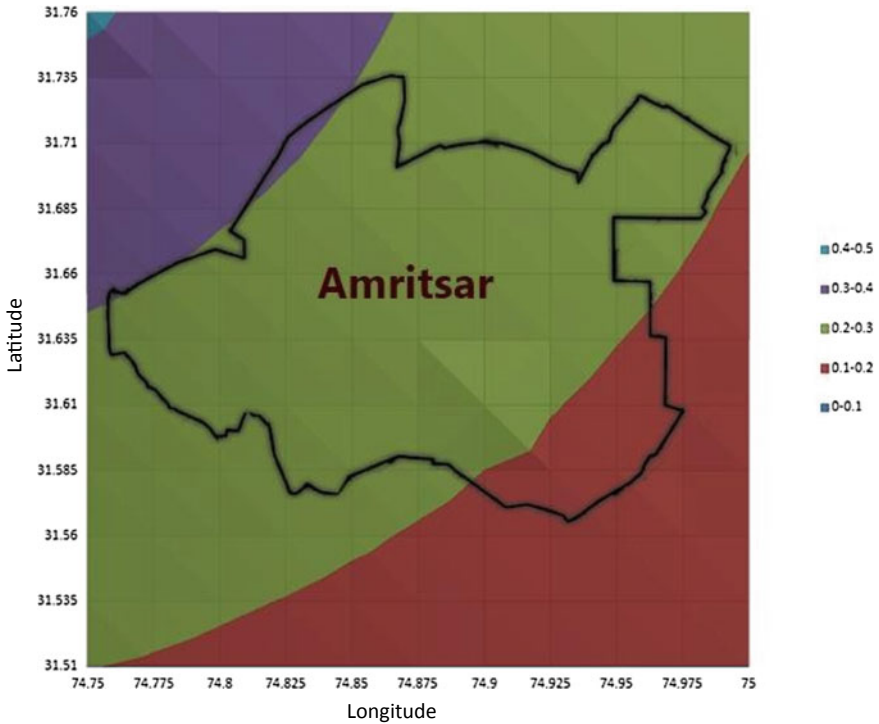


Fig. 8 Seismic contour map for smart city Amritsar

Table 4 PGA_{max} at bedrock level values for seismic sources of SSA

S.no.	Source	Abbreviations used	PGA (g)
1	Sargodha-Lahore-Delhi-Ridge	SLDR	0.414
2	Main boundary thrust	MBT	0.143
3	Main frontal thrust	MFT	0.02
4	Jwalamukhi thrust	JFT	0.061
5	Ropar fault	RF	0.006
6	Lineament 1	L1	0.038
7	Lineament 2	L2	0.044

The “zone factor” Z computed in this study is directly proportional to “design horizontal seismic coefficient” (A_h) [6]. Furthermore, the “base shear” (V_B) bears a direct relationship with A_h [6]. Thus, any increase in the value of Z will cause an increase in base shear, simply leading to increase in amount of reinforcement required. In addition to spectral acceleration, a special seismic contour map is also been constructed using interpolation technique and is depicted in Fig. 8.

7 Conclusion

1. There are total 14 structural highlights in the seismic investigation region out of which 7 structural highlights are chosen as most probable seismogenic sources.
2. The greatest capability of seismogenic sources that is the value of M_{\max} goes from M_w 5.94 to 8.5.
3. The PGA values have been determined utilizing the equation provided by NDMA. The sort of PGA_{\max} at bedrock level for the matrix goes from 0.006 to 0.414 g.
4. For the majority of the regions, the PGA_{\max} esteems determined are higher than the PGA esteems given in [6]. Henceforth, there is immediate requirement to update the codal values of zone factor for Amritsar (Punjab) and the abutting regions.
5. Response spectra have been plotted for six locales of selected region at which the greatest peril is required, and a seismic contour map is constructed to help specialists and town organizers in planning tremor safe constructions.

References

1. Bilham R (2004) Earthquakes in India and the Himalaya: tectonics, geodesy and history. *Ann Geophys* 47. <https://doi.org/10.4401/ag-3338>
2. Jade S (2004) Estimates of plate velocity and crustal deformation in the Indian subcontinent using GPS geodesy. *Curr Sci* 86:1443–1448
3. Kumar P, Yuan X, Kumar MR, Kind R, Li X, Chadha RK (2007) The rapid drift of the Indian tectonic plate. *Nature* 449:894–897
4. Kramer SL (1996) *Geotechnical earthquake engineering*. Prentice Hall
5. Gupta ID (2002) The state of the art in seismic hazard analysis. *ISET J Earthq Technol Pap No* 428(39):311–346
6. BIS-IS1893 (2016) *Criteria for earthquake resistant design of structures—part 1: general provisions and buildings*
7. Naik N, Choudhury D (2014) Deterministic seismic hazard analysis for the state of Goa, India. *Nat Hazards* 751, 75:557–580
8. Parvez IA, Vaccari F, Panza GF (2003) A deterministic seismic hazard map of India and adjacent areas. *Geophys J Int* 155:489–508
9. Sitharam TG, Anbazhagan P (2007) Seismic hazard analysis for the Bangalore region. *Nat Hazards* 40:261–278. <https://doi.org/10.1007/S11069-006-0012-Z>
10. Raghu Kanth STG, Iyengar RN (2007) Estimation of seismic spectral acceleration in Peninsular India. *J Earth Syst Sci* 1163, 116:199–214
11. Deep G, Naval S (2016) Deterministic seismic hazard analysis for proposed smart city, Jalandhar!Request PDF. In: *Int Geotech Eng Conf Sustain Geotech Eng Pract Relat Urban Issues*
12. Puri N, Jain A (2016) Deterministic seismic hazard analysis for the state of Haryana, India. *Indian Geotech J* 46:164–174
13. Chandan K, Naval S (2017) Deterministic seismic hazard analysis for proposed smart city, Ludhiana (India) Sanjeev Naval. *Electron J Geotech Eng* 22:4255–4270
14. Ganpathy G (2010) A deterministic seismic hazard analysis for the major cultural heritage sites of Tamil Nadu, India-Indian journals. *Int J Geomatics Geosci* 1:529–543

15. Gupta S, Naval S (2020) Analysis of orthotropic RC rectangular slabs supported on two adjacent edges—a simplistic approach. *Civ Eng J* 6:1992–2001
16. Gupta S, Singh H (2020) Analysis of reinforced concrete rectangular slabs with three-sides supported under uniformly distributed load, *Asian. J Civ Eng* 21:81–90
17. NDMA (2010) Development of probabilistic seismic hazard map of India
18. Dasgupta S (2000) *Seismotectonic atlas of India and its environs*, 59th edn. Geological Survey of India
19. Wells DL, Coppersmith KJ (1994) New empirical relationships among magnitude, rupture length, rupture width, rupture area, and surface displacement. *Bull Seismol Soc Am* 84:974–1002
20. Mark R, Bonilla M (1977) Statistical relations among earthquake magnitude, surface rupture length, and surface fault displacement. *Bull Seismol Soc Am* 74:0–47
21. Iyengar RN, Gosh S (2004) Microzonation of earthquake hazard in Greater Delhi area. *Curr Sci* 1193–1203

Ground Improvement and Transportation Geotechnics

Effect of Sand Blanket Reinforced with Geogrid Over the Stone Column in Compressible Clay Soils: 3D Numerical Study



Sudheer Kumar Jala, Sudhanshu Sharma, and Aijaz H. Bhat

Abstract The present study is on stiffening the soft cohesive soils with a sand blanket, sand reinforced with geogrid layer and reinforced with geotextile encased stone columns (GESCs). The three-dimensional numerical investigation was conducted on sand reinforced without and with a geogrid effect. And below the sand bed, the ordinary and encased columns are studied. The circular footing (uniform distributed load) rests on a multi-layered soil model. The significant parameters investigated through these models are load improvement factor (LIF), bearing capacity improvement ratio (BCR), settlement reduction ratio (SRR), modulus of subgrade reaction and stiffness improvement ratio. From the results, it is evident that sand bed with ordinary stone column and GESC cases gives a considerable improvement. The percentage of improvement in the case of sand bed reinforced with geogrid layer followed by GESC installed is 148% than the untreated cohesive soil. This study is useful for highway subgrades and raft slabs that rest on soft cohesive soils to control total settlement and non-uniform settlement.

Keywords Sand bed · Ordinary stone columns · Geotextile encased stone columns · Stiffness · Modulus of subgrade reaction

1 Introduction

Compressible soils like clay soil and peat with a higher plasticity index give an excessive settlement. Several methods are adopted to reduce the plasticity index of the soil. Particularly at foundation and pavement subgrade constructions, regular practice is to replace the expansive soils with the granular soil and reinforce the soil mass below the foundation/subgrade by various inclusions like a geosynthetic group

S. K. Jala (✉) · S. Sharma · A. H. Bhat
Department of Civil Engineering, DAV Institute of Engineering and Technology, Jalandhar, India
e-mail: sudheeritd@gmail.com

S. Sharma
e-mail: sudhir.jala@gmail.com

© The Author(s), under exclusive license to Springer Nature Singapore Pte Ltd. 2023
A. K. Agnihotri et al. (eds.), *Proceedings of Indian Geotechnical and Geoenvironmental Engineering Conference (IGGEC) 2021, Vol. 1*, Lecture Notes in Civil Engineering 280,
https://doi.org/10.1007/978-981-19-4739-1_36

397

of material, horizontal steel strips, fiber material, etc. And the famous practice in the recent past is to install the stone columns at shallow depths. They not only enhance the bearing strength but will also reduce the settlement of the footing/subgrade.

1.1 Background

Several researchers [1–4] have reported an increase in bearing capacity and reduced settlement behavior of foundations by the inclusion of reinforcements. Stone columns are constructed by replacing poor soil with crushed stone aggregate to construct a vertically resistant system. The stone column technique is a useful, environment-friendly and cost-effective method for resolving settlement issues in the ‘soft’ soils. Stone columns also increase the consolidation rate in soft soils because of high permeability. It is observed from the literature that the location of inclusions (influence depth) significantly affects the reinforcing action. Biaxial geogrids and granulated blast furnace slag (*GBS*) were tested to determine the optimum depth for the first layer of reinforcement from the footing base and its effect on bearing capacity ratio (BCR). Gill et al. [5] reported that the bearing capacity of a coal ash slope with coal ash used as an embankment fill material is found to yield an increase in bearing capacity using geogrids. The bearing capacity improvement with number of geogrid layers ($N = 1, 3, 4$) in sand underlain by silt clay reported as 44.44%, 61.11% and 72.22% respectively [6]. Laboratory model test results for the ultimate bearing capacity of a strip foundation supported by multi-layered geogrid-reinforced sand at one relative density were also compared with theoretical results.

The previous researchers worked experimentally and numerically on ordinary stone columns and geosynthetic stone columns. The published literature is proven that they are very effective in increasing the bearing capacity and controlling the settlement in expansive clay soils when they were at their liquid limit and undrained shear strength is less than 15 kPa [7–10].

Mehrannia et al. [11] examined a granular blanket with two thicknesses of 40 and 75 mm which were reinforced by geogrid and also use stone column which was reinforced by geotextile encasement which helps to increase stress concentration ratio, bearing capacity and the stiffness of stone column. Sudheer et al. [12] reduced the amount of lateral deformation up to 92 and 74% in the case of HC-2 and HC-1 encasement systems with a comparison of the OSC case. The bearing capacity of encased stone columns was done numerically. Hataf et al. [13] with the help of graphical representation showed that the maximum value of load factor which was equal to 1.4 means encasing the stone columns increases the bearing capacity of the stone column by 40%. Using loaded strip footing resting on mattress-strips fly ash slopes, [2] examined maximum to minimum percentage variation of bearing capacity from 6.96 to 0.54. Lateral bulging is reduced when horizontal reinforcement is used in stone columns because of additional support provided by frictional and interlocking interaction of geogrids [14]. It was found that under-reamed cemented stone columns are highly effective in enhancing the bearing capacity and stiffness of

soft clay ground. Bearing capacity improvement factor in case of under-reamed SC increases about 45–50% [15].

In the present study, authors are numerically comparing the load-carrying capacity of the sand blanket, geogrid at the interface of the two layers and vertical stone column without and with geosynthetic encasement in soft soils. The total six cases were studied in the current research that are presented graphically in Fig. 1. Case 1. clay without any reinforcement, case 2. compressible clay with 0.5m coarse sand blanket at top of the surface, case 3. geogrid was applied for reinforcing the soils at the interface of the two layers, case 4. ordinary stone column in the full thickness of clay underneath the sand blanket and there is no geogrid used at the interface of the two layers, case 5. encased stone column in the full thickness of clay underneath the sand blanket and there is no geogrid used at the interface of the two layers and case 6. encased stone column with geogrid at the interface clay -sand.

2 Materials

For the numerical analysis purpose, clay as foundation soil, sand blanket as a top layer, geogrid and stone aggregates are used in the column as fill material. Table 1 presented the properties of materials used for the study.

3 Numerical Modeling Considerations—Plaxis FE Analysis

Plaxis 3D program was used to perform finite element analyses. In all the FE analyses, the thickness of the soft soil was kept as 8 m in the 1st case and later a 0.5 m sand layer was laid on top of the clay. The stone column having a diameter of 1 m extends to the full depth of the clay layer. The Mohr–Coulomb parameters used in the numerical analyses are similar to the typical values used by other researchers. The clayey soil was also modeled as Mohr–Coulomb material. The geosynthetic was modeled as an elastic membrane element. The geosynthetic was assumed to be an isotropic linear material, with an assumed Poisson's ratio of 0.3. For the geosynthetic used to encase granular columns on different projects, the design tensile modulus (J) values ranged from 300 and 10,000 kN/m. Hence, a value of $J = 4500$ kN/m was used in the numerical analyses. The software which the authors used (Plaxis 3D) defines the interaction factor. The angle of shear resistance depends on the interaction coefficient value.

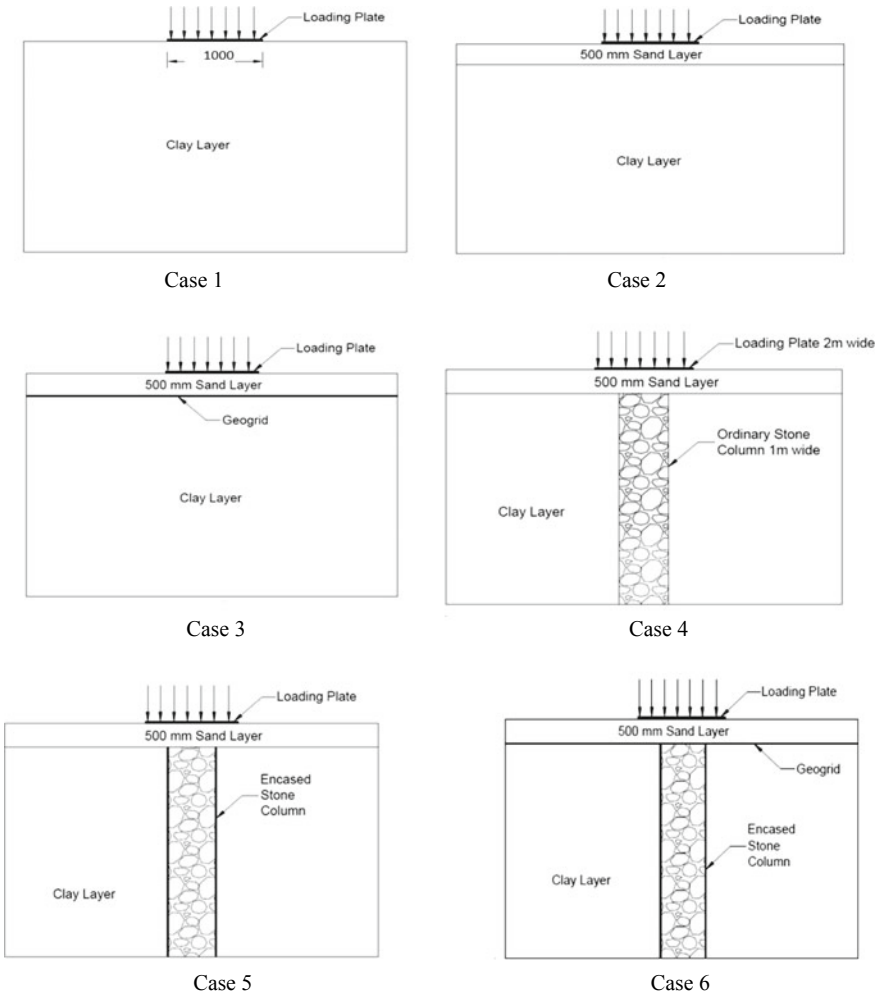


Fig. 1 Graphical representation of the cases studied

4 Results and Discussions

To determine the stress–settlement behavior on top of the soil model, soil nodal points corresponding to the top of the column were subjected to a series of vertical downward displacements by applying a uniformly distributed load.

The surrounding soil nodes were left to displace freely because the analysis was done to examine the behavior of a single column that is being used to support an applied structural load. Corresponding to the load applied at the top, the resultant settlement was recorded and a load-settlement graph was drawn for each case as shown in Fig. 2.

Table 1 Material properties used in the analysis [7–9]

Test parameter	Sand (drained)	Geogrid	Clay (undrained)	Stone aggregate (drained)
Eref (modulus of elasticity) kN/m ²	20,000	–	5000	40,000
Tensile strength (kN/m)	–	4500	–	–
V (Poisson’s ratio)	0.3	–	0.33	0.3
Φ (angle of internal friction)	34°	–	30°	44°
Ψ (psi)	4°	–	0	14°
C	1	–	15	0
Unsaturated unit weight (kN/m ³)	17	–	17	17
Saturated unit weight (kN/m ³)	20	–	18	22
K _x (m/day)	1	–	0.0100	1
K _y (m/day)	1	–	0.0100	1

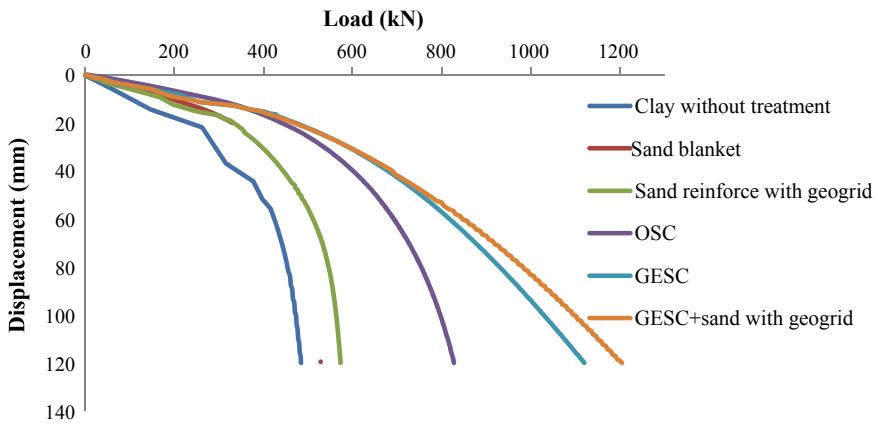


Fig. 2 Effect of sand blanket, geogrid and stone column on a load-carrying capacity of compressible clay soils

From Fig. 2, it is evident that untreated clayey soil undergoes larger deformations under smaller load values. The sand layer is provided at the top of the clay; it carries more load (12.5% more) for the same value of displacement. The geogrid is placed between the clay and the sand layer; the value of the load is 25% more than untreated soil. In another case, ordinary stone column (OSC) is placed in the clay underneath the sand layer without any geogrid and the load carried by the composite soil is 100% more than untreated soil. In another case, GESC is placed in the clay underneath the

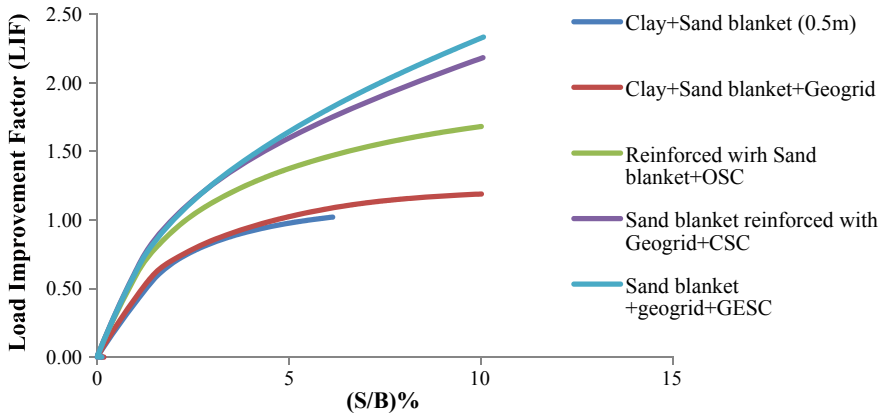


Fig. 3 Variation of load improvement factor with (S/B) ratios

sand layer without geogrid and the value of the load is 162% more than untreated soil. In the last case, GESC is placed in the clay-sand soil having an interface between them; the value of the load is 187% more than the untreated soil.

Figure 3 shows the plot between the load improvement factor (LIF) and the settlement upon width for all the cases discussed earlier. The value of LIF is lowest for clay soil having a top layer with a 0.5 m sand layer. The geogrid is placed between the sand and the clay layer, and the LIF increases by 20%. The OSC is placed in the clay under the sand layer without geogrid, and the LIF increases by 70%. When the OSC is encased, the LIF value increases by 120%. In the last case, GESC is placed with geogrid at the interface of the sand and clay layer, and the LIF value increases by 130%.

The relative improvement in the load-carrying capacity of various improvement techniques is computed in terms of bearing capacity improvement ratio or bearing capacity ratio (BCR) which is equal to the ratio of bearing capacity of treated soil to the untreated soil resulted presented in Fig. 4. The BCR value increases with different ground improvement techniques. The BCR value is high when soil is reinforced with GESC, and geogrid is placed in between the clay and sand layer. It is evident from Fig. 5 that the settlement reduction ratio increases from case 1 to case 6. The highest settlement reduction is possible with the OSC, GESC and sand reinforced with the geogrid followed by the GESC. This may be due to the geogrids, the settlement reduced considerably, and also because of interlocking and high tensile strength of the geogrid ribs in transverse and machine direction, it contributes to the load-carrying capacity of the soil.

Figure 6 shows the variation of stiffness of the treated soil which is an indicator to determine the tendency for material to return to its original position after being subjected to load. The stiffness is defined as the ratio of the load applied on a boundary through a loading area divided by the displacement experienced by the loaded area. From Fig. 6, the stiffness of the composite ground steadily increases in all cases

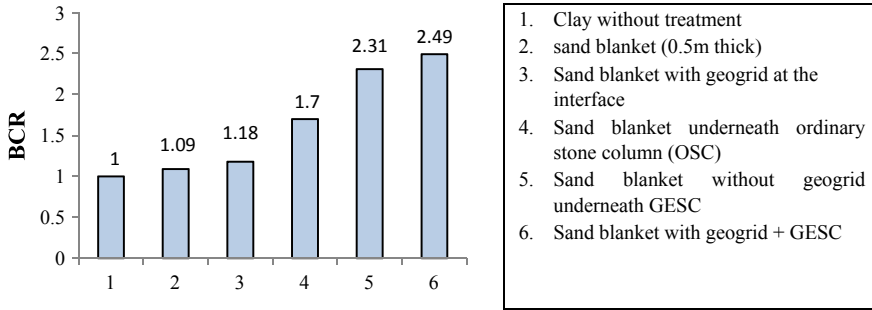


Fig. 4 Bearing capacity ratio variation with the treatment of the compressible clay soil

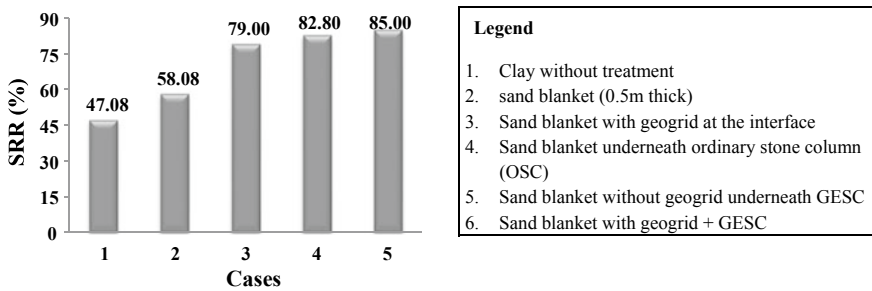


Fig. 5 Effect of the sand blanket, geogrid, CSC and GESC treatments of incompressible clay soils

when compared to the clay soil without treatment. The percentage increases of the stiffness when compared to the clay without treatment are 18% in the case of sand with geogrid, 70% in the case of OSC, 131% in the case of GESC and 148% in the case of sand reinforced with the geogrid plus GESC case. The stiffness of the subgrade and composite soil is a very important parameter to design the rigid pavements and raft or mat foundations. This study may be useful to improve the stiffness factor of the composite ground.

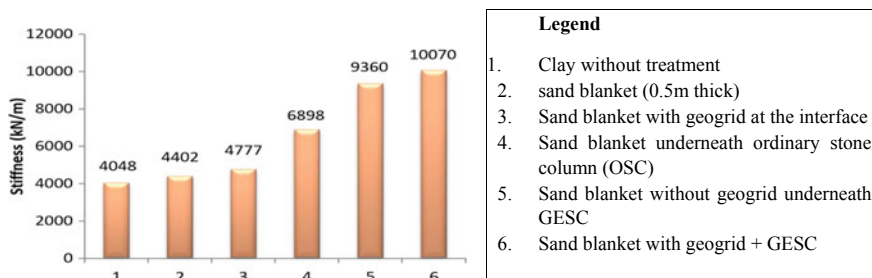


Fig. 6 Variation of stiffness of the treated compressible soils

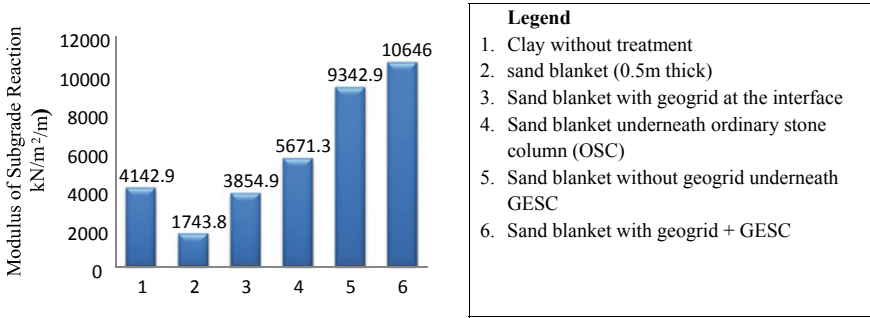


Fig. 7 Comparison of modulus of subgrade reaction of the treated compressible soils

Figure 7 shows the modulus of subgrade reaction of the treated compressible soils. The conceptual relationship between the applied pressures against settlement at that particular point is used vastly in the analysis of foundation members. It is expressed as $K_s = p/s$. It can be defined as the initial slope of the applied pressure to the settlement of the plate load test curve. The unit of the subgrade modulus is kN/m²/m. In the present study results, as shown in Fig. 6, the subgrade reaction is reported very less when the upper compressible layer is replaced with the 0.5 m thick sand. This may be due to the looseness of the granular particles, and compression is higher at the immediate of the footing load. Subgrade reaction is improved consistently in the remaining cases. The improvement of the subgrade reaction from OSC to GESC with a sand bed is significant. It is useful in piles subjected to lateral load, strip footing, mats and rigid pavement design and other types of foundation member’s design.

5 Failure Mechanism of Reinforced Soil

The mode of failures of all the six cases are presented in Fig. 8; it is evident that just below loading plate settlement is higher due to higher compression; and it is following Terzaghi’s failure model. The depth of the failure zone increases as reinforcement is incorporated through the sand, sand with geogrid, sand with OSC, sand with GESC and sand with geogrid and GESC cases.

6 Conclusions

The load-settlement characteristics of the parent clay soil can be enhanced by providing a sand blanket on the top of the clay by 12.5% more for the same value of displacement but when GESC is placed in the clay-sand soil having geogrid at the interface, the value of the carrying load is 187% more than the untreated soil. Encasing

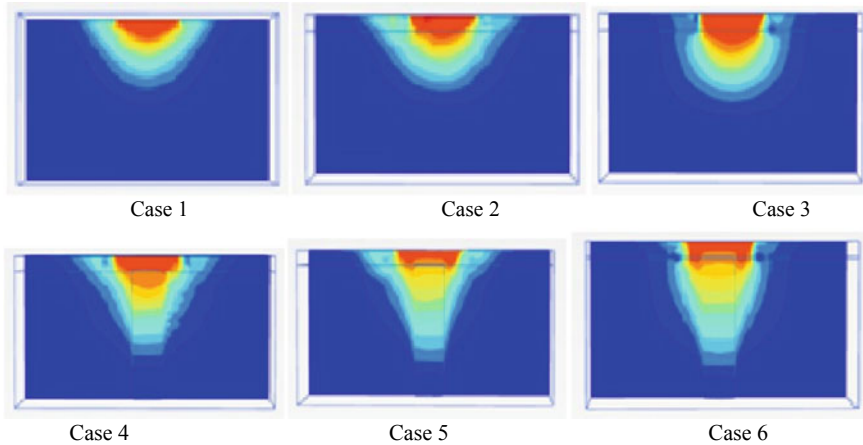


Fig. 8 Mode of failure of the clay without and with sand, geogrid and stone columns

the stone column with geogrid increases the bearing capacity of the composite foundation and reduces the settlement. The maximum value of bearing capacity is reported for an encased stone column with geogrid at the clay-sand interface.

Although the modulus of subgrade reaction was reported to be less when a sand blanket was applied on top of the clay, it significantly increases when a stone column was introduced. The modulus further increases when a stone column was encased and geogrid was introduced at the clay-soil interface.

This study shows the value of modulus of subgrade reaction of the last case as clay and sand with GESG and geogrid at interface is $10646 \text{ kN/m}^2/\text{m}$ which is more effective than other cases especially than clay and sand with CSC and geogrid at the interface by 14%.

The stiffness of the composite soil follows the same trend as the bearing capacity ratio. The stiffness is highest for an encased stone column with geogrid at the clay-sand interface.

References

1. Kumar A (2018) Behavior of strip footing resting on pretensioned geogrid reinforced ferrochrome slag subgrade. Doctoral dissertation, NIT, Jamshedpur
2. Nadaf MB, Mandal JN (2017) Model studies on fly ash slopes reinforced with planar steel grids. *Int J Geotech Eng* 11(1):20–31
3. Yadu L, Tripathi RK (2014) Effect of depth and number of layers of reinforcement on bearing-capacity ratio of strip footing resting on granulated blast-furnace slag reinforced with geogrid. In: *Geo congress: geo-characterization and modeling for sustainability*, pp 3605–3614
4. Prasad PS, Ramana GV (2016) Feasibility study of copper slag as structural fill in reinforced soil structures. *Int J Geotext Geomem* 44(6):623–640

5. Gill KS, Choudhary AK, Jha JN, Shukla SK (2013) Large model footing load test on multi-layer reinforced coal ash slope. In: *Geo-congress: stability and performance of slopes and embankments III*, pp 489–498
6. Kolay PK, Kumar S, Tiwari D (2013) Improvement of bearing capacity of shallow foundation on geogrid reinforced silty clay and sand. *J Const Eng*
7. Ghazavi M, Yamchi AE, Afsar JN (2018) Bearing capacity of horizontally layered geosynthetic reinforced stone columns. *Geotext Geomembre* 46:312–318
8. Murugesan S, Rajagopal K (2006) Geosynthetic-encased stone columns: numerical evaluation. *Geotext Geomembr* 24(6):349e358
9. Malarvizhi SN, Ilamparuthi K (2007) Comparative study on the behaviour of encased stone column and conventional stone column. *Soils Found* 47(5):873–885
10. Black JA, Sivakumar V, Madhav MR, Hamill GA (2007) Reinforced stone columns in weak deposits: laboratory model study. *J Geotech Geoenviron* 133(9):1154–1161
11. Mehrannia N, Kalantary F, Ganjian N (2018) Experimental study on soil improvement with stone columns and granular blankets. *J Cent South Univ* 25:866–878
12. Sudheer KJ, Rawat S, Gupta AK (2021) Loose ash fills reinforced with the high confined encased stone columns—experimental and numerical investigation. *Int J Geotech Geolog* 39:2503–2520
13. Hataf N, Nabipour N, Sadr A (2020) Experimental and numerical study on the bearing capacity of encased stone columns. *Int J Geo-Eng* 11:4
14. Naderi E, Asakereh A, Dehghani M (2018) Bearing capacity of strip footing on clay slope reinforced with stone columns. *Arabian J Sci Eng*
15. Fatma KS, Kolosov ES, Fattah MY (2019) Behavior of different materials for stone column construction. *J Eng Appl Sci* 14(4):1162–1168
16. Dash SK, Bora MC (2013) Influence of geosynthetic encasement on the performance of stone columns floating in soft clay. *Can Geotech J* 50:754–765
17. Prasad S, Satyanarayana PVV (2016) Improvement of soft soil performance using stone columns improved with circular geogrid discs. *Ind J Sci Techn* 9(30)

Use of Chitosan Biopolymer and Fly Ash to Enhance Mechanical Properties of Soil



Rohan M. Shinde, Shweta G. Jambhulkar, and Rupa S. Dalvi

Abstract For the stabilization of expansive soil, chemical stabilizers like cement and fly ash are more often used. But chemical stabilizers are not eco-friendly. Therefore, an attempt is toward an eco-friendly and sustainable additive possessing efficient property to replace such chemical additives. Thus, biological additive like biopolymers is studied. Biopolymer like chitosan is widely used in geotechnical concern giving effective strength gain results. In the present study, an optimum dosage of chitosan (CS) is found out performing UCS test by increasing chitosan of 0, 0.01, 0.0125, 0.025 and 0.05%. Then, the fly ash (FA) was amended to the soil by weight of 15, 20, 25 and 30% to find out the right amount that may provide strength characteristics. Laboratory tests like unconfined compressive strength test (UCS) and direct shear test (DST) are performed for dry condition curing of 0 day, 1 day, 3 days, 7 days and 28 days on clay soil, chitosan treated clay soil and fly ash amended clay soil. Results are compared between treated and untreated soil. Strength gain is achieved in stabilized soils with respect to an untreated BCS due to increase in cohesion of clay. Numerical model was tested using Plaxis 2D to analyze the settlement characteristics of the stabilized soil. It showed that the chitosan treated soil with 20% fly ash replacement (CS-FA) provided good results.

Keywords Biopolymer · Soil stabilization · Chitosan · Fly ash · Unconfined compressive strength · Direct shear test · California bearing ratio

R. M. Shinde (✉) · S. G. Jambhulkar · R. S. Dalvi
Geotechnical Engineering, College of Engineering, Wellesley Rd, Shivajinagar, Pune,
Maharashtra 411005, India
e-mail: shinderm19.civil@coep.ac.in

S. G. Jambhulkar
e-mail: jambhulkarsg18.civil@coep.ac.in

R. S. Dalvi
e-mail: rsd.civil@coep.ac.in

1 Introduction

Soil stabilization in a broad sense includes various methods used for modifying the properties of soil to enhance its engineering performance. By stabilization, the major properties of soil, i.e., volume stability, strength, compressibility, permeability, durability and dust control are improved, which makes the soil suitable for use. The mechanical properties of these naturally occurring soil are not enough to fulfill engineering application. To sustain and withstand the load of structure, the soil needs improvement. There are different methods of stabilization, which include physical, chemical and polymer methods of stabilization. Physical methods involve physical processes to improve soil properties. This includes compaction methods and drainage. Drainage is an efficient way to remove excessive water from soil by means of pumps, pipes and canal with an aim to prevent soil from swelling due to saturation with water. Compaction processes lead to increase in water resistance capacity of soil. Drainage is less common due to generally poor connection between method effectiveness and cost. But, compaction is very common method. Although it makes soil more resistant to water, this resistance will be reducing over time. Chemical soil stabilization uses chemicals and emulsions as compaction aids, water repellents and binders. The most effective chemical soil stabilization is one which results in non-water-soluble and hard soil matrix. Polymer methods of stabilization have several significant advantages over physical and chemical methods. These polymers are cheaper and are more effective and significantly less dangerous for the environment as compared to many chemical additives. Thus, as an alternative chitosan biopolymer is used to improve the soil efficiently.

2 Literature Reviewed

The soil stabilization is a strategy used to enhance soils to meet the requirements of different kinds of projects. Soil stabilization can be categorized to chemical, biological, electrical and mechanical. Traditional chemical soil stabilizers like lime and cement seem to be widely used in improvement of fine-grained soils for a long time as these stabilizers lead to pollution and have harmful environmental impacts. So, as biopolymers are abundant in nature, many are known to be harmless and beneficial (Kang et al. 2018). Because of their natural origins, they are synthesized from biological processes. These are eco-friendly sustainable material than chemical soil additives and can achieve the same amount of strengthen at much lower concentration than that of traditional stabilizer (Latifi et al. 2016). From various types of biopolymers used, in this study, focus is given to chitosan (CS) biopolymer and its behavior with expansive soil as it is present in most parts of central India, CS having potential to enhance the mechanical properties of soil (Agular et al. 2016; Latham and Lee 1995).

Chitosan is a biodegradable biopolymer obtained by deacetylation of chitin which is second most abundant naturally occurring polysaccharide synthesized from crustacean shell waste. It also has the tendency to degrade over a period in the aqueous environment (Hataf et al. 2018). Therefore, fly ash with biopolymer is used to stabilize the soil in an optimized way to attain the strength over the course of time (Latifi et al. 2016). The improved performance of such soil is analyzed with compaction tests, unconfined compression test and shear test. And to analyze the settlement characteristics, numerical model was prepared.

3 Materials

3.1 Soil

The expansive soil used in this study was collected from Loni Kalbhor, Pune. The soil was oven-dried and sieved through sieve opening of 4.75 mm to remove gravel with specific gravity $G_s = 2.8$. The grain size distribution curve was obtained through sieve analysis and hydrometer analysis in accordance with IS 2720. As shown in Fig. 1, the soil contains 22.1 wt% of gravel, 23.83 wt% of sand, 25.24 wt% of silt and 28.83 wt% of clay as per IS 2720. The gradation curve of fly ash shows it as silt type. Based on the gradation curve and Atterberg limits, the base soil was therefore classified as silty clay of intermediate plasticity in accordance with the Indian Standard Classification System. It has low shrink-swell capacity. Table 1 shows the properties of soil.

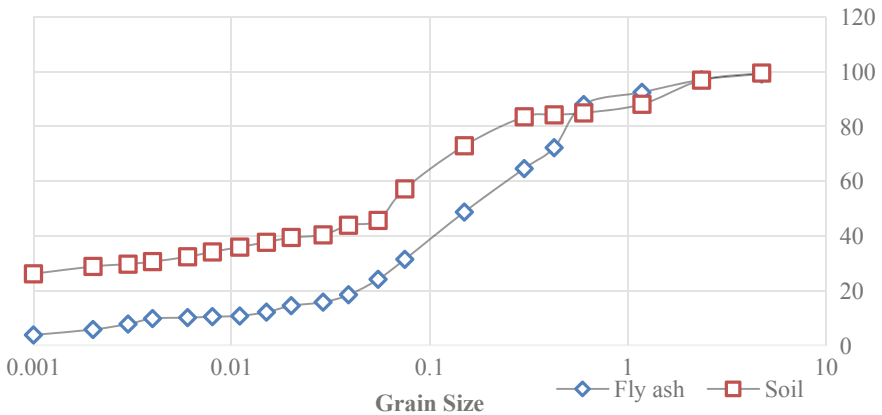
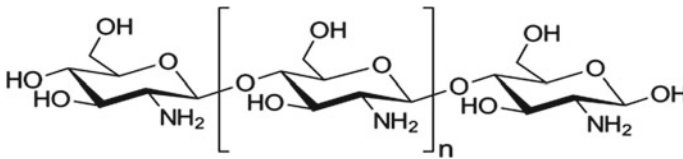


Fig. 1 Grain size analysis of virgin soil and fly ash

Table 1 Physical properties of soil

S. No.	Property	Value
1	Specific gravity	2.8
2	Liquid limit	40%
3	Plastic limit	21%
4	Plasticity index	19
5	Maximum dry density	1.705 g/cc
6	Optimum moisture content	19.4%
7	Cohesion	21.9 kN/sq m
8	Angle of internal friction (deg.)	10°

**Fig. 2** Chemical structure of chitosan biopolymer

3.2 Chitosan Biopolymer

Chitosan is a low soluble high viscous substance. It is a natural, biodegradable, biocompatible polymer with antimicrobial activity and has a wide range of applications in different fields such as membranes, medicine, drug delivery, hydrogels, water treatment, adhesives, food packaging, fuel cells and surface conditioner and also used effectively in geotechnical concern. Chitosan is usually obtained from discarded crustacean shells of seafood industry. It is a natural, biodegradable, biocompatible polymer.

The appearance is of whitish color in the powdered form. Chitosan possesses highly reactive amino and hydroxyl groups. The structure is shown in Fig. 2. The different concentrations of chitosan solutions were prepared, in all cases by dissolving predetermined mass of chitosan in a 1% (v/v) acetic acid solution. Solution was stirred for 5 h. to form uniform solution. Different solution was prepared for different percentage as 0, 0.01, 0.0125, 0.025 and 0.05%, and then, chitosan solutions were added to the soil.

3.3 Fly Ash

Fly ash used in experiment is classified as Class F, collected from locally available cement industries near Pune. It shows the SEM image of the Class F fly ash. It is

Table 2 Properties of fly ash

S. No.	Property	Value
1	Specific gravity	2.06
2	Maximum dry density	1.13 g/cc
3	Optimum moisture content	17.71%
4	Cohesion	28.3 kPa
5	Angle of internal friction (deg.)	27.5°

shown that most of the fly ash particles are smooth, with some relatively oversized and irregular shaped particles. Some vitreous unshaped fragments can also be seen in the fly ash samples. The fly ash particles ranged from few micrometers to a hundred micrometers. Small particles are attached to large particles, and the contact area varies significantly. The grain size distribution curves of the kaolinite clay and fly ash are shown in Fig. 1. In general, fly ash particle sizes are at microscale; however, kaolinite aggregates are much smaller. The specific gravity is found out to be 2.06 by density bottle method. The optimum moisture content was 17.71%, and the maximum dry density was 1.31 g/cm³ (Table 2).

4 Sample Preparation and Experimental Program

In this study of stabilization of black cotton soil, experimental program was carried out in four stages. At the first stage, the mechanical properties of an untreated soil were found out. In the second and third stage, mechanical properties of treated clay are found out for chitosan treated clay and fly ash amended clay, while in the last stage, numerical study was made and the variation in settlement was studied. For preparing the solution of 0.0125% (w/w) of chitosan content, it requires 0.175 gm (1400 soil wt × 0.0125%) of chitosan powder, 1.75 ml (100 × 0.175/10) of chitosan powder solution and 418.25 ml (480–1.75) of hot water. The water to be added should have pH value between 5.5 and 6 for proper deacetylation process of chitosan. Fly ash was mixed with soil in percentages of 15, 20, 25 and 30%. The 20% fly ash mix was found to be effective of all mixes, as it showed peak results. Then, the soil was treated with chitosan biopolymer solution of 0.0125% to the 20% FA-80% soil mix. To understand the improvement of the strength characteristics of polymer amended soil mixes, mechanical tests like Atterberg limits, Proctor compaction, unconfined compression and direct shear tests were conducted in accordance with IS 2720 and properties of mixes were found out for different curing period of 0 day, 1 day, 3 days, 7 days and 28 days.

4.1 Direct Shear Test

For fine-grained soils, the small box direct shear test is to be performed. This test is useful to find out shearing resistance of soil sample giving shearing factor parameters such as cohesion and angle of internal friction. The normal load is applied in either stress-controlled or strain-controlled condition. The strain rate was kept at 1.25 mm/m until the specimen failed or reached 20% longitudinal displacement with vertical loads of 0.5, 1 and 2 kg which were used for each soil sample. Small box shear test is performed in accordance with IS 2720.

4.2 Unconfined Compression Test

The unconfined compressive strength is determined in accordance with IS 2720. The strain rate was kept at 1.25 mm/m until the specimen failed or reached 20% shear strain. Soil samples were mixed at OMC in accordance with the data from standard Proctor test with specimen size 38 mm in diameter and 75 mm in height. Each specimen tested was compacted in 3 layers in a Proctor mold. Afterward, three specimens were extracted from each mold filled for immediate UCS test. Sample preparation and its quality control are provided in IS 2720.

5 Numerical Model

5.1 Model Description

The finite element model was built using the software *Plaxis 2D*. The used model is a concrete footing 3 m width and 0.50 m in thickness resting on 10 m layer of soil. The soil boundaries were extended horizontally for 10 m from the footings at both sides, with a total horizontal length of 23 m, and it also extended 10 m under the footings. The horizontal boundary was restrained in both horizontal and vertical directions, however; the vertical boundary was restrained just in the horizontal direction; and fifteen-node elements were used for both soil and footings. The model mesh was generated as a medium coarseness and then refined to be fine to increase the node numbers around the footing in the affected area as shown in Fig. 3.

The concrete footing was modeled as a linear elastic non-porous material, which is defined by the total unit weight (γ_{unsat}), modulus of elasticity (E) and Poisson's ratios (ν). The soil was simulated using the Moher-Coulomb model by defining the soil unit weight (γ), Young's modulus (E), cohesion stress (C) and friction angle (ϕ). The soil shear parameters that are needed for the Moher-Coulomb model were obtained from the direct shear results which were performed previously in this study.

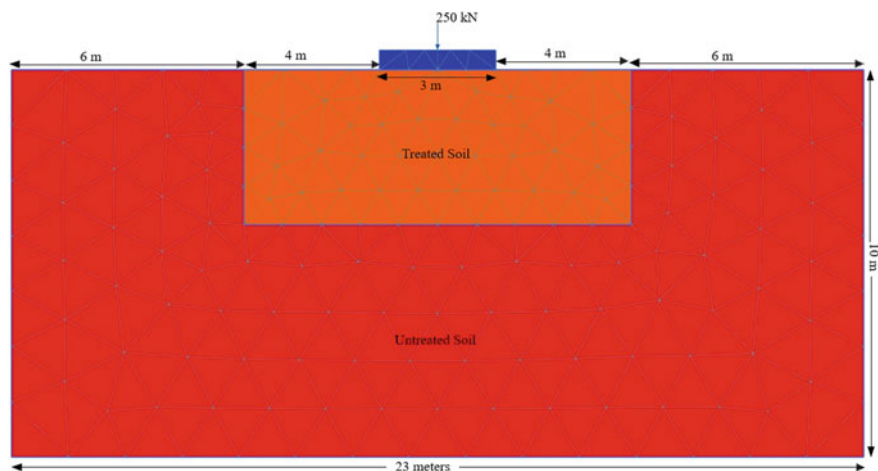


Fig. 3 Soil model

Young's modulus (E) was calculated from stress–strain curve obtained from UCS test according to Hooke's law.

The model was used after that to determine the stress/displacement curves for treated soils, which is essential to estimate the bearing capacity of the treated soil. It was also used to calculate the settlement under a loaded footing rested on treated soil.

6 Results and Discussion

Table 3 shows the comparison of optimum moisture content (OMC), maximum dry density (MDD) and 28th day compressive strength of untreated and soil amended with fly ash mixes as FA15, FA20, FA25 and FA30. As observed, the FA15 mix showed peak result with MDD of 17.44 kN/m^3 and least OMC at 18.25%, but with further increasing in fly ash content, lesser compaction was achieved by the other mixes and the required water content increased. But the 28th day UCS values of FA20 mix showed peak result with 17.25 g/cc of density achieved at 18.5% moisture content. The virgin soil replaced with amount of 15–20% proves to be beneficial as the gradation of soil is changed.

6.1 UCS Results

It is performed on different chitosan concentration stabilized soil mixes for 0-day curing period, and results are found out for optimum value of chitosan concentration

Table 3 Comparison of OMC, MDD and UCS for different fly ash mixes

Particular	Dry density kN/m ³	OMC %	28th day strength kPa
Untreated	16.72	19.4	207.77
FA15	17.44	18.25	241.1
FA20	17.25	18.5	262.9
FA25	17.05	21.2	218.2
FA30	17.02	23.4	167.3

solution to be analyzed further with different curing periods. The following Table 4 shows the 0-day UCS results of the different mixes from which the CS2 with 0.0125% chitosan solution in water and then mixed to soil mix showed peak results with 70% increment in compressive strength. This mix is further tested for UCS test and DST with different curing days.

Table 5 shows that as curing period increases, the UCS strength increases providing higher UCS strength at 28 days of curing. But if curing is proceeded further, then at some point after the peak value, it starts decreasing. From this graph, the peak value is observed at 28 days.

Table 5 shows the UCS results of CS2 mix and virgin soil with comparative % increase in strength values. At 28th day, the strength value of CS2 mix increases from 207.77 to 362.48 kPa with 74% increment compared to virgin soil.

Chitosan (CS)–fly ash (FA) treated soil is tabulated in the Table 6; it shows the results of untreated soil with CS-FA mix with different curing periods and the percentage increase in strength. The mix achieves more than 200% increase in compressive strength values for all curing periods which conclude it stabilizes the

Table 4 Comparison of UCS values for varied chitosan percentage

Mixes	Chitosan (%)	Chitosan solution used (ml)	UCS strength at 0 day (kPa)
CS1	0.01	1.4	222.55
CS2	0.0125	1.75	257.5
CS3	0.025	3.5	228.39
CS4	0.05	7	205.95

Table 5 UCS results for CS2 mix

Curing period (days)	Untreated soil (kPa)	Treated using chitosan 0.0125% (kPa)	Percentage increase %
0 day	148.2	257.5	73
1 day	177.57	299.19	68
3 days	211.39	312.86	47
7 days	187.62	337.64	80
28 days	207.77	362.48	74

Table 6 UCS results for CS-FA mix

Curing period (days)	Untreated soil (kPa)	Treated using Chitosan-fly ash mix (kPa)	Percentage increase %
1 day	148.2	302.5	204
3 days	187.39	474.2	253
7 days	211.62	497.8	235
28 days	207.77	512.59	247

soil better than with only either one of the additives as shown in Table 6. The strength gain is mainly due to increase in cohesion of clay soil due to the chitosan biopolymer and the hardness imparted by the fly ash.

Figure 4 shows the unconfined compressive strength results for untreated soil, 20% fly ash replaced soil (FA20), chitosan treated soil (CS2) and the chitosan-fly ash amended soil mixes. The fly ash replacement provided no significant change in the UCS values compared with untreated soil initially, but at 28th day, it increased by only 27%; thus, the chitosan biopolymer was used as a binder between the soil and fly ash. The chitosan treated soil with 0% fly ash replacement showed good results and provided with 70% increment in compressive strength values, and the DST results showed that the strength gain was due to increase in cohesion of clay soil. Further, chitosan treated soil with 20% fly ash replacement provided better results as the chitosan could bind the fly ash and soil particles together; thus, it provided more than 200% increment in compressive strength values.

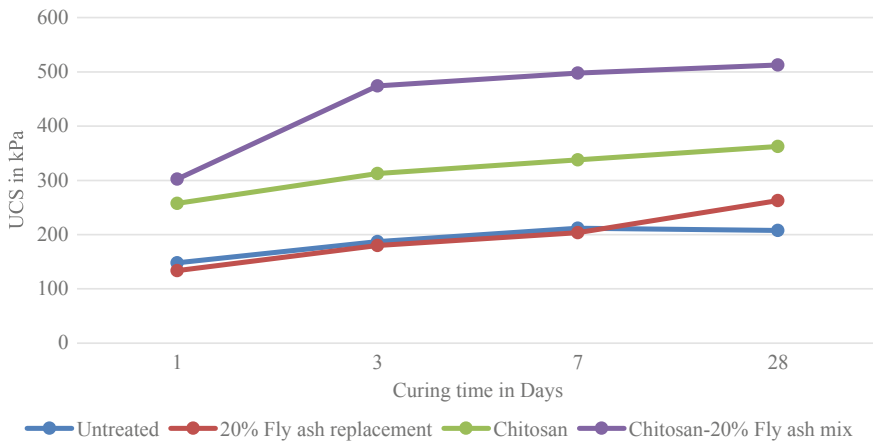


Fig. 4 Comparison of UCS results for different mixes at varying curing period

Table 7 Cohesion and frictional angle values from DST results

Case	C kN/m ²	φ°
Untreated soil	22	10
Fly ash	20	21.2
Chitosan	29.7	13.11
Chitosan–fly ash mix	28	26.5

6.2 DST Results

Direct shear test values are shown in Table 7, with replacement of fly ash in the soil decreased the cohesion value but the angle of internal friction increased from 10 to 21.2 due to which it showed some improvement in UCS value at 28th day. The chitosan addition in soil provided increment in cohesion as the biopolymer creates bond between the particles but the φ° value did not change. Thus, with both chitosan–fly ash amended, the C and φ values increased from 22 to 28 kPa and from 10 to 26.5, respectively. It shows that the chitosan and fly ash treatment to soil provides good shear strength.

6.3 CBR Test

The CBR test results of chitosan–fly ash treated clayey soil and fly ash–soil mix are shown in Fig. 5. It gives a clear indication of influence of chitosan on CBR values of clayey soil. The normal soil otherwise not suitable for pavement construction is found to have improved CBR value with the addition of chitosan. The CBR value with replacement of fly ash increases the value at 2.32% from 1.92% as the fly ash provides some nominal increase in shear strength but the chitosan–fly ash treated soil further increased the value to 2.91%. It does not show that good of an improvement in CBR value to be used as a pavement material. But it shows a considerable amount of improvement compared to virgin soil.

6.4 Numerical Model Calculations

From the tests performed, following are the test results as the parameters for the numerical model, the soil shear parameters that were needed for the Moher-Coulomb model were obtained from the direct shear results which were performed previously in this study. Young's modulus (E) was calculated from stress–strain curve obtained from UCS test according to Hooke's law. The unit weight of mixes was calculated from standard Proctor tests.

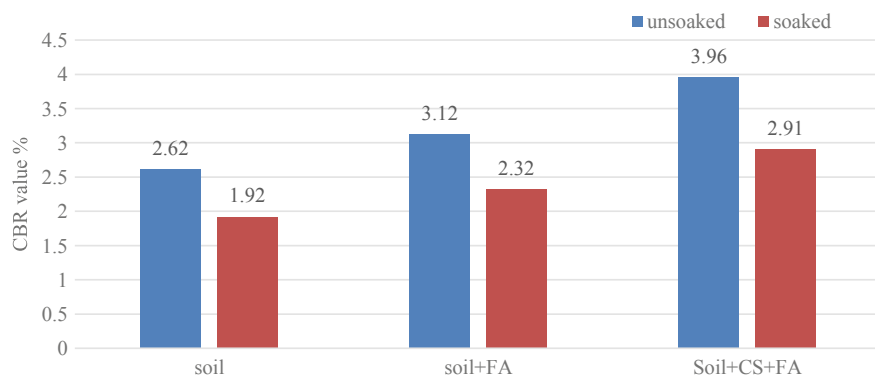


Fig. 5 CBR test results

The parameters used for numerical modeling of soil settlement model are shown in Table 8. The other required values were referred through literature and were given to each case. Thus, running the numerical analysis, the settlement versus load graphs were obtained as shown in Fig. 6. From the graph, it is observed that the virgin soil failed immediately with implication of load to the model without any resistance. With replacement of fly ash and chitosan treatment, the settlement was improved slightly but the CS-FA mix with 20% fly ash replacement and 0.0125% chitosan solution treated soil mix provided better resistance to the settlement in soil model.

Ultimate bearing capacity (q_{ult}) is the maximum stress that the soil can support before the shear fails and by dividing q_{ult} by factor of safety, the allowable bearing capacity ($q_{all, shear}$) can be calculated. However, in some types of soils which are expected to serve a large settlement or in some other kind of structures where it is required to control the settlement to a certain value, in these cases, the allowable bearing capacity ($q_{all, sett}$) can be considered according to the required settlement. Overall, the considered allowable bearing capacity ($q_{all, considered}$) is governed by both soil failure and allowable settlement the least of $q_{all, shear}$ and $q_{all, sett}$. Two methods were used to estimate the allowable bearing capacity from load settlement curves; in the first method, the ultimate bearing capacity was calculated from the intersection between the initial tangent and the steeper tangent, and then, the allowable bearing capacity $q_{all, shear}$ was calculated using a factor of safety with a value of 3.0, while in the

Table 8 Parameters used in numerical modeling for settlement analysis

Case	Additive concentration	Model parameters			
		γ kN/m ³	E kN/m ²	C kN/m ²	φ°
Untreated soil	–	16.72	1644	22	10
Fly ash	20%	16.25	8825	27	26
Chitosan	0.0125%	15.13	4145	29.7	13
Chitosan–fly ash mix	0.0125%C-20%FA	16.83	9568	28	26

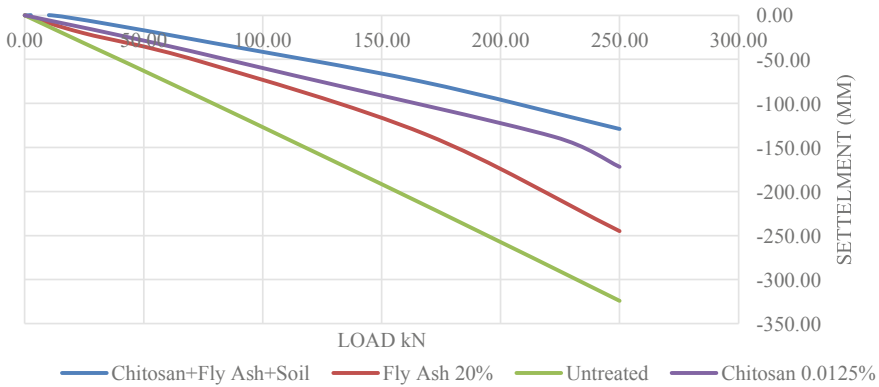


Fig. 6 Settlement Curves

second method, the allowable stress $q_{all,sett}$ at 10 cm settlement values was obtained for treated soil. For all soil treatments, $q_{all, shear}$ was more than $q_{all, sett}$. Therefore, $q_{all, sett}$ can be taken as the considered allowable bearing capacity ($q_{all, considered}$). From Fig. 7, the settlement values for the different mixes are shown. Firstly, with only replacement in soil with 20% fly ash the $q_{all, sett}$ showed minimum change from 25.72 to 34.26 kPa but considering the UCS values earlier obtained concludes it is not efficient in stabilizing the soil. With chitosan treatment, the $q_{all, sett}$ improved by 190% from 25.72 to 49.37 kPa and thus proved effective in resisting the settlement, but with both fly ash replacement and with chitosan treatment, it showed 240% improvement with $q_{all, sett}$ value of 63.54 kPa.



Fig. 7 $q_{all, sett}$ values for different mixes

7 Conclusion

This study investigates the use of chitosan biopolymer as an alternative soil stabilizer to conventional stabilizers particularly in case of clayey soil with fly ash replacement; following conclusion has been drawn from the presented study.

1. The dry density reduces with increase in replacement of fly ash (w/w) from 17.44 to 17.02 kN/m³, while the optimum water content increased from 18% to around 24%.
2. Biopolymer has proved highly efficient in improving the strength for both virgin and fly ash mixed soils.
3. Mixing the soil with 0.0125% biopolymer concentration leads to an increment in the UCS value of about 74%.
4. Despite the reduction in density, which was observed with increasing the concentration, the shear resistance of the treated soil has improved. The cohesion stress has increased by increasing the concentrations with a slight reduction in the friction angle. However, the total shear stress has increased with increasing the concentrations for chitosan.
5. Fly ash showed peak values for 20% replacement over virgin soil for increasing the soil frictional angle and reducing the settlement with a percentage of about 20%.
6. Chitosan treated fly ash–soil mix showed the better results with 250% increase in UCS and the CBR value by 2%.
7. The $q_{all,sett}$ for CS-FA mix increased from 25.72 to 63.54 kPa which provides good resistance against the settlement.

The experimental studies based on longer curing period should be studied further. Also durability with wet and dry cycles should be studied. Experimental model should be prepared and tested further than laboratory sample testing to observe the considerable results for usage of an eco-friendly biopolymer in the field to alternate chemical stabilizer. The work should be done on weak and affecting sides of biopolymer to utilize its significant uses for effective geotechnical concern.

References

1. Latifi N (2016) Improvement of problematic soils with biopolymer-an environmentally friendly soil stabilizer. *J Mater Civ Eng* 29. [https://doi.org/10.1061/\(ASCE\)MT.1943-5533.0001706](https://doi.org/10.1061/(ASCE)MT.1943-5533.0001706)
2. Aguilar R, Nakamatus J, Ramirez E, Elgegren M, Ayarza J, Kim S, Pando M, Ortega L (2016) The potential use of Chitosan as a biopolymer additive for enhanced mechanical properties and water resistances of earthen construction. *Constr Build Mater* 114:625–637. ISSN 0950-0618
3. Hataf N, Ghadir P, Ranjbar N (2018) Investigation of soil stabilization using chitosan biopolymer. *J Cleaner Prod* 170:1493–1500. ISSN 0959-6526
4. Kang X, Bate B, Chen P, Yang W, Wang F (2019) Physicochemical and mechanical properties of polymer amended kaolinite and fly-ash kaolinite mixtures. *J Mater Civ Eng* 31(6):04019064. ISSN 0899-1561

5. Cabalar AF, Awraheem MH, Khalaf MM (2018) Geotechnical properties of a low-plasticity clay with biopolymer. *J Mater Civ Eng* [https://doi.org/10.1061/\(ASCE\)MT.1943-5533.0002380](https://doi.org/10.1061/(ASCE)MT.1943-5533.0002380)
6. Ayeldeen M, Negm A, Kitazume M (2016) Enhancing the behavior of collapsible soil using biopolymers S1674-7755(16)30273-6. <https://doi.org/10.1016/j.jrmge.2016.11.007>

Analyze of Subgrade Soil Behavior Blended with Phosphogypsum and Fly Ash as Additive



Priyanka Saha and Vidya Sagar Khanduri

Abstract A road/pavement is a thoroughfare, route, or way on land between two places that has been paved or improved to allow travel by foot or some form of conveyance like motor vehicle, cart, or bicycle. The quality of roads dictates the economy of a country and hence the quality of our lives. Road transport of India covered more than 60% of the freight and 80% of the passenger road traffic. Roads are mainly used for the transport of goods and passengers. Village roads are dangerous for the basic connectivity for the upliftment of the social and economic condition of the rural area. Such roads provide access to employment, means of transporting agricultural produce and access to health care and social services. In transportation engineering, subgrade is the native material underneath a constructed road, pavement or railway (US: railroad) track. It is also called formation level. The term can also refer to imported material that has been used to build an embankment. For this present project work silty—sandy soil samples have been collected from different changes of newly constructed Kadapa-Renigunta express highway, Andhra Pradesh, India. Every soil samples have been collected from 15 cm. below the existing ground surface. The sample of fly ash has been collected through Thermanl power plant, (NTPC, Ramagundam). Several physical, as well as engineering properties tests, were done as per the necessities of IS-Codes. Output of the test results has concluded that soil stabilized with fly ash and phosphogypsum, the C.B.R. and UCS results are significantly more compared to without treated soil. Tests point toward that soil mixed with 30% FA and 6% PG may be used as an improved subgrade material. As the subgrade thickness reduced so the construction will be economic.

Keywords Standard proctor test · U.C.S. · Permeability

P. Saha (✉) · V. S. Khanduri
Department of Civil Engineering, Lovely Professional University, Phagwara,
Punjab 144411, India
e-mail: priyankasaha.mcet@gmail.com

V. S. Khanduri
e-mail: vidya.18579@lpu.co.in

© The Author(s), under exclusive license to Springer Nature Singapore Pte Ltd. 2023
A. K. Agnihotri et al. (eds.), *Proceedings of Indian Geotechnical and Geoenvironmental Engineering Conference (IGGEC) 2021, Vol. 1*, Lecture Notes in Civil Engineering 280,
https://doi.org/10.1007/978-981-19-4739-1_38

421

1 Introduction

We know that all civil engineering structures to be constructed on soil. Most of them are to be constructed on poor soil deposits. As we know poor deposit means soil exhibits low strength, more permeability, more compressibility, and excessive settlement. To overcome these hazardous conditions general conventional techniques are replacing the poor soil by a suitable material, provide deep foundation to bypass weak strata. But the above solutions require more time and also the construction cost should be high. So to overcome all the above problems improving the soil may be the excellent solution.

2 Literature Review

Keramatikerman et al. [1] Replacement of soil with by-product is very interesting due to positive geoenvironmental impact. This study considers the effect on the UCS values and compaction characteristics of fly ash mixed with PC and soil. The PC changed from 1 to 4%. The curing time considered as 3–28 days. Elhakim [2] Permeability of soil also known as hydraulic conductivity can be measured using various methods. For finding the permeability of soil in laboratory Constant head and falling head permeability tests are mostly used. The results of laboratory tests such as the grain size distribution we can empirically assume the coefficient of permeability of soil. In this present study, the permeability coefficient was measured at different depth using field falling head permeability test. Pumping tests also has been conducted at same site location to determine field permeability coefficient. Results obtained from different methods are compared to the values empirically presumed from the cone penetration test at same location. Likewise, the permeability values are obtained by using empirical relationships based on the different engineering properties of the confirmed sand for comparison with the measured values. Changizi et al. (2014), It was intended to study effect of addition recycled polyester fiber on soil properties, especially shear strength and CBR using clay soil with low liquid limit (CL) and atterberg limits used high liquid limit (CH). Reprocessed polyester fibers were mixed with soil in three diverse percentages 0.1, 0.3 and 0.5% (the portion of additive materials to soil net weight). The shear strength, CBR, atterberg limits of treated samples were measured by direct shear test and CBR test, and atterberg limits test. Through increase in fiber content, the CBR and the modulus of subgrade reaction of reinforced soil upturns in such a way that with addition of 0.5% recycled polyester fibers, the CBR and the modulus of subgrade reaction and elastic modulus of reinforced soil, become 1.59, 2.23, and 1.34 times of UCS of natural soil individually [3]. Punhutaech et al. (2006) while investigating change of volume behaviors in black cotton soils stabilized by recycled ash and fiber reported that bottom fly ash improved soils exhibit improved characteristics in soil atterberg's limit [4]. Bera et al. [5] observed the effect of specific gravity on MDD of pond ash during proctor density

test of pond ash and observed from the test data that specific gravity increases as well as maximum dry density (MDD) increases.

Subbarao and Ghosh (1997) reported pond ash collected from Kolaghat thermal power station, West Bengal, India. Chemical composition percentages are as follows SiO_2 : 52.80, Al_2O_3 : 29.80, Fe_2O_3 : 9.00, CaO : 1.00, and MgO : 0.10 [6].

3 Objective

Objective of the present work is by using low-cost admixture to improve locally available soil. Thus soil sample for this laboratory was collected from different changes at newly constructed Kadapa-Renigunta express highway, Andhra Pradesh, India. And fly ash used for improvement collected from NTPC, Ramagundam, Telangana, India. Fly ash is used at different percentages. The scope for this study is as follows:

- Find out the effect of fly ash on soil-specific gravity and compaction characteristics.
- Fly ash effect on soil permeability should be studied.

4 Methodology

Difficulties associated with fly ash are as follows:

- Gradually land decrease for fly ash disposal;
- Aquatic ecosystem will affect for fly ash disposal into sea;
- In dry state fly ash will fly in air;
- Fly ash toxic metals may contaminate groundwater or the surface water during leaching;
- Radioactive particles of fly ash may create dangerous health problems of mankind and other animals.

This brings us to the fact that in order to reuse or utilize this fly ash we have to understand and study it better. This will help us to utilize FA in an environment-friendly way. The chemical analysis was conducted in the lab for FA. Chemical composition was determined in accordance with ASTM standards (ASTM C618-93) and for determination of pH value the ASTM standards [ASTM D2976-71 (2004)] were followed. The percentages of the constituents present in the fly ash samples are within the following ranges:

Composition	Percentage of composition presence
Silicon dioxide	60.50–66.20
Ferric oxide	7.40–8.75

(continued)

(continued)

Composition	Percentage of composition presence
Aluminum oxide	11.65–18.25
Calcium oxide	3.75–6.50
Magnesium oxide	3.05–5.35
Letter of intent	3.25–3.85
Others	0.35–1.35

The predominant chemical constituent in the fly ash is silica (SiO_2). According to the ASTM C618-93, all fly ash for this present work are class F type. The pH values are above 7.00 (i.e., alkaline in nature) for seven fly ash samples and the pH value for the remaining samples, BBP and BAB, are 6.90 and 6.96, respectively.

5 Results and Discussions

Results of the present study are based on the specific gravity, proctor density, and permeability test. The most important test though is the proctor density test which determines the maximum proportion of fly ash content be added to natural soil. The test results are given in the following Fig. 1.

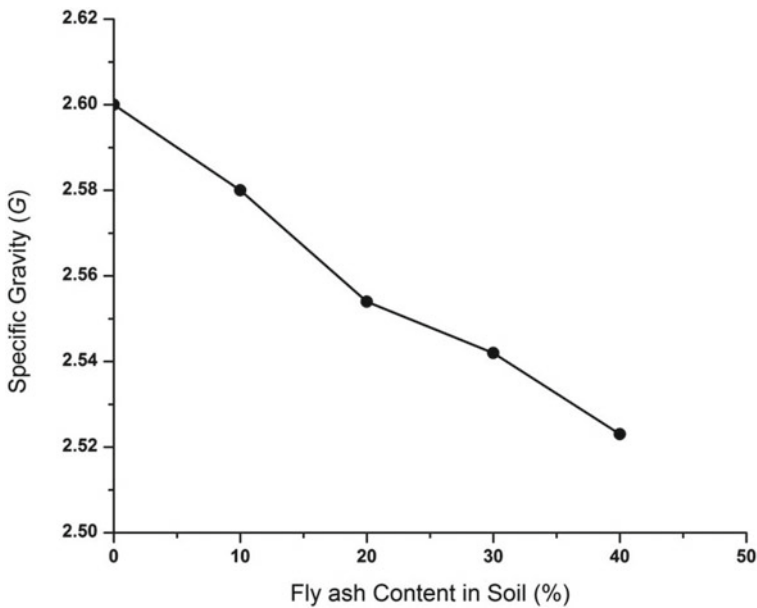


Fig. 1 Specific gravity test of soil-fly ash mixture

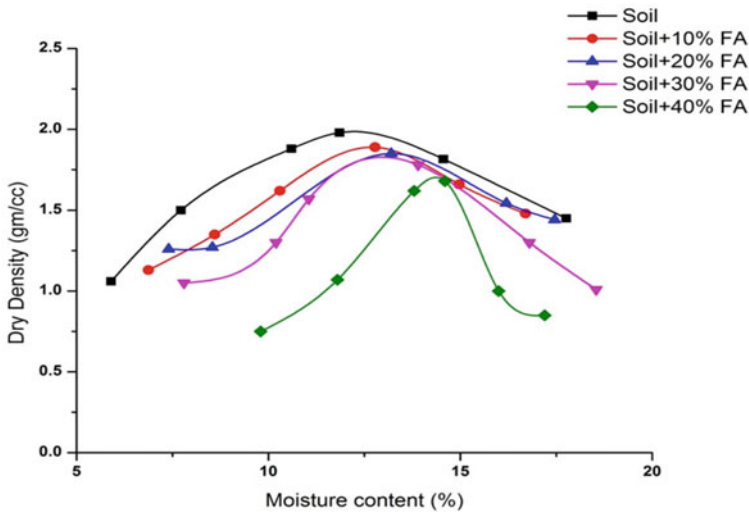


Fig. 2 Relationship of maximum dry density for soil-fly ash mix

Figure 2 shows that at 30% of fly ash blended with soil the dry density achieved is maximum. The further study is mainly based on this proportion of soil and fly ash (30%). As this fly ash content is giving us the maximum possible density, the permeability tests are based on this result only. The permeability test results are given in the following table:

Material composition	Permeability test results (cm/sec)
Untreated soil	1.776×10^{-07}
Treated soil (30% FA)	9.079×10^{-08}

References

1. Keramatikerman M, Chegenizadeh A, Nikraz H (2020) Strength of cemented fly ash soil. Int J Eng Appl Sci Technol
2. Elhakim FA (2016) Estimation of soil permeability. Alexandria Eng J 10. <https://doi.org/10.1016/j.aej.2016.07.034>
3. Inan G, Sezer A, Yilmaz R, Kambiz R (2016) Use of a very high lime fly ash for improvement of Izmir clay. The Elsevier, vol 10, pp 10. buildenv.2004.12.009
4. Rathana RR, Banupriya S, Dharani R (2016) Stabilization of soil using rice husk ash. Int J Comput Eng Res 06. ISSN (e): 2250–3005
5. Bera AK, Ghosh A, Ghosh A (2007) Compaction characteristics of pond ash. J Mater Civ Eng ASCE 19(4):349–357
6. Kim B, Prezzi M, Salgado R (2005) Geotechnical properties of fly ash and bottom ash mixtures for use in highway embankments. J Geotech Geoenviron Eng ASCE 131(7):914–924

Evaluation of Deviator Stress of Lime-Alcofine-Stabilized Fly Ash from Ultrasonic Pulse Wave Velocity



Rakesh Kumar Dutta  and Jitendra Singh Yadav 

Abstract The paper presents the correlation between the deviator stress and ultrasonic pulse wave velocity of fly ash stabilized with 6% lime and 2% alcofine content. Unconsolidated undrained and consolidated drained tests were performed on 7, 14, and 28 days cured specimen subjected to confining pressure of 49.1–196.2 kPa. The test results revealed that peak deviator stress of the mix increases with the increase in confining pressure for all curing period. Similarly, the improvement in initial tangent modulus and secant modulus was seen with the increase in curing period and confining pressure. Whereas, with the prolongation of curing period, an increase in the cohesion and decrease in friction angle of the mix were observed. An empirical relationship between the deviator stress of the mix and ultrasonic pulse wave velocity, confining pressure, and curing period was proposed and found satisfactory.

Keywords Lime-alcofine-fly ash mix · Shear strength · Ultrasonic pulse wave velocity · Empirical relationship

1 Introduction

Fly ash is by-product of the thermal power plants collected in electrostatic precipitator. The number of coal thermal power plants is continuously increasing in the country. It leads to enormous increase in the generation of fly ash. During the year 2019–2020, about 227 million tons of coal ash has been generated in India [1]. The disposal of such large quantity involves substantial expenditure as well as may cause environmental pollution. Therefore, the best way of large-scale utilization of fly ash in ecofriendly way is in the Geotechnical engineering applications. On the other hand, alcofine is new generation supplementary cementitious material manufactured by

R. K. Dutta · J. S. Yadav (✉)

Department of Civil Engineering, National Institute of Technology, Hamirpur, Himachal Pradesh, India

e-mail: jsyadav@nith.ac.in

Ambuja cement. It ranged in size from 0.1 to 0.17 μ with an average particle size less than 4 μ . It is manufactured by grinding granulated blast furnace slag with glass content more than 90%.

Fraay et al. [2] demonstrated that the low shear strength gain in fly ash-lime mix in the early stages of curing was due to low pH values of the pore fluid. The pozzolanic reaction accelerates at the later stage of curing and led to an increase in the shear strength. Consoli et al. [3] reported that the addition of carbide lime to the soil-fly ash mixture caused a reduction in the dry unit weight and an increase in the optimum moisture content. The drained triaxial compression of compacted soil-fly ash carbide lime mixtures was also studied by Consoli et al. [3] and showed increase in the friction angle, cohesion, and average modulus due to the addition of carbide lime to the soil-fly ash mixture. Ghosh and Subbarao [4] carried out unconsolidated undrained triaxial tests on fly ash modified with lime and gypsum. With the addition of lime or lime combined with gypsum, increase in the cohesion and angle of internal friction of fly ash was observed. To estimate the parameter like deviatoric stress at failure, and cohesion of the modified fly ash, the empirical relationship was proposed. Sivapullaiah and Moghal [5] examined the effect of lime content (1, 2.5, 5, and 10%) on the compaction behavior of fly ash through min compaction test and observed that the addition of lime to fly ash resulted in a marginal increase in dry unit weight and optimum moisture content. They found that strength of low lime fly ash increased with the lime content. The increase was significant up to a lime content of 5%. Mishra [6] documented that with the addition of lime to the fly ash, maximum dry density increased and the optimum moisture content decreased. There are very few studies on alccofine, which are related with the enhancement of the performance of concrete. There are no investigations of alccofine done yet in Geotechnical engineering applications.

With the above in view, the present study was planned to understand the strength characteristic of fly ash-lime-alccofine mix. Its behavior was examined thoroughly through unconsolidated undrained (UU) triaxial test, consolidated drained (CD) triaxial test, and ultrasonic pulse velocity test, and generalized equation was developed.

2 Material Used

The fly ash used in the study was procured from Ropar thermal power plant, Punjab, India. It had a specific gravity of 2.04. The maximum dry unit weight and optimum moisture content as obtained by standard proctor test were found to be 10.84 kN/m² and 33.18%, respectively. The fly ash is of class F type (as per ASTM C 618). Commercially available lime procured from the local market in Hamirpur, Himachal Pradesh, India, was used in this study. The lime used had a specific gravity of 2.33. Alccofine 1203 manufactured by Ambuja cement Limited was used in this study. It contains cementitious material, which has ungrounded granulated blast furnace slag, glass content more than 90%. It had a specific gravity of 2.94.

3 Experiment Methodologies

3.1 Preparation of Specimens

The fly ash was ground slightly by hand with a pestle to separate the individual particles. A metallic mold having size 38 mm inner diameter and 76 mm long with additional detachable collars at both ends were used to prepare cylindrical specimens for the unconsolidated undrained and consolidated drained triaxial tests. The required quantity of lime (6%) and alccofine (2%) corresponding to dry weight of fly ash was then mixed thoroughly, and the water [corresponding to optimum moisture content (OMC)] was added to the mix. The composite of fly ash + 6% Lime + 2% Alccofine was fixed as reference mix obtained from the compaction studies [7]. To ensure uniform compaction, specimen was compressed statically from both ends until the specimen just attained the required dimension. The specimen was then removed with a hydraulic compression machine with sample extrusion facility. The prepared specimens were cured for 7, 14, and 28 days using burlap curing method.

3.2 Unconsolidated Undrained Triaxial Test

Unconsolidated undrained (UU) triaxial test was carried out on the reference mix in accordance with IS 2720 (Part 11)-1971 [8]. A Perspex triaxial cell capable of withstanding confining pressure of more than 1 MPa and with the facility to test specimen of 38 mm diameter and 76 mm height was used. The confining pressure was applied and maintained with the means of air compressor. Further, axial loads were applied through a loading frame with deformation control system. The proving rings of capacity 2 kN and 10 kN were used for testing specimens cured for 7, 14, and 28 days, respectively. 7, 14, and 28 days cured specimens were tested under confining pressure of 49.05, 98, and 196.2 kPa.

3.3 Consolidated Drained Triaxial Test

Consolidated drained triaxial tests were performed in accordance with IS 2720 (Part 12)-1981 [9]. After the sample was prepared, it was placed on pedestal with porous stone and filter paper at both top and bottom. A 10 kN proving ring capacity, dial gauge with accuracy 0.01 mm, and 25 ml volume change measure device with 0.01 ml accuracy were used. Valve kept open during both consolidation and shearing stage. 7, 14, and 28 days cured specimens were tested under confining pressure of 49.05, 98, and 196.2 kPa.

3.4 Ultrasonic Pulse Wave Velocity Test

Ultrasonic pulse velocity test is used to determine the velocity of the P wave and S wave of laboratory sample. It is non-destructive test, which generates compression wave (P wave and S wave) in the frequency range 20 kHz–1 GHz through the specimen. Compression waves of frequency 54 kHz are used in this study. Ultrasonic pulse velocity measurements were done on the same specimens prior to unconsolidated undrained and consolidated drained test.

4 Results and Discussion

4.1 Shear Strength Parameters

The stress–strain curves for the reference mix cured for 7, 14, and 28 days and at confining pressure of 49.05–196.2 kPa both unconsolidated undrained (UU) and consolidated drained (CD) triaxial tests were shown in a research article published by the authors [7]. The unconsolidated undrained and consolidated drained triaxial test results were used to make p – q plots, and the values of shear strength parameters were calculated. The values of shear strength parameters obtained for UU test and CD tests are tabulated in Table 1.

Study of Table 1 reveals that the cohesion is increased and friction angle is decreased of the reference mix with the increase in curing period. For example, for UU test, the cohesion of 76.51 kPa of the reference mix cured for 7 days increased to 153.14 and 263.44 kPa when the curing period is raised to 14 and 28 days, respectively, and the friction angle of 32.33° of the reference mix cured for 7 days decreased to 32.14° and 28.23° when the curing period is raised to 14 and 28 days, respectively. Similarly, for CD test, the cohesion of 93.40 kPa of the reference mix cured for 7 days increased to 170.65 kPa and 268.93 kPa when the curing period is raised to 14 and 28 days, respectively, and the friction angle of 37.80° of the reference mix cured for 7 days decreased to 36.62° and 33.41° when the curing period is raised to 14 and 28 days, respectively. This increase in cohesion was due to the formation of calcium silicate hydrate and calcium aluminate hydrate gel formed in the mix, which gets transformed into more crystalline form with the extension of curing period [7]. This

Table 1 Shear strength parameters for the reference mix cured for 7, 14, and 28 days

Curing period (days)	UU test		CD test	
	c (kPa)	Φ (deg)	c (kPa)	Φ (deg)
7	76.51	32.33	93.40	37.80
14	153.14	32.14	170.65	36.62
28	263.44	28.23	268.93	33.41

transformation makes the sample more rigid and leads to the reduction in internal friction between particles corresponding to extended curing period.

4.2 Shear Strength Parameters

Deformation modulus is one of the most important mechanical properties of stabilized fly ash which links the stress and the corresponding strain. It is generally used in design problems as well as an input parameter various numerical tools to predict response of structure resting on such stabilized materials. The initial tangent modulus (determined at the peak strength) and secant modulus (determined at 50% of peak strength) determined from the UU and CD triaxial test are tabulated in Table 2.

Study of Table 2 reveals that the initial tangent modulus and secant modulus of the reference mix increased with the increase in curing period. For example, for UU triaxial test, for the reference mix cured at 7 days of curing in undrained condition at a confining pressure of 49.05, 98.1, and 196.2 kPa, the initial tangent modulus and secant modulus was 20.90, 22.27, 26.50 Mpa and 20.21, 21.90, 24.54 MPa, respectively, which increased to 27.91, 30.02, 38.28 MPa and 26.26, 29.51, 34.66 MPa and 51.41, 54.68, 57.29 MPa and 47.62, 50.67, 54.95 MPa when the curing period was raised to 14 and 28 days, respectively. Similarly, for CD triaxial test, for the reference mix cured at 7 days of curing at confining pressure of 49.05, 98.1 kPa, and 196.2 kPa, the initial tangent modulus and secant modulus were 25.22, 25.83, 39.99 MPa and 4.54, 25.72, 36.91 MPa, respectively, which increased to 28.07, 34.59, 40.42 MPa and 25.69, 34.25, 39.33 MPa and 55.30, 58.78, 59.44 Mpa and 52.88, 56.42, 56.73 MPa when the curing period was raised to 14 and 28 days, respectively. Further, Table 2 reveals that the initial tangent modulus and secant modulus increase with the increase in confining pressure at all curing periods. For example, for UU triaxial test, the reference mix cured at 7 days of curing in undrained condition at confining

Table 2 Deformation modulus (MPa) of reference mix

Curing cell UU test CD test period pressure					
(days)	σ_3 (kPa)	E_i (MPa)	E_s (MPa)	E_i (MPa)	E_s (MPa)
7	49.05	20.90	20.21	25.22	24.54
	98.1	22.27	21.90	25.83	25.72
	196.2	26.50	24.54	39.99	36.91
14	49.05	27.91	26.26	28.07	25.69
	98.1	30.02	29.51	34.59	34.25
	196.2	38.28	34.66	40.42	39.33
28	49.05	51.41	47.62	55.30	52.88
	98.1	54.68	50.67	58.78	56.42
	196.2	57.29	54.95	59.44	56.73

pressure 49.05 kPa, the initial tangent modulus and secant modulus were 20.90 and 20.21 MPa, respectively, which increased to 22.27 and 21.90 MPa and 26.50 and 24.54 MPa when the confining pressure was raised to 98.1 kPa and 196.2 kPa, respectively. Similarly, for CD test, the reference mix cured at 7 days of curing in undrained condition at confining pressure 49.05 kPa, the initial tangent modulus and secant modulus were 25.22 and 24.54 MPa, respectively, which increased to 25.83 and 25.72 MPa and 26.50 and 24.54 MPa when the confining pressure was raised to 98.1 kPa and 196.2 kPa, respectively. Similar trend of increase in initial tangent modulus and secant modulus with the increase in confining pressure was observed at other curing periods as evident in Table 2.

4.3 Proposed Correlations Between Triaxial and Ultrasonic Pulse Wave Velocity Test

In order to get the deviator stress (q_f) from ultrasonic pulse wave velocity (V_P), confining pressure (σ_3), and curing period (C_P), it is proposed to develop the correlation among these parameters. For this, a scatter plot between deviator stresses and ultrasonic pulse wave velocity for the reference mix cured for 7–28 days was drawn. Fig. 1a–b shows the scatter plot between deviator stresses and ultrasonic pulse wave velocity for the reference mix cured for 28 days. Based upon regression analysis, Eqs. 1 and 2 are proposed to predict deviator stress from ultrasonic pulse wave velocity, confining pressure, and curing period for the reference mix.

$$\text{UU Test } q_f = 0.08V_P + 2.01\sigma_3 + 9.57C_P + 146.43 \quad (1)$$

$$\text{CD Test } q_f = 0.09V_P + 2.76\sigma_3 + 5.59C_P + 267.94 \quad (2)$$

The values of the relevant statistical coefficients like coefficient of multiple determinations (R^2), adjusted coefficients of determination (R^2_{adjusted}), standard error (SE), and confidence level (CL) for Eq. 1 were 0.974, 0.954, 58.67, and 95%, respectively. Similarly, for Eq. 2, the statistical coefficients were 0.974, 0.958, 60.48, and 95%, respectively.

5 Conclusion

Based on the obtained results, the following conclusions can be drawn.

- The deviator stress, cohesion, initial tangent modulus, and secant modulus increased and friction decreased with the increase in curing period for unconsolidated undrained and consolidated drained triaxial test.

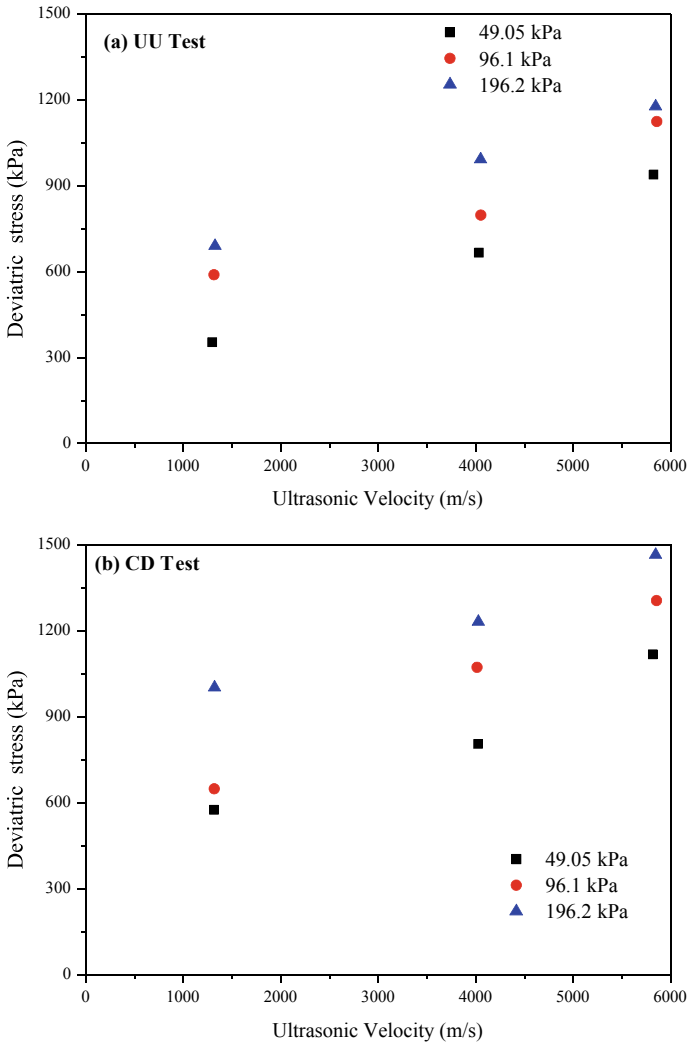


Fig. 1 Variation of deviator stress and ultrasonic pulse velocity at different confining pressure **a** UU test **b** CD test

- Empirical correlation between the deviator stress of the mix and ultrasonic pulse wave velocity, confining pressure, and curing period for unconsolidated undrained and consolidated drained triaxial test was found satisfactory.
- The empirical models presented in this paper were based on the experimental data within the range of curing period (7–28 days), and beyond this range of values, the models may be checked with experimental results.

References

1. Central Electricity Authority (2020) Report on fly ash generation at coal/lignite based thermal power stations and its utilization in the country for the year 2019–2020. https://cea.nic.in/wp-content/uploads/tcd/2021/01/flyash_2019-20.pdf. Last accessed on 15 Aug 2021
2. Fraay J, Bijen M, Vogelaar P (1990) Cement-stabilized fly ash base courses. *Cem Concr Res* 12:279–291
3. Consoli NC, Prietto PDM, Carraro JAH, Heineck KS (2001) Behavior of compacted soil-fly ash-carbide lime mixtures. *J Geotech Geoenviron Eng* 127(9):774–782
4. Ghosh A, Subbarao C (2007) Strength characteristics of class F fly ash modified with lime and gypsum. *J Geotech Geoenviron Eng* 133(7):757–766
5. Sivapullaiah PV, Moghal AAB (2011) Role of gypsum in the strength development of fly ashes with lime. *J Mater Civ Eng* 23(2):197–206
6. Mishra NK (2012) Strength characteristics of clayey sub-grade soil stabilized with fly ash and lime for road works. *Indian Geotech J* 42(3):206–211
7. Dutta RK, Yadav JS, Khatri VN, Venkataraman G (2021) A study on the suitability of fly ash–lime–alccofine mixtures in the construction of road pavement. *Transp Infrastruct Geotech* 1–27
8. IS: 2720-Part 11 (1971) Method of test for soils—determination of shear strength parameter by unconsolidated undrained triaxial compression without the measurement of pore water pressure. Bureau of Indian Standards, New Delhi
9. IS: 2720-Part 12 (1981) Method of test for soils—determination of shear strength parameter of soil from consolidated undrained triaxial compression test with measurement of pore water pressure. Bureau of Indian Standards, New Delhi

Strength Behaviour of Dredged Soil Stabilized with Cement and Fly Ash



Razia Sultan and M. Y. Shah

Abstract Any wastes that are produced by human activities that are solid in nature are categorized as solid wastes. In this research, solid waste was produced by dredging Kashmir's renowned Dal Lake. Dal Lake in Srinagar, Jammu and Kashmir, produces a significant amount of dredged dirt, presenting severe health and environmental issues. Concerns about the environmental impacts of dredging and disposal, as well as the growing scarcity of appropriate disposal locations, have increased the need for dredged material characterization. As such, the purpose of this research is to describe the waste material produced by Dal Lake by examining its different physical and mechanical characteristics. Dredged material was collected from the Shalimar site, which is located within the Dal Lake catchment, for the purpose of conducting various field and laboratory tests to determine field density, soil classification, compaction characteristics, and strength parameters such as unconfined compressive strength and direct shear test. The findings indicate that dredged material is mostly composed of silt, clay, and sand, and that strength characteristics indicate that dredged material cannot be utilized in its natural form as building and foundation material. As a result, appropriate and practical treatments should be applied to dredged material in order to enable its use in geotechnical applications.

Keywords Dredged material · Solid waste · Characterization · Geotechnical · Applications · Unconfined · Compressive strength

1 Introduction

In this research, solid waste was produced by dredging Kashmir's renowned Dal Lake. Dal Lake in Srinagar, Jammu and Kashmir, India, is the state's second-biggest lake and has long been an important part of the state's tourism and leisure. Dal Lake is basically the lifeblood of Kashmir Valley, serving as the foundation for all economic activity. Sewage from towns around the lake and houseboats enters the lake untreated.

R. Sultan (✉) · M. Y. Shah

National Institute of Technology, Srinagar, J&K 190006, India

e-mail: sultanrazia67@gmail.com; razia_03mtech19@nitsri.net

© The Author(s), under exclusive license to Springer Nature Singapore Pte Ltd. 2023
A. K. Agnihotri et al. (eds.), *Proceedings of Indian Geotechnical and Geoenvironmental Engineering Conference (IGGEC) 2021, Vol. 1*, Lecture Notes in Civil Engineering 280,
https://doi.org/10.1007/978-981-19-4739-1_40

435

Massive amounts of solid waste and excessive fertilizers entering from inlet channels create algal blooms, which eventually cause eutrophication. Additionally, the drains transport sludge and solid wastes into the lake from the neighbouring regions. In September 2014, when the River Jhelum reached a hazardous level owing to heavy rains, a large quantity of water entered the Dal Lake due to a breach in the embankment near Ram Munshi Bagh. This water introduced a significant quantity of sediment and biological load into the lake, resulting in its siltation and contamination. Due to continual garbage dumping, silt deposition, and encroachment, the lake's load-bearing capacity has been decreased, necessitating the dredging operation to preserve the lake. Thus, appropriate treatment of dredged material is necessary to reduce health and environmental risks [18]. Dredging the Dal Lake produces a huge number of dredged sediments, presenting severe health and environmental concerns. Dredged material is a precious resource that may be used for a variety of practical applications. Depending on its composition, it may be used for a variety of purposes, including fill material, subgrade construction, reclamation, landscaping, agriculture, covering landfills, creating wetlands to enhance water quality, and bank stabilization. Chemical stabilization using cement and fly ash is used in this research to enhance the soil's characteristics. Cement stabilization of soil is a widely used technique for pavement and earth structure construction globally. Stabilization starts by mixing cement and water required for compaction into the in situ soil in a reasonably dry condition. When soil is exposed to moisture and a cementing agent, it undergoes modification, in which particles cluster together as a result of physical–chemical interactions between the soil, cement, and water. Stabilization of problematic soils using industrial by-products such as fly ash [24] increases the strength and decreases the compressibility characteristics [3]. Additionally, lowering the cost of disposal and minimizing any negative environmental effects associated with fly ash (FA) may lower building costs and offer economic benefits [21]. The combination of cement with pozzolanic additives such as FA is definitely the best option, as the inclusion of FA enhances geotechnical characteristics through pozzolanic reactions, cation exchange, flocculation, and its function as a microfiller [21, 23]. Fly ash is a fine by-product of the combustion of pulverized coal in a thermal power plant. Fly ash disposal is a significant environmental problem that costs millions of rupees. Today, fly ash is utilized in a range of building applications, including compacted fills, concrete, bricks, and embankment construction in a number of nations, including India. While fly ash alone has a low cementation value, when combined with moisture, it chemically interacts to create cementitious compounds, thus improving the compressibility and strength properties of soils.

2 Materials and Methodology

2.1 Materials

In the present investigation, soil sample (in situ and disturbed) was collected from Shalimar site of Dal Lake. Disturbed samples of the dredged soil were collected for studying their strength behaviour on application of chemical additives, i.e. cement and fly ash (Table 1).

Mixture proportions

A series of control and experimental tests were carried out using only cement and a mixture of cement and FA. Table 2 shows the mixture proportions for all the specimens.

The soil samples were mixed with a range of different percentages of fly ash and cement as given in Table 2. The specimens were subsequently subjected to numerous strength tests such as unconfined compressive strength tests at immediate, 7 days, and 28 days of curing period. A comparative study of the change in the mechanical properties of the soil on adding cement and fly ash was performed. Compaction characteristics, unconfined compressive strength, and direct shear parameters of treated soil samples were studied. The unconfined compressive strength at different ranges

Table 1 Properties of dredged soil

Sr. No.	Properties	Shalimar site
1.	In situ water content, w_n (%)	35.09
2.	Field dry unit weight, γ_d (kN/m ³)	10.74
3.	Specific gravity, G	2.4
4.	Clay (%)	10.57
5.	Silt (%)	77.64
6.	Sand (%)	11.785
7.	Gravel (%)	0
8.	Coefficient of uniformity, c_u	15
9.	Coefficient of curvature, c_c	1.323
10.	Suitability number, s_n	911.61
11.	Liquid limit (%)	39.88
12.	Plastic limit (%)	29
14.	Plasticity index PI (%)	10.88
15.	PI A-line	15.1
16.	PI U-line	28.69
17.	Classification	MI
18.	Clay mineral	Kaolinite
19.	Flow index, I_f	10.10

Table 2 Mix proportions examined in the study

Symbol	Cement(%)	FA(%)
C4FA0	4	0
C8FA0	8	0
C12FA0	12	0
C16FA0	16	0
C8FA8	8	8
C8FA12	8	12
C8FA16	8	16
C8FA20	8	20

of curing revealed an optimum cement content of around 12% and optimum fly ash content of around 16% at a constant cement percentage of 8%.

2.2 Experimental Study

Two phases of testing were conducted. The first step included determining the fundamental characteristics of dredged material (physical and engineering parameters) using a variety of tests, including gradation, specific gravity, consistency indices, light compaction, unconfined compressive strength, and direct shear testing. The following sections describe the different tests.

Index properties

While determining the index properties, viz. liquid limit and plastic limit of the samples tested in this investigation, standard procedures recommended in the respective I.S. codes of practice (I.S. 2720 (Part-V)—1985 [10]) were followed.

Compaction properties

Optimum moisture content and maximum dry density of dredged soil were determined according to I.S. light compaction test (I.S. 2720 (Part-VII) 1980) [11].

Unconfined compressive strength test (UCT) and direct shear tests

Two levels of testing were done. The initial step involved a variety of tests, such as gradation, specific gravity, consistency indices, light compaction, unconfined compressive strength, and direct shear testing, to ascertain the fundamental characteristics of the dredged material (physical and engineering parameters).

In stage-II, the soil samples were mixed with different percentages of fly ash and cement as given in Table 2. The treated samples were put through strength tests like unconfined compressive tests at immediate, 7 days, and 28 days of curing period. A comparative study of the improvement in the mechanical properties of the soil was conducted when cement and fly ash were added. Compaction characteristics,

unconfined compressive strength, and direct shear parameters of treated soil samples were studied. The unconfined compressive strength at immediate, 7 days, and 28 days of curing period revealed an optimum cement percentage of around 12% and optimum fly ash percentage of around 16% at a constant cement percentage of 8%.

3 Results and Discussions

Effect of cement and fly ash on dry density and optimum moisture content

In general, a high level of soil compaction improves the geotechnical parameters of the soil; therefore, reaching the right degree of relative compaction required to achieve specified or desired properties of soil is very important [20]. The addition of cement to the soil increases the MDD and correspondingly decreases the OMC as shown in Fig. 1.

It is also seen that the addition of fly ash to the soil increases the MDD and correspondingly decreases OMC as can be seen from Fig. 2.

Unconfined compressive strength test

Effect of cement content

Figures 3, 4, and 5 show that raising the cement content (CC) increases the UCS value, due to pozzolanic interactions involving lime, silica, and aluminium in cement, which result in the formation of hydrated calcium silicate (C-S-H) and hydrated calcium aluminate (C-A-H). The following reactions cause the mixture to harden during the hydration process [2, 14].

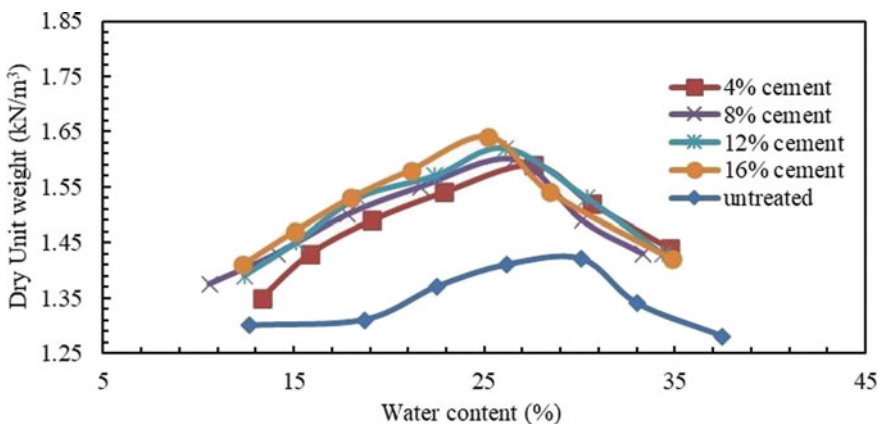
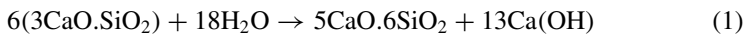


Fig. 1 Variation of MDD and OMC with varying percentage of cement content

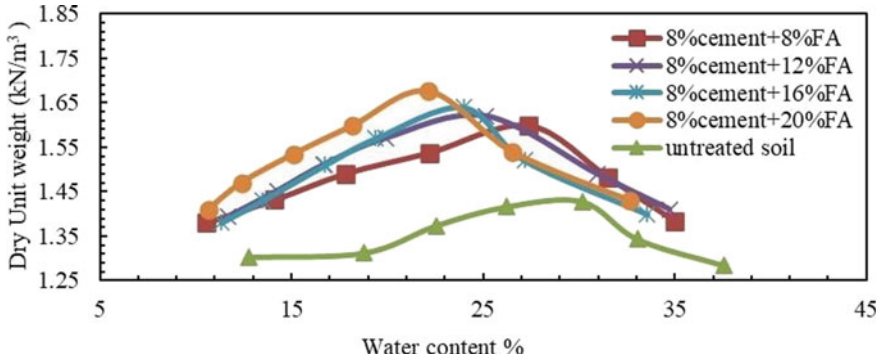


Fig. 2 Variation of MDD and OMC with varying percentage of fly ash content at constant cement content of 8%

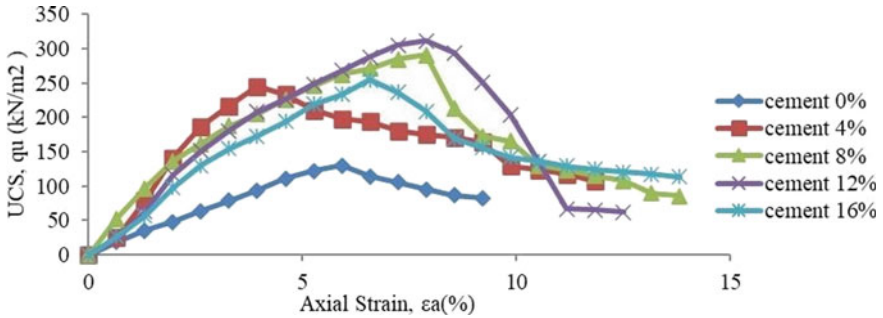


Fig. 3 Stress–strain curves for cement stabilized dredged soil (immediate)

Fig. 4 Stress–strain curves for cement stabilized dredged soil (7 day)

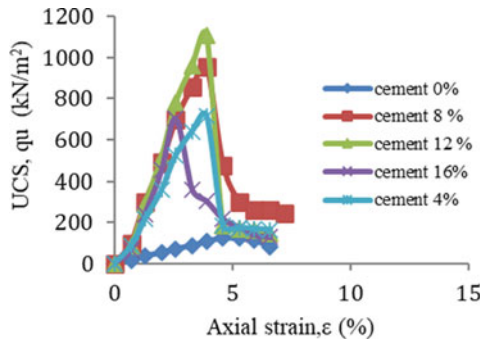
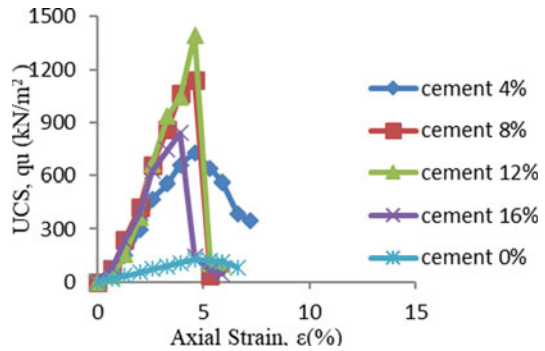


Fig. 5 Stress–strain curves for cement stabilized dredged soil (28 day)



After the setting and hardening stages, these chemical processes increase the PH of the mixture, form C-S-H and C-A-H cementation gels, and improve the mixture’s strength.

From the results, it can be seen that raising cement content (CC) increases the rate of growth in the UCS, increases hardness, reduces compressibility, and finally raises the slope of the stress–strain curves both before and after achieving the peak compressive stress value. This means that raising CC causes the material to become more brittle by lowering the failure strain.

Figures 6, 7, and 8 demonstrate the effect of fly ash on the UCS, illustrating that the rate of increase in the UCS at the same cement content increases with increasing fly ash content, largely identified in samples with 8% cement and 16% fly ash. Despite the increase in compressive strength, the failure strain does not alter significantly when compared to the increase in cement.

Similarly, Koliass et al. [16] found that increasing the fly ash content increased compressive strength.

Effect of fly ash content

When cement and fly ash (FA) are mixed with dredged sediments in the presence of water, a series of reactions occur, resulting in the dissociation of lime (CaO) in

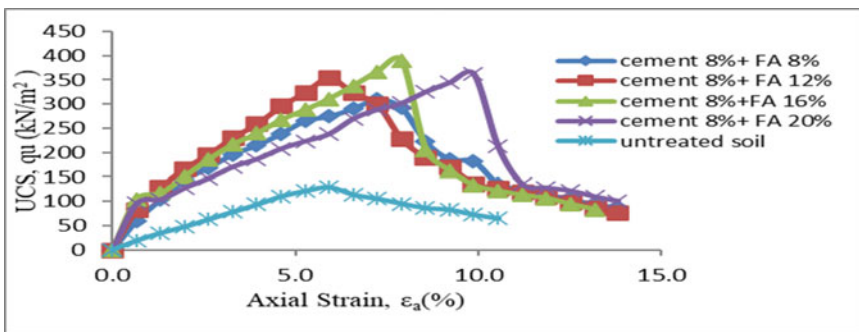


Fig. 6 Stress–strain curves for cement and FA stabilized dredged soil (immediate)

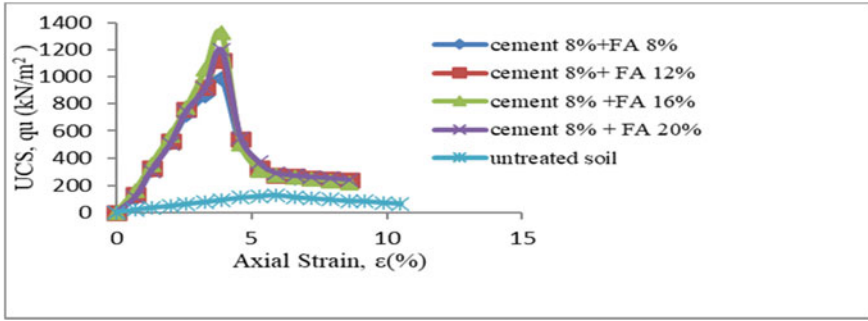


Fig. 7 Stress–strain curves for cement and FA stabilized dredged soil (7 day)

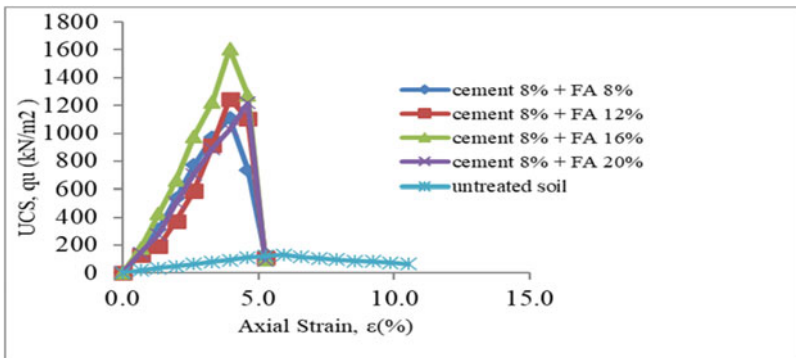


Fig. 8 Stress–strain curves for cement and FA stabilized dredged soil (28 day)

the cement and fly ash and the creation of cementitious and pozzolanic gels (calcium silicate hydrate gel, CSH). The cement hydration reaction is the first step, followed by the pozzolanic reaction. The solid particles are held together by CSH gels produced by hydration and pozzolanic processes. As a result of this binding, the sediment matrix becomes stronger, resulting in greater strength [22].

Because most of the CSH was induced from only the cement hydration reaction due to the lack of SiO₂ in fly ash, specimens stabilized with only cement had lower strength than specimens stabilized with a combination of cement and fly ash at the same cement content and curing period. Due to the presence of SiO₂ in the fly ash, CSH was induced by both cement hydration and pozzolanic processes in the specimens stabilized with a combination of cement and fly ash, producing a greater amount of CSH than utilizing OPC only.

However, in the range of 8–20% FA, the 16% FA content yielded the highest unconfined compressive (*q_u*) strength of all samples (C8FA8, C8FA12, C8FA16, and C8FA20); *q_u* tended to decrease above this fly ash content, as the 16% FA content provided the most suitable proportions of SiO₂ and CaOH₂ from FA and the cement hydration reaction, respectively, obtaining optimal performance for the

pozzolanic reaction caused by the increased formation of CSH. FA content of more than 16% may surround the cement granules, preventing water and OPC contact [4]. Consequently, the abundance of cementitious products and, in turn, q_u decreased when FA was greater than 16% (Figs. 9 and 10).

Direct shear test

From Figs. 11 and 12, it is seen that increasing cement content and fly ash content increases the cohesion and the friction angle of the sample by causing pozzolanic reactions and creating cementation gel.

Effect of curing period

When the curing duration is taken into consideration, the compressive strength of 28 days is greater than that of immediate and 7 days, as anticipated, due to the increased pozzolanic reactions and the production of extra cementation compounds over the extended curing period. Additionally, Marjive et al. [17], Kogbara et al. [15], and Kaniraj et al. [13] all indicated that extending the curing time results in an increase in compressive strength, as seen in Figs. 13 and 14. It can be stated that increasing the curing time increases stiffness, decreases compressibility, and increases the slope of stress–strain curves both before and after the peak compressive stress value, thereby lowering the failure strain of samples and resulting in a more brittle behaviour of the mixture, as illustrated in Figs. 6, 7, and 8.

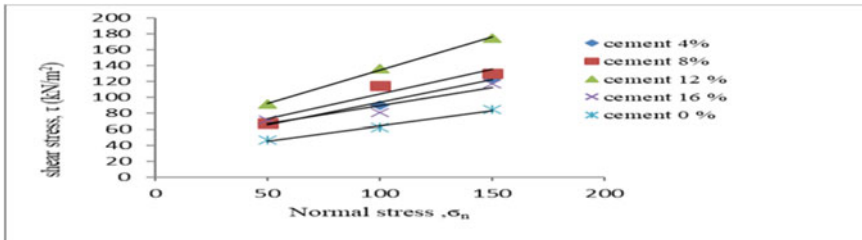


Fig. 9 Mohr failure envelope for cement stabilized dredged soil

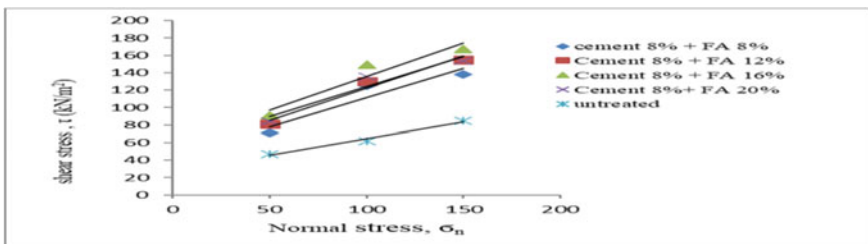


Fig. 10 Mohr failure envelope for fly ash stabilized dredged soil at a constant cement of 8%

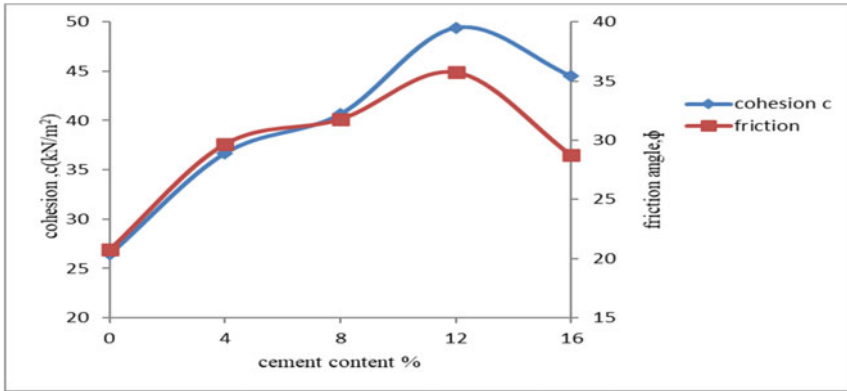


Fig. 11 Variation of c and ϕ with change in cement content

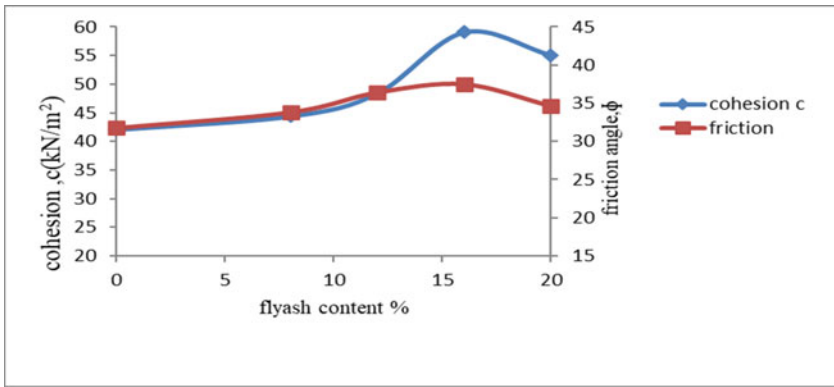


Fig. 12 Variation of c and ϕ with change in fly ash content at constant cement of 8%

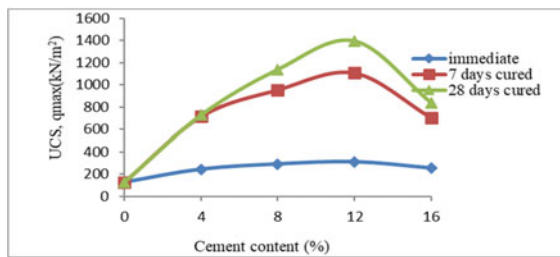
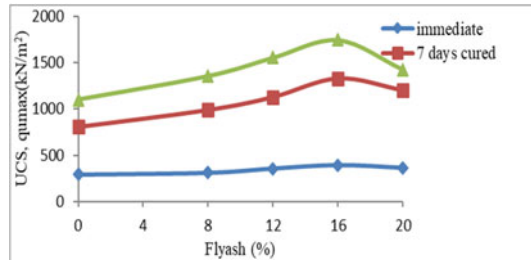


Fig. 13 Effect of curing period on strength with change in cement content

Fig. 14 Effect of curing period on strength with change in fly ash content at constant cement content of 8%



4 Conclusions

The main conclusions drawn are as follows:

1. Dredged material is made up of poorly graded inorganic silt with medium plasticity.
2. Dredged material in its in situ condition is unsuitable as a construction material as it has low compressive strength and shear strength.
3. At the same cement content and curing period, specimens stabilized purely with cement had lower q_u than specimens stabilized with a mixture of cement and FA.
4. Unconfined compressive strength showed the maximum increase in strength in sample with 8% cement and 16% fly ash as compared to the sample with only cement (8%) treatment. Beyond the optimum value, the strength decreased as fly ash and cement having no cohesion, and friction does not lead to increase in strength.
5. The sample exhibits brittleness when admixtures are added. As a result, it should be utilized cautiously in the field.
6. The curing time enhances interparticle bonding as a result of the pozzolanic processes that occur during the production of cementitious compounds. It is possible to assert that stabilized material may be beneficially used and is no longer considered a spoil or waste. Thus, utilizing dredged material has a dual benefit: first, it avoids the enormous environmental issues associated with its widespread disposal, and second, it allows for mass use of dredged material.

References

1. Aarninkhof S, Lujendijk A (2010) Safe disposal of dredged material in an environmentally sensitive environment. *Port Technol Int* 47:39–45
2. Brooks R, Udoeyo FF, Takkalapelli KV (2010) Geotechnical properties of problem soils stabilised with fly ash and limestone dust in Philadelphia. *J Mater Civ Eng* 23(5):711–716
3. Hassan HF, Taha R, Rawas AA, Shandoudi BA, Gheithi KA, Barami AMA (2005) Potential uses of petroleum-contaminated soil in highway construction. *Constr Build Mater* 19:646–652. *Engineering geology*, 267, p 105491

4. Horpibulsuk S, Phetchuay C, Chinkulkijniwat A, Cholaphatsorn A (2013) Strength development in silty clay stabilized with calcium carbide residue and fly ash. *Soils Found* 53(4):477–486
5. IS: 2720-part 10 (1973) Method of test for soils: determination of shear strength parameter by unconfined compression test. New Delhi: Bureau of Indian Standards
6. IS: 2720-part 3(1) (1980) Determination of specific gravity of fine grained soils. BIS, New Delhi
7. IS: 2720-part 3(2) (1980) Determination of specific gravity of fine, medium and coarse grained soils. BIS, New Delhi
8. IS: 2720-part 39 (1977) Method of test for soils: determination of shear strength parameter by direct shear test. Bureau of Indian Standards, New Delhi
9. IS: 2720-part 4 (1985) Determination of grain size distribution. BIS, New Delhi
10. IS: 2720-part 5 (1985) Determination of Atterberg limits. BIS, New Delhi
11. IS: 2720-part 7 (1980) Determination of water content-dry density relation using light compaction. BIS, New Delhi
12. Jan O, Mir BA (2018) Strength behaviour of cement stabilised dredged soil. *Int J Geosynthetics Ground Eng* 4(2)
13. Kaniraj SR, Havanagi VG (2001) The behavior of cement-stabilized fiber-reinforced fly ash-soil mixtures. *J Geotech Geoenviron Eng* 127(7):574–584
14. Kim SW, Yun HD (2013) Influence of recycled coarse aggregates on the bond behavior of deformed bars in concrete. *Eng Struct* 48(1):133–143
15. Kogbara RB, Al-Tabbaa A, Yi Y, Stegemann JA (2013) Cement- fly ash stabilisation/solidification of contaminated soil: performance properties and initiation of operating envelopes. *Appl Geochem* 33(1):64–75.
16. Kolia S, Kasselouri-Rigopoulou V, Karahalios A (2005) Stabilisation of clayey soils with high calcium fly ash and cement. *Cem Concr Compos* 27(2):301–313
17. Marjive VR, Ram Rathan Lal B (2016) An experimental study on stone dust and EPS beads based material. In: *Proceedings of the geo-Chicago 2016 conference, Chicago, Illinois, U.S.A., Aug.* Marjive VR, Rathan Lal B (2016) Compressive strength behaviour of stone dust and EPS beads-based material. In: *Proceedings of the geotechnical and structural engineering congress 2016, Phoenix, Arizona, U.S.A., Feb*
18. Mir BA (2005) Need for dredging and dredged material characterization from Dal Lake Srinagar—an overview. In: *Proceedings, IGC-2013, vol 1, Th-1, paper no 39. IIT Roorkee, India, pp 1–9*
19. Mir BA, Amin F, Majid B (2016) Some studies on physical and mechanical behavior of dredged soil from flood spill channel of Jhelum river, Srinagar. *Acta Ing Civil* 1(1):1–79
20. Nicholson P, Kashyap V, Fuji C (1994) Lime and fly ash admixture improvement of tropical Hawaiian soils. *Transp Res Rec Washington, DC* 1440:71–78
21. Silitonga E, Levacher D, Mezazigh S (2010) Utilization of fly ash for stabilization of marine dredged sediments. *Eur J Environ Civ Eng* 14(2):253–265
22. Tastan EO, Edil TB, Benson CH, Aydilek AH (2011) Stabilization of organic soils with fly ash. *J Geotech Geoenviron Eng* 137(9):819–833
23. Wang D, Abriak NE, Zentar R, Xu W (2012) Solidification/stabilization of dredged marine sediments for road construction. *Environ Technol* 33(1):95–100
24. Yoobanpot N, Jamsawang P, Poorahong H, Jongpradist P, Likitlersuang S (2020) Multiscale laboratory investigation of the mechanical and microstructural properties of dredged sediments stabilized with cement and fly ash

An Experimental Study on the Effect of RBI Grade 81 Additive on the Engineering Properties of Clayey Soils



Manisha Gunturi and P. T. Ravichandran

Abstract This article focuses on the study of influence of RBI grade 81 stabilizer on the improvement of the expansive soil properties with an emphasis on the micro-level analysis of the treated soils. The soil samples were treated with various dosages (2, 4 and 6%) of the stabilizer and cured under controlled conditions. The improvement in the treated soil properties in terms of effectiveness of dosage and effectiveness of curing periods was studied. An attempt has been made to understand the soil behavior and the efficiency of the stabilizer by comparing the laboratory test results with the micro-level analysis. The test results indicated reduction in free swell index of the soil samples and a significant increase in the strength parameters of the treated soils. The addition of RBI 81 stabilizer resulted in the improvement of about 500% and 300% in the UCS values for samples 1 and 2, respectively. The CBR values obtained from treated soil samples were observed to be around 50% for both the soils in soaked condition. The swell potential of the treated soil samples was reduced by 80% for both the soil samples.

Keywords Soil stabilization · UCS · CBR · RBI 81 · SEM

1 Introduction

The swell-shrink problem associated with expansive soils is a serious threat to the lightly loaded structures constructed on these soils. The most common types of structures affected by these types of soils are pavements, canal linings, compound walls, etc. The unpredictable ground movements caused by these soils induce large

M. Gunturi (✉)

Department of Civil Engineering, Gokaraju Rangaraju Institute of Engineering and Technology, Hyderabad, India
e-mail: manisha3897@gmail.com

P. T. Ravichandran

Department of Civil Engineering, SRM Institute of Science and Technology, Kattankulathur, Chennai, India

stresses on the structures found in them. The potential danger coupled with these soils is a worldwide problem and needs to be addressed.

Expansive soils are clayey soil which depict excessive volumetric changes on addition or removal of moisture Asuri and Keshavamurthy [1]. The volume change behavior is seen in some types of clays while other types do not depict any such variation in volumes which can be attributed to the mineralogical differences, mode of formation, occurrence, composition, etc. In most of the cases, the clays where montmorillonite mineral is predominant show excessive volume change behavior and hence known as expansive soils.

Other clay minerals such as kaolinite, illite and halloysite do not exhibit swell-shrink behavior but possess low bearing capacity. The expansive soils are sensitive to fluctuations in moisture content and also possess low bearing capacity. Therefore, these need to be stabilized for their volume change behavior and improved for other engineering properties.

Large number of stabilizing agents are available which can enhance the required properties of these soils. The choice of stabilizing agents further depends upon the type and depth of soil, type of problem, site conditions, etc. On the basis of the depth of soil layer requiring treatment, one can opt for physical or chemical methods of soil treatment. The former deals with complete or partial replacement of soil with non-cohesive fill material, while the latter deals with the addition of stabilizing agents to alter the existing soil properties. Usage of stabilizing agents for improving the expansive soils is the most commonly adopted method due to its advantages over other methods such as easy application, early strength gain and durability Firoozi et al. [2].

Depending upon the nature of soil–stabilizer reaction, the stabilization technique can be classified into calcium based and non-calcium based. The calcium-based stabilizers improve the soil properties by pozzolanic reactions to form hydrates of calcium silicates and aluminates Behnood [3], Jalal et al. [4], whereas in case of non-calcium-based stabilizers, the improvement in engineering properties can be achieved by means of soil reinforcement Wang et al. [5], alkali activation Shaquor et al. [6], etc. When calcium-based stabilizers are added, a series of chemical reactions occur in the soil such as cation exchange, flocculation and pozzolanic reactions resulting in the improvement of geotechnical properties of the soil Diamond and Kinter [7]. Although a wide range of calcium-based additives are available, lime and cement are most commonly adopted owing to their easy availability and economic factors. In addition to these, fly ash, rice husk ash Onyelowe et al. [8], phosphogypsum Divya Krishnan et al. [9], marble dust, calcium chloride, sodium meta-silicate, etc., are also widely adopted stabilizers.

RBI grade 81 is one such calcium-based stabilizer that can be used to stabilize the subgrade soils which is manufactured in powdered form with a small fraction fiber content for commercial purpose. The suitability of this eco-friendly and cost-effective stabilizer is confirmed by various researchers Kumar et al. [10], Kodicherla and Nandyala [11], Ravi Shankar and Panditharadhya [12], Gunturi [13], Anitha et al. [14], Harichane et al. [15], Ismeik and Shaqour [16], Sharo et al. [17]. Although a numerous soil stabilizers are commercially available that can be effectively used,

studies are still going on in search of a better stabilizer. Similar attempt is made in this study to evaluate the influence of calcium-based additive on the geotechnical properties of the expansive soils. This article presents the results of influence of RBI grade 81 stabilizer on the improvement of the expansive soil properties with an emphasis on the micro-level analysis of the treated soils.

2 Materials and Methods

2.1 Soils

Two types of soil samples were selected for the laboratory investigation, namely S1 and S2 from a depth of 60 cm below ground level after removing the debris and grit from the top surface. The soil samples were obtained from Thittaguti to Sirupakkam road and Perungudi, Chennai, India, respectively.

Series of tests were conducted on the soil properties in order to classify and to understand the behavior of these soils. The properties of soil like specific gravity, liquid limit, plastic limit, shrinkage limit and compaction characteristic were determined. In addition to this, UCC, free swell and CBR tests of untreated and treated soil were conducted as per BIS procedure.

The specific gravity of the soil samples S1 and S2 is obtained as 2.63 and 2.65, respectively. Clay and silt fraction predominated in both the soils with 70% and 26% in S1 and 66% and 32% in S2, respectively. The liquid limit and plasticity index of the soil samples are observed to be 75%, 38 for S1 and 72%, 39 for S2 and a shrinkage limit of 7% and 6% for samples S1 and S2, respectively, and the soils were classified as clay of high compressibility as per IS 1498 (1970) Asuri and Keshavamurthy, [1]. The free swell index tests on soil samples showed 110% and 105%, respectively, for S1 and S2. The test results depict excessive volume change behavior indicating damage potential of these soils.

The maximum dry density and optimum moisture content as obtained from compaction tests results for the samples were observed as 1.66 g/cc and 20% for S1 and 1.54 g/cc and 24.5% for S2. The unconfined compressive strength of the samples was recorded as 138 kPa and 122 kPa and California bearing ratio as 2% and 2.19%, respectively, for S1 and S2.

2.2 Stabilizer

In this investigation, RBI grade 81 is selected as the stabilizer for treating the soil samples. RBI grade 81 is commercially available in powdered form with a small fraction of fibers. It is a cementitious material which when added to the soil initiates irreversible pozzolanic reactions in the soil, thereby altering the soil properties. This

material is suitable for almost all the soil types and is proven efficient for stabilization of subgrade soils.

3 Preparation of Test Specimen

The test specimen was prepared by adding various dosages of the stabilizer at 2, 4 and 6% by weight of the soil sample for treatment. The treated soil samples were cured for 3, 7 and 14 days under controlled environment to prevent any moisture loss.

Test specimens were prepared for UCC and CBR tests strictly as per the codal specifications provided by the Bureau of Indian Standards.

3.1 Unconfined Compressive Strength

Cylindrical test specimens of 38 mm diameter and 76 mm height were compacted at the optimum moisture content to obtain a maximum dry density as determined by the compaction tests. The prepared specimens were secured in airtight plastic bags which were kept wetted rice husk covered with wetted gunny bags to ensure zero or minimum loss of moisture content. The specimens were tested at a controlled strain rate of 1.25 mm/min in the unconfined compression testing machine at 3, 7 and 14 days.

3.2 California Bearing Ratio

Cylindrical specimen of 150 mm diameter and 125 mm height was prepared at a predetermined optimum moisture content and maximum dry density. The prepared specimens were placed over wetted rice husk layer and covered with wetter gunny bags to ensure temperature control. The specimens were soaked for a duration of 96 hr prior to the testing. The average California bearing ratio values were recorded at 2.5 mm and 5 mm penetration by a plunger of 50 mm diameter and 100 mm length.

The specimens were tested at a strain rate of 1.25 mm/min in California testing machine after soaking for a 96-hr duration prior to the testing.

3.3 Free Swell Index

To conduct free swell index test, the sample was obtained from the tested UCC and CBR specimens. The sample was oven-dried at 60 °C to avoid any loss on ignition

for 24 hr. The oven-dried sample immersed in kerosene and water is then kept under observation for 24 hr.

3.4 Micro-Level Analysis

To understand the morphology and behavior of the soils, micro-level analysis was conducted on the untreated and treated soil samples. Both untreated soil samples and soil + RBI grade 81 composites were subjected to SEM analysis.

4 Results and Discussion

4.1 Unconfined Compressive Strength Test

The unconfined compressive strength tests were conducted on soil and soil + RBI grade 81 composites at 2, 4 and 6% dosages and at 3, 7 and 14 days of curing periods. Figures 1 and 2 show the typical stress-strain curves obtained from the unconfined compression tests on the specimens. It can be observed that the UCS values of the soil samples increase with the addition of RBI grade 81. The shift in yield point from the graph indicates increase in UCS values and change in the morphology of the soil on treatment. Both the soil samples have undergone brittle failure on treatment. With the increase in dosage of additive, higher stress values at lower strains can also be observed from the plots.

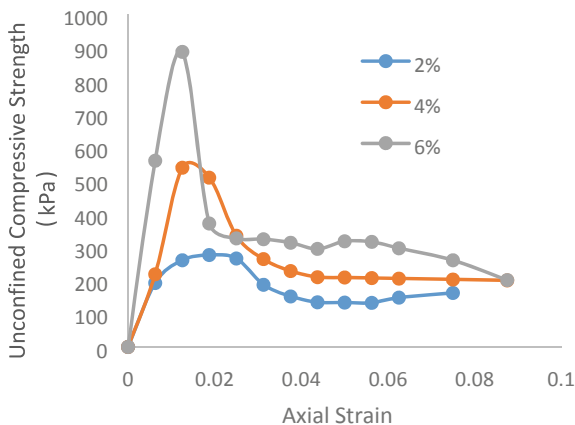


Fig. 1 Stress–strain curves from UCS test of 14 days of cured S1 + RBI grade 81 composites at various dosages

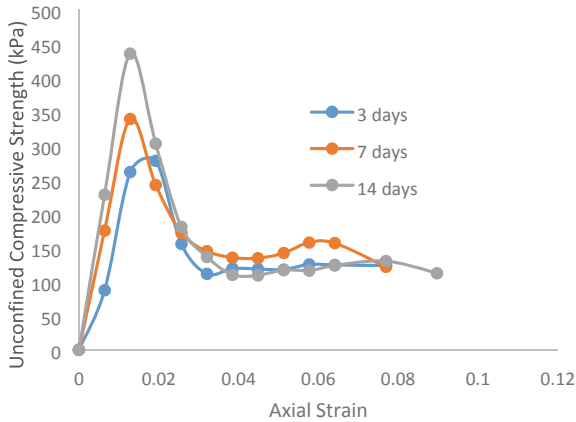


Fig. 2 Stress–strain curves obtained from UCS test of S2 + RBI grade 81 composites at various curing periods

4.2 California Bearing Ratio Test

California bearing ratio test was conducted on treated soil samples which were prepared using different percentages of additive 2, 4 and 6% for different curing periods of 3, 7 and 14 days. Thereafter, the prepared specimens were placed under a surcharge pressure of 2.5 kPa and the load was applied on the soil to determine the CBR values of treated soils. The test results conducted on soil + RBI grade 81 composites are depicted in Fig. 3. The CBR values of the treated soil samples increased significantly by 10-fold on treatment with 6% additive cured for 14 days. The variation in CBR values from 2% for untreated soil to 9, 16 and 20% in case of treated soils with 2, 4 and 6% additive cured for 14 days can be observed from the plot. Early strength gain in the treated soils can be observed from the test results which is favorable for the current demands in the construction industry.

4.3 Free Swell Index

The free swell index test was conducted on the pulverized soil obtained from tested UCC and CBR specimens. The pulverized samples passing through 75 μ were kept immersed in water and kerosene as prescribed in IS 2720 part 40, and the observations were recorded after 24-hr duration. Variation in free swell index values of soil sample S1+RBI composites at various curing periods is shown in Fig. 4. A gradual decrease in the free swell index values of the soil samples can be observed on treatment with the additive. The free swell values reduced by 50% on treatment with the additive.

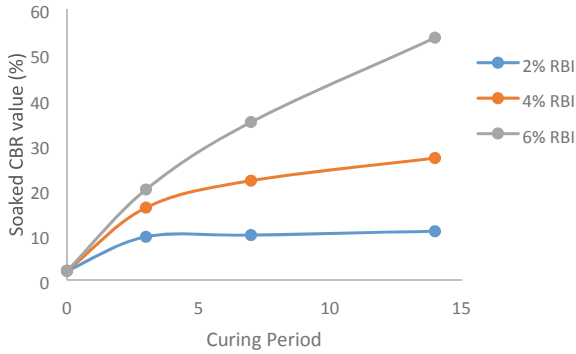


Fig. 3 Variation in CBR values of S1 + RBI grade 81 composites cured for 14 days

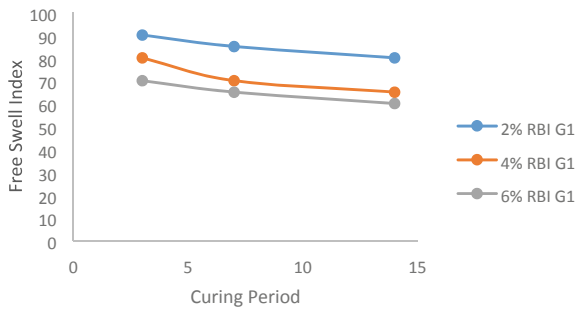


Fig. 4 Variation in free swell index values of S1 + RBI composites

5 Micro-Analysis

5.1 Scanning Electron Microscopy

The tested UCC specimens were pulverized and subjected to micro-level analysis for further assessment on the particle assembly and pore spaces of the soil samples on treatment. The SEM analysis on the composites gave a clear indication on the presence of cementitious compounds and reduction in pore spaces of the soil samples on treatment. Figure 5 indicates the variation in the particle arrangement and reduction in pore spaces on treatment with the RBI grade 81.

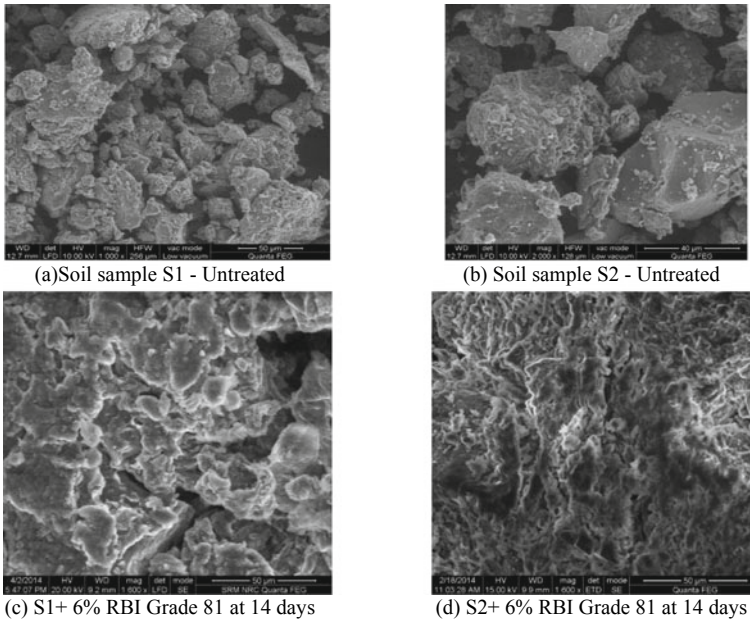


Fig. 5 SEM Images

6 Conclusion

The RBI grade 81 stabilizer was proven to be efficient in improving the strength of expansive soils. The stabilizer when added in traces was effective in reducing the swell-shrink behavior of the expansive soils.

The early strength gain as observed from the laboratory investigation is desirable in the construction industry by reducing the time required in the soil treatment in the pre-construction phase of the project.

The following conclusions can be drawn based on the experimental investigation:

1. The addition of RBI grade 81 stabilizer improved the geotechnical properties of the expansive soils and reduced the free swell index of the soil.
2. The soil composites depicted a change in the failure pattern of the specimens in the UCS test. A brittle failure was observed in the treated soils with a very high compressive strength values. On treatment, the soils depicted a 16-fold strength gain in the UCS values compared to the untreated soils.
3. A significant increase in the soaked CBR value is observed on adding the stabilizer. The maximum CBR value observed was 20–25% for the both the soils with the addition of 6% RBI additives at the curing period of 14 days.
4. SEM micrographs reveal the change in microstructure of the treated soil sample by the formation of cementitious material and reduction in the pore spaces which are filled by the former.

References

1. Asuri S, Keshavamurthy P (2016) Expansive soil characterisation: an appraisal. *INAE Lett* 1(1):2933. <https://doi.org/10.1007/s41403-016-0001-9>
2. Firoozi AA, Guney Olgun C, Baghini MS (2017) Fundamentals of soil stabilization. *Int J Geo-Eng* 8(1):26. <https://doi.org/10.1186/s40703-017-0064-9>
3. Behnood A (2018) Soil and clay stabilization with calcium- and non-calcium-based additives: a state-of-the-art review of challenges, approaches and techniques. *Transp Geotech* 17:14–32. <https://doi.org/10.1016/j.trgeo.2018.08.002>
4. Jalal FE, Xu Y, Jamhiri B, Memon SA (2020) On the recent trends in expansive soil stabilization using calcium-based stabilizer materials (CSMs): a comprehensive review. *Adv Mater Sci Eng* 10(2020):1510969
5. Wang J-Q, Hou S-L, Xue J-F, Lin Z-N, Tang Y (2021) Triaxial shear behavior of a gravelly sand with different forms of reinforcement. In: *Advances in civil engineering*, vol 2021, Article ID 8891400, p 11. <https://doi.org/10.1155/2021/8891400>
6. Shaqour F, Ismeik M, Esaifan M (2017) Alkali activation of natural clay using a $\text{Ca}(\text{OH})_2/\text{Na}_2\text{CO}_3$ alkaline mixture. *Clay Miner* 52:485–496. <https://doi.org/10.1180/claymin.2017.052.4.06>
7. Diamond S, Kinter EB (1965) Mechanisms of soil-lime stabilization. *Highway Res Rec*
8. Onyelowe KC, Jalal FE, Onyia ME, Onuoha IC, Alaneme GU (2021) Application of gene expression programming to evaluate strength characteristics of hydrated-lime-activated rice husk ash-treated expansive soil. Daneshvar Rouyendegh (B. Erdebilli) B (ed). *Appl Comput Intell Soft Comput* 2021(6686347)
9. Divya Krishnan K, Ravichandran PT, Janani V, Annadurai R, Gunturi M (2014) Effect of fly ash and phospho gypsum on properties of expansive soils. *Int J Sci Eng Technol* 3(5):592–596
10. Prasanna Kumar SMVS, Durga Prasad L, Sivanarayana C, Prasad DSV (2019) A study on stabilization of expansive soil by using agricultural by-products. *SSRG Int J Civ Eng* 5(8):17–21
11. Kodicherla SPK, Nandyala DK (2017) Effect of RBI Grade 81 on strength characteristics of clayey subgrade. *Geo-Engineering* 8:24. <https://doi.org/10.1186/s40703-017-0061-z>
12. Ravi Shankar A, Panditharadhya BJ (2017) Laboratory investigation of lateritic soil treated with terrasil and cement
13. Gunturi M (2014) Study on strength characteristics of soil using soil stabilizer RBI–81. *Int J Res Eng Technol* 03:201–204
14. Anitha KR, Ashalatha R, Johnson AS (2009) Effects of RBI grade 81 on different types of subgrade soil. In: 10th National conference on technological trends (NCTT09). pp 6–7
15. Harichane K, Ghrici M, Gadouri H (2019) Natural pozzolana used as a source of silica for improving the behaviour of lime-stabilised clayey soil. *Arab J Geosci* 12(15):447. <https://doi.org/10.1007/s12517-019-4635-2>
16. Ismeik M, Shaqour F (2020) Effectiveness of lime in stabilising subgrade soils subjected to freeze-thaw cycles. *Road Mater Pavement Des* 21(1):42–60. <https://doi.org/10.1080/14680629.2018.1479289>
17. Sharo AA, Alhowaidi YA, Al-Tawaha MS (2019) Improving properties of expansive soil using cement, quick lime and cement-lime blend. *Int Rev Civ Eng (IRECE)* 10(2):94. <https://doi.org/10.15866/irece.v10i2.16064>

A Study on the Effectiveness on the Polyethylene Strips in Cement-Treated Soil



Manisha Gunturi and Goutham Sarang

Abstract This paper presents the study conducted on the locally available clayey soil using plastic strips with and without cement. Low-density polyethylene obtained from shopping bags was cut into strips of aspect ratio (AR) 4 and 2 (length/width ratio). The plastic strips were uniformly mixed in the soil sample by adding 1, 2, and 3% by weight of the soil. The samples were tested for unconfined compression test. In order to compare the improvement in strength of the soil, a constant value of 2% cement was added along with the plastic strips. The cement-treated samples were cured for a period of 7, 14, 21, and 28 days prior to testing. The test results for untreated and treated soil samples with and without cement were compared. The samples treated with plastic strips showed slight improvement in the UCS values on comparison to the cement-treated soil samples. A maximum of 10 fold and 18-fold increase in the UCS values compared to untreated soils were observed for soil samples treated with plastic strips of AR2 and AR4, respectively. Similarly, the cement-treated soils showed better results than the soils without cement treatment. The UCS values of cement-treated soil samples was found to be 28-fold and 32-fold for AR2 and AR4, respectively.

Keywords UCS · Plastic strips · Soil reinforcement · Cement-treated soils

1 Introduction

Soil being one of nature's most abundant construction materials is used for almost all construction activities directly or indirectly. These naturally existing soils can be classified based on particle size, mode of formation, mode of deposition, index properties, etc. Utilization of a particular type of soil as construction material depends upon the material properties. All the soils that exist in nature cannot be used in the construction. Traditionally when such situations are encountered, the unsuitable soils

M. Gunturi (✉) · G. Sarang
School of Civil Engineering, VIT Chennai, Chennai, India
e-mail: manishag3897@gmail.com

© The Author(s), under exclusive license to Springer Nature Singapore Pte Ltd. 2023
A. K. Agnihotri et al. (eds.), *Proceedings of Indian Geotechnical and Geoenvironmental Engineering Conference (IGGEC) 2021, Vol. 1*, Lecture Notes in Civil Engineering 280,
https://doi.org/10.1007/978-981-19-4739-1_42

457

were replaced with the suitable soils. This method of replacement is proven expensive and requires lot of effort in terms of excavating the existing soil, transporting and dumping the refusal, identification, transportation, refilling, and compaction of suitable soils. In order to simplify the tedious process involved in soil replacement method, improving the properties of existing soils is necessary. This can be achieved by adopting the in-situ treatment techniques such as soil modification. Soil modification is an alternative technique to soil replacement where the existing soil is improved to make it suitable as a construction material. Such soils are known as modified soils.

Scarcity of suitable land for construction has led to the utilization of modified soils for engineering purposes all over the world. Soil modification refers to the changing the property of soil by increasing strength and durability. It is the process of treating soil using compaction, dewatering, and adding minerals to the soil.

Improving the existing soil's engineering properties is referred to as either "soil modification" or "soil stabilization." The term "modification" indicates a change or alteration in the properties of a soil, whereas stabilization indicates change in engineering properties of the soil so as to make these soils suitable for construction purposes.

A number of researches are being carried out across the world to come up with suitable and economic alternative treatment techniques for addressing the issues related to the soils in construction industry. Soil modification by densification, fiber reinforcement, proportioning, are commonly adopted nowadays. The densification methods include compaction, sand columns or stone columns by displacement or replacement techniques. In fiber reinforcement, a wide variety of fibers are being used such as coir fibers, jute fibers, synthetic fibers, etc. to provide reinforcement to the existing soils. Similarly in proportioning technique, the unsuitable soils is partially replaced with any suitable soil to obtain a mixture of desired properties. Utilization of fiber with or without industrial by-products and other wastes for enhancing the desirable properties of soils has been employed by many researchers Anupam et al. [1], Dutta and Sarda [3], Gupta and Kumar [4]. Geofibers along with synthetic fluids has improved the CBR values of fine-grained soils Hazirbaba and Gullu [5]. Addition of various types of fibers to subgrade soils and embankment soils resulted in improvement of soil properties and was found to be a cost-effective solution Hausmann [6], Jha et al. [7], Kumar et al. [8], Kumar et al. [9], Kumar and Singh [10], Kumar et al. [11]. In similar studies, coir fibers, as well as polypropylene fibers, were added to clayey soils where improvement in soil properties in terms of CBR values were observed Mohanty et al. [12], Muntohar [14], Pradhan et al. [16], Priyadarshree et al. [17], Sarbaz et al. [20]. Inclusion of various types of fiber reinforcement to different soil types is found to be effective in enhancing the strength characteristics of fine-grained soils Take et al. [21], Tang et al. [22], White et al. [23], Yetimoglu et al. [24], Zaimoglu and Yetimoglu [25]. Even though there are numerous solutions available to improve the existing soil properties, extensive researches are continuously being done to achieve better performance, cost-effective solutions, reusing the locally available waste materials, etc. In a similar manner this study focused on evaluating the

performance of waste plastic obtained from shopping bags on the geotechnical properties of expansive soils. A series of laboratory tests were conducted on the clayey soils with the inclusion of plastic strips with and without the addition of cement.

2 Soil Treatment Methods

2.1 Types of Soil Stabilization

The existing soil properties can be improved by adopting appropriate soil improvement techniques. Selecting of a suitable treatment techniques requires identification of the type, properties of the in-situ soils, and the project requirements. The methods of soil treatment can be broadly classified into: (a) Physical and Mechanical modification (b) Chemical modification (c) Hydraulic modification (d) Modification by inclusions. The physical and mechanical modifications include densification methods while chemical and hydraulic modification includes incorporating chemical additives and dewatering techniques, respectively. In case of modification by inclusions, the desirable properties of the existing properties are enhanced by providing suitable reinforcement in the form of fibers, strips, meshes, etc. Nguyen et al. [15].

Mechanical modification: This method involves improvement of existing soil properties by mechanical means such as densification techniques. This method is most widely adopted for loose strata and sandy soils. The densification techniques can be effectively employed for both shallow as well as deeper soil layers Hausmann [6].

Chemical modification: This method involves treatment of existing soils with the help of chemical additives. The main advantage of chemical modification is that setting time and curing time can be controlled. Most of the chemical treatment techniques being irreversible in nature, provide durability. Availability of wide range of chemicals for treatment techniques, cheaper industrial wastes, and by-products that can be used effectively has led to the increased usage of this method. Cement, Bitumen, Fly ash, Phosphogypsum, Lime, etc. are some of the examples of chemical stabilizers. The main principle behind the chemical stabilization is that the soil properties are altered by chemical reactions and thereby formation of cementitious materials within the soil.

Hydraulic modification: This method of soil modification involves dewatering and consolidation of the existing soils with or without vertical drains.

2.2 Modification by Inclusions and Confinement

This method involves addition of reinforcing materials to the soil in order to withstand the lateral component of the loads. Reinforcement by fibers, strips, bars, meshes, and

fabrics imparts tensile strength to a constructed soil mass Priyadharshini et al. [18], Muir Wood et al. [13]. In-situ reinforcement is achieved by nails and anchors. The use of natural fibers in geotechnical applications is a balancing act between the fulfillment of human needs and the protection of the natural environment. Reinforcing the soil with natural fibers is a cost-effective solution. Soil Reinforcement may be made with a number of materials like Woven geotextiles, Polymer Geogrids, Polyester and Fiberglass Geogrids, Steel Strips, Welded wire mesh, etc. Dave et al. [2], Salim et al. [19].

2.3 Applications

Stabilized soils with or without reinforcement is most commonly adopted nowadays in the construction industry due to the factors like economy, easy availability, speed and ease of construction, etc. Roadways, airport runways, landfills, retaining walls, embankments, etc. are few of the examples where these methods are being employed with effective results.

3 Materials Used

3.1 Soil Sample

To conduct the experimental investigation, clayey soil obtained from Kollur location in Hyderabad, Telangana is adopted. The top half meter of the soil layer contained debris and vegetation matter is removed before excavating the sample for investigation purposes. The soil sample obtained was air dried for a period of 7 days and then pulverized to remove visible lumps. Wet sieve analysis was conducted on a representative sample which indicated that the majority of the selected sample is finer than 75 μm .

Preliminary tests were conducted on soil sample in accordance with IS 2720 and the soil sample is classified as Clayey Sand (Table 1).

3.2 Fibers

Polyethylene fibers of 100 μm thickness are used in this investigation to study the effectiveness of the fibers on soil with and without cement content. The LDPE fibers with cut into two different aspect ratios (length to width ratio) to carry out the investigation. The fibers were cut to a size of 1 cm in length and 0.25 and 0.5 cm

Table 1 Properties of untreated soil sample

Parameters		Symbol	Sample
Grain size analysis	Sand	S	21.5%
	Silt and clay	M and C	78.5%
Liquid limit %		W_L	32
Plastic limit%		W_P	12.2
Plasticity index%		I_P	19.8
Shrinkage limit %		W_s	4.0
Specific gravity		G	2.37
Free swell index		FSI	30%
Optimum moisture content		OMC	15.5%
Maximum dry density		$\gamma_{d \max}$	1.6 g/cc
		q_u	1.045 kg/cm ²
Unconfined compressive strength		c_u	0.52 kg/cm ²
California bearing ratio		CBR	3.9%
Soil classification			SC—Clayey sand

in width for AR4 and AR2, respectively. The fibers were added at 1, 2, and 3% by weight of the soil sample.

3.3 Cement

In this investigation, cement is used as an additional material to test the effectiveness of fiber reinforcement. Ordinary Portland Cement of grade 33 is added to fiber-reinforced soil at a fixed rate of 2% by weight of the soil sample. The fiber-reinforced cement-treated soil samples are cured for four different curing periods of 7, 14, 21, and 28 days.

The constant value of 2% by weight of cement is selected based on the literature survey. This low quantity will ensure that the strength gain in case of treated soil is not due to the addition of cement alone. Addition of excess quantity of cement may result in the significant contribution of strength of treated soil by cement treatment.

4 Soil Classification

Based on the test results obtained from the laboratory tests on untreated soil samples, the sample was classified as clay of high compressibility. Table 1 shows the test results of untreated soil sample.

5 Methodology and Tests Conducted

The soil samples were added with 1, 2, and 3% by weight of the plastic fibers of AR4 and AR2. Two sets of reinforced soil samples were prepared with and without cement treatment. For samples with cement treatment, only 2% by weight of cement is added to the fiber-reinforced soil samples. Unconfined compressive test was planned on the treated soil sample. Soil specimen was prepared for the test in accordance with IS 2720 and samples were placed in air-tight plastic covers to retain the moisture content which are in turn covered with wetted clothes to control the temperature changes.

The prepared specimens were cured for 7, 14, 21, and 28 days in controlled conditions. At least three specimens were prepared for each test and all the tests were conducted according to the IS code specifications.

6 Results and Discussions

The series of UCC tests were done as planned in the experimental program. The test results indicate that in case of samples without cement treatment (WoCAR2 and WoCAR4), samples with AR2 gives better result than AR4 (Figs. 1, 2 and 3). In case of samples treated with 2% cement content (WCAR2 and WCAR4), an increasing trend was observed at first followed by a reduction in rate of strength increment as it can be observed from Figs. 1, 2 and 3.

An improvement in the unconfined compressive strength was observed even without the addition of cement. This can be attributed to the reinforcement provided to the soil samples in the form of plastic strips. It has been observed that the UCS values for the samples with aspect ratio 4 (AR4) showed lower values without cement. In addition of cement, an increase in the UCS was observed. This might be due to the limited cohesion in soils obstructed by fibers which was accounted by addition of cement, the formation of cementitious compounds within the composite enhanced the binding properties. In the samples with cement, the rate of increment in strength

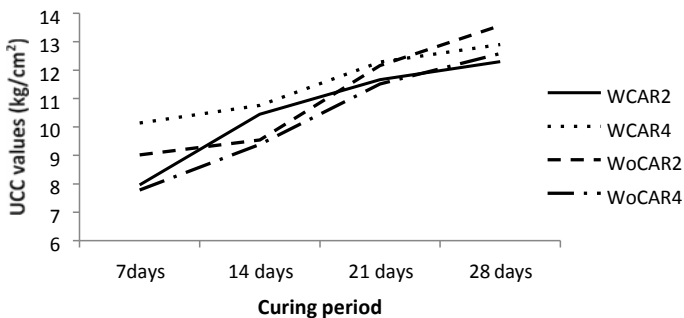


Fig. 1 Effect of curing period on UCC specimen with 1% fiber for soil sample

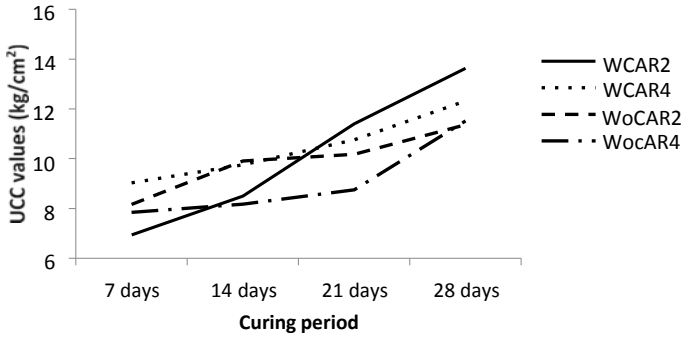
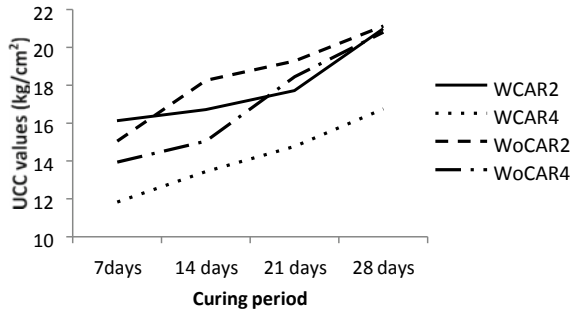


Fig. 2 Effect of curing period on UCC specimen with 2% fiber for soil sample

Fig. 3 Effect of curing period on UCC specimen with 3% fiber for soil sample



was low initially but was eventually increased by 28 days curing period. This can be due to the formation strength imparting calcium silicates and aluminate hydrates by the end of 28-day curing periods.

Though the material used in this study do not provide eco-friendly or sustainable solution for soil improvement, it does provide an alternative method for reusing the plastic waste. The waste plastic is extensively being used in the construction of pavements in many areas. In a similar manner, the plastic waste can also be used in enhancing the existing soil properties. To address the issue related to the non-biodegradable nature of the plastic waste can be addressed by addition of appropriate binding materials to arrest the mobility of the waste.

7 Conclusion

1. A minimum quantity of cement, i.e., 2% was added to the samples to ensure enough binding of soil particles and not to have significant influence on the soil properties.

2. It was observed that even as small as 2% by weight of fibers were enough to enhance the soil properties.
3. The test results indicate that in case of samples without cement treatment, samples with AR2 gives better result than AR4. It has been observed that with the increase in the aspect ratio, the cohesion between the soil particles is reduced and hence the reduction in strength.
4. Addition of cement for AR4 fibers showed better results than that of the sample without cement. The cement in this case compensated the loss in cohesion and hence the strength improvement.

References

1. Anupam AK, Kumar P, Ransinchung RINGD (2013) Use of various agricultural and industrial waste materials in road construction. *Procedia Soc Behav Sci* 104:264–273. <https://doi.org/10.1016/j.sbspro.2013.11.119>
2. Dave TN, Patel D, Saiyad G, Patolia N (2020) Use of polypropylene fibres for cohesive soil stabilization. In: Prashant A, Sachan A, Desai C (eds) *Advances in computer methods and geomechanics. Lecture notes in civil engineering*, vol 56. Springer, Singapore. https://doi.org/10.1007/978-981-15-0890-5_34
3. Dutta RK, Sarda VK (2007) CBR behaviour of waste plastic strip-reinforced stone dust/fly ash overlying saturated clay. *Turk J Eng Environ Sci* 31(3):171–182
4. Gupta D, Kumar A (2017) Performance evaluation of cement-stabilized pond ash-rice husk ash-clay mixture as a highway construction material. *J Rock Mech Geotech Eng* 9(1):159–169. <https://doi.org/10.1016/j.jrmge.2016.05.010>
5. Hazirbaba K, Gullu H (2010) California bearing ratio improvement and freeze–thaw performance of fine-grained soils treated with geofibre and synthetic fluid. *Cold Reg Sci Technol* 63(1):50–60. <https://doi.org/10.1016/j.coldregions.2010.05.006>
6. Hausmann MR (1990) *Engineering principles of ground modifications*. McGraw Hill, New York
7. Jha JN, Choudhary AK, Gill KS, Shukla SK (2014) Behaviour of plastic waste fibre-reinforced industrial wastes in pavement applications. *Int J Geotech Eng* 8(3):277–286. <https://doi.org/10.1179/1939787914Y.0000000044>
8. Kumar P, Chandra S, Vishal R (2006) Comparative study of different subbase materials. *J Mater Civil Eng* 18(4):576–580. [https://doi.org/10.1061/\(ASCE\)0899-1561](https://doi.org/10.1061/(ASCE)0899-1561)
9. Kumar P, Mehndiratta HC, Chandranarayana S, Singh SP (2005) Effect of randomly distributed fibres on flyash embankments. *J Inst Eng India Part CV Civil Eng Div Board* 86(3):113–118
10. Kumar P, Singh SP (2008) Fibre-reinforced fly ash subbase in rural roads. *J Transp Eng* 134(4):171–180. [https://doi.org/10.1061/\(ASCE\)0733-947X](https://doi.org/10.1061/(ASCE)0733-947X)
11. Kumar R, Kanaujia VK, Chandra D (1999) Engineering behaviour of fibre-reinforced pond ash and silty sand. *Geosynth Int* 6(6):509–518. <https://doi.org/10.1680/gein.6.0162>
12. Mohanty B, Chauhan MS, Mittal S (2011) California bearing ratio of randomly oriented fibre reinforced clayey subgrade for rural roads. In: *Proceedings of Indian geotechnical conference*. Kochi, India, pp 611–614
13. Muir Wood D, Diambra A, Ibraim E (2014) Fibres and roots for soil improvement. In: *Geomechanics from micro to macro—proceedings of the TC105 ISSMGE international symposium on geomechanics from micro to macro*, vol 2. CRC Press, IS-Cambridge, pp 1503–1508
14. Muntohar AS, Widiyanti A, Hartono E, Diana W (2013) Engineering properties of silty soil stabilized with lime and rice husk ash and reinforced with waste plastic fibre. *J Mater Civil Eng* 25(9):1260–1270. [https://doi.org/10.1061/\(ASCE\)MT.1943-5533.0000659](https://doi.org/10.1061/(ASCE)MT.1943-5533.0000659)

15. Nguyen G, Hrubešová E, Voltr A (2015) Soil improvement using polyester fibres. *Procedia Eng* 1(111):596–600
16. Pradhan PK, Kar RK, Naik A (2012) Effect of random inclusion of polypropylene fibres on strength characteristics of cohesive soil. *Geotech Geol Eng* 30(1):15–25. <https://doi.org/10.1007/s10706-011-9445-6>
17. Priyadarshree A, Gupta D, Kumar V, Sharma V (2015) Comparative study on performance of tire crumbles with fly ash and kaolin clay. *Int J Geosynth Ground Eng* 1(4):38. <https://doi.org/10.1007/s40891-0150033-3>
18. Priyadharshini B, Boopathiraj, Eshanthini P (2021) Experimental study on soil stabilization using fibres. *Mater Res Proc* 19:200–207
19. Salim NM, AL-Soudany KYH, Ahmed AA (2018) The impact of using recycled plastic fibres on the geotechnical properties of soft Iraqi soils. *IOP Conf Ser Mater Sci Eng* 433:012017
20. Sarbaz H, Ghiassian H, Heshmati AA (2014) CBR strength of reinforced soil with natural fibres and considering environmental conditions. *Int J Pavement Eng* 15(7):577–583. <https://doi.org/10.1080/10298436.2013.770511>
21. Take WA, Irving J, Bischoff PH, Valsangkar AJ (1997) Synthetic fibre reinforcement of clayey sand and silt subgrade and sand sub base. In: *Proceedings of the international conference on ground improvement techniques*, pp 547–552
22. Tang C, Shi B, Gao W, Chen F, Cai Y (2007) Strength and mechanical behaviour of short propylene fibre reinforced and cemented stabilized clayey soil. *Geotext Geomembr* 25(3):194–202. <https://doi.org/10.1016/j.geotextmem.2006.11.002>
23. White DJ, Vennapusa PKR, Becker P, White C, Engineers BC (2013) Cement stabilization with fibre reinforcement of subbase. Technical Brief, Centre for CEER Earthworks Engineering Research, Iowa State University, Institute of Transportation
24. Yetimoglu T, Inanir M, Inanir OE (2005) A study on bearing capacity of randomly distributed fibre- reinforced sand fills overlying soft clay. *Geotext Geomembr* 23(2):174–183. <https://doi.org/10.1016/j.geotextmem.2004.09.004>
25. Zaimoglu AS, Yetimoglu T (2012) Strength behaviour of fine grained soil reinforced with randomly distributed polypropylene fibres. *Geotech Geol Eng* 30(1):197–203. <https://doi.org/10.1007/s10706-011-9462-5>

Shear Strength Characteristics of Marble Dust-Lime Stabilized Marine Clay



B. Manjula Devi and H. S. Chore

Abstract Marine clay has a low load capacity and changes volume dramatically as an effect of water content. It may need to be treated before it can be utilized for road construction. Many types of waste materials are accumulating, and environmentalists are concerned for how to safely dispose of them. India's vast industrial network generates millions of metric tons of industrial wastes each year. The marble business produces marble dust as one of its products. The study is to examine the effect of marble dust as a stabilizer. First, an optimum value of marble dust (20%) was determined on the basis of unconfined compressive strength (UCS) properties of mixtures of marble dust and soil (marine clay). Then, lime was mixed up to 10% by weight with an increment of 2% in the optimized mixture (marine clay-marble dust). To examine the properties of Marble dust-Lime Stabilized Marine clay, various experiments such as Unconfined Compressive Strength (UCS), Triaxial Tests, and X-Ray Diffraction (XRD) were performed. The results obtained from the laboratory investigation, it is observed the ideal marble dust-lime proportion for the best stabilization effect is observed to be 4–20%.

Keywords Marine clay · Marble dust · Lime · UCS · Triaxial

1 Introduction

In recent years, the disposal of waste materials produced by industry has become a serious environmental challenge. These waste materials can be utilized to construct pavements since they have a high potential for strengthening the strength of the sub-grade soil beneath the pavement, allowing for a reduction in pavement thickness.

B. M. Devi

Department of Civil Engineering, Datta Meghe College of Engineering, Sector-3, Airoli, Navi Mumbai 400708, India

H. S. Chore (✉)

Department of Civil Engineering, Dr. B. R. Ambedkar National Institute of Technology, Jalandhar 144011, India

e-mail: chorehs@nitj.ac.in

Such a structure could be cost-effective. A thick soft marine clay deposit with poor shear strength and high compressibility covers vast areas, notably around the coast. Efforts to find solutions to the challenges of marine clay have been attempted all around the world.

On the other side, as the marble products grows, the amount of waste marble material generated climbs as well [1]. In quarries, the amount of marble dust released as by-product during block manufacturing ranges from 40 to 60% of total output volume [2]. Marble dust is created when a marble stone is cut and polished. Marble slurry is produced in the amount of 5–6 million tons per year [3].

Several researchers [4–9] deduced from laboratory investigations that in soil stabilization processes, marble dust is a useful industrial by product. Because it improves compaction, subgrade properties, swelling characteristics, compressive strength characteristics, of stabilized soil. Several geotechnical laboratory tests such as UCS, triaxial and shrinkage tests were performed to compare the findings and graphs of various mixtures in order to assess the impact of materials used to improve the soil quality [10]. The influence of marble dust on clayey soil stabilization was studied using Atterber's limits, compaction tests and UCS tests (curing). An increase in soil strength with addition of marble dust was observed [11].

As seen in some of the preceding sections, the utilization of marble dust in the construction of pavement will help in the preservation of the environment and will also result in sustainable development. Aim of this research is to examine the waste material (marble dust) along with lime to stabilize marine clay. The most essential reason for mixing marble dust with subgrade soil is to decrease the construction cost and reduce waste.

2 Materials and Experimental Program

2.1 Soil

It is collected from the Jawaharlal Nehru Port Trust (JNPT), Maharashtra State, India by about 50–60 m from the banks of the Uran River at a depth of 3–3.5 m. The soil index properties are listed in Table 1.

Marble dust is produced from the marble industry during the cutting and grinding of marble. Marble dust used for this study was collected from Navi Mumbai, Maharashtra. It has specific gravity of 2.5, sand sized particles 74.716%, silt sized particles 25.28%. MDU 18.87 kN/m³ and OMC 12.48%.

Table 1 Properties of marine clay marble dust

Sr. No.	Parameters	Value
1	Specific gravity	2.5
2	Liquid limit (%)	80
3	Plastic limit (%)	35
4	Plasticity index (%)	45
5	Shrinkage limit (%)	22.35
6	Sand (%)	3.9
7	Silt + Clay (%)	96.1 (47.1 + 49)
8	Unified soil classification	CH
9	Soil specification as per AASHTO	A-7-5
10	Optimum moisture content (%)	31
11	Maximum dry unit weight (kN/m ³)	13.73
12	Unsoaked CBR (%)	4.54
13	Soaked CBR (%)	1.85
14	Free swell index (%)	150

2.2 Lime

The quick lime utilized in this investigation was readily available in the area. It consisting of 74% CaO and 7.9% Silica.

2.3 Experimental Procedure

Marble dust was varied in the increment of 5% up to 30% by dry weight of marine clay. These samples/mixes were tested to standard Proctor compaction tests, UCS tests, as per Indian Standard codes to determine the ideal percentage of stabilizer. Furthermore, lime was added in 2% increments up to 10% to analyze the effect of lime with the ideal proportion of marble dust. Undrained triaxial test was conducted to determine the shear strength parameters of the unstabilized soil, marble dust stabilized soil and marble dust-lime stabilized soil. XRD tests were performed to establish the mineralogical composition.

2.4 X-ray Diffraction (XRD)

The XRD patterns of Marine clay and Marble dust are shown in Figs. 1 and 2, respectively. The major mineral components found in the marble dust are Dolomite [CaMg(CO₃)₂], Quartz (SiO₂) and Calcite (CaCO₃). The major mineral components

Fig. 1 XRD patterns for marble dust

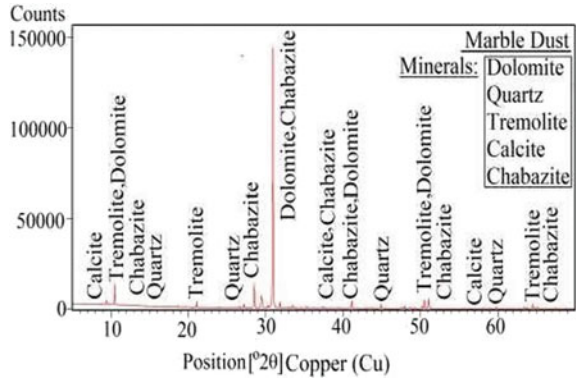
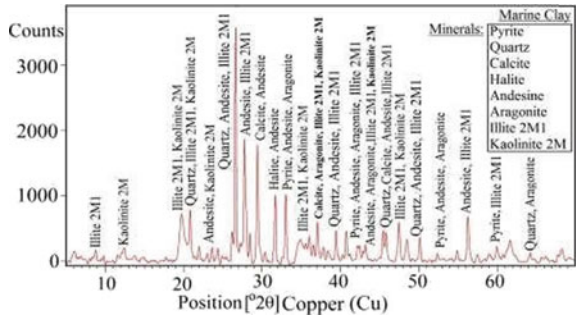


Fig. 2 XRD patterns for marine clay



found in the Marine clay are Quartz (SiO_2), Andesine ($(\text{Na}, \text{Ca})\text{Al}_{1-2}\text{Si}_{3-2}\text{O}_8$), Illite 2M1 ($\text{K}0.65\text{Al}_2.0[\text{Al}0.65\text{Si}_3.35\text{O}10](\text{OH})_2$), Kaolinite [$\text{M}(\text{Al}_2\text{Si}_2\text{O}_5(\text{OH})_4)$].

3 Analysis of Test Results

The results of the Standard Proctor Test and UCS Test values of Marine Clay-Marble Dust-Lime specimens are presented in Table 2.

Table 3 illustrates the different proportions of marble dust-lime influence the MDU and OMC of unstabilized and stabilized marine clay. MDU continues to increase despite of marble dust and lime added. The MDU of stabilized soil with 20% marble dust and 4% lime increased from 13.72 to 15.808 kN/m^3 . The fall in dry density beyond the ideal proportion could be attributed to the replacement of soil in the mixture by lime, which has a lower specific gravity than soil. The increase in MDU indicates that the qualities of stabilized soil have improved. As presented in Fig. 5, the OMC decreases despite of the proportion of Marble dust and Lime added. The OMC decreases to a value of 20.29% from 31%, when 20% marble dust and 4% lime were added to marine clay.

Table 2 Standard proctor and UCS test result

Marine clay + marble dust + lime	Optimum moisture content (%)	Maximum dry unit weight (kN/m ³)	UCS value (kN/m ²)	Percentage increase in strength (%)
(100 + 0 + 0)	31	13.729	23.045	–
(95 + 5 + 0)	30	14.249	24.644	6.936
(90 + 10 + 0)	29	14.435	40.893	77.446
(85 + 15 + 0)	27	14.611	48.140	108.89
(80 + 20 + 0)	25	14.906	53.083	130.344
(75 + 25 + 0)	24.5	15.102	46.179	100.383
(70 + 30 + 0)	24	15.396	41.776	81.276
(78 + 20 + 2)	23.6	15.317	87.279	278.723
(76 + 20 + 4)	20.3	15.808	91.591	297.446
(74 + 20 + 6)	21.2	15.435	85.317	270.212
(72 + 20 + 8)	24.5	15.004	77.472	236.170
(70 + 20 + 10)	28.2	14.101	72.569	214.893

Table 3 Modulus values for stabilized and unstabilized mixes

Particulars of the mixes	Modulus value at cell pressure (kPa)		
	50 kPa	100 kPa	150 kPa
Marine clay	1231.591	1529.585	1681.709
Marine clay + marble dust	2916.667	3026.813	3410.833
Marine clay + marble dust + lime	6792.59	6907.307	7380.33

3.1 Unconfined Compressive Strength (UCS)

The UCS for various combinations are illustrated in Fig. 3. It is seen that highest value of UCS is obtained for 20% marble dust and 4%lime contents which increases from 23.05 to 91.59 kPa. The production of cementitious compounds (calcium silicate hydrate) increase the UCS value initially further addition of stabilizers, the UCS decreases, indicating that the extra marble dust and lime do not play a substantial role in the marble dust-lime -soil reaction.

3.2 Triaxial Shear Test (U-U) Results

Triaxial shear test can be used to find out the elastic modulus of the soil. The unconsolidated undrained (U-U) triaxial tests were conducted for the 50, 100 and 150 kPa (cell pressure) on the samples of native marine clay, marble dust stabilized marine clay (80 + 20); and the marble dust-lime stabilized marine clay (76 + 20 + 4) as

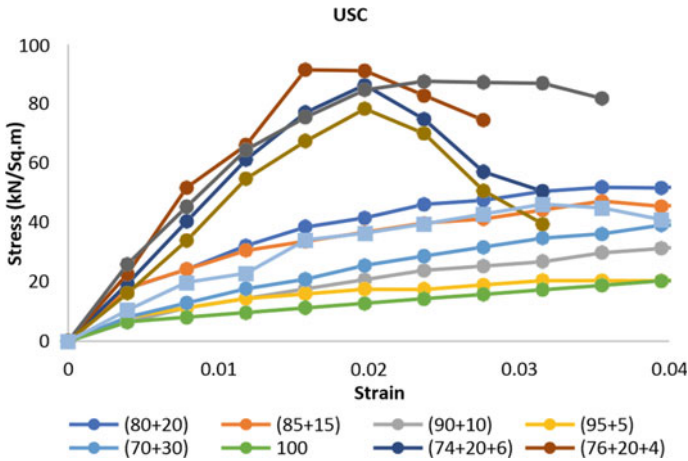


Fig. 3 Variation of UCS (marine clay-marble dust-lime)

per relevant Indian Standard specifications. Stress–strain curves are drawn from the test data, and Mohr circles are generated to determine cohesive and frictional angle, as shown graphically in Figs. 4, 5, 6, 7, 8 and 9.

The cohesion value and frictional angle of marine clay is found to increase with addition of marble dust and lime. This could be attributed to a higher percentage of fine particles in the mix, which minimizes the voids in the sample. In the entire triaxial tests, the samples were prepared corresponding to the respective OMC. It may be one of the reasons the sample attains its maximum dry unit weight and the void ratio with maximum contacts between the particles. The increase in friction angle is due to the inclusion of stiffer minerals namely, marble dust and lime. It will also decrease certain amount of clay minerals. For clay, it is cohesion while for the other mixes; it is the combination of cohesion and adhesion. The cohesion between the clay particles remains same; the adhesion may be the more for the other cases, resulting increase C and ϕ values.

Fig. 4 Stress–strain for marine clay

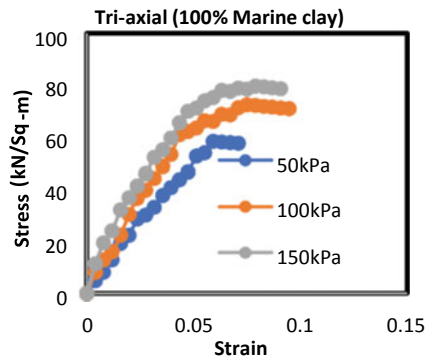


Fig. 5 Mohr's circle for marine clay

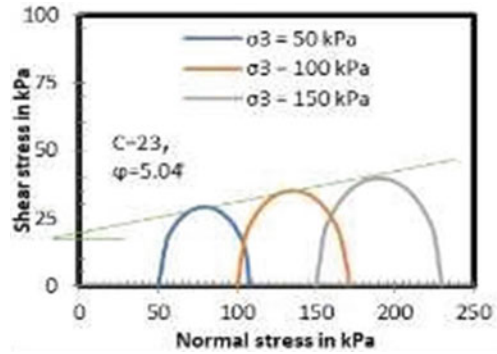


Fig. 6 Stress-strain for marble dust stabilized marine clay

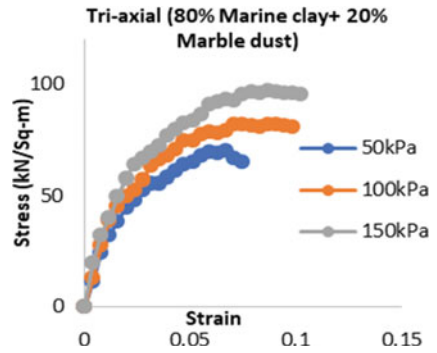


Fig. 7 Mohr's circle for marble dust stabilized marine clay

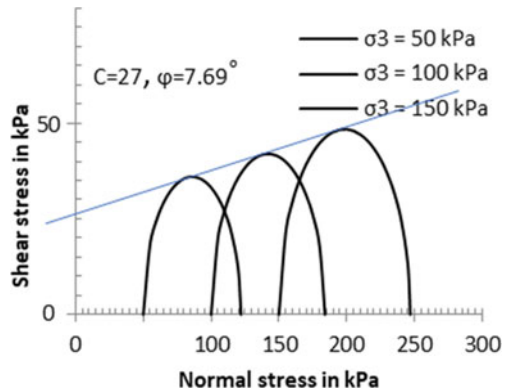


Fig. 8 Stress–strain for marble dust-lime stabilized marine clay

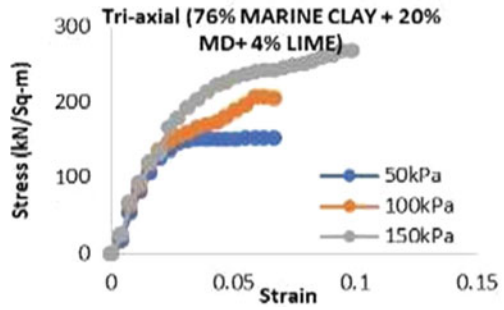
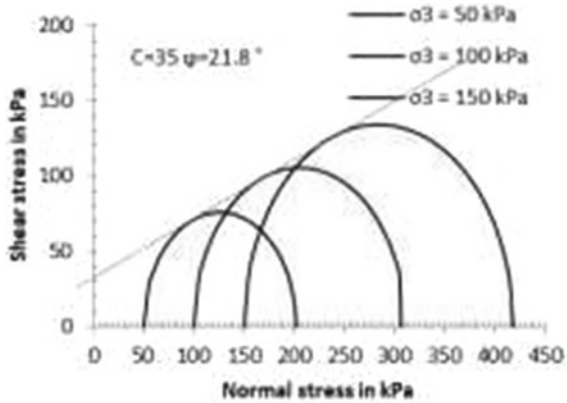


Fig. 9 Mohr's circle for marble dust-lime stabilized marine clay



3.3 Elastic Modulus

The secant modulus is defined as the ratio of the deviator stress to the corresponding axial strain at a given position on the stress–strain curve. The E_{50} secant modulus is calculated for each of the cases and presented in Table 3, and indicated in Fig. 10. The modulus is found to go on increasing with increase in cell pressure. Highest modulus is observed for stabilized soil (marble dust-lime) with 451% increase in modulus value compare to the unstabilized soil.

4 Conclusion

The following are some of the major results derived from the laboratory work on marble dust-lime stabilized marine clay.

- The O.M.C. of the marine clay was found to be reduced by 19.33% for 20% marble dust, further decreased by 34.54% on addition of 4% of lime.

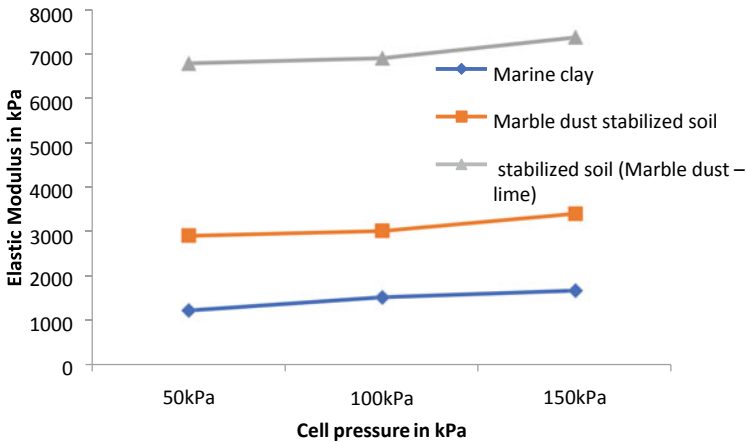


Fig. 10 Elastic modulus for marine clay, MD stabilized marine clay and MD-lime stabilized marine clay

- The M.D.D of the marine clay is improved by 8.57% for 20% marble dust, further improved 15.14% when 4% lime is added.
- The XRD patterns, the major mineral components found in the marble dust are Dolomite and Calcite. The major mineral components found in the marine clay are Quartz, Andesine, Illite and Kaolinite.
- The compressive strength (UCS) value of the marine clay is increased by 130.34% for 20% marble dust and further, improved by 297.466% when 4% lime is added.
- The cohesion value and frictional angle for the addition of marble dust and lime.
- Highest modulus is observed for the marble dust stabilized soil with 137% and 451% increase in modulus value further addition of 4% lime compare to the unstabilized soil.
- The ideal marble dust-lime proportion for the best stabilization effect is observed to be 4–20%.
- Industrial waste, such as marble dust, has the ability to change the properties of marine clay, making it ideal for a variety of geotechnical applications.

References

1. Muthu Kumar M, Tamilarasan VS (2015) Experimental study on expansive soil with marble powder. *Int J Eng Trends Technol* 22(11):504–507
2. Çelik MY (1996) M. S. Thesis, Afyon Kocatepe University. *Nat Appl Sci* 119
3. Central Pollution Control Board (2012) Guidelines for management and handling of marble slurry generated from marble processing plants in Rajasthan (Final Draft), New Delhi, India. <https://cpcb.nic.in>
4. Baser O (2009) Stabilization of expansive soils using waste marble dust. Master of science thesis, submitted to civil engineering department, middle east, technical university

5. Palaniappan KA, Stalin VK (2009) Utility effect of solid wastes in problematic soils. *Int J Eng Res Indus Appl* 2(1):313–321
6. Agrawal V, Gupta M (2011) Expansive soil stabilization using marble dust. *Int J Earth Sci Eng* 04(06):59–64, SPL. ISSN: 0974–5904
7. Sabat AK, Nanda RP (2011) Effect of marble dust on strength and durability of rice husk ash stabilised expansive soil. *Int J Civ Struct Eng* 1(4):939–948
8. Viswakarma A, Singh RR (2013) Utilization of marble slurry to enhance soil properties and protect environment. *J Environ Res Dev* 7(4A):1479–1483
9. Bansal H, Sidhu GS (2016) Influence of waste marble powder on characteristics of clayey soil. *Int J Sci Res (IJSR)* 5(8)
10. Singh K, Arora K (2017) Stabilization of black soil using lime stone, rice husk and fly ash. In: *ICRTESSM-2017*
11. Debnath A, Saha S, Chattaraj R (2021) Stabilization of clayey soil with marble dust. In: *Recent developments in sustainable infrastructure. Lecture notes in civil engineering, vol 75*. Springer, Singapore. https://doi.org/10.1007/978-981-15-4577-1_14

Evaluation of Bagasse Ash in Stabilization of Pavement Sub-Grade



Riddhi H. Jethwa, Sharmeen S. Momin, B. Manjula Devi, and H. S. Chore

Abstract India is one of the biggest countries, also called the “Indian subcontinent.” It is the second most populated country in the world. For managing such a huge population, the government provides many services, appropriate means of transportation being one of them. When a development’s sub-grade is discovered to be weak, it must be treated or stabilized to meet the project’s needs. The availability of waste materials from agriculture and industry, as well as the necessity to use this material in the field of road construction rather than typical stabilizing materials, has fueled research into sugarcane bagasse ash soil stabilization. Sugarcane bagasse ash provides a number of engineering advantages that make it an excellent stabilizer material. The goal of our project is to assess the potential benefits of bagasse ash as a sub-grade layer stabilizer material.

Keywords Bagasse ash · Black cotton soil · Soil stabilization

1 Introduction

When sub-grade at the project site is found to be weak, it has to be treated or stabilized to attain the required strength. Increasing or maintaining the strength and stability of soil is to enhance engineering properties of sub-grade materials from expansive clay (such as BLACK COTTON SOIL) to granular materials required various ground

R. H. Jethwa

Department of Civil Engineering, Datta Meghe College of Engineering, Navi Mumbai, India

S. S. Momin

Department of Civil Engineering, Anjuman-I-Islam’s Kalsekar Technical Campus, Panvel, India

B. M. Devi

Datta Meghe College of Engineering, Navi Mumbai, India

H. S. Chore (✉)

Department of Civil Engineering, Dr. B. R. Ambedkar National Institute of Technology,
Jalandhar 144011, India

e-mail: chorehs@nitj.ac.in

improvement methods. Advantages of the stabilization process include a decrease in permeability, increase in resistance value, lower plasticity, reduction of pavement thickness, elimination of handling and hauling of excavation material, etc. To improve the different features of soil, bagasse ash is used in this project.

A brief summary of the experiments and analysis of black cotton soil stabilized with bagasse ash by researchers are described below.

The effects of bagasse ash and cement on black cotton soil stabilization were investigated. Cement and bagasse ash was mixed in varied proportions with black cotton soil (i.e., 4, 8, and 12%). UCS and CBR were two of the strength parameters that were carried out. When a mixture of bagasse ash and varying percentages of cement was employed to stabilize black cotton soil, substantial changes in UCS, MDD, and CBR were observed. MDD value increases from 1.516 to 1.65 g/cc for 8% cement with 8% bagasse ash, while UCS value increases from 84.92 to 174.91 kN/m² for the same blend. CBR increased from 2.12 to 5.43 after using 8% cement and 4% bagasse [1].

Experimental analysis was carried out to investigate the impacts (physical characteristics) of bagasse ash on the (black cotton soil) Iraq, Duhook sub-grade layers. Atterberg's limit and compaction were among the tests carried out. The addition of bagasse ash to soil the MDD value falls 30% (1.59–1.1 g/cm³) in 30% bagasse ash stabilized soil. The OMC increased by 55.6%, going from 21.9 to 55.6% [2]. In order to identify the better admixture (fly ash, bagasse ash) conducted different laboratory experiments on the expansive soil. It was reported that for 10% fly ash and bagasse ash added with soil, the CBR values increased to 13.87% and 15.11%, respectively. They concluded that fly ash is a better stabilizer than bagasse ash as it consists of more pozzolanic substances [3]. Bagasse ash (BA) along with granulated blast furnace slag (GBFS) explored for the sub-base layer in flexible pavement construction. From the UCS and CBR results, it was reported that 60%BA and 40% GBFS satisfied the required strength properties [4]. The aim of this particular study is to stabilize the black cotton soil with bagasse ash. Standard proctor and CBR tests were conducted on various mixes and the test results were analyzed.

2 Materials and Methodology

2.1 Soil

Black cotton soils are expansive clays with a high degree of shrinkage and swelling due to changing moisture content. The main causes of swelling and shrinking in black cotton soil are mineralogical features. The mineral montmorillonite is responsible for the soil's instable nature. Black cotton soils have low strength and are prone to large volume variations, making them challenging to work with in infrastructure projects. Unpredictability and instability of soils tend to cause more damage and destruction to structures than any other natural hazard, such as floods and earthquakes. Due to

the extreme nature of this soil, the bearing capacity is negatively affected. When dry, black cotton soil is extremely hard which makes it difficult to pulverize the dried clods for treatment for using it in the construction of roads. This results in severe problems which affect the performance of the road.

The soil used in this project was procured from Susgaon, Pune. The soil properties are shown in Table 1.

Table 1 Properties of virgin soil

Sr. No.	Soil	Value
1.	Soil classification (as per AASHTO)	CH
2.	Plastic limit	34.2%
3.	Liquid limit	80.4%
4.	Plasticity index	46.2%
5.	Specific gravity	2.435%
6.	Optimum moisture content (OMC)	19.5%
7.	MDD	1.5 g/cc
8.	Free swell index	50%
9.	CBR	1.40%

2.2 Bagasse Ash

The fibrous ash collected after the burning of bagasse in the boiler during the cogeneration process is known as sugarcane bagasse ash. This fibrous waste material is found to have characteristics of a supplementary cementation material because it is rich in amorphous SiO_2 .

Bagasse ash was collected from Sakhar Karkhana Ltd., located at Kasarsai Darumbre Somatane Phata, Pune. The basic properties ash was shown in Table 2.

Table 2 Properties of bagasse ash

Sr. No.	Bagasse ash	Value
1.	Specific gravity	1.21
2.	Density	0.44 g/cc

2.3 Methodology

To disintegrate the lump, the soil was crushed with a wooden hammer and then sun-dried. The soil was then dried in the oven for 24 hr at 105–110 °C. Before being used, the bagasse ash was sieved at 600 μm . The performance of bagasse ash stabilized with soil was assessed using the California bearing ratio, a physical

strength performance test (soaked CBR). The test was carried out to see if the sub-grade soil’s strength qualities had improved. As a result, using such modern materials in road construction can be effective in enhancing soil strength while also lowering project costs. The samples were prepared for all the tests as per the parameters, and the results were recorded accordingly. The discussion was held, and the conclusions were prepared. 8% was obtained as the optimum percentage, and pavement was designed using the CBR value obtained for it.

3 Result and Discussion

The test results are plotted in the form of graphs to analyze and found out the optimum proportions. The results of the standard proctor and CBR with different mix proportions are as follows: Tables 3 and 4

The test result for the standard proctor test demonstrates that as the percentage of bagasse ash is raised, the OMC value increases and the MDD value decreases. The general decrease in MDD may be due to tiny particles of bagasse ash, flocculating and agglomerating and subsequently filling larger spaces, resulting in a fall in dry density [5, 6]. The MDD decrease for higher bagasse content indicates that more voids present in the mix. Eventually, it will observe the more water may be the reason for the increase in OMC (Fig. 1).

The CBR test findings reveal that there is a rise in CBR up to the addition of 8% bagasse ash, and then it declines after that until it reaches 16% bagasse ash. Bagasse ash’s pozzolanic action is responsible for the increase in strength since it contains a significant amount of silica and other essential oxides, which promotes good pozzolanic activity.

Table 3 Result of standard proctor

Mix proportions	OMC (%)	MDD (g/cc)
Virgin soil	19.50	1.500
Soil with 4% of BA	23.71	1.443
Soil with 8% of BA	23.60	1.400
Soil with 12% of BA	26.75	1.361
Soil with 16% of BA	28.11	1.313

Table 4 CBR test results

Mix proportions	CBR (%) soaking
Virgin soil	1.4
Soil with 4% of BA	10
Soil with 8% of BA	11.2
Soil with 12% of BA	9.1
Soil with 16% of BA	9.4

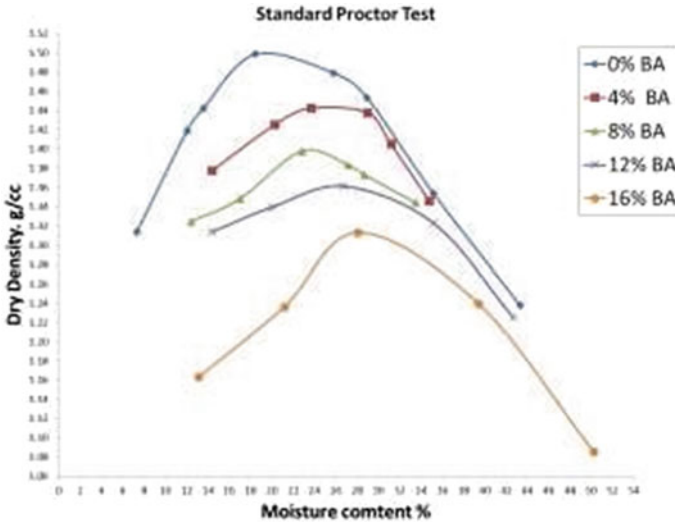


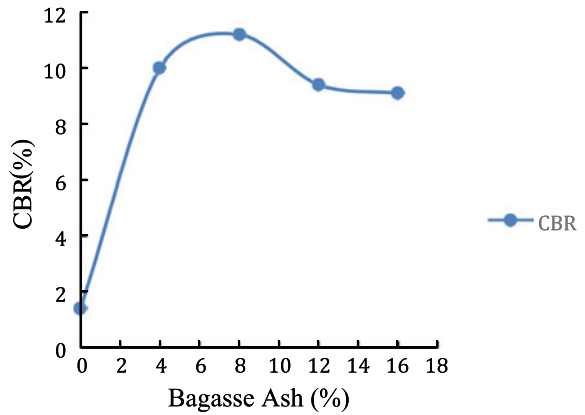
Fig. 1 Standard proctor test results

4 Conclusion

Some of the predominant conclusions are

- With higher bagasse ash concentration, the MDD and OMC of the treated sample generally decreased and increased, respectively. The addition of bagasse ash to soil lowers the MDD from (1.5 g/cc) for natural soil to (1.4 g/cc) for 8% bagasse ash stabilized soil, a drop of roughly 6.67%, and raises the OMC from (19.5%) to (23.6%), a 17.37% increase.
- California bearing ratio value got increased from 1.4 to 11.2% for the addition of 8% bagasse ash which shows an increase of 87.5%; further, addition of bagasse ash decreases the CBR value. An increase in CBR indicates a reduction in the settlement (Fig. 2).
- Hence, from the results above it can be concluded that an amount of 8% of bagasse ash, when added to black cotton soil, gives us an optimum result and can be used in stabilization of expansive soil or weak sub-grade. The interaction behavior of bagasse ash with soil can lead to viable solutions for its large-scale utilization and disposal.
- Bagasse ash can be utilized as a soil stabilizer in high-water-content soils, particularly in sugar-producing countries where it is abundant.

Fig. 2 Variation of CBR with different percentages of bagasse ash



References

1. Kiran RG, Kiran L (2013) Analysis of strength characteristics of black cotton soil using bagasse ash and additives as stabilizer. *Int J Eng Res Technol* 7
2. Masued GG (2017) Effect of sugarcane bagasse ash on the physical properties of sub-grade layer. *J Eng Sustain Dev* 21(5). ISSN: 2520-0917
3. Harun-Or-Rashid GM, Rahman MF, Siddique AB (2019) A comparative study on fly ash and bagasse ash using as a sub-grade material. *Am J Civ Eng* 7(4)
4. Manjuladevi B, Chore HS (2020) Feasibility study on bagasse ash as light weight material for road construction. In: International conference on advance light-weight materials and structures (ICALMS-2020)
5. Ola SA (1983) Geotechnical properties and behaviour of some Nigerian lateritic soils. In: Ola SA, Balkema AA (eds) *Tropical soils of Nigeria in engineering practice*. Balkema, Rotterdam
6. Osinubi KJ (1986) Permeability of lime-treated lateritic soil. *J Transp Eng* 124(5):465–469

An Experimental Study on the Strength Behaviour of Black Cotton Soil Stabilized with Industrial Waste Material (Zinc Slag) for Pavement Construction



Mohini Patel , P. S. Prasad , Pranav R. T. Peddinti ,
and Vijai Kumar Kanaujia 

Abstract Depletion of natural resources for construction material, abundant generation of industrial wastes, disposal problems and their environmental impact have resulted in a continuous research scope for reuse of industrial wastes for sustainable engineering practice. Among these practices, the utilization of industrial wastes from metal processing industry for pavement subgrade stabilization has gained significant global importance. Present research aims at investigating the potential of one such material zinc slag (ZS) in altering and enhancing the strength properties of black cotton soils (BCS) for possible pavement applications. Different dosages of ZS (25, 50 and 75%) and cement (3, 6 and 9%) are administered to the black cotton soil. The mechanistic performance of these stabilized soil–slag mixtures in the form of CBR and unconfined compressive strength (UCS) values has been observed and used as an indicator to investigate the suitability of these mixes as pavement subgrade and subbase roads having traffic intensity up to 5 msa. The proposed layer thicknesses due to the increased CBR/UCS values is calculated to meet the IRC: 372018 guidelines. The IITPAVE analysis is used to quantify the fatigue and rutting strains at perilous locations in the pavement during the desired service life.

Keywords Black cotton soil · Zinc slag · Cement · CBR · UCS · Utilization · Industrial waste · Pavement subgrade · Strain analysis · Low volume rural roads

M. Patel (✉) · P. R. T. Peddinti
Department of Civil Engineering, Pandit Deendayal Energy University, Gujarat, India
e-mail: mohinipatel16198@gmail.com

P. S. Prasad · V. K. Kanaujia
Geotechnical Engineering Division, CSIR-Central Road Research Institute, New Delhi, India

P. R. T. Peddinti
Department of Urban and Environmental Engineering, Ulsan National Institute of Science and Technology, Ulsan, South Korea

1 Introduction

In recent years, the problem of containing and disposing wastes is growing globally. Environmental conservation also seems to be becoming a prime concern because of the increase in waste materials such as by-products from the metal industries. Reutilization of these waste materials in a more economical and sustainable way is essential to avert these materials from damaging the nature [1]. Recycling of these industrial waste materials and by-products for sustainable engineering construction will decrease the need of generating new raw materials as well as the depletion of conventional materials. The effective consumption of these waste materials in road construction is recommended to find an alternate source of material supply to counterbalance the rising cost of typical natural aggregates and waste disposal [2]. India, being the second largest pavement network in the world, requires improved subgrade performance to cater the needs of ever-increasing traffic and axle loads. However, due to drastic urbanization and infrastructural demand, pavement engineers are forced to take up road construction even in the areas having problematic soils. On the other hand, India reportedly has a considerable stretch of black cotton soils which pose multifaceted problems because of their swell-shrink behaviour. Unforeseen construction of pavements on such subgrades results in severe pavement structural damages, rider inconvenience, financial loss and additional investments on maintenance.

BCS is a clay-rich soil that comprises calcium, potash and carbonate, and it holds moisture. Black colour of these soils is formed due to the existence of titaniferous magnetite. It is also rich in iron, lime and magnesium and has low amount of phosphorous and nitrogen including organic matter. These soils are extremely compressible under loading and expansive during saturation and have very low bearing capacity. Black cotton soils are susceptible to evident volume changes with varying water content and have great shrinkage and swelling characteristics. BCS is also having very low shear strength. These types of soils swell during the rainy season and form cracks in dry season due to shrinkage. Design and construction of road pavements on such soils have always been a thought-provoking assignment [3]. Approximately 20% of the total land area is covered with BC soil in India and encountered in Southern, Western and Central states of India including Madhya Pradesh, Maharashtra, Telangana, Andhra Pradesh, Karnataka and Gujarat [4]. Zinc slag (ZS) is a waste engendered during extraction of zinc from its pyro-metallurgical process. Chemical compositions of ZS mainly comprise Fe_2O_3 , CaO , ZnO , SiO_2 , Al_2O_3 and other elements. It is referred to as ISFS (Imperial Smelting Furnace Slag), which is a granulated, glassy material and dark in colour. ZS generated all over the world is mostly dumped in allocated dumping yards, as it does not have any major application [5]. Few literatures suggested that ZS can be used in place of conventional materials in transportation geotechnics' applications such as road construction [6]. Around one million tonnes of ZS is produced per annum worldwide, and in India, the annual production of ZS is about 720,000 tonnes [7]. Cement has the property to bind different materials together [8]. Ordinary Portland Cement (OPC) type of

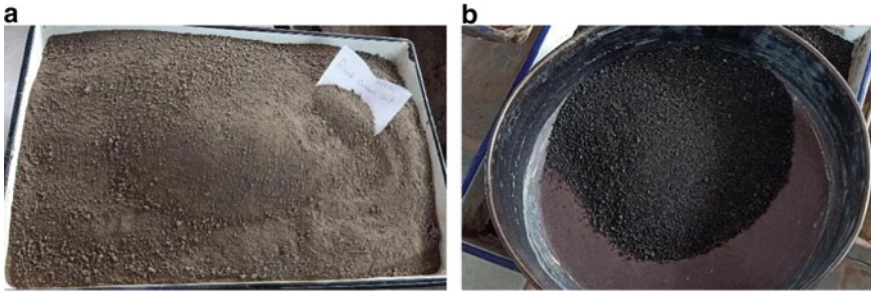


Fig. 1 a Black cotton soil. b Zinc slag

cement is the most commonly produced and used worldwide. Chemical composition of OPC consists of CaO , SiO_2 , Al_2O_3 , Fe_2O_3 , MgO , SO_3 , Na_2O and K_2O .

Copper slag, steel slag, jarofix and zinc slag/tailings are some of the waste materials from metal industries which can be efficiently used for subgrade and subbase applications in road construction particularly for the problematic soils. Though zinc slag has not been widely used for stabilizing the subgrade BC soil, the current study aims to analyse the behaviour of black cotton soil while adding zinc slag and cement. From the laboratory study on soil–slag mixtures with cement as a stabilizer, it was perceived that the CBR and UCS considerably improved up to the desired values to design a road pavement having traffic intensity up to 5 msa. Road pavements for the design traffic of 5 msa or less were designed accordingly.

2 Materials Used for the Current Study

Black cotton soil (Fig. 1a) was collected from Bhopal, Madhya Pradesh state, India. Coarse-grained zinc slag (industrial waste) was collected from Hindustan Zinc Limited, Chittorgarh, Rajasthan state, India, as shown in Fig. 1b. Ordinary Portland Cement of 43-Grade was used for stabilization purpose, and it has a compressive strength of 43 MPa.

3 Geotechnical Characterization

Geotechnical characteristics of BC soil, ZS and BC soil–ZS mixtures have been studied by conducting different laboratory experiments including grain size analysis, Atterberg limits, index properties, specific gravity, modified Proctor compaction test, California bearing ratio (CBR) test and unconfined compressive strength (UCS) test.

3.1 Physical Properties

Grain Size Distribution: Grain size analysis was done on BC soil and ZS by sieve analysis and hydrometer method according to the procedure provided in IS: 2720 (Part 4)—1985 [9]. The grain size analysis results are presented in Table 1 and shown graphically in Fig. 2.

Atterberg Limits, Index Properties and Specific Gravity: Liquid limit (W_L) and plastic limit (W_P) tests were performed on BCS as per IS: 2720 (Part 5)—1985 [10]. The results showed that the soil is plastic in nature and as per IS: 1498—1970 [11]. BC soil is classified as CH (clay with high plasticity), whereas zinc slag is classified as SP. Plasticity index of the BCS was determined to be 35.32%. Specific gravity of BCS and ZS was carried out as per IS: 2720 (Part 3/Section 1)—1980 [12]. The

Table 1 Results of grain size analysis for BC soil and zinc slag

Particle size (mm)	BCS	ZS
Gravel (>4.75)	–	1.09%
Sand (0.075–4.75)	4.33%	96.16%
Silt (0.002–0.075)	48.26%	2.75%
Clay (<0.002)	47.41%	–
Cu	–	
Cc	–	

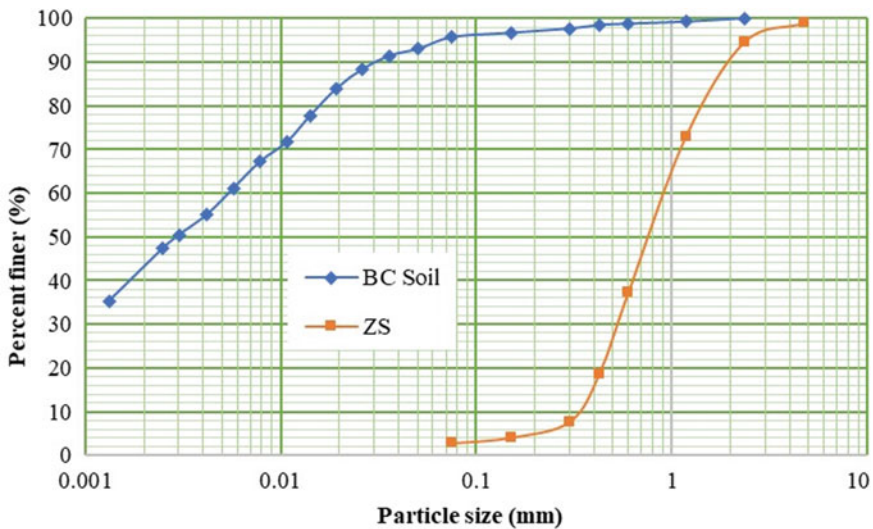


Fig. 2 Grain size distribution curves of BC soil and ZS

Table 2 Atterberg limits, index properties and specific gravity of soil and slag

Property	BCS	ZS
W_L	60.32%	Not possible
W_P	25%	Not possible
I_P	35.32%	Non-plastic
Shrinkage limit	12.2%	–
Free swell index	75%	–
Specific gravity	2.7	3.6
Activity	0.74	–
Soil classification	CH (clay with high plasticity)	SP (poorly graded sand)

results of Atterberg limits, index properties and specific gravity values of BCS and ZS are presented in Table 2.

Shrink and Swell Characteristics: The BCS was tested to observe its shrinking and swelling behaviour. Shrinkage limit test was done as per procedure of IS: 2720 (Part 6)—1972 [13]. Free swell index of the soil was observed to be 75% as per the method provided in IS: 2720 (Part 40)—1977 [14] which indicates that the BC soil is a medium swelling soil. The results of shrinkage and free swell index of BC soil are presented in Table 2.

3.2 Compaction Characteristics

Modified Proctor compaction tests were performed for BCS, zinc slag and BCS-ZS mixtures as per IS: 2720 (Part 8)—1983 [15]. Moisture-density relationship was derived as represented in Fig. 3. MDD and OMC values for the samples (BCS, ZS and BCS-ZS mixtures) are tabulated (Table 3). Test results specified that maximum dry density (MDD) increases and optimum water content (OMC) decreases with increase in percentage of ZS administered to the BC soil.

3.3 California Bearing Ratio

The CBR tests were conducted for the samples prepared at 97% MDD and OMC of BC soil, ZS and BC soil–ZS mixtures as per procedure of IS: 2720 (Part 16)—1987 [16]. The soaked CBR value of the BC soil was 3.35% which varied from 3.35 to 8.10% with the increase in percentage of zinc slag (25, 50, 75%) administered to the soil. Soaked CBR of zinc slag was found to be extremely high as 62.35. Figure 4 represents the CBR trend detected in the present study.

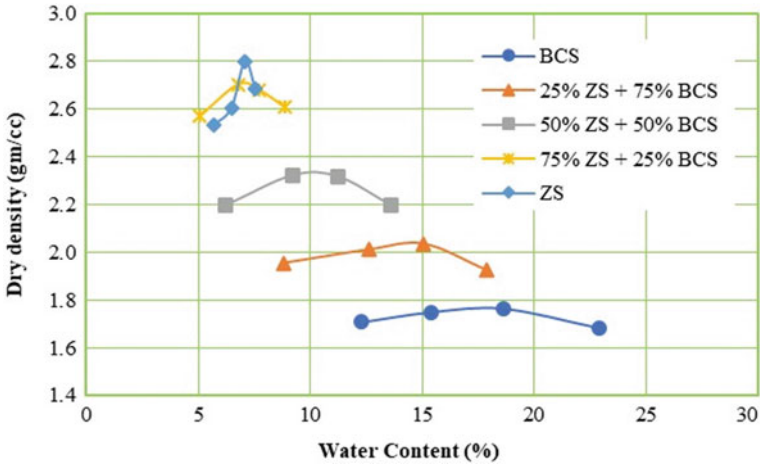


Fig. 3 Compaction curves for BCS, ZS and soil-slag mixtures

Table 3 Compaction characteristics of BC soil and BC soil-ZS mixtures

Material	MDD (gm/cc)	OMC (%)
BC soil	1.77	17.80
25% ZS + 75% BCS	2.04	14.55
50% ZS + 50% BCS	2.34	10.20
75% ZS + 25% BCS	2.71	7.10
ZS	2.80	7.09

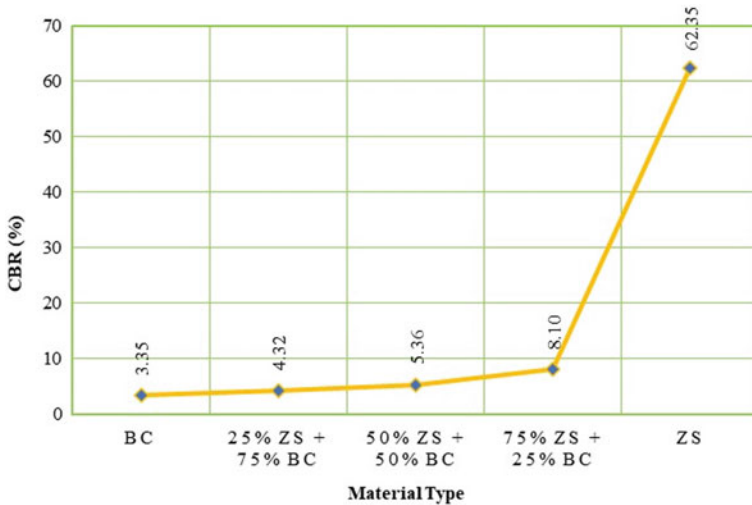


Fig. 4 CBR trend observed in the present study

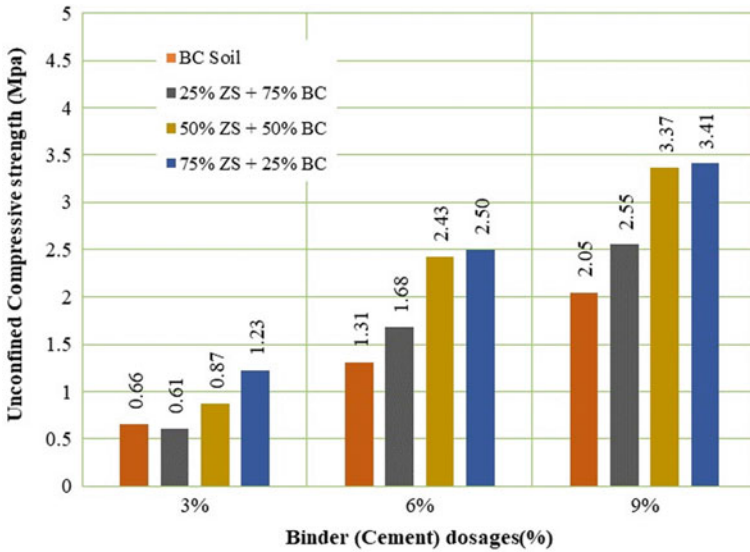


Fig. 5 Unconfined compressive test results with cement and slag

3.4 Unconfined Compressive Strength (UCS)

The UCS tests were performed at 97% MDD and OMC on BCS and BCS-ZS mixture blended with cement as per IS: 2720 (Part 10)—1991 [17]. Cylindrical specimens with a dia. of 5 cm and length of 10 cm were prepared and preserved in a closed desiccator for 7 days of curing before testing. The result of 7-day UCS was 0.33 MPa for the soil. It varied from 0.66 to 3.41 MPa when dosages of cement (3, 6, 9%) and zinc slag (25, 50, 75%) were administered to the BC soil. Figure 5 typically represents the results of UCS tests performed for the present study.

4 Design of Rural Road Pavement

Two different flexible pavement compositions were proposed considering traffic volume up to 5 million standard axles (msa) and design life of 15 years using guidelines provided in IRC: 37—2018 [18]. The existing subsoil is BC soil (CBR = 3.35%), and the effective CBR values for the improved subgrades used for the design, i.e. for 75% ZS + 25% BCS and 100% ZS, were determined to be 6.31% and 23.45%, respectively.

The combination of 50% ZS, 50% BCS and 3% cement having a UCS value of 0.87 MPa (as stated above) was used as a cement-treated subbase (CTSB) layer. Higher UCS values are attained in this study for higher dosages of cement; however,

Table 4 Layer thicknesses for pavement compositions proposed in the present study

Layer thickness (mm)		
	Pavement composition	Layer material
	1	2
Surface course (BC) (VG30)	40	40
Base course (WMM)	150	150
CTSB (cement-treated subbase)	200	200
Subgrade (75% ZS + 25% BCS)	500	–
Subgrade (zinc slag)	–	500

Table 5 Actual strain values obtained by IITPAVE analysis

	Pavement composition 1	Pavement composition 2	Allowable strains
ϵ_t ($\mu\epsilon$)	206.9	223.2	409.04
ϵ_v ($\mu\epsilon$)	671.2	502.7	784.38

it is not encouraged for design purposes because of the increase in cost of road construction.

Wet Mix Macadam as a base layer and VG30 Bituminous Concrete as a surface course were provided. Table 4 represents thicknesses of each layer provided for pavement compositions proposed in the present study.

These pavement compositions were analysed for the fatigue and rutting strains at critical locations using IITPAVE software and IRC: 37—2018 guidelines [18]. Allowable rutting strain (ϵ_v) and fatigue strain (ϵ_t) were determined to be 784.38 and 409.04 $\mu\epsilon$ (micro-strain), respectively, using equations provided in IRC guidelines [18]. Actual values of these strains for two different pavement compositions were derived from the analysis by IITPAVE software, and the results are presented in Table 5. The results show that the strains are within the calculated permissible limits in both the cases. Design of these compositions is shown in Fig. 6.

5 Conclusion

Utilization of zinc slag for stabilizing black cotton soils for road construction leads to eliminating the problem of dumping of industrial waste materials and minimizing the depletion of conventional materials and the cost of construction as well. Cement stabilized soil–slag mixture gives desired strength; therefore, the difficulty of constructing roads over problematic soils can be resolved. From the results of IITPAVE analysis, it can be concluded that the strains are within the permissible limits while using soil–slag mixtures (stabilized with cement) as a subbase material and ZS or BC soil mixed with ZS (75%) in subgrade applications for the design of roads having a traffic

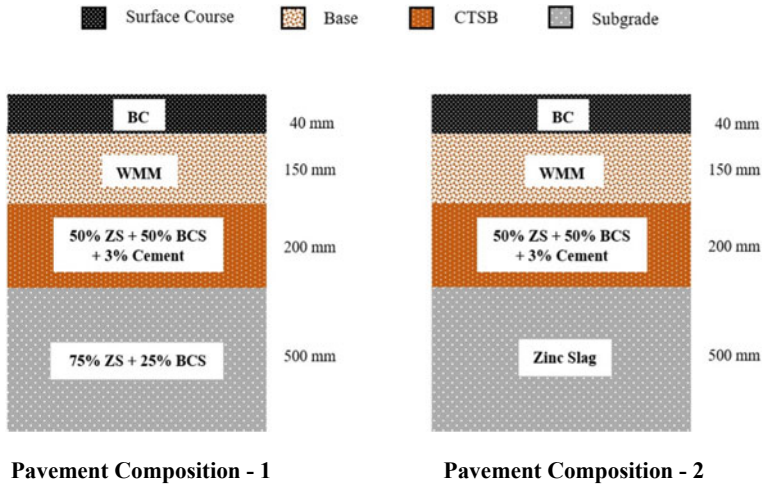


Fig. 6 Pavement compositions proposed in the present study

intensity up to 5 msa or less. Owing to high CBR and shear strength values, zinc slag is demonstrated to be effectively helpful for economical and sustainable road pavement constructions. Zinc slag is used for subgrade and subbase applications in the present study; however, further research can be carried out to check possibilities of using it for base course as well.

References

1. Aktas B, Aslan S (2016) Laboratory evaluation on waste slag produced zinc industry as mineral filler in stone mastic Asphalt. In: 6th Eurasphalt & Eurobitume Congress, E&E Congress, Prague
2. Ahmed I (1991) Use of waste materials in highway construction. Final report, FHWA/IN/JHRP-91/3, Indiana Department of Transportation and U. S Department of Transportation—Federal Highway Administration, West Lafayette, Indiana
3. Narendra Goud G, Hyma A, Shiva Chandra V, Sandhya Rani R (2018) Expansive soil stabilization with coir waste and lime for flexible pavement subgrade. In: ICRAMMCE 2017, IOP conference series: materials science and engineering, vol 330, Hyderabad, India, p 012130
4. Kumrawat N, Ahirwar SK (2014) Performance analysis of black cotton soil treated with calcium carbide residue and stone dust. *Int J Eng Res Sci Technol* 3(4). ISSN: 2319-5991
5. Yadav S, Veer J, Gupta R, Yadav P (2018) Review on utilisation on flyash, copper slag and zinc slag in road construction and embankment. *Int J Adv Res Sci Eng* 7(10). ISSN: 2319-8354
6. The World Bank Transport & ICT (T&I) (2016) Global practice of the world bank group: promoting the use of green construction materials in low volume roads in India. The International Bank for reconstruction and development/The World Bank, Washington DC, USA
7. Sharma PK, Tripathi B (2021) Properties of concrete containing industrial waste as a fine aggregate: a review. *Community based research and innovations in civil engineering, IOP conference series: earth and environmental science*, vol 796, Jaipur, Rajasthan, India, p 012040

8. Sutar SN, Patil PV, Chavan RV, Maske MM (2021) Study and review of ordinary Portland cement. *ASEAN J Sci Eng* 1(2):153–160
9. IS 2720-Part 4 (1985) Methods of test for soils—grain size analysis, Bureau of Indian Standards, New Delhi, India
10. IS 2720-Part 5 (1985) Methods of test for soils—determination of liquid and plastic limit, Indian Standards Institution, New Delhi, India
11. IS 1498 (1970) Classification and identification of soils for general engineering purposes, Bureau of Indian Standards, New Delhi, India
12. IS 2720-Part 3/Section 1 (1980) Methods of test for soils—determination of specific gravity (Fine Grained Soils), Bureau of Indian Standards, New Delhi, India
13. IS 2720-Part 6 (1972) Methods of test for soils—determination of shrinkage factors, Bureau of Indian Standards, New Delhi, India
14. IS 2720-Part 40 (1977) Methods of test for soils—determination of free swell index of soils, Bureau of Indian Standards, New Delhi, India
15. IS 2720-Part 8 (1983) Methods of test for soils—determination of water content-dry density relation using heavy compaction, Bureau of Indian Standards, New Delhi, India
16. IS 2720-Part 16 (1987) Methods of test for soils—laboratory determination of CBR, Bureau of Indian Standards, New Delhi, India
17. IS 2720-Part 10 (1991) Methods of test for soils—determination of unconfined compressive strength, Bureau of Indian Standards, New Delhi, India
18. IRC: 37 (2018) Guidelines for the design of flexible pavements, Indian Roads Congress, New Delhi, India

Effect of Resilient Modulus on Inverted Base Pavements—A Theoretical Study



Swagata Mishra, Pratik Jaiswal, and D. Sitarami Reddy

Abstract Inverted base pavement is a new type of pavement structure in which a good quality unbound granular aggregate base (GAB) layer is placed between a stiff cement treated base (CTB) layer and bituminous concrete (BC) layer. Inverted base pavements are being used in many countries due to its various advantages. The major advantage of inverted base pavements over conventional pavements includes thinner BC layer as compared to conventional pavements. Therefore in this paper, an attempt has been made to model an inverted base pavement section using finite element software and predicting its response by varying the resilient modulus of different layers. Though the response of pavement depends on both layer thickness and resilient modulus, this study is limited to study only the effect of resilient modulus on pavement performance. The approach of the study is to develop finite element model using ABAQUS software followed by validation of results of base model in IIT_PAVE software and then to study the response of a typical inverted base pavement using ABAQUS. By varying the resilient modulus of layers, total of 13 cases were considered in this study. The results indicated that BC modulus significantly affects strain values at the bottom of BC layer, GAB modulus affects the BC layer on its surface as well as at the bottom of BC layer and also the subgrade, whereas CTB modulus significantly affects the vertical strain in the subgrade and hence can be used to prevent excessive deformation problems in inverted base pavements.

Keywords Inverted base pavement · Finite element model · Resilient modulus

1 Introduction

Inverted base pavement is a new type of pavement structure in which a good quality unbound granular aggregate base (GAB) layer is placed between a stiff cement treated base (CTB) layer and bituminous concrete (BC) layer [1]. Nowadays, many countries like South Africa, U.S.A and Australia are adopting inverted base pavements

S. Mishra · P. Jaiswal (✉) · D. Sitarami Reddy
Visvesvaraya National Institute of Technology, Nagpur 440010, India
e-mail: pratikjaiswal25031996@gmail.com

© The Author(s), under exclusive license to Springer Nature Singapore Pte Ltd. 2023
A. K. Agnihotri et al. (eds.), *Proceedings of Indian Geotechnical and Geoenvironmental Engineering Conference (IGGEC) 2021, Vol. 1*, Lecture Notes in Civil Engineering 280,
https://doi.org/10.1007/978-981-19-4739-1_46

493

over conventional flexible pavements as it proves to be an economical option [2, 3]. The main difference between a conventional flexible pavement and an inverted base pavement lies in the sequence of different pavement layers. In conventional flexible pavements, the stiffer layers are typically placed at the top and the layer stiffness decreases with depth. But in case of inverted base pavement, a layer of compacted aggregate base is 'sandwiched' between two stiffer layers, i.e. BC layer at the top and CTB layer at the bottom. Inverted base pavements rely on the well-compact granular aggregate base to act as the primary load-bearing layer [3, 4]. Major advantages of inverted base pavements over conventional pavements include thinner BC layer as compared to conventional pavements; possibility of usage of inferior aggregates in CTB layer due to presence of binding cementitious material; provision of uniform surface of CTB layer for compaction of GAB layer; low maintenance and repair cost, etc. Therefore due to various advantages of inverted base pavement over conventional flexible pavement, this study has been done to predict the response of inverted base pavements under varying resilient modulus of different layers of inverted base pavements.

2 Literature Review

Finite Element (FE) method is one of the tools for mechanistic design and can be used in pavement design to model the viscoelasticity and anisotropy nature of materials [5]. Two kinds of model can be used to study the linear and non-linear behaviour of the material. In linear modelling, it is assumed that all the material will behave linearly, whereas in non-linear modelling, stress-dependent non-linear characteristics of material can be modelled. In non-linear models pavement analyses can be carried out at particle level hence gives much more realistic or accurate results. Accuracy of the result also depends upon the mesh size adopted in the model. Finer the mesh size more will be the accuracy in the analysis but computation time will also increase. Tyre contact pressure in finite element model (FEM) can be modelled as a uniformly distributed load considering contact shape either circular or rectangular [5]. Analyzing fatigue cracking behaviour of thin flexible pavement by replacing a set of dual wheels as an equivalent single tyre is unsafe because it underpredicts the horizontal tensile strain values at the bottom of thin bituminous layer [6]. Gupta and Kumar [7] studied the behaviour of a typical flexible pavement using FEM package, ANSYS and compared its results with KENPAVE. The study concluded that subgrade modulus controls vertical surface deflection in flexible pavement, but base course modulus and surface layer modulus does not have much effect on vertical surface deflection in flexible pavement. Sahoo and Reddy [8] analyzed the effect of nonlinearity in granular layer on critical pavement response of low volume roads by considering two non-linear models, i.e. Drucker-Prager model and k-theta model. Results from the study indicated that k-theta model gives much more realistic results as compared to drucker-prager model. Papadopoulos and Santamarina [1] concluded that in inverted base pavements, BC and CTB layers being stiffer deform as beams

and develop extensive tension, whereas the GAB layer which is under compression everywhere acts as a cushioning layer to support the BC layer and releases tension from the CTB layer, whereas the subgrade barely participates in the load distribution. In another study, the same author [2] concluded that the CTB limits the deformation of the GAB layer which allows it to develop increased stiffness under high loads, whereas well-compacted GAB layer reduces reflective crack propagation on BC layer. Cortes et al. [4] showed that granular layer is stress-dependent layer and due to repeated traffic loads, it experiences cyclic stresses which increases its stiffness. Good compaction of the granular layer above a stiff cemented base layer also increases the stiffness of this layer. It was also concluded from the study that, in case of inverted base pavements, the tensile stresses in the BC layer, CTB layer, as well as the compressive stress on the subgrade decrease as the stiffness of the GAB layer increases. Tutumluer and Barksdale [9] evaluated the field performance of inverted flexible pavement and did non-linear modelling in GT-PAVE software. Results indicated that inverted flexible pavement has outperformed the conventional flexible pavement. From the above literatures, it can be concluded that inverted base pavements has various advantages over conventional flexible pavements. Hence this study has been done to predict the response of inverted base pavements under varying resilient modulus of different layers of inverted base pavements.

3 Methodology

In this study, an attempt has been made to develop 3D FEM of inverted base pavement in ABAQUS software. Validation of base model is also done with IIT_PAVE software to check its accuracy. This study is based on the assumption that all layers are linearly elastic and isotropic in nature. An inverted base pavement section of length 2.4 m and width of 1.6 m as shown in Fig. 1 was taken for study. These dimensions of model were selected to avoid the effect of boundaries on the response of the pavements. Dual tyres loading assembly was selected to simulate wheel loading in the model. The dual tyres used in the study was approximated by two rectangular plates with each of dimension 240×160 mm and with centre to centre spacing as 320 mm. The contact pressure of tyre was taken as 0.56 MPa [10]. Materials in each layer are characterized by resilient modulus (E), Poisson's ratio (ν) and density. Table 1 shows the layer properties considered in the analysis for base model [1]. The elements used for modelling is taken as solid element-C3D8R. It is an 8-node brick element that has only displacement degree of freedom. Meshing is applied to all the layers before application of load to analyze the pavement model at every infinitesimal element. Finer the mesh size more will be the accuracy in the analysis but computation time will also increase [5]. Therefore separate meshing was adopted to reduce computational time and to get more accurate results in the analysis. Finer meshing was applied to the surface layer and coarser meshing was applied to the subsequent layers. As far as the boundary conditions of the pavement are concerned, the bottom of the pavement has all its displacements (X , Y , Z) completely restrained and the sides of the pavement

model has no restraints in vertical direction but completely restrained over the other two directions (X, Z). Figure 2 shows the model developed in ABAQUS. The effects of axle load and tyre pressure on pavement sections have been obtained by computing strains at the critical positions indicated in Fig. 3. In the present work, total of 13 cases were considered for the analysis by varying the resilient modulus of different layers as given in Table 2. The BC layer modulus is varied in the range of 1000–3000 MPa and the GAB layer modulus is varied in the range of 300–500 MPa, whereas the CTB layer modulus is varied in range of 5000–15,000 MPa [10]. In inverted base pavements, the contribution of subgrade to pavement deterioration is lesser [1]. Hence, only the effect of elastic modulus variation of BC layer, GAB layer and CTB layer is considered in this study. Model 1–5 were considered to analyze the effect of BC layer resilient modulus, whereas model 6–9 and model 10–13 were considered to analyze the effect of GAB layer resilient modulus and CTB layer resilient modulus on the response of the inverted base pavements.

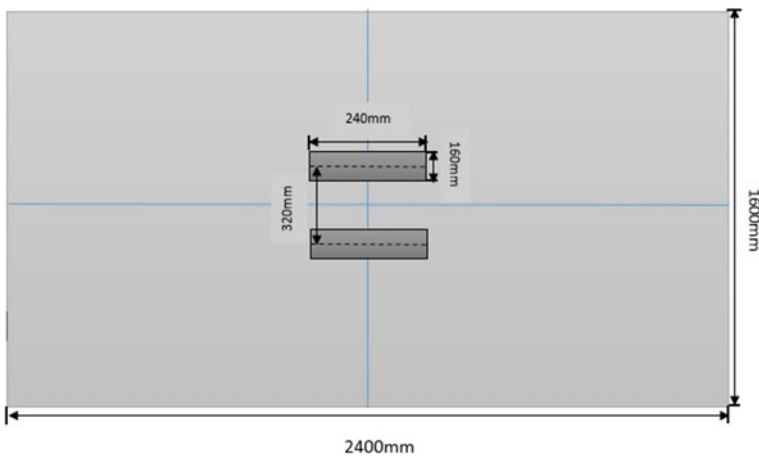


Fig. 1 Pavement section used in the stud

Table 1 Layer properties used for the base model [1]

Layer	Thickness (mm)	Resilient modulus (MPa)	Density (kg/m^3)	Poisson's ratio
BC	20	2000	2243	0.35
GAB	150	400	2200	0.35
CTB	160	10,000	2400	0.2
Subgrade	2000	50	1700	0.2

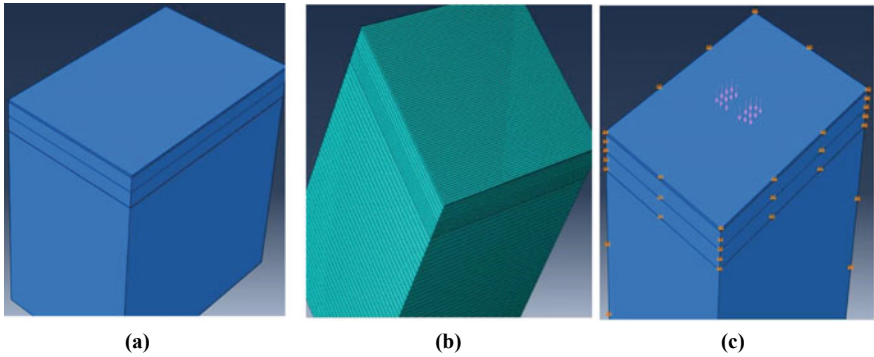


Fig. 2 Model development process using ABAQUS: **a** creation of pavement model. **b** Application of mesh. **c** Application of loading and boundary conditions

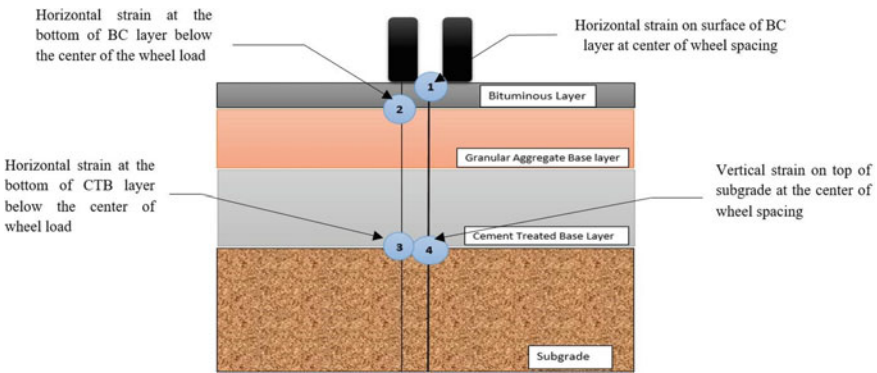


Fig. 3 Critical strain positions considered in study

4 Results and Discussions

The main objective of this study is to predict the response of inverted base pavement by varying resilient modulus of different layers. Hence total of 13 models is developed in ABAQUS by varying the resilient modulus of each layer of pavement. The effect of resilient modulus on the performance of inverted base pavements is evaluated by computing strains at the critical locations. The comparison of results obtained by ABAQUS and IIT_PAVE software is also done to check the accuracy of model. Table 3 shows the result obtained from ABAQUS and IIT_PAVE software for base model. The minor variations in the results obtained from ABAQUS and IIT_PAVE analysis may be attributed to the mesh size adopted. A smaller mesh size is expected to go into more detailed analysis and give more accurate results [5]. The error percentage of the values obtained from ABAQUS compared to values of IIT_PAVE is calculated using Eq. 1:

Table 2 Resilient modulus values of different layers used in the analysis

Case	BC modulus (MPa)	GAB modulus (MPa)	CTB modulus (MPa)	Subgrade modulus (MPa)
1	1000	400	10,000	50
2	1500	400	10,000	50
3	2000	400	10,000	50
4	2500	400	10,000	50
5	3000	400	10,000	50
6	2000	300	10,000	50
7	2000	350	10,000	50
8	2000	450	10,000	50
9	2000	500	10,000	50
10	2000	400	5000	50
11	2000	400	7500	50
12	2000	400	12,500	50
13	2000	400	15,000	

Table 3 Comparison of results between ABAQUS and IIT_PAVE for base model

S.No.	Strain location	ABAQUS	IIT_PAVE	Error (%)
1	Horizontal strain (ϵ_t) on surface of BC layer at centre of wheel spacing	1.84E-04	2.18E-04	15.6
2	Horizontal strain (ϵ_t) at the bottom of BC layer below the centre of the wheel load	1.67E-05	1.46E-05	14.4
3	Horizontal strain (ϵ_t) at the bottom of CTB layer below the centre of wheel load	4.08E-05	4.84E-05	15.7
4	Vertical strain (ϵ_c) on top of subgrade layer at centre of wheel spacing	-3.8E-04	-3.51E-04	7.27

$$\text{Error}\% = \frac{|\text{ABAQUS value} - \text{IIT_PAVE value}|}{\text{IIT_PAVE value}} \times 100 \quad (1)$$

4.1 Effect of Variation of Resilient Modulus of BC Layer

To analyze the effect of BC layer modulus on the response of inverted base pavements, models 1–5 are considered. Horizontal strains at the centre of spacing of wheel load on the top of BC layer and horizontal strains at the centre of wheel load at the bottom of BC layer are considered as the critical parameter for cracking in flexible pavement [10]. High horizontal strain on top of BC layer can cause top-down cracking and high horizontal strain on bottom of the BC layer can cause bottom-up cracking. Figure 4

shows the horizontal strain variation on top and bottom of BC layer at the respective critical locations for model 1–5.

From Fig. 4a, it is observed that variation in BC modulus have minor effect on the tensile strain values on the surface of BC layer at the critical point, i.e. at the centre of the wheel spacing. Tensile strain values on surface of BC slightly seem to decrease with increase in resilient modulus. With this result, it can be concluded that with increase in resilient modulus, strain values decrease. On the other hand, in Fig. 4b, horizontal strain values increases non-uniformly with increase in BC modulus values. Upto around 2000 MPa, the increase is rapid and after that the rate of increase in strain with variation of BC modulus values decreases. Therefore with these results, it is advisable to use high resilient modulus BC layer, especially in pavements with very thin bituminous layers. The critical point considered here is the point at the bottom of BC layer directly below the wheel load.

High horizontal strain at the centre of wheel load on the bottom of CTB base is mainly responsible for cracking in CTB, whereas high vertical compressive strain at centre of spacing of wheel loads on the top of subgrade layer is mainly responsible for rutting in pavements [10]. Figure 5 shows the horizontal strain variation on bottom of CTB and vertical compressive strain variation on top of subgrade layer at the respective critical locations for model 1–5.

From Fig. 5, variation in BC modulus does not show significant change on critical points at the bottom of CTB and top of subgrade, though slight decrease in strain values can be observed with increase in modulus values which can be attributed to the fact that with increase in stiffness, strain values decreases. The subgrade experiences the minimal effect due to BC layer. Hence it can be concluded that BC layer modulus has lesser yet prominent effect on subgrade.

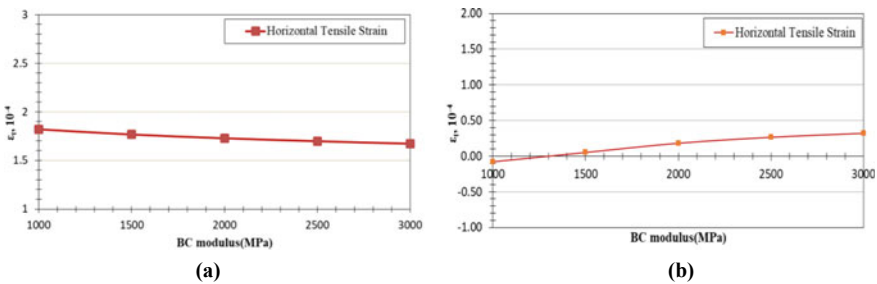


Fig. 4 Variation of critical parameters for model 1–5. **a** Horizontal strain variation with BC modulus on surface of BC layer at centre of wheel spacing. **b** Horizontal strain variation with BC modulus at the bottom of BC layer below the centre of the wheel load

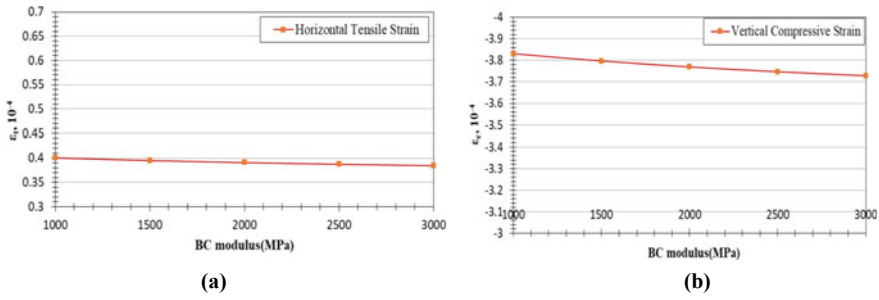


Fig. 5 Variation of critical parameters for model 1–5. **a** Horizontal strain variation with BC modulus at the bottom of CTB layer below the centre of wheel load. **b** Vertical strain variation with BC modulus on top of subgrade at the centre of wheel spacing

4.2 Effect of Variation of Resilient Modulus of GAB Layer

The response of inverted base pavements depends majorly on the GAB layer as it acts as the stress absorbing layer or as a cushioning layer to support the BC layer and releases tension from the CTB layer [1]. Hence it should be of good quality with a good degree of compaction to withstand the traffic loads. The elastic response of the granular base depends on many factors such as stress, density, gradation, particle size, moisture content, stress history, load duration, load frequency, etc. [4]. So the modulus values of GAB layer are varied with slight variations which may be the outcome of change in above factors. Figure 6 shows the variation of critical parameters at the respective critical locations for model 6–9.

From Fig. 6, it can be observed that variation in GAB modulus affects the strain values on the surface of BC layer, at the bottom of BC layer as well as the Subgrade. The strain values decrease with the increase in modulus values for all the critical points. But GAB modulus does not have much significant effect on the strain values in CTB. From the literatures it was concluded that the tensile stresses in the BC and in the CTB, as well as the compressive stresses on the subgrade, increase as the resilient modulus of the unbound granular base decreases [4]. Similarly from the above figures, for strains at the critical positions with increase in resilient modulus of GAB layer, the strain values decrease for BC layer at both its critical points and also at the critical point on top of subgrade. GAB modulus can be said to be significantly affecting the BC layer and subgrade. By increasing the modulus of GAB layer by usage of proper gradation and high-quality aggregates as well as good compaction of the layer, the excessive strain values at the critical location on bottom of BC layer and top of subgrade layer can be avoided which are mainly responsible for bottom-up cracking and rutting in pavements. In case of thin bituminous layer, on the surface of the layer, horizontal tensile stress are also developed near the edges of tyre and it is maximum at the centre of spacing of two tyres [1]. By increasing resilient modulus of GAB layer, the strain values on the surface of BC layer would decrease so initiation

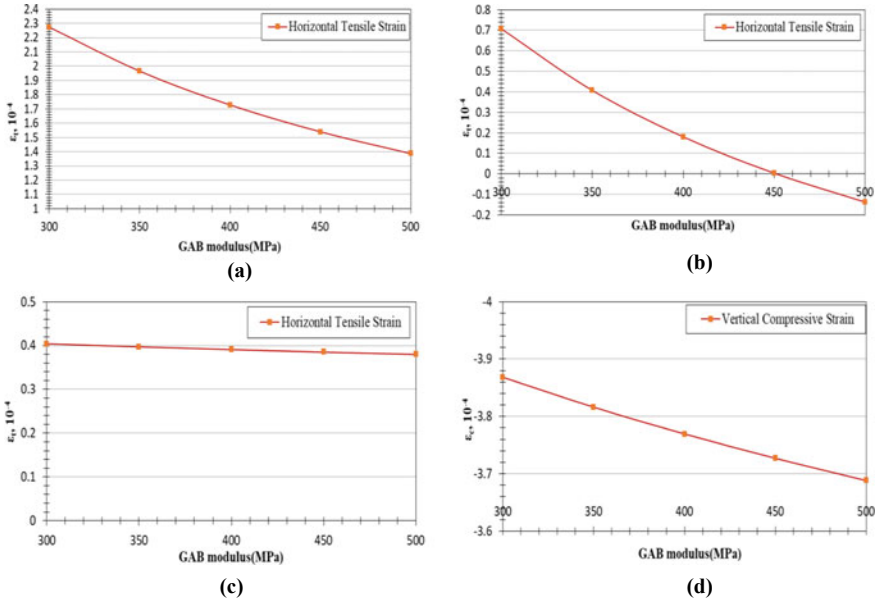


Fig. 6 Variation of critical parameters for model 6–9. **a** Horizontal strain variation with GAB modulus on surface of BC layer at centre of wheel spacing. **b** Horizontal strain variation with GAB modulus at the bottom of BC layer below the centre of the wheel load. **c** Horizontal strain variation with GAB modulus at the bottom of CTB layer below the centre of wheel load. **d** Vertical strain variation with GAB modulus on top of subgrade at the centre of wheel spacing

of top-down cracking, longitudinal surface cracking followed by transverse cracking can also be avoided.

4.3 Effect of Variation of Resilient Modulus of CTB Layer

A stiffer base, like CTB layer, reduces deformations due to traffic loads, resulting in lower strains on the pavement surface. CTB thickness are significantly less than the thickness required for granular bases carrying the same traffic load in pavement design. CTB continues to gain strength with age [10]. So the variation can account for the behaviour of CTB with its age. Figure 7 shows the variation of critical parameters at the respective critical locations for models 10–13.

From Fig. 7, it can be observed that with increase in CTB modulus, the strain values decrease at the bottom of CTB layer. The decrease is rapid upto 10,000 MPa and then the change is slow. In case of subgrade, with increase in the modulus values, there is decrease in the vertical compressive strain values. Therefore it is advisable to use high modulus CTB layers to prevent rutting in the pavements but at the same time

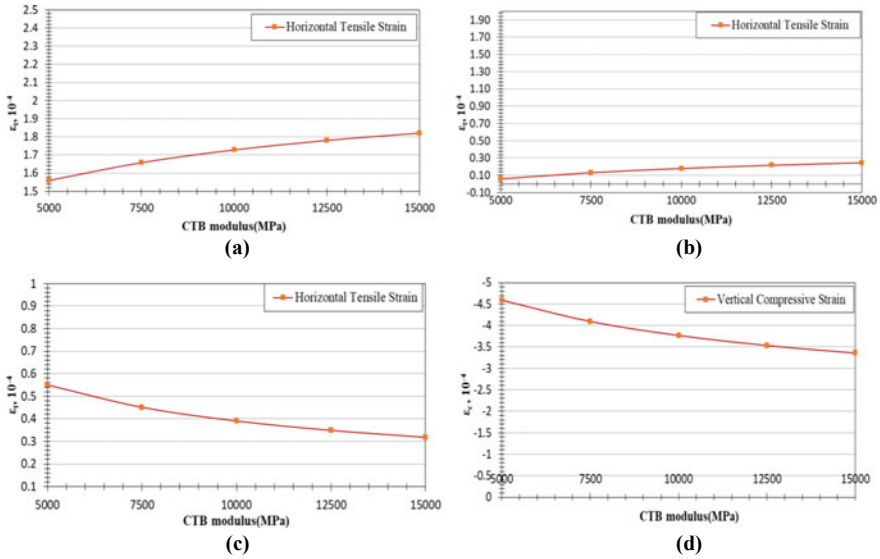


Fig. 7 Variation of critical parameters for model 10–13. **a** Horizontal strain variation with CTB modulus on surface of BC layer at centre of wheel spacing. **b** Horizontal strain variation with CTB modulus at the bottom of BC layer below the centre of the wheel load. **c** Horizontal strain variation with CTB modulus at the bottom of CTB layer below the centre of wheel load. **d** Vertical strain variation with CTB modulus on top of subgrade at the centre of wheel spacing

top-down cracking and bottom-up cracking susceptibility of pavements increases as horizontal strains on top and bottom of BC layer increase.

5 Conclusions

The main objective of this study is to predict the response of inverted base pavements under varying resilient modulus of pavement layers. Hence an attempt has been made to develop 3D FEM of inverted base pavement in ABAQUS software. Validation of model is also done with IIT_PAVE software to check its accuracy. From this study, the following conclusions are derived.

1. There are variations in the results obtained from ABAQUS and IIT-PAVE software which may be attributed to the mesh size adopted in FEA, different contact area shape, i.e. circular contact area in IIT-PAVE and rectangular contact area in FEA and also the method of calculation used by both software.
2. The BC layer modulus significantly affects the strain values at top and bottom of BC layer. Higher BC modulus reduces the strain on top of the pavements and can be used to arrest top-down cracking susceptibility in inverted base pavements.






3. GAB modulus affects the BC layer on its surface as well as at the bottom of BC layer and also subgrade. With increase in modulus values the layer stiffness increases and the strain values decreases.
4. The CTB modulus affects the CTB and Subgrade layers significantly along with BC layer. It helps reducing the deformations due to traffic loads, resulting in lower strains on the lower layers of the pavement and the pavement surface as well. Also, it helps in reducing rutting deformation due to subgrade and bituminous layers.

References

1. Papadopoulos E, Santamarina JC (2015) Analysis of inverted base pavements with thin-asphalt layers. *Int J Pavement Eng* 17(7):590–601. <https://doi.org/10.1080/10298436.2015.1007232>
2. Papadopoulos E, Santamarina JC (2017) Inverted base pavements: construction and performance. *Int J Pavement Eng*
3. Baskandi D (2020) Inverted pavements: an overview. *Int J Civil Struct Environ Infrastruct Eng Res Develop (IJCSEIERD)* 10(4):61–66
4. Cortes DD, Shin HS, Santamarina JC (2012) Numerical simulation of inverted pavement systems. *ASCE J Transp Eng* 138(12):1507–1519
5. Cho S, Toth C, Soos Z (2018) Finite element method analysis for mechanistic design in flexible pavement, review: from how to build a material in FE analysis to complexity in reality. *J Silic Based Compos Mater* 70:204–208
6. *Pavement Analysis and Design-Second Edition* by Yang H. Huang University of Kentucky
7. Gupta A, Kumar A (2014) Comparative structural analysis of flexible pavements using finite element method. *Int J Pavement Eng Asphalt Technol* 15(1). <https://doi.org/10.2478/ijpeat.2013-0005>
8. Sahoo UC, Reddy KS (2010) Effect of nonlinearity in granular layer on critical pavement responses of low volume roads. *Int J Pavement Res Technol*
9. Tutumluer E, Barksdale RD Inverted flexible pavement response and performance. *Transp Res Record* 1482:102–110
10. *Guidelines for the Design of Flexible Pavements (Fourth Revision)* (2018) Indian Roads Congress, New Delhi

Identification and Analysis of Factors of Delay in Road Construction Projects



Bishnu Kant Shukla , Vaishnavi Bansal , S. Varadharajan ,
Gaurav Bharti , Aparupa Shenoy , Udit Kumar Singh,
and S. V. Kirthanashri 

Abstract Delays are frequent in any civil engineering projects including the road projects. Project delays can result in cost overrun, time overruns, quality issues, etc. In this study, a national highway road project has been considered. A total of probable 90 delay factors were recognized and were characterized into nine foremost categories. A questionnaire was prepared, and it was filled by 101 respondents. Relative importance index technique has been used for the analysis of questionnaire data. The top and base 15 delay factors were recognized. The top five delay factors were found to be: consequence of sub-surface circumstances (rock, water table, soil, etc.), design related clashes/faults, provide the furnished site to the contractor, scarcity of skilled labour, resource allocation related delay, etc.

Keywords Road projects · Cost overrun · Time overrun · Delay factors · Relative importance index

1 Introduction

Delay in completion of road projects is frequent which results in cost overrun, time overrun, and many other issues. Construction projects most of the time fail to deliver projects on time. Delay in road projects depends upon a number of factors like based on the location of the project, size of the project, and many other factors. First part is identification of the delay factors, which will be done using questionnaire survey as it was found to be most suitable technique for identification of the factors involved. Delays are found to be present in every construction project which also affects budget of the project (usually results in overruns). Overall this affects all the stakeholders which are involved in the project, i.e. clients, consultants, and contractors. This study

B. K. Shukla (✉) · V. Bansal · S. Varadharajan · G. Bharti · A. Shenoy · U. K. Singh
Department of Civil Engineering, JSS Academy of Technical Education, Noida 201301, India
e-mail: bishnukantshukla@gmail.com

S. V. Kirthanashri
Amity Institute of Molecular Medicine and Stem Cell Research, Noida 201301, India

© The Author(s), under exclusive license to Springer Nature Singapore Pte Ltd. 2023
A. K. Agnihotri et al. (eds.), *Proceedings of Indian Geotechnical and Geoenvironmental Engineering Conference (IGGEC) 2021, Vol. 1*, Lecture Notes in Civil Engineering 280,
https://doi.org/10.1007/978-981-19-4739-1_47

focuses on the need to complete road projects on time by identifying critical delay factors present in road construction. Delay factors have been classified into number of categories by different authors in their studies. For this study, delay has been categorized into nine categories based on the originator of the delay and source of the delay.

2 Background Study

A number of definitions of delay were found in the literature, and the conclusion was that the delay is a problem which results in failure to deliver the project on time as per the contract documents or any other agreement. Delay results in number of problems which affects the project objectives. Bansal [1] studied delay factors in construction of highway project. In literature, various analytical techniques like relative importance index (RII), frequency index, severity index, average index, etc., were used to analyse the data. This thesis work has been analysed in this study using RII. Hamzah et al. [2] identified the delay causes in Malaysian construction industries. Questionnaire survey technique was used for this study. The respondents involved in survey consisted of consultants, developers, and contractors. This study identified 34 delay factors out of which 24 has been found as major delay factors. Lo et al. [3] focused on the study of the perception of different parties involved in projects, i.e. contractor, consultant, client individually as well as combined. Based on their perception, he concluded that how important are the delay causes. The different perspectives of the groups were analysed using rank agreement factor (RAF), percentage disagreement (PD), and percentage agreement (PA). In last, top delays were listed based on the combined results of the analysis. This delay was classified in two categories: excusable delays and inexcusable delays. Excusable delays are further classified into two categories, i.e. compensable (owner) and non-compensable category. All the delay factors identified were listed in these categories. Mahamid et al. [4] focused on the identification of delay causes and found 52 undecorated delay factors in road creation projects in construction industry in Palestine. A questionnaire investigation technique was used to categorize top factors. Top five factors identified were shortage of equipment, award to lowest bid, political situation, payment interruption by owner, and constrained movement between areas. Ogunlana et al. [5] studied delay factors in Cambodian construction industry. Sixty-four factors were initially identified and questionnaire survey technique was used to find top factors [6, 7]. In this analysis, firstly frequency index and severity index were calculated [7]. Based on the frequency index and severity index, importance index was calculated. Top delays were identified, recommendations and suggestions to minimize impact of delay was given against each critical delay factor identified [8].

The purpose of current study is to ascertain the factors contributing to delays in road construction, by identifying the top and base fifteen factors causing delays in road construction using questionnaire method and further analyse the data and rank

Table 1 Major categories of delay factors used based on originator and source

S.No.	Delay category
1	Owner related factor
2	Contractor related factor
3	Factor associated to consultant
4	Factor linked to materials
5	Factors associated designer
6	Factor associated to labour
7	Factors associated to equipment's
8	Factors associated projects
9	Other factor of delay

the delay factors using analytical and statistical tools. This study has been conducted on the Parwanoo–Solan road stretch in Himachal Pradesh, India.

3 Research Methodology

Research methodology used in this paper is listed in the following points: (1) Identification of delay factors based on the literature. These 90 delay causing factors were recognized and were characterized into nine groups namely factors related owner, factors related to contractor, factor related to consultant, factor related to materials, factors related designer, factor related to labour, factors related to equipment's, factors related projects, other factor of delay as shown in Table 1. (2) The questionnaire survey consisted of two parts: part A consists of respondent's information and part B was focused on delay factors response based on 5-point Likert scale. (3) The response of the questionnaire was analysed using RII. Statistical package for the social sciences (SPSS) was used to analyse data statistically. (4) To rank the top and base 15 delay factors and give recommendations and suggestions for these factors.

4 Questionnaire Survey

The questionnaire was prepared on the five-point scale of Likert based on severity of each factor, i.e. how much that factor contributes to delay in road projects. This questionnaire was filled by respondents included owner (4%), contractor (12%), consultant (5%), site engineer (36%), supervisor (33%), designer (6%), and project manager (5%) as shown in Table 2. A total of 145 questionnaires were distributed out of which 101 was received back which were analysed using RII. Response rate of 69.65% was observed.

Table 2 Number of participants in questionnaire survey

S.No.	Role of participant in company	Number of participants
1	Owner	4
2	Contractor	12
3	Consultant	5
4	Site engineer	36
5	Supervisor	33
6	Designer	6
7	Project manager	5
Total		101

5 Data Analysis and Ranking

As the data obtained from the questionnaire survey was in numeric form, therefore, qualitative analysis is done using RII using Eq. (1)

$$RII = \frac{\sum W}{A \times N} \tag{1}$$

where

- RII Relative importance index
- W Weightage given by respondent to each factor
- A Highest range, i.e. 5
- N Total number of respondents

Each of the respondent was having five options to choose from against each factor which are described as in Table 3. This was based on how much a factor effects in delay of road projects according to respondents.

RII for each of the delay factor was calculated based on the responses of the respondents received. Top 15 delay factors found are listed in Table 4 along with their RII score and delay group category. In top 15 delay factors, four were from other factors of delay category, three factors were from contractor related category, three were from owner related category, and rest were from mixed category.

Table 3 Scoring for RII in questionnaire

Scale	Scoring
Very low significance	1
Low significance	2
Moderate significance	3
High significance	4
Extreme significance	5

Table 4 Top 15 delay factors identified

Rank	Delay causes	R.I.I	Delay-groups
(i)	Consequence of sub-surface circumstances (soil, water table, rock, etc.)	0.871	Other factor related to delay
(ii)	Design errors and disputes	0.848	Associated with designer
(iii)	Delivery of furnish site to contractor	0.844	Owner associated
(iv)	Resource allocation delay	0.816	Contractor associated
(v)	Scarcity of skilled labour	0.812	Labour associated
(vi)	Late in approving and changing intended papers by owner	0.804	Owner associated
(vii)	Recurrent changes in project planning and scheduling	0.802	Contractor associated
(viii)	Labour slowdowns	0.796	Labour associated
(ix)	Delay due to abrupt amendment in alignment	0.788	Other factor related to delay
(x)	Absence of regulation in site supervision	0.784	Contractor associated
(xi)	Sluggish site clearances (public properties, forest department, etc.)	0.782	Other factor of delay
(xii)	Delayed conveyance of materials to chosen site	0.780	Material associated
(xiii)	Added extra work	0.778	Other factor related to delay
(xiv)	Variation in cost of material	0.776	Material associated
(xv)	Delay in growth payments	0.774	Owner associated

Similarly, base 15 delay factors were also listed based on their RII score. Base 15 delay factors along with their ranking are listed in Table 5. Along with their RII score and delay group category. Most of the base factors were from other factor of delay category. These results were based on the survey analysis performed, and ranking was based on the RII score. Reliability analysis was performed on the questionnaire to check the reliability. Reliability was checked using Cronbach alpha in statistical package for social sciences (SPSS).

Cronbach alpha score was found to be between 0.957 and 0.99 which is highly reliable. A questionnaire is said to be valid if its Cronbach alpha value is greater than 0.7. Further, Spearman's rank correlation coefficient analysis was also performed on the questionnaire results to check the relation between critical delay factors. The values were found lie between +0.932 and +0.562 that depicts positive correlation. Further on performing factor analysis, the 90 factors were divided into three groups. Group 1 consists of 46 factors, group 2 consists of 25 factors, and group 3 consists of 19 factors with good Cronbach alpha value.

Table 5 Base 15 delay factors identified

Rank of different factors	Various causes associated with delay	RII	Delay-groups
(i)	Consequence of societal and traditional causes	0.404	Other factor related to delay
(ii)	Insufficient documents related to project	0.419	Other factor related to delay
(iii)	Intervention of native public live in vicinity of location of construction	0.432	Other factor related to delay
(iv)	Alterations in lending policy by banks	0.440	Other factor related to delay
(v)	Problems arise during process of transport of material	0.452	Material associated
(vi)	Corrosion in material at the time of need	0.456	Material associated
(vii)	Deferral in execution examination and analysis	0.460	Consultant associated
(viii)	Site of the project	0.520	Other factor related to delay
(ix)	Constraint and control on traffic situation and its mobilization at job site	0.523	Other factor of delay
(x)	Problems associated with other agencies	0.535	Other factor related to delay
(xi)	Skirmishes among labours	0.539	Labour associated
(xii)	Mishaps in the course of construction and security features	0.574	Other factor related to delay
(xiii)	Community incursions and uprisings	0.576	Other factor related to delay
(xiv)	Price variations	0.578	Other factor related to delay
(xv)	On site sluggish deployment of labour	0.586	Labour associated

6 Conclusions and Recommendations

The top and base fifteen factors responsible for delay were ranked using RII established on the severity of the delay on conclusion of the project. In this, a total of 90 delay factors have been assessed in this research. The top fifteen delay factors found were: consequence of sub-surface circumstances (rock, water table, soil, etc.), disputes and errors associated with design, convey the furnish site to the person or organization awarding contract, scarcity of skilled labour, resource allocation delays, recurrent change in project planning and scheduling, delay in approving and changing

designed papers by the owner, delay due to abrupt alteration in alignment, labour incursions, sluggish site clearances (public properties, forest department, etc.), deficiency of supervision in site administration, additional extra work, delayed delivery of material to chosen site, and deferral in progress payments variation in material cost. The base fifteen delay factors found were: insufficient documents associated to project, effect of societal and ethnic factors, changes in lending policy by bankers, intervention of native public live in the vicinity of site of construction, corrosion of material during need hour, issues that arise during transportation of material, site of the project, delay in execution of testing and inspection, problematic issues with other agencies, restriction and control on traffic mobilization at job site, mishaps during construction and safety aspects, skirmishes among labours, price variations, public incursions and riots, and sluggish mobilization of on-site labours. This work is helpful for both researchers and practitioners as these factors can be considered directly and further research can be done location-specific with minor changes.

The delay in any project associated with construction depends on the assertiveness of the management (can be from owner, consultant, contractor, etc.) side. Each and every person involved in construction projects should understand their responsibilities towards their work. To deal with delays in a better manner, risk management frameworks can also be used and immediate suitable remedial measures should be undertaken. Delay checklists should be there to check progress during various stages of the project. Delay factors as categorized in this paper may be used to identify who is responsible for factors involved and thus responsibilities should be allotted according to it.

References

1. Bansal V (2019) Time delay in road construction project. Masters thesis, CED, Jaypee University of Information Technology (JUIT), Wagnaghat, Solan, HP, India
2. Hamzah N, Khoiry MA, Arshad I, Badaruzzaman WHW, Tawil NM (2012) Identification of the causes of construction delay in Malaysia. *World Acad Sci Eng Technol WASET, Int J Civ Sci Eng* 6(12):578–583
3. Lo TY, Fung IW, Tung KC (2006) Construction delays in Hong Kong civil engineering projects. *J Constr Eng Manag* 132(6):636–649
4. Mahamid I, Bruland A, Dmaidi N (2011) Causes of delay in road construction projects. *J Manag Eng* 28(3):300–310
5. Ogunlana SO, Promkuntong K, Jearkjirm V (1996) Construction delays in a fast-growing economy: comparing Thailand with other economies. *Int J Project Manage* 14(1):37–45
6. Aziz RF, Abdel-Hakam AA (2016) Exploring delay causes of road construction projects in Egypt. *Alex Eng J* 55(2):1515–1539
7. Kazaz A, Ulubeyli S, Tuncbilekli NA (2012) Causes of delays in construction projects in Turkey. *J Civ Eng Manag* 18(3):426–435
8. Aibinu AA, Odeyinka HA (2006) Construction delays and their causative factors in Nigeria. *J Constr Eng Manag* 132(7):667–677

Effect of Curing on Strength of Clayey Soil Stabilized with Marble Dust



Aditya D. Ahirwar and H. S. Chore

Abstract Marble is a versatile material used to enhance the artistic value of structures, sculptures, and monuments. Utilization of marble is not only restricted to traditional applications like internal and external walls and claddings, flooring work, but also includes non-traditional applications such as paint and agricultural lime. In India, Rajasthan accounts for 89% of the marble production of the country. There are almost 4000 marble mines in state of Rajasthan. During the mining and finishing operations, a substantial amount of marble waste is generated in order to obtain a well-finished product. In existing study, effort is made to assess the usefulness of marble dust for stabilization of clayey soil. Parameters like compaction characteristics, strength characteristics are assessed through experimental work. Laboratory investigations were carried out to assess the effect of curing period on strength of different combination of mixes. Test results indicates that the strength of composite mix increases with increase in proportion of marble dust and also, with the curing period.

Keywords Clayey soil · Marble waste · Curing period

1 Introduction

Marble is used in a wide range of projects to enhance the artistic value of structures, sculptures and monuments. To obtain a well-finished product, an enormous quantity of waste is generated throughout mining and finishing processes. This massive amount of waste is frequently dumped nearby processing units. The disposal of such waste on open land endangers both public health and the environment. A finer fraction of such marble waste can pollute the air and reduce visibility in nearby areas. It

A. D. Ahirwar (✉) · H. S. Chore
Department of Civil Engineering, Dr. B.R. Ambedkar National Institute of Technology,
Jalandhar 144011, India
e-mail: ahirwarad.ce.19@nitj.ac.in

H. S. Chore
e-mail: chorehs@nitj.ac.in

© The Author(s), under exclusive license to Springer Nature Singapore Pte Ltd. 2023
A. K. Agnihotri et al. (eds.), *Proceedings of Indian Geotechnical and Geoenvironmental Engineering Conference (IGGEC) 2021, Vol. 1*, Lecture Notes in Civil Engineering 280,
https://doi.org/10.1007/978-981-19-4739-1_48

513

can reduce soil porosity and have an impact on ground water recharge. Furthermore, it can raise the alkalinity of the soil, making it unsuitable for agriculture. However, the tendency of such industrial waste material to blend well with soil and improve the strength characteristics of composite mix makes it suitable for possible use in highway construction.

Celik and Sabah [1] stressed the importance of conducting research to identify potential applications of waste generated by marble industry. Almeida et al. [2] suggested possible utilization of marble by product in not only cement, tiles, concrete industry but also in pavement and embankment construction. They further recommended that marble waste can be utilized in paper industry, agriculture and water treatment.

Singh and Yadav [3], Akinwumi and Booth [4], Yilmaz and Yurdakul [5] and Saxena [6] have investigated effectiveness of utilization of marble waste for soil stabilization. Experimental investigation suggests improvement in index properties, compaction characteristics, strength of soil-marble dust composite mix.

Gurbuz [7] investigated the impact of addition of marble powder on strength and durability of composite mixes containing soil and marble dust. Saygili [8] identified that marble dust with higher calcium content plays vital role in hydration process. Formation of pozzolanic compound results in an increase in strength. He also found that size of pores in soil matrix reduces after addition of marble dust. After curing, it becomes extremely difficult for water to enter into clay matrix, thus reducing the swelling of the composite mix. Sabat and Nanda [9] examined the effect of curing on an expansive soil stabilized with marble waste and rice husk ash. Okagbue and Onyeobi [10] investigated the effect of 7 day and accelerated 24 h curing on soil stabilized with marble dust.

The purpose of the investigation was to analyze the compaction characteristics and strength of various mixes containing clayey soil and marble dust. Comprehensive laboratory testing was conducted to assess the effect of curing on unconfined compressive strength of composite mix.

2 Material and Method

In present study, clayey soil was mixed with different proportions of marble dust (5, 10, 15 and 20%). The soil and marble dust used for the experimental investigation was brought from local supplier. The geotechnical properties of different combinations of mixes were found out, which includes determination of plasticity characteristics, compaction characteristics and unconfined compressive strength of clay-marble dust composite mix. Table 1 illustrates particulars of clay-marble dust mixes, considered in the present study.

Table 1 Different combination of mixes

S. No.	Property	Value
1	PC (Plain Clayey Soil)	100% Clay
2	C5MD	Clay + 5% Marble dust
3	C10MD	Clay + 10% Marble dust
4	C15MD	Clay + 15% Marble dust
5	C20MD	Clay + 20% Marble dust

3 Discussion of Results

Experimental program includes preliminary tests to determine index properties of clayey soil. Table 2 presents index properties of the soil.

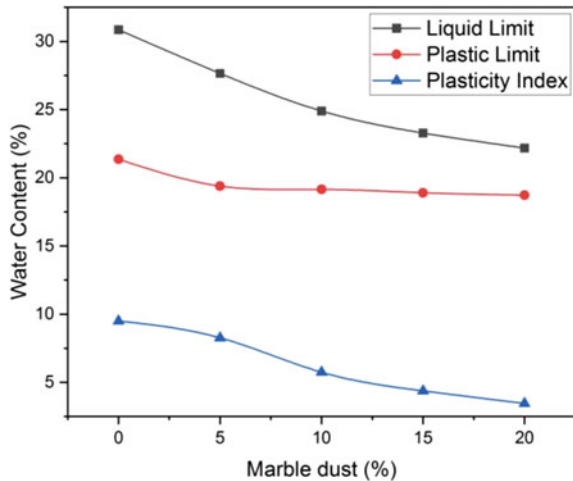
In the present study, Atterberg’s limits of various combinations of mixes were evaluated using Casagrande’s apparatus. Figure 1 illustrates the variation in Atterberg’s limit after addition of marble dust.

It is evident from Fig. 1 that the increase in the proportion of marble dust reduces LL and PL. As marble dust fills up voids of flocculated soil, reduction in water

Table 2 Index properties of clayey soil

S. No.	Property	Value
1	LL: liquid limit (%)	30.85
2	PL: plastic limit (%)	21.35
3	Specific gravity	2.61
4	OMC: optimum moisture content (%)	17.4
5	MDD: maximum dry density (gm/cc)	1.782

Fig. 1 Effect of addition of marble dust on LL, PL, PI



retention capacity of composite mix is observed. The improvement in soil property is indicated by reduction in plasticity index.

Compaction characteristics govern geotechnical properties of soil. Focus of current study is on analyzing the effect of addition of marble dust on maximum dry density (MDD) and optimum moisture content (OMC) of the different combinations of mixes.

As the proportion of marble dust in composite mix increases, the MDD of composite mix increases while OMC decreases (Fig. 2).

Tests were carried out to determine the effect of addition of marble dust on unconfined compressive strength (UCS) of various mixes (Fig. 3).

UCS of composite mix increases with increase in proportion of marble dust up to 15%. After further addition, UCS decreases. Similar trend is observed for the 7 and

Fig. 2 Variation in MDD and OMC of soil-marble dust composite mix

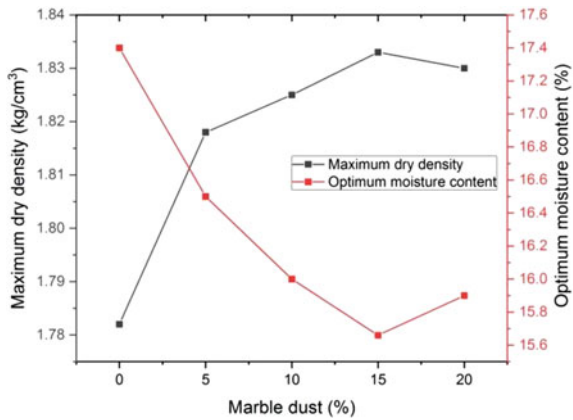


Fig. 3 Variation in UCS after addition of marble dust

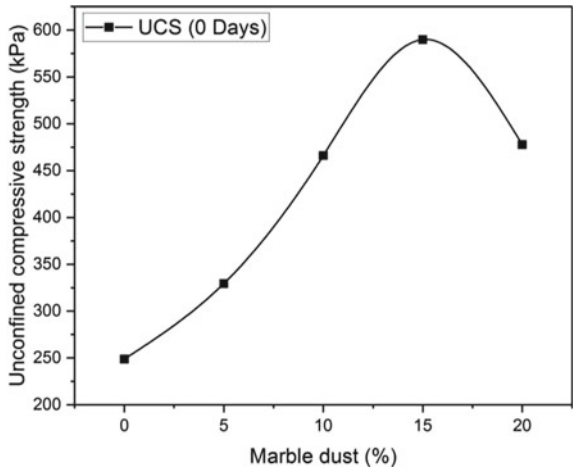
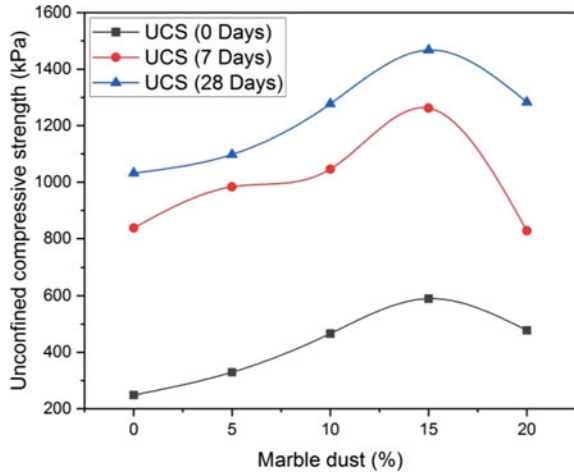


Fig. 4 Variation in UCS of composite mix for after 7 and 28 days curing



28 days curing period. From Fig. 4, it can further be noted that the UCS of composite mix increases with curing period.

4 Summary and Conclusions

From the experimental investigations on stabilized clay samples, following conclusion can be drawn:

1. After addition of marble dust, the LL, PL and PI of the composite mix decrease.
2. MDD of the composite mix increases while the optimum moisture content decreases, after addition of marble dust.
3. Strength of the clay- marble dust composite mix increases with addition of marble dust upto 15%. Based on result obtained from UCS test, mix with 15% marble dust found out to be optimum mix.
4. UCS of the composite mix increases significantly with curing period.

Thus, marble dust can be advantageously used to stabilize clayey soil based on strength characteristics of different combination of mixes. This will not only provide possible approach for safe disposal of waste by product but also will end up saving the conventional material that would have been used therein.

References

1. Celik MY, Sabah E (2008) Geological and technical characterization of iscehisar (Afyon-Turkey) marble deposits and the impact of marble waste on environmental pollution. *J Environ Manage* 87(1):106–116
2. Almeida N, Branco F, Santos JR (2007) Recycling of stone slurry in industrial activities: Application to concrete mixtures. *Build Environ* 42(2):810–819
3. Singh PS, Yadav RK (2014) Effect of marble dust on index properties of black cotton soil. *Int J Engg Res Sci Tech* 3:158–163
4. Akinwumi II, Booth CA (2015) Experimental insights of using waste marble fines to modify the geotechnical properties of a lateritic soil. *J Environ Eng Landsc Manag* 23(2):121–128
5. Yilmaz F, Yurdakul MUHAMMET (2017) Evaluation of marble dust for soil stabilization. *Acta Phys Pol, A* 132(3):710–711
6. Saxena, D., 2017. Effects of marble powder and fine sand on properties of expansive soil. *International Journal of Engineering Trends and Technology (IJETT)*–Volume, 52, 12–16
7. Gurbuz A (2015) Marble powder to stabilise clayey soils in sub-bases for road construction. *Road Materials and Pavement Design* 16(2):481–492
8. Saygili A (2015) Use of waste marble dust for stabilization of clayey soil. *Mater Sci* 21(4):601–606
9. Sabat AK, Nanda RP (2011) Effect of marble dust on strength and durability of Rice husk ash stabilised expansive soil. *Int J Civ Struct Eng* 1(4):939–948
10. Okagbue CO, Onyeobi TUS (1999) Potential of marble dust to stabilise red tropical soils for road construction. *Eng Geol* 53(3–4):371–380

Analysis of Bagasse Ash with GBFS as a Cement-Treated Sub-Base



B. Manjuladevi and H. S. Chore

Abstract Flexible pavements are easy to maintain, can be opened to traffic in a very short time, it also has a smooth surface, better riding comfort, low noise, short construction period, low cost and convenient maintenance. India, as the world's seventh-largest country by land, to serve its people, it requires a vast network of structures and highways. This imposes undue pressure on limited resources, in order to practise sustainable development and rather necessitates the use of industrial by-product (IBP) and locally available materials. The industrial by-product of sugarcane industry and steel plant are bagasse ash (BA) and granulated blast furnace slag (GBFS), respectively. To understand the possibility of these materials as cement-treated sub-base materials (CTSB), various physical, chemical analysis and permeability tests conducted on different proportion of these materials. From the strength characteristics, 60% of BA and 40% of GBFS found as an optimum combination and can be used as CTSB material for low-volume roads.

Keywords Bagasse ash · Granulated blast furnace slag · CTSB

1 Introduction

Pavement is a layered structure that consists of subgrade, sub-base, base and wearing courses in case of flexible pavement and subgrade, base and concrete slab in case of rigid pavement. India has the world's second largest road network, with 1.70 km of road per square kilometre of land. In 2019, India crossed more than 5.9 million kilometres (58.98 lakh km). Paved Indian roads now comprise for almost 62.5% of all Indian highways [1].

B. Manjuladevi

Department of Civil Engineering, Datta Meghe College of Engineering, Sector-3, Airoli, Navi Mumbai 400708, India

H. S. Chore (✉)

Department of Civil Engineering, Dr. B. R. Ambedkar National Institute of Technology, Jalandhar 144011, India

e-mail: chorehs@nitj.ac.in

The major issues faced by road transport authority are scarcity of good quality of conventional materials. India's ever increasing population needs an extensive system of roads to absorb the high traffic volume. Aggregates are a significant part of the pavement structure and also a major materials used in pavement construction. Due to the rapid depletion of naturally occurring materials for construction, the road development organisations are looking for other substitutes for these materials due to rising prices of conventional construction materials. Hence, it is global necessity to find alternate materials that are cost-effective, eco-friendly and function in a better way. In the coming years, road pavements are expected to go through a major change with respect to the usage of materials and procedure of construction and operation. Guidelines on sustainable development are going to be enforced by the government. There is a push to identify, examine local soil and industrial waste material that could be used in place of conventional construction materials.

In our country, flexible pavements are designed and constructed by using conventional materials and its strength qualities. However, nowadays, the focus has shifted towards the industrial by-products in different layers of pavements construction. This clearly indicates from the revised IRC 37 (2012 and 2018) codes considered some of the industrial by-products, and its specifications are given. Still, there is a need of such research with some waste materials which have not been tried either partly or fully. The use of IBP in pavement construction will contribute in the preservation of natural resources and will also result in sustainable development.

Bagasse ash, fly ash, rice husk ash and other pozzolanic materials have been widely used for the stabilisation along with lime and cement [2–10]. Bagasse ash has been found to possess a high amount of silica and other important oxides, which promote good pozzolanic activity [11, 12].

Stability analysis was carried out on copper slag and pond ash mixes to analyse its possibility as an embankment materials [13]. Physical and chemical analysis was carried out on (steel slag—fly ash) mix to explore these materials for the construction of sub-base [14]. GBFS used for stabilisation of weak soil. CBR and UCS tests were performed with the different proportions ranging from 3 to 12% in the increment of 3%. They discovered that the ideal level of GBFS, which is 9%, gives a 28% improvement in the strength of soft soil when compared to unstabilised soil [15]. Horizontal and vertical permeability tests were conducted on the crushed stone aggregates and granular slag in different combinations for the construction of GSB layer in flexible pavement to determine its permeability characteristics, concluding that all crushed stone—slag mixes meet the necessary permeability criteria in both horizontal and vertical directions [16]. The strength (UCS, CBR) and permeability requirements for Grade I materials that consist of coarse aggregate mixed with stone dust were analysed. Good gain in the strength was observed, but the mix failed to satisfy the permeability criteria specified in the IRC and AASHTO codes [17]. Experimental investigation carried out on the electric arc furnace slag and ground granulated blast furnace slag for the construction on base/sub-base in low-volume roads [18]. From the literature review, the BA and GBFS for the sub-base layer construction was not observed; most of the researchers have used these materials for soil stabilisation. On

this backdrop, the possibility of BA and GBFS as a CTSB layer in flexible pavement construction was analysed; different laboratory experiments were conducted.

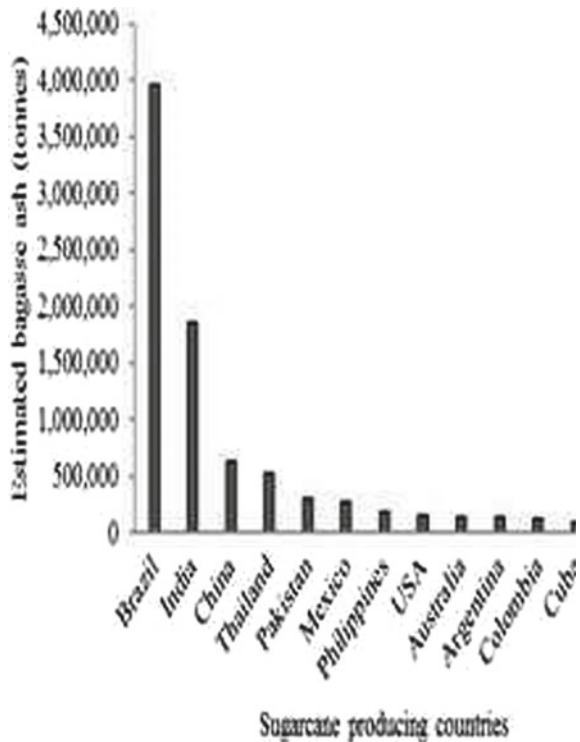
2 Materials and Methodology

2.1 Bagasse Ash

Bagasse is the leftover fibrous substance after crushing sugarcanes in sugar mills and extracting juice from processed cane by milling. In cogeneration boilers, bagasse is used as a fuel. Bagasse ash is the residue collected using a baghouse filter after burning. The bagasse ash (BA) quantity in India is (44,000 t/day), and it creates lot of problem for disposal as it affects the environment [19]. Figures 1 and 2 show the expected amount of bagasse ash produced by various countries and states in India.

From this chart, Uttar Pradesh and Maharashtra produce the highest quantity of BA. Shri Sant Tukaram Sakhari Sakhar Karkhana Limited, Pune, supplied the bagasse ash for this project (Maharashtra).

Fig. 1 Different countries sugarcane bagasse ash production [19]



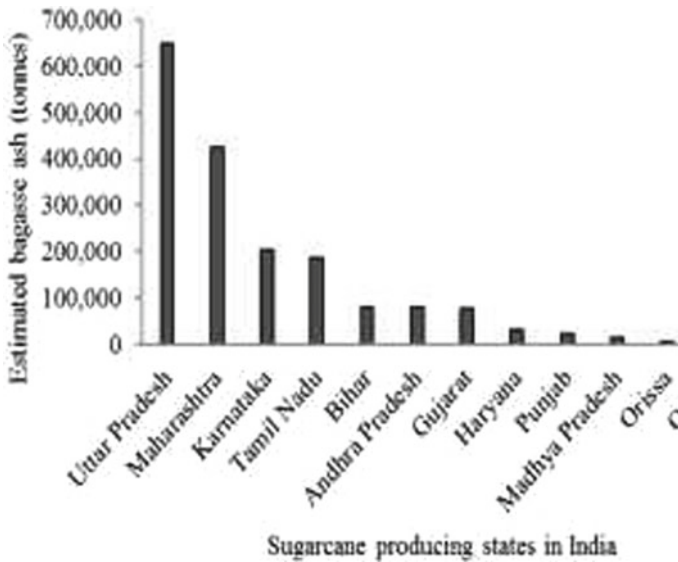


Fig. 2 Different states sugarcane bagasse ash production in India [19]

2.2 Granulated Blast Furnace Slag (GBFS)

Steel companies produce GBFS as a by-product. Most countries use GBFS in road construction to replace natural aggregate in the wearing course, base and sub-base layers, either partially or completely. GBFS was approved by the Ministry of Roads and Transportation in 2013 for the building of sub-base and base course layers. In India, integrated iron and steel industries generate over 270 million tonnes of industrial solid waste each year, with just 30% of that being used (meconlimited.co.in). The GBFS was collected from Coke Oven Plant, JSW Steel Limited, Pune, Maharashtra.

2.3 Physical Characteristics of the Materials

Various laboratory experiments like sieve analysis, specific gravity, standard Proctor test and permeability tests were conducted on these materials according to the relevant IS code. The basic properties were shown in Table 1.

The sieve analysis results of BA and GBFS are plotted in Fig. 3.

Table 1 Engineering properties of BA and GBFS

Sr.No.	Property	GBFS	BA
1	Specific gravity	2.49	2.02
2	MDU (kN/m ³)	14	7.13
3	OMC (%)	6.5	54
4	Sand-sized particles (%)	98.55	95.65
5	Silt and clay-sized particles (%)	1.45	4.35

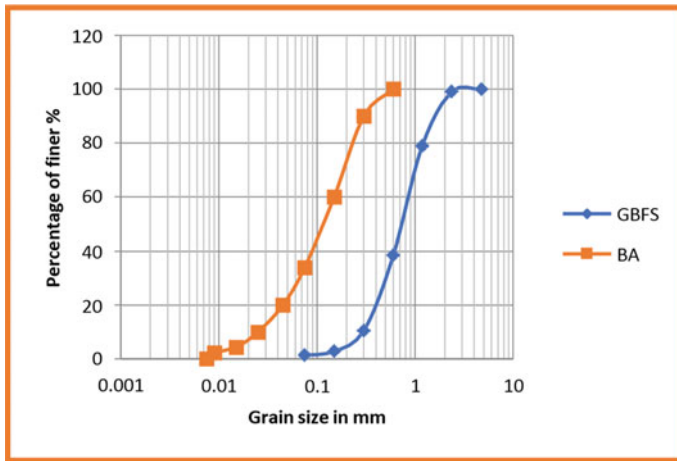


Fig. 3 Sieve size distribution of BA and GBFS

2.4 XRD Analysis of BA and GBFS

To understand the chemical composition of the materials (BA and GBFS), XRD test was conducted and shown in Figs. 4 and 5. In BA, quartz (Q) and cristobalite (C) were found to be present. Higher diffraction angle was observed between 15° and 35° (2θ).

In GBFS, the slag primarily consists of gehlenite (2CaOAl₂O₃SiO₂) and calcite (CaCO₃). “The slag is primarily vitreous because of the halo located in the range between 2θ values of 23 and 37°”. Similar pattern was observed in the GBFS of this study.

2.5 Testing Procedure

To find out the optimum mix of BA and GBFS, GBFS varied from 10 to 50% in the increment of 10%. Particle size distribution test, standard Proctor test, UCS and falling head permeability tests were performed as per the Indian standard code. To

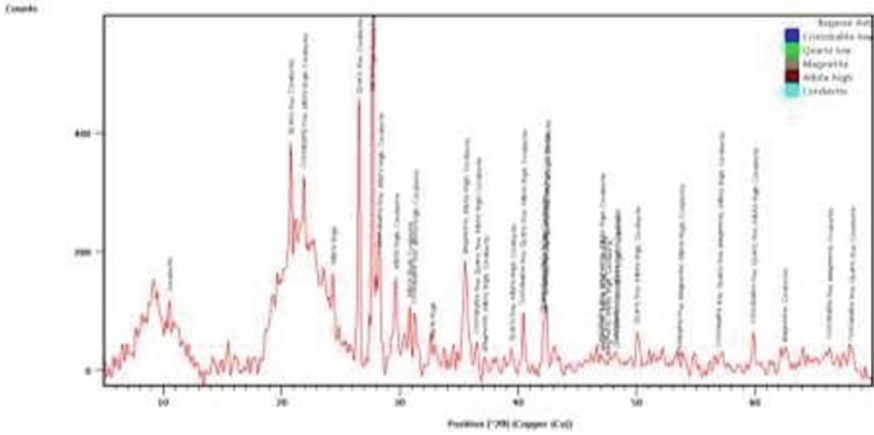


Fig. 4 X-ray diffraction patterns for BA

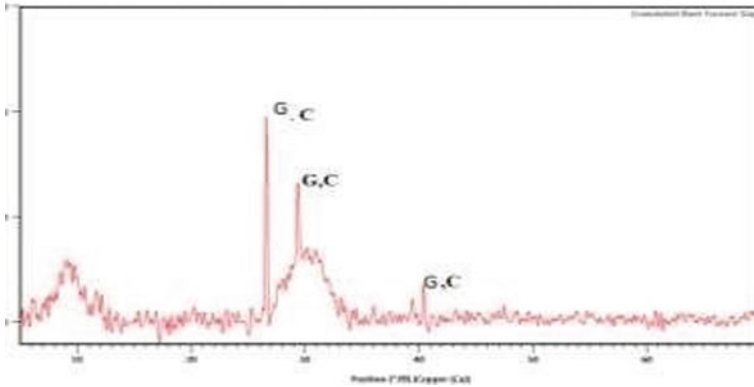


Fig. 5 X-ray diffraction patterns for GBFS

understand the effect of curing for the optimum mix, UCS test performed for 7, 14, 28 days curing. The tests results were compared with IRC and MoRTH specifications, to confirm the mix for the CTSB layer in the flexible pavement.

3 Discussion of Results

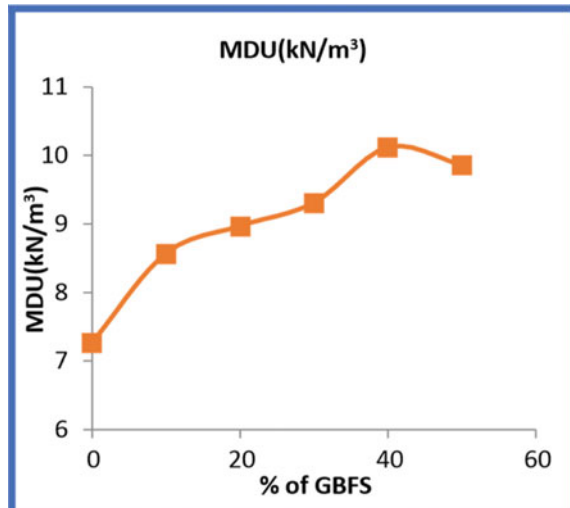
The test results of BA GBFS mix presented in Table 2. From Fig. 6, the maximum dry unit weight and UCS values are high for the 60% BA and 40% GBFS combination.

From the results, the MDU of BA increases from 7.27 kN/m³ at 54% OMC for the BA to 10.12 kN/m³ at 43% OMC for the optimum mix. Because of the higher particle

Table 2 Results of standard Proctor and UCS

FA + GBFS	OMC (%)	MDU (kN/m ³)	UCS (kN/m ²)	Permeability coeff Kv m/day
(100 + 0)%	54	7.27	46.62	0.06448
(90 + 10)%	53	8.57	57.12	0.086115
(80 + 20)%	50	8.97	63.21	0.119837
(70 + 30)%	47	9.31	66.93	0.509328
(60 + 40)%	43	10.12	78.69	1.595808
(50 + 50)%	46	9.86	67.67	5.09328

Fig. 6 Variation of MDU for BA with different contents of GBFS



size of GBFS blended with the BA attained the mix more density resulted increase MDU up to 40% of GBFS. The maximum dry unit weight is found to increase with increase in the contents of GBFS up to 40%, beyond which further addition of GBFS is found to reduce the maximum dry unit weight. This could be attributed to the fact that the GBFS is coarser than BA and therefore, when the GBFS is added up to 40%, the mix is rendered to be compact with less voids. Any more addition of GBFS in BA increases the voids in the mix and the maximum dry unit weight reduces (Fig. 7).

The UCS value increases up to 40% of GBFS due to the presence of gehlenite (2CaOAl₂O₃SiO₂), calcite (CaCO₃) in GBFS and Quarts (SiO₂) in BA that reacts with water to form CaO, SiO₂, H₂O (C–S–H) gel which is a cementitious compounds, namely calcium-silicate-hydrate. The decrease in UCS values above 40% of GBFS could probably be attributed to the formation of more voids as GBFS have more sand-sized particles (Fig. 8).

Falling head permeability test was performed for all the mix and represent in Table 2 and Fig. 9. It was observed that when GBFS increases, the permeability coefficient

Fig. 7 Variation of OMC for BA with different contents of GBFS

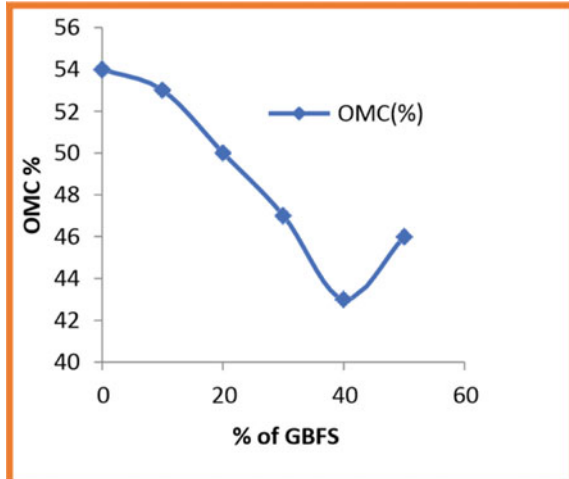
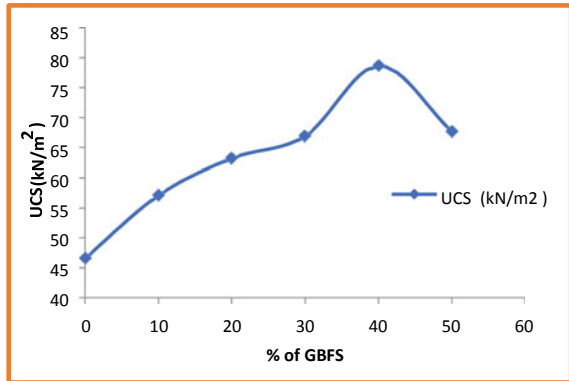


Fig. 8 Effect of GBFS on UCS



also increasing. It may be due to the more percentage of sand particle present in GBFS attributing the more voids in the mix.

4 Analysis of the Materials as CTSB Layer

4.1 Particle Size Requirements

Particle size requirements of CTSB layer as per IRC 37-2018 [20] and MoRTH are compared with the present study. The results were shown in Table 3 and Fig. 10.

From Table 3 and Fig. 10, the mix of 60% BA and 40% mix satisfy the particle size requirement as a CTSB layer for the flexible pavement.

Fig. 9 Coefficient of permeability for varying % of GBFS mix

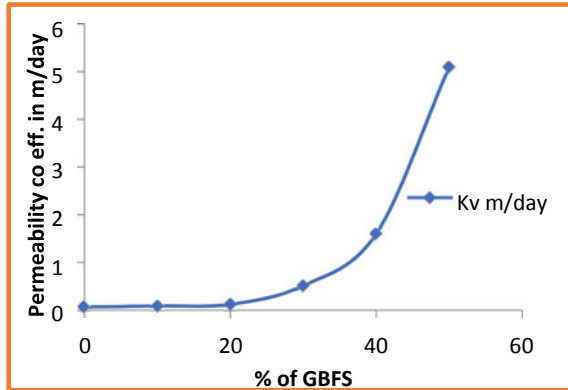
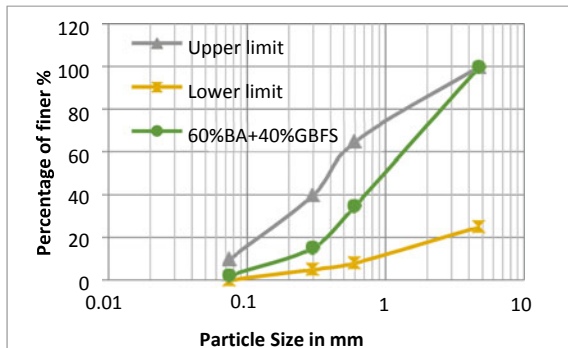


Table 3 Requirements of CTSB layer (grading IV of table 400-1, MoRTH)

Sieve size in mm	Upper limit of CTSB (as per MoRTH)	Lower limit of CTSB (as per MoRTH)	Present study cumulative % finer (N) (60%BA + 40%GBFS)
4.75	100	25	99.9
0.6	65	8	34.8048
0.3	40	5	15.2048
0.075	10	0	2.1892

Fig. 10 Particle size distribution curve for CTSB layer



4.2 UCS Requirements

The UCS test was performed for the optimum mix of 60% BA and 40% of GBFS for 7, 14 and 28 days to understand the curing effects and shown in Fig. 11. From the results, the strength of optimum mix increases with curing period clearly indicates that the strength gain. This is due to the pozzolonic reaction between the calcite

Fig. 11 UCS for different curing periods

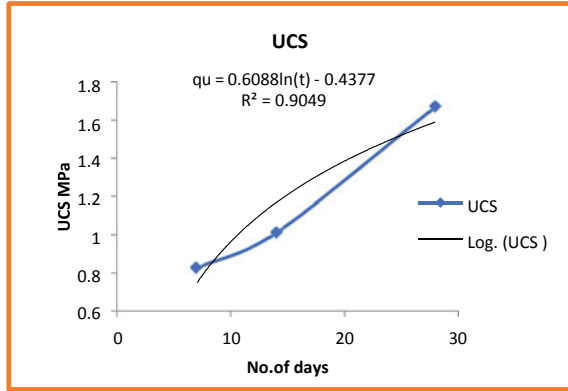


Table 4 Typical UCS values required for CTSB layer [20]

References	Typical UCS ranges (MPa)	Curing period	Applications
IRC 37-2018 [20] and IRC SP: (2018)	1.5–3	7 days	Cementitious sub-base layer (CTSB) (drainage or filter/separation layer)
IRC 37-2018 [20] and IRC SP: (2018)	0.75–1.5	7 days	Cumulative standard axial (CSA) less than 10 msa (CTSB with grading IV)
Present work	0.826	7 days	It can be used the roads
(60%BA + 40%GBFS)	1.67	28 days	With cumulative standard axial (CSA) less than 10 msa (Million standard axle)

(CaCO₃) in GBFS and Quarts (SiO₂) in BA forms C–S–H gel. Table 4 shows the UCS requirements of CTSB layer as per IRC 37-2018 [20] in section 7.3.

The generalised equation developed from the UCS values as shown in Fig. 11

$$q_u = 0.6088 \ln(t) - 0.4377 \tag{1}$$

4.3 Permeability Requirements

As per MoRTH [21] and IRC 37 [20] specifications, the required permeability is 300 m/day. Based on that it was observed that this mix may not be suitable as a drainage layer. It is clearly stated in the IRC and MoRTH specifications regarding CTSB layer; these material can be used in lower sub-base layer as a separation/filter

layer. In that case, any kind of geocomposite materials can be used in the upper layer for drainage purpose. (IRC 37-2018 [20], section 3.1).

5 Summary

Some predominant conclusions from the present experimental works are given below.

- The MDU of BA increases from 7.27 kN/m³ at 54% OMC to 10.12 kN/m³ at 43% OMC for the optimum mix.
- The UCS value increases up to 40% of GBFS due to the formation of calcium-silicate-hydrate.
- The permeability coefficient increases with increasing GBFS mix due to more percentage of sand particle present in GBFS attributing the more voids in the mix.
- From the strength characteristics, 60% of BA and 40% of GBFS found as an optimum combination and can be used as CTSB material for low-volume roads.

References

1. Basic Road Statistics in India, 2019–20, Ministry of Road Transport and Highways, Transport Research Wing, Government of India, New Delhi, pp 29–30
2. Anupam AK, Kumar P, Ransinchung GD (2013) Use of various agricultural and industrial waste materials in road construction. *Procedia-Soc Behav Sci* 104:264–273
3. Anupam AK, Kumar P, Ransinchung GD (2017) Study on performance and efficacy of industrial waste materials in road construction: fly ash and bagasse ash. *Airfield and Highway Pavements*, ASCE, pp 45–56
4. Amu O, Solomon O, Olawale O (2011) Geotechnical properties of lateritic soil stabilized with sugarcane straw ash. *Am J Sci Ind Res* 2(2):323–331
5. Jasvir S, Harpreet SM (2017) Soil stabilization using fly ash and rice husk ash. *Int J Innov Res Sci Eng Tech* 6(7):14412–14419
6. Chittaranjan M, Vijay M, Keerthi D (2011) Agricultural wastes as soil stabilizers. *Int J Earth Sci Eng* 4(6)(Special Publication):50–51
7. Laxmikant Y, Rajesh KT, Dharamveer S (2011) Comparison of fly ash and rice husk ash stabilized black cotton soil. *Int J Earth Sci Eng* 4(6)(Special Publication):42–45
8. Muazu MA (2007) Evaluation of plasticity and particle size distribution characteristics of bagasse ash on cement treated lateritic soil. *Leonardo J Sci* 10:137–152
9. Osinubi KJ, Thomas S (2007) Influence of compactive effort on bagasse ash treated soils. *Nigerian J Soil Environ Res* 7:92–101
10. Sabat AK (2012) Utilization of bagasse ash and lime sludge for construction of flexible pavements in expansive soil areas. *Electron J Geo Eng (EJGE)* 17:1037–1046
11. Nuntachai C, Napongsatorn L, Chai J (2009) Development of bagasse ash as a pozzolanic material in concrete. *Asian J Energy Environ* 10:149–159
12. Hailu B (2011) Bagasse ash as cement replacing material. M.Sc thesis (unpublished), Addis Ababa University, Addis Ababa
13. Havanagi VG, Sinha AK, Mathur S, Prasad P (2008) Experimental study on the use of copper slag wastes in Embankment and pavement construction. Symposium on engineering of ground & environmental geotechnics (S EG2), Hyderabad, Feb 29–March 1, 2008

14. Patel S, Vakharia PP, Raval SM (2007) Use of copper slag and fly ash mix as subgrade and embankment fill material. *J Indian Highw* 35(11):17–22
15. Yadu L, Tripathi RK (2013) Effects of granulated blast furnace slag in the engineering behaviour of stabilized soft soil. *Procedia Eng* 51:125–131
16. Kavitha G, Krishnamurthy, Srinivasamurthy BR (2015) Laboratory permeability testing of granular slag and gravel sub base courses (GSB). In: 6th international conference on structural engineering and construction management 2015, Kandy, Sri Lanka, 11th–13th Dec 2015
17. Puzara R, Sachdeva SN (2017) Laboratory studies on Granular sub base grade-I. *J Basic Appl Eng Res* 4(1):64–66. ISSN: 2350-0077; e-ISSN: 2350-0255
18. Gonawala RJ, Khapre S, Kumar R, Chauhan AK (2019) Suitability of EAF slag and GGBFS mix as cementitious base/subbase layer for low volume road construction. *Inter J Geotech Eng.* <https://doi.org/10.1080/19386362.2019.1621458>
19. Bahurudeen A, Wani K, Basit M, Santhanam M (2016) Assesment of pozzolanic performance of sugarcane bagasse ash. *ASCE J Mat Civ Eng* 28(2):1–11
20. IRC, Guidelines for the design of flexible pavements, IRC: 37-2018, Indian Roads Congress
21. MORTH (2013) Specifications for road and bridge works, Ministry of Road Transport and Highways, Government of India

Strength Characteristics of Copper Slag and Lime Stabilized Clayey Soil



Aditya D. Ahirwar and H. S. Chore

Abstract Flexible pavement is multi-layered structure which helps in distributing traffic load over wider area of subgrade. Stability of pavement depends on strength of the subgrade soil. Non-availability of suitable material for construction of pavement is one of the major reasons which hampers the completion of the highway construction project. The disposal of waste generated in various industries like steel and copper is a major environmental and ecological issue. These waste materials can be used effectively in pavement construction because they have the potential to improve the strength of the subgrade soil. Utilization of such material to enhance strength characteristics of the subgrade soil will not only help in reducing pavement thickness but also will provide substitute for conventional material either independently or as stabilizer. Locally available soft clay was stabilized with copper slag and experimental investigations were carried out to evaluate consistency limits, compaction characteristics and strength characteristics of different combination of mixes. The strength of clay is found to increase with the addition of copper slag up to 30%. California bearing ratio (CBR) of various mixes increases with addition of lime.

Keywords Clayey soil · Copper slag · CBR

1 Introduction

The main concern in the construction sector is the scarcity of suitable soil for the construction of transportation facilities. As a result, alternative materials must be discovered. Rapid industrialization, on the other hand, has a negative impact on the environment because it generates large amounts of waste material, such as steel making slag, copper slag and zinc slag. Copper slag is a by-product of the smelting

A. D. Ahirwar (✉) · H. S. Chore
Department of Civil Engineering, Dr. B. R. Ambedkar National Institute of Technology,
Jalandhar 144011, India
e-mail: ahirwarad.ce.19@nitj.ac.in

H. S. Chore
e-mail: chorehs@nitj.ac.in

© The Author(s), under exclusive license to Springer Nature Singapore Pte Ltd. 2023
A. K. Agnihotri et al. (eds.), *Proceedings of Indian Geotechnical and Geoenvironmental Engineering Conference (IGGEC) 2021, Vol. 1*, Lecture Notes in Civil Engineering 280,
https://doi.org/10.1007/978-981-19-4739-1_50

531

and refining process. Huge quantity of such waste is disposed of near the processing units and plants which cause environmental problems.

According to a review of the literature, various experimental investigations have been carried out in the past to evaluate the performance of problematic soft soil stabilized with various industrial by products. Gorai and Jana [1] and Murari et al. [2] highlighted the characteristics of the copper slag along with its possible applications. Ravi et al. [3] and Qureshi et al. [4] explored the viability of utilizing the copper slag as a stabilizer. Shahiri and Ghasemi [5] and Kumar et al. [6] inspected the effect of addition of copper slag on Atterberg's limits, California bearing ratio, compaction characteristics of expansive soil. Bharati and Chew [7] concluded that copper slag can be utilized to treat problematic marine clay.

Kavisri et al. [8] and Nelson and Parvathy [9] concluded that addition of copper slag as stabilizer increases the strength of the soil. After identifying some of the gaps in available literature and identifying the problems related to utilization of problematic soft clay and disposal of waste by products, experimental investigations were conducted to evaluate the compaction and strength properties of soft clay after addition of copper slag as the stabilizer.

2 Material and Method

In the existing study, the soft clay was admixed with the different proportions of copper slag (10, 20, 30 and 40%). The soil used for the project was brought from local supplier. The geotechnical properties of different combinations of mixes were found out. The geotechnical investigations involved the determination of plasticity characteristics, compaction characteristics and strength (CBR) of clay–copper slag and clay–slag–lime composite mix. Table 1 shows particulars of mixes, considered in the present work.

Table 1 Different combination of mixes

S. No.	Property	Variables
1	Plain clayey soil (PC)	–
2	Clay–copper slag mix	(a) Copper slag (10, 20, 30 and 40%)
3	Clay–copper slag–lime mix	(a) Copper slag (10, 20, 30 and 40%) (b) Lime (4, 8 and 12%)

3 Discussion of Results

The experimental programme comprises of conducting the preliminary tests to attain the engineering properties of clay. Table 2 shows geotechnical properties of the clay used in the study.

Consistency limits of various combinations of mixes were evaluated using Atterberg’s limit test. Figure 1 illustrates the variation in index properties such as LL, PL and PI of various mixes containing copper slag.

From Fig. 1, it can be observed that the LL, PL and PI reduce after addition of copper slag. The reduction in the PI is an indication of an improvement of soil property.

The MDD and OMC are the two most important factors for determining geotechnical properties of soil. Attempt has been made to determine the effect of addition

Table 2 Geotechnical properties

S. No.	Property	Value
a	LL: liquid limit (%)	154.0
b	PL: plastic limit (%)	43.5
c	OMC: optimum moisture content (%)	36.9
d	MDD: maximum dry density (gm/cc)	1.28
e	CBR: California bearing ratio (%)	6.02

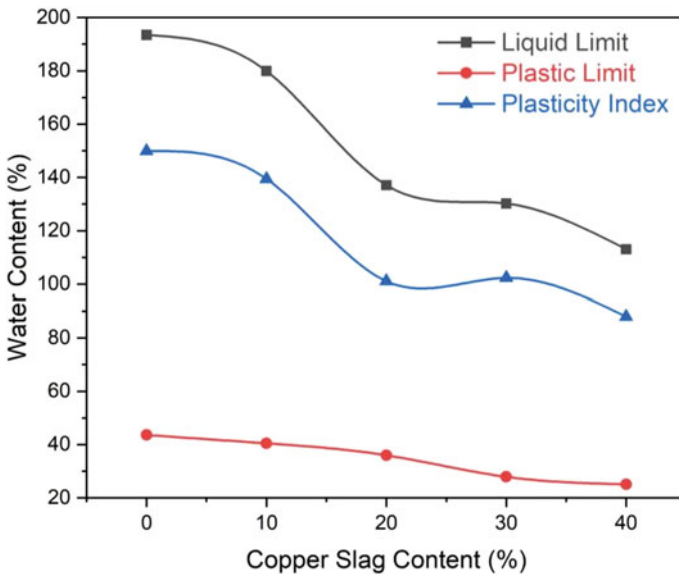


Fig. 1 Effect of addition of copper slag on LL, PL, PI

of slag on compaction properties of various mixes. With increase in proportion of copper slag, MDD of the composite mix increases, OMC decreases (Fig. 2).

The laboratory work was extended to gauge the effect of addition of lime on OMC and MDD of various combinations of clay–slag–lime mixes. Result of the study (Fig. 3a and b) indicates that, with addition of copper slag, OMC decreases, whereas MDD increases.

The study also seeks to ascertain the effect of slag addition on the CBR of various mixes. Figure 4 shows the variation in CBR of soil–copper slag mix. Enhancement in CBR of composite mixes is observed with the addition of slag up to 30%.

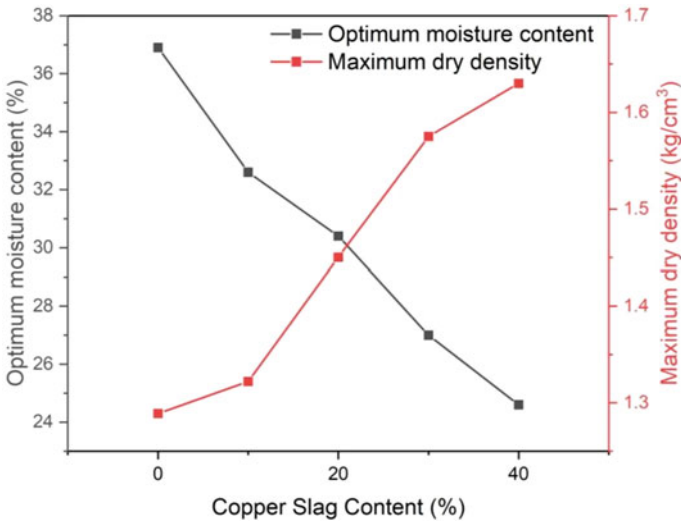


Fig. 2 Variation in OMC and MDD of soil-slag composite mix

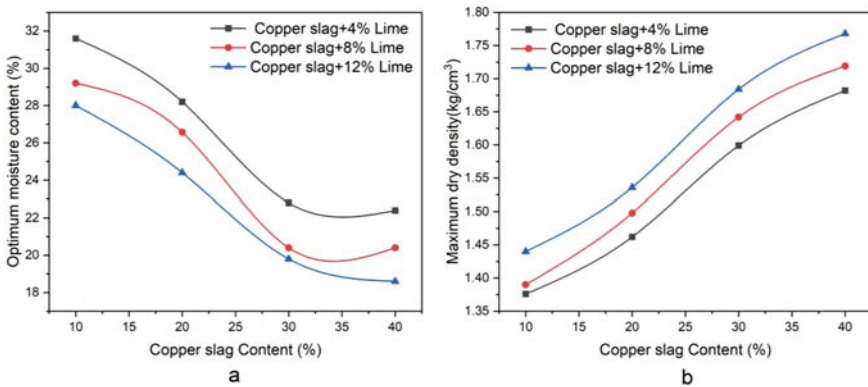


Fig. 3 Variation in compaction characteristics of soil–slag–lime mix

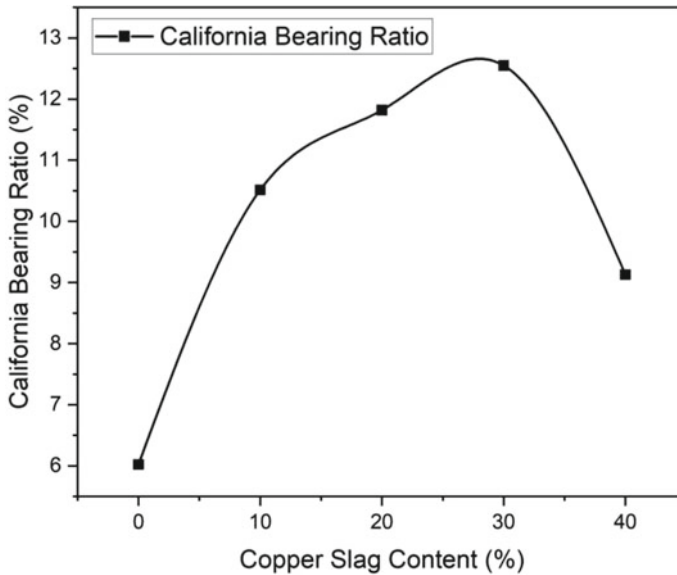


Fig. 4 Effect of addition of copper slag on CBR

Present study also aims to govern the effect of addition of lime on CBR of various mixes. Copper slag is added in magnitude of 10, 20, 30 and 40% whereas lime was added in the range of 4, 6 and 8%. Figure 5 depicts the effect of addition of copper slag and lime on CBR of the various mixes. After comparing Figs. 4 and 5, it can be concluded that CBR of the various combination of mixes increases with addition of lime.

Figure 5 indicates that, with addition of copper slag to soil stabilized with 4% lime, CBR increases up to increase in copper slag content up to 30%, thereafter decrease in CBR is observed. Similar pattern can be seen in case of soil stabilized with 6 and 8% of lime.

4 Summary and Conclusion

Following conclusions can be deduced from the laboratory investigations conducted on clay samples stabilized with copper slag and lime:

1. The values of the index properties (LL, PL and PI) of composite mix decrease after addition of slag, thereby making the composite mix more workable.
2. Addition of slag increases MDD of soil–slag composite mix and reduces OMC.
3. With addition of lime to soil–copper slag mix, MDD of the mix increases and OMC decreases.
4. The CBR of the soil–copper slag mixes increase with addition of slag up to 30%.

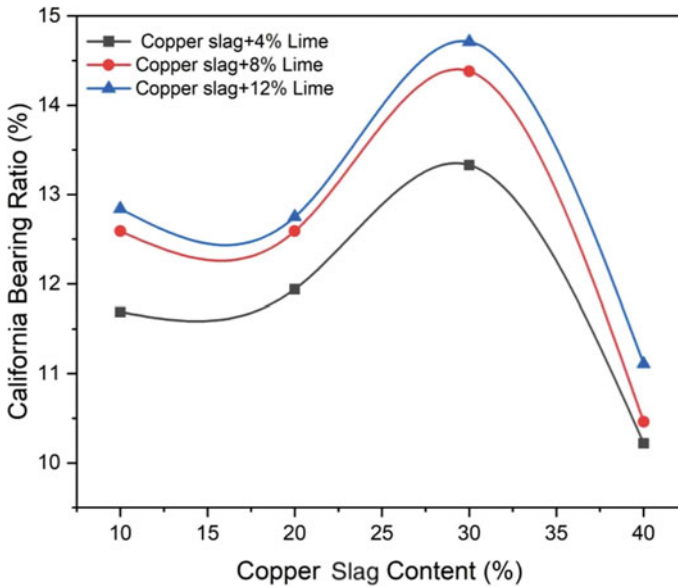


Fig. 5 Effect of addition of copper slag and lime on CBR

5. Lime improves CBR of the composite mix.
6. The CBR of the lime treated clayey soil increases with addition of slag up to 30%.

Thus, industrial waste materials such as copper slag can prove as the sustainable road construction material to stabilize clayey soil. This will not only provide an alternate solution for safe disposal of the waste by-product, but will also will provide suitable alternative to raw materials which would have been used in highway construction.

References

1. Gorai B, Jana RK (2003) Characteristics and utilization of copper slag—a review. *Resour Conserv Recycl* 39(4):299–313
2. Murari K, Siddique R, Jain KK (2015) Use of waste copper slag, a sustainable material. *J Mater Cycles Waste Manage* 17(1):13–26
3. Ravi E, Udhayasakthi R, Vadivel TS (2016) Enhancing the clay soil characteristics using copper slag stabilization. *J Adv Chem* 12(26):5725–5729
4. Qureshi MA, Mistry HM, Patel VD (2015) Improvement in soil properties of expansive soil by using copper slag. *Int J Adv Res Eng Sci Technol* 2(07):125–130
5. Shahiri J, Ghasemi M (2017) Utilization of soil stabilization with cement and copper slag as subgrade materials in road embankment construction. *Int J Transp Eng* 5(1):45–58
6. Kumar PR, Kumar PSP, Maheswari G (2017) Laboratory study of black cotton soil blended with copper slag and fly ash. *Int J Innov Res Sci Eng Technol* 6(2):19601967

7. Bharati SK, Chew SH (2016) Geotechnical behavior of recycled copper slag-cement-treated Singapore marine clay. *Geotech Geol Eng* 34(3):835–845
8. Kavisri M, Senthilkumar P, Gurukumar MS, Pushparaj KJ (2018) Experimental study on effects of stabilization of clayey soil using copper slag and GGBS. *Rasayan J Chem* 11:111–117
9. Nelson AA, Parvathy S (2016) Study on the effect of copper slag on lime stabilized clay. *Int J Eng Res Technol* 5(9):536–540

Influence of Fines Content on the Strength and Compaction of the Poorly Graded Soil



Vaibhav Sharma, Arvind Kumar, Pritesh Patel, and Dheeraj Kumar

Abstract This paper is aimed to study the effect of fines content on the compaction and strength aspects of soil. Fine soil (Kaolin clay) and coarse soil (sand) were used in this paper. The fines content was varied as 0, 15, 20, 25, 30, 35, 40, 45, 50, 55, 60, 65, 70, 75, 80, 85, and 100%, by weight of the mix. To study compaction characteristics, modified proctor compaction test was performed. To study the strength aspect, CBR tests were carried out. From the test results it was discovered that the optimum moisture content (OMC) of the mix kept on increasing as the fines content was increased in the mix. Moreover, the maximum dry unit weight (MDUW) first increases up to the fines content of 30% and then starts decreasing, after adding more fines to the mix. In addition to this, CBR values also show increasing trend until the fines content reaches 30–35% and then it starts decreasing, afterwards. This trend of CBR was similar for both the un-soaked and soaked samples.

Keywords Soil stabilization · Poorly graded sand · CBR · Compaction · Optimum moisture content · Maximum dry density

1 Introduction

Subgrade has an imperative affect for the economical construction of pavement. In practice, it is often advised to use locally available material. This material is normally collected and transported from the nearby borrow pits. This, as a consequence, results in a low lying areas. The leftover soil at these sites may have poor geotechnical properties. So, in order to utilize these soils, soil stabilization techniques can become very handy.

V. Sharma (✉)

School of Civil Engineering, Lovely Professional University, Phagwara, Punjab, India
e-mail: civil.vaibhav.sharma@gmail.com

A. Kumar · P. Patel · D. Kumar

Dr. B R Amberkar National Institute of Technology, Jalandhar, Punjab, India
e-mail: agnihotriak@nitj.ac.in

Most of the studies pertaining to soil stabilization are done to stabilize the soil type which is clayey in nature. Chen and Lin [1] used sewage sludge ash, Pourakbar et al. [2] used ultrafine palm oil fuel and cement, Priyadarshee et al. [3] used tyer crumbles, fly ash and cement, Kumar and Gupta [4] used rice husk ash (RHA), pond ash (PA), cement and polypropylene fibers, Ta'negonbadi and Noorzad [5] used lignosulfonate, Etim et al. [6] used lime and iron ore tailing admixtures, Dalal et al. [7] used agricultural and industrial waste, Dahale et al. [8] used lime and fly ash, Ghadir and Ranjbar [9] used geopolymer and Portland cement, Gupta et al. [10] used PA and RHA, Patel et al. [11] reviewed various type of stabilizing agents, Gobinath et al. [12] used a novel SiO_2 combination as a stabilizing agent, Ghavami et al. [13] used sodium chloride and cement-kiln dust and Mohanty et al. [14] used an industrialized by-products like ground granulated blast furnace slag (GGBS), fly ash and cement clinker as a stabilizing agent for dispersive soil. It can be observed that most of the studies are focused on stabilizing problematic soils by using natural, industrial by-product or binder element (cement).

However, poorly-graded granular soils are mostly found through the coastline and floodplains of waterway gorges. Cementation is one technique which is often applied to improve its condition [15]. Therefore, very limited effort has been offered to advance the mechanical features of poorly graded soils [15, 16]. Hence, keeping this in view the present study is undertaken. In this study, the effect of fines content on the compaction and strength characteristics of poorly graded soil is studied. The fines content was varied as 0, 15, 20, 25, 30, 35, 40, 45, 50, 55, 60, 65, 70, 75, 80, 85, and 100%, by weight of the mix. To study compaction characteristics, modified proctor compaction test was performed. To study the strength aspect, California bearing ratio (CBR) tests were carried out.

2 Materials

Sand (coarse soil) used in the study (Fig. 1a) was obtained from Nasrula (Punjab), in which all the grain sizes are greater than 75μ . Kaolin was used as a fine soil in this study (Fig. 1b). It has smooth texture and particles sizes were less than 75μ . The physical properties of sand are shown in Table 1. Consistency limits of fine soil are presented in Table 1. The grain-size distribution of sand and Kaolin clay is presented in Fig. 2.

3 Testing Program and Sample Preparation

Testing program consists of two stages. In the first stage, preliminary tests were carried out to obtain the physical properties of the soils. In second stage, the compaction and the strength characteristics were obtained by conducting Modified

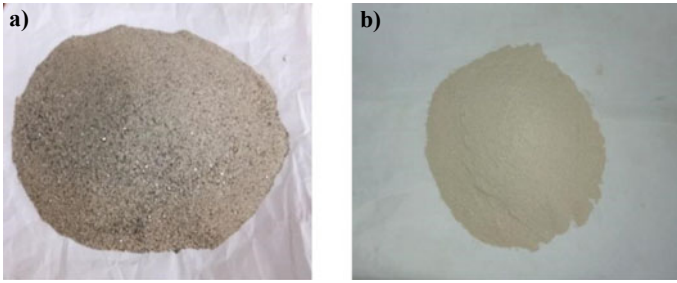


Fig. 1 Appearance of soils used

Table 1 Properties of soils used

Property	Sand	Kaolin clay
Specific gravity (G)	2.67	2.73
MDUW, γ_d (kN/m^3)	17.50	18.40
OMC, w (%)	8.50	18.00
Uniformity coefficient, C_u	2.15	–
Curvature coefficient, C_C	0.99	–
Classification	<i>SP</i>	<i>CI</i>
Liquid limit, W_L (%)	–	41.00
Plastic limit, W_P (%)	–	21.00

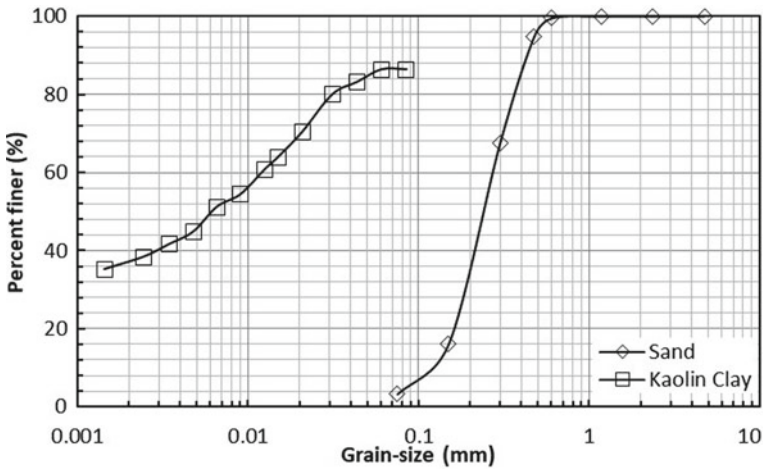


Fig. 2 Grain-size distribution of soils used

Table 2 Testing program

Mix type		Characteristics	Total tests
S0C100	S55C45	Liquid limit, Plastic limit, Compaction, Soaked CBR Un-soaked CBR	85
S15C85	S60C40		
S20C80	S65C35		
S25C75	S70C30		
S30C70	S75C25		
S35C65	S80C20		
S40C60	S85C15		
S45C55	S100C0		
S50C50			

Note S and C stands for Sand and Clay, respectively (%)
Curing time for soaked test = 4 days

Proctor compaction [17] and CBR [18] tests, respectively, as per the Indian standards. Testing program is presented in Table 2.

Depending on the MDUW of the mix, the required amount of the soil mix can be calculated. Knowing the volume of the CBR mold, the mass of the soil mix can be obtained. It can be done by simply multiplying the MDUW with the volume of the mold. After obtaining the weight of the whole mix, the weight of its individual ingredients can be calculated.

In this paper, first the sand and kaolin clay were mixed in dry condition until it gives a uniform appearance. Then required amount of water was added to the mix, depending on its OMC. The soil sample was prepared using the relevant standard [18].

4 Results and Discussion

In this section, the results obtained from consistency, compaction and CBR test are presented and discussed.

4.1 Consistency Characteristics

Figure 3 shows the deviation of liquid and plastic limit of soil mixed with fines content. It is clear from Fig. 3 that the mix is non-plastic in nature up to 30% fines content and on further increasing the fines content, that is, between 30 and 35%, it starts gaining some plasticity. Thereafter, it goes on increasing almost linearly. With no fines content in coarse soil, the liquid limit is 0% and on addition of fines content in the coarse soil, it shows almost linear increment. Liquid limit of coarse soil is increasing with increases of fines content because fine particle has more surface area and it required more water to wet their surface. As fines content increases, plasticity index increases, which means plasticity of coarse soil can be increased by increase

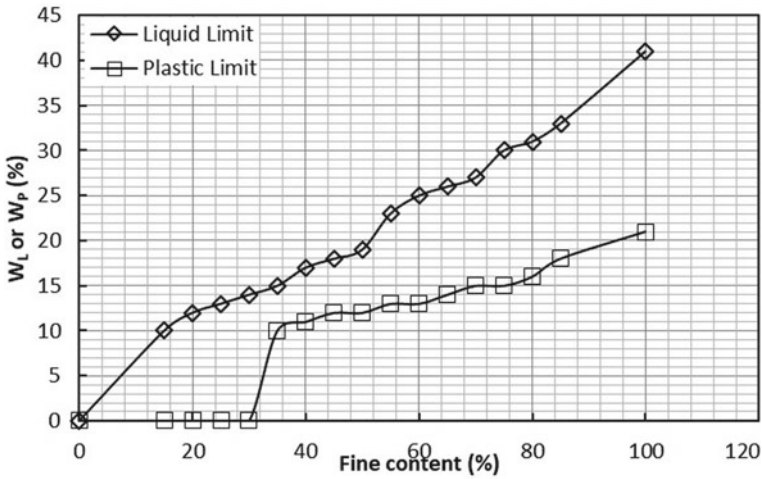


Fig. 3 Variation of liquid and plastic limit with fines content

the fines content. Up to 30% fines content soil behaves non-plastic. This may be due to the fact that the content of fines is very less and the properties of coarser soil dominated until the fines content reaches 25%. Moreover, the role of fines up to this content is just to fill the voids and nothing else. Soil starts gaining plasticity with further increase in fines content. Thereafter, continuous increase in Plasticity has been observed till fines content in soil reaches 100%.

4.2 Compaction Characteristics

Figure 4 shows the relation of MDUW and OMC. When fines content increases from 0 to 30%, MDUW increased because the voids in coarse soil gets filled by the fines content and with further increase in fines content, the void ratio is increasing. Hence, results in decrease in MDUW. It is clearly visible that maximum of MDUW has been achieved when 30% of finer content is added in coarse soil that is 21.1 KN/m³, and the corresponding OMC is 11.5%. When fines content increases in coarse soil then fine particle fill the voids and it result in to increase in the surface area. When surface area increases then water required in wetting the soil is also increased. Figure 4 is showing same behavior when finer content increases optimum moisture content is increases linearly. The OMC is consistently increasing as the fines content increases, and is due to increase in surface area and water required in wetting the soil is also increased.

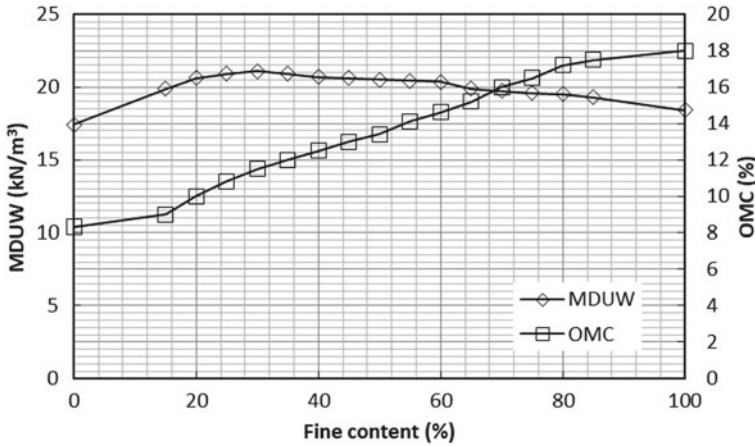


Fig. 4 Variation of MDUW and OMC with fines content

4.3 Strength Characteristics

Figure 5 displays the variation of soaked and un-soaked CBR values obtained for different mixes. From these figures, it can be perceived that with the accumulation of fine soil in coarse soil, the mix soil starts resisting more loads even at same penetration value. This increase in resistance is increasing till 35% fines content has been added to the coarse soil. On further increasing the fines content, i.e., by 5%, there is not much significant change in the resistance offered, but further increase in fines content starts decreasing the resistance offered at same penetration value. Unsoaked CBR value obtained for coarse soil is equal to 9.02% analogous to 2.5 mm permeation. The strength is found to surge with escalation in the proportion of fines content, thus 35% fine proportion is the particular value where unsoaked CBR displayed an improvement of 76.94% over plain soil. An increase in strength can significantly lessen the pavement’s overall depth.

Furthermore, soaked CBR value for plain coarse soil is equal to 6.5% corresponding to 2.5 mm permeation. Soaked strength is also found to surge with the surge in the fraction of fines content, thus 35% fine fraction is the particular value where strength improvement of 86.15% was observed than plain soil.

Moreover, on comparing both the values, it can be observed that for all the mix proportions, soaked strength is observed to be lesser than the un-soaked CBR. It is because of the fact that in soaked condition, i.e., due to submergence under water, the moisture content of the soil sample increases which results in the increase in lubricating effect. Due to this increase in lubricating effect, the resistance offered to the penetration of plunger is decreased and hence, results in lower CBR value than the unsoaked condition.

Naeini and Baziar [19] studied the effect of fines content on steady-state strength of mixed and layered samples of a sand, which is similar to this study. Unlike the present

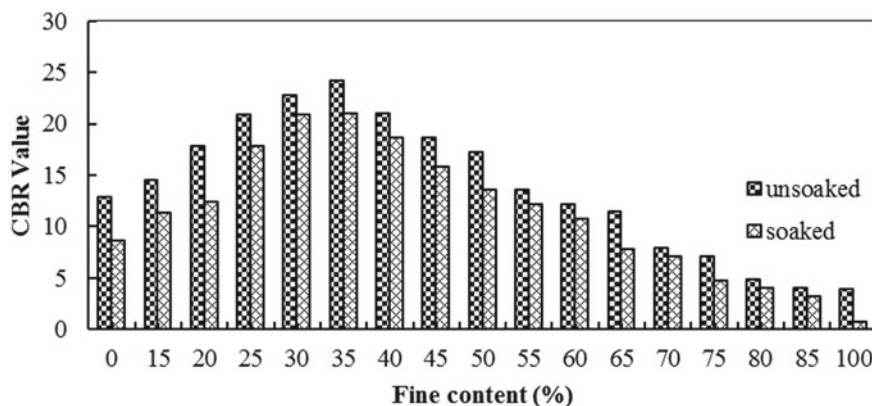


Fig. 5 Unsoaked and soaked CBR value obtained for various mixes

study, undrained triaxial compression tests were conducted to study the strength aspect of the soil. This study also pointed out that up to fine content of 35%, the peak as well as residual strength changes its behavior, which is similar to this study. However, the type of material may affect the result significantly. Therefore, it is advised to conduct preliminary test to arrive at any conclusions.

5 Conclusions

A study has been carried out to examine the effect of fines content on the consistency, compaction and CBR of coarse soil. From the experiments, following conclusions can be drawn:

- Up to 30% finer content, mix is behaving non-plastic in nature. After adding 30% fines content, it became plastic and plastic limit reached 10% at 35% finer content. Liquid limit shows a linear variation with addition of fines in coarse soil. Maximum liquid and plastic limits are 41% and 21%, respectively, and minimum for both are 0%.
- By introducing finer content in sand maximum dry density is first increasing up to 30% and thereafter starts decreasing, i.e., maximum of maximum dry density is 21.1 kN/m³ and maximum dry density at 0% finer content is 17.4 kN/m³, and at 100% finer content is 18.4 kN/m³.
- By introducing finer content in sand optimum moisture content is increases linearly, i.e., minimum moisture content is 8.5% and maximum is 18%.
- Un-soaked and Soaked strength obtained for coarse soil is equal to 9.02% and 6.5%, respectively. The strength is found to surge with surge in the fraction of fines content, thus 35% fine fraction is the particular value where strength displayed and improvement of 76.94% and 86.15%, respectively, than the plain soil.

Although study is carried out using CBR tests, which has its own limitations. It is a well-known fact that this test does not reflect whether the road is multi-lane single or dual carriage way and does not consider the result of heavier loads and their frequency in the wheel load variety. In addition, total thickness of pavement is obtained corresponding to different intensity of traffic and subgrade's CBR value. Furthermore, to have a more economical pavement design; thickness of subbase, base and surfacing must be calculated separately. However, the results obtained from the study provides a fair share of information which will guide the designers that the fines content can greatly influence the strength aspect of the soil.

References

1. Chen L, Lin DF (2009) Stabilization treatment of soft subgrade soil by sewage sludge ash and cement. *J Hazard Mater* 162(1):321–327. <https://doi.org/10.1016/j.jhazmat.2008.05.060>
2. Pourakbar S, Asadi A, Huat BBK, Fasihnikoutalab MH (2015) Stabilization of clayey soil using ultrafine palm oil fuel ash (POFA) and cement. *Transp Geotech* 3:24–35. <https://doi.org/10.1016/j.trgeo.2015.01.002>
3. Priyadarshree A, Gupta D, Kumar V, Sharma V (2015) Comparative study on performance of tire crumbles with fly ash and kaolin clay. *Int J Geosynth Gr Eng.* 1(4):1–7. <https://doi.org/10.1007/s40891-015-0033-3>
4. Kumar A, Gupta D (2016) Behavior of cement-stabilized fiber-reinforced pond ash, rice husk ash-soil mixtures. *Geotext Geomembranes* 44(3):466–474. <https://doi.org/10.1016/j.geotextmem.2015.07.010>
5. Ta'negonbadi B, Noorzad R (2017) Stabilization of clayey soil using lignosulfonate. *Transp Geotech* 12:45–55. <https://doi.org/10.1016/j.trgeo.2017.08.004>
6. Etim RK, Eberemu AO, Osinubi KJ (2017) Stabilization of black cotton soil with lime and iron ore tailings admixture. *Transp Geotech* 10:85–95. <https://doi.org/10.1016/j.trgeo.2017.01.002>
7. Dalal SP, Patel R, Dalal PD (2017) Effect on engineering properties of black cotton soil treated with agricultural and industrial waste. *Mater Today Proc* 4(9):9640–9644. <https://doi.org/10.1016/j.matpr.2017.06.240>
8. Dahale PP, Nagarnaik PB, Gajbhiye AY (2017) Engineering behavior of remolded expansive soil with lime and flyash. *Mater Today Proc* 4(9):10581–10585. <https://doi.org/10.1016/j.matpr.2017.06.423>
9. Ghadir P, Ranjbar N (2018) Clayey soil stabilization using geopolymer and Portland cement. *Constr Build Mater* 188:361–371. <https://doi.org/10.1016/j.conbuildmat.2018.07.207>
10. Gupta D, Kumar A, Kumar V, Sharma V (2019) Performance of pond ash and rice husk ash in clay: a comparative study. pp 145–153. https://doi.org/10.1007/978-981-13-7017-5_17
11. Patel P, Kumar A, Sharma V (2019) Influence of admixtures on the CBR value of soil: a review. *Lect Notes Civ Eng* 31:265–271. https://doi.org/10.1007/978981-13-7010-6_26
12. Gobinath R, Raja G, Prasath E, Shyamala G, Viloría A, Varela N (2020) Studies on strength characteristics of black cotton soil by using novel SiO₂ combination as a stabilizing agent. *Mater Today Proc* 27:657–663. <https://doi.org/10.1016/j.matpr.2020.01.597>
13. Ghavami S, Jahanbakhsh H, Saeedi Azizkandi A, Moghadas Nejad F (2021) Influence of sodium chloride on cement kiln dust-treated clayey soil: strength properties, cost analysis, and environmental impact. *Environ Dev Sustain* 23(1):683–702. <https://doi.org/10.1007/s10668-020-00603-6>
14. Mohanty S, Roy N, Singh SP, Sihag P (2021) Effect of industrial by-products on the strength of stabilized dispersive soil. *Int J Geotech Eng* 15(4):405–417. <https://doi.org/10.1080/19386362.2019.1654281>

15. Hossein Rafiean A, Najafi Kani E, Haddad A (2020) Mechanical and durability properties of poorly graded sandy soil stabilized with activated slag. *J Mater Civ Eng* 32(1):04019324. [https://doi.org/10.1061/\(asce\)mt.1943-5533.0002990](https://doi.org/10.1061/(asce)mt.1943-5533.0002990)
16. Basha EA, Hashim R, Mahmud HB, Muntohar AS (2005) Stabilization of residual soil with rice husk ash and cement. *Constr Build Mater* 19(6):448–453. <https://doi.org/10.1016/j.conbuildmat.2004.08.001>
17. IS-2720 (PART-8) Methods of test of soils: determination of water content-dry density relation using heavy compaction
18. IS-2720 (Part-16) Methods of test of soils: laboratory determination of CBR
19. Naeini SA, Baziar MH (2004) Effect of fines content on steady-state strength of mixed and layered samples of a sand. *Soil Dyn Earthq Eng* 24(3):181–187. <https://doi.org/10.1016/j.soildyn.2003.11.003>

Modification of Engineering Properties of Soil Using Waste Materials: A Review



Alka Shah  and Tejas Thaker

Abstract In recent decades, changes in lifestyle, industrialization, urbanization, migration, etc., affected the ecosystem of the earth due to the generation of post-consumer wastes. The amount of waste generation is leading to a huge challenge for the disposal of wastes. The direct dumping of wastes in water bodies and land created a major impact on ambient. A refined analysis was carried out based on studies available on the effect of natural and synthetic waste materials on the geotechnical properties of soils. This paper presents the review of various types of wastes used as an admixture with soil and its behavior. Looking to the problem of waste dumping, one of the potential use of wastes in developing country is to utilize wastes in ground improvement looking to the large-scale infrastructure construction. The addition of wastes in different amount, form, etc., shows the significant modification in the properties of virgin soil.

Keywords Soil · Modification · Natural waste · Synthetic wastes

1 Introduction

Development of facilities plays significant role in the growth of any country but one negative aspect of it is the generation of different waste like municipal solid waste, E-waste, plastic waste, construction and demolition waste and disposal issue of such wastes. There are negative impacts to the environment due to the disposal of wastes. As per CPCB report 2019, 152,076 TPD solid waste generated in India and also per capita waste generation has increased at an exponential rate (0.26–0.85 kg/day). Moreover, 2019 report of Central Pollution Control Board shows that around 26,000 tones of plastic waste generated in India every day and out of which

A. Shah (✉)

Nirma University and Pandit Deendayal Energy University, Ahmedabad, Gujarat, India
e-mail: alkamurarishah@gmail.com

T. Thaker

Pandit Deendayal Energy University, Ahmedabad, Gujarat, India

10,400 tones remains uncollected from the source and littered [1]. As per the report published in UNPD, “The world produces around 300 million tons of plastic waste, only 9% of the generated plastic waste is recycled, ~ 14% collected for recycling while the rest reaches the ocean annually” [2]. E-waste, C&D waste also joining the community. Generally, due to unawareness, for easy disposal and system the wastes are directly dumped into the open land area and water bodies consequently creating land and water pollution. The scarcity of land, transportation cost, taxes are the addition to this problem. So it is burning issue to utilize such waste which is proving threat to environment. One of the potential solution to utilize waste in the soil modification/stabilization process. The utilization of wastes as additives in soil or concrete not only improves the performance of soil or concrete but also saves the natural resources by reducing the disposal problems as well as made eco-friendly and economical end products [3]. From past few years, there is interest in utilizing such waste materials which harming the ambient environment severely to achieve the goal of sustainable development [4–8]. Waste material reusing/recycling is the potential solution to minimize waste and preserving the natural resources from further depletion and future generation. Sustainable development takes into consideration simultaneous economic, environmental, and social growth [3]. This practice has become very important in today’s reference as rapid growth has sidelined conservation and protection of the natural resources [9].

Earlier, there were many admixtures to stabilize the local soils. From last few years, advancement and demand of economy push alternative materials over conventional to pave their way in soil stabilization [4]. Soil modification is a technique to modify properties of weak soil. It is being used from ancient time to gain enough strength to soil to bear the imposed load [4, 9]. The stabilized soil by using additives can be successfully used in road, airport, and others works [4, 9, 10]. In this paper, the various possible natural and synthetic waste to modify soil materials are presented, which will be a useful study to utilize waste material in construction.

2 Soil Modification Using Waste Materials

Many studies exist in which use of waste material like synthetic and natural waste is investigated to study the behavior of soil with the inclusion of different waste materials which may be applicable for various geostructure application [4–8, 10–15]. Among this agricultural waste is the natural waste generated at the end of any agricultural process. Agricultural waste like rice husk ash (RHA), bagasse ash, chicken eggshells, and seeds can be used for the purpose. Other natural waste includes the fibrous material from the various plants and trees like natural palm empty fruit bunch (PEFB), natural bihul and chir, corn, hemp, natural reed plant, jute, and wood residue. Synthetic waste can be defined as all other waste which cannot be categorized as natural waste. Mohan et al. said in the study that “synthetic materials being non-biodegradable is either openly burnt or being dumped in the land and water beds causing major environmental issues” [4]. Examples of synthetic wastes are

fly ash (FA), ground granulated blast furnace slag (GGBFS), marble powder (MP), plastic waste, polymeric materials, lime, sand, waste glass, bacteria, construction and demolition (C&D) waste, lime, etc.

2.1 *Natural Waste*

Maher et al. [5] studied the effect of natural fibers from reed plant and palm tree showing the behavior of soil under repeated load condition. Results show the significant improvement in the soil behavior. Babu et al. [6] used coir fiber as admixtures with soil. Series of triaxial test was carried out with different confining pressure ranging from 50 to 150 kPa. Comprehensive experimental results in terms of stress–strain response, major principal stress at failure and stiffness for various fiber contents, fiber lengths, fiber diameters, and confining pressures are obtained. Inclusion of fiber showed the significant improvement in the stress–strain response.

Ahmad et al. [7] studied the effect of palm empty fruit bunch (OPEFB) fiber was mixed with silty sand soil to investigate the increase of shear strength during triaxial compression test. The addition of OPEFB fibers can significantly increase the peak shear strength of silty sand soil. Increasing fiber content leads to increasing strain at failure and, consequently, to more ductile behavior. Sharma et al. [8] studied the soil mixture with the natural fibers of *grewia optiva* (bihul) and *pinus roxburghii* (chir). Series of UCS test was carried out to investigate the strength of soil mixtures. Rahgozar et al. [40] experiment on the jute fiber, coir fiber, and sabai grass. Result shows that increase in fiber content decreased the MDD and increased OMC. Increase in fiber upto 2% increased the CBR and UCS. Rangwala et al. [10] the effect of the inclusion of jute fibers as reinforcement on the various properties of soil, i.e., OMC & MDD and CBR values. The outcome of the design shows that the inclusion of reinforcements decreases the thickness of the subgrade layer [10]. Maity et al. [11] studied the effect of RHA on OMC & MDD and CBR values. Result shows increase in RHA content increased OMC and decreased MDD. RHA and OPC improved the UCS and CBR values accordingly. Tran et al. [12, 16] also studied the effect of waste corn silk on the unconfined compressive strength and splitting tensile strength. Results show that the compressive and tensile strength of soil, cement and cornsilk fibers mixture are improved with the addition of fibers. The most improvements in compressive strength and splitting tensile are 177% and 88%, respectively. The optimum fiber contents of 0.25–0.5% should be used to improve the compressive and splitting tensile strength of cemented soil reinforced by cornsilk fibers. Hiral et al. [13] studied the effect of coir fiber on unconfined compressive strength, CBR value and swelling pressure. From the study, it can be said that the fiber content has effective modification on the parameters under consideration. Ammar et al. [14] used hemp fiber used as an admixture and direct box shear test and single fiber pullout test was carried out. Sharma et al. [15] studied effect of RHA and C&D on the resilient modulus of soil with and without lime. RHA increased the OMC and reduced the MDD of the soil. RHA (12%) and lime (5%) increased the CBR value and resilient

Table 1 Types, forms, size, and content of natural wastes

Name of author	Waste material	Waste forms	Waste size	Waste content
Maher et al. [5]	Reed plant and palm tree and glass	Fibers	$D = 0.3\text{--}1.1$ mm AR = 53–125	1, 3, 4 and 5%
Babu et al. [6]	Coir	Fiber	$D = 0.15, 0.25$ and 0.35 mm	0.5, 1, 1.5, 2, and 2.5%
Ahmad et al. [7]	Palm empty fruit brunch (PEFB)	Fiber	$D = 0.40$ mm	0, 0.25, and 0.50%
Sharma et al. [8]	Grewia Pinus, Bihul and chir	Fiber	$D = 0.48$ mm AR = 0.00148 mm $L = 324$ mm $D = 0.03$ mm $L = 730$ mm AR = 0.000041	1.0, 0.0, 1.50, 0.50, and 2.0%
Maity et al. [11]	RHA	Powder	–	0, 2, 4, 6, and 8%
Rangwala et al. [10]	Jute	Fibers	$L = 0.5$ cm	0.0, 2, 4, 6, and 8%
Rahgozar et al. [40]	Jute, coir and sabai grass	Fibers	$L = 0.5$ cm	1, 1.5, 2, and 2.5%
Modha et al. [13]	Coir	Fiber	$L = 0.5$ cm	0, 2, 4, 6, and 8%
Ammar et al. [14]	Hemp	Fiber	$T = 0.13$ mm $B = 0.65$ mm	–
Sharma et al. [41]	RHA	Powder	–	12%

modulus of clayey soil. Table 1 is representing the type, form, size, and content of waste used in the study.

2.2 Synthetic Waste

Polypropylene fiber type of waste is the most common waste used widely to study the soil modification. Rosa et al. [17] conducted the series of UCS test to investigate the effect of polypropylene fiber dosage and fiber length on performance of fiber-stabilized soil. Results show that the inclusion of fiber significantly increased the unconfined comprehensive strength of sand specimen. Consoli et al. [18–20] studied in detailed the effect of polypropylene fibers content, form on the different parameters with the addition of cement. He conducted the plate load test, triaxial test with different stress path and UCS test to investigate the behavior. In all the testing, it was reflect that there is improvement in parameters of soil under consideration. The failure envelope shows the bilinear behavior in case of reinforced sand with different values of shear parameters at low-pressure part and high-pressure part.

Failure is due to stretching and yielding of fiber and no fiber found break. The scope of the study of Abuel-Maaty [21] was to investigate the effect of polypropylene fiber dosage and elastic modulus of the soil on subgrade normal strength, the modulus of subgrade reaction “Ks” and the plastic deformation. Fatahi et al. [22] considered the combination of three types of fiber—polypropylene, recycled carpet, and steel to study the mechanical properties of cement-treated clay through USC. The unconfined compression test results indicate that the shear strength increases with the addition of fibers, and the brittle cement-treated kaolinite is changed to a more ductile material. Olgun [23] used polypropylene–cement–fly ash mixture. Unconfined compressive and split tensile strength tests were carried out after 7- and 28-day curing periods. The volume change characteristics of the reinforced stabilized soil were determined using shrinkage limit and crack reduction values. In the experimental investigation, the significant increases observed, especially in tensile strength values. Ibrahim et al. [24] and Wang et al. [25] also studied the effect of polypropylene on soil behavior. Other polymeric waste materials like polyester, nylon also are used as an admixture. Kaniraj et al. [26] carried out UCS tests on fly ash–soil specimens prepared with 3% cement content alone and also with 3% cement and 1% fiber contents. The study shows that cement stabilization and fiber inclusion increases the strength of the raw fly ash–soil specimens and change their brittle behavior to ductile behavior. Estabragh et al. [27] carried out series of UCS test on the cemented and cemented-fiber clay sample. Results show that the inclusion of fibers results in an increase in the peak strength, but the amount of the increase in strength is dependent on the fiber content. The strength increased with fiber content up to about 1%, beyond which further increase in fiber content did not have a significant effect on the strength.

After the polypropylene, scrap tire waste, scrap rubber is the second type of waste materials widely used for the soil modification. Yadav et al. [28] conducted compaction, unconfined compressive strength, split tensile strength, California bearing ratio, swelling pressure, wet/dry cycles durability along with the scanning electron microscopy to ascertain the suitability of rubber fibers with cement stabilized clay. The addition of rubber fibers up to 2.5% increases the unconfined compressive strength and split tensile strength but decreases the CBR values after 2.5%. Pamukcu et al. [42] and Nakhaei et al. [29] studied the granular form of rubber waste. Amanta et al. [30] investigated the response of scrap tire chips on the generation of the excess pore pressure. Sand-tire chip mixtures by weight, were examined to get an optimum ratio having maximum resistance towards the liquefaction. The mix with 40% tire chip content was found to be the most effective mix against liquefaction. Abbaspour et al. [31] carried out compaction, direct shear, unconfined compressive strength (UCS), California bearing ratio (CBR), and repeated load triaxial (RLT) using waste tire fibers, which are produced during the shredding process of worn. WTTf incorporation with an optimum content of 1–2% under low normal stresses led to a 17–17.5% increase in the peak shear strength. 2% brought about a 117% increase in cohesion and marginal reduction in internal friction angle.

Plastic waste management becomes the serious affair for the entire world. An overview shows that 1500 bottles are dumped and discarded in landfills every second. PET and HDPE were reported to be one of the most abundant plastics in urban solid

waste production which has become one of the major concerns environmentally [32]. Choudhary et al. [33] investigated the effect of plastic waste (HDPE—high-density polyethylene stripes) reinforcement in sandy soil through CBR test with different aspect ratio. Results show that the maximum improvement in CBR and secant modulus is obtained when the strip content is 4% and the aspect ratio is 3 but the improvement in CBR is also appreciable even at 2% strip content. Series of Proctor compaction, unconfined compression, and triaxial compression tests were carried out using PET bottle strips to examine the undrained shear strength of clayey soil. UCS of fiber mixed soil increases with increase in fiber content but it occurs up to its addition of 1% when other parameters do not alter. Optimum value comes at aspect ratio 2. Modulus of elasticity of fiber mixed soil increases with increase in fiber content but it occurs up to addition of 1% of plastic strips when other parameters do not alter. Optimum value is achieved at aspect ratio 2 [43]. Engineering properties of high plastic silt was investigated with the addition of waste plastic bag (Polypropylene—PP), lime, and RHA. UCS, split tensile test, triaxial test, and CBR test was carried out. Brittle behavior of the plastic-waste fiber reduced due to inclusion. Addition of 0.1% fiber was enough to decrease the brittleness of the stabilized soil. In general, inclusion of the plastic-waste fiber increased the secant modulus E_{50} of the stabilized soil specimen. CBR value increases by 3.6% by mixing lime and RHA [44]. Babu et al. [34] carried out the consolidation, CBR and Cu test to investigate the mixture of only fly ash and plastic waste. Consolidation test results that reveal decrease in compressibility was consistently higher for higher percentages of plastic waste. CBR values of fly ash mixed with waste found more than the plain fly ash. First study was carried out on the different type of plastic waste to study the behavior of soil with different plastic waste [35]. Fathi et al. [32] conducted shake table tests to investigate the dynamic properties of the Sand-PET mixtures. Study shows that addition of the plastic waste strips to the sand and could change the soil brittle behavior under low overburden pressures. Damping ratio of mixture increased and shear modulus decrease with the increase of the plastic waste strips content. Tafreshi et al. [36] used the full plastic bottle filled with sand as a bed below the foundation. Results showed that the bottle bed performed well at the higher pressure. Shah et al. [37, 38] studied the effect of plastic waste on the properties of soil by converting plastic waste into geogrid, geocell, and strips. Study shows that inclusion of plastic waste improves the weak soil. Table 2 presents the type of waste, its content and forms used for the studies on the soil waste mixture.

3 Conclusions and Future Outlook

Following are the observation derived from the above exhaustive literature review:

- Polypropylene is the type of waste which highly studied by the researches under the different load conditions like static and dynamic.

Table 2 Types, forms, size, and content of synthetic wastes

Name of author	Waste material	Waste forms	Waste size	Waste content
Rosa et al. [17]	Synthetic polypropylene	Monofilament, fibrillated, tape, and mesh fibers	Monofilament round: $L = 13, 19, 25,$ and 51 mm Fibrillated flat narrow: $L = 13, 25, 51,$ and 76 mm Tape wide flat wide: 51 and 76 mm Mesh fibers round grid: 51×102 mm	0.2, 0.4, 0.6, 0.8, and 1.0%
Kaniraj et al. [26]	Polyester	Fibers	Round fiber $D = 0.075$ mm Aspect ratio = 267	1%
Consoli et al. [18]	Polypropylene	Fibers	$L = 24$ mm $D = 0.023$ mm	0.5%
Pamukcu et al. (2006)	Rubber	Granular	2 mm	5, 7.5, 10, 12.5, and 15%
Consoli et al. [19]	Polypropylene	Fiber	$L = 24$ mm $D = 0.023$ mm	0.5
Consoli et al. [19]	Polypropylene	Monofilament fiber	$L = 24$ mm $D = 0.023$ mm	0.5%
Choudhary et al. [33]	HPDE	Strips	$B = 12$ mm $L = 12, 24$ and 36 mm $T = 0.40$ mm $AS = L/B = 1, 2$ and 3	0.0, 0.25, 0.50, 1.0, 2.0, and 4.0%
Abuel-Maaty [21]	Polypropylene	Fiber	$L = 24$ mm $D = 0.023$ mm	0.0, 0.25, 0.50, 1.0, 2.0, and 4.0%
Ibraim et al. [24]	Polypropylene	Crimped fiber	$L = 35$ mm $D = 0.1$ mm	0.3, 0.6, and 0.9%
Estabragh et al. [27]	Nylon	Fiber	$L = 20$ mm $D = 0.28$ mm	0.5, 0.75, 1, and 1.25%
Fatahi et al. [22]	Polypropylene, recycled carpet, and steel	Fiber	Polypropylene $L = 20$ mm $D = 0.28$ mm Recycled carpet $L = 10$ mm Steel $0.4 \times 3 \times 0.3 \times 18.4$ mm	Polypropylene fibers = 0.1, 0.2, and 0.5% Carpet fibers = 0.5, 0.75, and 1% Steel = 5, 7.5, and 10%

(continued)

Table 2 (continued)

Name of author	Waste material	Waste forms	Waste size	Waste content
Acharyya et al. [43]	Plastic waste (PET)	Strips	$L = 5, 10, 15$ mm $B = 5$ mm $T = 0.5$ mm	0.5, 1, 1.5, and 2%
Muntohar et al. [44]	Waste plastic beg made from polypropylene	Strips	$L = 20-30$ mm $B = 2-2.5$ mm	0.1, 0.2, 0.4, 0.8, and 1.2%
Olgun [23]	Polypropylene	Fiber	$L = 6, 12$ and 20 mm $D = 0.034$ mm	0.25, 0.50, 0.75, and 1.0%
Wang et al. [47]	Polypropylene	Crimped fiber	$L = 53$ mm $D = 0.1$ mm	–
Acharyya et al. [43]	Plastic waste (PET)	Strips	$L = 5, 10, 15$ mm $B = 5$ mm $T = 0.5$ mm	0.5, 1, 1.5, and 2%
Babu et al. [34]	Plastic waste (PET bottles)	Chips	$L = 10-20$ mm $T = 0.2$ mm $AR = 20-40$	0, 0.50, 0.75, and 1.0%
Sadeghi et al. [39]	Polypropylene	Monofilament fibers	$L = 2$ mm $D = 0.023$ mm	0, 0.5, and 1%
Bo Li et al. [46]	Shredded waste tire rubber	Rubber crumb	$D = 0.2-0.8$ mm	0.0, 5, 10, and 20%
Yadav et al. [28]	Waste tire rubber	Fiber	$L = 15$ mm $B = 2-3$ mm	2.5, 5, 7.5, and 10%
Amanta et al. [30]	Scrap tire	Chips	$C/S = 10 \times 10$ mm $L = 20$ mm	0–100%
Abbaspour et al. [31]	Waste tire	Fibers	$L = 0-70$ mm $D = 0.030-1.50$ mm	0, 0.5, 1, 2, 3, and 4%
Mukhtar et al. [44]	HDPE, LDPE, PET, and PP	Ground, Pellet, Flake	Pellet 3.3 mm Flake 7×8.8 mm in diameter and 0.7 mm in thickness	1–10%
Fathi et al. [32]	Plastic waste (PET bottles)	Strips	$L = 10$ and 50 mm $B = 10$ mm $AR = 1$ and 5	0, 0.5, 0.75, and 1%
Tafreshi et al. [36]	Plastic waste (PET bottles)	Soil filled bottle used as a full bottle reinforcement		

- Different forms of scrap tire waste also the most common type of waste used to investigate the behavior of different soil.
- A very few studies were available on the plastic waste; there is urgent need to explore this field.
- It was also found that majority of the study shows the potential application of plastic waste recycling in the construction of pavements. These all study were carried out considering static load condition. Pavements are vulnerable to dynamic loading/repeated loading. But rarely the study available in which actual field condition i.e. dynamic loading may be considered.
- So there is scope to use the plastic waste in the dynamic characterization of soil by looking to the field conditions.

References

1. Muyen Z, Barna T, Hoque M (2016) Strength properties of plastic bottle bricks and their suitability as construction materials in Bangladesh. *Progress Agric* 27(3):362–368
2. Kumar A, Agrawal A (2020) Recent trends in solid waste management status, challenges, and potential for the future Indian cities—a review. *Curr Res Environ Sustain* 2:100011
3. Dima DN, Ansrei R, Boboc V, Scabteianu I (2008) Evaluation of the sustainability of farms. *Bul Institutului Politeh DIN IAS_I* 63:293–296
4. Mohan HT, Jayanarayanan K, Mini KM (2021) Recent trends in utilization of plastics waste composites as construction materials. *Constr Build Mater* 271:121520
5. Maher BMH, Member A, Woods RD (1990) Dynamic response of sand reinforced with randomly distributed fibers. *J Geotech Eng* 116(7):1116–1131
6. Babu GLS, Vasudevan AK (2008) Strength and stiffness response of coir fiber-reinforced tropical soil. *J Mater Civ Eng* 571–577
7. Ahmad F, Bateni F, Azmi M (2010) Performance evaluation of silty sand reinforced with fibres. *Geotext Geomembr* 28(1):93–99
8. Sharma V, Vinayak HK, Marwaha BM (2015) Enhancing compressive strength of soil using natural fibers. *Constr Build Mater* 93:943–949
9. Gautam PK, Kalla P, Jethoo AS, Agrawal R (2018) Sustainable use of waste in flexible pavement: a review. *Constr Build Mater* 180:239–253
10. Rangwala HM, Kamplimath HM, Kanara A, Ratlami M, Kothari M, Khatri M (2017) Effect of randomly distributed jute fibers on design of soil subgrade. In: 6th Nirma University international conference on engineering (NUICONE)
11. Maity J, Chattopadhyay BC, Mukherjee SP (2017) Improvement of characteristics of clayey soil mixed with randomly distributed natural fibers. *J Inst Eng (India) Ser A* 99:55–65
12. Tran KQ, Satomi T, Takahashi H (2018) Effect of waste consilk fiber reinforcement on mechanical properties of soft soils. *Transp Geotech* 16(2018):76–84
13. Modha H, Shah A (2018) Randomly distributed coir fiber effect on sub grade soil—An experimental study. *I-Manager's J Civ Eng* 8(4):1–6
14. Ammar A, Najjar S, Ph D, Asce AM, Sadek S, Ph D, Asce M (2019) Mechanics of the interface interaction between hemp fibers and compacted clay. *Int J Geomech* 19(4):1–15
15. Sharma RK, Hymavathi J (2016) Effect of fly ash, construction demolition waste and lime on geotechnical characteristics of a clayey soil: a comparative study. *Environ Earth Sci* 75:377
16. Tran KQ, Satomi T, Takahashi H (2018) Improvement of mechanical behavior of cemented soil reinforced with waste consilk fibers. *Constr Build Mater* 178:204–210
17. Santoni RL, Tingle JS, Webster SL (2001) Engineering properties of sand-fiber mixtures for road construction. *J Geotech Geoenviron Eng ASCE* 127(3):258–268

18. Consoli NC, Vendruscolo MA, Prietto PDM (2003) Behavior of plate load tests on soil layers improved with cement and fiber. *J Geotech Geoenviron Eng* 129(1):96–101
19. Consoli NC, Heineck KS, Casagrande MDT, Coop MR (2007) Shear strength behavior of fiber-reinforced sand considering tri-axial tests under distinct stress paths. *J Geotech Geoenviron Eng ASCE* 133(11):1466–1469
20. Consoli NC, Winter D, Leon HB, Scheuermann Filho HC (2010) Durability, strength, and stiffness of green stabilized sand. *J Geotech Geoenviron Eng* 144(9):04018057–1–10
21. Abuel-Maaty AE (2010) Evaluation of characteristics of subgrade stabilized with random polypropylene short fiber. *J Eng Appl Sci* 57(3):167–183
22. Fatahi B, Khabbaz H (2012) Mechanical characteristics of soft clay treated with fibre and cement. *Geosynth Int* 19:252–262
23. Olgun M (2013) Effects of polypropylene fiber inclusion on the strength and volume change characteristics of cement-fly ash stabilized clay soil. *Geosynth Int* 20(4):263–275
24. Ibraim E, Diambra A, Wood DM, Russell AR (2010) Static liquefaction of fibre reinforced sand under monotonic loading. *Geotext Geomembr* 28:374–385
25. Wang Y, Guo P, Ren W, Yuan B, Yuan H, Zhao Y (2018) Laboratory investigation on strength characteristics of expansive soil treated with jute fiber reinforcement. *Int J Geomech* 17(11):1–12
26. Kaniraj BSR, Havanagi VG (2001) Behavior of cement stabilized fiber reinforced fly ash soil mixtures. *J Geotech Geoenviron Eng* 127(July):574–584
27. Estabragh AR, Bordbar AT, Javadi AA (2011) Mechanical behavior of a clay soil reinforced with nylon fiber. *Geotech Geol Eng* 29(5):899–908
28. Yadav JS, Tiwari SK (2017) Effect of waste rubber fibres on the geotechnical properties of clay stabilized with cement. *Appl Clay Sci* 149(May):97–110
29. Nakhaei A, Marandi SM, Kermani SS, Bagheripour MH (2012) Dynamic properties of granular soils mixed with granulated rubber. *Soil Dyn Earthq Eng* 43:124–132
30. Amanta AS, Dasaka SM (2019) A numerical study on the dynamic response of scrap tire chips-sand mixture under undrained condition, conference. In: Silvestri, Moraci (eds.) *Earthquake geotechnical engineering for protection and development of environment and constructions*. Associazione Geotecnica Italiana, Rome
31. Abbaspour M, Narani SS, Aflaki E, Nejad FM (2020) Behavior of a subgrade soil reinforced by waste tire textile fibers under static and cyclic loading. *J Mater Civ Eng* 32(8)
32. Fathi H, Jamshidi Chenari R, Vafaeian M (2020) Shaking table study on pet strips-sand mixtures using laminar box modelling. *Geotech Geol Eng* 38(1):683–694
33. Choudhary AK, Jha JN, Gill KS (2010) Utilization of plastic wastes for improving the subgrades in flexible pavements. In: *Geoshanghai 2010 international conference*, pp 320–326
34. Babu GLS, Jaladurgam M (2014) Strength and deformation characteristics of fly ash mixed with randomly distributed plastic waste. *J Mater Civ Eng* 26(12):1–7
35. Abukhettala M, Fall M (2021) Geotechnical characterization of plastic waste materials in pavement subgrade applications. *Transp Geotech* 27:100472
36. Tafreshi SNM, Omran MP, Rahimi M, Dawson A (2021) Experimental investigation of the behavior of soil reinforced with waste plastic bottles under cyclic loads. *Transp Geotech* 26:100455
37. Shah A, Modha H (2020) Improving the soil subgrade with plastic waste reinforcement—an experimental study, lecture notes in civil engineering. In: *Advances in sustainable construction materials and geotechnical engineering*, pp 153–161, Springer, Singapore
38. Solanki Y, Jambudia M, Shah A (2021) Analysis and modification of engineering behavior of soil using plastic waste materials. In: Patel S, Solanki CH, Reddy KR, Shukla SK (eds.) *Proceedings of the Indian geotechnical conference 2019*. Lecture notes in civil engineering, vol 136. Springer
39. Sadeghi MM, Beigi FH (2014) Dynamic behavior of reinforced clayey sand under cyclic loading. *Geotext Geomembr* 42:564–572
40. Rahgozar MA, Saberian MH, Li J (2018) Soil stabilization with non-conventional eco-friendly agricultural waste materials: an experimental study. *Transp geotech* 14:52–60

- 41 Sharma A, Sharma, RK (2021) Sub-grade characteristics of soil stabilized with agricultural waste, constructional waste, and lime. *Bull eng geol environ* 80:2473–2484
- 42 Pamukcu S, Akbulut S (2006) Thermoelastic enhancement of damping of sand using synthetic ground rubber, *j geotech and geoenviron eng, ASCE* 132(4):501–510
- 43 Acharyya R (2013) Improvement of undrained shear strength of clayey soil with pet bottle strips, *indian geotechnical conference-2013, Indian Inst Tech, Roorkee*
- 44 Muntohar AS, Widiyanti A, Hartono E, Diana W (2013) Engineering Properties of Silty Soil Stabilized with Lime and Rice Husk Ash and Reinforced with Waste Plastic Fiber, *J geotech and geoenviron eng, ASCE*, 25(9):1260–1270
- 45 Abukhettala M, Fall M (2020) Geotechnical characterization of plastic waste materials in pavement subgrade applications, *Transp geotech* 27:100472
- 46 Li B, Huang M, Zeng X (2016) Dynamic Behavior and Liquefaction Analysis of Recycled-Rubber Sand Mixtures, *J geotech and geoenviron eng, ASCE*, 04016122–1
- 47 Wang K, Brennan AJ (2013) Dynamic response of saturated fibre-reinforced sand, *young eng conf, UK*

Suction Analysis at Soil-Geocell Interface for a Clayey Soil



Bhavita S. Dave, Chandresh H. Solanki, and Atul K. Desai

Abstract The soils of the Greater Himalayas are predominantly found in Leh and Ladakh, Lahaul and Spiti, and Uttarakhand's upper ranges. The humidity regime is erratic. The arid zone begins from Baralacha pass in Lahaul and extends throughout the Spiti valley in the Himachal Pradesh district of Lahaul and Spiti. The purpose of this study is to establish the suction value of soil taken from the arid zone of the Spiti valley during various freezing–thawing cycles, taking into account the climate variations of the Spiti valley. The most basic and important parameter that impacts the behaviour of an unsaturated soil is suction. Before doing further tests such as shear and permeability, it is critical to know the suction value of an unsaturated soil. In a nutshell, it is the negative pore water pressure in partially saturated soil expressed in terms of water column height. The study employed the filter paper method as a cost-effective way to assess suction. It is the only approach that can determine both contact and noncontact suction. To get a wide range of suction, soil specimens were treated to 0, 1, 3, and 5 freezing–thawing (F-T) cycles for various degrees of saturation, and soil freezing characteristic curves (SFCC) were developed for all F-T cycles. For each SFCC, the data obtained from the experiments revealed the best fitting values using the Fredlund and Xing model.

Keywords Suction · Arid region soil · Soil freezing characteristic curve · Freezing–thawing cycle

B. S. Dave (✉) · C. H. Solanki · A. K. Desai
Department of Civil Engineering, Sardar Vallabhbhai National Institute of Technology, Surat,
Gujarat, India
e-mail: davebhavitas@gmail.com

C. H. Solanki
e-mail: chs@amd.svnit.ac.in

A. K. Desai
e-mail: akd@amd.svnit.ac.in

1 Introduction

When the temperature drops below the freezing point of a soil, a fraction of the water in the soil changes phase and freezes solid. Adsorbed coatings over particles, fissures between particles, and pores with small enough diameters are all places where unfrozen water can be found. As the temperature drops, more water freezes, leaving the rest in thinner adsorbed layers and smaller holes and crevices. Because matric forces produced by soil on water diminish the energy status of the water, which lowers the freezing point, soil water can remain unfrozen at temperatures well below freezing. Water potential is significantly depending on temperature where liquid water and ice coexist in frozen soil; their relationship may be determined from thermodynamics. The link between water potential and (liquid) water content in frozen soil is called the soil freezing content (SFC), which is similar to the idea of soil moisture content (SMC) for unfrozen soil [10].

Researchers have been attempting to characterize unsaturated soil masses by measuring suction and establishing the soil water characteristics curve (SWCC), which is a relationship between soil suction and gravimetric or volumetric water content of the soil mass [3, 5–7, 9–15]. The SWCC's usefulness in solving numerous problems in geotechnical engineering has long been recognized, and its precise determination is now required. In addition, a critical review of the literature reveals that soil type [2, 6, 8, 9, 13], fabric [11, 17], initial void ratio (Kawai e [16]). Furthermore, the fitting functions used to build SWCCs and derive appropriate fitting parameters are heavily influenced by the form and slope of the SWCC [3–5]. The pore-size distribution, compressibility, and stress history of the soil are also important factors that influence the SWCC [8].

The drying and wetting reactions of unfrozen soil are strikingly similar to the freezing and thawing reactions of frozen soil. As the soil dries, water evaporates and is replaced by air, leaving the water that remains with a lower matric potential. When soil freezes, a similar thing happens, but liquid water transforms into ice. The mechanisms that prevent soil water from draining also prevent it from freezing. Because of this apparent similarity, it has been suggested that the SMC and SFC contain the same information and that the soil water retention qualities can be determined by either drying and wetting or freezing and thawing [10, 12, 18].

2 Material

For the purpose of the research, soil sample was procured from Kaza, Lahaul and Spiti, Himachal Pradesh, which can be categorized as frozen soil. This type of soil can be found in the arid zone of the greater Himalayas mostly pertain to Leh and Ladakh, and Lahaul and Spiti. Soil sample was kept in an oven and dried at 105 °C for 24–48 h before use. To classify the soil composition collected and to determine its

Table 1 Physical properties of soil

Property	Soil
Specific gravity (G)	2.31
<i>Grain size</i>	
Gravel fraction (%)	0.00
Fine sand fraction (%)	55.36
Medium sand fraction (%)	0.35
Coarse sand fraction (%)	0.19
<i>Atterberg Limits</i>	
Liquid limit (LL) (%)	33.75
Plastic limit (PL) (%)	18.84
Plasticity Index (IP) (%)	14.19
<i>Compaction parameters</i>	
Optimum moisture content (OMC) (%)	16.64
Maximum dry density (MDD) (gm/cc)	1.76
Soil classification	CL

3 Result and Discussion

The results of SFCCs were attained by performing filter paper method and are presented [1]. All specimens were prepared at varied water content of 90, 80, 70, 60, 50, and 40% of degree of saturation and at dry density of 1.76 gm/cc (MDD) for soil and soil-geocell interface. The results presented are in terms of water content and matric suction. All results of SFCCs are fitted using Fredlund and Xing [5] model.

The fitting parameters α , A_f , n , and m for specimen tests of soil and soil-geocell interface at Proctor density for different freezing–thawing cycles (0, 1, 3, 5, 7) by FX model are shown in the Tables 2 and 3, respectively.

Figure 3 shows the graph of degree of saturation v/s suction for soil and soil-geocell interface. The graph of pure soil for each FTC shows the haphazard nature, whereas for soil-geocell interface, the curves for different freezing–thawing cycles

Table 2 Fitting parameters for soil specimen at proctor density for FX model (soil)

FX model					
Soil–matric suction					
F-T cycles	0	1	3	5	7
A_f	283.1519	192.94	195.6422	0.0002	283.9464
R^2	0.8600	0.8870	0.7013	0.7254	0.9239
Air entry (kPa)	224.48	18.74	156.88	27.98	18.31
N	18.3460	0.4509	0.1403	19.9997	0.4838
M	0.1563	1.1597	0.1538	0.0374	1.1778

Table 3 Fitting parameters for soil specimen at Proctor density for FX model (soil-geoell interface)

FX model					
Soil-geocell interface—matric suction					
F-T cycles	0	1	3	5	7
A_f	507.8990	0.0364	717.0357	214.4134	1046.85 76
R^2	0.8163	0.0169	0.7998	0.7576	0.8553
Air entry (kPa)	335.18	39,973.41	836.21	193.73	166.09
N	2.7647	2.2914	0.4116	20.0000	0.6983
M	0.3171	0.1907	1.2000	0.1642	0.1349

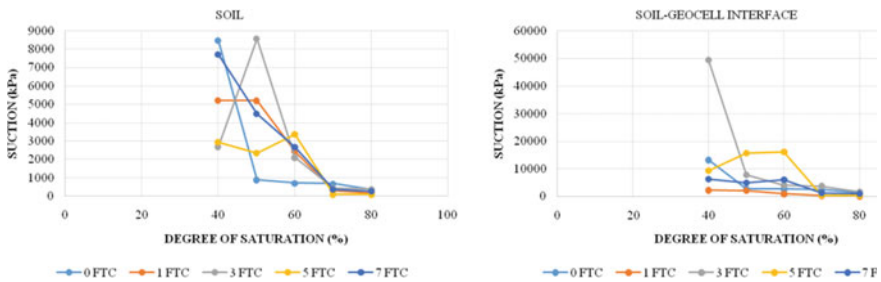


Fig. 3 Effect of degree of saturation on matric suction for each FTC

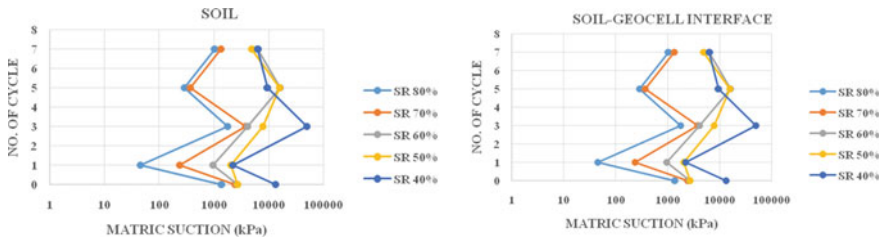


Fig. 4 Freezing–thawing behaviour of soil and soil-geocell interface

are nearly of same nature. It has been observed that the freezing–thawing process affects matric suction measured for both soil and soil-geocell interface. Figure 4 represents freezing–thawing behaviour of soil specimens.

4 Conclusion

It has been discovered that soil specimens of appropriate consistency are particularly effective in determining the SFCC of the soil and the soil-geocell interface. These

specimens have also been proven to improve suction measurement uniformity, which contributes in obtaining a unique SFCC. The shape of the SFCC is not affected by the thickness of the geocell. The air entrance value of the soil-geocell interface has been shown to be higher than that of pure soil specimens. Freezing and thawing of specimens generates a density contrast in the specimen, which might result in a longer equilibration period and, as a result, inaccurate results.

References

1. ASTM D5298 (2007) Test method for measurement of soil potential (suction) using filter paper. ASTM International, West Conshohocken
2. Baker R, Frydman S (2009) Unsaturated soil mechanics: critical review of physical foundations. *Eng Geol* 106(1–2):26–39
3. Bulut R, Leong EG (2008) Indirect measurement of suction. *Geotech Geol Eng* 26(6):633–644
4. Fredlund MD, Wilson GW, Fredlund DG (2002) Use of grain size distribution curve for estimation of the soil water characteristics curve. *Can Geotech J* 39(5):1103–1117
5. Fredlund DG, Xing A (1994) Equations for the soil-water characteristic curve. *Can Geotech J* 31(4):521–532
6. Fredlund DG, Fredlund MG, Wilson GW (1997) Prediction of the soil-water characteristic curve from grain-size distribution and volume-mass properties. In: 3rd Brazilian symposium on unsaturated soils, Freitas Editora, Rio de Janeiro, Brazil, pp 1–12
7. Hanumantha Rao B, Singh DN (2010) Application of thermal flux for establishing soilwater characteristic curve of kaolin. *Geomech Geoeng* 5(4):259–266
8. Marinho F (2005) Nature of soil–water characteristic curve for plastic soils. *J Geotech Geoenviron Eng*. *J Geotech Geoenviron Eng* 131. [https://doi.org/10.1061/\(ASCE\)1090-0241\(2005\)131:5\(654\)](https://doi.org/10.1061/(ASCE)1090-0241(2005)131:5(654))
9. Miller CJ, Yesiller N, Yaldo K, Merayyan S (2002) Impact of soil type and compaction conditions on soil water characteristic. *J Geotech Geoenviron Eng* 128(9):733–742
10. Miller RD (1966) Phase equilibria and soil freezing. In: Proceedings of the Second International Conference in Permafrost. National Academy of Sciences, National Research Council, Washington, DC, pp 193–197
11. Ng CWW, Pang YW (2000) Experimental investigations of the soil-water characteristics of a volcanic soil. *Can Geotech J* 37(6):1252–1264
12. Schofield RK (1935) The pF of water in soil. *International Congress on Soil Science, Trans. 3rd (Oxford, G.B.)*, vol 2, pp 37–48
13. Thakur VKS, Sreedeeep S, Singh DN (2005) Parameters affecting soil–water characteristic curves of fine-grained soils. *J Geotech Geoenviron Eng* 131(4):521–524
14. Thakur VKS, Sreedeeep S, Singh DN (2006) Laboratory investigations on extremely high suction measurements for fine-grained soils. *Geotech Geol Eng* 24(3):565–578
15. Toker NK, Germaine JT, Sjoblom KJ, Culligan PJ (2004) A new technique for rapid measurement of continuous soil moisture characteristic curves. *Geotechnique* 54(3):179–186

16. Uchaipichat A, Khalili N (2009) Experimental investigation of thermo-hydro mechanical behaviour of an unsaturated silt. *Geotechnique* 59(4):339–353
17. Vanapalli SK, Pufahl DE, Fredlund DG (1998) The effect of stress state on the soilwater characteristic behavior of a compacted sandy-clay till. In: *Proceeding of 51st Canadian geotechnical conference Canadian geotechnical society, Montreal*, pp 81–86
18. Williams PJ (1964) Unfrozen water content of frozen soils and soil moisture suction. *Géotechnique* 14(3):246. <http://dx.doi.org/10.1680/geot.1964.14.3.231>

Potential of Coconut Shell Powder on Geotechnical Characteristics of Stabilized Soil



Pratik Ranjan Yadav and Mahesh Patel

Abstract The area around Karnataka is mostly comprised of lateritic soils and many irregular lateritic hillocks. It consists of lithomargic clay sandwiched between the weathered laterite which is located at the top and hard-granitic gneiss beneath it. These soils are structurally unstable and are highly prone to erosion. A lot of engineering problems such as foundation problems, subgrade problems, erosion and slope stability problems are being faced due to the presence of these soils. Therefore, this kind of soil is not much stable and could not be used directly for heavy construction work. So far, various attempts have been made to stabilize the engineering properties of these type of soil using different materials. Fibers like nylon, polypropylene strips and agents like cement and lime were also used. Due to the addition of above substances and modifiers, it usually improves the bearing capacity and strength characteristics of the soil mass. In some cases, the liquid limit also drastically decreased. With the introduction of reinforcements like coconut shell in the backfill, several parameters of the retaining wall system may be improved; for example, the use of reinforcements in soil in the form of geotextile or geogrid reduces the lateral earth pressure. In this study, we have compared the variation in properties between natural soil and soil stabilized with coconut shell. Coconut shell was reduced to sizes of 2–4.75 and 4.75–10 mm and was used at different percentages up to 10.

Keywords Lateritic soils · Stabilization · Reinforced soil · Coconut shell

P. R. Yadav (✉) · M. Patel
Department of Civil Engineering, Dr. B.R. Ambedkar National Institute of Technology, Jalandhar,
Punjab 144011, India
e-mail: pratikry.gg.20@nitj.ac.in

M. Patel
e-mail: patelm@nitj.ac.in

© The Author(s), under exclusive license to Springer Nature Singapore Pte Ltd. 2023
A. K. Agnihotri et al. (eds.), *Proceedings of Indian Geotechnical and Geoenvironmental Engineering Conference (IGGEC) 2021, Vol. 1*, Lecture Notes in Civil Engineering 280,
https://doi.org/10.1007/978-981-19-4739-1_54

569

1 Introduction

Soil is an earthen and unconsolidated material which has numerous applications and is widely used in the construction industry. It is used in foundation of buildings and bridges, culverts, embankment, dams, retaining walls, tunnels and others. One of the major issues in soil is its expansive behavior. When soil comes in contact with water or any liquid, it swells results in significant reduction in the bearing capacity. Soil in contact with water tends to flow and making it difficult to use for construction activities [1, 2]. Even such behavior of soil can lead to differential settlements, cavities and slope failure over time. Therefore, this type of soil cannot be used directly for construction purposes, but for its application, the soil needs to be treated through the application of any technique or equipment, which would strengthen the soil [2]. However, due to the expenditure and other constraints involved in strengthening the soil, there is a need to find an alternative method which is both sustainable as well as cost effective. One of the ways could be to use the concept of soil stabilization. Soil stabilization is a technique in which an additive or a foreign matter is introduced to enhance engineering properties of a soil [3, 4]. Soil stabilization is broadly classified into three categories, namely physical, chemical and biological soil stabilization. Depending upon the site conditions, constraints and the resources available, one of above methods could be incorporated [5, 6].

In recent times, many techniques such as geo-synthetics [7, 8] microbial activity [9, 10] and application of waste materials [11, 12] have proven to be highly effective, but due to the higher expenditure and cost associated with first two methods, practically it is not feasible to use them in all conditions. Whereas, waste materials such as plastics [13, 14], fly ash [15–17], sugarcane bagasse ash [18, 19], rice husk ash [20, 21] and natural fibers [22, 23] have been successfully been used for enhancing the soil characteristics. In a similar manner, coconut shell is an agricultural waste and a non-food component of coconuts. Coconut shell possesses high strength and modulus values, making it a highly potential material to stabilize the soil [24]. Coconut shell mainly consists of four parts such as coconut husk, shell, skin and copra. Also, coconut coir is extracted from coconut husk and has number of applications both in and out of construction industry [25, 26]. It is used in slope stabilization, reinforcement of soil, geotextile, yarn, insulation panels, packaging and others. Coconut shell has number of advantages as it is weather resistant, absorbs less moisture and has high strength and modulus. One major drawback of using coconut shell is its non-biodegradable behavior as problem arises mainly in its dumping. Every year thousands of tons of coconut shells are generated all over the world and their dumping remains a big challenge [27]. There is a need to manage coconut waste and harness their energy in one form or the other [28–30].

Numerous studies have been conducted on waste materials [31–33], but there have been limited research to understand behavior of coconut shell on the strength and other characteristics of soil. Moreover, most of the authors have focused only on increasing the strength of the soil using coconut shells. After thoroughly analyzing and identifying gaps in the use of coconut shell as a stabilizing agent, the current

experimental study is focused on the influence of coconut shell powder on various engineering properties of soil and to compare the results with conventional soil. In addition, investigations will be conducted on impact of coconut shell powder on the bearing capacity, cohesive strength and angle of shearing resistance, permeability and lateral earth pressure of soil.

1.1 Problems with the Soil

There are predominantly lithomargic clays along the west coast of southern India (commonly known as Shedi soil) sandwiched between weathered laterite on top and hard-granitic gneiss beneath. On the entire stretch of the Konkan belt, in southern India, there are widespread deposits of lateritic soil. When soil becomes moist, it tends to lose part of its strength and tends to flow with water. This results in the formation of cavities, uneven settlements and ultimately slope failure [1]. Engineers need extreme caution while working with this type of soil. Typically, these soils consist of silty sand and/or sandy silt with higher moisture content, causing them to lose strength under wet conditions and tend to flow with the water resulting in cavities and unsettlements. Silt deposits in such high concentrations cause many problems, such as slope failures, foundation failures, embankment failures and uneven settlements and many other [1, 2].

2 Materials and Methodology

2.1 Coconut Shell

In the current experimental study, coconut shells have been crushed using standard proctor rammer in the size range of 2–4.75 mm and 4.75–10 mm. In the process, sieve analysis has been done after crushing in order to validate the desired size range. In this study, to obtain the desired size range of coconut shell, it has been made to pass through sieves of 1.18 mm, 4.75 mm and 10 mm to check % retained and % passing. Coconut shell is mainly made up of Lignin, Pentosam and Cellulose. Lignin contributes around 29.4%, whereas Cellulose and Pentosam contribute around 26.6% and 27.7% each. It also consists of moisture, ash, Uronic hydroxides and solvent extractives. The chemical composition of coconut shell is represented in Table 1 (Fig. 1).

Table 1 Chemical composition of coconut shell

Chemical composition	Value (%)
Cellulose	26.6
Pentosam	27.70
Moisture	8%
Lignin	29.4
Ash	0.6
Uronic hydroxides	3.5
Solvent extractives	4.2

Fig. 1 Coconut shell and coconut shell powder



2.2 Lithomargic Clay

Lithomargic clay has been collected from a site named moodubelle, and undisturbed sample has been extracted using the sampler. Table 2 represents the results of tests conducted on soil.

Table 2 Test data corresponding to natural soil (Lithomargic clay)

Tests	Results
In-situ density using core cutter	1.55 g/cm ³
Dry density	1.2 g/cm ³
Liquid limit	41.2%
Specific gravity	2.54
Water content	30%
Soil gradation	SM-MI
Plastic imit	27.25%
Shrinkage limit maximum dry density	23.24% 1.68 g/cm ³
OMC	21%
pH	6.05
Free swell index	50%
Permeability	6.63*10 ⁻⁶ cm/s
Shear strength characteristics	C = 0.01 Mpa
Friction angle	27°

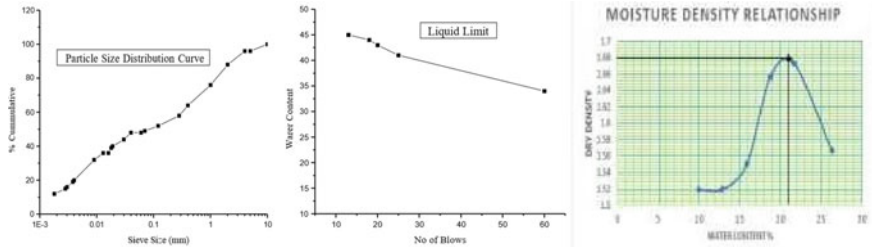


Fig. 2 Particle size distribution, moisture density relationship and liquid limit of soil

For the gradation of soil, sieve analysis has been conducted. The graph is plotted between IS sieve size and % cumulative. The output of sieve analysis has been drawn in semi-log scale to obtain desired variation and shape of the curve. The obtained curve is S-shaped, which is as per the guidelines in the code. From the above analysis, soil has been classified as SM-MI. From Figure 2 below, liquid limit is determined with respect to 25 number of blows, which is the standard, and 41% water content is achieved. Generally, number of blows varies between 15 and 35, with 25 being the optimum number of blow. Higher number of blows indicates that the soil is relatively stiffer, whereas lower values indicate soil being relatively weak and less stiff. From the standard proctor test, maximum dry density (MDD) of 1.68 g/cm³ and optimum moisture content (OMC) of 21% have been obtained.

2.3 Water

In this experimental study, mainly distilled water has been used. The water was found to be free of any organic matter or impurities.

3 Methodology

In this experimental study, various tests such as standard proctor test, specific gravity, falling head, direct shear and UCS have been conducted on the soil with and without the addition of coconut shell powder in the laboratory. The obtained results were compared with the reference soil to check performance of soil amended with coconut shell powder. The combination used in the current study is presented in the following Table 3.

Table 3 Combination of lithomargic clay with % CSP

Mixes	Clay	Coconut shell powder (CSP)
Mix 1 (CSP 0%)	100	0
Mix 2 (CSP 2%)	98	2
Mix 3 (CSP 4%)	96	4
Mix 4 (CSP 6%)	94	6
Mix 5 (CSP 8%)	92	8
Mix 6 (CSP 10%)	90	10

3.1 Tests Conducted on Lithomargic Clay

On natural soil, several tests have been conducted namely in-situ density using core cutter method, dry density, water content, specific gravity, liquid limit, plastic limit, shrinkage limit, maximum dry density, OMC, pH, free swell index, soil gradation, permeability and shear strength characteristics.

3.2 Tests to Be Conducted on the Mixture of Lithomargic Clay and Coconut Shell Powder of Different Size and Percentages

The natural soil is mixed with coconut shell of different size range and at varying percentages from 0 to 10. standard proctor test, optimum dry density (OMC) and maximum dry density (MDD) are conducted on soil stabilized with and without coconut shell powder and at different sizes and percentage.

4 Results and Discussion

4.1 Results of the OMC of Soil Stabilized with Coconut Shell of Size 2–4.75 mm and 4.75–10 mm

Standard proctor test on natural soil stabilized with coconut shell of size 2–4.75 mm has been conducted to observe the variation in optimum moisture content (OMC). Natural soil has an OMC of 21%. For the OMC with coconut shell in the size range of 2–4.75 mm, it attains peak value at 4% CSP. In the beginning, OMC increases, attains peak and decreases till 10% CSP. The reason for non-uniform trend might be due to varying moisture retaining capacity of clay particles and coconut shells in powdered form. Coconut shell absorbs relatively less water than the clay. In the

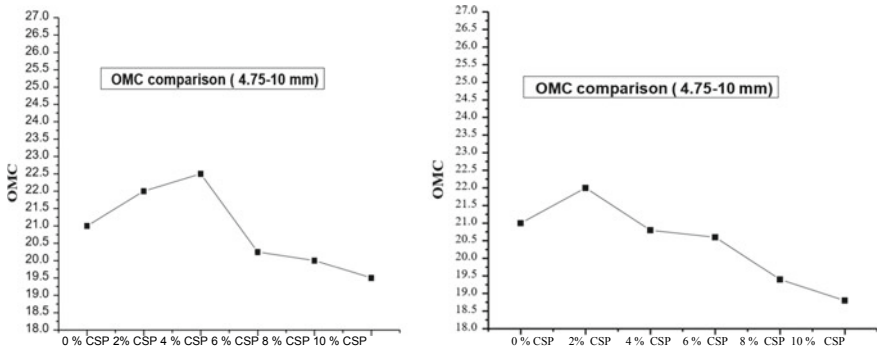


Fig. 3 OMC Comparison (2–4.75 mm) and (4.75–10 mm)

previous studies, OMC was obtained at 1% addition of CSP with no regular trend observed. Also, in other experimental study, OMC was obtained at 5% addition of coconut shell [34] (Fig. 3).

Standard proctor test on natural soil stabilized with coconut shell of size 4.75–10 mm has been conducted to observe the variation in optimum moisture content (OMC). In the curve obtained above, for OMC with 4.75–10 mm, peak is attained at 2% CSP, and then, decreasing trend is observed up to 10%. In one of the previous studies, 20% OMC was achieved on addition of CSP. The trend in the curve could be explained again on the basis of ability of clay particles and coconut shell powder to absorb the moisture. And it could also be attributed to the consistency and fineness of the mixture obtained. Larger the size of coconut shells used, lesser the consistency of the mixture [34].

4.2 Results of the Soil Stabilized with Coconut Shell of Size 2–4.75 mm (MDD Comparison)

Standard proctor test on natural soil stabilized with coconut shell of size 2–4.75 mm and 4.75–10 mm has been conducted to obtain maximum derv density (MDD) value, and results are presented in Fig. 4. Natural soil has MDD value of 1.64 g/cc. Decreasing trend has been observed in dry density values till 6% CSP. After that, dry density increased slightly till 10% addition. The reason for above behavior could be that in the beginning, on the addition of coconut shell powder, most of the voids in the clay particles might be filled with CSP, and CSP along with clay particles mixed and compacted quite well [24], thus increasing the density of the soil mixed with coconut shell powder. The curve obtained follows the expected trend as dry density increases in the beginning, attains its peak and then starts decreasing [35].

In the given curve, maximum dry density first increases and then starts decreasing, and this is as per the variation recommended. The above trend could be attributed to

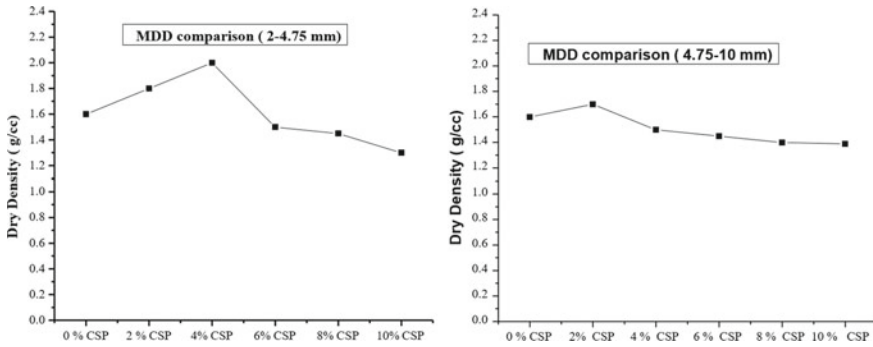


Fig. 4 a MDD comparison (2–4.75 mm), b MDD Comparison (4.75–10 mm)

the degree of compaction attained and how seamlessly coconut shell powder mixes fills in to the pore spaces of the clay particles [1, 24].

4.3 Permeability Test

Permeability test is performed on the soil stabilized with coconut shell, between the size range of 2–4.75 and 4.75–10 mm at 2, 4, 6, 8 and 10%, and results are presented in Fig. 5. For CSP in the range of 2–4.75, at 4% CSP, permeability increased all of a sudden, and then at 6%, it decreased. On the other hand, for 4.75–10 mm, peak was obtained at 6% with the same trend as that of CSP with 2–4.75 mm. The behavior of clay particles shown in the curve might well be due to the variation in void ratio and porosity of the clay particles on addition of coconut shell powder [24, 35]. If void ratio and porosity are closer to each other, then regular trend could have been obtained. Also, movement of CSP through the interconnected voids of clay particles also plays an important role in determination of permeability.

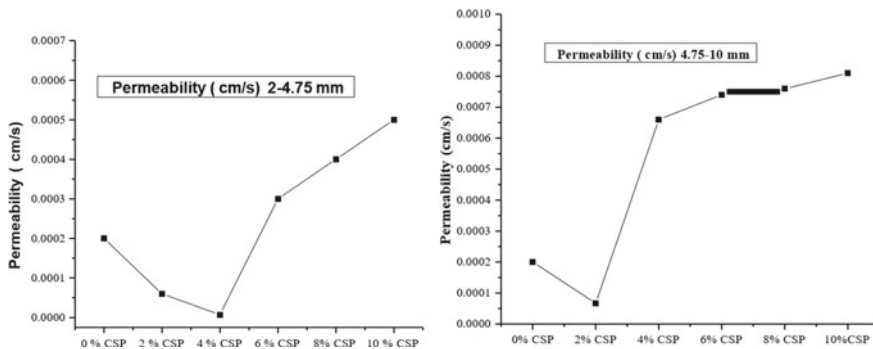


Fig. 5 Variation in permeability corresponding to % CSP (2–4.75 and 4.75–10 mm)

4.4 Unconfined Compressive Strength Test (UCS)

Unconfined compressive strength test has been conducted on the soil sample both with and without the coconut shell. Different percentages of coconut have been used along with varying percentage. In UCS, soil sample is subjected to compression, and reading is noted until the soil specimen fails or cracks. Then along the failure plane, we measure the angle of shear failure and with the help of Mohr circle, both cohesion and angle of shear resistance are determined. The results of angle of internal friction and cohesion for the CSP of different sizes and percentages are presented in Figs. 6 and 7.

There was increase in cohesive strength and decrease in angle of friction after stabilization [35]. Due to the fineness of the coconut shell powder, it perfectly fits into the void of the soil and owing to its similar size as that of soil; it seamlessly mixes with the soil, hence replacing water or any other material finer than it. Also, if we use coconut shell charcoal powder, due to the presence of SiO₂ in sufficient quantity, resulting in stronger bond between particles and cohesion values increases [2].

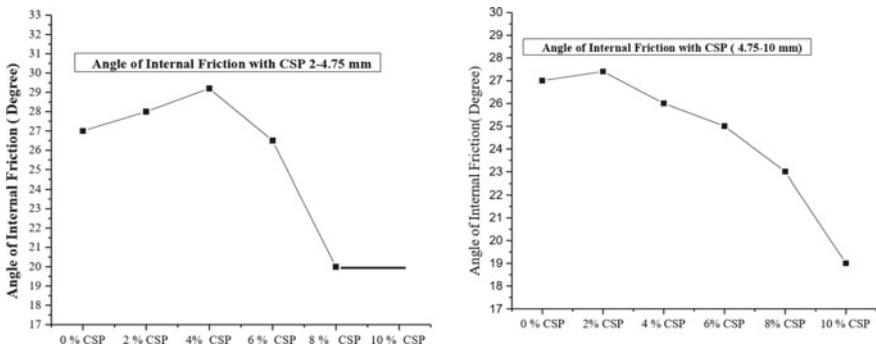


Fig. 6 Angle of internal friction (2–4.75 mm and 4.75–10 mm)

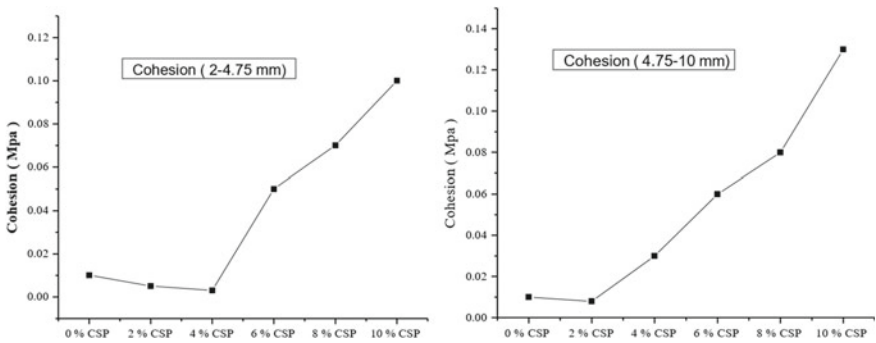


Fig. 7 Cohesion value corresponding to soil type (2–4.75 and 4.75–10 mm)

According to previous experimental studies, maximum angle of shearing resistance was observed at 5% crushed coconut shell powder [36].

5 Conclusion

Based on the results, it can be concluded that on the addition of different proportions and sizes of coconut shell powder in the soil, significant improvement in the performance of the soil has been observed. The properties such as OMC, MDD, permeability, cohesion and angle of internal friction of soil mixed with coconut shell powder were improved in comparison with the normal soil. When coconut shell powder of size 2–4.75 mm and 4.75–10 mm has been used, best results have been observed at 4% and 2%, respectively. The increase in the performance of the soil amended with the coconut shell powder is due to the high strength characteristics, less permeable, weather resistant and high modulus of coconut shell powder. Also, when natural soil mixed with coconut shell is used as a backfill material in retaining wall, permeability of the entire soil mass reduces due to presence of high quantity of lignin in coconut shell used in powdered form. Considering the positive impact of coconut shell powder on the soil, it can be inferred that for cost effective and environment-friendly stabilizations, locally available coconut shell powder can be used (2–4%) to avoid the problematic behavior of soil in retaining wall.

References

1. Radhika B (2017) Variation of properties in Shedi soil on addition of lime and coconut. 8(6):932–938
2. Nayak D (2021) Geotechnical characterization of lithomargic clays of Uttara Kannada District, Karnataka. XIII 7:168–176
3. Firoozi AA, Guney Olgun C, Firoozi AA, Baghini MS (2017) Fundamentals of soil stabilization. *Int J Geo-Eng* 8(1). <https://doi.org/10.1186/s40703-017-0064-9>
4. Winterkorn HF, Pamukcu S (1991) Soil Stabilization and Grouting. *Found Eng Handb* 317–378. https://doi.org/10.1007/978-1-4757-5271-7_9
5. Afrin H (2017) A review on different types soil stabilization techniques. *Int J Transp Eng Technol* 3(2):19. <https://doi.org/10.11648/j.ijtet.20170302.12>
6. Ramaji AE (2012) A review on the soil stabilization using low-cost methods. *J Appl Sci Res* 8(4):2193–2196
7. Koerner RM, Hwu BL, Wayne MH (1987) Soft soil stabilization designs using geosynthetics. *Geotext Geomembr* 6(1–3):33–51. [https://doi.org/10.1016/0266-1144\(87\)90056-2](https://doi.org/10.1016/0266-1144(87)90056-2)
8. Pinto MIM (2003) Applications of geosynthetics for soil reinforcement. *Gr Improv* 7(2):61–72. <https://doi.org/10.1680/grim.7.2.61.37503>
9. Harris RF, Allen ON, Chesters G, Attoe OJ (1963) Evaluation of microbial activity in soil aggregate stabilization and degradation by the use of artificial aggregates. *Soil Sci Soc Am J* 27(5):542–545. <https://doi.org/10.2136/sssaj1963.03615995002700050022x>
10. Saneiyani S, Ntarlagiannis D, Werkema DD, Ustra A (2018) Geophysical methods for monitoring soil stabilization processes. *J Appl Geophys* 148:234–244. <https://doi.org/10.1016/j.japgeo.2017.12.008>

11. Jamiolkowski M (2019) Recent thoughts in geoenvironmental engineering
12. Wu J et al (2021) A generic framework of unifying industrial by-products for soil stabilization. *J Clean Prod* 321(September):128920. <https://doi.org/10.1016/j.jclepro.2021.128920>
13. Ogawa K, Taguchi K, Kinoshita K (1999) Stabilization of soil surface
14. Prasanna S (2019) Utilization of waste plastic shreds for stabilization of soil, vol 29. Springer Singapore
15. Ghais A, Ahmed A (2014) Fly Ash utilization in soil stabilization. 76–78. <https://doi.org/10.15242/iicbe.c514601>
16. Edil TB, Acosta HA, Benson CH (2006) Stabilizing soft fine-grained soils with fly ash. *J Mater Civ Eng* 18(2):283–294. [https://doi.org/10.1061/\(asce\)0899-1561\(2006\)18:2\(283\)](https://doi.org/10.1061/(asce)0899-1561(2006)18:2(283))
17. Prabakar J, Dendorkar N, Morchhale RK (2004) Influence of fly ash on strength behavior of typical soils. *Constr Build Mater* 18(4):263–267. <https://doi.org/10.1016/j.conbuildmat.2003.11.003>
18. Using S, Pozzolans N (2017) Enhancing the engineering properties of expansive soil using bagasse ash Enhancing the engineering properties of expansive soil using bagasse ash. *J Phys Conf Ser*
19. Dang LC, Khabbaz H, Ni BJ (2021) Improving engineering characteristics of expansive soils using industry waste as a sustainable application for reuse of bagasse ash. *Transp Geotech* 31(July):100637. <https://doi.org/10.1016/j.trgeo.2021.100637>
20. Rahman ZA, Ashari HH, Sahibin AR, Tukimat L, Razi IWM (2014) Effect of rice husk ash addition on geotechnical characteristics of treated residual soil. *Am J Agric Environ Sci* 14(12):1368–1377. <https://doi.org/10.5829/idosi.ajeaes.2014.14.12.12462>
21. Mohammed YF, Falah HR, Kawther A-S, YH (2012) Improvement of clayey soil characteristics using rice husk Ash.pdf. *J Civ Eng Urban* 3(1):12–18 [Online]. Available: <http://www.ojceu.ir/main/%5Cn19> visited on 02/04/2014
22. Sharma V, Vinayak HK, Marwaha BM (2015) Enhancing compressive strength of soil using natural fibers. *Constr Build Mater* 93:943–949. <https://doi.org/10.1016/j.conbuildmat.2015.05.065>
23. Zhao L-S, Zhou W-H, Su L-J, Garg A, Yuen K-V (2019) Selection of physical and chemical properties of natural fibers for predicting soil reinforcement. *J Mater Civ Eng* 31(10):04019212. [https://doi.org/10.1061/\(asce\)mt.1943-5533.0002850](https://doi.org/10.1061/(asce)mt.1943-5533.0002850)
24. Arathy VB, Jery C, Raj J, Lekshmi VS, Chacko A (2015) Effect of coconut shell powder on the strength of soil. 3(2):35–40
25. Oluremi JR, Osuolale OM, Adeoye TT, Abiola A (2016) Strength development in lateritic soil stabilised with coconut shell ash for highway pavement construction, *nnovative Syst. Des Eng* 7(11):49–56
26. Adeel S, Kiran S, Shahid M, Habib SR, Habib N, Hussaan M (2021) Ecofriendly application of coconut coir (*Cocos nucifera*) extract for silk dyeing. *Environ Sci Pollut Res*. <https://doi.org/10.1007/s11356-021-15669-6>
27. Nunes LA, Silva MLS, Gerber JZ, Kalid RDA (2020) Waste green coconut shells: Diagnosis of the disposal and applications for use in other products. *J Clean Prod* 255:120169. <https://doi.org/10.1016/j.jclepro.2020.120169>
28. Kabir Ahmad R., Anwar Sulaiman S, Yusup S, Sham Dol S, Inayat M, Aminu Umar H (2021) Exploring the potential of coconut shell biomass for charcoal production. *Ain Shams Eng J* xxxx. <https://doi.org/10.1016/j.asej.2021.05.013>
29. Bolivar-Telleria M et al (2018) Second-Generation bioethanol from coconut husk. *Biomed Res Int* 2018. <https://doi.org/10.1155/2018/4916497>
30. Banzon JA (1980) The coconut as a renewable energy source. *Philipp J Coconut Stud* 11–27
31. Dahale PP, Nagarnaik PB, Gajbhiye AR (2012) Utilization of solid waste for soil stabilization: a review. *Electron J Geotech Eng* 17(January):2443–2461
32. Kamon BM, Nontananandh S (1991) 117(1):1–17
33. Puppala A, Hoyos L, Viyanant C, Musenda C (2000) Fiber and fly ash stabilization methods to treat soft expansive soils. *Proc United Eng Found ASCE Geo-Institute Soft Gr Technol Conf Soft Gr Technol GSP* 112, 301:136–145. [https://doi.org/10.1061/40552\(301\)11](https://doi.org/10.1061/40552(301)11)

34. Zumrawi M, Johnson A, IJERT-Expansive soil stabilization using coconut shell powder and lime. Related papers Soil Stabilization as an Avenue for Reuse of Solid Wastes: A Review Jijo James Effect of Bitumen and Fly Ash on Expansive Soil Properties Expansive Soil Stabilization. IJERT J Int J Eng Res Technol
35. Athira T, Johnson A, Krishnankutty SV (2017) Expansive soil stabilization using coconut shell powder and lime. Int J Eng Res 6(03):541–543.<https://doi.org/10.17577/ijertv6is030512>
36. Science E (2020) Analysis of shear strength clay using coconut shell charcoal powder as stabilization material analysis of shear strength clay using coconut shell charcoal powder as stabilization material. <https://doi.org/10.1088/1755-1315/599/1/012068>

Unconfined Compressive Strength of Fly Ash-Soil-lime-Fiber System



Bhupati Kannur, Hemant S. Chore, and Swati Yede

Abstract The objective of the present study was to investigate the strength of soil-fly ash-fiber-lime system. More specifically to study the effect of different materials such as soil, fly ash, lime, and fiber on the strength of the system in terms of unconfined compressive strength (UCS). The combinations of fly ash stabilized with soil by 15, 25, and 10, 15, and 20% lime added with polypropylene fiber contents of about 0.1, 0.2, and 0.4% were prepared and tested for their strength at curing periods of 7 and 28 days.

Keywords Soil · Fly ash · Lime · Polypropylene fiber · Unconfined compressive strength

1 Introduction

The industrialization is necessary for the development of the country, but the environmental pollution due to the by-products or the waste materials of the industries is unavoidable. The solution is to reuse such materials in the construction industry which also saves the original materials and proves to be cost economic. Fly ash is one such industrial waste which has the potential to improve the strength of soil. Further, there might be scarcity of locally available quality materials nearby the construction locations and procuring the materials from long distances increases the project cost. The tones of fly ash being generated by the thermal power plants can be promisingly utilized in the geotechnical constructions like structural landfills, road sub base, embankments, etc., in replacement to the conventional weak earth material. On the other hand, the use of fibers renders the reinforcing effect. The utilization of

B. Kannur (✉) · S. Yede
Department of Civil Engineering, Dr. B. R. Ambedkar National Institute of Technology Jalandhar,
Jalandhar, Punjab, India
e-mail: bhupati.kmt@gmail.com

H. S. Chore
Datta Meghe College of Engineering, Airoli, Navi Mumbai, Maharashtra, India

the fly ash-soil-fiber system solves both the problems of elimination of solid waste firstly, and provision of a huge amount of needed construction material secondly.

There are many studies on the fly ash-soil-reinforced with fibers. Kar and Pradhan [1] studied the UCS of soil reinforced with randomly distributed fibers. Singh and Goswami [2] studied the compaction properties of lateritic soil with low calcium fly ash and lime. Singh and Kalita [3] studied the California bearing ratio (CBR) behavior of fine grained lateritic soil. Khan [4] studied the swelling pressure of clayey soil-fly ash system. Kaniraj and Gayatri [5] concludes that the samples of raw fly ash have increased strength due to inclusion of fibers as reinforcement. Kumar et al. [6] studied the fly ash embankments with randomly distributed polypropylene fibers. Kumar and Singh [7] studied the UCS, CBR, shear strength, and modulus of elasticity of the fly ash with polypropylene fibers. There are ample studies on randomly distributed and discrete fibers such as [8–10].

2 Materials

Fly ash was procured from Nashik Thermal Power Station. The chemical and physical properties of the same are presented in the Table 1. The polypropylene fibers of length 12 mm and diameter 34 μm were used in the study were obtained from build core chemicals, Andheri, Mumbai. The density of fibers is about 0.91 g/cm^3 . The lime used in the study was purchased from retailer shop in Airoli, Navi Mumbai. The soil used in the research was brought from Ratnagiri. The index properties of the soil are tabulated as in the Table 2.

Table 1 Physical and chemical properties of fly ash

Physical properties	
Specific gravity	2.13
Liquid limit	21
Shrinkage limit	29
Loss on ignition	1.06
Moisture (%)	0.21
<i>Chemical composition</i>	
Silica (SiO_2)	58.04
Alumina (Al_2O_3)	25.71
Ferric Oxide (Fe_2O_3)	5.31
Sulfur trioxide (SO_3)	0.676
Calcium Oxide (CaO)	5.60
Magnesium Oxide (MgO)	1.589

Table 2 Index properties of soil

Liquid limit [11]	63.8%
Plastic limit [11]	33.36%
Shrinkage limit	25%
OMC [12]	36.31%
MDD (gm/cm ³) [12]	1.396
Specific gravity	2.7

3 Experimental Program

The present study carried a series of tests on various materials for their physical, chemical, and geotechnical properties along with important tests to evaluate the strength of the system. In total, 18 combinations have been formed of fly ash stabilized with 15 and 25% of soil, lime of about 10, 15, and 20% and polypropylene contents of about 0.1, 0.2, and 0.4% as shown in Table 3.

Standard proctor tests have been conducted to evaluate the maximum dry density (MDD) and optimum moisture content (OMC) [12]. Unconfined compression strength (UCS) [13] test on all the combinations in both soaked and unsoaked conditions have been performed.

3.1 Unconfined Compression Strength

3.1.1 Sample Preparation

A cylindrical mold of 38.1 mm diameter and height of 76.2 mm has been utilized for the preparation of samples. The samples were cured for 7 and 28 days. The stabilized fly ash may be subjected to inundation in the field to access the effect of soaking.

Table 3 Combinations of fly ash–soil–lime–fiber system

S. No.	Soil (%)	Lime (%)	Fiber (%)	S. N	Soil (%)	Lime (%)	Fiber (%)
1	15	10	0.1	10	25	10	0.1
2	15	15	0.1	11	25	15	0.1
3	15	20	0.1	12	25	20	0.1
4	15	10	0.2	13	25	10	0.2
5	15	15	0.2	14	25	15	0.2
6	15	20	0.2	15	25	20	0.2
7	15	10	0.3	16	25	10	0.3
8	15	15	0.3	17	25	15	0.3
9	15	20	0.3	18	25	20	0.3

Thus, tests were conducted in both soaked and unsoaked conditions on the samples compacted at OMC. For soaked tests, the specimens were kept immersed in water for 8–10 h after required curing period.

3.1.2 Testing of Samples

The UCS testing machine with a proving ring of capacity of 2–30 kN was used for the UCS test. For each combination three samples were prepared, one was kept for soaked condition, and other two specimens were used for un-soaked condition. All the specimens were tested after curing for 7 and 28 days.

4 Results and Discussion

4.1 Compaction Behavior

The values of MDD and OMC of all the fly ash-soil-lime mixes with fiber reinforcement are as shown in the Table 4. It can be observed that the MDD decreases with increase in fiber content. From the initial trials, it was observed that the MDD of un-reinforced combinations were less than those of reinforced combinations.

Table 4 Compaction properties of fly ash-soil–lime fiber system

Compaction properties for fly ash-soil–lime fiber system with 15% soil						
% of fibers	UCS-10%L		UCS-15%L		UCS-20%L	
	MDD (g/cc)	OMC (%)	MDD (g/cc)	OMC (%)	MDD (g/cc)	OMC (%)
0.1	1.23	29	1.25	28	1.25	30
0.2	1.22	28	1.23	28	1.23	30
0.4	1.21	30	1.22	31	1.22	32
Compaction properties for fly ash-soil–lime fiber with 25% soil						
% of fibers	UCS-10%L		UCS-15%L		UCS-20%L	
	MDD (g/cc)	OMC (%)	MDD (g/cc)	OMC (%)	MDD (g/cc)	OMC (%)
0.1	1.42	30	1.45	29	1.47	31
0.2	1.42	30	1.45	31	1.45	32
0.4	1.41	30	1.42	30	1.43	32

Table 5 UCS (kg/cm²) for different fiber contents for fly ash with 15% soil (7-Days Curing)

% of fibers	UCS-10%L		UCS-15%L		UCS-20%L	
	Soaked	Unsoaked	Soaked	Unsoaked	Soaked	Unsoaked
0.1	1.45	3.26	2.46	3.94	2.52	4.52
0.2	1.72	3.51	2.89	4.31	3.01	5.55
0.4	1.67	5.58	3.27	5.95	3.59	7.02

4.2 Unconfined Compressive Strength

The results of UCS tests for various fly ashsoillimefiber systems with 15% and 25% of soil at 7 days curing are presented as in the Tables 5 and 6, and the same are graphically represented with bar charts as shown in Figs. 1 and 2, respectively. Similarly, Tables 7 and 8 shows the UCS results of various combinations of fly ash soillimefiber systems with 15% and 25% soil at 28 days of curing with bar charts as in Figs. 3 and 4, respectively.

Table 6 UCS (kg/cm²) for different fiber contents for fly ash with 25% soil (7-Days curing)

% of fibers	UCS-10%L		UCS-15%L		UCS-20%L	
	Soak ed	Unsoaked	Soak ed	Unsoaked	Soak ed	Unsoaked
0.1	4.3	5.13	4.65	6.1	5.15	6.15
0.2	3.54	6.66	4.7	6.79	5.28	7.61
0.4	3.6	7.57	4.87	8.09	5.71	8.41

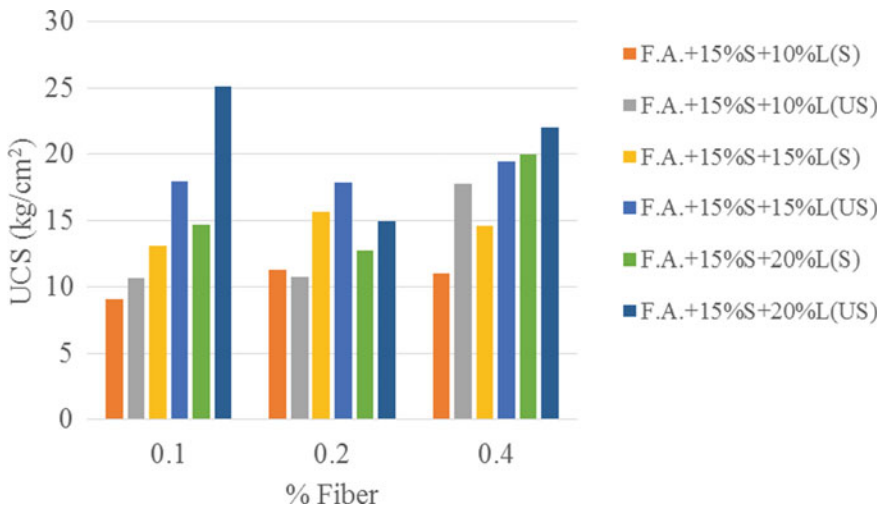


Fig. 1 Variation in UCS with fiber content for fly ash with 15% of soil for 7 days of curing

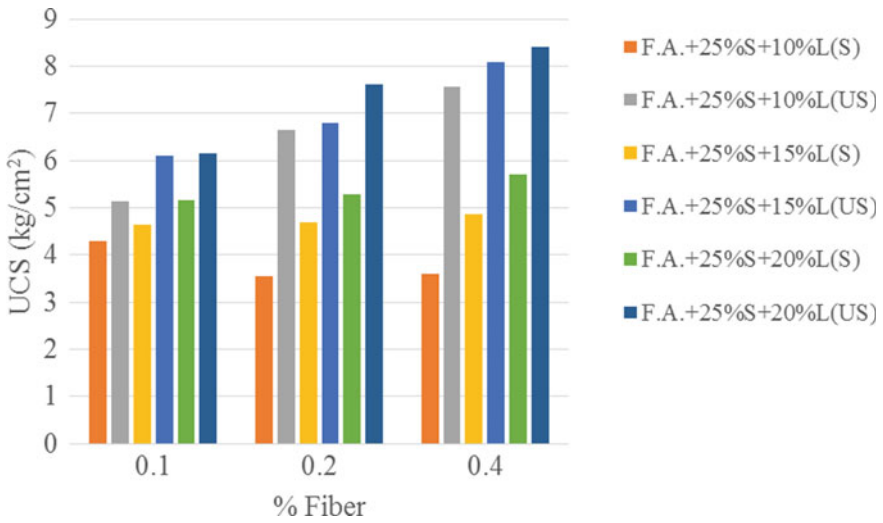


Fig. 2 Variation in UCS with fiber content for fly ash with 25% of soil for 7 days of curing

Table 7 UCS (kg/cm²) for different fiber contents for fly ash with 15% soil (28 days curing)

% of fibers	UCS-10%L		UCS-15%L		UCS-20%L	
	Soaked	Unsoaked	Soaked	Unsoaked	Soaked	Unsoaked
0.1	9.15	10.71	13.12	17.92	14.72	25.17
0.2	11.3	10.75	15.64	17.91	12.71	14.94
0.4	11.08	17.8	14.58	19.44	19.95	22.03

Table 8 UCS (kg/cm²) for different fiber contents for fly ash with 25% soil (28 days curing)

% of fibres	UCS-10%L		UCS-15%L		UCS-20%L	
	Soake d	Unsoaked	Soaked	Unsoaked	Soaked	Unsoaked
0.1	22.24	20.74	22.46	34.83	30.85	32.71
0.2	22.04	18.22	18.32	24.22	20.29	29.55
0.4	11.09	18.45	24.7	28.18	18.9	20.51

4.2.1 Effect of Different Factors on UCS of Fly Ashsoil-Limefiber System

(a) Effect of Soaking

From all the Figs. 1, 2, 3 and 4, it can be observed that in general the unsoaked specimens showed the higher UCS values as compared to those of soaked specimens. There is reduction in the strength of stabilized specimens due to soaking irrespective of mix proportion and curing periods. The reason for the higher strength of unsoaked

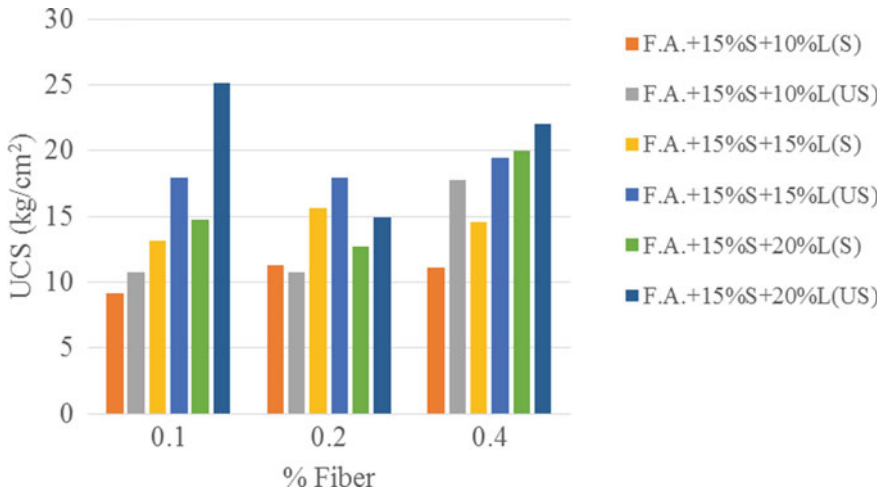


Fig. 3 Variation in UCS with fiber content for fly ash with 15% of soil for 28 days of curing

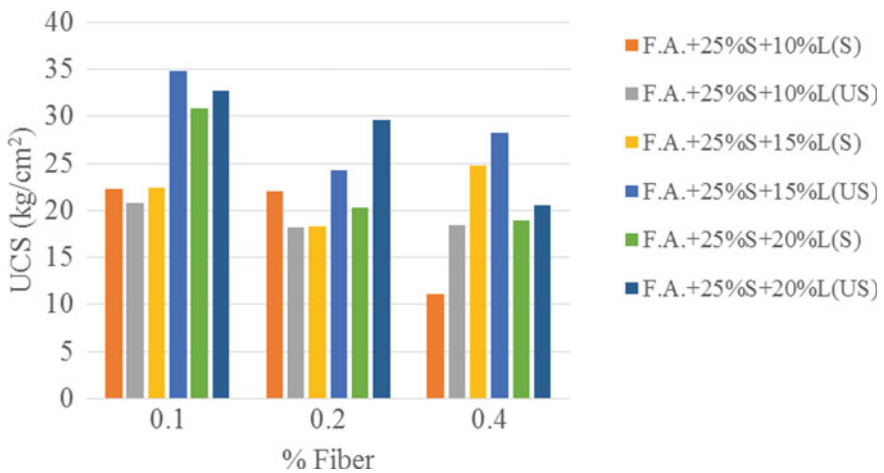


Fig. 4 Variation in UCS with fiber content for fly ash with 25% of soil for 28 days of curing

specimens may be the possible suction developed in the pore fluid which gives rise to high compressive strength.

(b) Effect of lime

In early ages (at 7 days curing) in all the cases, there was increase in the UCS values with increase in the lime content from 10 to 20%. But, at the later ages at 28 days curing the values of UCS of fly ash combinations with 15% of soil reveal that there is increase in the UCS with increase in the lime contents from 10 to 15%. Further addition of lime decreases the UCS at 20% of lime content. Whereas for

stabilized fly ash with 25% soil the increase in the lime content constantly increases the UCS values.

(c) Effect of fiber contents

From the Figs. 1, 2, 3 and 4, it is observed that the compressive strength of the stabilized fly ash-soil-lime mixture varies with randomly distributed polypropylene fibers. In respect of 7 days UCS results, the strength is found to increase significantly with increase in fiber contents from 0.1% to 0.4% respectively. The compositions with 0.4% of fiber showed the maximum strength.

But, for the specimens tested at 28 days of curing the trends were completely different for both the cases with 15% soil and 25% soil as compared to the trend of 7 days UCS values in view of the effect of the fiber contents. From Fig. 3 of UCS values with 15% soil at 28 days, it can be observed that there is decrease in the UCS value as fiber content increases from 0.1% to 0.2%. While on further addition of the fibers, i.e., at 0.4% fiber contents the compressive strengths were again found to increase. On the other hand from Fig. 4 for the 28 days UCS of fly ash-soil-lime system with fiber reinforcement it is clear that the addition of fiber up to 0.1% increases the strength, while further addition of fibers consistently were found to reduce the UCS values at 0.2% and 0.4% fiber contents, respectively.

5 Conclusion

On the basis of the laboratory investigation and the regression analysis following conclusions are drawn

1. The compressive strength increases up to 0.4% fibers for 7 days curing, whereas for 28 days of curing 0.1% of fiber content gives the higher values of UCS.
2. The UCS values increases with increased curing period.
3. The technique of fly ash stabilization with lime alone or with polypropylene fibers is effective method to improve the strength.
4. The unsoaked UCS values are higher than those of soaked samples.
5. About 20% of lime and 0.4% of fiber content gives the optimum strength results in both soaked and unsoaked conditions.

References

1. Kar RK, Pradhan PK (2011) Strength and compressibility characteristics of randomly distributed fiber-reinforced soil. *Int J Geotech Eng IJGE* 5:235–243
2. Singh B, Goswami RK (2012) Compaction characteristics of lateritic soil mixed with fly ash and lime. *Int J Geotech Eng IJGE* 6:437–444
3. Singh B, Kalita A (2013) Influence of fly ash and cement on CBR behaviour of lateritic soil and sand. *Int J Geotech Eng IJGE* 7(2):173–177

4. Khan MA (2013) A CBR based study evaluating subgrade strength of flexible pavements having soil fly ash interface. *Int J Civ Eng Trans B Geotech Eng* 11(1):1–18
5. Kaniraj and V. Gayatri, (2003) Geotechnical behavior of fly ash with randomly oriented fiber inclusions. *J Geotext Geomembr* 21:123–140
6. Kumar A, Walia BS, Mohan J (2005) Compressive strength of fiber reinforced highly compressible clay. *Construct Build Mater*
7. Kumar P, Singh SP (2008) Fiber reinforced fly ash sub-bases in rural roads. *J Transp Eng ASCE* 134(4):171–180
8. Chauhan M.S., Mittal S., and Mohanty B. (2008) Performance evaluation of silty sand and sub grade reinforced with fly ash and fiber. *J Geotext Geomembr*
9. Sadek S, Najjar SS, Freiha F (2010) Shear strength of fiber reinforced sand. *J. Geotech. Eng. Geomech. ASCE* 136(3):490–499
10. Chore HS et al (2011) Performance evaluation of polypropylene fibers on sand-fly ash mixtures in highways. *J Civ Eng (IEB)* 39(1):91–102
11. IS: 2720 Part 5-1970, “Determination of Liquid limit and Plastic limit”, Bureau of Indian Standards (BIS)
12. IS: 2720 Part 7-1983, “Determination of water content—dry density relation using light compaction”, Bureau of Indian Standards (BIS)
13. IS: 2720 Part 10-1973, “Determination of Unconfined Compressive Strength”, Bureau of Indian Standards (BIS)

Bearing Capacity of Geocell Reinforced Model Fly Ash Slope



Vidya N. Patil, Hemant S. Chore, and Vishwas A. Sawant

Abstract A bulk utilization of pozzolonic material in the geotechnical construction is in demand for sustainable infrastructural development as it is economical, and further, it also reduces pollution. This paper focuses on the experimental investigations of only fly ash and single geocell-layered fly ash with slope angle $\beta = 45^\circ$ and footing edge distances ($D_e = 1B, 2B, 3B$). This is done in laboratory and with model instrument. From the experiment, load and settlement are measured, and from this data, load-settlement curves are reported. Ultimate bearing capacity of reinforced fly ash slope with geocell is compared with unreinforced fly ash slope by using load-settlement characteristics for slope. Test results show that load carrying capacity increases with increase in footing location from crest of the slope in all cases. Also, there is ample increase in bearing capacity with addition of single geocell reinforcement at first location of geocell layer ($Z/B = 0.30$). The study demonstrates bearing capacity improvement with the inclusion of geocell reinforcements.

Keywords Bearing capacity · Embedment depth · Fly ash · Geocell

1 Introduction

With the increasing land cost and decreasing availability of good construction sites for infrastructural developments, there is a need to use available sites like landfills, the pozzolonic waste disposal. These sites require large land area for disposal which

V. N. Patil (✉)

Department of Civil Engineering, All India ShriShivaji Memorial Society's College of Engineering, Pune, Maharashtra, India
e-mail: vidya_patil55@rediffmail.com

H. S. Chore

Department of Civil Engineering, Dr. B.R. Ambedkar National Institute of Technology Jalandhar (NITJ), Jalandhar, Punjab, India
e-mail: chorehs@nitj.ac.in

V. A. Sawant

Department of Civil Engineering, Indian Institute of Technology, Roorkee, Uttarakhand, India

is serious environmental problem as these pozzolonic waste materials posing a great environmental problem in changing the air, water, and the land cycles. These sites can be used after filling it with better material fills and/or some reinforcements as well as some modifications. Infrastructural developments on such land areas require special considerations, e.g., foundations on waste embankments, road construction, bridge abutment on waste slopes. The load carrying capacity of the footings and their position with respect to crest of the slope crest are critical in all circumstances as the constructions undertaken on such slope might be unsafe owing to slope failure.

Theme: Sustainable Infrastructure and Engineering Researchers [1–22] have widely worked on utilization of different types of reinforcements for improvement of the strength of such embankment fill.

2 Literature Review

Few researchers [1–5] conducted extensive experimental research with respect to the safe utilization of FA as a fill material. They concluded that inclusion of random geosynthetic fibers significantly improved the strength of fly ash and inferred that FA can be effectively and economically used for constructing stable embankments and fills. These investigations concluded that pulverized coal ash with no cementing properties can be used as a structural fill.

Some of the researchers [4–10] studied load carrying of footings on reinforced slopes via laboratory model testing and found improvement in the capacity, but it depends on selection of type of reinforcement and its embedment depths feasible for the case.

A significant research has been in progress in the area of bearing capacity of reinforced deposits [11, 12] and reported the optimization of variables, length of reinforcing strips, depth of top reinforcing layer from the surface, number of strips, vertical spacing among the consecutive layers. Considerable advantages of reinforcements can be obtained by including the reinforcing layer below footing at optimum embedment depth (z/B) of reinforcement [13]. These investigations are carried out on the utility of FA when subjected to monotonic or static loading have established clearly the effectiveness of FA as backfill material [14–18].

Effect of the confinement of geocell was studied on improvement of strength, and stiffness of granular soil was noted [19]. A study [20] evaluated the performance of different types of reinforcements when placed in sand beds under strip footing. Geocell-reinforced sand cushions were found to reduce the settlement of soft soil [21]. Effect of geocells, when placed in retaining structures, was studied on the failure mechanism under surcharge [22].

Table 1 Geotechnical characteristics of FA [14–17]

S. No	Properties	Value
1	Specific gravity	2.09
2	Liquid limit	NP
3	Plastic limit	NP
4	Maximum dry unit weight (g/cc)	1.35
5	Optimum moisture content (%)	20
6	Angle of internal friction, $\phi = (^{\circ})$	12.95
7	Cohesion, $C = (\text{kN/m}^2)$	7.85

3 Model Tests

3.1 Material Used

The fly ash (FA) procured from a TPP located near Nashik (India) was used in this study. The FA was tested for chemical composition as per IS: 3812 [23] and ASTM C 618 [24]. The FA procured for the purpose of the study meets requirement of Class F fly ash. The tests were undertaken for evaluating physical, index and compaction properties, and shear strength parameters of FA as per IS:2720 [25]. These are already published by the authors [14–17] and reproduced below in Table 1.

3.2 Geocell

It is lightweight, strong, a three-dimensional honeycomb-like cellular confinement system, which offer unique reinforcement for sub-base, sub-grade and embankment. Geocell used in the investigation is StrataWeb® SW 356. The standard physical properties of StrataWeb® SW 356 are provided by the supplier and presented in Table 2. Texture of geocell is polythelene strip which perforated with horizontal rows of maximum 10-mm-diameter holes. The cell perforations area is less than 12% of cell surface area. This is done with a 102-mm weld joint. The required size of geocell with model test tank was 700×300 mm. The cell was cut manually and arranged in model test tank as shown in Fig. 1.

3.3 Geometry of the Model Testing

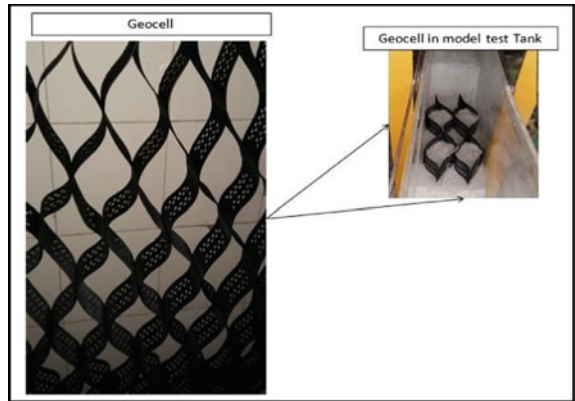
The model test setup was prepared for studying load carrying capacity of axially loaded strip footing when placed on unreinforced and reinforced slope with geometry as shown in Fig. 2. This set up was fabricated and fixed in laboratory (Fig. 4). Different locations of footing relative to the slope crest (D_e) are planned for unreinforced and

Table 2 Properties of geocell reinforcement (as provided by supplier)

Physical Properties	Unit	Typical Value
Nominal-expanded size of cell (width × length)	mm	259 × 224
Nominal-expanded area of cell	cm ²	289
Nominal-expanded section (width × length)	m	0.68 × 2.56
Depth of a cell	N	200
Seam peel strength		2840

Seam hang strength A 102-mm weld joint supporting a load of 72.5 kg for 30 days minimum or a 102-mm weld joint supporting a load of 72.5 kg for 7 days minimum

Fig. 1 Geocell in model test tank



reinforced slope with inclination ($\beta = 45^\circ$) (Fig. 3). The geocell layer with length, $L_r = 0.7B$, was placed as a reinforcement at $z/B = 0.30$ from top of slope (Figs. 2 and 3).

Fig. 2 Geometry considered in the study

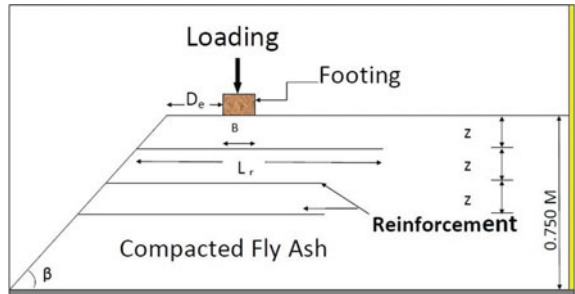


Fig. 3 Schematic of experimental setup

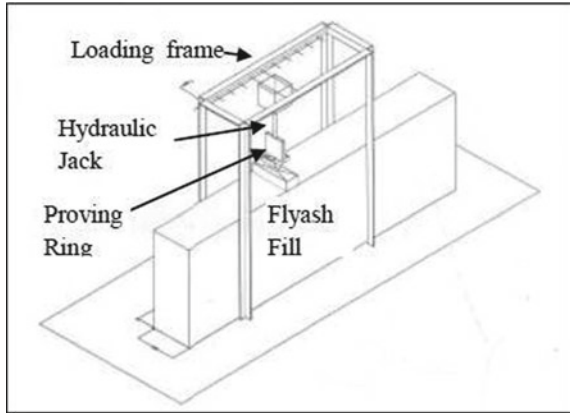


Fig. 4 Experimental setup



3.4 Model Instrument and Experimental Procedure

The authors have already explained the particulars of the model test tank and footing in their earlier publications (Fig. 4) [14, 15, 17]. The experimental procedure is also available [14, 15, 17]. For the sake of brevity, the particulars of the model instrument, test tank, footing, and the experimental procedure are not furnished here. The tests were conducted with the model instrument (Figs. 3, 4 and 5).

A model footing (300 mm × 100 mm × 100 mm) made of Sal wood was made use of. Its base was roughed by fixing a thin layer of sand. Width of the model footing in this testing is $B = 0.1$ m. Based on the experimental observations, load-settlement curves were deduced, and ultimate bearing capacity of footing was evaluated [26]. The parameters used in the test are presented in Table 3.

Fig. 5 Close up while the measurements being taken



Table 3 Parameters considered in the study

Type of slope	Constant parameter	Variable parameter
Unreinforced	$B = 100 \text{ mm}$ $\beta = 45^\circ$	$D_e/B = 1.0$ $D_e/B = 2.0$ $D_e/B = 3.0$
Reinforced	$B = 100 \text{ mm}$ $N = 1$ $L_r = 7B$ $\beta = 45^\circ$, $z/B = 0.03$	$D_e/B = 1.0$ $D_e/B = 2.0$ $D_e/B = 3.0$

4 Results and Discussion

The tests were conducted for different locations of the footing (D_e) with respect to crest of the slope in the context of unreinforced and reinforced slope. The tests continued until settlement of footing got stabilized, and corresponding load and settlement were recorded. The results are compared for two series of unreinforced and reinforced slope with three different footing locations and same slope inclination 45° . The load-settlement characteristics of unreinforced and reinforced slope were obtained for set parameters (Table 3) as shown in Fig. 6.

Several investigations with unreinforced slope have been done by the authors in respect of other type of reinforcements [14–17] and found the slope inclination, $\beta = 45^\circ$ as a critical inclination. Pursuant to this, the work is extended with critical slope $\beta = 45^\circ$ and different footing locations ($D_e = 1, 2, \text{ and } 3B$) for unreinforced and geocell-reinforced fill. Embedment depth for geocell was kept same for all reinforced slope testing, $z/B = 0.03B$. The load carrying capacity of footing placed at a location from the slope’s crest is found to have been increased significantly with increase in D_e and inclusion of geocell at $z/B = 0.03 \text{ m}$.

Ultimate load bearing capacity is found to be improved with a layer of the geocell reinforcement model slope testing. The comparison of the results in respect of reinforced and unreinforced slopes is shown in Fig. 6. The load-settlement analysis

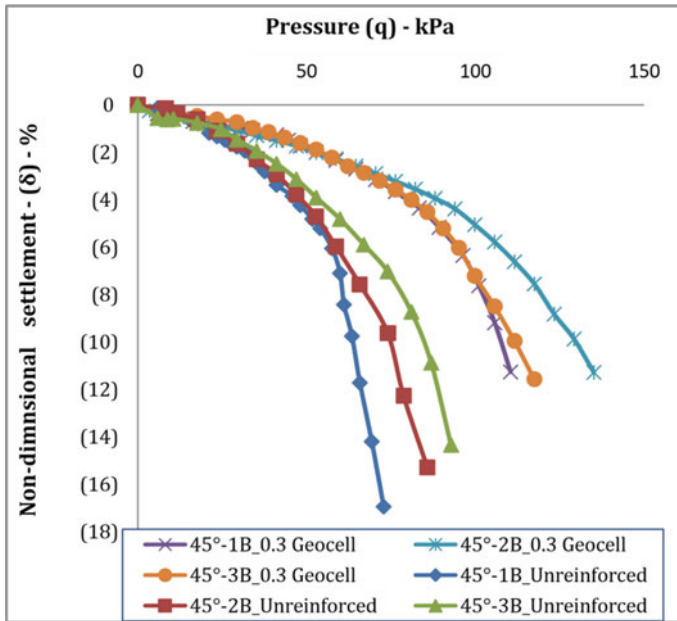


Fig. 6 Load-settlement characteristics for $Z = 0.30$

is compared for all parameters and found ultimate bearing capacity with Adam Colin [14] technique. The ultimate capacity of geocell-reinforced slope is more when compared with the unreinforced one (Fig. 6). It is found to go on increasing with edge distance in respect of both the embedment depth ratios in case of geocell-reinforced slope. This is true in case of all the values edge distances and the embedment ratio, considered in the present study.

When ultimate capacity of geocell-reinforced fill is compared with that of unreinforced one, it is found to be 24% at $z/B = 0.3$ with respect to the edge distance of $1B$. For the next edge distance, $2B$, the increase at the corresponding embedment depth ratios is found to be 20%, and at $3B$, the increase at either embedment depth ratio is same, i.e., 13.5%. The difference between the bearing capacities observed between the two values of the embedment depth ratios goes on decreasing with the edge distance.

5 Conclusions

- i. Improvement in bearing capacity of a model footing is noticed with location of a footing succeeding from the crest of a slope.
- ii. The footing location has a significant effect on the bearing capacity of slopes as it increases with gap between footing location and slope crest.

- iii. The inclusion of single geocell reinforced at $z/B = 0.30$ confirms improvement in bearing capacity as compared to that in unreinforced one.
- iv. The strength in of geocell-reinforced sloped fill is found to be more as compared to that of unreinforced one.

Acknowledgements The authors acknowledge the financial support rendered by Savitribai Phule Pune

University under the research scheme of Board of University Colleges and Development (BCUD 2014-16) and StrataWeb® for providing geocell for experimentation work.

References

1. Madhavi LG, Murthy VS (2007) Effects of reinforcement form on the behavior of geosynthetic reinforced sand. *Geotext Geomembr* (25):23–32
2. Bhardwaj DK, Mandal JN (2008) Study on polypropylene fiber reinforced fly ash slopes. In: The 12th international conference of international association for computer methods and advances III geomechanics (IACMAG) 1(6):3778–3787
3. Kim B, Prezzi M (2008) Compaction characteristics and corrosively of Indiana Class- F fly ash and bottom ash mixtures. *Constr Build Mater* (22):694–702
4. Chaudhary AK, Jha JN, Gill KS (2010) Shear Strength characteristics of fiber reinforced fly ash, *Indian Geotech Conf*
5. Tejaswini BR, Gangadara HC, Muddaraju BK (2014) A study on the performance of circular footing embedded in geogrid reinforced fly ash beds under cyclic loading. *Int J Res Eng Technol* 3(06):76–80
6. Yoo C (2001) Laboratory investigation of bearing capacity behavior of strip footing on geogrid reinforced sand slope. *Geotext Geomembr* (9):279–298
7. El Sawwaf MA (2007) Behavior of strip footing on geogrid-reinforced sand over a soft clay slope. *Geotext Geomembr* 25:50–60
8. Alamshahi S, Hataf N (2009) Bearing capacity of strip footings on sand slopes reinforced with geogrid and grid anchors. *Geotext Geomembr* 27:217–226
9. Mittal S, Shah MY, Verma NK (2009) Experimental study of footing on reinforced earth slope. *Int J Geotech Eng* 3(2):251–260
10. Shukla SK, Sivakugan N, Das BM (2011) A state of the art review of geosynthetic reinforced slopes. *Int J Geotech Eng* 5(1):1732
11. Kumar A, Saran S (2006) Parametric study of footing resting on reinforced soil. *Civ Eng Constr Rev Found Spec Issue* 19(2):4857
12. Shukla SK, Sivakugan N, Das BM (2009) Fundamental concepts of soil reinforcement- an overview. *Int J Geotechn Eng* 3(3):329342
13. Yoo C (2001) Laboratory investigation of bearing capacity behavior of strip footing on geogrid-reinforced sand slope. *Geotext Geomembr* 19(2001):279–298
14. Patil VN, Chore HS (2016) Bearing capacity of embedded strip footing on geogrid reinforced fly ash slope. *Open J Civ Eng* 6:179–187
15. Patil VN, Chore HS (2017) Bearing capacity behavior of a strip footing on model slopes made up of fly ash and furnace slag. *Int J Geotech Eng* 11(5):431–440
16. Patil VN, Chore HS, Sawant VA (2020) Numerical analysis of reinforced embankment slopes made up of pozzolanic waste materials. *Int J Geo-Eng* 11:1–28
17. Patil VN, Chore HS, Sawant VA (2021) Bearing capacity of reinforced embankment slope models of fly ash and furnace slag. *Transp Infrastruct Geotechnol* 1–32

18. Ram Rathan Lal BR, Manda I JN (2012) Feasibility study of fly ash as backfill material in cellular reinforced walls. *Electron J Geotech Eng (EJGE)* 17:1437–1458
19. Latha GM, Dash SK, Rajagopal K (2009) Numerical simulation of the behavior of geocell reinforced sand in foundations. *Int J Geomech* 9:143–152
20. Dash SK, Rajagopal K, Krishnaswamy NR (2004) Performance of different geosynthetic reinforcement materials in sand foundations. *Int J Geosynthetics* 11(1):35–42
21. Zhou H, Xuejun W (2008) Model studies on geogrid- or geocell-reinforced sand cushion on soft soil. *Geotext Geomembr* 26(3):231–238
22. Chen RH, Chiu YM (2008) Model tests of geocell retaining structures. *Geotext Geomembr* 26(1):56–70
23. IS:3812 (Part 1) Pulverized Fuel Ash—specification, Bureau of Indian Standards (BIS), New Delhi (2013).
24. ASTM C618–12a: Standard Specification for Coal Fly Ash and Raw or Calcined Natural Pozzolan for Use in Concrete
25. IS:2720 (Part I) Methods of test for soils. Bureau of Indian Standards (BIS), New Delhi (1983)
26. Adams MT, Collin JG (1997) Large model spread footing load tests on geosynthetic reinforced soil foundation. *ASCE J Geotech Geoenvironmental Eng* (123)1:6672

Unconfined Compressive Strength of Clayey Soil Stabilized with Marble Dust



H. S. Chore, Anurag M. Khadse, and Aditya D. Ahirwar

Abstract Marble is used to enhance the artistic value of structures, sculptures, and monuments. In India, Rajasthan accounts for 89% of the marble production of the country. There are almost 4000 marble mines in state of Rajasthan. During the mining and finishing operations, a substantial amount of marble waste is generated in order to obtain a well-finished product. In existing study, effort is made to judge the usefulness of marble dust for stabilization of clayey soil. Parameters like compaction characteristics, unconfined compressive strength are assessed through experimental work. Laboratory investigations were carried out to assess the effect of curing period on strength of different combination of mixes. Test results indicates that the strength of composite mix increases with increase in proportion of marble dust and also, with the curing period.

Keywords Clayey soil · Marble dust · Unconfined compressive strength · Curing period

1 Introduction

Marble dust is the by-product of the marble industry which is generated from cutting and grinding of the marble. “The waste generation is approximately 40% of the total marble handled per annum. It has relevance because annually about 68 million of marbles are manufactured all over the world.” To obtain a well-finished product, an enormous quantity of waste is generated throughout mining and finishing processes.

H. S. Chore (✉) · A. M. Khadse · A. D. Ahirwar
Department of Civil Engineering, Dr. B.R. Ambedkar National Institute of Technology,
Jalandhar 144011, India
e-mail: chorehs@nitj.ac.in

A. M. Khadse
e-mail: anuragmk.gg.20@nitj.ac.in

A. D. Ahirwar
e-mail: ahirwarad.ce.19@nitj.ac.in

Although notified sites have been established for dumping, the marble cutting plants are dumping the waste marble powder in any neighboring spaces near their facility. The disposal of marble waste on open ground creates serious threats for public health and for the environment as well. Besides, marble wastes may contaminate the water and cause diseases if mixed with the surface water sources. It may also percolate through the soil and affect the ground water. It also causes clogging of soil by lowering its permeability and reduces the productivity of the soil.

However, the tendency of such industrial waste material to blend well with soil and improve the strength characteristics of composite mix makes it suitable for possible use in ground improvement.

Celik et al. [1] emphasized on importance of conducting research to identify potential applications of waste generated by marble industry. Baser [2]; Palaniappan and Stalin [3] and Agrawal et al. [4] proved that the marble dust utilization in ground improvement.

Singh et al. [5]; Akinwumi et al. [6] and Yilmaz et al. [7] have investigated effectiveness of utilization of marble waste for soil stabilization. Experimental investigation suggests improvement in index properties, compaction characteristics, strength of soil-marble dust composite mix.

Gurbuz [8] investigated the impact of addition of marble powder on strength and durability of composite mixes containing soil and marble dust. Saygili [9] identified that marble dust with higher calcium content plays vital role in hydration process. Formation of pozzolanic compound results in an increase in strength. Okagbue [10] investigated the effect of 7 day curing on soil stabilized with marble dust.

The purpose of the investigation was to analyze the compaction characteristics and strength of variety of mixes containing clayey soil and marble dust. Comprehensive laboratory testing was conducted to assess the effect of curing on unconfined compressive strength of composite mix.

2 Material and Method

In present study, clayey soil was mixed with different proportions of marble dust (10, 20, 30 and 40%). The soil and marble dust used for the experimental investigation was brought from local supplier. The engineering properties of different combinations of mixes were found out, which includes determination of compaction characteristics and unconfined compressive strength of clay stabilized with marble dust. Table 1 illustrates particulars of clay-marble dust mixes, considered in the present study.

3 Discussion of Results

Experimental investigation includes preliminary tests to determine index properties of clay. Table 2 presents index properties of the soil.

Table 1 Different combination of mixes

S. No.	Property	Value
1	PC (Plain Clayey Soil)	100% Clay
2	C10MD	Clay + 10% Marble dust
3	C20MD	Clay + 20% Marble dust
4	C30MD	Clay + 30% Marble dust
5	C40MD	Clay + 40% Marble dust

Table 2 Index properties of clayey soil

S. No.	Property	Value
1	LL: Liquid limit (%)	43.10
2	PL: Plastic limit (%)	24.50
3	Specific gravity	2.601
4	OMC: Optimum moisture content (%)	18.05
5	MDD: Maximum dry density (gm/cc)	1.72

Compaction characteristics govern geotechnical properties of soil. Focus of current study is on analyzing the effect of addition of marble dust on maximum dry density (MDD) and optimum moisture content (OMC) of the different combination of mixes.

As the proportion of marble dust in composite mix increases, the MDD of composite mix increases while OMC decreases (Fig. 1).

Tests were carried out to determine the effect of addition of marble dust on unconfined compressive strength (UCS) of various mixes. From Fig. 2, it can be noted that

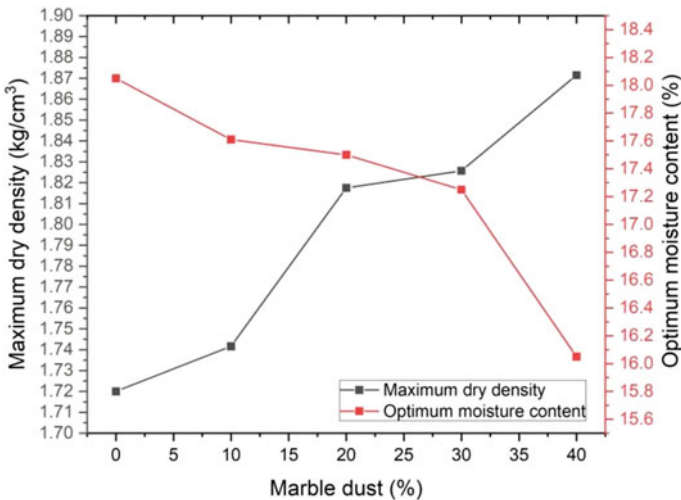


Fig. 1 Variation in MDD and OMC of soil-marble dust composite mix

as the amount of MD increases, the UCS of clay-marble dust mix increases up to addition of marble dust up to 20%, thereafter rate of increase in strength reduces.

The increment in UCS is 65.22% after addition of 20% marble dust and 40.86% after addition of 30% marble fines. Akinwumi identified the possible reason behind increase in strength as cation exchange process which helps in formation of pozzolanic compound.

Investigation is further extended to evaluate the effect of 7 and 14 days curing on UCS of the composite mix. Impact of curing period on UCS of stabilized mix is presented in Fig. 3.

UCS of composite mix increases with increase in proportion of marble dust up to 20%. After further addition, UCS decreases. Similar trend is observed for the 7 and

Fig. 2 Variation in UCS of uncured composite mix

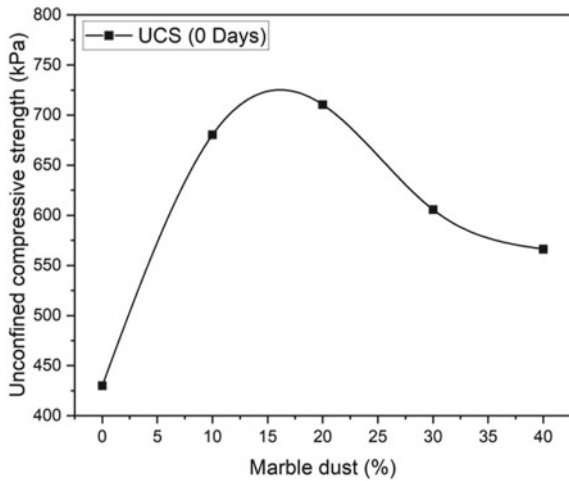
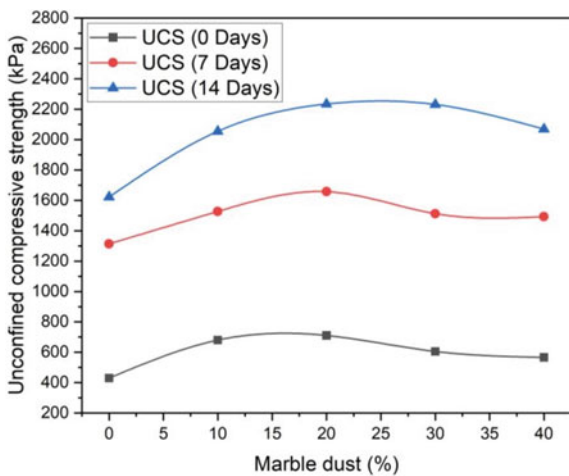


Fig. 3 Variation in UCS of composite mix for after 7 and 14 days curing



14 days curing period. From Fig. 3, it can further be noted that the UCS of composite mix increases with curing period.

4 Summary and Conclusions

From the experimental investigations on stabilized clay samples, following conclusion can be drawn:

1. MDD of the composite mix increases while the optimum moisture content decreases, after addition of marble dust.
2. Strength of the clay-marble dust composite mix increases with addition of marble dust up to 20%.
3. Based on result obtained from UCS test, mix with 20% marble dust found out to be optimum mix.
4. UCS of the composite mix increases significantly with curing period.

Thus, marble dust can be advantageously used to stabilize clayey soil based on strength characteristics of different combination of mixes. This will not only provide possible approach for safe disposal of waste by product but also will end up saving the conventional material that would have been used therein.

References

1. Celik MY, Sabah E (2008) Geological and technical characterization of iscehisar (Afyon-Turkey) marble deposits and the impact of marble waste on environmental pollution. *J Environ Manage* 87(1):106–116
2. Baser O (2009) Stabilization of expansive soils using waste marble dust. Master of Science Thesis submitted to civil engineering department, Middle East, Technical University
3. Palaniappan KA, Stalin VK (2009) Utility effect of solid wastes in problematic soils. *Int J Eng Res Ind Appl* 2(1):313–321
4. Agrawal V, Gupta M (2011) Expansive soil stabilization using marble dust. *Int J Earth Sci Eng* 04(06):59. ISSN 0974-5904
5. Singh PS, Yadav RK (2014) Effect of marble dust on index properties of black cotton soil. *Int J Engg Res Sci Tech* 3:158–163
6. Akinwumi II, Booth CA (2015) Experimental insights of using waste marble fines to modify the geotechnical properties of a lateritic soil. *J Environ Eng Landsc Manag* 23(2):121–128
7. Yilmaz F, Yurdakul MUHAMMET (2017) Evaluation of marble dust for soil stabilization. *Acta Phys Pol, A* 132(3):710–711
8. Gurbuz A (2015) Marble powder to stabilise clayey soils in sub-bases for road construction. *Road Mater Pavement Des* 16(2):481–492
9. Saygili A (2015) Use of waste marble dust for stabilization of clayey soil. *Mater Sci* 21(4):601–606
10. Okagbue CO, Onyeobi TUS (1999) Potential of marble dust to stabilise red tropical soils for road construction. *Eng Geol* 53(3–4):371–380